Methods in Molecular Biology 1324

Springer Protocols

Ülo Langel *Editor*

Cell-Penetrating Peptides

Methods and Protocols

Second Edition

Humana Press

METHODS IN MOLECULAR BIOLOGY

Series Editor
John M. Walker
School of Life and Medical Sciences
University of Hertfordshire
Hatfield, Hertfordshire, AL10 9AB, UK

For further volumes:
http://www.springer.com/series/7651

Cell-Penetrating Peptides

Methods and Protocols

Edited by

Ülo Langel

Department of Neurochemistry, Stockholm University, Stockholm, Sweden

Humana Press

Editor
Ülo Langel
Department of Neurochemistry
Stockholm University
Stockholm, Sweden

ISSN 1064-3745 ISSN 1940-6029 (electronic)
Methods in Molecular Biology
ISBN 978-1-4939-2805-7 ISBN 978-1-4939-2806-4 (eBook)
DOI 10.1007/978-1-4939-2806-4

Library of Congress Control Number: 2015944509

Springer New York Heidelberg Dordrecht London

Printed on acid-free paper

Humana Press is a brand of Springer
Springer Science+Business Media LLC New York is part of Springer Science+Business Media (www.springer.com)

Preface

In the late 1980s and early 1990s, it began to become evident that the old dogma asserting the impermeability of the cell plasma membrane to proteins and peptides was not valid in several new and important cases [1]. First, in 1988, two independent research groups demonstrated the shuttling properties for an HIV tat trans-activator protein [2, 3]. Second, in 1991, the group of Alain Prochiantz reported [4] on cellular internalization of the 60 aa homeodomain of Antennapedia (a *Drosophila* homeoprotein), followed in 1994 by the report on a short 16 aa peptide, pAntp(43–58), later named penetratin, which was necessary and sufficient for this translocation [5].

These reports are usually considered the starting events for the research field of cell-penetrating peptides, or CPPs.[1] My personal preference tends to also see 1994 as another defining year with the publication of the first scientific report on 16 aa pAntp/penetratin. On the other hand, the sequence of pAntp was patented and studied several years before 1994, so the exact date for the CPP field is, hence, more difficult to define by any single event.

To declare a starting moment for CPP research is even more complicated if we recall that several short peptides were earlier reported to induce intracellular events in receptor dependent or independent manner when exposed to cell cultures. It had been speculated even before the "era of CPPs" that toxins or cell surface receptor ligands should be good drug candidates on their own or as delivery vectors for connected drugs (reviewed for blood-brain barrier delivery by TfR in [6]). We can refer to examples such as the peptide toxins mastoparan (from wasp venom), melittin (from bee venom), as well as neuropeptides bradykinin and substance P, which were demonstrated to activate mast cells receptor independently by interaction with plasma membranes or initiating G-protein activation (reviewed in [7]). Recent reports [8] demonstrate the involvement of glycosaminoglycans in cellular uptake of the arginine-rich pituitary adenylate-cyclase-activating polypeptide (PACAP), an endogenous peptide neuro-hormone, and its plasma membrane translocation in a specific receptor-independent manner as well as its efficient mediation of the uptake of various cargoes being even more efficient than TAT peptide. Hence, in future, these known peptides and hormones might be defined as novel members of CPP family, although it sounds unconventional yet.

Comprehensive work was carried out in the 1980s (and perhaps even before) to characterize these peculiar effects of the short peptides. The many antimicrobial peptides are other cases where short peptides dose dependently influence cells by processes such as forming membrane pores or through interacting directly with intracellular targets such as DNA, RNA, and components of protein synthesis [9], suggesting their possible use as drug delivery vectors at nontoxic doses. Recent report on cell-penetrating synthetic nontoxic antimicrobial peptides gives promise to further development of the field [10]. Moreover, several of these peptides were later connected to different bioactive cargos, and intracellular delivery/bioactivity of these cargos has been demonstrated such as in the cases of mastoparan

[1] Also known as protein/peptide transduction domains (PTD), Trojan peptides etc.

[11] or substance P (discussed in [12]). It seems in general that several cell-penetrating peptides carry more than single function exemplified by antimicrobial peptides, neuropeptides, or short protein mimics.

Obviously, this repertoire of internalized cargos should be enlarged to include small or large fluorescent labels conjugated to CPPs, currently used often as tools for visualization of internalization and intracellular/tissue localization. Therefore, although usually not defined as CPPs, all these short peptides could be seen as cell penetrating and the term CPP might need to be redefined in order to cover more properties and functions, even if uncertainties remain in characterizing the specific translocating mechanisms of CPPs. A definition that would incorporate these expanded properties would be as follows.

Cell-penetrating peptides (CPPs) are relatively short peptides, 4–40 aa, with the ability to gain access to the cell interior by means of different mechanisms, mainly including endocytosis, and/or with the capacity to promote the intracellular effects by these peptides themselves, or by the delivered covalently or noncovalently conjugated bioactive cargoes.

The inclusion in the above definition of CPPs [1] of the sentence "with the capacity to promote the intracellular effects by these peptides themselves" is certainly necessary due to multiple demonstrations that short peptides contain motifs that might influence multiple intracellular interactions. CPP mechanisms are very likely to be multiple as well, including the spectra from direct cell membrane penetration to endocytotic internalization of the peptides or CPP/cargo complexes and conjugates. In the latter case, one might argue that there is little difference as compared to cellular signaling cascades initiated by classical ligand-receptor interactions. However, I believe that this difference between CPPs and classical ligands is obvious due to the demonstrations that, in many cases, endosomal escape of the peptides or conjugated cargo is the prerequisite for initiation of intracellular effects. It has been demonstrated that such endosomal escape occurs in cases of CPP-initiated delivery, and hence the promotion of endosomal escape seems to be the essential characteristics of CPPs.

This leads to an intriguing, and even philosophical question: how does one define/distinguish the cargo and CPP? Some short CPPs are concealed in the sequence of a protein like in case of pAntp/penetratin or Tat peptides, being also called peptide/protein transduction domains (PTD). Such PTDs are, to my personal preference, an important subclass of CPPs, and they have been an excellent tool in CPP research. However, the existence of PTDs makes it more complicated to define a CPP, since we must decide whether the short peptide or the whole protein should be called the CPP/PTD. To avoid having the definition become diffuse, we have introduced the requirement that CPPs be a relatively short, 4–40 aa peptide, well understanding that such a definition is somewhat arbitrary, at least for now. The lower length of the peptides, 4 aa, is set by a novel cell-permeable antioxidant peptide, SS31 [13] and the others; the higher length, 40 aa, is here defined as an arbitrary border between the peptides and proteins, although everybody knows that such border is very diffuse.

Another question of definition concerns the cargo. The statement that CPPs "promote the intracellular effects by these peptides themselves, or … conjugated bioactive cargoes" will hopefully cover the problems with CPP definitions as well as enable us to include even small fluorescent labels as intracellularly active cargos.

Of course, there remains much to discover concerning CPP-aided cargo delivery in vivo. Critically, the CPP field is suffering from lack of proper understanding of how to manage with in vivo administration of CPP-based drug candidates. Although, there are multiple reports on in vivo administration of different peptides with CPP properties or as

delivery vectors of bioactive cargos, several hurdles exist on a way to translate the research results into clinical trials, such as toxicity and degradation problems, optimization of the administration, tissue targeting, and others. Careful in vivo studies are underway that seeks to address these issues. Hopefully, this revised edition of the book will enable us to get a sense of where we stand on this and will inspire further applications of CPPs in drug development.

This book is divided into three parts, summarizing the most important areas of CPP research and hopefully raising relevant questions for further development. Part I briefly presents the historical background of CPP studies and the classifications of the available CPPs, and then summarizes the approaches for prediction of novel CPPs. An overview of penetratin studies is also included due to the importance of this CPP for the whole field.

To provide an update of existing CPP methods and where the mechanisms of CPP uptake are still not totally clarified, the methods for testing CPP mechanisms are discussed in Part II. The structure of CPPs and their interactions with phospholipid membranes are important factors in their functioning and, hence, the methods to study these are an essential part of this handbook. Part II mainly describes the methods for studies of "naked" CPPs, that is, CPPs without conjugated cargos. I believe that, although often not including the CPP/cargo internalization mechanisms, such studies are highly relevant since, among multiple interactions of CPP/cargo complexes, there usually occur the steps of "naked" CPP interactions with internalization machinery. These include possible CPP membrane disturbance or interactions with membrane-bound proteins/glycoproteins. Various approaches for the testing of endocytotic pathways of CPP uptake are also described, among these fluorescent and electron microscopy, together with functional splice correction assay and toxicity methods. Different CPP uptake experiments are also compared since it is becoming clear that it is often best to apply several methods in a complementary manner in order to most comprehensively evaluate CPP uptake mechanisms due to the complexity of these processes.

The largest part, Part III presents a representative and brief summary of functionality issues of CPPs, both in vitro and in vivo. Of special interest is the mimicry of proteins by short peptides in their sequences. Several examples of such protein mimicry are available and the methods for these are presented here, starting with an overview chapter of the field. I believe that this is one of the most exciting CPP applications, possibly becoming an important therapeutic approach for interfering with intracellular protein-protein interactions. This goal is certainly achievable only when we will learn to unite the CPP and protein mimicking properties of these peptides. I hope the selected chapters will serve to stimulate work toward this goal.

The quickly growing field is summarized on applications of CPPs to improve the delivery of the oligonucleotides involved in gene modulation, particularly for gene silencing by antisense or siRNA oligonucleotides. The application of splice correcting oligonucleotides is the modern antisense strategy where several different chemically modified oligonucleotides serve as efficient splice redirectors. Since it is hoped that this approach may lead to novel gene therapies, I am especially pleased to present some siRNA delivery strategies using CPPs. It seems that we are not far from siRNA therapies that harness CPPs to improve and precisely target delivery in vivo based upon the efficient in vitro applications already available today. In parallel, the methods for transfection of plasmids by CPPs or their chemically modified analogs are developing efficiently and quickly.

The ideas are discussed for turning CPP-based strategies into drugs. Tumor-selective targeting with flexible CPP technologies has been fueling the CPP research for years, and

now the first fruit of these studies has become available. Additional organ-selective delivery strategies are also described, demonstrating that the combination of CPPs with novel nanoparticles and polymer systems is an efficient method for drug delivery. This point is underscored by the contributions of authors based at pharma companies who have contributed their ideas about CPP applications in drug development to this book.

In summary, the short history of research of cell-penetrating peptides has clearly demonstrated that CPPs have helped us to expand beyond several long held dogmas. This presents us with superb opportunities to study in new ways many intracellular mechanisms and promote the future development of novel drugs.

Stockholm, Sweden ***Ülo Langel***

References

1. Langel Ü (2011) Cell-penetrating peptides. Methods and protocols. Preface. Methods in molecular biology, Humana Press, vol 683, v–vi
2. Frankel AD, Pabo CO (1988) Cellular uptake of the tat protein from human immunodeficiency virus. Cell 55:1189–1193
3. Green M, Loewenstein PM (1988) Autonomous functional domains of chemically synthesized human immunodeficiency virus tat trans-activator protein. Cell 55:1179–1188
4. Joliot A, Pernelle C, Deagostini-Bazin H, Prochiantz A (1991) Antennapedia homeobox peptide regulates neural morphogenesis. Proc Natl Acad Sci USA 88:1864–1868
5. Derossi D, Joliot AH, Chassaing G, Prochiantz A (1994) The third helix of the Antennapedia homeodomain translocates through biological membranes. J Biol Chem 269:10444–10450
6. Pardridge WM (2015) Blood-brain barrier drug delivery of IgG fusion proteins with a transferrin receptor monoclonal antibody. Expert Opin Drug Deliv 12:207–222
7. Mousli M, Bueb JL, Bronner C, Rouot B, Landry Y (1990) G protein activation: a receptor-independent mode of action for cationic amphiphilic neuropeptides and venom peptides [see comments]. Trends Pharmacol Sci 11:358–362
8. Tchoumi Neree A, Nguyen PT, Chatenet D, Fournier A, Bourgault S (2014) Secondary conformational conversion is involved in glycosaminoglycans-mediated cellular uptake of the cationic cell-penetrating peptide PACAP. FEBS Letters, in press
9. Guilhelmelli F, Vilela N, Albuquerque P, Derengowski LDS, Kyaw CM (2013) Antibiotic development challenges: the various mechanisms of action of antimicrobial peptides and of bacterial resistance. Front Microbiol 4, article 353:1–12
10. Sharma A, Pohane AA, Bansal S, Bajaj A, Jain V, Srivastava A (2015) Cell penetrating synthetic antimicrobial peptides (SAMPs) exhibiting potent and selective killing of mycobacterium by targeting its DNA. Chemistry. doi: 10.1002/chem.201404650
11. Jones S, Howl J (2012) Enantiomer-specific bioactivities of peptidomimetic analogues of mastoparan and mitoparan: characterization of inverso mastoparan as a highly efficient cell penetrating peptide. Bioconj Chem 23:47–56
12. Oehlke J, Lorenz D, Wiesner B, Bienert M (2005) Studies on the cellular uptake of substance P, and lysine-rich, KLA-derived model peptides. J Mol Recogn 18:50–59
13. Cho S, Szeto HH, Kim E, Kim H, Tolhurst AT, Pinto JT (2007) A novel cell-permeable antioxidant peptide, SS31, attenuates ischemic brain injury by down-regulating CD36. J Biol Chem 282:4634–4642

Contents

Preface . . . . . *v*
Contributors . . . . . *xiii*

PART I INTRODUCTION

1 Classes of Cell-Penetrating Peptides 3
Margus Pooga and Ülo Langel

2 Penetratin Story: An Overview 29
Edmond Dupont, Alain Prochiantz, and Alain Joliot

3 Prediction of Cell-Penetrating Peptides 39
Mattias Hällbrink and Mati Karelson

4 Computer-Aided Virtual Screening and Designing of Cell-Penetrating Peptides 59
Ankur Gautam, Kumardeep Chaudhary, Rahul Kumar, and Gajendra Pal Singh Raghava

PART II METHODS TO TEST MECHANISMS OF CELL-PENETRATING PEPTIDES

5 Investigating Membrane Interactions and Structures of CPPs 73
Fatemeh Madani and Astrid Gräslund

6 Determining the Effects of Membrane-Interacting Peptides on Membrane Integrity 89
William C. Wimley

7 Study of CPP Mechanisms by Mass Spectrometry 107
Sandrine Sagan, Chérine Bechara, and Fabienne Burlina

8 Methods to Study the Role of the Glycocalyx in the Uptake of Cell-Penetrating Peptides 123
Samuel Schmidt, Rike Wallbrecher, Toin H. van Kuppevelt, and Roland Brock

9 Toxicity, Immunogenicity, Uptake, and Kinetics Methods for CPPs 133
Julia Uusna, Kent Langel, and Ülo Langel

10 Unraveling the Mechanisms of Peptide-Mediated Delivery of Nucleic Acids Using Electron Microscopy 149
Helerin Margus, Carmen Juks, and Margus Pooga

11 SCARA Involvement in the Uptake of Nanoparticles Formed by Cell-Penetrating Peptides 163
Henrik Helmfors, Staffan Lindberg, and Ülo Langel

PART III APPLICATIONS OF CPPS IN VITRO AND IN VIVO

12 Protein Mimicry and the Design of Bioactive Cell-Penetrating Peptides 177
John Howl and Sarah Jones

13 Pepducins and Other Lipidated Peptides as Mechanistic Probes and Therapeutics 191
Ping Zhang, Lidija Covic, and Athan Kuliopulos

14 Identification and Characterization of Homing Peptides Using In Vivo Peptide Phage Display 205
Maija Hyvönen and Pirjo Laakkonen

15 The Antimicrobial and Antiviral Applications of Cell-Penetrating Peptides 223
Kalle Pärn, Elo Eriste, and Ülo Langel

16 Visualizing Actin Architectures in Cells Incubated with Cell-Penetrating Peptides 247
Lin He, Peter D. Watson, and Arwyn T. Jones

17 Cell-Penetrating Peptides as Carriers for Transepithelial Drug Delivery In Vitro 261
Stine Rønholt, Mie Kristensen, and Hanne Mørck Nielsen

18 A Pathway Toward Tumor Cell-Selective CPPs? 279
Isabel D. Alves, Manon Carré, and Solange Lavielle

19 PepFects and NickFects for the Intracellular Delivery of Nucleic Acids 303
Piret Arukuusk, Ly Pärnaste, Mattias Hällbrink, and Ülo Langel

20 In Vitro Assays to Assess Exon Skipping in Duchenne Muscular Dystrophy 317
Prisca Boisguerin, Liz O'Donovan, Michael J. Gait, and Bernard Lebleu

21 Applications of ApoB LDLR-Binding Domain Approach for the Development of CNS-Penetrating Peptides for Alzheimer's Disease 331
Eliezer Masliah and Brian Spencer

22 CPP-Based Delivery System for In Vivo Gene Delivery 339
Kaido Kurrikoff, Kadi-Liis Veiman, and Ülo Langel

23 Application of CPPs for Brain Delivery 349
Artita Srimanee, Jakob Regberg, and Ülo Langel

24 Intracellular Delivery of Nanoparticles with Cell Penetrating Peptides 357
Giuseppina Salzano and Vladimir P. Torchilin

25 Multifunctional Oligoaminoamides for the Receptor-Specific Delivery of Therapeutic RNA 369
Judith Weber, Ulrich Lächelt, and Ernst Wagner

26 Cell Penetrating Peptides for Chemical Biological Studies 387
Ikuhiko Nakase, Toshihide Takeuchi, and Shiroh Futaki

27 Experiences with CPP-Based Self Assembling Peptide Systems for Topical Delivery of Botulinum Toxin 397
Jane Lee, Phil Kennedy, and Jacob M. Waugh

28 Applications of CPPs in Genome Modulation of Plants 417
Alicja Ziemienowicz, Jordan Pepper, and François Eudes

29 DNA Transfer into Animal Cells Using Stearylated CPP Based Transfection Reagent 435
Kristiina Karro, Tiiu Männik, Andres Männik, and Mart Ustav

30 Live Cell Genomics: Cell-Specific Transcriptome Capture in Live Tissues and Cells 447
Thomas J. Bell and James Eberwine

31 Live Cell Genomics: RNA Exon-Specific RNA-Binding Protein Isolation 457
Thomas J. Bell and James Eberwine

Index *469*

Contributors

Isabel D. Alves • *Institute of Chemistry & Biology of Membranes & Nanoobjects, CBMN CNRS UMR 5248, University of Bordeaux, Pessac, France*

Piret Arukuusk • *Laboratory of Molecular Biotechnology, Institute of Technology, Tartu University, Tartu, Estonia*

Chérine Bechara • *Sorbonne Universités, UPMC Univ Paris 06, LBM, Paris, France; Département de ChimieEcole Normale Supérieure-PSL Research University, Paris, France; CNRS, UMR 7203 LBM, Paris, France*

Thomas J. Bell • *Department of Systems Pharmacology and Translational Therapeutics, University of Pennsylvania Perelman School of Medicine, Philadelphia, PA, USA*

Prisca Boisguerin • *Centre de Recherche de Biochimie Macromoléculaire, UMR 5235 CNRS, Montpellier, France*

Roland Brock • *Department of Biochemistry, Radboud University Medical Centre, Nijmegen, The Netherlands*

Fabienne Burlina • *Sorbonne Universités, UPMC Univ Paris 06, LBM, Paris, France; Département de Chimie, Ecole Normale Supérieure-PSL Research University, Paris, France; CNRS, UMR 7203 LBM, Paris, France*

Manon Carré • *Centre de Recherche en Oncologie Biologique et Oncopharmacologie, INSERM, CRO2 UMR S 911, Aix-Marseille Université, Marseille, France*

Kumardeep Chaudhary • *Bioinformatics Centre, CSIR-Institute of Microbial technology, Chandigarh, India*

Lidija Covic • *Center for Hemostasis and Thrombosis Research, Tufts Medical Center, Tufts University School of Medicine, Boston, MA, USA*

Edmond Dupont • *College de France, Center for Interdisciplinary Research in Biology (CIRB), Labex Memolife, PSL Research University, Paris, France; CNRS, UMR, Paris, France; INSERM, Paris, France*

James Eberwine • *Department of Systems Pharmacology and Translational Therapeutics, University of Pennsylvania Perelman School of Medicine, Philadelphia, PA, USA*

Elo Eriste • *Laboratory of Molecular Biotechnology, Institute of Technology, Tartu University, Tartu, Estonia*

François Eudes • *Agriculture and Agri-Food Canada, Lethbridge, AB, Canada*

Shiroh Futaki • *Institute for Chemical Research, Kyoto University, Kyoto, Japan*

Michael J. Gait • *Medical Research Council, Laboratory of Molecular Biology, Cambridge, UK*

Ankur Gautam • *Bioinformatics Centre, CSIR-Institute of Microbial technology, Chandigarh, India*

Astrid Gräslund • *Department of Biochemistry and Biophysics, Stockholm University, Stockholm, Sweden*

Mattias Hällbrink • *Department of Neurochemistry, Stockholm University, Stockholm, Sweden*

Lin He • *Cardiff School of Pharmacy and Pharmaceutical Sciences, Cardiff University, Cardiff, Wales, UK*

Henrik Helmfors • *Department of Neurochemistry, Stockholm University, Stockholm, Sweden*
John Howl • *Research Institute in Healthcare Science, Faculty of Science and Engineering, University of Wolverhampton, Wolverhampton, UK*
Maija Hyvönen • *Research Programs Unit, Translational Cancer Biology, Biomedicum Helsinki, University of Helsinki, Helsinki, Finland*
Alain Joliot • *College de France, Center for Interdisciplinary Research in Biology (CIRB), Labex Memolife, PSL Research University, Paris, France; INSERM U1050, Paris, France; Homeoproteins and Plasticity, CIRB, CNRS UMR 7241/INSERM U1050, Labex Memolife, PSL Research University, Collège de France, Paris, France*
Arwyn T. Jones • *Cardiff School of Pharmacy and Pharmaceutical Sciences, Redwood Building, Cardiff University, Cardiff, Wales, UK*
Sarah Jones • *Research Institute in Healthcare Science, Faculty of Science and Engineering, University of Wolverhampton, Wolverhampton, UK*
Carmen Juks • *Institute of Molecular and Cell Biology, University of Tartu, Tartu, Estonia*
Mati Karelson • *Institute of Chemistry, University of Tartu, Tartu, Estonia*
Kristiina Karro • *Icosagen AS, Icosagen Group, Tartumaa, Estonia*
Phil Kennedy • *Revance Therapeutics Inc., Newark, CA, USA*
Mie Kristensen • *Department of Pharmacy, Faculty of Health and Medical Sciences, University of Copenhagen, Copenhagen, Denmark*
Athan Kuliopulos • *Center for Hemostasis and Thrombosis Research, Tufts Medical Center, Tufts University School of Medicine, Boston, MA, USA*
Rahul Kumar • *Bioinformatics Centre, CSIR-Institute of Microbial technology, Chandigarh, India*
Toin H. van Kuppevelt • *Department of Biochemistry, Radboud University Medical Center, Nijmegen, The Netherlands*
Kaido Kurrikoff • *Laboratory of Molecular Biotechnology, Institute of Technology, Tartu University, Tartu, Estonia*
Pirjo Laakkonen • *Research Programs Unit, Translational Cancer Biology, Biomedicum Helsinki, University of Helsinki, Helsinki, Finland*
Ulrich Lächelt • *Pharmaceutical Biotechnology, Center for System-based Drug Research, Ludwig-Maximilians-University Munich, Munich, Germany; Nanosystems Initiative Munich, Munich, Germany*
Ülo Langel • *Department of Neurochemistry, Stockholm University, Stockholm, Sweden; Laboratory of Molecular Biotechnology, Institute of Technology, Tartu University, Tartu, Estonia*
Kent Langel • *Laboratory of Molecular Biotechnology, Institute of Technology, Tartu University, Tartu, Estonia*
Solange Lavielle • *Sorbonne Universités UPMC Univ Paris 06, UMR 7203 ENS - CNRS, Laboratoire des Biomolécules, Paris, France*
Bernard Lebleu • *Centre de Recherche de Biochimie Macromoléculaire, UMR 5235 CNRS, Université Montpellier 2, Montpellier, France*
Jane Lee • *Revance Therapeutics Inc., Newark, CA, USA*
Staffan Lindberg • *Department of Neurochemistry, Stockholm University, Stockholm, Sweden*
Fatemeh Madani • *Department of Clinical Neuroscience, Center for Molecular Medicine, Karolinska Institutet, Stockholm, Sweden*
Tiiu Männik • *Icosagen Cell Factory OÜ, Icosagen Group, Tartumaa, Estonia*

Andres Männik • *Icosagen Cell Factory OÜ, Icosagen Group, Tartumaa, Estonia*
Helerin Margus • *Institute of Molecular and Cell Biology, University of Tartu, Tartu, Estonia*
Eliezer Masliah • *Departments of Neuroscience and Pathology, University of California – San Diego, La Jolla, CA, USA*
Ikuhiko Nakase • *Nanoscience and Nanotechnology Research Center, Research Organization for the 21st Century, Osaka Prefecture University, Osaka, Japan*
Hanne Mørck Nielsen • *Section for Biologics, Department of Pharmacy, Faculty of Health and Medical Sciences, University of Copenhagen, Copenhagen, Denmark*
Liz O'Donovan • *Medical Research Council, Laboratory of Molecular Biology, Cambridge, UK*
Kalle Pärn • *Laboratory of Molecular Biotechnology, Institute of Technology, Tartu University, Tartu, Estonia*
Ly Pärnaste • *Laboratory of Molecular Biotechnology, Institute of Technology, Tartu University, Tartu, Estonia*
Jordan Pepper • *Agriculture and Agri-Food Canada, Lethbridge, AB, Canada*
Margus Pooga • *Institute of Molecular and Cell Biology, University of Tartu, Tartu, Estonia*
Alain Prochiantz • *College de France, Center for Interdisciplinary Research in Biology (CIRB), Labex Memolife, PSL Research University, Paris, France; CNRS, Paris, France; INSERM, Paris, France*
Gajendra Pal Singh Raghava • *Bioinformatics Centre, CSIR-Institute of Microbial technology, Chandigarh, India*
Jakob Regberg • *Department of Neurochemistry, Stockholm University, Stockholm, Sweden*
Stine Rønholt • *Department of Pharmacy, Faculty of Health and Medical Sciences, University of Copenhagen, Copenhagen, Denmark*
Sandrine Sagan • *Sorbonne Universités, UPMC Univ Paris, LBM, Paris, France; Département de Chimie, Ecole Normale Supérieure-PSL Research University, Paris, France; CNRS, UMR 7203 LBM, Paris, France*
Giuseppina Salzano • *Center for Pharmaceutical Biotechnology and Nanomedicine, Northeastern University, Boston, MA, USA*
Samuel Schmidt • *Department of Biochemistry, Radboud University Medical Center, Nijmegen, The Netherlands*
Brian Spencer • *Department of Neuroscience, University of California – San Diego, La Jolla, CA, USA*
Artita Srimanee • *Department of Neurochemistry, Stockholm University, Stockholm, Sweden*
Toshihide Takeuchi • *Institute for Chemical Research, Kyoto University, Kyoto, Japan*
Vladimir P. Torchilin • *Center for Pharmaceutical Biotechnology and Nanomedicine, Northeastern University, Boston, MA, USA; Department of Pharmaceutical Sciences, Bouve College of Health Sciences, Boston, MA, USA; Department of Biochemistry, Faculty of Science, King Abdulaziz University, Jeddah, Saudi Arabia*
Mart Ustav • *Icosagen Cell Factory OÜ, Icosagen Group, Tartumaa, Estonia*
Julia Uusna • *Laboratory of Molecular Biotechnology, Institute of Technology, Tartu University, Tartu, Estonia*
Kadi-Liis Veiman • *Laboratory of Molecular Biotechnology, Institute of Technology, Tartu University, Tartu, Estonia*

Ernst Wagner • *Pharmaceutical Biotechnology, Center for System-based Drug Research, Ludwig-Maximilians-University Munich, Munich, Germany; Nanosystems Initiative Munich, Munich, Germany; Department of Pharmacy and Center for Nanoscience (CeNS), Ludwig-Maximilians-University, Munich, Germany*
Rike Wallbrecher • *Department of Biochemistry, Radboud University Medical Center, Nijmegen, The Netherlands*
Peter D. Watson • *Cardiff School of Biosciences, Cardiff University, Cardiff, Wales, UK*
Jacob M. Waugh • *Revance Therapeutics Inc., Newark, CA, USA*
Judith Weber • *Pharmaceutical Biotechnology, Center for System-based Drug Research, Ludwig-Maximilians-University Munich, Munich, Germany; Nanosystems Initiative Munich, Munich, Germany*
William C. Wimley • *Department of Biochemistry and Molecular Biology, Tulane University School of Medicine, New Orleans, LA, USA*
Ping Zhang • *Center for Hemostasis and Thrombosis Research, Tufts Medical Center, Tufts University School of Medicine, Boston, MA, USA*
Alicja Ziemienowicz • *Agriculture and Agri-Food Canada, Lethbridge, AB, Canada*

Part I

Introduction

Chapter 1

Classes of Cell-Penetrating Peptides

Margus Pooga and Ülo Langel

Abstract

During the three decades of cell-penetrating peptides era the superfamily of CPPs has rapidly expanded, and the quest for new sequences continues. CPPs have been well recognized by scientific community and they have been used for transduction of a wide variety of molecules and particles into cultured cells and in vivo. In parallel with application of CPPs for delivering of active payloads, the mechanisms that such peptides take advantage of for gaining access to cells' insides have been in the focus of intense studies. Although the common denominator "cell penetration" unites all CPPs, the interaction partners on the cell surface, evoked cellular responses and even the uptake mechanisms might greatly vary between different peptide types. Here we present some possibilities for classification of CPPs based on their type of origin, physical-chemical properties, and the extent of modifications and design efforts. We also briefly analyze the internalization mechanisms with regard to their classification into groups based on physical-chemical characteristics.

Key words Cell-penetrating peptide, CPP classes, CPP kinetics, CPP mechanisms, Second-generation CPPs, Lipidated CPPs

1 Introduction, CPPs, and Their Place in the Space of Macromolecule Delivery

The features and behavior of cell-penetrating peptides have intrigued researchers from the very beginning of their discovery about a quarter of century ago. The studies on the mechanism that some viral proteins [1, 2] and homeoprotein-type transcription factors [3, 4] use to overcome the plasma membrane barrier and for gaining access to the cell interior allowed definition of a novel and complex mechanism for the translocation of macromolecules to mammalian cells: penetration [5, 6]. The research groups, which discovered the phenomenon of penetration of extracellular proteins into the cells cytoplasm and nucleus, were initially not confident about the biological relevance of their finding; still they prophesized the significance of discovery for biotechnological applications [4]. However, the rapid progress in harnessing of CPPs for delivery of proteins, nucleic acids, and other bioactive macromolecules into cultured living cells did neither directly nor

Ülo Langel (ed.), *Cell-Penetrating Peptides: Methods and Protocols*, Methods in Molecular Biology, vol. 1324,
DOI 10.1007/978-1-4939-2806-4_1,

quickly transform to immense success in vivo [7, 8]. Still, the refinement of the CPP design and cargo coupling strategies and perhaps better knowledge about the mechanisms of how such peptides slip into cells and carry payloads are starting to open the real potential of these delivery vehicles for in vivo use [9–11]. Nowadays CPPs represent a viable alternative for methods that have been elaborated earlier for the cellular delivery of bioactive macromolecules, like lipid- or polymer-based and nanoparticle-based chemical methods, viral methods, and physical strategies, including electroporation and magneto- and photo transfection [12, 13]. CPP-based strategies have enabled regulation of gene expression by delivery of nucleic acids with antisense, siRNA, and splicing switching activities, expression from mRNA and plasmid vectors both in vitro and in vivo [13–15]. In parallel CPPs are harnessed for transport of proteins [16, 17] and peptide hormones (insulin) across the barriers in living organism [18]. Although by first definition universal and unselective, CPPs have been turned to specifically targeting delivery vehicles by designing activatable peptides that respond to the particular milieu of pathologic conditions, like activated proteases [19–22] and increased acidity [23–25] around tumors or enhanced protease activity at atherosclerotic lesions [20, 26]. The selective targeting is also achieved using chimerism: by fusion of CPP to the "zip codes of organism"—the peptide sequences, which accumulate in a particular tissue [27] or lesion [28, 29] after systemic administration (homing sequences and receptor ligands) or translocate inside cells to a particular organelle (e.g., nucleus or mitochondria localizing sequence) [30–32]. The ability to first concentrate at the site of action and deliver the active payload into targeted cells endows CPPs a unique position among other methods for the macromolecule delivery, especially in multifunctional nanoparticle formulations [33].

2 Classification of CPPs

2.1 Historical Approach

The name "cell-penetrating peptide" nowadays designates a large superfamily of peptides that differ in length, charge, hydrophobicity, flexibility, solubility, etc. [34, 35]. On the first glance CPPs have less common features than differing ones, except the capability of transducing exogenous molecules or particles into cells. The highly diverse nature of CPPs in physical-chemical and also biological means have complicated the elaboration of an exact definition for cell-penetrating peptides and also division into classes.

The first and simplest classification of cell-penetrating peptides was straightforward, and was based on their origin, grouping CPPs to protein-derived and the synthetic peptides [36]. The sequences of the former were found in the proteins of different origin and function, like in viral and mammalian RNA/DNA-binding

proteins, transcription factors, and fusogenic and antimicrobial sequences [34]. In concordance with their function, such sequences were named as the protein transduction domains (PTD), Trojan peptides, and membrane translocation sequences (MTS) that were used in parallel with CPP, although less frequently nowadays [37].

The first discovered protein-derived CPPs, Tat peptide from the transcription transactivating protein from HIV-1 [38, 39] and penetratin from the Antennapedia homeotic transcription factor [4, 40], specified the major characteristics of a typical CPP. The sequence responsible for the translocation of protein from outside to insides of cells was rather short encompassing 10–30 amino acids and highly positively charged [41]. The discovery of novel natural peptide sequences with the cell-penetrating activity has shifted the length limits in both directions, and also neutral and even some anionic CPPs have been found or designed [34]. Still the majority of CPPs known and actively used for the delivery of bioactive cargoes obey the rules postulated two decades ago. The family of protein-derived CPPs quickly expanded including novel highly cationic peptides deduced from vascular epithelial cadherin (pVEC) [42], herpes (VP22) [43] and other viruses [44], and homeoproteins Islet-1 [45], Engrailed-2 [46], and others [47]. The sequences from human calcitonin [48, 49] and lactoferrin [50] have also been intensely investigated and developed as well as peptides from toxins crotamine [51] and maurocalcine [52, 53]. The family of protein-derived CPPs is still the largest, and since the quest for novel cell-penetrating sequences continues, it continues expanding.

The second class in historical grouping of CPPs, chimeric peptides, can be considered as a transition from the natural to the purely synthetic/artificial peptides since they combine sequences from two different naturally occurring proteins. This "two-in-one" rationale was used for designing transportan by fusing amphipathic peptide mastoparan from bee venom to the fragment of human neuropeptide galanin [54]. The peptides constructed for delivery of nucleic acids or proteins by simple complex formation, MPG and Pep-1, respectively, combined highly cationic nuclear localization signal (NLS) of SV40 T-antigen and a hydrophobic peptide (e.g., signal peptide of transmembrane proteins), which have high affinity to cellular membranes [31, 55]. Integration of cationic, hydrophobic, and amphipathic sequences in different combinations has been later exploited for creating numerous efficient CPPs and delivery constructs, like CADY [56] and Pip (PNA internalizing) peptides [57] if to name just a few.

The receptor-independent effect of substance P in the mast cell activation, which might involve intracellular effects of peptide, was discovered before reports about the translocation of Tat protein and fragment of Antennapedia protein into cultured cells in active form and triggering relevant biological response. The amphiphilic

character [58] of this cationic neuropeptide inspired design of the first synthetic CPP—the model amphipathic peptide (MAP or KLAK) [59]. Remarkably, the arrangement of amino acids in MAP peptide allowed discovery of amphipathicity as one of the general features that might govern cell penetration. The positive charge was not the only determining factor for the model amphipathic peptides since the charge-neutral and anionic peptides, which contained instead of basic lysine glutamine or acidic glutamate residue, respectively, translocated into cells and their nuclei. Disruption of the helicity, in contrary, substantially reduced the internalization of peptides to cells [60].

Among synthetic/designed CPPs polyarginine 8–10-mers are the most widely used, due to high cellular uptake-inducing activity [61, 62].

The classification of cell-penetrating peptides to protein-derived, chimeric, and synthetic ones is useful for understanding the relevance of cell penetration phenomenon and mechanisms for some proteins in physiological processes or biological responses in very general means, e.g., trafficking of homeoproteins between cells during development of a multicellular organism and for brain plasticity [63, 64], and for translocation of pro-apoptotic proteins into cells [65]. Still it does not allow correlation of the properties of CPPs with the interaction with cells or their working principle. Therefore in the next section we group CPPs according to chemical-physical features, which determine the interaction and effects of these peptides.

2.2 Physical-Chemical Character of CPPs as Basis for Classification

Notwithstanding the very high diversity, the cell-penetrating peptides can be grouped into three categories according to the physical-chemical properties: the charge and hydrophobicity, and the distribution of these descriptors along the peptide sequence. Classification of CPPs as cationic, amphipathic, and hydrophobic correlates fairly well with their interaction pattern with membranes and other cellular structures; hence it might be associated with effects on the cellular machinery and the uptake mechanisms [66, 67]. Chimeric CPPs can be typically categorized into two different peptide classes at the same time, and this also applies to longer bipartite peptides. The behavior and internalization mechanism of the chimeric peptides tends to be more difficult to predict, especially if coupled to a cargo [14].

The vast majority of peptides in all three CPP classes carry a positive charge at physiological conditions, whereas anionic peptides contribute rather marginally to CPP superfamily [34]. In order to distinguish from the amphipathic and hydrophobic, typically to the group of cationic CPPs are classified only peptides that contain a continuous stretch of basic amino acids. This strongly cationic region should also be responsible for the cellular uptake of peptide, and not form upon folding to a helical conformation.

2.2.1 Cationic CPPs

The first, serendipitously discovered cell-penetrating protein, Tat from HIV-1, contains sequence RKKRRQRRR, which can be considered a prototypic cationic CPP. It carries eight positive charges which is a minimal number for an efficiently penetrating cationic CPP [68]. The quintessence of this sequence and many other DNA/RNA-binding motif-based CPPs, oligoarginines, penetrate into cells remarkably better than oligolysines with the same length and charge. Analysis of arginine polymers with different length revealed that from 8-mer (R8), these peptides are efficiently taken into cells [61, 62], although the shorter are also internalized to some extent starting from arginine 6-mer. The internalization of oligoarginines increases with their length, but for the delivery purposes the optimal are R8–R10. Above this value the side effects like the interference with the cell viability and irreversible interactions with plasma membrane also increase, reducing their overall efficacy as transport vehicles [61, 69].

The polycationic stretches are common in DNA-, RNA-, and heparan-binding proteins of all taxa from viruses to mammals, and thus are a rich source for CPP sequences (*see* Table 1) [44, 70, 71]. CPPs found in the RNA-binding proteins form viruses and phages as well as protamines [72] and histones [73] from mammals are especially arginine rich and quite monotonous. However, cationic CPPs present in metazoan transcription factors of leucine-zipper and homeoprotein family contain also hydrophobic amino acids, which might contribute to the cellular uptake and increase their affinity towards membranes [74]. For instance the sequence of penetratin RQIKIWFQNRRMKWKK contains two tryptophans which are crucial for the cellular uptake and replacement of W14 to F abolishes internalization of peptide by neuronal cultures [75, 76]. Significant contribution of tryptophans to the cellular uptake has also been demonstrated in case of other cationic CPPs and their presence allows internalization of peptides with less than 7–8 positive charges [77–79].

Another common cationic motif in CPPs is the arginine- and lysine-rich sequences of NLS. The basic amino acids, typically 5–6, can be arranged in NLS in one or two clusters, but as CPPs, predominantly monopartite NLS have been used. NLS by itself are poor CPPs due to the moderate positive charge, but combination of these with hydrophobic or amphipathic sequences might yield very efficient and versatile carriers of amphipathic character, like $S4_{13}$-PV, MPG, and Pep-1, which contain NLS from simian virus 40T-antigen [80, 81].

2.2.2 Amphipathic CPPs

Amphipathic molecules possess two different faces, which in CPPs are typically a positively charged and/or hydrophilic area and hydrophobic region. Amphipathic class of CPPs is the most numerous, accounting for more than 40 % of CPPs known so far and also contains peptides with negative overall charge [34]. The

Table 1
Selection of best known cell-penetrating peptides

Sequence	Name (origin)	Type[a]	Ref.
Cationic			
RKKRRRESRKKRRRES	DPV3	N	[71]
GRPRESGKKRKRKRLKP	DPV6	N	[71]
RKKRRQRRR	HIV-1 pTat(49–57)	N	[38]
RRRRNRTRRNRRRVR[b]	FHV coat	N	[44, 70]
TRQARRNRRRRWRERQR[b]	HIV-1 Rev	N	[44, 70]
PRRRRSSSRPVRRRRRPRVSRRRRRRGGRRRR	Protamine 1	N	[72]
RIKAERKRMRNRIAASKSRKRKLERIAR	Human cJun	N	[44, 70]
RQIKIWFQNRRMKWKK	Penetratin	N	[4]
RVIRVWFQNKRCKDKK	Islet-1	N	[45]
SQIKIWFQNKRAKIKK	Engrailed-2	N	[47]
RQVTIWFQNRRVKEKK	HoxA-13	N	[46]
$(R)n$[b]; $n = 6–12$	Polyarginine	S	[44, 61]
Amphipathic			
MVKSKIGSWILVLFVAMWSDVGLCKKRPKP	BPrPp(1–30)	N	[85]
KCFQWQRNMRKVRGPPVSCIKR[b]	hLF peptide(19–40)	N	[50]
TRSSRAGLQWPVGRVHRLLRK	Buforin 2	N	[176]
YKQCHKKGGKKGSG	Crotamine	N	[177]
NAATATRGRSAASRPTQRPRAPARSASRPRRPVQ	VP22	N	[43]
DPKGDPKGVTVTVTVTVTGKGDPKPD	VT5	N	[89]
MVRRFLVTLRIRRACGPPRVRV	ARF(1–22)	N	[83]
MVTVLFRRLRIRRACGPPRVRV[b]	M918	N	[86]
LLIILRRRIRKQAHAHSK[b]	pVEC	N	[42]
LSTAADMQGVVTDGMASG	Azurin p18	N	[178]
KFHTFPQTAIGVGAP[b]	hCT peptide18-32	N	[179]
ALWKTLLKKVLKAPKKKRKV	$S4_{13}$-PV_{rev}	C	[81]
KETWWETWWTEWSQPKKKRKV[c]	Pep-1	C	[31]
GALFLGFLGAAGSTMGA[c]	MPG	C	[55]
GWTLNSAGYLLGKINLKALAALAKKIL[b]	Transportan	C	[54]
AGYLLGKINLKALAALAKKIL[b]	TP10 (transportan analogue)	C	[82]

(continued)

Table 1
(continued)

Sequence	Name (origin)	Type[a]	Ref.
Stearyl-AGYLLGK(ε-TMQ)INLKALAALAKKIL[b]	PepFect 6	S	[154]
Stearyl-AGYLLGKLLOOLAAAALOOLL[b]	PepFect 14	S	[155]
Stearyl-AGY(PO3)LLGKTNLKALAALAKKIL[b]	NickFect 1	S	[130]
δ-(St-AGYLLG)OINLKALAALAKKIL[b]	NickFect 51	S	[151]
GLWRALWRLLRSLWRLLWRA[c]	CADY	S	[56]
RRWWRRWRR	W/R	S	[180]
KLALKALKALKAALKLA[b]	MAP (model amphipathic peptide)	S	[181]
QLALQLALQALQAALQLA	MAP17	S	[182]
(PPR)3, (PPR)4, (PPR)5, (PPR)6	(PPR)*n*	S	[183]
VRLPPPVRLPPPVRLPPP	SAP	S	[184]
YTAIAWVKAFIRKLRK[b]	YTA2	S	[185]
IAWVKAFIRKLRKGPLG[b]	YTA4	S	[185]
Palmitoyl-SFLLRN	PAR1		[186]
Palmitoyl-KIHKKGMIKS	$F2Pal_{10}$	S	[187]
Hydrophobic			
AAVLLPVLLAAP	K-FGF	N	[188]
VPTLK (PMLKE, VPALR, VSALK, IPALK)	Bip	N	[189, 190]
PFVYLI	C105Y	N	[96]
SDLWEMMMVSLACQY	Pep-7	S	[94]
PLILLRLLRGQF	Pept1	S	[191]
Anionic			
LKTLTETLKELTKTLTEL	MAP12	S	[192]
VELPPPVELPPPVELPPP	SAP(E)	S	[184]
TSF[d]EYWYLL[d]	Stapled p53 peptide MO6	S	[193]

St stearyl
[a] *N* natural, *C* chimeric, *S* synthetic
[b] C-terminal amide
[c] C-terminal cycteamide
[d] Staple tethering site

amphipathic CPPs can be further split into primary and secondary amphipathic peptides based on their sequence, length, and association with lipids [66]. However, this division is not very strict and different authors may assign some CPPs to different group, based on the biological effects and structural considerations. In primary amphipathic CPPs (paCPP) the areas with different character are separated either in primary structure, like in chimeric MPG and Pep-1, or in stable secondary α-helical structure, like in transportan and TP10 [82]. The secondary amphipathic CPPs (saCPP) are not structured in solution, and acquire amphipathic character only after changing the secondary structure upon interaction with polyanions [67].

Primary amphipathic CPPs are in general longer than cationic or saCPP, encompassing 20 amino acids or more. They strongly associate with both neutral and anionic membranes and are theoretically long enough to span the hydrophobic core of membranes. PaCPPs insert into membranes, and may induce rearrangements of lipids and disturbances in membrane organization. Although paCPPs are mainly chimeric or synthetic, some such sequences are derived from proteins. For example paCPP, ARF(1–22) peptide corresponds to the N-terminal domain of tumor-suppressor p14ARF protein [83], and bPrPr(1–28) and mPrPr(1–30) are derived from prion proteins [84, 85].

The amphipathic features of saCPPs reveal after rearrangement of peptide to α-helical structure upon interaction with negatively charged membranes or glycosaminoglycans. This leads to the formation of cationic patch on one side of peptide, and to the exposure of hydrophobic amino acids on the other as can be well distinguished on helical wheel projection of CPP. SaCPPs, like MAP, pVEC, and M918 [86], are typically shorter than paCPPs and associate stably only with negatively charged, but not neutral, membranes, although the hydrophobic face could in principle allow that. Despite formation of an amphipathic structure saPPCs do not insert into membrane deeply and they cause less disturbances in biological membranes as compared to paCPPs [87]. Still, at higher concentrations and in more anionic membranes saCPPs can induce leakage in membranes [88].

Transition to a β-sheet structure can also lead to amphipathic structure and cell penetration properties [89]. Excellent example of secondary structure variability is penetratin that in aqueous solution is in random coil configuration but upon interaction with anionic lipids can form amphipathic secondary structures: α-helical at lower peptide to lipid ratios and β-sheet at higher ratios [90].

Class of saCPPs comprises also anionic peptides, the analogues of MAP and KALA peptide with reversed charge, MAP17 and GALA [91], respectively. The proline-rich amphipathic sequences with specific properties form a subgroup of CPPs that differ from others by quite many means [92].

Although amphipathicity is a common feature of many CPPs, the cell-penetrating properties are characteristic only for a negligible fraction of amphipathic peptides or regions of proteins.

2.2.3 Hydrophobic CPPs

The class of hydrophobic CPPs (hCPP) has the lowest number of representatives among all CPPs. hCPPs contain either only nonpolar or possess very few charged amino acids, typically cationic, and they have been used for cargo delivery rather seldom. Among these the 12 amino acids long hydrophobic region of Kaposi fibroblast growth factor (FGF4) was harnessed for transducing into cell mainly peptides that interfere with the intracellular signaling pathways, but also for delivering proteins [93]. However, the hydrophobic stretches are often crucial for the cellular uptake of saCPPs and chimeric sequences. For instance, replacement of any leucine or isoleucine in the hydrophobic patch of pVEC (originating from the transmembrane region of cadherin) by alanine dramatically reduced the cellular uptake of CPP. Substitution of arginines with alanine, in contrary, enhanced internalization of pVEC, emphasizing the significance of nonpolar cluster for functioning of this CPP [42]. As mentioned earlier, fusion of hydrophobic sequences with cationic peptides has been a fruitful strategy for designing novel efficacious CPPs. Novel hCPPs have also been found by phage or plasmid display, e.g., Pep-7 and SG3 [94, 95]. Remarkably, the highest accumulation into spermatozoa was recently demonstrated for an hCPP, C105Y [96], that strongly excelled cationic and amphipathic CPPs in endocytosis-excluding conditions [97].

3 Cell Translocation Mechanisms of CPPs

The models and hypotheses about how CPPs can translocate from the outside to cells' inside, finally reaching cytosol and nucleus, have continuously evolved and are often debated [11, 13, 98–100]. Distinguishing between two possible pathways, endocytosis and direct translocation/penetration across the plasma membrane, should, in principle, be simple. Penetration of fluorescently labeled CPP into living cells should yield a uniform and diffuse labeling of cells, whereas endocytosis results in granular/punctuate pattern due to entrapment of peptide and label in vesicular organelles. Indeed, both these localization types have been documented in scrupulously designed experiments, and intriguingly, even for the same peptide in same cells. Variation of experimental conditions, such as increase of peptide concentration, leads to a switch from endocytic mechanism to direct translocation into HeLa cells in case of pTat and R8 peptides [101]. Analogous effect can be evoked by temperature modulation in KG1a suspension cells with R8 peptide. At physiological temperature CPP was internalized by endocytosis, but at temperatures lower than 20 °C, direct

translocation took over [102]. Such behavior illustrates the versatility of CPPs to swiftly adapt to the environmental conditions, and their ability to use radically different mechanisms for entering cells. In more general means, the internalization mechanism of CPP depends on the properties of peptide and associated cargo; type, confluence, viability of cells, and the composition of their plasma membrane and extracellular matrix; and environmental factors like temperature, ionic strength, and pH [103].

Under standard tissue culture conditions and moderate peptide concentrations that are commonly used in CPP-mediated delivery experiments, endocytosis is a vastly prevailing internalization mechanism. CPPs have shown to take advantage of all major internalization routes: clathrin- or caveolin-dependent endocytosis, macropinocytosis, and clathrin- and caveolin-independent pathway [104–107]. Typically the majority of CPP mechanisms were assigned by using pharmacologic inhibitors of endocytosis pathways. Only recently a more specific technique—siRNA-induced knockdown of proteins that control particular endocytosis routes—was applied for unraveling CPP internalization mechanisms [108, 109].

In order to pinpoint the internalization pathways of cationic CPPs, Al Soraj et al. examined in a systematic study the impact of siRNA and pharmacological inhibition of endocytosis pathways on the cellular uptake of R8 and pTat. The internalization of defined probes for clathrin-, caveolin-, and flotillin-dependent endocytosis was significantly suppressed by both the pharmacological inhibitors of the respective pathways and RNA interference. The cellular uptake of R8 and pTat, in contrary, was not markedly influenced by either type of inhibition. Only suppression of macropinocytosis by downregulation of Pak-1 kinase and inhibitor with wide range of activities, blebbistatin, interfered with the uptake of R8 and pTat by HeLa and A431 cells, suggesting that only macropinocytic mechanism cannot be compensated by other internalization routes [109]. Also the earlier studies have demonstrated the prevalence of this uptake mechanism for cCPPs in cultured cell lines. CCPPs activate Rac-1 to induce macropinocytosis [110] and it has been suggested that clustering of heparan sulfate proteoglycans might trigger this activation, and that syndecans could be involved [111]. Recently the cellular uptake of R12 peptide and induction of endocytosis were found to be dependent on the chemokine receptor CXCR4 [112]. The necessity of a receptor protein for the cellular uptake of pTat-protein constructs was also postulated earlier [113] and surprisingly a protein component of the plasma membrane is ultimately required for the direct translocation of R9 and pTat into giant plasma membrane vesicles (GPMV) [114]. Still it does not seem too probable that CXCR4 serves as universal vector for cationic CPPs in different cell types and perhaps more proteins involved in internalization of CPPs would be pinpointed. Although

macropinocytosis is one of the key mechanisms in the endocytic uptake of CPPs by commonly used immortal cell lines [115], it is not clear how efficient macropinocytosis is in primary cells and in in vivo conditions. For example the conjugates of Pip6a peptide with splicing switching PMO were endocytosed by caveolin-dependent pathway in murine primary myotubes and by clathrin-mediated route in cardiomyocytes in mdx mouse model [116].

The cationic CPPs do not associate with non-charged model membranes or interfere with the organization of the plasma membrane of cells [87]. Primary amphipathic CPPs in contrary associate with neutral membranes and upon interaction with plasma membrane interfere with its packing in a concentration-dependent manner. At higher concentrations aCPPs induce influx of Ca ions into cytosol, which trigger plasma membrane repair response by cells [88], and perhaps compensatory endocytosis. As expected, aCPPs also harness other endocytic routes to enter cells, in addition to macropinocytosis.

Although the mechanisms of CPP penetration across the biological membranes are not so well defined yet as endocytosis, still several principles for facilitating endocytosis-independent translocation can be outlined. The hydrophobic core of biological membranes poses the major barrier for direct crossing of charged molecules; thus not surprisingly the changes in the membrane composition and density of packing strongly modulate the penetration efficiency. For example, depletion of cholesterol from membranes facilitates translocation of CPPs across plasma membrane [117] and its supplementation drastically suppresses penetration [114]. Penetration of CPPs into cells or across the membrane of GPMV is also substantially increased by generation of ceramide, a negative curvature-inducing lipid, in membranes [77, 114, 118]. A rather universal mechanism of arginine-rich CPPs for penetration across biological membranes could be ion-pair formation with free fatty acids of plasma membrane [119] or added pyrene butyrate [120], which drastically increases translocation of peptides and proteins into cell cytoplasm. The arginine-rich peptides are suggested to form a short-living hydrophilic channel in the plasma membrane of cells upon translocation [119, 121, 122]. Intriguingly, this is not accompanied by Ca influx to cells even at very high R9 or pTat concentration [87]. Temporary pores are formed in the plasma membrane of cells also by aCPPs, but their properties and lifetime should be different, since influx of Ca to cells could be detected [123, 124]. It is tempting to speculate that at certain loci, the requirements for efficient penetration of CPPs and their cargoes across membranes (high concentration of peptide and favorable lipid composition) are also met in living cells.

As suggested earlier by pioneers of the cell penetration research, cell-penetrating proteins might represent a very ancient mechanism of communication between cells [125]. Instead of activating

sophisticated receptor systems on the cell surface and triggering signal transduction cascades inside cells and finally leading to changes in the gene expression pattern, the homeotic transcription factors can be shuttled between cells or signal from outside to reach the same goal [126, 127]. Analogous strategy could also use cytotoxic proteins to penetrate into target cells and trigger apoptosis [65].

4 Kinetics of CPP Cellular Uptake

The speed of cell entry is an essential characteristic of CPPs. Peptides have rather short half-life in biological fluids, and CPPs are not an exception [128]. Therefore under standard cell culture conditions, and especially in vivo, the CPPs that can faster fulfil their task—deliver payloads into cells—should have advantage over the slowly acting carriers, since the latter could be degraded before sufficient amounts of cargo are taken up by cells. The reliably estimated cellular uptake kinetics should also hint when the wanted biological effect in cultured cells and especially in vivo can be expected to occur. Unfortunately the cell internalization kinetics of CPPs was addressed in quite a few studies and the published results are often contradictory [14]. Certainly, it is a difficult task to design a perfect assay for the characterization of the CPP or cargo translocation kinetics from the extracellular medium to cell interior, and to target organelle/molecule due to very high complexity of the process and variability in the properties of CPPs and used payloads. We have to consider that in different assays CPP might function as a monomer, as associated with proteins of the blood plasma [62], or as a nanoparticle [129] in complex (or conjugate) with its payload molecule [130], depending on the used media and particular cargo. Obviously, the state of CPP (molecular or in particle) predisposes its degradation speed and strongly influences the mechanism of uptake by cells. Interpretation of internalization kinetics data is further complicated by the ability of CPPs to activate several cellular uptake pathways in parallel, and entrapment/escape in/from endosomal organelles [131]. Therefore the CPP uptake by cells is typically modeled to follow first-rate kinetics [132].

The first studies that estimated the internalization speed of CPPs were based on the quantification of the label coupled to peptide. In initial studies the radioactive label was used to assess the kinetics of CPP internalization, e.g., ^{125}I transportan for uptake by Bowes melanoma [54] and [^{99m}Tc]-pTat in Jurkat cells [133]. However, in the majority of cases the fluorescent reporter has been exploited, like NBD for penetratin in K562 [76, 134], fluorescein for pTat in Jurkat cells [104], and polyarginine [135] or rhodamine for pTat, polyarginine, transportan, and penetratin [136, 137].

These studies helped definition of the time frame for CPP cellular uptake, revealing the half-times for some CPPs, like MAP and TP within 2–15 min, but for the majority about 20–60 min. However, quantification of label does not reflect the availability of the cargo molecules at the site of their activity, which typically lies in cytosol or nucleus of cell, and usually leads to overestimation of the putative biological effect [138]. Quantification of the pre-labeled cargo molecules provides slightly more relevant information about the expected impact of payloads inside cells [139], but still tends to overvalue the biological effects [140].

In order to estimate the concentration of cargo molecules that reach cytosol after being delivered into cells by CPPs, Hällbrink et al. introduced the quenched fluorescence method [141]. For this assay the peptide cargo was labeled with aminobenzoic acid, whose fluorescence signal is quenched by nitrotyrosine group added to CPP, which is conjugated to cargo peptide by disulfide bond. Fluorescence of the reporter can be regained only when the disulfide bond between the cargo and CPP is dissociated, which in cells occurs in reducing environment of cytosol, maintained by high concentration of glutathione. Thereby this method enables quantification of the cargo in the cytoplasm (and nuclei) of living cells in real time, and the payload molecules entrapped in endosomes or outside of cells do not interfere with quantification. Among the studied four peptides MAP and TP quicker transduced the model peptide (CLKANL) into Bowes melanoma cells, whereas its delivery by pTat and penetratin was slower and yielded a lower concentration of cargo in cells. On the other hand, both MAP and TP induced more efflux from cells at higher concentrations than penetratin or pTat, suggesting that higher delivery efficiency to cytosol of cells in case of MAP and TP was also accompanied by higher disturbances of Bowes cell membranes. The study also clearly pointed out that delivery of even a small cargo into cells was not as fast process as internalization of CPPs themselves [141]. This method was later refined by using a more efficient quencher group and performing the measurements in serum-containing tissue culture medium, i.e., in more natural conditions [142]. Comparison of three novel CPPs revealed higher transduction efficiency, and also the internalization speed of M918 peptide, as compared to pVEC or TP10. As expected, delivery of model peptide was more efficient at higher concentrations of conjugates with CPP. Remarkably, at higher concentrations the uptake rate constants and the plateau values of intracellular cargo concentration were rather comparable for all three studied peptides. The pharmacological inhibitors of endocytosis, chlorpromazine, wortmannin, sucrose and cytochalasin D reduced the amount of internalized cargo peptide for all used CPPs. Surprisingly inhibitors increased the values of kinetic constants, i.e., accelerated delivery of peptide cargo to cytoplasm of cells [142].

CPP-assisted delivery to cytoplasm has been measured in real time also by using peptide conjugates with releasable luciferase substrate in reporter HeLa cells [143]. The reduction-sensitive linkage between the peptide and substrate ensures that luciferin liberates only in the cell cytoplasm, where it is metabolized by luciferase and the emitted light can be quantified, which allows to consider this assay background free. This method classified the commonly used CPPs to be very quickly acting—luminescence was detectable in cells already in seconds or minutes after application of a high concentration of substrate conjugated with MAP, pTat, and TP10, and moderate ones. Penetratin, pVEC, EB1, and M918 lead to highest degradation rate of substrate in cytoplasm after 30–120 min. One might speculate that the very fast uptake observed at 10 μM concentration of quickly acting CPPs is due to direct penetration to cell cytoplasm, which has been observed earlier for pTat [101]. Still, the inhibitors of endocytosis also affected the cellular uptake of fast CPPs, suggesting the involvement of endocytosis processes. Macropinocytosis was considered a major internalization mechanism for all CPP-luciferin conjugates with some contribution of clathrin- and caveolin-mediated endocytosis in these studies. We have to also bear in mind that the releasable luciferin tag that is exploited in this assay might have an analogous effect with fluorescent reporters and can alter the properties of CPP and augment their uptake [99, 144]. For example the used tag coupled to the N-terminus of pTat might turn the construct more chimeric as compared to the original peptide and modulate its internalization.

Translocation of CPPs into cells has also been quantified by mass-spectrometry-based methodology. Internalization of penetratin analogue P1 by CHO wild-type cells reached steady state after 50 min and in pgsA-745 derivative line that lacks proteoglycans after 30 min, and the final concentration of CPP was substantially lower in mutant CHO [145]. Thereby the kinetic parameters measured by MS are quite well in line with the results from fluorescence-based assays.

In general the CPP conjugates with payload are internalized by cells at lower pace than carrier peptides itself. However, in rare cases the opposite has been observed. Sasaki and colleagues found that the conjugate of a cyclic hydrophobic (CH) peptide CPFKQC with CPP (CWR_8K) was internalized by Jurkat cells faster than the used R_8 analogue itself [146]. The CH peptide was identified from phage library as XIAP (X-linked inhibitor of apoptosis protein) inhibitor and its cell-permeable construct (CHCPP) potently inhibited proliferation of Jurkat cells. Both fluorescein-labeled peptides were incorporated into cells rapidly, in 5–10 min, and CHCPP showed higher uptake rate than CPP. Remarkably the hydrophobic amino acid (phenylalanine or dimethyl-phenylalanine) was necessary for the inhibition of cell proliferation. The cyclized peptide

cargo might also contribute to the facilitated cellular translocation of CHCPP, since cyclization of R_{10} and R_6 peptides significantly increase penetration of these CPPs into cells [147, 148].

5 Second-Generation CPPs

The name "second-generation CPP" might sound too ambitious or provocative, since we introduce it here in order to distinguish the classical CPPs that are built up using 20 natural amino acids included in proteins from CPPs modified with small organic molecules or comprising non-ribosomal amino acids and non-peptide bonds, rigidified by stapling, etc. On one hand, from the peptide chemistry viewpoint, such CPPs do not contain really novel modifications. On the other, the abovementioned derivatizations have conferred these CPPs several advantages over "the first-generation CPPs."

5.1 Fatty Acid-Modified CPPs

Modification of CPP with fatty acid or other hydrophobic moiety can be considered as introduction of chimerism in the peptide and it was first applied for arginine-rich cCPPs, like Tat, R8, Rev, and others [149]. Coupling of fatty acid to the N-terminus of these peptides increased drastically their efficiency at delivering into COS-7 cells luciferase-encoding pDNA by forming a non-covalent complex, and revelation of respective enzymatic activity. The most prominent effect was obtained by modification of peptides with stearic acid, whereas lauryl and cholesteryl group enhanced plasmid delivery at lower extent. Analogous strategy was recently also applied for amphipathic CPPs $(RXR)_4$ and TP10 and the stearylated (st) analogues were used for cellular delivery of nucleic acids. Remarkably, st$(RXR)_4$ induced higher luciferase expression from cell-delivered pDNA compared to stR8, and led to EGFP expression from plasmid in higher number of CHO cells than Lipofectamine2000 [140]. Moreover, st$(RXR)_4$ condensed splicing correcting oligonucleotides (SCO) to particles, which after cellular uptake escaped from endosomes and liberated SCO rescued expression of luciferase in HeLa reporter cell line. Although the same amount of SCO complexes with unmodified $(RXR)_4$ were internalized by cells, these had no detectable effect on splicing, emphasizing the beneficial effect of stearyl modification [140].

Stearylation of TP10 and further derivatization have yielded two novel families of powerful agents for cellular delivery of nucleic acids: PepFects (PF) [150] and NickFects (NF) [151]. In analogy with $(RXR)_4$, modification of the TP10 N-terminal with stearic acid substantially stabilized peptide-nucleic acid complexes. The resultant PF3 efficiently delivered into cells SCO and pDNA [152, 153]. The next members of this CPP family were equipped with pH-sensitive groups in PF6 [154] and NF1 [130], contained amino acids not coded by DNA in PF14 [155] and NF51, or were

crooked by switching the synthesis of peptide from α-amino group to the side chain NH_2 of ornithine [151] and others. PepFect- and NickFect-type delivery vehicles transfect into cell nucleic acids with different size and activity [15]: single-stranded oligonucleotides with splicing switching or antisense activity [155], double-stranded siRNA for knockdown of gene expression [154], and pDNA for expression of exogenous genes [156]. However, a particular type of gene expression-modulating nucleic acid requires to own PF or NF for the highest effect to be revealed. For instance, the highest efficacy of functional siRNA delivery has been achieved with PF6 [154] and protein production from pDNA with NF51. Importantly, PF and NF complexes with NA can be used in serum-containing growth media and in vivo implying the stability and activity of formed nanocomplexes under such conditions [154]. Typically the efficacy of PF and NF in NA transduction exceeds that of lipofection agents and they are less toxic for cultured cells [150]. In general the CPP-NA complexes have positive overall charge and induce cellular uptake after binding to heparan sulfate-containing proteoglycans. Surprisingly the nanoparticles of nucleic acids with NF and PF have a positive zeta potential and their cellular uptake is dependent on the type A scavenger receptors [157, 158].

5.2 Pepducins

In parallel with the introduction of stearyl group into CPPs another class of lipid-modified peptides with the cell-penetrating features was invented: pepducins [159]. Pepducins are designed to target the intracellular regions of G-protein-coupled receptors (GPCR) and modulate their signaling. Pepducins are created by coupling palmitoyl, other acyl chain, or a steroid group to the N-terminus of peptide whose sequence corresponds to intracellular loop (i1–i4) of GPCR. The lipid group is suggested to first anchor pepducin to the plasma membrane and induce "flip" across the lipid bilayer. In contrary to the majority of CPPs, pepducins remain attached to the plasma membrane in cells where they modulate the signaling of GPCR of interest. Pepducins can function as agonists or antagonists of targeted GPCR, and have been designed for a variety of receptors, e.g., protease-activated receptors (PAR1, 2, 4), chemokine receptors (CXCR1, 2, 4), adrenergic receptor (ADRA1B), and others [160]. Pepducins have been used for controlling various physiological processes: platelet-dependent hemostasis and thrombosis [161], tumor growth, invasion and angiogenesis [162], and others [163].

5.3 Prenylated CPPs

Protein prenylation, addition of farnesyl (C15) or geranylgeranyl (C20) isoprenoid moiety to the C-terminus of polypeptide, is a common hydrophobic posttranslational modification, present in about 2 % of mammalian proteins, which localizes proteins to plasma membrane. Addition of farnesyl group to the C-terminus gives cell penetration ability to various peptides, which cannot

enter cells by themselves. Prenylated peptides are suggested to translocate directly into the cell cytosol, in an ATP- and endocytosis-independent manner [164, 165].

5.4 Stapled CPPs

Stabilization of the peptide in α-helical conformation by covalently connecting the adjacent turns of structure by a hydrophobic chemical linker improves the proteolytic stability of peptide [166, 167]. Such stapling can increase the affinity of peptide to interacting proteins and often allows their cellular uptake [168]. Although stapling does not guarantee that peptide is converted to cell penetrating, most peptides gain this ability. Remarkably, not only cationic but also charge-neutral and anionic stapled α-helical peptides can be CPPs and some anionic impermeable peptides acquire cell-penetrating ability after substitution of negatively charged amino acids by neutral or cationic ones. A good example of stapled peptide application is the activation of p53 tumor-suppressor protein by SAH-8 [166] and sMTide peptides [168]. Both these peptides activate p53 by inhibiting repression by Mdm2, and contain α-helical conformation stabilizing staple. However, their sequence and charge are different; the former is derived from the Mdm2-binding domain of wild-type p53 and is cationic. The latter was discovered by phage display; it is anionic, is efficient at lower concentrations, and possesses less unrelated activities [168].

The majority of modifications introduced in sgCPPs render peptides more hydrophobic, once more emphasizing the importance of interactions of CPPs with membranes for both: the cell penetration and endosomal escape. On one hand the potential of turning peptides more hydrophobic in order to facilitate their cellular uptake is probably not fully exploited yet. On the other, the results of the most popular technique in CPP studies—fluorescence microscopy—might be biased due to the hydrophobic nature of all organic fluorophores, which can intensify and facilitate cellular uptake of labeled peptides [99, 144].

6 Third-Generation CPPs

CPPs of third generation are hoped to combine all positive features of peptide-based delivery systems in one molecule:

- Efficient delivery of active payloads at low concentration and with minimal side effects
- Facile escape from endocytic compartment into cell cytosol, or direct penetration into cells
- Selective targeting of cargoes to specified tissue/organ in living organism

Each of these requirements is met in several CPPs already and in some peptides even pairwise. Hopefully in near feature we will witness whether all these features can be merged in a magic CPP, or a multifunctional nanoparticle approach has to be applied to reach these goals.

7 Conclusions

The research in the peptide-based delivery of bioactive payloads has reached several important milestones in last years:

- The CPP conjugates with exon skipping PMOs rescued dystrophin expression in all muscle types in mouse models of Duchenne muscular dystrophy, including heart. The systemically administered conjugates are efficient at low doses and in therapeutic settings [169, 170].
- Peptides that selectively accumulate in solid tumors and quickly penetrate deeper into malignant tissue were discovered by phage display [171, 172].
- Designed peptides targeted siRNA containing endosomes into mouse brain with concomitant knockdown of targeted genes in neurons, microglia, and oligodendrocytes [173, 174].
- The first receptor that associates polyarginine CPPs was discovered [112].
- Sophisticated systems for delivery of nucleic acids that have therapeutic relevance were introduced [9, 150]. Some of the transport platforms also target the cell-surface receptors enabling addressing of cargoes to cell types of interest [157].

In addition to the abovementioned, the scope of cell penetration has remarkably widened: novel strategies like stapling and lipidation can transform membrane-impermeable peptides to penetrating ones. Methods that modify the lipid composition of membranes and also facilitate direct penetration of peptides across the plasma membrane have been elaborated. Furthermore, CPPs that augment endosomal escape have been designed, and the cell penetration mechanisms better understood. We hope that the progress made in CPP research in last years should enable better harnessing of immense potential of peptides in cellular delivery of various bioactive molecules on organism level and medicinal settings [14].

Authors are optimistic about the future of CPPs in delivery of bioactive drug-like molecules in vivo. For example, very recently a membrane-permeable peptide mimic of the protein-tyrosine phosphatase σ (PTPσ) promoted efficient recovery from spinal cord injury. PTPσ wedge domain was converted to membrane permeable by coupling pTat. The systemic delivery of this peptide

construct restored substantial serotonergic innervation of injured spinal cord and led to functional recovery of locomotor and urinary systems [175]. We believe that more exciting and elegant approaches/examples will follow soon and CPPs start to fulfil the hopes laid on them.

Acknowledgements

We are grateful to Dr. A. Lorents for the help with table and citations. The authors were supported by grants from the Estonian Science Foundation (ESF 8705), the Estonian Ministry of Education and Research (0180019s11, 0180027s08), and European Union Regional Development Fund (grant EU30020) through the Competence Centre on Reproductive Medicine and Biology.

References

1. Frankel AD, Pabo CO (1988) Cellular uptake of the tat protein from human immunodeficiency virus. Cell 55:1189–1193
2. Green M, Loewenstein PM (1988) Autonomous functional domains of chemically synthesized human immunodeficiency virus tat trans-activator protein. Cell 55: 1179–1188
3. Joliot A, Pernelle C, Deagostini-Bazin H et al (1991) Antennapedia homeobox peptide regulates neural morphogenesis. Proc Natl Acad Sci U S A 88:1864–1868
4. Derossi D, Joliot AH, Chassaing G et al (1994) The third helix of the Antennapedia homeodomain translocates through biological membranes. J Biol Chem 269: 10444–10450
5. Derossi D, Calvet S, Trembleau A et al (1996) Cell internalization of the third helix of the Antennapedia homeodomain is receptor-independent. J Biol Chem 271: 18188–18193
6. Derossi D, Chassaing G, Prochiantz A (1998) Trojan peptides: the penetratin system for intracellular delivery. Trends Cell Biol 8:84–87
7. Lee SH, Castagner B, Leroux JC (2013) Is there a future for cell-penetrating peptides in oligonucleotide delivery? Eur J Pharm Biopharm 85:5–11
8. Abes R, Arzumanov AA, Moulton HM et al (2007) Cell-penetrating-peptide-based delivery of oligonucleotides: an overview. Biochem Soc Trans 35:775–779
9. Cerrato CP, Lehto T, Langel Ü (2014) Peptide-based vectors: recent developments. Biomol Concepts 5:479–488
10. Vasconcelos L, Parn K, Langel Ü (2013) Therapeutic potential of cell-penetrating peptides. Ther Deliv 4:573–591
11. Brock R (2014) The uptake of arginine-rich cell-penetrating peptides: putting the puzzle together. Bioconjug Chem 25:863–868
12. Wang F, Wang Y, Zhang X et al (2014) Recent progress of cell-penetrating peptides as new carriers for intracellular cargo delivery. J Control Release 174:126–136
13. Copolovici DM, Langel K, Eriste E et al (2014) Cell-penetrating peptides: design, synthesis, and applications. ACS Nano 8:1972–1994
14. Shi NQ, Qi XR, Xiang B et al (2014) A survey on "Trojan Horse" peptides: opportunities, issues and controlled entry to "Troy". J Control Release 194C:53–70
15. Margus H, Padari K, Pooga M (2012) Cell-penetrating peptides as versatile vehicles for oligonucleotide delivery. Mol Ther 20: 525–533
16. Fu A, Tang R, Hardie J et al (2014) Promises and pitfalls of intracellular delivery of proteins. Bioconjug Chem 25:1602–1608
17. Margus H, Padari K, Pooga M (2013) Insights into cell entry and intracellular trafficking of peptide and protein drugs provided

by electron microscopy. Adv Drug Deliv Rev 65:1031–1038

18. Liu E, Sheng J, Ye J et al (2014) CPP mediated insulin delivery: current status and promising future. Curr Pharm Biotechnol 15:240–255
19. Metildi CA, Felsen CN, Savariar EN et al (2015) Ratiometric activatable cell-penetrating peptides label pancreatic cancer, enabling fluorescence-guided surgery, which reduces metastases and recurrence in orthotopic mouse models. Ann Surg Oncol 22:2082–2087
20. Nguyen QT, Tsien RY (2013) Fluorescence-guided surgery with live molecular navigation – a new cutting edge. Nat Rev Cancer 13:653–662
21. Olson ES, Jiang T, Aguilera TA et al (2010) Activatable cell penetrating peptides linked to nanoparticles as dual probes for in vivo fluorescence and MR imaging of proteases. Proc Natl Acad Sci U S A 107:4311–4316
22. Jiang T, Olson ES, Nguyen QT et al (2004) Tumor imaging by means of proteolytic activation of cell-penetrating peptides. Proc Natl Acad Sci U S A 101:17867–17872
23. Koren E, Torchilin VP (2012) Cell-penetrating peptides: breaking through to the other side. Trends Mol Med 18:385–393
24. Torchilin VP (2008) Cell penetrating peptide-modified pharmaceutical nanocarriers for intracellular drug and gene delivery. Biopolymers 90:604–610
25. Andreev OA, Engelman DM, Reshetnyak YK (2010) pH-sensitive membrane peptides (pHLIPs) as a novel class of delivery agents. Mol Membr Biol 27:341–352
26. Chen B, Friedman B, Whitney MA et al (2012) Thrombin activity associated with neuronal damage during acute focal ischemia. J Neurosci 32:7622–7631
27. Zhang L, Hoffman JA, Ruoslahti E (2005) Molecular profiling of heart endothelial cells. Circulation 112:1601–1611
28. Teesalu T, Sugahara KN, Ruoslahti E (2012) Mapping of vascular ZIP codes by phage display. Methods Enzymol 503:35–56
29. Ruoslahti E (2000) Targeting tumor vasculature with homing peptides from phage display. Semin Cancer Biol 10:435–442
30. Chaloin L, Vidal P, Heitz A et al (1997) Conformations of primary amphipathic carrier peptides in membrane mimicking environments. Biochemistry 36:11179–11187
31. Morris MC, Depollier J, Mery J et al (2001) A peptide carrier for the delivery of biologically active proteins into mammalian cells. Nat Biotechnol 19:1173–1176
32. Stewart KM, Horton KL, Kelley SO (2008) Cell-penetrating peptides as delivery vehicles for biology and medicine. Org Biomol Chem 6:2242–2255
33. Shaheen SM, Akita H, Nakamura T et al (2011) KALA-modified multi-layered nanoparticles as gene carriers for MHC class-I mediated antigen presentation for a DNA vaccine. Biomaterials 32:6342–6350
34. Milletti F (2012) Cell-penetrating peptides: classes, origin, and current landscape. Drug Discov Today 17:850–860
35. Reissmann S (2014) Cell penetration: scope and limitations by the application of cell-penetrating peptides. J Pept Sci 20:760–784
36. Lindgren M, Hällbrink M, Prochiantz A et al (2000) Cell-penetrating peptides. Trends Pharmacol Sci 21:99–103
37. Prochiantz A (2000) Messenger proteins: homeoproteins, TAT and others. Curr Opin Cell Biol 12:400–406
38. Vives E, Brodin P, Lebleu B (1997) A truncated HIV-1 Tat protein basic domain rapidly translocates through the plasma membrane and accumulates in the cell nucleus. J Biol Chem 272:16010–16017
39. Schwarze SR, Ho A, Vocero-Akbani A et al (1999) In vivo protein transduction: delivery of a biologically active protein into the mouse. Science 285:1569–1572
40. Derossi D, Prochiantz A (1995) Internalization of macromolecules by live cells. Restor Neurol Neurosci 8:7–10
41. Langel Ü (2002) Cell-penetrating peptides, processes and applications. CRC Press, Boca Raton, FL
42. Elmquist A, Lindgren M, Bartfai T et al (2001) VE-cadherin-derived cell-penetrating peptide, pVEC, with carrier functions. Exp Cell Res 269:237–244
43. Elliott G, O'Hare P (1997) Intercellular trafficking and protein delivery by a herpesvirus structural protein. Cell 88:223–233
44. Futaki S, Suzuki T, Ohashi W et al (2001) Arginine-rich peptides. An abundant source of membrane-permeable peptides having potential as carriers for intracellular protein delivery. J Biol Chem 276:5836–5840
45. Kilk K, Magzoub M, Pooga M et al (2001) Cellular internalization of a cargo complex with a novel peptide derived from the third helix of the islet-1 homeodomain. comparison with the penetratin peptide. Bioconjug Chem 12:911–916
46. Balayssac S, Burlina F, Convert O et al (2006) Comparison of penetratin and other homeodomain-derived cell-penetrating

peptides: interaction in a membrane-mimicking environment and cellular uptake efficiency. Biochemistry 45:1408–1420

47. Han K, Jeon MJ, Kim KA et al (2000) Efficient intracellular delivery of GFP by homeodomains of Drosophila Fushi-tarazu and Engrailed proteins. Mol Cells 10: 728–732
48. Machova Z, Muhle C, Krauss U et al (2002) Cellular internalization of enhanced green fluorescent protein ligated to a human calcitonin-based carrier peptide. Chembiochem 3:672–677
49. Rennert R, Neundorf I, Beck-Sickinger AG (2008) Calcitonin-derived peptide carriers: mechanisms and application. Adv Drug Deliv Rev 60:485–498
50. Duchardt F, Ruttekolk IR, Verdurmen WP et al (2009) A cell-penetrating peptide derived from human lactoferrin with conformation-dependent uptake efficiency. J Biol Chem 284:36099–36108
51. Radis-Baptista G, Kerkis I (2011) Crotamine, a small basic polypeptide myotoxin from rattlesnake venom with cell-penetrating properties. Curr Pharm Des 17:4351–4361
52. Esteve E, Mabrouk K, Dupuis A et al (2005) Transduction of the scorpion toxin maurocalcine into cells. Evidence that the toxin crosses the plasma membrane. J Biol Chem 280: 12833–12839
53. Tisseyre C, Bahembera E, Dardevet L et al (2013) Cell penetration properties of a highly efficient mini maurocalcine Peptide. Pharmaceuticals (Basel) 6:320–339
54. Pooga M, Hällbrink M, Zorko M et al (1998) Cell penetration by transportan. FASEB J 12:67–77
55. Morris MC, Vidal P, Chaloin L et al (1997) A new peptide vector for efficient delivery of oligonucleotides into mammalian cells. Nucleic Acids Res 25:2730–2736
56. Crombez L, Aldrian-Herrada G, Konate K et al (2009) A new potent secondary amphipathic cell-penetrating peptide for siRNA delivery into mammalian cells. Mol Ther 17:95–103
57. Ivanova GD, Arzumanov A, Abes R et al (2008) Improved cell-penetrating peptide-PNA conjugates for splicing redirection in HeLa cells and exon skipping in mdx mouse muscle. Nucleic Acids Res 36:6418–6428
58. Repke H, Bienert M (1987) Mast cell activation – a receptor-independent mode of substance P action? FEBS Lett 221:236–240
59. Oehlke J, Beyermann M, Wiesner B et al (1997) Evidence for extensive and non-specific translocation of oligopeptides across plasma membranes of mammalian cells. Biochim Biophys Acta 1330:50–60
60. Scheller A, Wiesner B, Melzig M et al (2000) Evidence for an amphipathicity independent cellular uptake of amphipathic cell-penetrating peptides. Eur J Biochem 267:6043–6050
61. Mitchell DJ, Kim DT, Steinman L et al (2000) Polyarginine enters cells more efficiently than other polycationic homopolymers. J Pept Res 56:318–325
62. Futaki S (2006) Oligoarginine vectors for intracellular delivery: design and cellular-uptake mechanisms. Biopolymers 84:241–249
63. Sugiyama S, Di Nardo AA, Aizawa S et al (2008) Experience-dependent transfer of Otx2 homeoprotein into the visual cortex activates postnatal plasticity. Cell 134: 508–520
64. Wizenmann A, Brunet I, Lam JS et al (2009) Extracellular Engrailed participates in the topographic guidance of retinal axons in vivo. Neuron 64:355–366
65. Metkar SS, Marchioretto M, Antonini V et al (2015) Perforin oligomers form arcs in cellular membranes: a locus for intracellular delivery of granzymes. Cell Death Differ 22:74
66. Ziegler A (2008) Thermodynamic studies and binding mechanisms of cell-penetrating peptides with lipids and glycosaminoglycans. Adv Drug Deliv Rev 60:580–597
67. Madani F, Lindberg S, Langel Ü et al (2011) Mechanisms of cellular uptake of cell-penetrating peptides. J Biophys 2011:414729
68. Tünnemann G, Martin RM, Haupt S et al (2006) Cargo-dependent mode of uptake and bioavailability of TAT-containing proteins and peptides in living cells. FASEB J 20: 1775–1784
69. Verdurmen WP, Brock R (2011) Biological responses towards cationic peptides and drug carriers. Trends Pharmacol Sci 32: 116–124
70. Nakase I, Hirose H, Tanaka G et al (2009) Cell-surface accumulation of flock house virus-derived peptide leads to efficient internalization via macropinocytosis. Mol Ther 17:1868–1876
71. De Coupade C, Fittipaldi A, Chagnas V et al (2005) Novel human-derived cell-penetrating peptides for specific subcellular delivery of therapeutic biomolecules. Biochem J 390: 407–418
72. Reynolds F, Weissleder R, Josephson L (2005) Protamine as an efficient membrane-translocating peptide. Bioconjug Chem 16:1240–1245

73. Rosenbluh J, Hariton-Gazal E, Dagan A et al (2005) Translocation of histone proteins across lipid bilayers and Mycoplasma membranes. J Mol Biol 345:387–400
74. Joliot A (2005) Transduction peptides within naturally occurring proteins. Sci STKE 2005:pe54
75. Christiaens B, Symoens S, Verheyden S et al (2002) Tryptophan fluorescence study of the interaction of penetratin peptides with model membranes. Eur J Biochem 269:2918–2926
76. Drin G, Mazel M, Clair P et al (2001) Physico-chemical requirements for cellular uptake of pAntp peptide. Role of lipid-binding affinity. Eur J Biochem 268: 1304–1314
77. Bechara C, Pallerla M, Burlina F et al (2015) Massive glycosaminoglycan-dependent entry of Trp-containing cell-penetrating peptides induced by exogenous sphingomyelinase or cholesterol depletion. Cell Mol Life Sci 72:809
78. Thoren PE, Persson D, Esbjorner EK et al (2004) Membrane binding and translocation of cell-penetrating peptides. Biochemistry 43:3471–3489
79. Konate K, Crombez L, Deshayes S et al (2010) Insight into the cellular uptake mechanism of a secondary amphipathic cell-penetrating peptide for siRNA delivery. Biochemistry 49:3393–3402
80. Hariton-Gazal E, Feder R, Mor A et al (2002) Targeting of nonkaryophilic cell-permeable peptides into the nuclei of intact cells by covalently attached nuclear localization signals. Biochemistry 41:9208–9214
81. Mano M, Henriques A, Paiva A et al (2006) Cellular uptake of S413-PV peptide occurs upon conformational changes induced by peptide-membrane interactions. Biochim Biophys Acta 1758:336–346
82. Soomets U, Lindgren M, Gallet X et al (2000) Deletion analogues of transportan. Biochim Biophys Acta 1467:165–176
83. Johansson HJ, El-Andaloussi S, Holm T et al (2008) Characterization of a novel cytotoxic cell-penetrating peptide derived from p14ARF protein. Mol Ther 16:115–123
84. Lundberg P, Magzoub M, Lindberg M et al (2002) Cell membrane translocation of the N-terminal (1-28) part of the prion protein. Biochem Biophys Res Commun 299:85–90
85. Magzoub M, Sandgren S, Lundberg P et al (2006) N-terminal peptides from unprocessed prion proteins enter cells by macropinocytosis. Biochem Biophys Res Commun 348:379–385
86. El-Andaloussi S, Johansson HJ, Holm T et al (2007) A novel cell-penetrating peptide, M918, for efficient delivery of proteins and peptide nucleic acids. Mol Ther 15: 1820–1826
87. Lorents A, Kodavali PK, Oskolkov N et al (2012) Cell-penetrating peptides split into two groups based on modulation of intracellular calcium concentration. J Biol Chem 287:16880–16889
88. Palm-Apergi C, Lorents A, Padari K et al (2009) The membrane repair response masks membrane disturbances caused by cell-penetrating peptide uptake. FASEB J 23: 214–223
89. Oehlke J, Krause E, Wiesner B et al (1997) Extensive cellular uptake into endothelial cells of an amphipathic beta- sheet forming peptide. FEBS Lett 415:196–199
90. Magzoub M, Eriksson LE, Gräslund A (2002) Conformational states of the cell-penetrating peptide penetratin when interacting with phospholipid vesicles: effects of surface charge and peptide concentration. Biochim Biophys Acta 1563:53–63
91. Li W, Nicol F, Szoka FC Jr (2004) GALA: a designed synthetic pH-responsive amphipathic peptide with applications in drug and gene delivery. Adv Drug Deliv Rev 56: 967–985
92. Sadler K, Eom KD, Yang JL et al (2002) Translocating proline-rich peptides from the antimicrobial peptide bactenecin 7. Biochemistry 41:14150–14157
93. Rojas M, Donahue JP, Tan Z et al (1998) Genetic engineering of proteins with cell membrane permeability. Nat Biotechnol 16:370–375
94. Gao C, Mao S, Ditzel HJ et al (2002) A cell-penetrating peptide from a novel pVII-pIX phage-displayed random peptide library. Bioorg Med Chem 10:4057–4065
95. Gao S, Simon MJ, Hue CD et al (2011) An unusual cell penetrating peptide identified using a plasmid display-based functional selection platform. ACS Chem Biol 6: 484–491
96. Rhee M, Davis P (2006) Mechanism of uptake of C105Y, a novel cell-penetrating peptide. J Biol Chem 281:1233–1240
97. Jones S, Lukanowska M, Suhorutsenko J et al (2013) Intracellular translocation and differential accumulation of cell-penetrating peptides in bovine spermatozoa: evaluation of efficient delivery vectors that do not compromise human sperm motility. Hum Reprod 28:1874–1889

98. Sagan S, Burlina F, Alves ID et al (2013) Homeoproteins and homeoprotein-derived peptides: going in and out. Curr Pharm Des 19:2851–2862
99. Jones AT, Sayers EJ (2012) Cell entry of cell penetrating peptides: tales of tails wagging dogs. J Control Release 161:582–591
100. Räägel H, Säälik P, Pooga M (2010) Peptide-mediated protein delivery - which pathways are penetrable? Biochim Biophys Acta 1798:2240–2248
101. Duchardt F, Fotin-Mleczek M, Schwarz H et al (2007) A comprehensive model for the cellular uptake of cationic cell-penetrating peptides. Traffic 8:848–866
102. Fretz MM, Penning NA, Al-Taei S et al (2007) Temperature-, concentration- and cholesterol-dependent translocation of L- and D-octa-arginine across the plasma and nuclear membrane of CD34+ leukaemia cells. Biochem J 403:335–342
103. Bechara C, Sagan S (2013) Cell-penetrating peptides: 20 years later, where do we stand? FEBS Lett 587:1693–1702
104. Richard JP, Melikov K, Vives E et al (2003) Cell-penetrating peptides. A reevaluation of the mechanism of cellular uptake. J Biol Chem 278:585–590
105. Fittipaldi A, Ferrari A, Zoppe M et al (2003) Cell membrane lipid rafts mediate caveolar endocytosis of HIV-1 Tat fusion proteins. J Biol Chem 278:34141–34149
106. Wadia JS, Stan RV, Dowdy SF (2004) Transducible TAT-HA fusogenic peptide enhances escape of TAT-fusion proteins after lipid raft macropinocytosis. Nat Med 10:310–315
107. Padari K, Säälik P, Hansen M et al (2005) Cell transduction pathways of transportans. Bioconjug Chem 16:1399–1410
108. Säälik P, Padari K, Niinep A et al (2009) Protein delivery with transportans is mediated by caveolae rather than flotillin-dependent pathways. Bioconjug Chem 20:877–887
109. Al Soraj M, He L, Peynshaert K et al (2012) siRNA and pharmacological inhibition of endocytic pathways to characterize the differential role of macropinocytosis and the actin cytoskeleton on cellular uptake of dextran and cationic cell penetrating peptides octaarginine (R8) and HIV-Tat. J Control Release 161:132–141
110. Gerbal-Chaloin S, Gondeau C, Aldrian-Herrada G et al (2007) First step of the cell-penetrating peptide mechanism involves Rac1 GTPase-dependent actin-network remodelling. Biol Cell 99:223–238
111. Letoha T, Keller-Pinter A, Kusz E et al (2010) Cell-penetrating peptide exploited syndecans. Biochim Biophys Acta 1798:2258–2265
112. Tanaka G, Nakase I, Fukuda Y et al (2012) CXCR4 stimulates macropinocytosis: implications for cellular uptake of arginine-rich cell-penetrating peptides and HIV. Chem Biol 19:1437–1446
113. Gump JM, June RK, Dowdy SF (2010) Revised role of glycosaminoglycans in TAT protein transduction domain-mediated cellular transduction. J Biol Chem 285: 1500–1507
114. Pae J, Säälik P, Liivamägi L et al (2014) Translocation of cell-penetrating peptides across the plasma membrane is controlled by cholesterol and microenvironment created by membranous proteins. J Control Release 192:103–113
115. Bryant KL, Mancias JD, Kimmelman AC et al (2014) KRAS: feeding pancreatic cancer proliferation. Trends Biochem Sci 39:91–100
116. Lehto T, Castillo Alvarez A, Gauck S et al (2014) Cellular trafficking determines the exon skipping activity of Pip6a-PMO in mdx skeletal and cardiac muscle cells. Nucleic Acids Res 42:3207–3217
117. Watkins CL, Schmaljohann D, Futaki S et al (2009) Low concentration thresholds of plasma membranes for rapid energy-independent translocation of a cell-penetrating peptide. Biochem J 420:179–189
118. Verdurmen WP, Thanos M, Ruttekolk IR et al (2010) Cationic cell-penetrating peptides induce ceramide formation via acid sphingomyelinase: implications for uptake. J Control Release 147:171–179
119. Herce HD, Garcia AE, Cardoso MC (2014) Fundamental molecular mechanism for the cellular uptake of guanidinium-rich molecules. J Am Chem Soc 136:17459
120. Takeuchi T, Kosuge M, Tadokoro A et al (2006) Direct and rapid cytosolic delivery using cell-penetrating peptides mediated by pyrenebutyrate. ACS Chem Biol 1:299–303
121. Mishra A, Lai GH, Schmidt NW et al (2011) Translocation of HIV TAT peptide and analogues induced by multiplexed membrane and cytoskeletal interactions. Proc Natl Acad Sci U S A 108:16883–16888
122. Chen X, Sa'adedin F, Deme B et al (2013) Insertion of TAT peptide and perturbation of negatively charged model phospholipid bilayer revealed by neutron diffraction. Biochim Biophys Acta 1828:1982–1988
123. Deshayes S, Plenat T, Charnet P et al (2006) Formation of transmembrane ionic channels

of primary amphipathic cell-penetrating peptides. Consequences on the mechanism of cell penetration. Biochim Biophys Acta 1758: 1846–1851

124. Rydstrom A, Deshayes S, Konate K et al (2011) Direct translocation as major cellular uptake for CADY self-assembling peptide-based nanoparticles. PLoS One 6:e25924
125. Joliot A, Prochiantz A (2008) Homeoproteins as natural penetratin cargoes with signaling properties. Adv Drug Deliv Rev 60:608–613
126. Layalle S, Volovitch M, Mugat B et al (2011) Engrailed homeoprotein acts as a signaling molecule in the developing fly. Development 138:2315–2323
127. Prochiantz A, Fuchs J, Di Nardo AA (2014) Postnatal signalling with homeoprotein transcription factors. Philos Trans R Soc Lond B Biol Sci 369:pii: 20130518. doi:10.1098/rstb.2013.0518
128. Palm C, Jayamanne M, Kjellander M et al (2007) Peptide degradation is a critical determinant for cell-penetrating peptide uptake. Biochim Biophys Acta 1768:1769–1776
129. Padari K, Koppel K, Lorents A et al (2010) S4(13)-PV cell-penetrating peptide forms nanoparticle-like structures to gain entry into cells. Bioconjug Chem 21:774–783
130. Oskolkov N, Arukuusk P, Copolovici DM et al (2011) NickFects, phosphorylated derivatives of transportan 10 for cellular delivery of oligonucleotides. Int J Pept Res Ther 17: 147–157
131. Regberg J, Eriksson JN, Langel Ü (2013) Cell-penetrating peptides: from cell cultures to in vivo applications. Front Biosci (Elite Ed) 5:509–516
132. Zorko M, Langel Ü (2005) Cell-penetrating peptides: mechanism and kinetics of cargo delivery. Adv Drug Deliv Rev 57:529–545
133. Polyakov V, Sharma V, Dahlheimer JL et al (2000) Novel Tat-peptide chelates for direct transduction of technetium-99m and rhenium into human cells for imaging and radiotherapy. Bioconjug Chem 11:762–771
134. Drin G, Cottin S, Blanc E et al (2003) Studies on the internalization mechanism of cationic cell-penetrating peptides. J Biol Chem 278:31192–31201
135. Tünnemann G, Ter-Avetisyan G, Martin RM et al (2008) Live-cell analysis of cell penetration ability and toxicity of oligo-arginines. J Pept Sci 14:469–476
136. Suzuki T, Futaki S, Niwa M et al (2002) Possible existence of common internalization mechanisms among arginine-rich peptides. J Biol Chem 277:2437–2443
137. Jones SW, Christison R, Bundell K et al (2005) Characterisation of cell-penetrating peptide-mediated peptide delivery. Br J Pharmacol 145:1093–1102
138. Järver P, Mäger I, Langel Ü (2010) In vivo biodistribution and efficacy of peptide mediated delivery. Trends Pharmacol Sci 31: 528–535
139. Säälik P, Elmquist A, Hansen M et al (2004) Protein cargo delivery properties of cell-penetrating peptides. A comparative study. Bioconjug Chem 15:1246–1253
140. Lehto T, Abes R, Oskolkov N et al (2010) Delivery of nucleic acids with a stearylated (RxR)4 peptide using a non-covalent co-incubation strategy. J Control Release 141:42–51
141. Hällbrink M, Florén A, Elmquist A et al (2001) Cargo delivery kinetics of cell-penetrating peptides. Biochim Biophys Acta 1515:101–109
142. Mäger I, Eiriksdottir E, Langel K et al (2010) Assessing the uptake kinetics and internalization mechanisms of cell-penetrating peptides using a quenched fluorescence assay. Biochim Biophys Acta 1798:338–343
143. Mäger I, Langel K, Lehto T et al (2012) The role of endocytosis on the uptake kinetics of luciferin-conjugated cell-penetrating peptides. Biochim Biophys Acta 1818:502–511
144. Hirose H, Takeuchi T, Osakada H et al (2012) Transient focal membrane deformation induced by arginine-rich peptides leads to their direct penetration into cells. Mol Ther 20:984–993
145. Jiao CY, Delaroche D, Burlina F et al (2009) Translocation and endocytosis for cell-penetrating peptide internalization. J Biol Chem 284:33957–33965
146. Sasaki Y, Minamizawa M, Ambo A et al (2008) Cell-penetrating peptide-conjugated XIAP-inhibitory cyclic hexapeptides enter into Jurkat cells and inhibit cell proliferation. FEBS J 275:6011–6021
147. Lättig-Tünnemann G, Prinz M, Hoffmann D et al (2011) Backbone rigidity and static presentation of guanidinium groups increases cellular uptake of arginine-rich cell-penetrating peptides. Nat Commun 2:453
148. Oh D, Nasrolahi Shirazi A, Northup K et al (2014) Enhanced cellular uptake of short polyarginine peptides through fatty acylation and cyclization. Mol Pharm 11:2845–2854
149. Futaki S, Ohashi W, Suzuki T et al (2001) Stearylated arginine-rich peptides: a new class of transfection systems. Bioconjug Chem 12:1005–1011

150. Lehto T, Kurrikoff K, Langel Ü (2012) Cell-penetrating peptides for the delivery of nucleic acids. Expert Opin Drug Deliv 9:823–836
151. Arukuusk P, Pärnaste L, Oskolkov N et al (2013) New generation of efficient peptide-based vectors, NickFects, for the delivery of nucleic acids. Biochim Biophys Acta 1828:1365–1373
152. Mäe M, El Andaloussi S, Lundin P et al (2009) A stearylated CPP for delivery of splice correcting oligonucleotides using a non-covalent co-incubation strategy. J Control Release 134:221–227
153. Lehto T, Simonson OE, Mäger I et al (2011) A peptide-based vector for efficient gene transfer in vitro and in vivo. Mol Ther 19:1457–1467
154. Andaloussi SE, Lehto T, Mäger I et al (2011) Design of a peptide-based vector, PepFect6, for efficient delivery of siRNA in cell culture and systemically in vivo. Nucleic Acids Res 39:3972–3987
155. Ezzat K, Andaloussi SE, Zaghloul EM et al (2011) PepFect 14, a novel cell-penetrating peptide for oligonucleotide delivery in solution and as solid formulation. Nucleic Acids Res 39:5284–5298
156. Arukuusk P, Pärnaste L, Margus H et al (2013) Differential endosomal pathways for radically modified peptide vectors. Bioconjug Chem 24:1721–1732
157. Ezzat K, Helmfors H, Tudoran O et al (2012) Scavenger receptor-mediated uptake of cell-penetrating peptide nanocomplexes with oligonucleotides. FASEB J 26:1172–1180
158. Lindberg S, Munoz-Alarcon A, Helmfors H et al (2013) PepFect15, a novel endosomolytic cell-penetrating peptide for oligonucleotide delivery via scavenger receptors. Int J Pharm 441:242–247
159. Covic L, Gresser AL, Talavera J et al (2002) Activation and inhibition of G protein-coupled receptors by cell-penetrating membrane-tethered peptides. Proc Natl Acad Sci U S A 99:643–648
160. Tressel SL, Koukos G, Tchernychev B et al (2011) Pharmacology, biodistribution, and efficacy of GPCR-based pepducins in disease models. Methods Mol Biol 683:259–275
161. Leger AJ, Jacques SL, Badar J et al (2006) Blocking the protease-activated receptor 1-4 heterodimer in platelet-mediated thrombosis. Circulation 113:1244–1254
162. Boire A, Covic L, Agarwal A et al (2005) PAR1 is a matrix metalloprotease-1 receptor that promotes invasion and tumorigenesis of breast cancer cells. Cell 120:303–313
163. Kaneider NC, Agarwal A, Leger AJ et al (2005) Reversing systemic inflammatory response syndrome with chemokine receptor pepducins. Nat Med 11:661–665
164. Ochocki JD, Mullen DG, Wattenberg EV et al (2011) Evaluation of a cell penetrating prenylated peptide lacking an intrinsic fluorophore via in situ click reaction. Bioorg Med Chem Lett 21:4998–5001
165. Wollack JW, Zeliadt NA, Ochocki JD et al (2010) Investigation of the sequence and length dependence for cell-penetrating prenylated peptides. Bioorg Med Chem Lett 20:161–163
166. Bernal F, Tyler AF, Korsmeyer SJ et al (2007) Reactivation of the p53 tumor suppressor pathway by a stapled p53 peptide. J Am Chem Soc 129:2456–2457
167. Walensky LD, Kung AL, Escher I et al (2004) Activation of apoptosis in vivo by a hydrocarbon-stapled BH3 helix. Science 305:1466–1470
168. Brown CJ, Quah ST, Jong J et al (2013) Stapled peptides with improved potency and specificity that activate p53. ACS Chem Biol 8:506–512
169. Betts C, Saleh AF, Arzumanov AA et al (2012) Pip6-PMO, a new generation of peptide-oligonucleotide conjugates with improved cardiac exon skipping activity for dmd treatment. Mol Ther Nucleic Acids 1:e38
170. Järver P, Coursindel T, Andaloussi SE et al (2012) Peptide-mediated cell and in vivo delivery of antisense oligonucleotides and siRNA. Mol Ther Nucleic Acids 1:e27
171. Sugahara KN, Teesalu T, Karmali PP et al (2009) Tissue-penetrating delivery of compounds and nanoparticles into tumors. Cancer Cell 16:510–520
172. Teesalu T, Sugahara KN, Kotamraju VR et al (2009) C-end rule peptides mediate neuropilin-1-dependent cell, vascular, and tissue penetration. Proc Natl Acad Sci U S A 106:16157–16162
173. Alvarez-Erviti L, Seow Y, Yin H et al (2011) Delivery of siRNA to the mouse brain by systemic injection of targeted exosomes. Nat Biotechnol 29:341–345
174. El-Andaloussi S, Lee Y, Lakhal-Littleton S et al (2012) Exosome-mediated delivery of siRNA in vitro and in vivo. Nat Protoc 7:2112–2126
175. Lang BT, Cregg JM, DePaul MA et al (2015) Modulation of the proteoglycan receptor PTPsigma promotes recovery after spinal cord injury. Nature 518:404–408

176. Kobayashi S, Takeshima K, Park CB et al (2000) Interactions of the novel antimicrobial peptide buforin 2 with lipid bilayers: proline as a translocation promoting factor. Biochemistry 39:8648–8654
177. Kerkis A, Kerkis I, Radis-Baptista G et al (2004) Crotamine is a novel cell-penetrating protein from the venom of rattlesnake Crotalus durissus terrificus. FASEB J 18: 1407–1409
178. Taylor BN, Mehta RR, Yamada T et al (2009) Noncationic peptides obtained from azurin preferentially enter cancer cells. Cancer Res 69:537–546
179. Trehin R, Krauss U, Beck-Sickinger AG et al (2004) Cellular uptake but low permeation of human calcitonin-derived cell penetrating peptides and Tat(47-57) through well-differentiated epithelial models. Pharm Res 21:1248–1256
180. Delaroche D, Aussedat B, Aubry S et al (2007) Tracking a new cell-penetrating (W/R) nonapeptide, through an enzyme-stable mass spectrometry reporter tag. Anal Chem 79:1932–1938
181. Oehlke J, Scheller A, Wiesner B et al (1998) Cellular uptake of an alpha-helical amphipathic model peptide with the potential to deliver polar compounds into the cell interior non- endocytically. Biochim Biophys Acta 1414:127–139
182. Scheller A, Oehlke J, Wiesner B et al (1999) Structural requirements for cellular uptake of alpha-helical amphipathic peptides. J Pept Sci 5:185–194
183. Daniels DS, Schepartz A (2007) Intrinsically cell-permeable miniature proteins based on a minimal cationic PPII motif. J Am Chem Soc 129:14578–14579
184. Martin I, Teixido M, Giralt E (2011) Design, synthesis and characterization of a new anionic cell-penetrating peptide: SAP(E). Chembiochem 12:896–903
185. Lindgren M, Rosenthal-Aizman K, Saar K et al (2006) Overcoming methotrexate resistance in breast cancer tumour cells by the use of a new cell-penetrating peptide. Biochem Pharmacol 71:416–425
186. Covic L, Misra M, Badar J et al (2002) Pepducin-based intervention of thrombin-receptor signaling and systemic platelet activation. Nat Med 8:1161–1165
187. Forsman H, Bylund J, Oprea TI et al (2013) The leukocyte chemotactic receptor FPR2, but not the closely related FPR1, is sensitive to cell-penetrating pepducins with amino acid sequences descending from the third intracellular receptor loop. Biochim Biophys Acta 1833:1914–1923
188. Lin YZ, Yao SY, Veach RA et al (1995) Inhibition of nuclear translocation of transcription factor NF-kappa B by a synthetic peptide containing a cell membrane-permeable motif and nuclear localization sequence. J Biol Chem 270:14255–14258
189. Gomez JA, Gama V, Yoshida T et al (2007) Bax-inhibiting peptides derived from Ku70 and cell-penetrating pentapeptides. Biochem Soc Trans 35:797–801
190. Gomez JA, Chen J, Ngo J et al (2010) Cell-penetrating penta-peptides (CPP5s): measurement of cell entry and protein-transduction activity. Pharmaceuticals (Basel) 3:3594–3613
191. Marks JR, Placone J, Hristova K et al (2011) Spontaneous membrane-translocating peptides by orthogonal high-throughput screening. J Am Chem Soc 133:8995–9004
192. Oehlke J, Birth P, Klauschenz E et al (2002) Cellular uptake of antisense oligonucleotides after complexing or conjugation with cell-penetrating model peptides. Eur J Biochem 269:4025–4032
193. Chee SM, Wongsantichon J, Soo Tng Q et al (2014) Structure of a stapled peptide antagonist bound to nutlin-resistant Mdm2. PLoS One 9:e104914

Chapter 2

Penetratin Story: An Overview

Edmond Dupont, Alain Prochiantz, and Alain Joliot

Abstract

Cell-penetrating peptides are short, often hydrophilic peptides that get access to the intracellular milieu. They have aroused great interest both in academic and applied research. First, cellular internalization of CPPs often involves the crossing of a biological membrane (plasma or vesicular), thus challenging the view of the non-permeability of these structures to large hydrophilic molecules. Secondly, CPPs can drive the internalization of hydrophilic cargoes into cells, a rate-limiting step in the development of many therapeutic substances. Interestingly, the two most used CPPs, TAT and penetratin peptides, are derived from natural proteins, HIV Tat and Antennapedia homeoprotein, respectively. The identification of the penetratin peptide, summarized in this review, is intimately linked to the study of its parental natural protein.

Key words Penetratin, Cell-penetrating-peptide, Homeodomain, Homeoprotein

1 Introduction

It is extremely striking that the transgression of the dogma of membrane impermeability to hydrophilic molecules at the origin, 20 years ago, of the cell-permeable peptide field stems from the study of two unrelated transcriptional regulators, HIV Tat protein and Antennapedia homeoprotein. In both cases, the necessity to verify their purely intracellular activity had motivated the addition of these proteins in the extracellular medium, with unexpected results that suggested internalization by cultured cells. These results have led to the development of the first cell-permeable peptides, to expression strategies based on direct protein delivery—instead of classical nucleic acid transfection—and to the search for the underlying biological function of protein transduction.

Ülo Langel (ed.), *Cell-Penetrating Peptides: Methods and Protocols*, Methods in Molecular Biology, vol. 1324,
DOI 10.1007/978-1-4939-2806-4_2,

2 The Origin of an Unexpected Observation

In 1988, the capture of HIV-TAT by cells and its transport to the nucleus were described [1, 2]. At the same time, our laboratory was trying to correlate neuronal shape and position and in this position/shape context had started to investigate the function of homeoprotein transcription factors.

In the mid-1980s, we observed that brain neurons in culture adopt different polarity patterns depending on the origin of the astrocytes on which they were plated [3, 4]. It was particularly striking that dendrites would only develop when neurons and astrocytes were derived from the same structure. This allowed us to establish a theoretical link between developmental morphogenetic programs and positional information. At the time, the homeoprotein family of transcription factors that link organ shape to their positional information was discovered in Drosophila. We asked whether morphogenetic programs acting at the multicellular levels might also act at the single-cell level, on neuronal shape.

Homeoproteins are defined by nature of their DNA-binding domain, the homeodomain. This domain is highly conserved across homeoproteins and species, and is composed of three α-helices, the third helix being more particularly dedicated to the recognition of the DNA target site [5]. We wanted to test our hypothesis by injecting a homeodomain within live neurons. The logic was that the injected homeodomain would gain access to the nucleus and displace endogenous homeoproteins away from their cognate sites, thus revealing their morphological function at the single-cell level. We used the homeodomain of Antennapedia for practical reasons and on the basis of the strong sequence conservation between homeodomains. To analyze the role of homeoproteins in neuronal morphogenesis we developed a protocol aimed at antagonizing transcriptional activity of endogenous homeoproteins. This was achieved through the mechanical internalization of FITC-labeled homeodomains into live post-mitotic neurons [6–8]. The addition of exogenous Drosophila Antennapedia homeodomain (AntpHD) induced strong neurite outgrowth as expected that was attributed to a competition between the homeodomain and endogenous homeoproteins for their binding sites [8]. But the surprise was total when adding the homeodomain into the culture medium, for a control, we observed the same phenotype. This suggested either that the effect of the injected homeodomain was due to its leakage outside of the cells—an artifact—or that the homeodomain was internalized. We verified the latter possibility and observed, much to our surprise, that the 60-amino acid-long polypeptide was captured by the cells and addressed to their nuclei [8].

3 Homeodomain Translocation

In an attempt to analyze the neurite-promoting function of the homeodomain and its mechanism of action, two different point mutations affecting the specificity of protein/DNA interactions (AntpHD 50A) or the structure of the homeodomain (AntpHD 48S) were introduced [9–11]. The DNA-binding capacity of the three mutants is either decreased (AntpHD 50A) or completely abolished (AntpHD 48S) and the biological activity (neurite outgrowth stimulation) is lost in all cases [9–11]. Most importantly, translocation into live cells is lost only in the AntpHD 48S mutant, into which a single-serine residue replaces three amino acids (tryptophan 48, phenylalanine 49, and glutamine 50). Tryptophan 48 (Trp 48) and phenylalanine 49 (Phe 49) are conserved in all homeodomains, and important for the homeodomain structure [10].

This observation was so unexpected and disturbing that we decided to identify the mechanism involved in homeodomain capture. Interestingly, the intracellular distribution showing uniform cytoplasmic staining and nuclear accumulation was at odd with endocytosis. Indeed, uptake was observed at 4 °C, with the same uniform cytoplasmic staining. To preclude that this diffusion was due to AntpHD redistribution following fixation, the same experiments done with an FITC-tagged homeodomain, on live cells, and with the help of confocal microscopy gave identical results [8]. Finally, it was verified that the AntpHD was retrieved, intact, from the cells at both temperature, demonstrating very limited degradation [12].

4 The Penetratin Peptide

The results with AntpHD 48S suggested the presence of a cell translocation sequence in the third helix. The 16 amino acids of the helix (amino acids 43–58 of the homeodomain) were synthesized and internalization into live cells was followed thanks to an N-terminal biotin [13]. Shorter versions of the same peptide, with N-ter or C-ter deletions, are not internalized suggesting that this sequence, thereafter penetratin, is necessary and sufficient for internalization.

Similarly to AntpHD, penetratin can be internalized by an energy-independent mechanism at both 4 and 37 °C and has access to the cytoplasm and nucleus from which it is retrieved without apparent degradation [13]. Penetratin's high content in basic amino acids is reminding of TAT and oligoarginine peptides. In contrast, a unique feature of penetratin is the presence of hydrophobic residues, in particular tryptophans, which are critical to the translocation process [13]. Indeed, penetratin and other basic

PTDs differ in their cellular behaviors, even in the same experimental setup [14–17]. More strikingly, significant differences have been reported between penetratin-like sequence issues from different homeoproteins, despite extensive conservation of this motif among homeoproteins [18, 19]. Although biophysical and biological studies have greatly helped to our comprehension of penetratin behavior, a full understanding of its mechanism of translocation is still in wait.

4.1 Charge and Hydrophobicity: A Dual Mode of Interaction

Because penetratin composed of D-amino acids (D-penetratin) and an *inverso* form of the peptide are internalized as efficiently as penetratin [20], it was concluded that a chiral membrane receptor (usually a protein) is not required for cellular translocation. On the other hand, the specific ability of penetratin to form multimers in the presence of ionic detergents has led to a close examination of penetratin/lipid interactions [13]. Biophysical studies have established that penetratin preferentially interacts with anionic phospholipids mainly through electrostatic interactions, followed by limited peptide insertion into the bilayer [21–23]. Although the first studies strongly suggested that penetratin binds to the lipid headgroups, a situation not in favor of direct translocation across pure lipid bilayers, a more recent diversification of the experimental models and techniques has revealed a different picture [24, 25]. Penetratin actually crosses pure lipid bilayers, either in the presence of an applied transmembrane pH gradient [26, 27] or in response to a self-generated potential resulting from asymmetric peptide aggregation at one side of the bilayer (electroporation-like mechanism) [21]. The spontaneous insertion of non-aggregated penetratin in the inner leaflet of lipid bilayers was also reported using a novel solid-state NMR technique [28]. In these experimental setups, the behavior of penetratin greatly depends on the lipid composition of the vesicles. The absence of penetratin translocation reported by other groups could reflect an unfavorable lipid composition [29–31].

It must be kept in mind that penetratin/lipid interaction is a reciprocal process affecting both partners. Penetratin adopts a random coil structure in an aqueous environment but becomes structured in the presence of anionic phospholipids. At a low peptide/lipid ratio (1/325), the peptide adopts an α-helical conformation [13, 32–35]. At a high peptide/lipid ratio (1/10), the peptide forms antiparallel β-sheets [23, 35, 36]. Conversely, penetratin alters the organization of lipid bilayers and the orientation of lipid acyl chains is modified upon the deep insertion of penetratin into membrane bicelles [37]. When applied on a brain lipid mixture preparation, penetratin induces the formation of hexagonal phases [33]. We have proposed that this transient remodeling of lipid organization induced by penetratin places the peptide in a pseudo-hydrophilic environment and allows its transfer from the extracellular

medium to the cytoplasm of the cell. Other perturbations of the lipid bilayer upon penetratin addition have been reported, which can account for the translocation process. Penetratin induces a negative curvature of the lipid bilayer of giant unilamellar vesicles that contains liquid disordered domains [38] and has been shown to stimulate a membrane repair response, following the transient perturbation of plasma membrane integrity [39].

4.2 Influence of Structural Parameters on Peptide Translocation

Mutation analysis has confirmed the contribution of both hydrophobic and electrostatic properties to penetratin translocation. Mutation of basic residues favors peptide insertion in the acyl chains but destabilizes the bilayer [40]. A similar situation is observed upon addition of fluorescent probes to penetratin, which increases its hydrophobicity [41], and induces a transient destabilization of the plasma membrane in live cells demonstrated by the uptake of a cell-impermeant DNA dye and the appearance of phosphatidylserine at the cell surface [42]. Taken together many arguments suggest that a subtle balance between hydrophobic and electrostatic properties of penetratin is required for its translocation. In fact, even minimal modifications, such as substitution of the two Trp residues by two Phe residues, modify peptide/lipid interactions and impair translocation in live cells [13, 37, 41, 43]. By contrast neither peptide helicity nor amphipathicity seems to be required for peptide internalization [20]. Indeed, increasing the amphipathicity of penetratin by mutations increases the toxicity of the peptide rather than its translocation efficiency [44].

A common feature of basic CPPs, including penetratin, is their strong electrostatic interaction with the complex carbohydrates that decorate the cell surface, likely preceding the interaction with the lipid bilayer. It was shown that the presence of Trp residues also modulates this very early step along the internalization process and consequently impacts on the internalization pathway used [45].

4.3 One or More Mechanisms of Penetratin Internalization

Recent studies on the mechanism of internalization of penetratin in live cells have revealed a more complex picture than previously thought, and concluded to a predominant endocytic uptake and vesicular localization of this peptide [14, 15]. This proposal is at odd with a direct translocation process demonstrated by several internalization protocols, in particular at 4 °C, and biophysical studies. In fact there is no reason to exclude that penetratin can be captured by endocytosis depending on cell type and tagging procedure. It remains that, in contrast with Tat, endocytosis is not a prerequisite for penetratin transfer into the cytoplasm and nucleus. Among modifiers of penetratin uptake are the highly negatively charged carbohydrates that surround most cells, in particular glycosaminoglycans (GAGs) [46]. The complex sugars could restrict penetratin access to the membrane, promote penetratin

aggregation [47], and induce endocytosis, with the possibility (or not) that the peptide crosses the bilayer later, once within endosomes. Indeed, penetratin escape from artificial vesicles driven by a proton gradient has been reported, supporting this mechanism [48]. Moreover, the non-endocytic component of penetratin internalization (i.e., observed at 4 °C) is poorly affected by the absence of GAGs, while the endocytic component dramatically decreases [46].

The diversity of mechanisms has also been illustrated by several studies [40, 49, 50]. For example, the intracellular distribution of internalized penetratin greatly differs between Hela and MC57 cell lines, or the macropinocytosis inhibitor ethylisopropylamiloride (EIPA) decreases penetratin uptake added at high (50 μM) but not low (10 μM) concentration [17, 51].

5 The First Applications

Soon after the observation of homeodomain translocation, we have demonstrated the use of this process for the efficient cell delivery and biological activity of hydrophilic molecules was published. Both antisense oligonucleotides (against the β-amyloid precursor protein) and protein domains (C-terminus domain of rab3a) were efficiently internalized by cells in culture upon fusion to AntpHD [52, 53]. The first in vivo application of AntpHD-mediated vectorization was the induction of T-cell responses by a peptide derived from the HLA-cw3 cytotoxic T cell epitope [54]. It appeared very quickly that the 16-amino acid-long peptide penetratin could substitute advantageously for AntpHD, both for oligopeptide and oligonucleotide delivery [55, 56]. Since this time, this vectorization strategy has expanded dramatically [57], and proven to be highly versatile toward the nature of the transported cargo (from small drugs to nanoparticles) and the biological context (both ex vivo and in vivo). Most importantly, a large panel of peptides has been characterized on the basis of their cell-penetrating behavior although only some of them have been validated with a biological cargo.

In physiological situations, many of the successful applications of penetratin-driven delivery rely on the topical or targeted delivery of the compound. Improvement of the bio-distribution and bioavailability will consist in one of the major challenges for the therapeutical development of this promising strategy.

6 Conclusion

More than 10 years after the initial reports, one can ask whether CPP-based cellular delivery has reached maturity. The naïve view of a universal magic CPP bullet that delivers any hydrophilic

molecule into the cell has been replaced by a more complex picture, where for instance the nature of the transported cargo, its mode of linkage to the CPP, or the targeted intracellular compartment have to be considered. Our knowledge in this field still remains largely empirical, rather than predictive, and often relies on the setting up of dedicated experimental protocols, such as those described in this book.

References

1. Frankel AD, Pabo CO (1988) Cellular uptake of the tat protein from human immunodeficiency virus. Cell 55:1189–1193
2. Green M, Loewenstein PM (1988) Autonomous functional domains of chemically synthesized human immunodeficiency virus tat trans-activator protein. Cell 55:1179–1188
3. Denis-Donini S, Glowinski J, Prochiantz A (1984) Glial heterogeneity may define the three-dimensional shape of mouse mesencephalic dopaminergic neurones. Nature 307: 641–643
4. Chamak B, Fellous A, Glowinski J, Prochiantz A (1987) MAP2 expression and neuritic outgrowth and branching are coregulated through region-specific neuro-astroglial interactions. J Neurosci 7:3163–3170
5. Gehring WJ, Qian YQ, Billeter M, Furukubo-Tokunaga K, Schier AF, Resendez-Perez D, Affolter M, Otting G, Wüthrich K (1994) Homeodomain-DNA recognition. Cell 78: 211–223
6. Ayala J, Touchot N, Zahraoui A, Tavitian A, Prochiantz A (1990) The product of rab2, a small GTP binding protein, increases neuronal adhesion, and neurite growth in vitro. Neuron 4:797–805
7. Borasio GD, John J, Wittinghofer A, Barde YA, Sendtner M, Heumann R (1989) ras p21 protein promotes survival and fiber outgrowth of cultured embryonic neurons. Neuron 2: 1087–1096
8. Joliot A, Pernelle C, Deagostini-Bazin H, Prochiantz A (1991) Antennapedia homeobox peptide regulates neural morphogenesis. Proc Natl Acad Sci U S A 88:1864–1868
9. Bloch-Gallego E, Le Roux I, Joliot A, Volovitch M, Henderson CE, Prochiantz A (1993) Antennapedia homeobox peptide enhances growth and branching of embryonic chicken motoneurons in vitro. J Cell Biol 120: 485–492
10. Le Roux I, Joliot AH, Bloch-Gallego E, Prochiantz A, Volovitch M (1993) Neurotrophic activity of the Antennapedia homeodomain depends on its specific DNA-binding properties. Proc Natl Acad Sci U S A 90:9120–9124
11. Le Roux I, Duharcourt S, Volovitch M, Prochiantz A, Ronchi E (1995) Promoter-specific regulation of gene expression by an exogenously added homeodomain that promotes neurite growth. FEBS Lett 368: 311–314
12. Joliot A, Triller A, Volovitch M, Pernelle C, Prochiantz A (1991) alpha-2,8-Polysialic acid is the neuronal surface receptor of antennapedia homeobox peptide. New Biol 3: 1121–1134
13. Derossi D, Joliot A, Chassaing G, Prochiantz A (1994) The third helix of the Antennapedia homeodomain translocates through biological membranes. J Biol Chem 269:10444–10450
14. Duchardt F, Fotin-Mleczek M, Schwarz H, Fischer R, Brock R (2007) A comprehensive model for the cellular uptake of cationic cell-penetrating peptides. Traffic 8:848–866
15. Maiolo JR, Ferrer M, Ottinger EA (2005) Effects of cargo molecules on the cellular uptake of arginine-rich cell-penetrating peptides. Biochim Biophys Acta 1712:161–172
16. Manceur A, Wu A, Audet J (2007) Flow cytometric screening of cell-penetrating peptides for their uptake into embryonic and adult stem cells. Anal Biochem 364:51–59
17. Nakase I, Niwa M, Takeuchi T, Sonomura K, Kawabata N, Koike Y, Takehashi M, Tanaka S, Ueda K, Simpson JC et al (2004) Cellular uptake of arginine-rich peptides: roles for macropinocytosis and actin rearrangement. Mol Ther 10:1011–1022
18. Balayssac S, Burlina F, Convert O, Bolbach G, Chassaing G, Lequin O (2006) Comparison of penetratin and other homeodomain-derived cell-penetrating peptides: interaction in a membrane-mimicking environment and cellular uptake efficiency. Biochemistry 45: 1408–1420
19. Harreither E, Rydberg HA, Amand HL, Jadhav V, Fliedl L, Benda C, Esteban MA,

Pei D, Borth N, Grillari-Voglauer R et al (2014) Characterization of a novel cell penetrating peptide derived from human Oct4. Cell Regen (Lond) 3:2

20. Derossi D, Calvet S, Trembleau A, Brunissen A, Chassaing G, Prochiantz A (1996) Cell internalization of the third helix of the Antennapedia homeodomain is receptor-independent. J Biol Chem 271:18188–18193
21. Binder H, Lindblom G (2003) Charge-dependent translocation of the Trojan peptide penetratin across lipid membranes. Biophys J 85:982–995
22. Christiaens B, Symoens S, Verheyden S, Engelborghs Y, Joliot A, Prochiantz A, Vandekerckhove J, Rosseneu M, Vanloo B, Vanderheyden S (2002) Tryptophan fluorescence study of the interaction of penetratin peptides with model membranes. Eur J Biochem 269:2918–2926
23. Persson D, Thorén PE, Nordén B (2001) Penetratin-induced aggregation and subsequent dissociation of negatively charged phospholipid vesicles. FEBS Lett 505:307–312
24. Fragneto G, Bellet-Amalric E, Charitat T, Dubos P, Graner F, Perino-Galice L (2000) Neutron and X-ray reflectivity studies at solid-liquid interfaces: the interaction of a peptide with model membranes. Phys Rev B Condens Matter 276–278:501–502
25. Fragneto G, Graner F, Charitat T, Dubos P, Bellet-Amalric E (2000) Interaction of the third helix of antennapedia homeodomain with a deposited phospholipid bilayer: a neutron reflectivity structural study. Langmuir 16: 4581–4588
26. Björklund J, Biverståhl H, Gräslund A, Mäler L, Brzezinski P (2006) Real-time transmembrane translocation of penetratin driven by light-generated proton pumping. Biophys J 91:L29–L31
27. Magzoub M, Pramanik A, Gräslund A (2005) Modeling the endosomal escape of cell-penetrating peptides: transmembrane pH gradient driven translocation across phospholipid bilayers. Biochemistry 44:14890–14897
28. Su Y, Mani R, Hong M (2008) Asymmetric insertion of membrane proteins in lipid bilayers by solid-state NMR paramagnetic relaxation enhancement: a cell-penetrating Peptide example. J Am Chem Soc 130:8856–8864
29. Bárány-Wallje E, Keller S, Serowy S, Geibel S, Pohl P, Bienert M, Dathe M (2005) A critical reassessment of penetratin translocation across lipid membranes. Biophys J 89:2513–2521
30. Persson D, Thorén PEG, Esbjörner EK, Goksör M, Lincoln P, Nordén B (2004) Vesicle size-dependent translocation of penetratin analogs across lipid membranes. Biochim Biophys Acta 1665:142–155
31. Terrone D, Sang SLW, Roudaia L, Silvius JR (2003) Penetratin and related cell-penetrating cationic peptides can translocate across lipid bilayers in the presence of a transbilayer potential. Biochemistry 42:13787–13799
32. Drin G, Mazel M, Clair P, Mathieu D, Kaczorek M, Temsamani J (2001) Physico-chemical requirements for cellular uptake of pAntp peptide. Role of lipid-binding affinity. Eur J Biochem 268:1304–1314
33. Berlose JP, Convert O, Derossi D, Brunissen A, Chassaing G (1996) Conformational and associative behaviours of the third helix of antennapedia homeodomain in membrane-mimetic environments. Eur J Biochem 242: 372–386
34. Lindberg M, Gräslund A (2001) The position of the cell penetrating peptide penetratin in SDS micelles determined by NMR. FEBS Lett 497:39–44
35. Magzoub M, Kilk K, Eriksson LE, Langel U, Gräslund A (2001) Interaction and structure induction of cell-penetrating peptides in the presence of phospholipid vesicles. Biochim Biophys Acta 1512:77–89
36. Bellet-Amalric E, Blaudez D, Desbat B, Graner F, Gauthier F, Renault A (2000) Interaction of the third helix of Antennapedia homeodomain and a phospholipid monolayer, studied by ellipsometry and PM-IRRAS at the air-water interface. Biochim Biophys Acta 1467: 131–143
37. Zhang W, Smith SO (2005) Mechanism of penetration of Antp(43-58) into membrane bilayers. Biochemistry 44:10110–10118
38. Lamazière A, Chassaing G, Trugnan G, Ayala-Sanmartin J (2009) Tubular structures in heterogeneous membranes induced by the cell penetrating peptide penetratin. Commun Integr Biol 2:223–224
39. Palm-Apergi C, Lorents A, Padari K, Pooga M, Hällbrink M (2009) The membrane repair response masks membrane disturbances caused by cell-penetrating peptide uptake. FASEB J 23:214–223
40. Christiaens B, Grooten J, Reusens M, Joliot A, Goethals M, Vandekerckhove J, Prochiantz A, Rosseneu M (2004) Membrane interaction and cellular internalization of penetratin peptides. Eur J Biochem 271:1187–1197
41. Esbjörner EK, Lincoln P, Nordén B (2007) Counterion-mediated membrane penetration: cationic cell-penetrating peptides overcome Born energy barrier by ion-pairing with

phospholipids. Biochim Biophys Acta 1768:1550–1558

42. Dupont E, Prochiantz A, Joliot A (2007) Identification of a signal peptide for unconventional secretion. J Biol Chem 282:8994–9000
43. Magzoub M, Eriksson LEG, Gräslund A (2003) Comparison of the interaction, positioning, structure induction and membrane perturbation of cell-penetrating peptides and non-translocating variants with phospholipid vesicles. Biophys Chem 103: 271–288
44. Drin G, Déméné H, Temsamani J (2001) Translocation of the pAntp peptide and its amphipathic analogue AP-2AL. Biochemistry 40:1824–1834
45. Bechara C, Pallerla M, Zaltsman Y, Burlina F, Alves ID, Lequin O, Sagan S (2013) Tryptophan within basic peptide sequences triggers glycosaminoglycan-dependent endocytosis. FASEB J 27:738–749
46. Jiao CY, Delaroche D, Burlina F, Alves ID, Chassaing G, Sagan S (2009) Translocation and endocytosis for cell-penetrating peptide internalization. J Biol Chem 284: 33957–33965
47. Ghibaudi E, Boscolo B, Inserra G, Laurenti E, Traversa S, Barbero L, Ferrari RP (2005) The interaction of the cell-penetrating peptide penetratin with heparin, heparansulfates and phospholipid vesicles investigated by ESR spectroscopy. J Pept Sci 11:401–409
48. Madani F, Perálvarez-Marín A, Gräslund A (2011) Liposome model systems to study the endosomal escape of cell-penetrating peptides: transport across phospholipid membranes induced by a proton gradient. J Drug Deliv 2011:897592
49. Letoha T, Gaal S, Somlai C, Czajlik A, Perczel A, Penke B (2003) Membrane translocation of penetratin and its derivatives in different cell lines. J Mol Recognit 16:272–279
50. Letoha T, Gaál S, Somlai C, Venkei Z, Glavinas H, Kusz E, Duda E, Czajlik A, Peták F, Penke B (2005) Investigation of penetratin peptides. Part 2. In vitro uptake of penetratin and two of its derivatives. J Pept Sci 11:805–811
51. Fischer R, Waizenegger T, Köhler K, Brock R (2002) A quantitative validation of fluorophore-labelled cell-permeable peptide conjugates: fluorophore and cargo dependence of import. Biochim Biophys Acta 1564:365–374
52. Allinquant B, Hantraye P, Mailleux P, Moya K, Bouillot C, Prochiantz A (1995) Downregulation of Amyloid Precursor Protein inhibits neurite outgrowth in Vitro. J Cell Biol 128:919–927
53. Perez F, Lledo PM, Karagogeos D, Vincent JD, Prochiantz A, Ayala J (1994) Rab3A and Rab3B carboxy-terminal peptides are both potent and specific inhibitors of prolactin release by rat cultured anterior pituitary cells. Mol Endocrinol 8:1278–1287
54. Schutze-Redelmeier MP, Gournier H, Garcia-Pons F, Moussa M, Joliot A, Volovitch M, Prochiantz A, Lemonnier FA (1996) Introduction of exogenous antigens into the MHC class I processing and presentation pathway by Drosophila antennapedia homeodomain primes cytotoxic T cells in vivo. J Immunol 157:650–655
55. Théodore L, Derossi D, Chassaing G, Llirbat B, Kubes M, Jordan P, Chneiweiss H, Godement P, Prochiantz A (1995) Intraneuronal delivery of protein kinase C pseudosubstrate leads to growth cone collapse. J Neurosci 15:7158–7167
56. Troy CM, Derossi D, Prochiantz A, Greene LA, Shelanski ML (1996) Downregulation of Cu/Zn superoxide dismutase leads to cell death via the nitric oxide-peroxynitrite pathway. J Neurosci 16:253–261
57. Dupont E, Prochiantz A, Joliot A (2006) Penetratins. CRC, Boca Raton, FL

Chapter 3

Prediction of Cell-Penetrating Peptides

Mattias Hällbrink and Mati Karelson

Abstract

The in silico methods for the prediction of the cell-penetrating peptides are reviewed. Those include the multivariate statistical methods, machine-learning methods such as the artificial neural networks and support vector machines, and molecular modeling techniques including molecular docking and molecular dynamics.

The applicability of the methods is demonstrated on the basis of the exemplary cases from the literature.

Key words Cell-penetrating peptides, Multivariate statistics, Artificial neural networks, Support vector machines, Molecular docking, Molecular dynamics

1 Introduction

Cheminformatics and molecular modeling have become an almost inseparable part in studies of complex biomolecular systems and in drug design. Whereas the prediction of cell-penetrating peptides (CPPs) using such rational approach is still in rather early stage, the interest in the application of various computational methods for this purpose is rapidly increasing.

Theoretical models at different levels of abstraction can be applied for the study of complex systems including peptides. The most fundamental level is the ab initio quantum chemistry [1]. Despite tremendous increase in modern computational power, realistic calculations on large molecular complexes of biological significance are still extremely difficult, especially for the applications requiring the use of post-Hartree-Fock theory. Therefore, less fundamental semiempirical methods such as Austin Model 1 (AM1) or Parameterized Model 3 (PM3) employing parameterizations from experimental data and various approximations have been mostly used for these applications.

Another, less fundamental level of theoretical description of complex molecular systems proceeds from molecular mechanics

Ülo Langel (ed.), *Cell-Penetrating Peptides: Methods and Protocols*, Methods in Molecular Biology, vol. 1324,
DOI 10.1007/978-1-4939-2806-4_3,

and molecular dynamics methods [2]. Both methods are based on the potentials reflecting electrostatic and van der Waals forces between the molecules in condensed media. In most cases, these potential functions are obtained by fitting some suitably chosen empirical data. In the case of biomolecular systems involving peptides, these methods can be used as the basis for molecular docking modeling.

The most widespread approach for the computational description of complex molecular systems has been the use of (quantitative) structure-activity/property relationships (QSAR/QSPR). The main objective of the QSPR methodology is to quantify and relate determining factors for a particular measured property with molecular features of a given system or chemical compound. To achieve this purpose, usually a mathematical model that connects experimental property values with a set of features (molecular descriptors) derived from the molecular structures is employed. The QSAR models are developed using multivariate statistical methods or various machine-learning algorithms.

The number of CPP sequences in the literature is continuously increasing. Thus, the possible dataset that can be used to construct predictive models expands. However, the plethora of methods used to measure cellular penetration make a direct comparison between experiment, and hence peptides, difficult. As a consequence most data on the cell penetration of small peptides have binary nature; that is, a given peptide either enters the cell or does not (1 vs. 0).

Depending on the origin and mechanism of action, some methods may be more suitable than others for the description of the particular property of CPPs. It has been noted that most data on the cell penetration of small peptides have binary nature; that is, a given peptide either enters the cell or does not (1 vs. 0). The machine-learning methods such as the artificial neural networks (ANNs) or support vector machines (SVMs) are appropriate for developing the predictive computational models based on such data. The multivariate statistical methods applying the molecular descriptors at different complexity are also applicable for this purpose, giving additionally some insight into the possible mechanism of the cell membrane penetration. Molecular docking and molecular dynamics modeling can be helpful in the elucidation of the detailed mechanism of the interaction between CPPs and membrane but also between a CPP and bound cargo molecule (e.g., a nucleic acid).

Stalmans and colleagues [3] attempted a unifying measure of cell penetration: the CP response. Taking advantage of the fact that the penetratin is often used as positive control in uptake experiments, peptides were normalized, over a wide range of experimental methods and parameters, against this peptide. In cases where penetratin was not included, the positive control CPPs for which

the CP response could be calculated were used to normalize the penetration to penetratin. The authors compared the calculated CP response both with articles giving a numerical value to the uptake and more subjective measures, such as "extremely effective." In both cases the CP response was shown to be predictive of the effectiveness of the cellular penetration.

In the following, a general overview of the computational methods applied for the prediction of the CPPs and their properties is given, together with the reference to the specific applications.

2 Molecular Descriptors in Structure-Activity Models

The predictive power of the quantitative structure-activity relationships depends critically on the quality of the molecular descriptors involved in the mathematical model. The presence of one or another descriptor in the model may also give valuable information about the molecular interactions determining the particular property.

The molecular descriptors can be divided into several classes based on their origin and level of abstraction (Table 1). Some of these are more appropriate than others for the description of relatively large and elongated compounds such as CPPs.

The simplest are the *constitutional descriptors* that represent the chemical composition of a molecule and are independent of molecular connectivity and geometry. They are fragment additive and therefore suited for the description of peptides that consist of distinct fragments, i.e., amino acid residues. The descriptors such as the number of certain chemical groups or particular amino acid residues can be used in simple Free-Wilson type of structure-activity relationships.

The *topological descriptors* or topological indices are graph invariant numbers calculated from a graph representing a molecule [4]. In most cases, the atom and bond types are neglected when the molecular graph is built. The topological indices are calculated either proceeding from the atom-atom connectivity or from topological distances between atom nodes in the graph. While the topological indices suite well for the prediction of the physicochemical parameters of hydrocarbon isomers, the presence of steric effects, polar functional groups, hydrogen bonding, and similar compounds limits the applicability of those molecular descriptors. Peptides contain all these features and therefore the topological indices are less suitable for the prediction of their different properties.

Peptides have multiple charged groups and therefore the *electrostatic descriptors* encoding the charge distribution in the molecules and reflecting Coulomb's interactions between molecules are

Table 1
Exemplary molecular descriptors [4–7]

Class	Descriptor (example)	Notation (formula)
Constitutional	Total number of atoms in the molecule	N_a
	Total number of bonds in the molecule	N_b
	Absolute and relative numbers of atoms of certain chemical identity (C, H, O, N, F, etc.) in the molecule	$N(C)$, $N(O)$, etc.
	Absolute and relative numbers of certain chemical groups and functionalities in the molecule (e.g., $-NH_2$, –OH groups, Arg, Lys residues)	$N(NH_2)$ $N(Arg)$, $N(Lys)$, etc.
	Absolute and relative numbers of single, double, triple, aromatic, or other bonds in the molecule	N_S, N_D, N_{Ar}, etc.
	Total number of rings, number of rings divided by the total number of atoms	N_{ring}
	Molecular weight and average atomic weight in the molecule	MW
Topological	Wiener index	$W = \frac{1}{2}\sum_{(i,j)}^{NSA} d_{ij}$
	Randić's molecular connectivity index	$\chi = \sum_{edges\,ij} \left(D_i D_j\right)^{-1/2}$
	Randić indices of different orders	${}^{m}\chi = \sum_{path} \left(D_i D_j \ldots D_k\right)^{-1/2}$
	Balaban's J index	$J = \frac{q}{\mu + 1} \sum_{edges\,ij} \left(S_i S_j\right)^{-1/2}$
	Kier and Hall valence connectivity indices	${}^{m}\chi^{v} = \sum_{i=1}^{N_s} \prod_{k=1}^{m+1} \left(\frac{1}{\delta_k^v}\right)^{1/2}$
	Kier flexibility index	$f = \left({}^{1}\kappa\, {}^{2}\kappa\right) / \mathrm{NSA}$
	Atom connectivity index	$\mathrm{ABC}(G) = \sum_{u \sim v} \sqrt{\frac{d_u(G) + d_v(G) - 2}{d_u(G)\, d_v(G)}}$

Geometrical	Molecular surface area	$S_{\mathrm{M}} = \sum_i S_{\mathrm{VW}}^{(i)} - S_{\mathrm{ov}}$
	Solvent-accessible molecular surface area	$S_{\mathrm{SA}} = A_+ + A_{\mathrm{s}} + A_-$
	Molecular volume	$V_{\mathrm{M}} = \sum_i V_{\mathrm{VW}}^{(i)} - V_{\mathrm{ov}}$
	Solvent-excluded molecular volume	$V_{\mathrm{mol(SE)}} = V_{\mathrm{p}} + \sum V_+ + \sum V_{\mathrm{s}} + \sum V_- + V_{\mathrm{ac}} + V_{\mathrm{nc}}$
	Gravitational index	$G_{\mathrm{p}} = \sum_{i<j}^{N_{\mathrm{a}}} \frac{m_i m_j}{r_{ij}^2}$
	Principal moments of inertia of a molecule	$I_k = \sum_i m_i r_{ik}^2$
	Shadow areas of a molecule	$S_k = \frac{1}{2} \cdot \oint_{(\mathrm{C})} (v\,\mathrm{d}\rho - \rho\,\mathrm{d}v)$

(continued)

Table 1
(continued)

Class	Descriptor (example)	Notation (formula)
Electrostatic	Mulliken atomic partial charges	$Q_{\mathrm{A}} = Z_{\mathrm{A}} - \sum_{k,l} P_{kl}$
	Minimum (most negative) and maximum (most positive) atomic partial charges	$Q_{\min} = \min(Q^{-})$ $Q_{\max} = \max(Q^{+})$
	Polarity parameters	$P' = \frac{Q_{\max} - Q_{\min}}{R_{mm}}$
	Dipole moment	$\mu = -\sum_{i=1}^{occ} \int_{(V)} \phi_i \check{r} \phi_i \mathrm{d}v + \sum_{a=1}^{M} Z_a \vec{R}_a$
	Molecular polarizability	$\mu' = \mu + \alpha \boldsymbol{E}$
	Molecular hyperpolarizability	$\mu' = \mu + \alpha \boldsymbol{E} + \frac{1}{2} \beta \boldsymbol{E}^2 + \cdots$
	Partial positively charged surface area	$\mathrm{PPSA1} = \sum_{A} S_A$ $A \in \{\delta_A > 0\}$
	Partial negatively charged surface area	$\mathrm{PNSA1} = \sum_{A} S_A$ $A \in \{\delta_A < 0\}$
	Difference between partial positively and negatively charged surface areas	$\mathrm{DPSA1} = \mathrm{PPSA1} - \mathrm{PNSA1}$
	Hydrogen bonding donor ability of the molecule	$\mathrm{HDSA1} = \sum_{D} S_D$ $D \in H_{\mathrm{H\ donor}}$
	Hydrogen bonding acceptor ability of the molecule	$\mathrm{HASA1} = \sum_{A} S_A$ $A \in H_{\mathrm{H\ acceptor}}$

Molecular orbital	Highest occupied molecular orbital (HOMO) energy	$\varepsilon_{\mathrm{HOMO}} = \phi_{\mathrm{HOMO}} \lvert \hat{\mathbf{F}} \rvert \phi_{\mathrm{HOMO}}$
	Lowest unoccupied molecular orbital (LUMO) energy	$\varepsilon_{\mathrm{LUMO}} = \phi_{\mathrm{LUMO}} \lvert \hat{\mathbf{F}} \rvert \phi_{\mathrm{LUMO}}$
	HOMO-LUMO gap	$\varepsilon_{\mathrm{HOMO}} - \varepsilon_{\mathrm{LUMO}}$
	Fukui atomic nucleophilic reactivity index	$N_A = \sum_{i \in A} c_{i\mathrm{HOMO}}^2 / \left(1 - \varepsilon_{\mathrm{HOMO}}\right)$
	Fukui atomic electrophilic reactivity index	$E_A = \sum_{j \in A} c_{j\mathrm{LUMO}}^2 / \left(\varepsilon_{\mathrm{LUMO}} + 10\right)$
	Fukui atomic one-electron reactivity index	$R_A = \sum_{i \in A} \sum_{j \in A} \frac{c_{i\mathrm{HOMO}} c_{j\mathrm{LUMO}}}{\varepsilon_{\mathrm{LUMO}} - \varepsilon_{\mathrm{HOMO}}}$
	Mulliken bond orders	$P_{AB} = \sum_{i=1}^{\mathrm{occ}} \sum_{\mu \in A} \sum_{\nu \in B} n_i c_{i\mu} c_{i\nu}$
	Free valence	$V_{fi} = V_{\max} - P_A$
Quantum chemical	Total energy of the molecule	$E_{\mathrm{tot}} = E_{\mathrm{el}} + \sum_{A \neq B} \frac{Z_A Z_B}{R_{AB}}$
	Total electronic energy of the molecule	$E_{\mathrm{el}} = 2\mathrm{Tr}(\mathbf{RF}) - \mathrm{Tr}(\mathbf{RG})$
	Standard heat of formation	$H_f^0 = H_f - \sum_a H_f^a$
	Electron–electron repulsion energy for a given atomic species	$E_{\mathrm{ee}}(A) = \sum_{B \neq A} \sum_{\mu,\nu \in A} \sum_{\lambda,\sigma \in B} P_{\mu\nu} P_{\lambda\sigma} \langle \mu\nu \lvert \lambda\sigma \rangle$
	Nuclear-electron attraction energy for a given atomic species	$E_{\mathrm{ne}}(AB) = \sum_B \sum_{\mu,\nu \in A} P_{\mu\nu} \left\langle \mu \lvert \frac{Z_B}{R_{iB}} \rvert \nu \right\rangle$

(continued)

Table 1
(continued)

Class	Descriptor (example)	Notation (formula)
Thermodynamic	Vibrational enthalpy of the molecule	$H_{\text{vib}} = \frac{1}{2}\sum_{j=1}^{a} h\nu_j + \frac{h\nu_j \exp\left(-h\nu_j / 2kT\right)}{1-\exp\left(-h\nu_j / 2kT\right)}$
	Translational enthalpy of the molecule	$H_{\text{tr}} = \int_{-\infty}^{\infty} \frac{p^2}{2m} e^{\frac{p^2}{2mkT}} \mathrm{d}p$
	Vibrational entropy of the molecule	$S_{\text{vib}} = \sum_{j=1}^{\alpha} \left\{ \frac{h\nu_j \exp\left(-h\nu_j / 2kT\right)}{kT\left[1-\exp\left(-h\nu_j / 2kT\right)\right]} - \ln\left[1-\exp\left(-h\nu_j / 2kT\right)\right] \right\}$
	Rotational entropy of the molecule	$S_{\text{rot}} = Nk \ln\left[\frac{\pi^{1/2}}{\sigma} \prod_{j=1}^{3} \left(\frac{8\pi^2 I_j kT}{h^2} \right)^{1/2} \right]$

more fitting for the development of structure-activity relationships [5]. The charge distribution in the molecules can be calculated directly from the quantum-chemical wavefunction of the molecule or proceeding from various semiempirical schemes based on the electronegativity of the atoms involved. The charge partitioning schemes of molecular systems can be divided into three groups: (1) wave function-based methods (Mulliken population analysis, natural population analysis); (2) molecular electrostatic potential fitting-based methods (such as the CHELPG and Merz-Singh-Kollman scheme); and (3) electron density-based methods (such as AIM).

A large class of the molecular descriptors can be derived from the results of the quantum-mechanical calculations [6, 7]. The typical *molecular orbital related descriptors* are energies of the HOMO (highest occupied molecular orbital) and LUMO (lowest unoccupied molecular orbital). These orbitals play a major role in governing many chemical reactions, determining electronic band gaps in solids and intermolecular interactions, particularly those related to the charge transfer. The HOMO-LUMO gap, i.e., the difference in energy between the HOMO and LUMO, is an important molecular stability index. In the case of CPPs, these descriptors may be important in describing the complex formation between a CPP and the cargo molecule but also its interactions with the cell membrane. The same is valid for more sophisticated Fukui reactivity indices.

The further important *quantum-chemical descriptors* are related to the calculated energies of molecules. In addition to the total molecular energy, electronic energy, and heat of formation, it is possible to derive energy components corresponding to different Coulombic and exchange energy contributions.

Peptides are constructed from a rather limited set of molecular fragments—amino acids. Therefore, specific descriptors have been proposed for the amino acids, i.e., the so-called *z-scales*. Hellberg et al. [8] have described the variation in amino acid sequence within sets of peptides by three principal properties, $z1$, $z2$, and $z3$, per varied amino acid position. These principal properties were derived from a principal component analysis of a matrix of 29 physicochemical variables for the 20 amino acids coded in mRNA. These scores were interpreted to represent hydrophilicity, side chain bulk/molecular size, and electronic properties of amino acid residues, respectively. The *z*-scales were further developed and refined by Sandberg et al. [9] for a set 87 amino acids. Altogether 26 physicochemical descriptor variables were used for each amino acid in the respective principal component analysis. These descriptor variables included experimentally determined retention values in seven thin-layer chromatography (TLC) systems, three nuclear magnetic resonance (NMR) shift variables, and 16 calculated variables, namely six semiempirical molecular orbital indices, total,

polar, and nonpolar surface area, van der Waals volume of the side chain, log *P*, molecular weight, four indicator variables describing hydrogen bond donor and acceptor properties, and side chain charge. The *z*-scales have been used for the QSAR modeling of various properties of peptides, including angiotensin-I-converting enzyme inhibitory dipeptides [10], bradykinin-potentiating pentapeptides, and cationic antimicrobial pentadecapeptides [11], for the analysis of drug receptor interactions and in design of new ligands [12, 13] and for the elucidation of antibodies' recognition of peptide antigens [14].

The *z*-scales have been effectively used also for the prediction of CPPs. Using the Sandberg's expanded *z*-scales, Hällbrink et al. [15] created an algorithm to predict CPPs in proteins or random peptide sequences. Bulk property values ($z\Sigma/n$) were assembled for the training set of 24 published cell-penetrating peptides and 17 non-penetrating analogues, and averaged over the total number of amino acids in the sequence. The most relevant descriptors for CPP prediction appeared to be $z1$, $z2$, and $z3$, describing lipophilicity, steric bulk, and polarity, respectively. It was also found that the bulk of the amino acid side chain, calculated as the number of heavy atoms (C, N, S, and O) in the side chain of the amino acid, together with net donated hydrogen bonds of the side chain, calculated as the accepted hydrogen bonds of the side chains subtracted from the donated hydrogen bonds, was necessary in order to predict CPPs. The average CPP prediction efficiency with *z*-scales was 68 %.

A structural topology scale (STscale) has been developed as a novel structural topological descriptor derived from principal component analysis on 827 structural variables of 167 amino acids [16]. By using partial least squares (PLS), the ST scale was applied for the study of quantitative sequence-activity models on three peptide datasets (58 angiotensin-converting enzyme (ACE) inhibitors, 34 antimicrobial peptides (AMPs), and 89 elastase substrates (ES)), with the improved results as compared to the earlier studies.

Mauri et al. [17] have proposed another special scale for the amino acids, based on traditional constitutional and topological 2D autocorrelation molecular descriptors. Instead of atomic representation, the amino acid residues were taken as the structural units and descriptors were calculated by applying two different kinds of weights (the first based on physicochemical properties of the amino acids, the second based on WHIM descriptors [4]). The prediction of two biological responses, i.e., the activated partial thromboplastin time (APTT) and thromboplastin time (TBPL) on a dataset of 20 peptide sequences using these descriptors, was successful.

van Westen et al. have recently carried out benchmarking on 13 different peptide descriptor scales, developed analogously to

z-scales for each amino acid [18, 19]. The comparison was of how similar or differently the available amino acid descriptor sets behave when converting structure to property space. The results obtained are expected to help researchers to select suitable amino acid descriptor sets for structure-activity analyses, e.g., those showing complementary behavior.

However, no attempt has been taken to predict the CPPs using these above-given descriptor sets.

Arguably the simplest method of CPP prediction, selecting peptides based on high arginine content, is nevertheless highly successful. Gautam and colleagues [20] selected protein-derived peptides which contain 8 or 9 Arg, in a 15-mer. The selection was further refined by removing sequences that contain negatively charged amino acids. From the candidates eight were selected and tested and seven performed equal to or better than the positive control, tat (48–60). Futaki and colleagues [21] tested ten arginine-rich peptides derived from RNA-binding domain of proteins. Nine of the sequences were considered to display CPP activity. Moreover, the internalization efficiency was dependent on the number of Arg in the sequence. Thus it appears possible to predict an arginine-rich CPP sequence with an at least 80 % probability using pen and paper.

For the target sequence ascertain that:

Number of aa <25

Number of Arg >6

Number of Arg/number of aa >0.5

It is a practical method for finding CPPs of this subset. However, most confirmed CPPs fall outside these structural constraints.

3 Multivariate Regression Methods

The most common and historically first mathematical QSAR models are developed as multiple linear relationships (MLR) between the experimental property of the interest and the molecular descriptors. Multiple linear regression is applied to determine the regression coefficients in MLR for each independent variable, i.e., molecular descriptor involved in the model. The regression coefficients are determined under condition that the sum of the squares of the errors between the original and predicted property values is minimized. Thus, the general multiple linear equation can be written in the following form as in Eq. 1:

$$y = b_0 + b_1 x_1 + b_2 x_2 + \cdots + b_p x_p \qquad (1)$$

where y is the property to be modeled; x_1, x_2, …, and x_p represent the independent variables (molecular descriptors); b_1, b_2, …, and b_p are the regression coefficients; and b_0 is the intercept. Stepwise regression routines are aimed to identify the "best" set of x variables, i.e., the set of given (minimum) variables, which explains the greater part of the data variance. The squared correlation coefficients, R^2; squared cross-validated correlation coefficients, R^2_{cv}; Fisher criterion value, F; and standard deviation, s, are used to describe the statistical quality of the regression model. A QSPR study starts routinely with a large number of molecular descriptors. The search for the best MLR model in such a large descriptor space is therefore not a trivial task. The number of all possible combinations of descriptors increases dramatically with the increase of descriptor scales in the model, making the "brute force" search for the best model computationally expensive. Therefore, various regression techniques coupled with variable selection procedures have been proposed for the selection of the "best set" of regression predictors, such as backward elimination, forward selection, and ridge regression. The best multilinear regression (BMLR) method has been implemented to find the "best" regression in a short computational time in a descriptor space of thousands of variables [22]. This method is based on the starting selection of the orthogonal descriptor pairs and further extension of the correlation with the addition of new descriptors improving the statistical parameters of the model. A cutoff value determining the improvement of R^2 is used to limit the number of descriptors entering the equation. It is important to take into account that the number of descriptors in the equation should not exceed certain limits because it could lead to an overfitted model. This problem can be controlled by exploring the improvement of R^2 or R^2_{cv} as a function of the number of descriptors in the model. Typically, a break point in this dependence determines the "optimum" number of the descriptors in the model. When the number of possible independent variables (descriptors) considered becomes very large, it may become possible that a correlation with the property under investigation will occur purely by chance. The possibility of chance correlations can be minimized so as to be negligible by using appropriate procedures. For instance, the collinearity of natural descriptor scales needs to be strictly controlled during the forward selection processing. The criteria used in the BMLR procedure have been proven to be sufficient for the elimination of chance correlations due to the non-orthogonality of the scales.

The multiple linear QSAR approach has been used for the prediction of the properties of CPPs. Robust QSAR models ($R^2 \approx 0.94$) including in each case just two descriptors were obtained for a relatively small set of CPPs [23]. The first of these descriptors, the number of N atoms, can be related just to the length of the peptide and the relative number of amino side groups

in peptide. The second descriptor reflecting the partial surface charge is directly related to the electrostatic interactions adjacent to the cellular uptake.

4 Machine-Learning Methods for Predicting the Properties of CPPs

The binary nature of the data on cell-penetrating peptides makes them particularly convenient for the structure-activity model building using machine-learning methods. The ANNs [24] and SVMs [20] have been used most for the CPP model building.

Various types of ANNs have been used to develop structure-activity relationships, including multilayer perceptron (MLP), Kohonen self-organizing maps (Kohonen SOMs), Bayesian probabilistic, radial basis function (RBF) networks, and entropy machines [25]. Those ANNs differ by their ideology and topology. Notably, in contrast to multiple linear statistics, ANNs are capable of recognizing highly nonlinear relationships. The CPPs have been modeled by using neural networks based on the back-propagation MLP learning algorithm, RBF, or Bayesian regularized networks.

An ANN is formed from artificial neurons or processing elements, connected with weight coefficients, which constitute the neural structure and are organized in layers. A typical example for three-layered MLP ANN with feed-forward learning is shown in Fig. 1. The first layer is usually termed as the input layer. In structure-activity modeling, this layer consists of molecular descriptors (so-called predictors of the network). The last layer of an ANN is the output layer in which the neurons are directly connected to

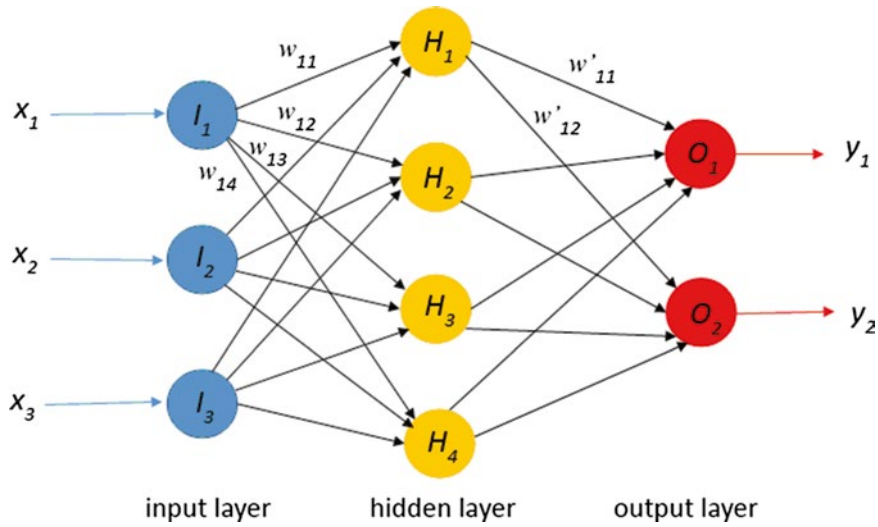

Fig. 1 A typical [3-4-2] multilayer perceptron ANN with feed-forward learning

the activity being predicted. The layers of neurons between the input and output layers are called hidden layers and their number can be varied depending on size and structure of the data. To each of the hidden and output neurons, one virtual neuron can be assigned called bias used as reference to activate or deactivate a neuron. Associated with each node is an internal state or activation function designated by I_i, H_h, and O_m functions for the input, hidden, and output layers, respectively. The net input to a neuron in hidden layer can be expressed as the weighted sum of the input activation functions (Eq. 2):

$$f_h = \sum_{i=1}^{n} w_{ih} I_i \tag{2}$$

where w_{ih} denote the weights between the two neurons from the input layer and hidden layer. Analogously, the net input from the hidden layer to an output neuron is given as follows (Eq. 3):

$$f_m = \sum_{h=1}^{N} w'_{hm} H_h \tag{3}$$

where w'_{ih} are the weights between the two neurons from the hidden and output layers. In the case of MLP neural networks, the output activation functions are commonly calculated using the sigmoid transformation as follows (Eq. 4):

$$H_i \text{ or } O_i = \frac{1}{1 - e^{-f_i}} \tag{4}$$

The network training is an iterative process where the information is fed back from the output neurons to neurons in hidden layers up to input layer in order to adjust the weights on the connections, w_{ij} and w'_{ij}. The initial values of the weights can be chosen randomly within interval [0,1] or determined from some independent considerations.

The feedback from the output layer to hidden layer or to input layer is usually the error in the output (Eq. 5), modified appropriately according to some useful paradigm:

$$E = \sum_p E_p + \frac{1}{2} \sum_p \sum_m \left(a_{pm} - O_{pm} \right)^2 \tag{5}$$

where E_p is the error of the pth training pattern, defined as the set of descriptors and activity corresponding to the pth data points, or chemical compounds, and a_{pm} corresponds to the experimentally measured value of the mth dependent variable. The process of feedback continues through the subsequent cycles of operation of the neural network and ceases when the training is completed. One of the standard algorithms for minimizing E is the delta rule introduced by Rumelhart which is based on an iterative procedure for

updating the weights of the neural network from their initially assigned random values.

Radial basis function (RBF) networks are similar to MLP networks, with the difference in the way how hidden units combine values coming from preceding layers in the network. Instead of sigmoid functions, an RBF network uses Gaussian activation function in the case of hidden layer neurons (Eq. 6):

$$H_i = \exp\left[\frac{1}{2\sigma^2} f_i - m_i^2\right] \tag{6}$$

where m_i and σ are the center and the width of the Gaussian function, respectively. The output layer is linear, supplying the response of the network to the activation pattern of the input layer. An advantage of the RBFs is that they can be trained faster than the MLPs in most of the cases. Bayesian regularized artificial neural networks (BRANNs) are another type of neural networks that make use of Bayesian probability.

Dobchev et al. [26] have developed an MLP neural network with two hidden layers (a 6-4-3-1 network) to predict the cell-penetrating peptides. Using the principal component analysis, six traditional descriptors referring to the whole molecule were chosen as the input to the network. These descriptors characterize the size of the peptide (molecular weight), its topology (Schultz average vertex), charge distribution and electrostatic interactions (differences in charged partial surface areas, topographic electronic index for all bonds), and hydrogen bonding ability (hydrogen acceptor-dependent charged surface area). The dataset was divided into training and validation sets of 71 and 30 data points, respectively. The first training of ANN showed 83 % accuracy of the model for the total data. This accuracy was further improved by removing the inaccurate predictions and rebuilding a new ANN model again based on new PCA descriptors. After training the ANN model, an excellent classification was obtained with almost 100 % correct prediction for all the CPPs except only one mispredicted.

Holton et al. [27] have introduced a web server called CPPpred [28] for the prediction of CPPs using an N-to-1 neural network. The server takes one or more peptide sequences, between 5 and 30 amino acids in length, as input and returns a prediction of how likely each peptide is to be cell penetrating. CPPpred was developed with redundancy-reduced training and test sets, giving to the ANNs developed higher stability. The reduced training set for CPPred included 74 CPPs and 30 non-CPPs. The test set consisted of 47 CPPs of 5–30 amino acids in length, labeled as having either “Greater,” “High,” or “Higher” uptake efficiency according to the classification of CPPsite and 47 randomly selected bioactive peptides. The CPPpred algorithm correctly predicted 17 of the 29 CPPs and 27 of the 29 non-CPPs.

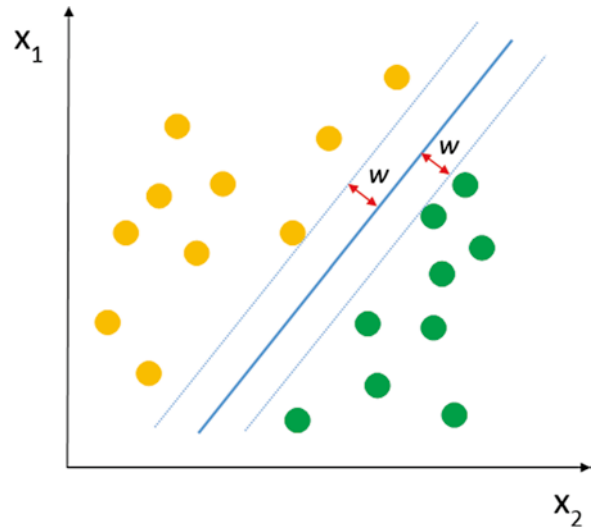

Fig. 2 The simplest case of the division of the data (*yellow* and *green*) into two groups in two-dimensional (x_1;x_2) space. A support vector machine is trained to maximize the distance 2*w* between two groups

Likewise to the ANN, SVMs [29] are particularly suitable for building the predictive models on binary data. SVM carries out a classification of data by constructing an *n*-dimensional hyper plane that optimally separates the data into two categories. SVM minimizes the empirical classification error and the respective geometric margin; that is, the distance between the hyper plane and the data from each group is maximized (cf. Fig. 2).

Sanders et al. have used SVMs for the classification of peptides as cell penetrating and non-penetrating [30]. Starting from 111 known CPPs and 34 known non-penetrating peptides from the literature and commercial vendors, several approaches were examined to build training datasets for the classifiers. Features were calculated from the datasets using a set of basic biochemical properties combined with features from the literature determined to be relevant in the prediction of CPPs. Those included the length of the peptide, net charge, hydrophobicity and lipophilicity, number of donated hydrogen bonds, and others, altogether 23 characteristic properties of peptides. A particular attention was given to the balance of the training sets of data. The SVM was trained using a sequential minimal optimization (SMO) algorithm in conjunction with the Pearson VII universal kernel [31]. The SVM classifications were validated by the synthesis and testing of a subset of peptides classified as either penetrating or non-penetrating. Of the synthesized peptides predicted to be CPPs, 100 % of these peptides were shown to be penetrating.

Gautam et al. [20] have also developed SVM models for predicting and designing highly cell-penetrating peptides. Various

features such as amino acid composition, dipeptide composition, binary profile of patterns, and physicochemical properties were used as input features. The main dataset used consisted of 708 peptides in total. In addition, various motifs in cell-penetrating peptides were identified, and used for developing a hybrid prediction model. On the basis of the obtained results, it was claimed that the discrimination of cell-penetrating peptides from non-cell-penetrating peptides was possible based only on amino acid composition. A maximum accuracy of 97.40 % was achieved using the hybrid model that combines motif information and binary profile of the peptides. On independent dataset, the maximum accuracy was 81.31 % with MCC of 0.63.

5 Molecular Modeling Approaches

A class of cell-penetrating peptides are active through their internalization by certain receptors. These include such receptor types as chemokine receptors, syndecans, neuropilins, the family of integrins, homing sequences, and the positively charged scavenger receptors [32].

When the 3D crystal structure of the receptor is known, the automated docking of peptides to these macromolecular targets can be useful for the elucidation of the cell-penetrating process as well as for the prediction of new CPPs. A variety of software are available both freely [33] and commercially [34] to carry out the docking calculations using different intermolecular force fields and docking algorithms.

Baumgärtner et al. [35] found that the cellular internalization of the serpin protein C inhibitor (PCI) is supported by plasma membrane PE, which enables its rapid targeting to the nucleus both in vitro and in vivo. Therefore, PCI was considered as an excellent candidate for the nuclear supply of cargo. As the crystallographic structure of PCI was known, the molecular docking was carried out to characterize the structural components of PCI enabling its distinctive interaction with phospholipids. Extensive blind molecular docking (over 25 million calculations) enabled to reveal the details of the binding site that could be useful for the prediction of CPPs employing the same internalization mechanism.

In another work [36], the internalization mechanism of a peptide derived from the TIRAP (toll-interleukin 1 receptor (TIR) domain containing adaptor protein), called pepTIRAP, and peptide pepTIRAPALA, where some of its cationic amino acids were changed to alanine, has been modeled in order to identify the effect of changes in electrostatic potential on peptide internalization. The modeling experiments indicated that the replacement of cationic amino acids with alanine resulted in a decrease in the

positive electrostatic potential in the peptide. The docking calculations also confirmed that interactions between pepTIRAP and negatively charged molecules on the cellular surface, such as heparan sulfate, are stronger than the ones exhibited by pepTIRAPALA. Therefore, it was suggested that mostly the electrostatic interactions between the peptide and molecules on the membrane are triggering the peptide internalization.

Molecular docking has also been used to examine the binding affinity of a series of cell-penetrating peptides with silencing RNAs (siRNAs) in order to predict the ability of peptides to bind and deliver the cargo nucleic acid into the cell [37]. The new ranking of the peptides based on docking was consistent with their experimentally determined efficiency to bind and deliver the siRNA into the cell. The stability and binding affinity of peptide-siRNA complexes were related to the side chains and modifications of the CPPs, with the stearyl and quinoline groups improving affinity and stability. The reranking of the peptides docked to siRNA, together with explicit water molecular dynamics simulations, gives a solid basis for the description and prediction of the interaction of CPPs with siRNA.

Molecular dynamics simulation consists of the numerical, step-by-step, solution of the classical equations of motion, which for a simple atomic system may be written (Eq. 7) as follows [38]:

$$m_i \ddot{r}_i = f_i \qquad f_i = \frac{\partial}{\mathrm{d}r_i} \tag{7}$$

where m_i denote the atomic masses and $r^N = (r_1, r_2, \ldots, r_N)$ represents the complete set of 3N atomic coordinates. The forces fi acting on the atoms are usually derived from a potential energy $U(r^N)$ that depends on the atomic coordinates. The differential equations (Eq. 7) are solved numerically to get the trajectory of the system in time. The potential energy for non-bonded interactions consists of usually a sum of a Lennard-Jones-type potential and Coulombic potential describing the interaction between the charges on atoms in molecules. Special potentials are also used for the description of intramolecular bonding interactions in molecules. The most common force fields used in the modeling of large biomolecular systems are AMBER [39], CHARMM [40], and OPLS [41]. Apart from the dynamics of the system in time, the molecular dynamics simulations may be used to determine macroscopic thermodynamic properties of the system as the time averages of an ergodic system correspond to microcanonical ensemble averages.

The molecular dynamics simulations could be very informative for predicting CPPs, provided that the molecular structure of the biological counterpart (receptor, membrane) enabling the internalization of the peptide is known. The lack of such information

has restricted, however, the use of molecular dynamics for CPP modeling. However, recently several charged cationic CPPs have been studied using the molecular dynamics simulations. Proceeding from the assumption that the internalization of nonaarginine peptide (Arg9) is a purely diffusive process [42] the underlying free energetics of the translocation of a nonaarginine peptide (Arg9) into a model DPPC bilayer was studied using the molecular dynamics approach [43]. The umbrella sampling molecular dynamics simulations were carried out with coarse-grained Martini lipids, polarizable coarse-grained water, and peptide. Significant barriers for Arg9 translocation from bulk aqueous solution to bilayer center were observed and discussed.

In another study [44], translocation of short, charged cationic oligo-arginine peptides (mono-, di-, and triarginine) from bulk aqueous solution into model DMPC bilayers was again studied using molecular dynamics simulations. The results demonstrate close similarity in the structure of the ensemble of configurations generated using the all-atom and coarse-grain force fields. Both resolutions show that oligo-arginine peptides adopt preferential orientations as they translocate into the bilayer.

References

1. Levine IN (2008) Quantum chemistry, 6th edn. Prentice Hall, New York, NY
2. Sabin JR, Brändas E (2010) Combining quantum mechanics and molecular mechanics. Some recent progresses in QM/MM methods. Adv Quant Chem 59:1–416
3. Stalmans S, Wynendaele E, Bracke N et al (2013) Chemical-functional diversity in cell-penetrating peptides. PLoS One 8:e71752
4. Todeschini R, Consonni V (2000) Molecular descriptors for chemoinformatics, 2 vols. Wiley-VCH, New York, NY
5. Karelson M (2000) Molecular descriptors in QSAR/QSPR. J. Wiley & Sons, New York, NY
6. Karelson M, Lobanov VS, Katritzky AR (1996) Quantum-chemical descriptors in QSAR/QSPR studies. Chem Rev 9:1027–1043
7. Karelson M (2004) Quantum-chemical descriptors in QSAR. In: Bultinck P et al (eds) Computational medicinal chemistry and drug discovery. Dekker Inc., New York, NY, pp 641–668
8. Hellberg S, Sjöström M, Skagerberg B et al (1987) Peptide quantitative structure-activity relationships, a multivariate approach. J Med Chem 30:1126–1135
9. Sandberg M, Eriksson L, Jonsson J et al (1998) New chemical descriptors relevant for the design of biologically active peptides. A multivariate characterization of 87 amino acids. J Med Chem 41:2481–2491
10. He R, Ma H, Zhao W et al (2012) Modeling the QSAR of ACE-inhibitory peptides with ANN and its applied illustration. Int J Pept 2012:620609
11. Zhou P, Chen X, Wu Y et al (2010) Gaussian process: an alternative approach for QSAM modeling of peptides. Amino Acids 38: 199–212
12. Prusis P, Lundstedt T, Wikberg JE (2002) Proteo-chemometrics analysis of MSH peptide binding to melanocortin receptors. Protein Eng 15:305–311
13. Prusis P, Uhlén S, Petrovska R et al (2006) Prediction of indirect interactions in proteins. BMC Bioinform 22:167
14. Mandrika I, Prusis P, Yahorava S et al (2007) Proteochemometric modelling of antibody-antigen interactions using SPOT synthesised peptide arrays. Protein Eng Des Select 20: 301–307
15. Hällbrink M, Kilk K, Elmquist A et al (2005) Prediction of cell-penetrating peptides. Int J Pept Res Ther 11:249–259
16. Yang L, Shu M, Ma K et al (2010) ST-scale as a novel amino acid descriptor and its application in QSAM of peptides and analogues. Amino Acids 38:805–816

17. Mauri A, Ballabio D, Consonni V et al (2008) Peptides multivariate characterisation using a molecular descriptor based approach. MATCH Commun Math Comput Chem 60:671–690
18. van Westen GJP, Swier RF, Wegner JK et al (2013) Benchmarking of protein descriptor sets in proteochemometric modeling (part 1): comparative study of 13 amino acid descriptor sets. J Cheminform 5:41
19. van Westen GJP, Swier RF, Cortes-Ciriano I et al (2013) Benchmarking of protein descriptor sets in proteochemometric modeling (part 2): modeling performance of 13 amino acid descriptor sets. J Cheminform 5:42
20. Gautam A, Chaudhary K, Kumar R et al (2013) Open source drug discovery consortium and *in silico* approaches for designing highly effective cell penetrating peptides. J Transl Med 11:74
21. Futaki S (2006) Oligoarginine vectors for intracellular delivery: design and cellular-uptake mechanisms. Biopolymers 84:241–249
22. Katritzky AR, Mu L, Lobanov VS, Karelson M (1996) Correlation of boiling points with molecular structure. 1. A training set of 298 diverse organics and a test set of 9 simple inorganics. J Phys Chem 100:10400–10407
23. Regberg J, Srimanee A, Erlandsson M et al (2014) Rational design of a series of novel amphipathic cell-penetrating peptides. Int J Pharm 464:111–116
24. Dobchev DA, Karelson M (2011) Using artificial neural networks to predict cell-penetrating compounds. Exp Opin Drug Discov 6: 783–796
25. Dobchev DA, Pillai GG, Karelson M (2014) In silico machine learning methods in drug development. Curr Top Med Chem 14:1913–1922
26. Dobchev DA, Mäger I, Tulp I et al (2010) Prediction of cell-penetrating peptides using artificial neural networks. Curr Comput Aid Drug Des 6:79–89
27. Holton TA, Pollastri G, Shields DC et al (2013) CPPpred: prediction of cell penetrating peptides. Bioinformatics 29:3094–3096
28. http://bioware.ucd.ie/cpppred
29. Vapnik V (1992) Principles of risk minimization for learning theory. In: Moody JE, Hanson SJ, Lippmann RP (eds) Advances in neural information processing systems, vol 4. Morgan Kaufmann, Burlington, MA
30. Sanders WS, Johnston CI, Bridges SM et al (2011) Prediction of cell penetrating peptides by support vector machines. PLoS Comput Biol 7:e1002101
31. Ustun B, Melssen W, Buydens L (2005) Facilitating the application of support vector regression by using a universal Pearson VII function based kernel. Chemom Intell Lab Syst 81:29–40
32. Reissmann S (2014) Cell penetration: scope and limitations by the application of cell-penetrating peptides. J Pept Sci 20:760–784
33. AutoDock4.2.6, The Scripps Institute, 2014.
34. (2014) Small-Molecule Drug Discovery Suite 2014-4: Glide, version 6.5, New York, NY: Schrödinger, LLC
35. Baumgärtner P, Geiger M, Zieseniss S et al (2007) Phosphatidylethanolamine critically supports internalization of cell-penetrating protein C inhibitor. J Cell Biol 179:793–804
36. Flores KA, Salgado JC, Zapata-Torres G et al (2012) Effect of the electrostatic potential on the internalization mechanism of cell penetrating peptides derived from TIRAP. Biotech Bioproc Eng 17:485–499
37. García-Sosa AT, Tulp I, Langel K, Langel Ü (2014) Peptide-ligand binding modeling of siRNA with cell-penetrating peptides. BioMed Res Int 2014:257040
38. Allen MP (2004) Introduction to molecular dynamics simulation. NIC Ser 23:1–28
39. Cornell WD, Cieplak P, Bayly CI et al (1995) A second generation force field for the simulation of proteins, nucleic acids, and organic molecules. J Am Chem Soc 117:5179–5197
40. MacKerell AD Jr, Feig M, Brooks CL III (2004) Extending the treatment of backbone energetics in protein force fields: limitations of gas-phase quantum mechanics in reproducing protein conformational distributions in molecular dynamics simulations. J Comput Chem 25:1400–1415
41. Jorgensen WL, Maxwell DS, Tirado-Rives J (1996) Development and testing of the OPLS all-atom force field on conformational energetics and properties of organic liquids. J Am Chem Soc 118:11225–11236
42. Säälik P, Niinep A, Pae J et al (2011) Penetration without cells: membrane translocation of cell-penetrating peptides in the model giant plasma membrane vesicles. J Control Rel 153:117–125
43. Hu Y, Liu X, Sinha SK, Sandeep P (2014) Translocation thermodynamics of linear and cyclic nonaarginine into model DPPC bilayer via coarse-grained molecular dynamics simulation: implications of pore formation and non-additivity. J Phys Chem B 118:2670–2682
44. Hu Y, Sinha SK, Sandeep P (2014) Reconciling structural and thermodynamic predictions using all-atom and coarse-grain force fields: the case of charged oligo-arginine translocation into DMPC bilayers. J Phys Chem B 118:11973–11992

Chapter 4

Computer-Aided Virtual Screening and Designing of Cell-Penetrating Peptides

Ankur Gautam, Kumardeep Chaudhary, Rahul Kumar, and Gajendra Pal Singh Raghava

Abstract

Cell-penetrating peptides (CPPs) have proven their potential as versatile drug delivery vehicles. Last decade has witnessed an unprecedented growth in CPP-based research, demonstrating the potential of CPPs as therapeutic candidates. In the past, many in silico algorithms have been developed for the prediction and screening of CPPs, which expedites the CPP-based research. In silico screening/prediction of CPPs followed by experimental validation seems to be a reliable, less time-consuming, and cost-effective approach. This chapter describes the prediction, screening, and designing of novel efficient CPPs using "CellPPD," an in silico tool.

Key words Cell-penetrating peptides, Drug delivery system, Machine learning approach, Virtual screening, Support vector machine, Prediction

1 Introduction

Therapeutic peptides have emerged as a very promising area of modern research. Previously, peptides were not considered as ideal therapeutic molecules, though the therapeutic peptide market emerged almost 40 years back in 1974, when Novartis launched the first therapeutic peptide-based drug, Lypressin, a vasopressin analog. In the last decade, a number of peptide databases [1–7] have been developed suggesting a restoration of interest in therapeutic peptides as potential drug candidates [8–10]. In this context, cell-penetrating peptides (CPPs) have attracted a significant scientific attention [11]. An increasing number of patents and research articles pertaining to CPPs have demonstrated how popular CPPs are as therapeutic peptides.

CPPs are small peptides (<50 amino acids) and have an inherent ability to penetrate a variety of cells [12]. In addition, CPPs are capable of transporting different types of cargoes like small molecules, nanoparticles, peptides, proteins, and nucleic acids and

Ülo Langel (ed.), *Cell-Penetrating Peptides: Methods and Protocols*, Methods in Molecular Biology, vol. 1324,
DOI 10.1007/978-1-4939-2806-4_4,

thus are being used widely in various drug delivery applications [13]. Since their inception in 1988, several hundreds of novel CPPs and their derivatives have been identified so far [14]. However, rational designing and identification of novel highly efficient CPPs is still a very challenging task.

In general, in the wet lab, identification of novel CPPs by high-throughput screening of modified analogs of existing CPPs is a time-consuming and labor-intensive approach. On the other hand, in silico screening/prediction of modified CPPs followed by experimental validation (integrative approach) is a more reliable approach, which has higher success rate, as compared to the traditional wet lab approach. In the past, substantial efforts have been made to develop in silico methods for the prediction of CPPs [15–19]. In 2005, Hallbrink et al. developed the first in silico prediction method. Since then, seven prediction methods have been developed (Fig. 1), but most of these methods are not freely available, and no web interface has been provided.

Two methods, CellPPD [20] and CPPpred [21], have been published recently and both are freely available to public. CPPpred is a neural network-based in silico method, which can predict cell-penetrating potential of peptides having length between 5 and 30 amino acids. But it cannot help in designing novel CPP analogs, while CellPPD can predict, as well as is helpful in designing novel efficient CPP analogs of parent CPP. This chapter describes the various modules of CellPPD for the prediction and designing of CPPs.

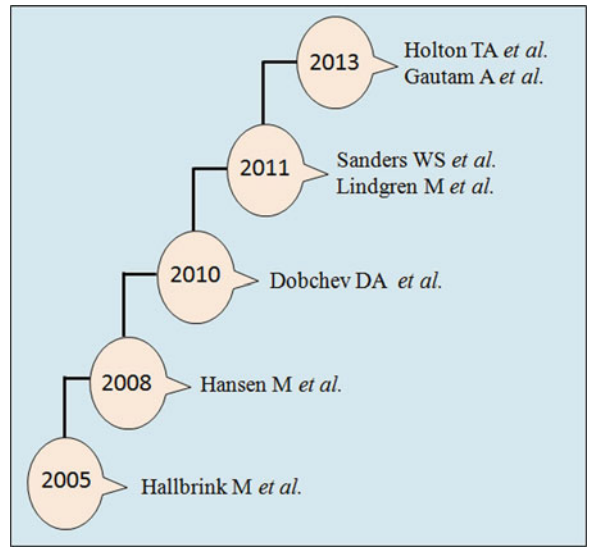

Fig. 1 Progress in the development of in silico tools for CPP prediction

2 Materials

2.1 CPPsite

CPPsite is a unique and the only repository of experimentally validated CPPs [14]. This database was developed with an aim to provide comprehensive information on experimentally tested CPPs. Apart from CPP sequences, it provides information about uptake mechanism, intracellular localization of CPPs, tested cell lines, uptake efficiency, etc. One of the essential features of this database is that it also provides predicted structures of all CPPs. Various tools for data retrieval and analysis were integrated, which makes it a very user-friendly resource. One of the major aims of this database is to provide latest datasets of CPPs for the analysis and development of CPP prediction methods. Two methods, CellPPD and CPPpred, which have been developed recently, have utilized the datasets generated from CPPsite.

3 Methods

3.1 CellPPD: Tool for the Prediction and Designing of Cell-Penetrating Peptides

CellPPD is a support vector machine-based in silico tool, which can predict whether a peptide will be CPP or non-CPP [20]. CellPPD is freely available at http://crdd.osdd.net/raghava/cellppd/. Prediction using CellPPD was based on peptide sequence information like amino acid composition, dipeptide composition, binary patterns, and motif information. Apart from prediction, CellPPD also provides the facility to design novel efficient CPPs. There are four modules: Design Peptide, Multiple Peptides, Protein Scanning, and Motif Scanning. The description of these modules is as follows.

3.2 Prediction and Designing of CPPs

One of the modules in CellPPD is "Design Peptide," which allows prediction of a query peptide as CPP or non-CPP according to the threshold cutoff chosen by the user (Fig. 2). In this module, user can submit single peptide at a time as a query in single-letter code. For the in silico prediction of the input sequence, there are two different prediction models provided (*see* **Note 1**), namely "SVM" and "SVM + motif" (hybrid model) based. Since the hybrid model is based on both motif information and SVM-based model, user can also select hybrid model for more reliable prediction. The selection of model leads to further more filters like setting of SVM threshold and *E*-value (*see* **Notes 2** and **3**); for example, selecting higher SVM threshold leads to greater stringency of prediction of cell-penetrating capacity.

One of the important features of this module is that it allows users to design novel analogs of existing CPP. In wet lab, after getting a suitable CPP lead, one uses to generate all possible analogs of the lead in order to have better and efficient CPPs. CellPPD

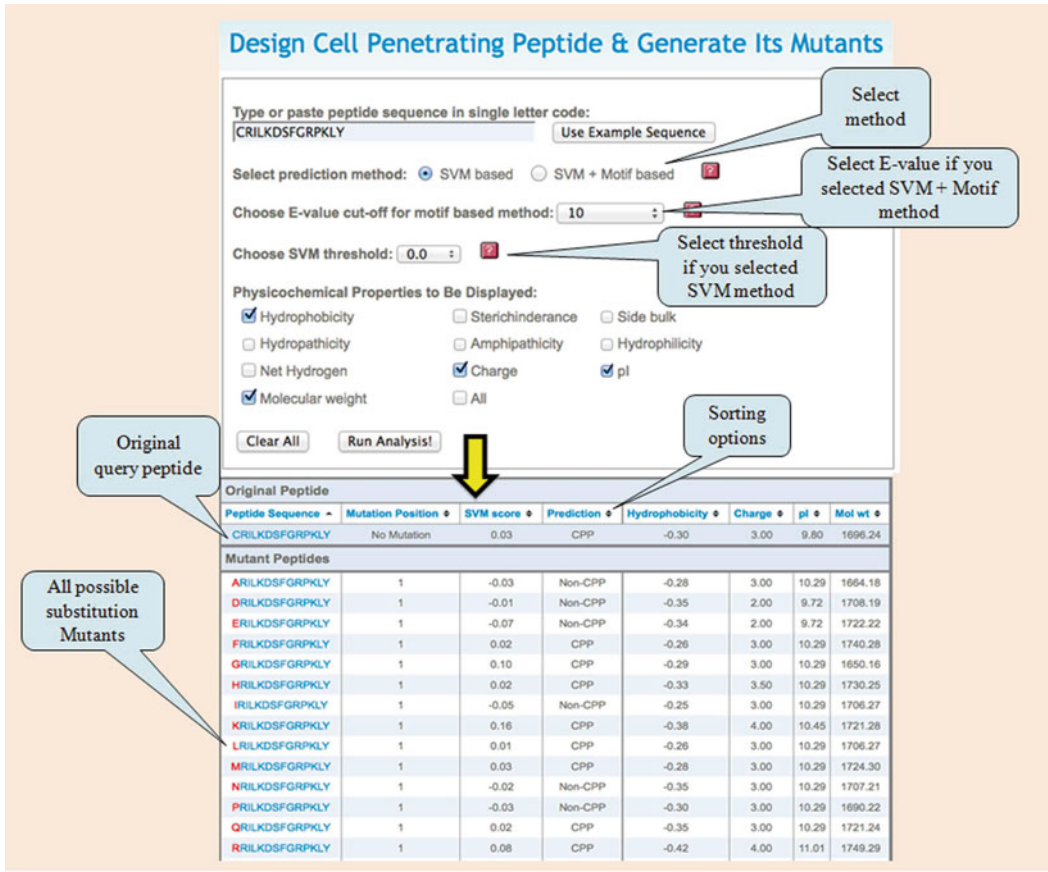

Fig. 2 Schematic representation of "Design Peptide" module and its output

works in the same manner and after submission of a query peptide, first it will predict whether the query peptide is CPP or not. In addition, server also generates all possible substitution mutants (mutated residues are depicted in red color) of the query peptide along with their SVM score, prediction status, and physicochemical properties, like hydrophobicity, charge, and molecular weight. User can sort any of these properties and select the best analog as CPP candidates. All these mutants are clickable and user can select any of the analogs and further generate all possible mutants of selected analog by clicking on that sequence (Fig. 3). In this manner, user can design novel CPP analogs with desired physicochemical properties.

3.3 Virtual Screening of CPPs

Another relevant module of CellPPD is "Multiple Peptides," which enables the users to predict large numbers of peptides at a time (Fig. 4). User can virtually screen libraries of a large number of peptides in order to identify novel efficient CPP candidates. It is just an extended version of "Design Peptide" module, which was

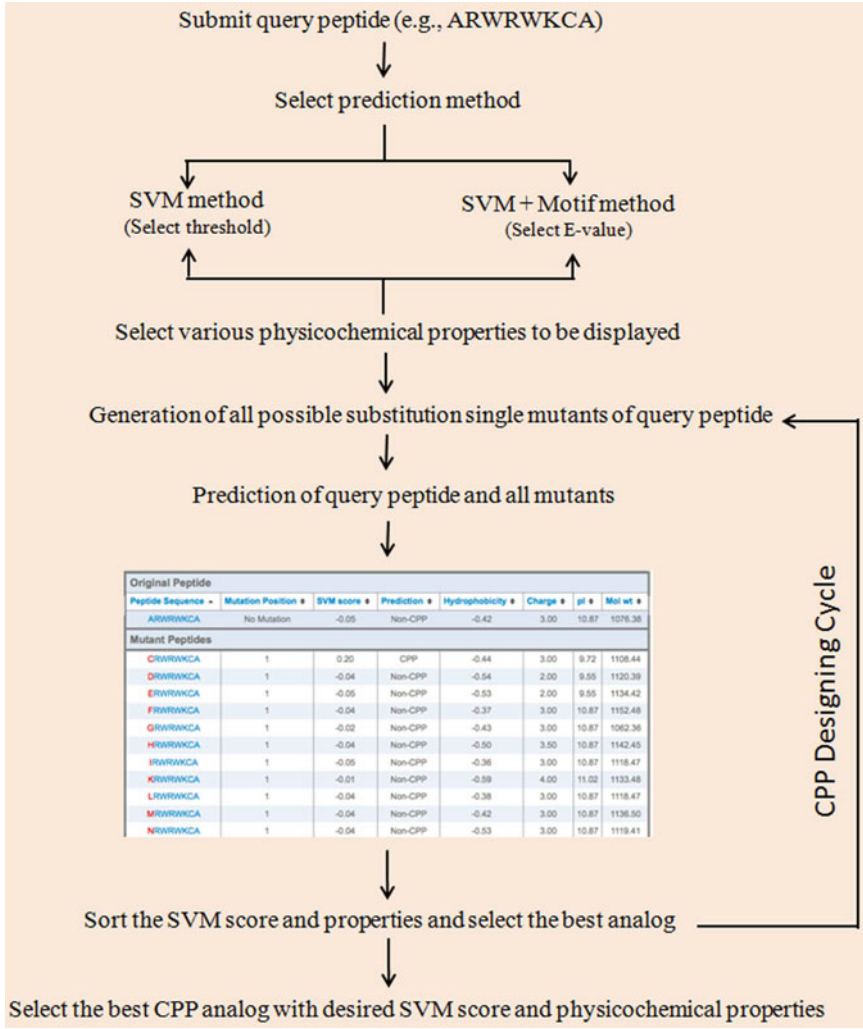

Fig. 3 Flow chart showing functioning of "Design Peptide" module for designing of CPP analogs (Color figure online)

built to save time and effort, if users have large numbers of peptides to predict. Interface of this module asks the users to select the method of prediction, i.e., "SVM" and "SVM + Motif" based. Then users have to define the *E*-value (*see* **Note 3**) if they are using "SVM + Motif"-based method as shown in Fig. 4.

Next is to select the SVM threshold; higher threshold leads to higher stringency (*see* **Note 2**). Users can also select the physicochemical properties, which they wish to display in outputs. Result table shows the prediction result and physicochemical properties, which users have selected (Fig. 4). In the result table, users can further click the individual peptide, which was submitted with multiple peptides earlier to generate its mutants. This facility of "Multiple Peptides" is homologous to "Design Peptide" module.

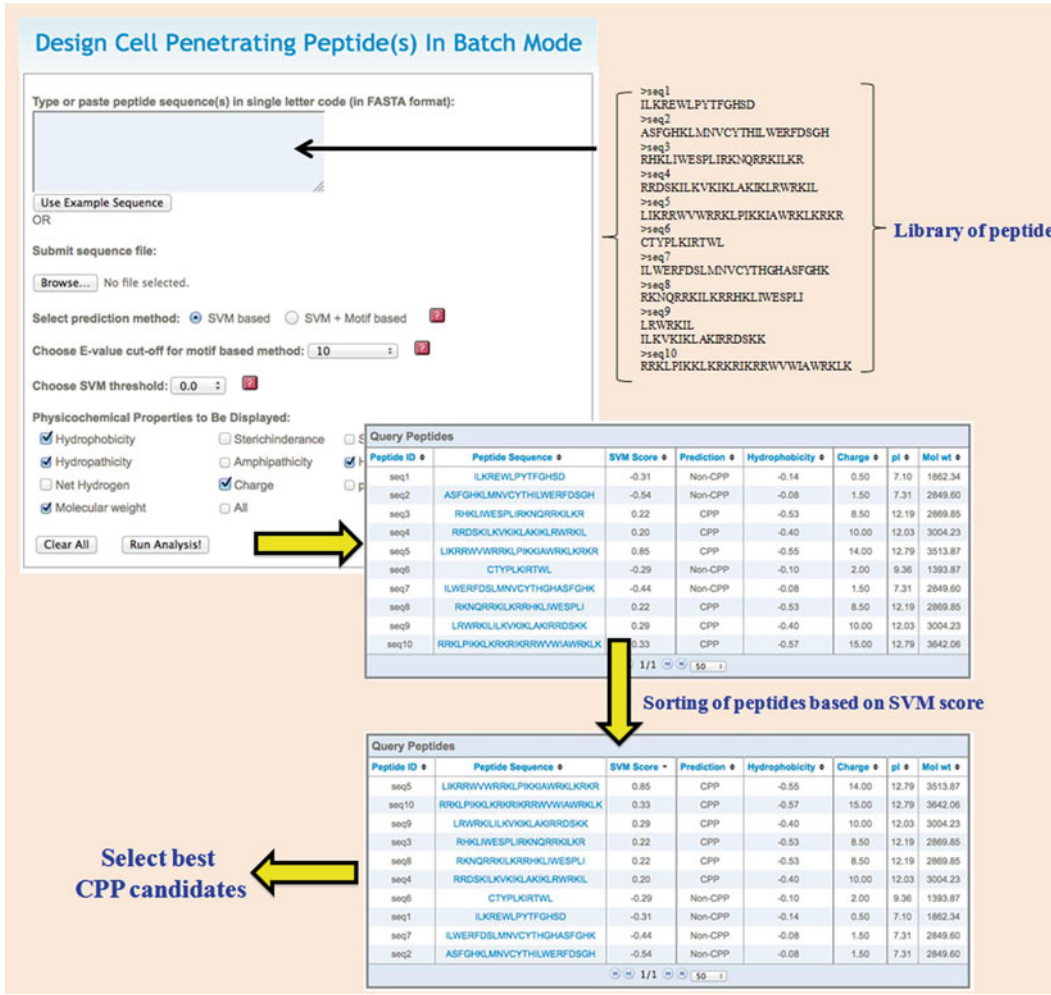

Fig. 4 Schematic representation of working flows of "Multiple Peptides" module of CellPPD

3.4 Protein Scanning

Since many of the CPPs are derived from natural proteins, user may be interested to identify novel CPPs that are derived from natural proteins. To identify those sections of a protein of interest, it has to be scanned throughout its length and resulting fragments can be identified as CPPs/non-CPPs based upon SVM score. For a protein of length l, a total number of overlapping fragments (n) is given by the equation $n = l - w + 1$, where w is the size of each fragment.

To capitalize this concept, "Protein Scanning" module has been integrated into "CellPPD" web server (Fig. 5). Here, the user can give protein sequence in plain one-letter amino acid format and can select the window length of fragments in which the protein has to be fragmented in sliding window fashion. Output can be obtained in tabular or graphical format based upon the selected model ("SVM" based or "SVM + Motif" based). Tabular output contains all the fragments of a query protein along with

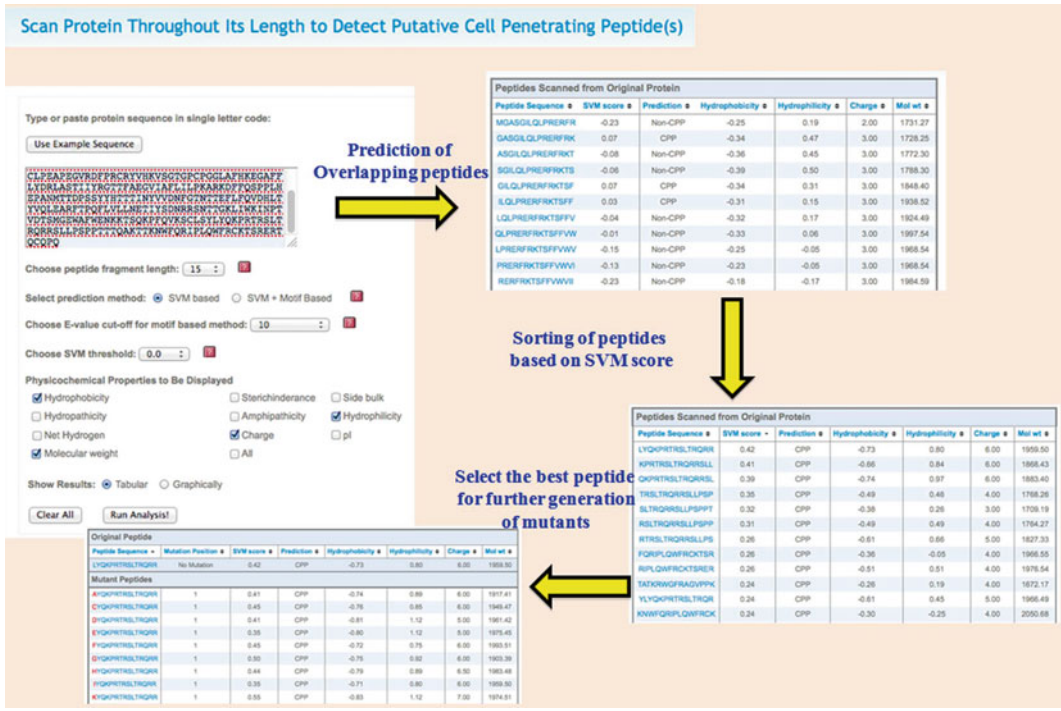

Fig. 5 Schematic representation of functioning of "Protein Scanning" module

their prediction score and prediction status, which is further accompanied by the user-selected physicochemical properties (hydrophobicity, hydrophilicity, molecular weight, etc.). These fragments are further clickable to generate single-point mutants/analogs along with their prediction scores. Parent peptide fragment is displayed in the top panel and respective analogs are in the lower panel of the sortable table. In this manner, user can reiterate and can select the best possible fragments and their analogs. Graphical output is more intuitive as it makes a clear picture of the trend of SVM scores and physicochemical properties of all generated fragments. Plots can be seen by clicking on the range of fragments given at the bottom, where plot's *y*-axis is the SVM score/property value and *x*-axis represents the fragments generated. Graphs are also supplemented with the tabular output.

3.4.1 *Example*

For a given Ebola protein, **Q66811**, if a user wants to see the CPP-rich regions of size 15 in above protein, then "Protein Scanning" module is useful. This query protein has a length of 365 amino acids and generates a total of 351 fragments (size = 15). If the user selects other default parameters and SVM-based model, then he or she gets the tabular output as shown in Fig. 5. Further output can be sorted based upon SVM score to get most potent CPP in the query protein and latter can be subject to generate single-point mutation analog generation (Fig. 5). Also to see the

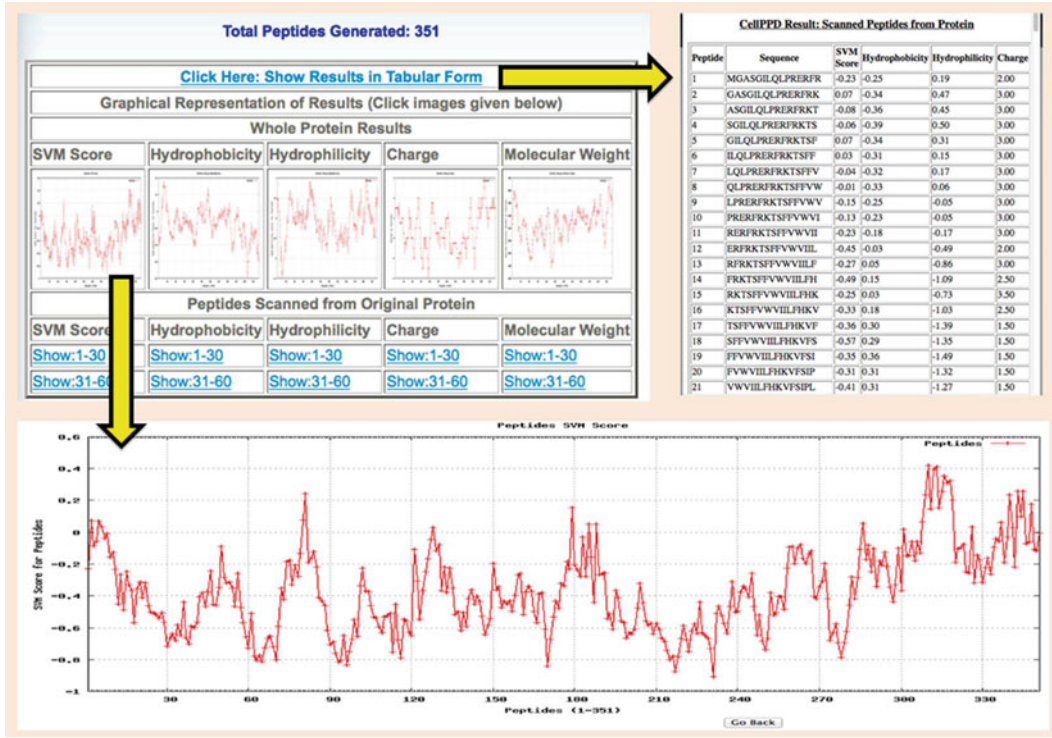

Fig. 6 Tabular and graphical output of "Protein Scanning"

plots of fragments having different SVM scores and physicochemical property values, user has to select graphical output (Fig. 6).

3.5 Motif Scanning

During preliminary analysis, it was observed that CPPs have significant sequence motifs, which are common to most of the CPPs. We have deduced a list of 120 significant motifs ranging from 4 to 30 in length using MEME suite. Whole list of CPP motifs is available at crdd.osdd.net/raghava/cellppd/. These 120 CPP motifs were further used for scanning of unknown proteins for any putative CPP activity, which leads to the concept of "Motif Scanning" module in CellPPD. In this module, user can submit any unknown protein to scan its sequence for the presence of known CPP motifs (Fig. 7). Along with the query sequence(s), user has to select few more options available at the CellPPD interface as shown in Fig. 7. These options are crucial for the scanning of significant motif in query protein sequence. User has to choose the *E*-value cutoff for motif scanning. This parameter is required by the MAST module of MEME suite, which CellPPD uses at the backend to scan motifs in a protein sequence. Users also have to define the length of the putative motifs they are looking for. As a case study, we used 43 protein sequences from five Ebola virus strains and scanned CPP motifs of different lengths in these protein sequences (Table 1).

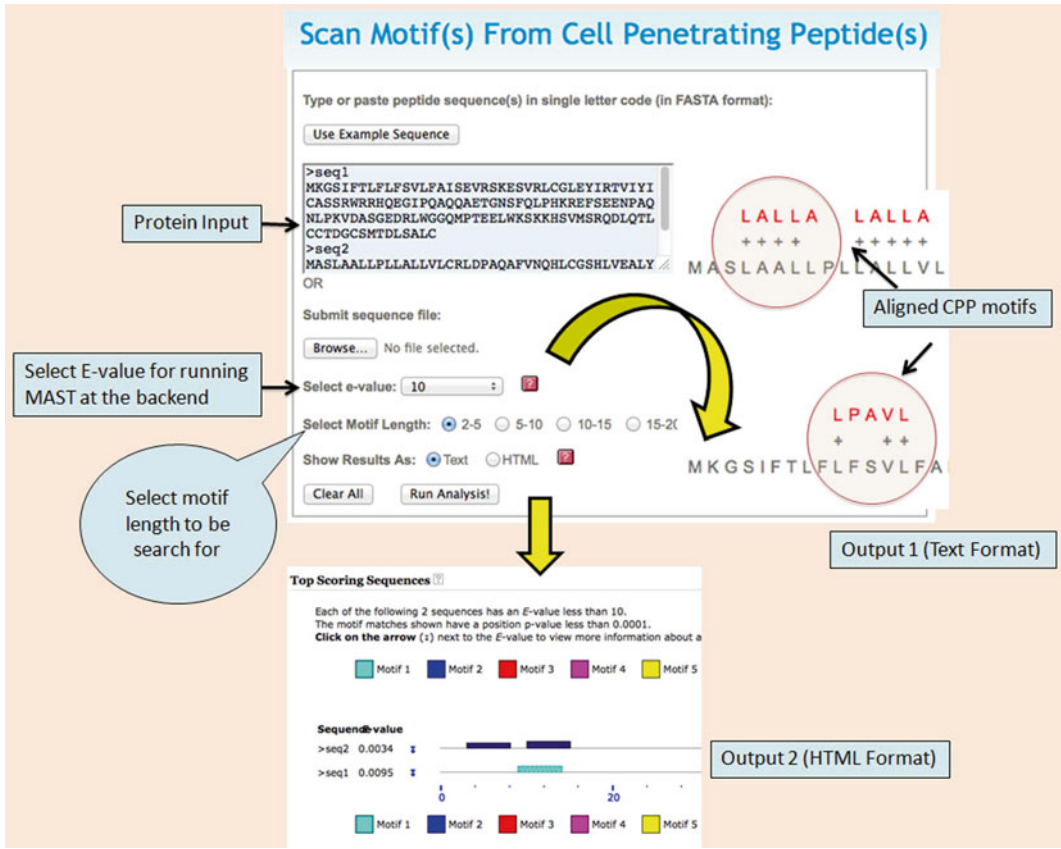

Fig. 7 Schematic representation of "Motif Scanning" module

Table 1
Ten most prominent CPP motifs (of different length) available in the Ebola protein sequences

S. no.	Motif sequence	*E*-value
1	YSPTT	1.70*E*–12
2	GNGYC	1.80*E*–07
3	MIIYR	3.50*E*–05
4	LALLA	2.00*E*–05
5	VALLPAVLLA	4.30*E*–07
6	KKTTTKPTKK	7.50*E*–06
7	ALWVTLWRDV	3.40*E*–05
8	GRQLRIAGKRLEGRS	1.10*E*–07
9	DSDCPGACICNGNGY	9.80*E*–05
10	GLWRALWRLLESLWWLLWEV	9.70*E*–06

4 Notes

1. All modules of CellPPD provide mainly two types of prediction models: (1) SVM based and (2) SVM + Motif based.
2. In the SVM-based model, the prediction status is assessed using the threshold of prediction score ranging nearly from −1 to +1. Default threshold is the one at which learning of a model is the best. If a user wants to shift from default threshold, then sensitivity and specificity also change accordingly. If a user wishes to get more accurate true positives rate (i.e., sensitivity) and false positive rate (i.e., specificity), then the user can move threshold towards +1 and −1, respectively.
3. In the case of motif-based models, users have to select *E*-values. Lower the *E*-value selected, the higher the stringency for that motif to be found in that sequence. But in that case, coverage of the samples decreases. So to compensate less coverage from motif-based approach, SVM and motif (hybrid) approach gives better performance than SVM-based approach, where the lower coverage is compensated by SVM performance and additional motif information attributes higher confidence.

5 Limitations and Future Prospects

Though CPPs are highly efficient and versatile delivery vehicles, their physicochemical properties often restrict their progression from bench to bedside. One of the major limitations is their low stability. Another limitation in CPP-based drug delivery is that most of the internalized CPP cargoes are entrapped in endosomes following endocytosis and the bioavailability is, therefore, severely reduced.

In order to overcome these limitations, novel CPPs with modified and nonnatural amino acids have been developed over the last decade. The in silico methods, which have been developed to date, can predict cell-penetrating potential of peptides consisting of only L-amino acids. Despite the enormous information on modified CPPs, no in silico method has been developed so far, which can predict peptides having modified or nonnatural amino acids. Also, there is a need to develop in silico tools, which can predict, as well as design CPPs with enhanced abilities to promote endosomal escape. Computational methods predicting intracellular localization of CPPs will also be useful for the scientific community, and thus provide momentum to peptide-based drug delivery.

References

1. Tyagi A, Tuknait A, Anand P et al (2014) CancerPPD: a database of anticancer peptides and proteins. Nucleic Acids Res 43:D837–43
2. Kumar R, Chaudhary K, Sharma M et al (2015) AHTPDB: a comprehensive platform for analysis and presentation of antihypertensive peptides. Nucleic Acids Res 43:D956–D962
3. Gautam A, Chaudhary K, Singh S et al (2014) Hemolytik: a database of experimentally determined hemolytic and non-hemolytic peptides. Nucleic Acids Res 42:D444–D449
4. Mehta D, Anand P, Kumar V et al. (2014) ParaPep: a web resource for experimentally validated antiparasitic peptide sequences and their structures. Database (Oxford) 2014
5. Van Dorpe S, Bronselaer A, Nielandt J et al (2012) Brainpeps: the blood-brain barrier peptide database. Brain Struct Funct 217: 687–718
6. Wynendaele E, Bronselaer A, Nielandt J et al (2013) Quorumpeps database: chemical space, microbial origin and functionality of quorum sensing peptides. Nucleic Acids Res 41: D655–D659
7. Waghu FH, Gopi L, Barai RS et al (2014) CAMP: collection of sequences and structures of antimicrobial peptides. Nucleic Acids Res 42:D1154–D1158
8. Vlieghe P, Lisowski V, Martinez J et al (2010) Synthetic therapeutic peptides: science and market. Drug Discov Today 15:40–56
9. Craik DJ, Fairlie DP, Liras S et al (2013) The future of peptide-based drugs. Chem Biol Drug Des 81:136–147
10. Kaspar AA, Reichert JM (2013) Future directions for peptide therapeutics development. Drug Discov Today 18:807–817
11. Cerrato CP, Lehto T, Langel U (2014) Peptide-based vectors: recent developments. Biomol Concepts 5:479–488
12. Milletti F (2012) Cell-penetrating peptides: classes, origin, and current landscape. Drug Discov Today 17:850–860
13. Copolovici DM, Langel K, Eriste E et al (2014) Cell-penetrating peptides: design, synthesis, and applications. ACS Nano 8:1972–1994
14. Gautam A, Singh H, Tyagi A et al. (2012) CPPsite: a curated database of cell penetrating peptides. Database (Oxford) bas015
15. Hällbrink M, Kilk K, Elmquist A et al (2005) Prediction of cell-penetrating peptides. Int J Pept Res Ther 11:249–259
16. Hansen M, Kilk K, Langel U (2008) Predicting cell-penetrating peptides. Adv Drug Deliv Rev 60:572–579
17. Dobchev DA, Mager I, Tulp I et al (2010) Prediction of cell-penetrating peptides using artificial neural networks. Curr Comput Aided Drug Des 6:79–89
18. Lindgren M, Langel U (2010) Classes and prediction of cell-penetrating peptides. Methods Mol Biol 683:3–19
19. Sanders WS, Johnston CI, Bridges SM et al (2011) Prediction of cell penetrating peptides by support vector machines. PLoS Comput Biol 7:e1002101
20. Gautam A, Chaudhary K, Kumar R et al (2013) In silico approaches for designing highly effective cell penetrating peptides. J Transl Med 11:74
21. Holton TA, Pollastri G, Shields DC et al (2013) CPPpred: prediction of cell penetrating peptides. Bioinformatics 29:3094–3096

Part II

Methods to Test Mechanisms of Cell-Penetrating Peptides

Chapter 5

Investigating Membrane Interactions and Structures of CPPs

Fatemeh Madani and Astrid Gräslund

Abstract

Despite many studies made on cell-penetrating peptides (CPPs), the mechanism of their cellular uptake and endosomal escape has not been completely resolved. This is even more unclear when the CPP is bound either covalently or non-covalently to the cargo molecules. To answer remaining questions, we require a combination of different methods, model systems, and experiments since there is no single method which could give a complete answer to all questions. Biophysical investigations of CPPs have a significant impact on CPP research considering their molecular mechanisms of action. In this chapter, we present different membrane model systems suitable for biophysical studies as well as the basic practical aspects underlying several common biophysical methods and experiments. The methods include fluorescence spectroscopy, circular dichroism spectroscopy, and dynamic light scattering and concern peptide-membrane interactions and vesicle model membrane leakage. We have also described the potential and limitations of biophysical studies on the CPP-membrane interactions and their impact on our understanding of how CPPs mediate the transport of cargoes into living cells.

Key words Large unilamellar vesicle, Circular dichroism, Dynamic light scattering, Nuclear magnetic resonance, Bacteriorhodopsin, pH gradient, Calcein leakage, Proton pumping

1 Introduction

Due to the complexity of the native biological plasma membrane, studying molecular mechanisms of the cell-penetrating peptide (CPP) underlying membrane interactions becomes very complicated. Circular dichroism (CD) and nuclear magnetic resonance (NMR) are biophysical techniques which are applicable to model membrane systems and provide information regarding the mechanistic aspects of CPPs, but they are difficult or not possible to use for an intact biological cell membrane. This chapter describes several model membrane systems used for biophysical studies of CPP-membrane interactions and CPP-induced membrane destabilization and leakage by methods such as CD, NMR, and fluorescence spectroscopies.

Ülo Langel (ed.), *Cell-Penetrating Peptides: Methods and Protocols*, Methods in Molecular Biology, vol. 1324,
DOI 10.1007/978-1-4939-2806-4_5,

1.1 Membrane Model Systems

Phospholipid vesicles are the most commonly used model membrane systems in biophysical studies. They are small spherical objects consisting of one (unilamellar) or more (multilamellar) lipid bilayers made of either natural or synthetic lipids [1, 2]. Major types of vesicles with different sizes are small unilamellar vesicles (SUV; typically 20–50 nm in diameter), large unilamellar vesicles (LUV; typically 100–200 nm in diameter), and onion-like multilamellar vesicles (MLV; 0.1–4 μm in diameter). Giant unilamellar vesicles (GUV) are large vesicles with diameters of about 10–100 μm and are observable under the optical microscope [1, 2]. Each model system has individual advantages and drawbacks when applied for biophysical applications. The main limitation is light scattering for applications such as fluorescence and CD methods. SUVs have the lowest light scattering propensity and are used in many biophysical studies, but their high surface curvature may influence the membrane-peptide interactions. LUVs have been extensively used as membrane model systems to study CPP-membrane interaction and perturbation. The small surface curvature and a high encapsulation efficiency means that this membrane model system may reasonably well mimic the biological cell membrane [1].

Dynamic light scattering has been widely employed to measure the diameter and stability of LUVs in solution [3]. This method is based on the fact that particles scatter light in different directions which helps to determine the size and molecular weight of particles. The intensity fluctuation of scattered light due to the particle motion is measured by DLS [4, 5]. The average hydrodynamic radius of typical LUVs as obtained by DLS is about 50 nm at 25 °C [6].

Besides the selected model system, the lipid concentration and lipid components of the membrane model are important factors that may influence the observed results. Various types of phospholipids with varying head-groups and their mixtures can be used to prepare the particular vesicles depending on the experiment. Due to the negatively charged nature of biological cell membrane, mixtures of neutral zwitterionic such as 1-palmitoyl-2-oleoyl-snglycero-3-phosphocholine (POPC) and negatively charged such as 1-palmitoyl-2-oleoyl-sn-glycero-3-phosphoglycerol (POPG) phospholipids are often used to make LUVs with negative surface charge. In this chapter the focus is on LUVs and their preparation procedures are described in detail.

1.2 Structure Induction of CPPs

The secondary and three-dimensional structures of the CPPs in different membrane models can be determined using CD and NMR methods, respectively [7–12]. CD spectroscopy gives information about the overall secondary structures of the proteins or peptides in solution as well as their conformational changes in different environments. It is generally based on the fact that optically

active molecules (such as peptides) have different extinction coefficients for left- and right-handed circularly polarized light, a phenomenon known as circular dichroism [13, 14]. Several groups have studied the structural induction in different CPPs in the presence of membrane mimetic models and the aim is to classify the CPPs according to the correlation between the induced structure and their uptake mechanisms [15]. Most CPPs form a random coil structure in aqueous solution and they may form α-helix or β-sheet conformations in the presence of different membrane model environments depending on the membrane surface charge [7–10, 15]. Recently, it has been shown that CPPs with stearic acid at the N-terminus such as PepFects and NickFects adopt an α-helical structure in aqueous solution [16]. CD spectroscopy is also used to determine the secondary structure of the CPPs in complex with the cargo in buffer and in the presence of the phospholipid membrane. Differences in the chemical structure of the peptide/cargo complex influence the peptide secondary structure and possibly the peptide-membrane interaction [11, 16].

NMR provides information of the three-dimensional structure and molecular dynamics of biological macromolecules such as peptides and proteins [12, 17, 18]. In contrast to CD, NMR provides atomic level structural information. In addition, studies of dynamic properties of the CPPs and their localization in the model membrane are possible with NMR spectroscopy [9, 10]. A three-dimensional structure by NMR will be obtained by following certain procedures including preparation of the appropriate sample, multidimensional NMR measurements, chemical shift assignment (backbone and side chain assignments), structure constraint generation, and structure calculation using the computer programs for interpretation of NMR data [19–21]. There are several studies which have determined the structure of CPPs both in solution and in the presence of membrane model systems [7, 22–24]. However, it is not simple to identify any correlation between the particular structure induced by the membrane model systems and the observed mechanism of cellular internalization for different CPPs.

1.3 Model Membrane Interactions of CPPs

Membrane models as simplified mimetic system for biological cell membranes have been successfully used to study CPP-membrane interactions. Both electrostatic interactions and peptide hydrophobicity are found to be important but, due to the lack of intrinsic negatively charged cellular components such as proteoglycans in membrane model systems, hydrophobicity often plays an important role for peptide-model membrane interactions [25].

Peptide-induced vesicle leakage is one common experiment to study the degree of membrane perturbation generated by different CPPs via fluorescence spectroscopy. Leakage experiments can be performed in several ways. Figure 1 shows one such experiment in which LUVs encapsulated a fluorophore are first prepared in a

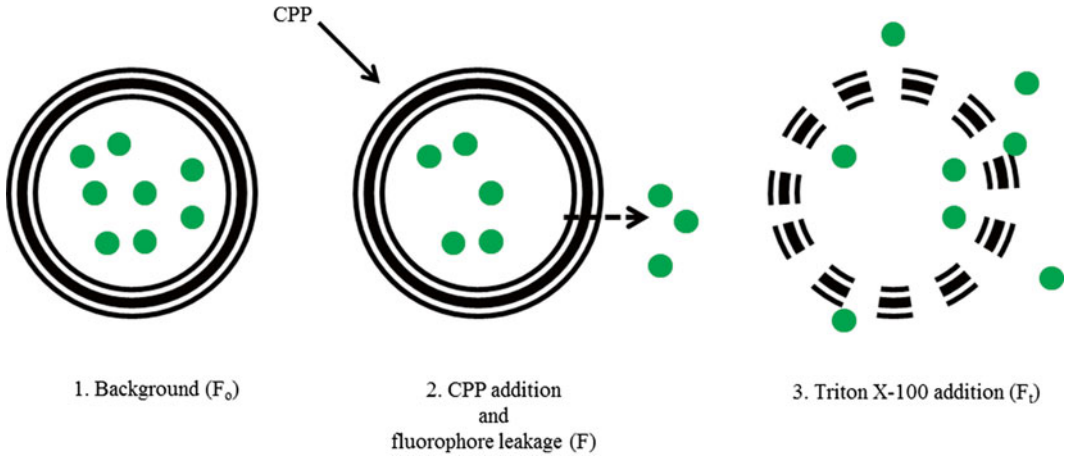

Fig. 1 Schematic overview of the leakage experiment. *Picture 1* shows LUVs encapsulated high concentration of a fluorophore (such as calcein). Fluorescence intensity at this stage is low and it is recorded as the background fluorescence intensity (*Fo*). *Picture 2* shows addition of the selected CPP and subsequent fluorophore leakage. Fluorescence intensity at different time points may be recorded at this stage. At *picture 3*, Triton X-100 is added and 100 % leakage may be recorded (*Ft*)

buffer containing a relatively high concentration of the fluorophore. Free residual fluorophore outside the vesicles should be carefully removed. High concentration of fluorophore inside the LUVs and subsequent self-quenching of fluorescence decrease the fluorescence intensity which should then increase upon fluorophore leakage and dilution in the outside medium. Addition of the CPP to the outside of the LUVs may induce leakage of the fluorophore from inside of the LUVs which can be recorded using fluorescence spectrometer [26, 27]. Studies have shown that primary amphipathic CPPs such as transportan and TP10 have higher degree of membrane perturbation and leakage. However, non-amphipathic or hydrophilic CPPs like TAT(48–60) and polyarginines induce no or less leakage compared with hydrophobic CPPs [25]. In contrast to model leakage studies, both groups of CPPs are cell penetrating and they have high activity in biological cell membranes [28]. These different results indicate that the potential effects of other components present in biological cell membranes may be important and suggest the presence of mechanisms more related to a receptor-protein-mediated uptake [29, 30].

In a second type of experiment a leakage-modulating molecule such as pyrenebutyrate (PB) is added into the fluorophore-encapsulated LUVs [25]. The results may highlight different characteristics that influence the peptide-membrane interaction and perturbation. In this experiment, one should optimize the CPP concentration that induces a minor fluorophore leakage. Next, the leakage-modulating molecule (PB) can be added to the LUVs followed by a certain incubation time. Finally, the selected

CPP is added and the leakage of the fluorophore is recorded using a fluorometer [25].

Generally, in all fluorophore leakage experiments, two important features are the presence of sealed vesicles and a suitable fluorophore entrapped inside the vesicles so that the fluorophore does not leak out in the absence of the leakage-causing peptide. In addition, experimental conditions such as peptide concentration and lipid composition are important factors affecting the result of the experiments. The balance among these variables is difficult to predict, which indicates that one needs to be careful when performing experiments and interpreting results obtained by fluorescence. Calcein is a synthetic fluorophore appropriate for membrane-leakage studies. Since calcein is negatively charged, its interaction with the phospholipid membrane and spontaneous membrane leakage occurs on a slower time scale than with fluorophores of less charge such as fluorescein.

In the third type of experiment, instead of the fluorophore, a fluorophore-labeled peptide can be encapsulated inside the vesicles and leakage of the peptide promoted by different factors such as a pH gradient across the membrane can be recorded by measuring the fluorescence intensity [22, 31–34].

CPP-endosomal escape is one major challenge in CPP cargo delivery and several studies have focused on investigating the mechanisms of endosomal escape of CPPs [35]. In an elegant experiment, the biological endosome can be modeled using the bacteriorhodopsin (BR)-reconstituted LUV system (BR-LUV). The proton pumping activity of BR simulates a pH decrease inside the late endosome and creates a pH gradient over the membrane. Translocation ability of different CPPs in the presence of the pH gradient can be investigated using BR-LUV model endosome. It has been shown that light-induced proton pumping activity of BR facilitates the vesicular escape of hydrophobic CPPs such as penetratin [36].

In summary, BR is reconstituted into the performed vesicles using detergent-mediated reconstitution method [37]. According to this method, asymmetrically oriented BR in the membrane pumps protons from the outside to the inside of the vesicles upon illumination. The pH can be recorded with LUVs in the dark and after a certain time of illumination by using a xenon lamp and a pH meter [6]. Upon illumination of the sample, the pH measured outside the vesicles should increase and reach a maximum, due to the fact that in the presence of light, BR pumps protons from the outside to the inside of the vesicles. In the dark, protons leak out across the membrane resulting in decrease of the pH outside the LUVs. Proton pumping efficiency depends on the orientation of the BR incorporated into the LUVs. The detergent-mediated reconstitution method results in 95 % inside-out orientation with maximum proton pumping [37]. Figure 2 shows a schematic

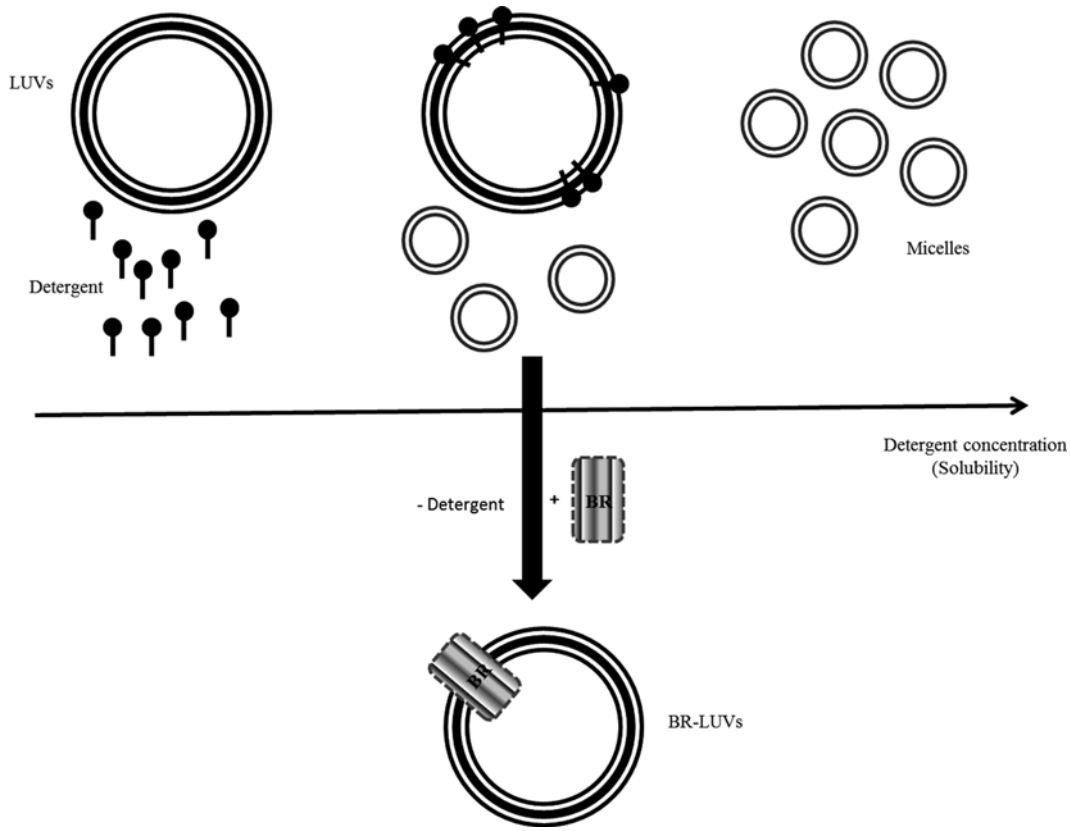

Fig. 2 Schematic overview for the method of detergent-mediated reconstitution of BR into the LUVs. For optimal reconstitution efficiency, BR should be added when both micelles and lipid-detergent vesicles are present in the solution

picture illustrating the time point when BR should be added to the LUVs to obtain high proton pumping efficiency.

Studies on CPP-membrane interaction performed so far have focused mainly on the effect of peptide alone, and few studies have focused on the peptide/cargo complexes [38, 39]. Understanding the effect of various cargo molecules on the CPP model membrane interaction is fundamental to understand the mechanistic aspects of CPPs especially on CPP endosomal escape efficiency. The effect of cargo molecules on CPP-membrane interactions can be evaluated using membrane models. It has been shown that the cargo decreases cellular uptake and membrane translocation efficiency [38, 40] and this observation has also been shown in the presence of the membrane model system [41]. In this respect, both the type of CPP and the cargo will affect the cargo/peptide complex formation and also affect the peptide-membrane interactions. Whether the impact of a non-covalently bound CPP/cargo complex on the CPP-membrane perturbation involves a direct interaction between peptide in

complex and membrane or if there are some free peptides that destabilize the membrane is not yet clear. Answer to this question requires unraveling the complexity of the peptide/cargo complexes in mechanistic details.

2 Materials

2.1 Preparation of the Large Unilamellar Vesicle

1. Phospholipids, typically neutral zwitterionic 1-palmitoyl-2-oleoyl-sn-glycero-3-phospho-choline (POPC) and negatively charged 1-palmitoyl-2-oleoyl-sn-glycero-3[phospho-rac-(1-glycerol)] (POPG) (Avanti Polar Lipids, Alabaster, Alabama, USA), without any extra purification.
2. Lyophilizer.
3. 50 mM Potassium phosphate buffer, pH around 7.4.
4. Vortexer.
5. Avanti mini extruder with polycarbonate filter, 100 nm pore size (Avanti Polar Lipids, Alabaster, Alabama, USA).

2.2 Circular Dichroism Spectroscopy

1. 10 mM Potassium phosphate buffer, pH 7.4.
2. LUVs in 10 mM phosphate buffer, pH 7.4.
3. Hellma Quartz cell.
4. A CD spectrometer.

2.3 Calcein Leakage Experiment

1. LUVs in 50 mM potassium phosphate buffer, pH 7.4.
2. Fluorophore, Calcein (AnaSpec, California, USA).
3. 50 mM potassium phosphate buffer containing 55 mM calcein. Final pH is adjusted to 7.4 by addition of NaOH (10 M).
4. PD-10 desalting column (GE Healthcare, Buckinghamshire, UK).
5. The detergent, Triton X-100 (Sigma-Aldrich, Stockholm, Sweden).
6. A fluorescence spectrometer.

2.4 BR-Induced pH Gradient Over the Model Membrane

1. LUV in 20 mM potassium phosphate buffer, 100 mM KCl, pH 7.2.
2. 0.68 M n-octyl-β-D-glucopyranoside, OG (Glycon Biochemicals, Luckenwalde, Germany).
3. Bacteriorhodopsin can be produced and purified essentially according to a published protocol [42]. Solubilize BR in detergent (OG) to give final concentrations of 1 mg/mL and 100 mM for BR and OG, respectively.
4. Bio-Beads (BIO-RAD, California, USA).

5. PD-10 desalting column (GE Healthcare, Buckinghamshire, UK).
6. Xenon lamp.
7. A pH meter.

2.5 Modeling the Endosomal Escape of CPPs

1. LUV in 20 mM potassium phosphate buffer, 100 mM KCl, pH 7.2.
2. Potassium iodide (KI).
3. Fluorescein-labeled CPP.
4. Bacteriorhodopsin can be produced and purified essentially according to a published protocol [42]. Solubilize BR in detergent (OG) to give final concentrations of 1 mg/mL and 100 mM for BR and OG, respectively.
5. Bio-Beads (BIO-RAD, California, USA).
6. PD-10 desalting column (GE Healthcare, Buckinghamshire, UK).
7. A fluorescence spectrometer.

3 Methods

3.1 Preparation of the Large Unilamellar Vesicle (Extrusion Method)

The extrusion method is a common means of vesicle production, which produces a relatively homogeneous solution of LUVs with a narrow size distribution of 100 nm in diameter. The resulting LUVs mimic the biological cell membrane in the size and packing density [43–45].

1. Dissolve the phospholipids in an organic solvent such as chloroform to obtain a homogeneous mixture. Both saturated and unsaturated phospholipids can be used to make vesicles, provided that the temperature is above the gel-fluid transition temperature [43]. Also, depending on the application, neutral zwitterionic lipids or mixture of zwitterionic and negatively charged lipids (e.g., 30 % negatively charged) may be used (*see* **Note 1**). Total lipid concentration is typically 1 mM.
2. Evaporate the solvent under high vacuum for 3 h in order to remove all residual organic solvent and obtain a dry lipid film (*see* **Note 2**).
3. Resuspend the dried lipid film in 55 mM potassium phosphate buffer, pH 7.4 to give a total lipid concentration of 1 mM. The solution is vortexed for 10 min. Multilamellar vesicles (MLVs) are formed at this stage.
4. Subject the solution to five times freeze-thaw with liquid nitrogen to reduce the lamellarity and obtain more aqueous trapped volumes [46].

5. Use an Avanti manual extruder and push the lipid solution containing MLVs 20 times through two polycarbonate filters (100 nm pore size) (*see* **Note 3**). At this stage, LUVs form with a well-defined diameter of 100 nm and a narrow size distribution (*see* **Note 4**).
6. Diameter and size distribution of vesicles may be determined by dynamic light scattering (DLS) (*see* **Note 5**).

3.2 Circular Dichroism Spectroscopy

Circular dichroism (CD) is used to obtain information on the secondary structure of the peptides in solution as well as information on the conformational changes of peptides in the presence of membrane model systems and in complex with different cargo molecules.

1. Record the CD spectra of the "blank" sample which can be the buffer, water, or vesicle solution to ensure that the background solution does not cause any artifacts (*see* **Note 6**).
2. Dissolve the peptide with desired concentration in buffer to obtain a homogeneous solution. The optimal peptide concentration depends on the path length of the cuvette (*see* **Note 7**).
3. After measuring the "blank" sample, CD spectra of the peptides in buffer can be recorded on a Chirascan CD spectrometer at 20 °C. Spectra are recorded at wavelengths between 190 and 260 nm, using a bandwidth of 2 nm. A quartz cuvette with an optical path length of 2 mm is used, requiring approximately 500 μL of sample. The temperature is adjusted using a TC 125 temperature control.
4. The background spectra of the buffer solution are then subtracted from the peptide spectra. Spectra are usually collected and averaged over several measurements.
5. For measuring peptide structure in vesicle solution, add different concentrations of the peptide to the LUV solution and measure the CD spectra of the peptide with LUVs. The CD spectrum of the peptide is obtained after subtracting the blank (LUVs) spectrum.

3.3 Calcein Leakage Experiment

Calcein leakage experiment is a fluorescence assay to qualitatively investigate the degree of membrane destabilization and perturbation caused by different peptides. Effect of cargo molecules on peptide-membrane interaction may also be studied using this method.

1. Dissolve the phospholipids in an organic solvent and prepare a dry lipid film as described in Subheading 3.1, **steps 1** and **2**.
2. Pass the potassium phosphate buffer containing calcein through a 100 nm polycarbonate filter to remove any large particles.

3. Resuspend the dried lipid film from **step 1** in the filtered buffer containing calcein to give a total lipid concentration of 5 mM. The solution is vortexed for 10 min. Multilamellar vesicles (MLVs) perform at this stage.
4. Subject the solution to five times freeze-thaw with liquid nitrogen to reduce the lamellarity and obtain more aqueous trapped volumes.
5. Use an Avanti manual extruder and push the lipid/calcein solution containing MLVs 20 times through two polycarbonate filters (100 nm pore size) (*see* **Note 3**).
6. Remove the calcein which is not entrapped inside the LUVs by filtering the LUV solution through Sephadex-G25 columns three times (*see* **Note 8**). Dilution factor for lipids is about 1.4 per each passage.
7. Record the fluorescence intensity of LUVs (usually with the total lipid concentration of 100 μM) encapsulating calcein using the fluorescence spectrometer, with wavelengths set at 494 nm for excitation and 516 nm for emission. The fluorescence intensity for a solution of 55 mM calcein should be low due to self-quenching (*see* **Note 8**).
8. After measuring the background intensity, different concentrations of peptides are added to the vesicle solution, which consisted of neutral zwitterionic vesicles such as POPC LUVs or partially negatively charged LUVs such as POPC/POPG LUVs (100 μM lipid concentration) at 25 °C.
9. Monitor the release of calcein from the vesicles over a period of time as an increase in the fluorescence intensity. One hundred percent leakage (i.e., destruction of the vesicles) is induced by addition of 10 % (w/v) Triton X-100. The degree of leakage induced by different peptides is calculated using the following equation: $\%\text{leakage} = [(F - Fo)/(Ft - Fo)] \times 100$, where Fo and Ft are the fluorescence intensities initially observed without peptide (background) and after treatment with Triton X-100, respectively. F is the fluorescence intensity in the presence of the peptide (*see* Fig. 1).

3.4 Transmembrane pH Gradient Experiment

Transmembrane pH gradient experiment can be used to investigate the mechanisms of endosomal escape of CPPs. Bacteriorhodopsin is used to induce a proton gradient across the lipid bilayer of the LUVs and simulate the biological endosome [37, 47–49].

1. Dilute the LUVs prepared by extrusion method (Subheading 3.1) in the buffer used for their preparation to the desired concentration. 2.3 mL vesicle suspension of 5 mM phospholipid concentration can be used.
2. Add 90 μL of OG detergent to the diluted LUVs. Final concentrations of lipids and OG are 4.8 and 25.6 mM, respectively.

As shown in Fig. 2, LUV solubilization takes place in three stages. First the detergent monomers start to diffuse among bilayers and there are also some free detergent monomers in the solution. Further addition of detergent saturates the vesicle bilayer, and transition from monomers to mixed lipid/detergent micelles will occur when detergent monomer concentration reaches its cmc value. At higher concentration of the detergent, all LUVs have disappeared and only micelles are present in the solution.

3. Add the BR monomers resulting from detergent solubilization of purple membrane (BR 1 mg/mL, OG 100 mM) to the solubilized LUV suspension and incubate for 5–10 min in the dark. Mixture of BR/lipid/detergent vesicles and lipid/detergent micelles with the final concentrations of 4 μM, 4.3 mM, and 29 mM for BR, lipid, and detergent, respectively, is the resulting suspension. At this stage, BR may be incorporated into the detergent-saturated vesicles. It has been shown that the partly detergent-saturated LUVs are optimal in reconstitution of BR which provides higher proton pumping efficiency [37].
4. Add pre-wet Bio-Beads (80 mg/mL) directly to the BR-lipid-detergent suspension and lightly stir the mixture at room temperature for 3 h. At this stage, the transition from micellar to lamellar phase may take place. Add a second portion of slightly wet beads and mix them overnight with a small shaker and the rate of around 400 rpm to remove detergents. Use two PD-10 columns to remove Bio-Beads and residual detergents from the sample (*see* **Note 9**).
5. Use a PD-10 column to equilibrate the BR-reconstituted vesicle suspension in 120 mM KCl pH 7.4 buffer. Monitor the pH changes outside the vesicle using a xenon lamp to illuminate the sample and the pH meter to record the values of the pH. Prior to the measurement, the sample is kept in the dark for at least 30 min to ensure the dark adaptation of the sample. Record the pH in the dark as the baseline. Light-induced pH changes of BR-LUVs are measured in a cuvette under agitation (*see* **Note 10**).

3.5 Preparation of CPP-Encapsulated LUVs and pH Gradient Experiment

1. Prepare 20 μM fluorescein-labeled CPP solution in 20 mM potassium phosphate, 100 mM KCl (pH 7.2), and 100 mM potassium iodide (KI). KI is used as a quencher.
2. Prepare the LUVs containing the peptide as described in Subheading 3.1 by using the abovementioned solution as a buffer.
3. Reconstitute the BR into the LUVs according to the procedure described in Subheading 3.4.

4. Wash the LUV suspension twice using two PD-10 columns to remove non-encapsulated fluorescein-labeled CPP and quencher from the outside of the LUVs (*see* **Note 11**).
5. Use a xenon lamp to illuminate the sample (CPP encapsulated in BR-LUVs) under agitation. Prior to the measurement, the sample is kept in the dark for at least 30 min to ensure the dark adaptation of the sample, and the fluorescence intensity is recorded in the dark as the baseline.
6. Light-induced pH changes of BR-LUVs and subsequent release of the labeled CPP from the vesicles over a period of time are recorded as an increase in the fluorescence intensity.

4 Notes

1. The permeability and stability of the LUVs are strongly affected by the lipid purity. Always use lipids with high purity. Oxidized lipids may change the vesicle permeability.
2. It is very important to remove all of the organic solvent before addition of the buffer to the dry lipid film. Residual solvent may affect the vesicle properties.
3. A certain number of passages (generally 20) is necessary to produce a homogeneous size distribution [45]. Obtained stability in the flow rate of the passages indicates that the number of passages is enough to obtain homogeneous size distributed LUVs.
4. LUVs may be stored for weeks at room temperature, particularly when they encapsulate only the buffer solution. LUVs are less stable when they are encapsulating fluorophores (such as calcein) or peptides.
5. For DLS measurements, the sample should be free of any particles such as dust, unwanted aggregates, and bubbles.
6. It is essential to minimize light absorption due to other components (buffers and LUV solution) in the mixture. Potassium phosphate buffer at low concentrations (e.g., 10 mM) has low absorbance above 190 nm.
7. The total absorbance of the sample at the selected wavelength should not be greater than about one unit to avoid the spectral noises.
8. Free residual fluorophore outside the vesicles should be carefully removed by passing through Sephadex-G25 columns (generally two or three times). Residual calcein outside the LUVs may interact with the peptide and change the peptide-membrane interaction.

9. Complete removal of detergent and examining the size and stability of LUVs with DLS are recommended to further improve the results in terms of proton pumping efficiency.
10. ΔpH inside the vesicles can be calculated based on the change in pH (ΔpH) outside the vesicles, the proton concentration, and the estimated inner volume of all vesicles in the solution.
11. Detergent changes the membrane permeability of the LUVs. Therefore, it is important to remove components outside the vesicles, such as peptides or quencher, after the detergent removal stage. KI as a quencher minimizes the background fluorescence intensity. Any increase in background fluorescence is due to the leakage of the labeled peptide from the LUVs.

Acknowledgment

Research in this field in the author's laboratory is supported by the Swedish Research Council.

References

1. Szoka F, Papahadjopoulos D (1980) Comparative properties and methods of preparation of lipid vesicles (liposomes). Annu Rev Biophys Bioeng 9:467–508
2. Lasic DD (1988) The mechanism of vesicle formation. Biochem J 256:1–11
3. Jin AJ, Huster D, Gawrisch K, Nossal R (1999) Light scattering characterization of extruded lipid vesicles. Eur Biophys J 28:187–199
4. Bruce J, Berne RP (1976) Dynamic light scattering with applications to chemistry, biology and physics. Dover, Mineola, NY
5. Clark NA, Lunacek JH, Benedek GB (1970) A study of Brownian motion using light scattering. Am J Physiol 38:575–585
6. Madani F, Perálvarez-Marín A, Gräslund A (2011) Liposome model systems to study the endosomal escape of cell-penetrating peptides: transport across phospholipid membranes induced by a proton gradient. J Drug Deliv 2011:1–7
7. Magzoub M, Kilk K, Eriksson LEG, Langel Ü, Gräslund A (2001) Interaction and structure induction of cell-penetrating peptides in the presence of phospholipid vesicles. Biochim Biophys Acta 1512:77–89
8. Bárány-Wallje E, Andersson A, Gräslund A, Mäler L (2004) NMR solution structure and position of transportan in neutral phospholipid bicelles. FEBS Lett 567:265–269
9. Lindberg M, Järvet J, Langel Ü, Gräslund A (2001) Secondary structure and position of the cell-penetrating peptide transportan in SDS micelles as determined by NMR. Biochemistry 40:3141–3149
10. Lindberg M, Biverståhl H, Gräslund A, Mäler L (2003) Structure and positioning comparison of two variants of penetratin in two different membrane mimicking systems by NMR. Eur J Biochem 270:3055–3063
11. Vasconcelos L, Madani F, Arukuusk P, Pärnaste L, Gräslund A, Langel Ü (2014) Effects of cargo molecules on membrane perturbation caused by transportan10 based cell-penetrating peptides. Biochim Biophys Acta 1838: 3118–3129
12. Salomone F, Cardarelli F, Di Luca M, Boccardi C, Nifosì R, Bardi G, Di Bari L, Serresi M, Beltram F (2012) A novel chimeric cell-penetrating peptide with membrane-disruptive properties for efficient endosomal escape. J Control Release 163:293–303
13. Marshall AG (1978) Biophysical chemistry, principles, techniques and applications, 1st edn. John Wiley, New York, NY, pp 364–367
14. Berova N, Nakanishi K, Woody RW (2000) Circular dichroism, principles and applications, 2nd edn. Wiley-VCH Inc, New York, USA, pp 1–35, 55–95, 601–620

15. Eiríksdóttir E, Konate K, Langel Ü, Divita G, Deshayes S (2010) Secondary structure of cell-penetrating peptides controls membrane interaction and insertion. Biochim Biophys Acta 1798:1119–1128
16. Arukuusk P, Pärnaste L, Margus H, Eriksson NK, Vasconcelos L, Padari K, Pooga M, Langel Ü (2013) Differential endosomal pathways for radically modified peptide vectors. Bioconjug Chem 24:1721–1732
17. Mäler L (2013) Solution NMR studies of cell-penetrating peptides in model membrane systems. Adv Drug Deliv Rev 65:1002–1011
18. Wüthrich K (2001) The way to NMR structures of proteins. Nat Struct Biol 8:923–925
19. Wüthrich K (1986) NMR of proteins and nucleic acids. Wiley & Sons, USA
20. Wüthrich K, Wider G, Wagner G, Braun W (1982) Sequential resonance assignments as a basis for determination of spatial protein structures by high-resolution proton nuclear magnetic-resonance. J Mol Biol 155:311–319
21. Wüthrich K (1990) Protein-structure determination in solution by NMR-spectroscopy. J Biol Chem 265:22059–22062
22. Thorén PEG, Persson D, Esbjörner EK, Goksör M, Lincoln P, Nordén B (2004) Membrane binding and translocation of cell-penetrating peptides. Biochemistry 43: 3471–3489
23. Magzoub M, Eriksson LEG, Gräslund A (2002) Conformational states of the cell-penetrating peptide penetratin when interacting with phospholipid vesicles: effects of surface charge and peptide concentration. Biochim Biophys Acta 1563:53–63
24. Magzoub M, Eriksson LEG, Gräslund A (2003) Comparison of the interaction, positioning, structure induction and membrane perturbation of cell-penetrating peptides and non-translocating variants with phospholipid vesicles. Biophys Chem 103:271–288
25. Guterstam P, Madani F, Hirose H, Takeuchi T, Futaki S, El Andaloussi S, Gräslund A, Langel Ü (2009) Elucidating cell-penetrating peptide mechanisms of action for membrane interaction, cellular uptake, and translocation utilizing the hydrophobic counter-anion pyrenebutyrate. Biochim Biophys Acta 1788:2509–2517
26. Niesman MR, Khoobehi B, Peyman GA (1992) Encapsulation of sodium fluorescein for dye release studies. Invest Ophthalmol Vis Sci 33: 2113–2119
27. Schwarz G, Arbuzova A (1995) Pore kinetics reflected in the dequenching of a lipid vesicle entrapped fluorescent dye. Biochim Biophys Acta 1239:51–57
28. Futaki S, Suzuki T, Ohashi W, Yagami T, Tanaka S, Ueda K, Sugiura Y (2001) Arginine-rich peptides. An abundant source of membrane-permeable peptides having potential as carriers for intracellular protein delivery. J Biol Chem 276:5836–5840
29. Ziegler A, Seeling J (2011) Contributions of glycosaminoglycan binding and clustering to the biological uptake of the nonamphipathic cell-penetrating peptide WR_9. Biochemistry 50:4650–4664
30. Ziegler A (2008) Thermodynamic studies and binding mechanisms of cell-penetrating peptides with lipids and glycosaminoglycans. Adv Drug Deliv Rev 60:580–597
31. Bárány-Wallje E, Keller S, Serowy S, Geibel S, Pohl P, Bienert M, Dathe M (2005) A critical reassessment of penetratin translocation across lipid membranes. Biophys J 89:2513–2521
32. Magzoub M, Pramanik A, Gräslund A (2005) Modeling the endosomal escape of cell-penetrating peptides: transmembrane pH gradient driven translocation across phospholipid bilayers. Biochemistry 44:14890–14897
33. Björklund J, Biverståhl H, Gräslund A, Mäler L, Brzezinski P (2006) Real-time transmembrane translocation of penetratin driven by light-generated proton pumping. Biophys J 91:29–31
34. Terrone D, Sang SLW, Roudaia L, Silvius JR (2003) Penetratin and related cell-penetrating cationic peptides can translocate across lipid bilayers in the presence of a transbilayer potential. Biochemistry 42:13787–13799
35. Madani F, Lindberg S, Langel Ü, Futaki S, Gräslund A (2011) Mechanisms of cellular uptake of cell-penetrating peptides. J Biophys 2011:414729
36. Madani F, Abdo R, Lindberg S, Hirose H, Futaki S, Langel Ü, Gräslund A (2013) Modeling the endosomal escape of cell-penetrating peptides using a transmembrane pH gradient. Biochim Biophys Acta 1828: 1198–1204
37. Rigaud JL, Pitard B, Levy D (1995) Reconstitution of membrane-proteins into liposomes—application to energy-transducing membrane-proteins. Biochim Biophys Acta 1231:223–246
38. Maiolo JR, Ferrer M, Ottinger EA (2005) Effects of cargo molecules on the cellular uptake of arginine-rich cell-penetrating epeptides. Biochim Biophys Acta 1712:161–172
39. Biondi B, Calderan A, Guiotto A, Ruzza P (2008) A comparative studies on lipid affinity of cell penetrating peptides in presence or absence of cargo. J Pept Sci 14:178–178

40. El-Andaloussi S, Järver P, Johansson HJ, Langel Ü (2007) Cargo-dependent cytotoxicity and delivery efficacy of cell-penetrating peptides: a comparative study. Biochem J 407:285–292
41. Bárány-Wallje E, Gaur J, Lundberg P, Langel Ü, Gräslund A (2007) Differential membrane perturbation caused by the cell penetrating peptide Tp10 depending on attached cargo. FEBS Lett 581:2389–2393
42. Oesterhelt D, Walther S (1974) Isolation of the cell membrane of *Halobacterium halobium* and its fractionation into red and purple membrane. Methods Enzymol 31:667
43. Nayar R, Hope MJ, Cullis PR (1989) Generation of large unilamellar vesicles from long-chain saturated phosphatidylcholines by extrusion technique. Biochim Biophys Acta 986:200–206
44. Macdonald RC, Macdonald RI, Menco BPM, Takeshita K, Subbarao NK, Hu LR (1991) Small-volume extrusion apparatus for preparation of large, unilamellar vesicles. Biochim Biophys Acta 1061:297–303
45. Frisken BJ, Asman C, Patty PJ (2000) Studies of vesicle extrusion. Langmuir 16:928–933
46. Mayer LD, Hope MJ, Cullis PR (1986) Vesicles of variable sizes produced by a rapid extrusion procedure. Biochim Biophys Acta 858: 161–168
47. Paternostre MT, Roux M, Rigaud JL (1988) Mechanisms of membrane-protein insertion into liposomes during reconstitution procedures involving the use of detergents. 1. Solubilization of large unilamellar liposomes (prepared by reverse-phase evaporation) by Triton X-100, octyl glucoside, and sodium cholate. Biochemistry 27:2668–2677
48. Rigaud JL, Paternostre MT, Bluzat A (1988) Mechanisms of membrane-protein insertion into liposomes during reconstitution procedures involving the use of detergents. 2. Incorporation of the light-driven proton pump bacteriorhodopsin. Biochemistry 27: 2677–2688
49. Heberle J (2000) Proton transfer reactions across bacteriorhodopsin and along the membrane. Biochim Biophys Acta 1458:135–147

Chapter 6

Determining the Effects of Membrane-Interacting Peptides on Membrane Integrity

William C. Wimley

Abstract

In the study of cell-penetrating and membrane-translocating peptides, a fundamental question occurs as to the contribution arising from fundamental peptide–membrane interactions, relative to the contribution arising from the biology and energy of the cell, mostly occurring in the form of endocytosis and subsequent events. A commonly used approach to begin addressing these mechanistic questions is to measure the degree to which peptides can interact with, and physically disrupt, the integrity of synthetic lipid bilayers. Here, we describe a set of experimental methods that can be used to measure the potency, kinetics, transience, and the effective size of peptide-induced membrane disruption.

Key words Vesicle leakage, Bilayer permeabilization, Pore formation, Leakage assay, Terbium, ANTS, DPX, Transient leakage, Pore size

1 Introduction

Cell-penetrating peptides (CPPs), including membrane-translocating peptides (MTPs), have shown significant promise in the laboratory over the last couple of decades [1–9]. There are examples of peptide-dependent in vitro delivery of small molecules, peptides, proteins, oligonucleotides, and nanoparticles. CPPs and MTPs, by definition, enable the movement of polar molecules across membrane barriers, but there are many possible mechanisms by which this can happen. Some are active, driven by cellular processes such as endocytosis, and some are passive, driven directly by the physical chemistry of peptide–membrane interactions. Understanding the contribution of these two possible mechanisms is the key to improving and refining peptide-dependent delivery strategies.

To assess the contribution of peptide–membrane interactions to the biological activity of CPPs and MTPs, cell membranes can be modeled by synthetic lipid vesicles. While synthetic bilayers are not exact mimics of cell membranes, there is much overlap in the

Ülo Langel (ed.), *Cell-Penetrating Peptides: Methods and Protocols*, Methods in Molecular Biology, vol. 1324,
DOI 10.1007/978-1-4939-2806-4_6,

physical chemistry of peptide interactions with synthetic and natural membranes. Thus, synthetic bilayers can be used as a simple and convenient model system with which to explore the fundamental interactions, and to explore the effects of peptides on membrane integrity. There are many experimental methods that have been developed to explore these effects. The information provided by such methods provide important information about the potential mechanisms of action of cell-penetrating and membrane-translocating peptides.

Here, we will describe a set of protocols that can be used to probe the effects of cell-penetrating and membrane-translocating peptides on the integrity of lipid bilayer membranes, both as a test of potential cytotoxicity and as a way of inferring mechanism of action. First, we will describe the *ANTS/DPX assay* [10, 11] and the *Tb3+/DPA assay* [12] that both can be used to measure the leakage of small-molecule probes from lipid vesicles. Second, we will describe the *equilibrium pore assay* [13] that can be used to measure probe leakage and simultaneously assess whether the leakage pathway in vesicles is a transient or an equilibrium phenomenon. This is an important clue to mechanism. Third, we will describe a *dextran escape assay* [14] that can be used to assess whether the peptide-induced pathways through lipid bilayers can enable the passage of macromolecules. The molecules used in these assays are shown in Fig. 1.

Some researchers have modeled membrane-permeabilizing peptides as membrane-spanning, proteinacious pores, sometimes drawing them as rings of parallel helices in a barrel-stave pattern across the membrane. However, experimental support for the existence of such explicit peptide pores is very rare [15–18]. Even the archetypal "pore-forming peptide," melittin, cannot be described accurately with a proteinaceous pore model under many conditions [15, 19, 20]. As a result, alternate, overlapping mechanistic models have been proposed that describe most peptide-induced membrane leakage as cooperative destabilization of membrane integrity, perhaps in the vicinity of peptide-rich domain in the bilayer [18, 21]. Even for the macromolecule-sized poration observed for a few peptides [14], long-lived, "barrel-stave" pores seem improbable as that structure would require a stable, continuous "ring" of 20 or more peptides to enable macromolecule passage through the bilayer. Instead, "pores" formed by peptides, including CPPs, will likely be caused by dynamic, cooperative destabilization of membrane structure within peptide-rich membrane domains, perhaps similar to the "toroidal pores" described by some researchers [22–24].

To fully communicate the effect that a peptide has on the integrity of a lipid bilayer, four properties must be described: potency, kinetics, transience, and pore size. The *potency of a peptide* describes the ability of a peptide to disrupt a lipid bilayer, on a

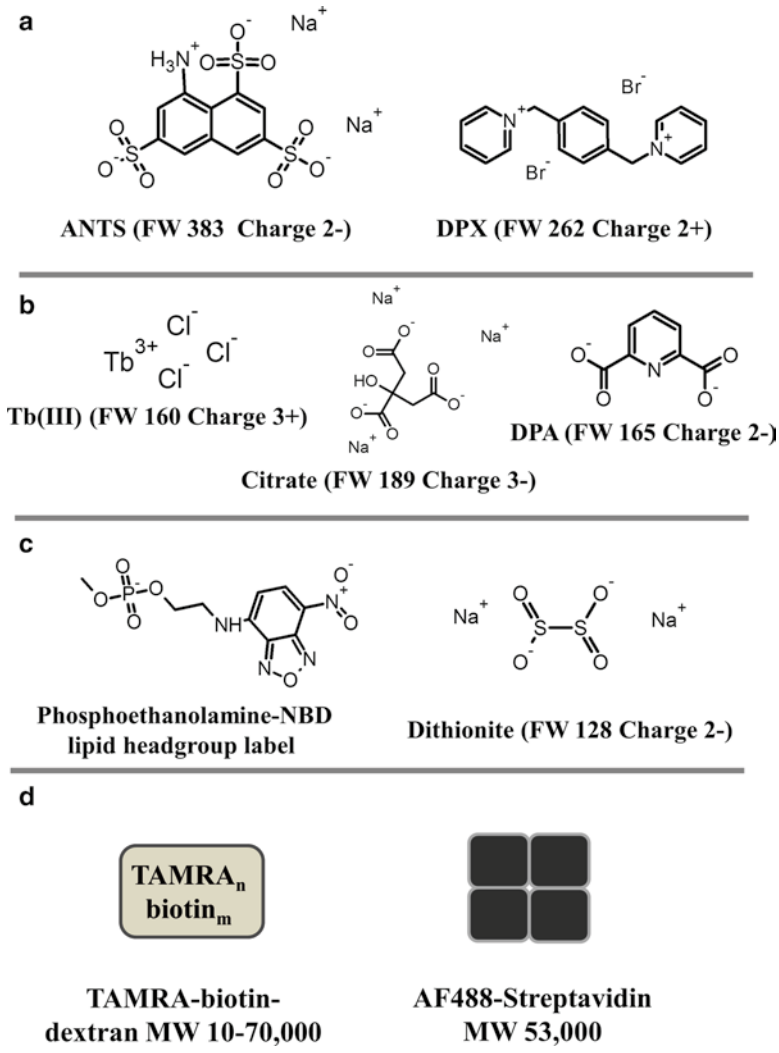

Fig. 1 The probe compounds used in the vesicle leakage assays described in this chapter. Counterions are shown when they contribute to osmolarity. Formula weights (FW) are for the probe without counterions to indicate the size of the molecule that must pass through the membrane to report on permeabilization. (**a**) ANTS/DPX assay; (**b**) Tb^{3+}/DPA assay; (**c**) The second part of the equilibrium pore assay, which also uses the Tb^{3+}/DPA assay; (**d**) Dextran release assay

peptide per lipid basis. Potency is best described using the ratio of *bound* peptide to total lipid (P_{bound}:L). The overall sample P:L sets only an upper limit on the possible P_{bound}:L. In order to determine P_{bound}, membrane binding must be measured. Fractional peptide binding can be measured by equilibrium dialysis [25], fluorescence titration [26], circular dichroism titration, filter binding, and other methods. Potency is important to note because almost any membrane-interacting peptide will disrupt bilayers at a high

enough P_{bound}:L (P:L ≥1:50), a concentration range that is likely not relevant to the biological activity of CPPs and MTPs. The most informative way to express potency is to record the P_{bound}:L that causes 50 % effect, or PL_{50}. This parameter ranges from ≥1, for peptides that have no effect on bilayers, to ≤1:2000, for the most potent membrane-disrupting peptides known [13, 27]. Real examples of potency measurements are shown in Fig. 2. Note that all the curves have a similar shape, an observation that holds true across many studies.

The *kinetics of leakage* describe the rate at which leakage occurs and the rate at which it stops. Rate measurements provide important information about the permeabilization mechanism. Peptide-induced leakage of solutes from lipid vesicles can range from almost instantaneous ($t_{1/2}$ < 30 s) to very slow with $T_{1/2}$ > 10 h. However, most peptide-induced leakage occurs within 2–30 min after

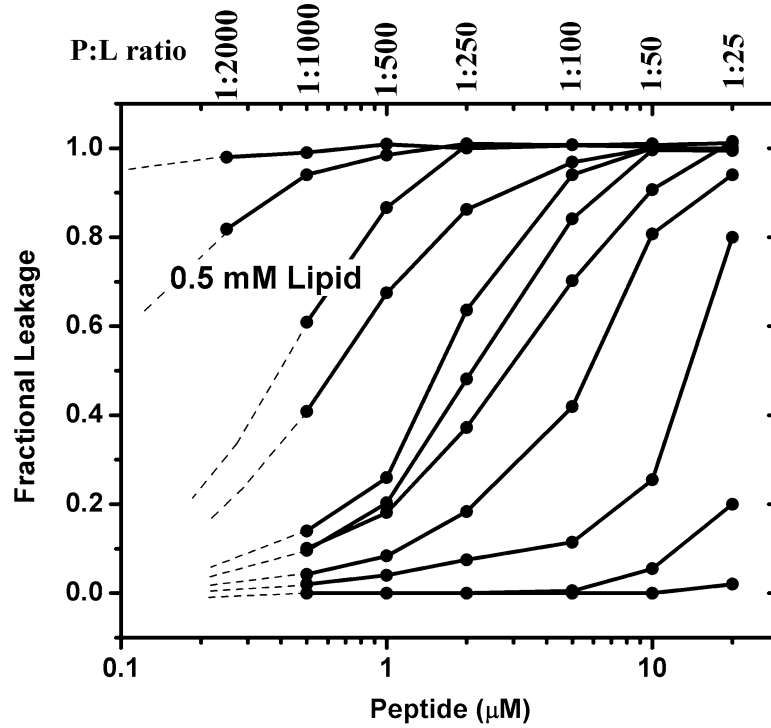

Fig. 2 Various leakage potency curves for membrane-active peptides. These data are from the author's laboratory and were selected from multiple papers and unpublished experiments. They were not all collected under the same conditions but are plotted together and scaled to 0.5 mM lipid. The plots show the range of possible potencies. The most potent peptides known can permeabilize vesicles efficiently at P:L ≤ 1:1000. However, most membrane active peptides cause permeabilization at P:L ≥ 1:100. Under some conditions, cell-penetrating peptides permeabilize lipid vesicles, usually in the range P:L ≥ 1:100

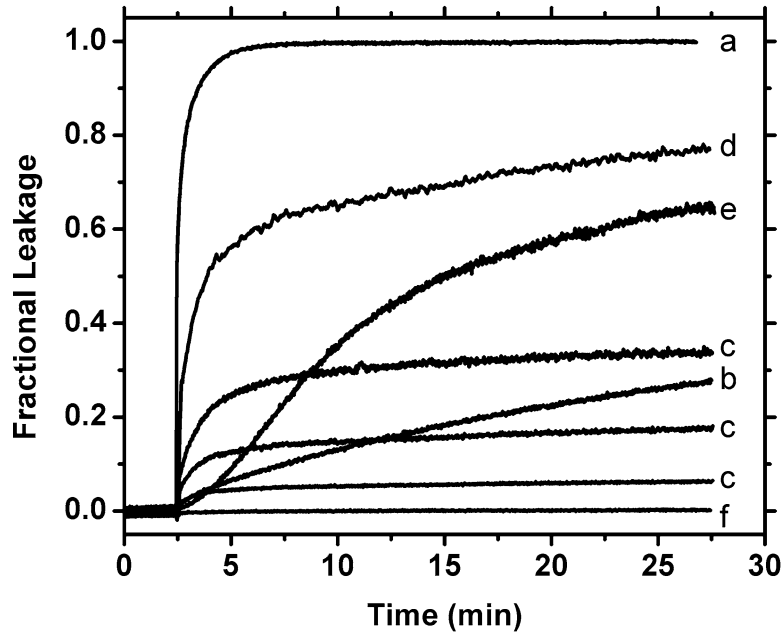

Fig. 3 Various leakage time course curves from the author's laboratory. These data, which were selected from multiple papers and unpublished experiments, show a variety of possible kinetic behaviors. They are not all collected under the same conditions but are plotted together here to serve as examples of the range of possible kinetic behaviors. Behaviors include (*a*) rapid total permeabilization, (*b*) slow total permeabilization, (*c*) transient burst of leakage with zero background leakage (three examples are shown for three P:L values), (*d*) transient burst with slow background leakage, (*e*) delayed leakage, and (*f*) no leakage. Leakage kinetics provide information about possible mechanisms of membrane permeabilization by peptides. Note that curves *c*, *d*, and *e* can only be explained by transient permeabilization

peptide addition. Various real examples of leakage time courses are shown in Fig. 3, demonstrating the range of likely behaviors.

The *transience of permeabilization* describes the lifetime of the disruption of bilayer integrity. Surprisingly, the majority of published examples of peptide-induced membrane permeabilization occur through transient, non-equilibrium processes [13, 28]. *Leakage occurs only in the minutes immediately after peptide addition*. The system then relaxes to a state where leakage slows or stops completely despite the continued presence of the peptides in the bilayer and the continued presence of entrapped probes. *Transient leakage cannot be correctly modeled as an equilibrium state of the membrane*. Even the archetypal pore-forming peptide melittin causes transient, non-equilibrium permeabilization at moderate peptide concentrations (P_{bound}:L ≤ 1:100). The reason for transient leakage has not been definitively proven. The leading hypothesis is that the initial binding of peptide to the surface of the

bilayer causes an imbalance of mass, charge or surface tension, which is dissipated by the stochastic, transient failure of the bilayer structure. When the asymmetry of peptide distribution has been relieved, the permeabilization no longer occurs. Transient membrane disruption means that simulations and structural modeling based on equilibrium phenomena are unlikely to reveal true mechanistic details.

The "*pore*" *size* allows a description of the size of the disruption of bilayer integrity. Peptide-induced release of molecules from lipid vesicles is generally probed using small-fluorescent probes of a few hundred Daltons. But important information on the characteristics of the membrane disruption can also be obtained by examining the dependence of membrane permeabilization on the size of the probe. Some membrane-permeabilizing peptides, at high concentration (P_{bound}:L ≥ 1:50), disrupt vesicles catastrophically [19, 29, 30], such that all entrapped probes escape equally well, independent of size. However, most peptides do not release macromolecules at all, indicating that only small pores are formed. A few peptides show a distinct size dependence for leakage, indicating a more well defined pathway for solute escape [31]. Information on pore size provides important clues to the mechanism of peptide-induced disruption of lipid bilayer membranes.

In the sections that follow, methods are described for characterizing the peptide-induced disruption of lipid bilayer membranes with respect to the four parameters described above. Specifically we describe two methods for assaying the potency and kinetics of probe release, a method for measuring both the potency and the transience of membrane disruption in the same vesicles, and a method for measuring the release of macromolecules from lipid vesicles, which can be used to probe the size of the "pore" in the membrane.

2 Materials

2.1 ANTS/DPX Leakage Assay

1. Vesicle preparation buffer: 10 mM phosphate or other buffer compound, 6 mM ANTS (8-aminonaphthalene-1,3,6-trisulfonic acid disodium salt), 20 mM DPX (*p*-xylene-bis-pyridinium bromide). No added NaCl (*see* **Note 1**). Any pH between 4.0 and 8.0.
2. Vesicle elution buffer: 10 mM phosphate or other buffer compound, 40 mM NaCl (*see* **Note 1**).
3. Lipids of user's choice dissolved in chloroform at 25 mg/ml.
4. 10 % v/v reduced Triton X-100 in water (*see* **Note 2**).
5. Lipid extruder, with drain disks and 0.1 μm pore size Nuclepore polycarbonate filters.

6. Sephadex G200 gel filtration resin or 5 ml 100 k MWCO centrifugal concentrator filter units.
7. Glass column for gel filtration of 25 × 2.5 cm.

2.2 Tb^{3+}/DPA Leakage Assay

1. Vesicle preparation buffer: 10 mM TES, pH 7.2, 50 mM sodium citrate, 25 mM $TbCl_3$ (Terbium(III) chloride, hexahydrate). No added NaCl (*see* **Notes 3** and **4**).
2. Vesicle elution buffer: 10 mM TES pH 7.2, 150 mM NaCl (*see* **Note 4**).
3. Terbium assay buffer: 150 μM dipicolinic acid (DPA) in vesicle elution buffer.
4. Lipids of user's choice dissolved in chloroform at 25 mg/ml.
5. 10 % v/v Reduced Triton X-100 (*see* **Note 2**).
6. Lipid extruder, with drain disks and 0.1 μm pore size Nuclepore polycarbonate filters.
7. Sephadex G200 gel filtration resin or 5 ml 100 k MWCO centrifugal concentrator filter units.
8. Glass column for gel filtration of 25 × 2.5 cm.

2.3 The Equilibrium Pore Assay

1. All materials for the Tb^{3+}/DPA assay, above.
2. DOPE-NBD(1,2-dioleoyl-sn-glycero-3-phosphoethanolamine-*N*-(7-nitro-2-1,3-benzoxadiazol-4-yl) (ammonium salt)), 1 mg/ml in chloroform.
3. Sodium dithionite (sodium hydrosulfite), 0.6 M, freshly prepared, in 1.0 M dibasic sodium phosphate buffer, pH 10.0 (*see* **Note 5**).

2.4 Synthesis of TAMRA-Biotin-Dextran

1. Reaction buffer: 50 mM potassium phosphate buffer, pH 8.4.
2. Tentagel-S-NH2 solid phase peptide synthesis resin.
3. 10,000, 40,000, or 70,000 Da amino dextran with at least 4, 10, or 12 amino groups per dextran molecule, respectively.
4. TAMRA-SE (5-and 6-TAMRA (mixed isomers) succinamidyl ester).
5. Biotin-SE (biotin succinamidyl ester).

2.5 Dextran Release Assay

1. Vesicle preparation (and elution) buffer: Any buffer of user's choice with 1 mg/ml TAMRA-biotin-dextran.
2. Vesicle elution buffer: Same as vesicle preparation except without TAMRA-biotin-dextran.
3. Dextran assay buffer: Vesicle preparation buffer with 40 nM AlexaFluor488-streptavidin.
4. Biotin, 0.1 mM in buffer.
5. Lipids of user's choice dissolved in chloroform at 25 mg/ml.

6. 10 % v/v reduced Triton X-100 in water.
7. Sephadex G200 gel filtration resin or 5 ml 100 k MWCO centrifugal concentrator filter units.
8. Glass column, 25 × 2.5 cm.

3 Methods

All the methods described below rely on the preparation of unilamellar (single bilayer) lipid vesicles, with a probe molecule, or probe molecules, entrapped inside. The probe molecules are removed from the external solution after vesicle preparation as described such that the release of entrapped probes can be measured by fluorescence. The so-called "large" unilamellar vesicles (LUV) of 0.1 μm diameter, made by extrusion [32], are the most commonly used synthetic vesicle system.

3.1 Preparation of Large Unilamellar Vesicles with Entrapped Probes

1. Mix a total of 250 μmol of lipids in chloroform in an appropriate glass vessel. The lipid composition is defined by the user's experimental questions. Dry off the bulk of the chloroform under a stream of nitrogen or in a rotary evaporator. Place the vessel in high vacuum for at least 4 h to evaporate any traces of remaining solvent.
2. Add 5 ml of the appropriate vesicle preparation buffer containing the probes to be entrapped (see below). This will make a suspension of 50 mM lipids (*see* **Note 6**). Gently warm and swirl the buffer until the dried lipid film is completely suspended (*see* **Note 7**).
3. To properly entrap the solutes and buffer ions within the lipid bilayers, repeatedly freeze the lipid suspension in liquid nitrogen, or in a dry ice/ethanol bath, and thaw the suspension in a warm (50 °C) water bath. Repeat this 10 times for small-molecule probes, 20 times for macromolecule probes.
4. Repeatedly extrude the lipid suspension through two stacked Nuclepore polycarbonate membranes, with 0.1 μm diameter pores, placed on top of a polymer mesh drain disk.
5. Separate the vesicles with their entrapped contents from external non-entrapped probe molecules using gel filtration chromatography. Prepare a 25 × 2.5 cm low pressure, clear glass column of Sephadex G200. Slowly add vesicles and continue buffer flow through the column. Monitor the movement of vesicles and probes through the column visually, or with a handheld UV light. The leading vesicle band will be opalescent. The trailing external probe band (if it is ANTS or TAMRA-biotin-dextran) band will be visibly fluorescent when illuminated with long wave UV light. The trailing Tb^{3+}/citrate

band will not be visible under these conditions. Manually collect the fractions containing the highest concentration of lipid (*see* **Note 8**).

6. As an alternative method of separating external probes from entrapped probes, 5 ml 100 kDa MWCO centrifugal sample concentrators can be used. Concentrate the vesicle samples, replace the lost buffer with vesicle elution buffer, and resuspend the vesicles. Repeat at least ten times using a refrigerated centrifuge. Save the individual flow-through fractions after repeat number 5 for analysis (*see* **Notes 1** and **4**). Assay the flow-through fractions for external probe concentration. Measure entrapped probe by lysing an aliquot of vesicles with 0.2 % v/v reduced Triton X-100 (*see* **Note 9**). Stop replacing buffer when the external probe concentration is less than 5 % of the entrapped probe concentration in the vesicles.
7. Measure lipid concentration in the final solution using the method of Bartlett [33] or Stewart [34].

3.2 ANTS/DPX Leakage Methods

1. Prepare a dried lipid sample as described in Subheading 3.1.
2. Suspend the lipids in the vesicle preparation buffer, containing ANTS and DPX.
3. Freeze–thaw and extrude lipid suspension as described in Subheading 3.1 to make large unilamellar vesicles (LUV).
4. Separate vesicles from external ANTS/DPX using gel filtration (Subheading 3.1, **step 5**) or centrifugal filtration (Subheading 3.1, **step 6**). The external solution should be vesicle elution buffer (*see* **Notes 1** and **10**).
5. To measure the leakage of ANTS/DPX, dilute vesicles in vesicle elution buffer to a concentration of 0.5 mM lipid. Add peptide to individual samples at concentrations from 0.5 μM (P:L = 1:1000) to 50 μM (P:L = 1:10) (*see* **Note 11**).
6. Monitor ANTS fluorescence using a fluorimeter (excitation = 350 nm; emission = 530 nm) or a fluorescence plate reader (excitation filter wavelength/bandpass = 340/11; emission 530/25). In a plate reader, do not use a dichroic mirror, and make sure there is no default UV filter in the excitation path) (*see* **Note 12**).
7. When leakage has stopped or slowed significantly (generally 10–60 min) measure the final ANTS fluorescence. Then add 2 % v/v of 10 % Triton X-100 (0.2 % v/v final concentration of Triton) to lyse the vesicles and measure fluorescence corresponding to 100 % ANTS release.
8. Calculate fractional leakage as $(F_{\text{sample}} - F_{\text{initial}})/(F_{\text{lysed}} - F_{\text{initial}})$ (*see* **Note 13**).

3.3 Tb^{3+}/DPA Leakage Methods

1. Prepare a dried lipid sample as described in Subheading 3.1.
2. Suspend the lipids in vesicle preparation buffer, containing Tb^{3+} and citrate.
3. Freeze–thaw and extrude the lipid suspension as described in Subheading 3.1 to make large unilamellar vesicles (LUV).
4. Separate vesicles from external Tb^{3+}/citrate using gel filtration (Subheading 3.1, **step 5**) or centrifugal filtration (Subheading 3.1, **step 6**). The external solution in either case should be vesicle elution buffer (*see* **Notes 4** and **10**).
5. To measure leakage of Tb^{3+} and DPA, dilute vesicles to a concentration of 0.5 mM in terbium assay buffer which contains 150 μM DPA. Add peptide to individual samples at concentrations from 0.5 μM (P:L = 1:1000) to 50 μM (P:L = 1:10) (*see* **Note 11**).
6. Monitor Tb^{3+}/DPA phosphorescence using a fluorimeter (excitation = 270 nm; emission = 490 nm or 545 nm) or a plate reader (excitation filter wavelength/bandpass 270/15; emission 540/30; use no dichroic mirrors or default UV filters) (*see* **Note 12**).
7. When leakage has stopped or slowed significantly (typically 10–60 min) measure final Tb^{3+}/DPA phosphorescence. Then add 2 % v/v of 10 % reduced Triton-X100 (final concentration 0.2 % v/v) to lyse the vesicles and measure 100 % Tb^{3+}/DPA phosphorescence corresponding to 100 % release.
8. Calculate fractional leakage as $(F_{sample} - F_{initial})/(F_{lysed} - F_{initial})$.

3.4 The Equilibrium Pore Assay Methods

In the equilibrium pore assay, an additional measurement is added to the Tb^{3+}/DPA assay described above in Subheading 3.3.

1. Prepare Tb^{3+}-containing vesicles exactly as described above, except replace 1 mol% of the PC lipid with NBD-DOPE lipid.
2. Measure Tb^{3+}/DPA leakage exactly as described above, except that the experimental samples are not lysed with Triton X-100. A separate sample is lysed to determine the Tb^{3+}/DPA intensity for 100 % leakage.
3. Allow transient processes to reach completion in experimental samples by equilibrating for at least 4 h. Overnight equilibration is also possible.
4. Add 5 % v/v of the fresh 0.6 M dithionite solution to the experimental samples.
5. Measure the NBD intensity loss in samples as a function of time for 60 min after adding dithionite. Also measure NBD loss in intact vesicles and in Triton X-100 lysed vesicles. The two control samples provide measurements of the rate of NBD fluorescence loss in intact vesicles, when some of it is not

exposed to the dithionite, and in Triton X-100, when it is 100 % exposed (*see* **Note 14**).

6. Determine the % NBD that is quenchable from the breakpoint between rapid quenching and slow quenching. In intact, control vesicles about 55 % of the NBD lipids are exposed on the outer monolayer and are rapidly quenched by dithionite. The remainder of the NBD lipids are on the inner monolayer, not exposed to dithionite. They are quenched very slowly as small amounts of dithionite equilibrate across the bilayer. In Triton-lysed vesicles 100 % of the NBD is effectively "exposed" and is rapidly quenched. Peptides that cause transient pores will not (at equilibrium) substantially increase the fraction of NBD that is accessible. Peptides that cause equilibrium pores allow for most of the NBD to be rapidly quenched at equilibrium because equilibrium pores enable uninhibited entry of dithionite into the vesicle interior.

3.5 Synthesis of TAMRA-Biotin-Dextran

1. Prepare 50 mg dextran, 10 mg TAMRA-SE, and 2 mg of biotin-SE in separate vials.
2. Dissolve the dextran in 2 ml reaction buffer just prior to labeling.
3. Dissolve each of the two labels in 0.4 ml of reaction buffer just prior to labeling. Mix the two labels together first, and then add them immediately to the dextran solution.
4. React at room temperature for 4 h with gentle mixing.
5. After 4 h, add 0.3 g of the peptide synthesis resin to react with the remaining unreacted labels. Mix well for 30 min, spin down the resin and remove the supernate.
6. Split the supernatant into two 15 ml tubes, with ~1.5 ml of reaction mixture in each tube.
7. Add 12 ml of cold methanol to each tube to precipitate the dextran. Mix and incubate at 4 °C for 15 min.
8. Pellet the large amount of colored, dextran precipitate by centrifugation. Discard the supernate.
9. Wash pellet as above 5–10 times with 10 ml cold methanol. Stop washing when the supernatant is colorless.
10. Dry the methanol from the dextran pellet under vacuum, and then dissolve the dextran in distilled water and lyophilize.
11. If blockage of all available amino groups on the dextran is critical, dissolve the dual-labeled dextran at 100 mg/ml in water and add 5 % diisopropylethylamine and 5 % acetic anhydride. React for 30 min with mixing to acetylate amino groups. Precipitate the dextran with cold methanol as above, and wash at least five times with cold methanol. Dry the methanol off, dissolve the dextran in distilled water, and lyophilize.

3.6 Dextran Escape Methods

1. Prepare a dried lipid sample as described in Subheading 3.1.
2. Suspend the lipids in the vesicle preparation buffer containing TAMRA-biotin-dextran.
3. Freeze–thaw the lipid suspension 20 times and extrude as described in Subheading 3.1 to make large unilamellar vesicles (LUV).
4. Separate vesicles from external dextran using gel filtration (Subheading 3.1, **step 5**) or centrifugal filtration (Subheading 3.1, **step 6**).
5. To measure leakage of dextran, dilute vesicles to a concentration of 0.5 mM into assay buffer which contains 40 nM AlexaFluor488-Streptavidin (*see* **Note 10**). To individual samples, add peptide at concentrations from 0.5 μM (P:L = 1:1000) to 50 μM (P:L = 1:10) (*see* **Note 11**).
6. Monitor AlexaFluor488 fluorescence using a fluorimeter (excitation = 488 nm; emission = 510 nm) or a fluorescence plate reader (excitation filter wavelength/bandpass 480/30; emission 520/30; 505 nm dichroic mirror) (*see* **Note 12**).
7. Release of TAMRA-biotin-dextran causes a decrease in Alexafluor488 intensity due to quenching. When dextran leakage has stopped (typically 10–60 min) measure final AlexaFluor488 fluorescence. Then add 2 % v/v of 10 % reduced Triton-X100 (final concentration 0.2 % v/v) to lyse the vesicles. Measure AlexaFluor488 fluorescence corresponding to complete dextran release (*see* **Note 15**).
8. Calculate fractional leakage as $(F_{\text{initial}} - F_{\text{sample}})/(F_{\text{initial}} - F_{\text{lysed}})$.

4 Notes

1. The osmolarity of the ANTS and DPX in the vesicle preparation buffer must equal the osmolarity of the NaCl in the vesicle elution buffer. Assuming osmotic coefficients of 1 then 3× [ANTS] + 3× [DPX] must equal 2× NaCl. In this protocol 6 mM ANTS and 20 mM DPX = ~40 mM NaCl. The buffers recommended here have 0 NaCl in the vesicle preparation buffer and 40 mM in the vesicle elution buffer. However, osmotic balance will be maintained in any buffer system in which the vesicle elution buffer has 40 mM *more* monovalent salt than the vesicle preparation buffer.
2. It is critical to use "reduced" Triton X-100 for all applications where fluorescence is being used. Ordinary Triton X-100 from scientific supply companies has a very large fluorescent background signal.

3. Terbium (III) is not very soluble in water unless it is chelated. Citrate is used to chelate the metal, but is readily displaced by DPA when DPA is present. Furthermore, Tb^{3+} cannot be used in the presence of phosphate, so an organic buffer such as TES or HEPES must be used.
4. The osmolarity of the $TbCl_3$ and Na_3Citrate in the vesicle preparation buffer must equal the osmolarity of the NaCl in the vesicle elution buffer. Assuming osmotic coefficients of 1, and ignoring the complex formation between Tb^{3+} and citrate, then 4× [$TbCl_3$] + 4× [Na_3Citrate] must equal 2× [NaCl]. In this protocol, 25 mM $TbCl_3$ and 50 mM Na_3Citrate = 150 mM NaCl. The buffers recommended here have 0 NaCl in the vesicle preparation buffer and 150 mM NaCl in the vesicle elution buffer. However, osmotic balance will be maintained in any buffer system in which the vesicle elution buffer has 150 mM *more* monovalent salt than the vesicle preparation buffer. In some work we have used 50 mM $TbCl_3$ and 100 mM Na citrate in vesicle preparation and thus used 300 mM NaCl in vesicle elution.
5. Sodium dithionite should be handled and stored with special care as it can spontaneously heat and combust when exposed to air or atmospheric humidity.
6. The values for lipid amount and buffer volume are for a preparation of 5 ml of 50 mM lipid. Reduce both proportionally if smaller volumes are needed.
7. For some lipid compositions, as much as 15 min will be required to get the lipid film into suspension. Do not vortex lipids at any time, as this can lead to foaming.
8. It is important at this point to verify that a good separation between entrapped and external probe has been obtained. This can be measured by separating an aliquot of vesicles using a filter or spin concentrator and measuring the concentration of the probe (ANTS,Tb^{3+},TAMRA-biotin-dextran) in the flow-through. Compare the flow-through concentration to the concentration in the retained vesicles (measured after lysing with 0.2 % final v/v of Triton X-100). The external probe concentration should be less than 5 % of the entrapped probe concentration. External ANTS can also be measured by titrating DPX into a sample of intact vesicles and measuring the quenching of ANTS fluorescence [10, 11]. External Tb^{3+} can be measured by adding DPA and measuring the increase in fluorescence. External TAMRA-biotin-dextran can be measured by adding external AlexaFluor488-streptavidin and measuring the quenching of AF488 relative to a parallel sample with no TAMRA-biotin-dextran.

9. Gel filtration and centrifugal concentration each have advantages and disadvantages. Gel filtration can be used to process large vesicle samples, and subjects the vesicles to fewer strong shear forces than centrifugation. However, gel filtration significantly dilutes the vesicles. Occasionally, due to imperfections in column packing, for example, separation of vesicles and external probe will be poor, leading to an entire failed batch of vesicles. Centrifugal buffer exchange is harsher on the vesicles due to physical shear forces of pelleting and resuspension, as well as temperatures of ~45 °C during long centrifugation. However, we have found little or no evidence that vesicles are negatively affected by these conditions. This approach also allows the final vesicle concentration to be determined by the researcher at the final dilution step.
10. One can estimate the concentration of entrapped probe molecules in an experiment using trapped volume measurements. For standard PC lipid vesicles, a typical fractional probe entrapment is about ~0.0032 per mM lipid. Thus, if lipid concentration is expressed in mM units, then

$$[\text{Probe}]_{\text{Experiment}} = 0.0032 \times [\text{Probe}]_{\text{Original}} \times [\text{Lipid(mM)}]_{\text{Experiment}}$$

As an example calculation, assume vesicles are prepared in the presence of 6 mM ANTS. Then the external ANTS is removed by gel filtration, and an experiment is performed at 0.5 mM lipid. We expect to have about $0.0032 \times 6 \times 0.5 = 0.010$ mM, or 10 μM, ANTS in the experimental sample. Similarly, entrapment of 1 mg/ml TAMRA-biotin-dextran (25 μM) gives 40 nM dextran in an experiment with 0.5 mM lipid.

11. An LUV with an 0.1 μm diameter will have roughly 100,000 lipids, calculated by determining the sum of the inner and outer vesicle surface area and dividing by the area of a typical lipid molecule (~70 Å^2). Thus at P:L = 1:1000 there are about 100 peptides per vesicle. At P:L = 1:50 there are about 2000 peptides per vesicle. Furthermore, the entrapped volume of a single vesicle is about 4.5×10^{-19} l. Thus, entrapment of 6 mM ANTS, for example, places about 2000 ANTS molecules inside each vesicle. Entrapment of 1 mg/ml TAMRA-biotin-dextran (40 μM) entraps about 10 dextrans in each vesicle (*see* Table 1).
12. One should always assess whether a peptide is causing large-scale aggregation/fusion of vesicles by examining the sample for peptide-induced changes in light scattering and physical appearance (loss of opalescence, formation of visible peptide-vesicle aggregates, lipidic material falling out of suspension, etc.). Aggregation and fusion are extremely common artifacts in the cell-penetrating peptide literature because, in a typical experiment, polycationic peptides are mixed with anionic bilayers at

Table 1
The number of probe molecules entrapped per vesicle, and the number released per peptide (assuming 100 % release) for typical ranges of concentrations

		Peptide bound to lipid ratio					
Probe concentration (mM)	**Probes per vesicle**	**1:1000**	**1:500**	**1:250**	**1:100**	**1:50**	**1:25**
0.01	2.7	0.03	>0.1	>0.1	>0.1	>0.1	>0.1
0.1	27	0.27	0.1	0.1	>0.1	>0.1	>0.1
1	270	2.7	1.4	0.7	0.3	0.1	>0.1
10	2700	27	14	6.8	2.7	1.4	0.7
100	27,000	270	135	68	27	14	7

Notice that even relatively "potent" leakage only requires the release of a few probe molecules per peptide. Typical experimental conditions (e.g. 10 mM probe and P:L = 1:50) require that only 1–2 probe molecules are released per peptide over the course of a 20–60 min incubation

high concentration. This single artifact has likely caused decades of confusion about CPP mechanism of action because leakage of entrapped probes due to peptide-induced aggregation and fusion, while a common experimental observation, is likely to be completely unrelated to the biological activity of CPPs. To separate true membrane permeabilization from artifacts caused by aggregation and fusion, vesicle–vesicle interactions can be blocked by the addition of 4 mol % of PEG2000 lipids [35]. The effects of PEG2000 lipids on peptide-induced aggregation of vesicles are shown in Fig. 4. The effects of 4 % PEG lipids on membrane permeabilization, if it is not dependent on fusion, are small.

13. ANTS quenching is not a linear function of DPX concentration [10, 11] as assumed in this commonly used equation. If leakage is "all-or-none" then the fluorescence will nonetheless be a linear function of leakage [10, 11]. However, if the leakage is "graded" then the fluorescence will not be linear with leakage. One can correct for this nonlinearity using a standard curve of ANTS intensity versus DPX concentration [10] but only if the mechanism is known. In the literature linearity is generally assumed because the mechanism, graded versus all-or-none, is unknown. In any case, the discrepancy is not significant as long the initial quenching is not more than about 80 %. This is the reason the protocol described here uses DPX concentrations of only 20 mM.
14. Depending on the lipid composition and other factors, dithionite may slowly enter vesicles and quench internal NBD lipids. External NBD is quenched much more rapidly. The protocol is designed to detect the fraction of NBD that is quenched

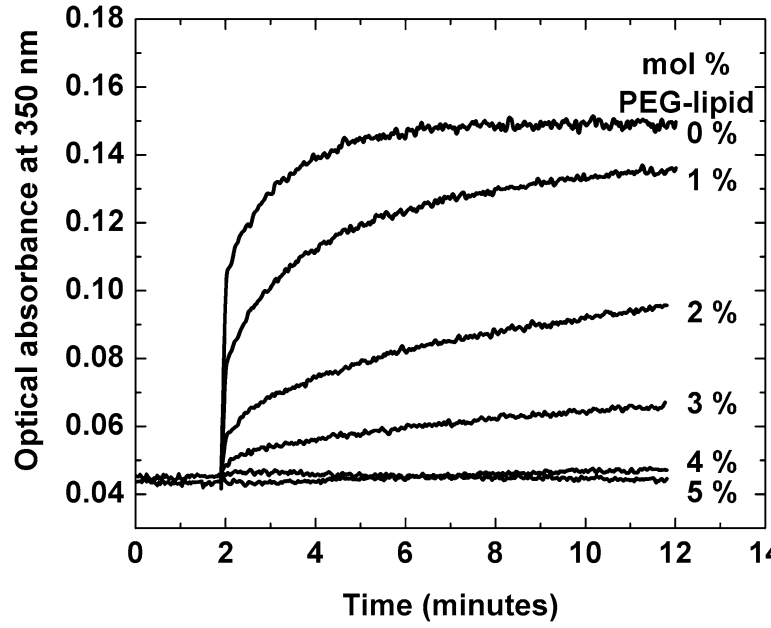

Fig. 4 Aggregation of anionic lipid vesicles by a cationic peptide can be blocked by PEG lipids. These vesicles contain 10 mol% anionic PG lipids and 90 % PC lipids and are at 1 mM concentration. At 2 min, 20 μM of a membrane-permeabilizing peptide with a net charge of +4 was added. In the absence of PEG lipids, the sharp increase in light scattering showed that large-scale aggregation occurs. Vesicles made with 1, 2, and 3 mol % of PEG2000 lipids showed sequentially less aggregation. Incorporation of ≥4 mol% PEG2000 lipids inhibited aggregation entirely

quickly, even when background quenching rate is relatively high, by identifying the breakpoint between rapid and slow quenching.

15. To verify that the AlexaFluor488-streptavidin, TAMRA-biotin-dextran system is functioning as expected, one can carry out two parallel leakage experiments: One experiment in the presence, and one in the absence, of 100 μM free biotin. The biotin-blocked sample should show no effect of leakage while the biotin-free system should show 60–90 % quenching of AF488-dex upon vesicle lysis. The exact amount of quenching depends on the ratio of the probes and the loading of TAMRA and biotin on the dextran.

References

1. Montrose K, Yang Y, Sun X, Wiles S, Krissansen GW (2013) Xentry, a new class of cell-penetrating peptide uniquely equipped for delivery of drugs. Sci Rep 3:1661
2. Dupont E, Prochiantz A, Joliot A (2011) Penetratin story: an overview. Methods Mol Biol 683:21–29
3. Schmidt N, Mishra A, Lai GH, Wong GC (2010) Arginine-rich cell-penetrating peptides. FEBS Lett 584:1806–1813
4. Chugh A, Eudes F, Shim YS (2010) Cell-penetrating peptides: nanocarrier for macromolecule delivery in living cells. IUBMB Life 62:183–193

5. Said HF, Saleh AF, Abes R, Gait MJ, Lebleu B (2010) Cell penetrating peptides: overview and applications to the delivery of oligonucleotides. Cell Mol Life Sci 67:715–726
6. Heitz F, Morris MC, Divita G (2009) Twenty years of cell-penetrating peptides: from molecular mechanisms to therapeutics. Br J Pharmacol 157:195–206
7. He J, Kauffman WB, Fuselier T, Naveen SK, Voss TG, Hristova K, Wimley WC (2013) Direct cytosolic delivery of polar cargo to cells by spontaneous membrane-translocating peptides. J Biol Chem 288:29974–29986
8. He J, Hristova K, Wimley WC (2012) A highly charged voltage sensor helix translocates spontaneously across membranes. Angew Chem Int Ed 51:7150–7153
9. Marks JR, Placone J, Hristova K, Wimley WC (2011) Spontaneous membrane-translocating peptides by orthogonal high-throughput screening. J Am Chem Soc 133:8995–9004
10. Ladokhin AS, Wimley WC, Hristova K, White SH (1997) Mechanism of leakage of contents of membrane vesicles determined by fluorescence requenching. Methods Enzymol 278: 474–486
11. Ladokhin AS, Wimley WC, White SH (1995) Leakage of membrane vesicle contents: determination of mechanism using fluorescence requenching. Biophys J 69:1964–1971
12. Rausch JM, Wimley WC (2001) A high-throughput screen for identifying transmembrane pore-forming peptides. Anal Biochem 293:258–263
13. Krauson AJ, He J, Wimley WC (2012) Determining the mechanism of membrane permeabilizing peptides: identification of potent, equilibrium pore-formers. Biochim Biophys Acta 1818:1625–1632
14. Wiedman G, Fuselier T, He J, Searson PC, Hristova K, Wimley WC (2014) Highly efficient macromolecule-sized poration of lipid bilayers by a synthetically evolved peptide. J Am Chem Soc 136:4724–4731
15. Wimley WC (2010) Describing the mechanism of antimicrobial peptide action with the interfacial activity model. ACS Chem Biol 5:905–917
16. Wimley WC, Hristova K (2011) Antimicrobial peptides: successes, challenges and unanswered questions. J Membr Biol 239:27–34
17. Bechinger B, Lohner K (2006) Detergent-like actions of linear amphipathic cationic antimicrobial peptides. Biochim Biophys Acta 1758:1529–1539
18. Shai Y, Oren Z (2001) From "carpet" mechanism to de-novo designed diastereomeric cell-selective antimicrobial peptides. Peptides 22:1629–1641
19. Ladokhin AS, White SH (2001) 'Detergent-like' permeabilization of anionic lipid vesicles by melittin. Biochim Biophys Acta 1514: 253–260
20. Wiedman G, Herman K, Searson P, Wimley WC, Hristova K (2013) The electrical response of bilayers to the bee venom toxin melittin: evidence for transient bilayer permeabilization. Biochim Biophys Acta 1828:1357–1364
21. Shai Y (2002) Mode of action of membrane active antimicrobial peptides. Biopolymers 66:236–248
22. Sengupta D, Leontiadou H, Mark AE, Marrink SJ (2008) Toroidal pores formed by antimicrobial peptides show significant disorder. Biochim Biophys Acta 1778:2308–2317
23. Ludtke SJ, He K, Heller WT, Harroun TA, Yang L, Huang HW (1996) Membrane pores induced by magainin. Biochemistry 35: 13723–13728
24. Yang L, Harroun TA, Weiss TM, Ding L, Huang HW (2001) Barrel-stave model or toroidal model? A case study on melittin pores. Biophys J 81:1475–1485
25. White SH, Wimley WC, Ladokhin AS, Hristova K (1998) Protein folding in membranes: determining the energetics of peptide-bilayer interactions. Methods Enzymol 295:62–87
26. Ladokhin AS, Jayasinghe S, White SH (2000) How to measure and analyze tryptophan fluorescence in membranes properly, and why bother? Anal Biochem 285:235–245
27. Parente RA, Nir S, Szoka F (1990) Mechanism of leakage of phospholipid vesicle contents induced by the peptide GALA. Biochemistry 29:8720–8728
28. Krauson AJ, He J, Wimley WC (2012) Gain-of-function analogues of the pore-forming peptide melittin selected by orthogonal high-throughput screening. J Am Chem Soc 134:12732–12741
29. Hristova K, Selsted ME, White SH (1997) Critical role of lipid composition in membrane permeabilization by rabbit neutrophil defensins. J Biol Chem 272:24224–24233
30. Goñi FM, Ostolaza H (1998) *E. coli* a-hemolysin: a membrane-active protein toxin. Braz J Med Biol Res 31:1019–1034
31. Ladokhin AS, Selsted ME, White SH (1997) Sizing membrane pores in lipid vesicles by

leakage of co-encapsulated markers: pore formation by melittin. Biophys J 72:1762–1766

32. Nayar R, Hope MJ, Cullis PR (1989) Generation of large unilamellar vesicles from long-chain saturated phosphatidylcholines by extrusion technique. Biochim Biophys Acta 986:200–206
33. Bartlett GR (1959) Phosphorus assay in column chromatography. J Biol Chem 234:466–468
34. Stewart JC (1980) Colorimetric determination of phospholipids with ammonium ferrothiocyanate. Anal Biochem 104:10–14
35. Hristova K, Kenworthy AK, McIntosh TJ (1995) Effect of bilayer composition on the phase behavior of liposomal suspensions containing poly(ethylene glycol)-lipids. Macromolecules 28:7693–7699

Chapter 7

Study of CPP Mechanisms by Mass Spectrometry

Sandrine Sagan, Chérine Bechara, and Fabienne Burlina

Abstract

Studying the mechanisms of entry of cell-penetrating peptides (CPPs) requires reliable methods to measure their cellular uptake efficiency, monitor their metabolic stability, and identify their intracellular localization. We describe here a protocol based on the direct detection of peptides by matrix-assisted laser desorption/ionization time-of-flight mass spectrometry (MALDI-TOF MS), which allows the absolute quantification of the intact internalized species and the analysis of their intracellular degradation. This protocol can be easily applied to the simultaneous quantification of different species, for example mixtures of CPPs.

Key words Cell-penetrating peptide, Mass spectrometry, Stable isotopically labeled internal standard, Peptide quantification, Metabolic stability

1 Introduction

MALDI-TOF MS is now widely used for the analysis of peptides obtained from biological samples since this technique is simple, fast and sensitive, allowing the detection of femtomole quantities. MALDI-TOF MS is not directly quantitative and the signal intensity on the mass spectrum does not exclusively depend on the analyte concentration in the sample [1]. This is due to several factors including the non-linear response of the detector and signal suppression phenomena that can occur when analyzing peptide mixtures. In addition, the co-crystallization of the peptide with the matrix can lead to heterogeneous deposits responsible for low shot-to-shot and spot-to-spot reproducibility. However, these problems can be overcome and accurate peptide quantification can be performed by MALDI-TOF MS by using an internal standard corresponding to the same peptide labeled with a stable isotope (^{2}H, ^{15}N, …) [1–3]. Because peptides can be partially lost during their recovery from biological samples, it is important to introduce the internal standard in the early stages of the extraction procedure. Being chemically equivalent, the analyte and the internal standard

Ülo Langel (ed.), *Cell-Penetrating Peptides: Methods and Protocols*, Methods in Molecular Biology, vol. 1324,
DOI 10.1007/978-1-4939-2806-4_7,

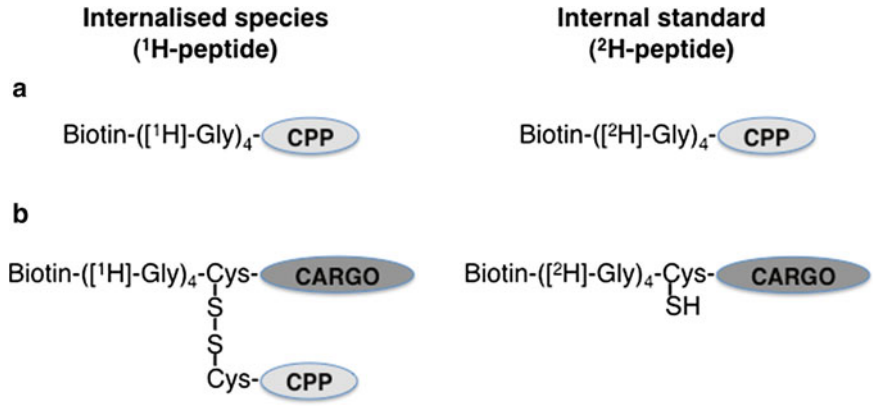

Fig. 1 Structure of the species incubated with cells and internal standards used in the experiments of quantification by MALDI-TOF MS. [^{1}H]-Gly = non-deuterated glycine, [^{2}H]-Gly = bi-deuterated glycine. (**a**) CPP quantification. The CPP is functionalized by the isotope labeling tag for MS quantification. (**b**) Cargo quantification using ^{1}H-Cargo-SS-CPP disulfide conjugate in the cellular uptake experiment. The cargo is functionalized with the isotope labeling tag. The non-conjugated deuterated cargo (^{2}H-Cargo-SH) is used as internal standard because disulfide bonds can be reduced in some cell compartments (in particular the cytosol). In addition, disulfide bonds can be fragmented during MALDI-TOF MS analysis. It should also be noted that when studying the cellular uptake of disulfide conjugates, the biotinylated species are recovered in reducing conditions before MS analysis

will be recovered with the same efficiency, exhibit identical behavior during the step of co-crystallization with the matrix and have the same desorption/ionization efficiency. Nevertheless, they will be distinguishable because of their mass difference. The relative intensity of their signals in the mass spectrum is therefore directly correlated to their relative abundance in the sample.

In the method described here to measure CPP internalization, the CPP is functionalized on its N-terminus by an isotope-labeling affinity tag (biotin-Gly_4) and synthesized using standard peptide solid-phase protocols in two versions: the ^{1}H-CPP containing four non-deuterated glycine residues (internalized peptide, the analyte) and the ^{2}H-CPP containing four bi-deuterated glycine residues (the internal standard) (Fig. 1a) [4, 5]. The biotin moiety enables the recovery from the biological sample of the peptides of interest (internalized peptide, internal standard, and their potential digests). The 8 mass units difference between the ^{1}H- and ^{2}H-peptide is sufficient to avoid the overlap of both peptide signals in the mass spectra for peptides with $m/z < 4000$. Internalization of proteins can also be evaluated using as internal standard the corresponding ^{15}N-labeled species. This has been applied before to study apo-neocarzinostatin (12,500 Da) internalization and both unlabeled and ^{15}N-labeled protein signals were found to be well separated in the mass spectra [6]. Here, the biotin was specifically introduced on a Cys residue of the expressed proteins by using a biotin-PEG-maleimide derivative.

The protocol described here can also be easily applied for the quantification of a delivered peptide cargo [7–9]. In this case, the biotin-Gly_4 tag is introduced on the cargo (Fig. 1b). When the CPP and cargo are linked by a reversible bond, for example a disulfide bond, the non-conjugated deuterated cargo (^{2}H-Cargo-SH) is used as internal standard for MALDI-TOF MS quantification (Fig. 1b). This strategy is particularly useful to compare the efficiency of different CPPs to deliver a given peptide cargo in its intact form. The integrity of the cargo is often required for its biological activity, measuring the amount of intact internalized cargo therefore gives a valuable information that can then be correlated with an observed biological activity. Interestingly, we have previously observed that the pattern of intracellular degradation of the cargo varies depending on the carrier used. This is most probably due to different intracellular targeting when using different carriers [9].

The quantification protocol is illustrated in Fig. 2. After incubation of the cells with the ^{1}H-peptide (CPP or conjugate) and removal of the membrane-bound peptide, a known amount of internal standard (^{2}H-peptide) is added. Cell lysis is performed and the peptides are recovered from the cell lysate using streptavidin-coated magnetic beads. After bead washing to remove the non-biotinylated species, the purified peptides are eluted from the beads by incubation with the MALDI matrix and directly analyzed by MALDI-TOF MS. The absolute amount of intact internalized peptide can then be simply calculated from the area of the ^{1}H- and ^{2}H-peptide signals. Biotinylated digests will also be recovered and can be easily characterized by MALDI-TOF MS.

Two steps are critical for the accuracy of the quantification of the internalized species. First, the membrane-bound peptide must be removed to prevent the overestimation of the internalization efficiency. This is classically performed by a short treatment with proteases (trypsin or pronase) [5, 10]. For CPPs or peptide cargoes that are not efficiently digested by proteases, chemical treatments that change the mass of the extracellular peptide are available to distinguish by mass spectrometry the internalized species from the membrane-bond species [11, 12]. It is of course essential to use a treatment that respects cell integrity, gives a complete peptide modification in a short time (<10 min) and only modifies the extracellular species. We have successfully used a combination of TCEP and *N*-ethylmaleimide to modify the Cys residues of CPPs and disulfide conjugates. In addition, treatment with diazotized-nitroaniline at 4 °C was used to modify peptides containing Cys, Lys, and Trp residues. Secondly, the conditions used for cell lysis are also important to ensure a correct quantification of the cellular uptake. Conditions have been optimized in this protocol in order to instantly inhibit intracellular proteases that are released during lysis, thus preventing degradation of the peptides of interest.

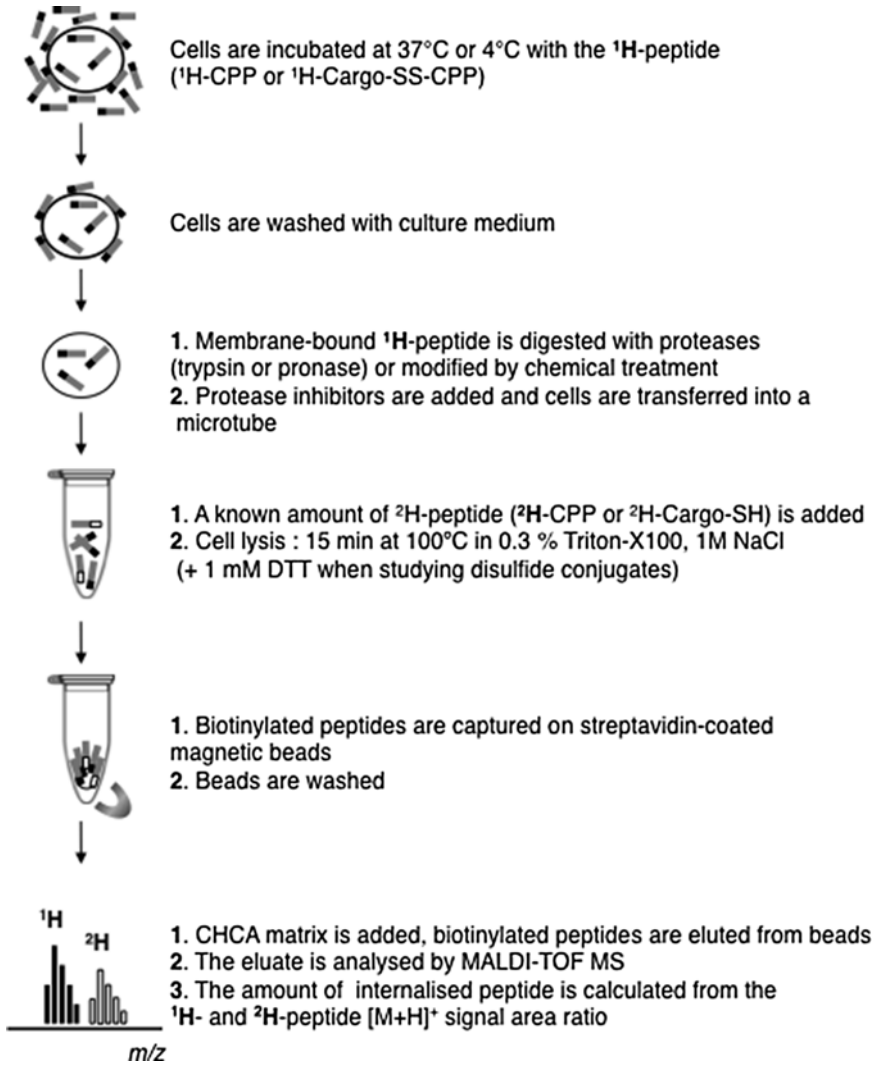

Fig. 2 Protocol of quantification by MALDI-TOF MS of the internalized CPP or cargo

This is performed by boiling the sample in the presence of detergent. Since the deuterated internal standard is added before cell lysis, it is easy to define the step at which peptide degradation took place. Intracellular degradation of the internalized peptides can indeed be differentiated from artifactual degradation that might occur during sample preparation: in the first case only ^{1}H-digests are observed whereas in the second case both ^{1}H and ^{2}H-digests would be detected. Boiling the sample also ensures that both ^{1}H- and ^{2}H-peptide are exposed to the same interactions with lysate components and are then recovered with streptavidin-coated beads with the same efficiency.

Various CPPs have been studied using this method including the classical CPPs Penetratin, Tat, R_9 and R_6/W_3 [5, 13, 14] and lipopeptides [8, 9]. Although the internalization efficiency can

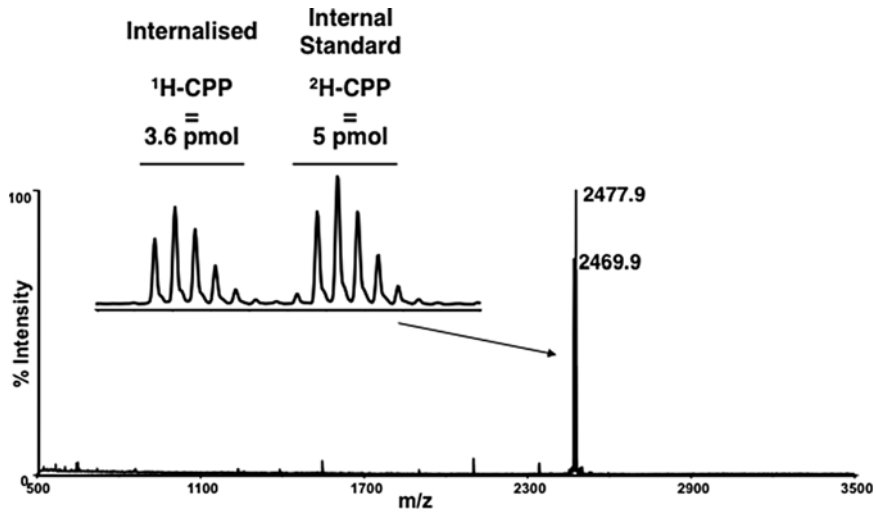

Fig. 3 Example of a mass spectrum obtained for the cellular uptake of the CPP Eng (corresponding to the third helix of the human Engrailed-2 homeodomain). The *insert* shows a zoom on the intact ^{1}H- and ^{2}H-CPP signals. Amounts of added internal standard and experimentally measured internalized CPP are indicated. The CPP (7.5 μM in DMEM) was incubated with 10^{6} CHO-K1 cells for 1 h 15 at 37 °C. The calculated intracellular concentration of intact CPP is 3.6 μM (using as estimated volume for 1 CHO-K1 cell: 1 pL)

vary between CPPs, intracellular concentrations usually observed are in the μM range when using extracellular peptide concentrations ranging from 5 to 10 μM. Noteworthy, for some CPPs, the measured intracellular concentration was higher than the concentration applied outside cells [8, 13]. In all cases, negligible intracellular degradation of the CPPs was observed after 1 h incubation with cells (Fig. 3). Intracellular degradation was analyzed over time for R_6/W_3 and it was shown that after overnight incubation, the intact CPP remained the most abundant species [15]. It was also investigated if once internalized this CPP was able to exit cells. No exit was observed [15].

The mechanism of entry of different CPPs and their conjugates has been studied using the protocol described below [8, 10, 14–16]. The respective contribution of direct translocation across the plasma membrane and endocytosis could be measured by comparing cellular uptake at 37 and 4 °C. While at 37 °C both mechanisms can co-exist, at 4 °C endocytotic pathways are inhibited but direct translocation can still occur although it might be reduced. The peptides entering at this low temperature will therefore end up first in the cytosol. The protocol of quantification can also be combined with the use of specific endocytosis inhibitors to further characterize the route of entry as performed with other techniques to study CPP cellular uptake [17, 18]. In addition, the involvement of cell-surface glycosaminoglycans (GAGs), which are major effectors in endocytosis, can be evaluated by comparing the entry in wild-type cells and in cells with defective GAG biosynthesis or

treated with enzymes to selectively remove GAGs (heparinase, chondroitinase). We have shown with this quantification strategy combined with DLS studies, that self-association of lipidated tetra-arginine CPPs was necessary to promote their GAG-dependent endocytosis [8]. This highlighted that the clustering of the basic residues of these small CPPs was crucial for efficient GAG recruitment. Moreover, when combining this quantification protocol to isothermal titration calorimetry, NMR spectroscopy and phase contrast microscopy, we demonstrated a specific role of Trp residues in the efficient clustering of GAGs. Enhanced CPP internalization by GAG-dependent endocytosis was correlated to the number of Trp residues in the peptide sequences. Circular dichroism studies confirmed that the presence of Trp residues promoted a β-strand conformation of the peptides in the presence of GAGs in vitro, further demonstrating CPP/GAG clustering [14, 16]. Finally, aggregation of GAGs was also enhanced when modifying the composition of the plasma bilayer. Using this quantification protocol as well as phase contrast microscopy, we showed that formation of ceramide-enriched domains and depletion of cholesterol induced massive GAG-dependent endocytosis of CPP containing Trp residues [16].

In summary, the method described here gives access to the total amount of internalized CPP or cargo, all intracellular compartments included. It therefore allows to fully and directly evaluate the contribution of a given route of entry by studying the impact of inhibitors or low temperatures. Since this method is based on direct detection and characterization of the internalized species by MALDI-TOF MS, it is possible to analyze their degradation and also to study the cellular uptake of mixtures of CPPs (as long as the CPPs have different masses) for screening or competition experiments [5]. Therefore, this method is complementary to fluorescence-based techniques commonly used to analyze the intracellular localization of CPPs. It is also complementary to methods monitoring the biological activity of the cargo [19, 20], the biological activity being dependent on several factors including the cargo co-localization and affinity for the intracellular target.

2 Materials

Prepare all solutions using ultrapure distilled or deionized water. All solutions and reagents can be stored at 4 °C unless mentioned otherwise.

2.1 Cell Seeding Reagents

1. Dulbecco's modified eagle medium (DMEM) or other culture medium depending on the cell line used.
2. Fetal calf serum (FCS).

3. Hank's balanced salt solution without Ca^{2+} and Mg^{2+} (HBSS).
4. Trypsin/EDTA solution: 0.05 % trypsin, 0.02 % EDTA (commercial solution for cell culture).
5. Complete medium: DMEM containing 5–10 % FCS.

2.2 Buffers and Solutions for the CPP Cellular Uptake Experiments

1. Peptide stock solutions: prepare stock solutions of the ^{1}H-peptides (^{1}H-CPP or ^{1}H-Cargo-SS-CPP conjugate) and ^{2}H-peptides (^{2}H-CPP or ^{2}H-Cargo-SH) (Fig. 1) at the concentration of 1 mM in H_2O (or DMSO for compounds presenting solubility problems). The solutions can usually be stored for long periods at −20 °C (*see* **Notes 1** and **2**).
2. 0.5 M Tris–HCl, pH 7.5.
3. BSA solution: 1 mg/mL bovine serum albumin in H_2O.
4. 4 M NaCl in H_2O.
5. 10 % Triton X-100 in H_2O.
6. 10 % sodium dodecyl sulfate (SDS) in H_2O. Store at room temperature.
7. 1 mM biotin in H_2O. Store at −20 °C.
8. 50 mM dithiothreitol (DTT) in H_2O. This solution is only required if peptides containing Cys residues are studied. It is best to prepare the solution freshly the day of the peptide internalization experiment.
9. Use these stock solutions to prepare the diluted solutions listed below.
10. TCEP solution: 2 mM tris(2-carboxyethyl)phosphine in 50 mM Tris–HCl pH 7.5. This solution is only required if peptides containing Cys residues are studied. Prepare freshly the day of the internalization experiment.
11. Trypsin/EDTA solution: 0.05 % trypsin, 0.02 % EDTA (commercial solution for cell culture) (*see* **Note 3**).
12. Pronase solution: 1 mg/mL pronase in 50 mM Tris–HCl pH 7.5 (*see* **Note 3**). The solution should be prepared freshly the day of the internalization experiment.
13. Trypsin inhibitor solution: 5 mg/mL soybean trypsin inhibitor in H_2O. This solution should be prepared freshly the day of the internalization experiment.
14. Pronase inhibitor solution: we have found that the cocktail of inhibitors Complete Mini (Roche) was efficient. Dissolve 1 tablet of Complete Mini in 1.5 mL H_2O. This solution should be prepared freshly the day of the internalization experiment.
15. Lysis solution A: 0.3 % Triton X-100, 1 M NaCl. This solution is used when studying peptides with no Cys residue.

16. Lysis solution B: 0.3 % Triton X-100, 1 M NaCl, 1 mM DTT. This solution is used when studying peptides with Cys residues. It should be prepared freshly the day of the internalization experiment.
17. Streptavidin-coated magnetic beads: For non-conjugated CPPs (Fig. 1a), both Dynabeads® M-280 Streptavidin and Dynabeads® MyOne™ Streptavidin C1 (Invitrogen) were found to give good results regarding the detection sensitivity of the peptides by MALDI-TOF MS. For CPP–cargo disulfide conjugates (Fig. 1b), Dynabeads® M-280 Streptavidin usually give better results limiting non-specific binding of the non-biotinylated CPP.
18. 10 μM biotin in H_2O.
19. Buffer A: 50 mM Tris–HCl, pH 7.5, 0.1 mg/mL BSA.
20. Buffer B: 50 mM Tris–HCl, pH 7.5, 0.1 mg/mL BSA, 0.1 % SDS.
21. Buffer C: 50 mM Tris–HCl, pH 7.5, 0.1 mg/mL BSA, 1 M NaCl.
22. Buffer D: 50 mM Tris–HCl, pH 7.5, 0.1 mg/ml BSA, 2 mM DTT. This buffer is only required when studying CPP–cargo disulfide conjugates. It should be freshly prepared the day of the internalization experiment.
23. Tris buffer 1×: 50 mM Tris–HCl, pH 7.5.
24. CHCA matrix solution: 5 mg/mL α-cyano-4-hydroxycinnamic acid in acetonitrile/H_2O/trifluoroacetic acid (50:50:0.1).

3 Methods

3.1 Cell Seeding

Below is given a standard protocol to prepare for the CPP internalization experiment 12-well plates with confluent CHO-K1 cells (10^6 cells/well). Cell culture conditions depend on the cell type. The procedure for cell seeding should therefore be adapted to the cell type of interest by using the appropriate growth medium and cell number and taking into account the cell doubling time. All steps for cell seeding must be performed in sterile conditions (*see* **Note 4**).

1. Grow CHO-K1 cells to confluence in complete medium in 100 mm Petri dishes or 75 mm^2 flasks in a humidified atmosphere containing 5 % CO_2 at 37 °C.
2. Pre-warm HBSS, DMEM, FCS, and the trypsin/EDTA solution at room temperature.
3. Remove the medium from the cultured cells with a pipette.
4. Wash adhering cells with 10 mL HBSS.

5. Discard the HBSS and add 2 mL of trypsin/EDTA solution.
6. Incubate cells at 37 °C for 2–3 min. Control under a microscope that cells are detached from the plate. If cells are not sufficiently detached, place the plate at 37 °C for one more minute.
7. Add 8 mL of complete medium to inhibit trypsin. Draw cell suspension into a Pasteur pipette several times to completely dissociate cells and to detach any remaining adherent cells. Check under a microscope that all cells are detached and properly dissociated.
8. Count cells with a hematocytometer-like or cell counter and dilute with complete medium to a density of 250,000 cells/mL.
9. Add 2 mL of the cell suspension to each well of a 12-well plate to have 500,000 cells/well.
10. Incubate for 20–24 h in a humidified 37 °C, 5 % CO_2 incubator.

3.2 CPP Cellular Uptake Experiment and MALDI-TOF MS Analysis

Sterile conditions are not required unless long incubation times with the peptide (>24 h) are used.

1. From the peptide stock solutions, prepare the solution(s) of ^{1}H-peptide (^{1}H-CPP or ^{1}H-Cargo-SS-CPP conjugate) diluted at the desired concentration (typically 1–20 μM, *see* **Note 5**) in DMEM (with or without FCS as wanted). Note that the volume required per well to properly cover cells when using 12-well plates is 1 mL. Also prepare the diluted solutions of ^{2}H-peptide (^{2}H-CPP or ^{2}H-Cargo-SH) in H_2O (typically 1–10 μM) (*see* **Note 6**).
2. Wash each well containing adherent cells with 2 mL HBSS (*see* **Note 7**).
3. Add to each well, 1 mL of the solution of ^{1}H-peptide and incubate at the chosen temperature (4 or 37 °C) and in the desired conditions. At the end of the incubation, check cell aspect under a microscope (*see* **Note 8**).
4. Wash cells three times with 1 mL HBSS.
5. The procedure then used to remove the membrane-bound peptide depends on the peptide and conditions tested:
   (a) CPPs or conjugates with no Cys residue incubated with cells at 37 °C (*see* **Note 3**):
      - Add to each well 500 μL of protease solution (trypsin/EDTA or pronase) and incubate at 37 °C for 3–5 min. At the end of incubation all cells must be detached, if not extend the incubation for 1–2 min.
      - Place the 12-well plate on ice and add to each well 100 μL of the BSA solution and 100 μL of the

appropriate protease inhibitor solution (trypsin or pronase inhibitor).

(b) CPPs or conjugates with no Cys residue incubated with cells at 4 °C (*see* **Note 3**):

- Add to each well 500 µL of the pronase solution and incubate at 4 °C for 5–10 min. At the end of incubation cells must be detached from the well surface, if not extend the incubation at 4 °C for 1–2 more minutes.
- Add to each well 100 µL of the pronase inhibitor solution and 100 µL of the BSA solution.

(c) Peptides or conjugates containing reduced or oxidized Cys (*see* **Note 9**):

- Incubate cells at room temperature for 2 min with 200 µL of the TCEP solution.
- Wash cells twice with 1 mL HBSS.
- Perform the protease digestion and inhibition steps as described above in (a) or (b) depending on the peptide sequence and incubation temperature.

6. Suspend cells gently in the well with a micropipette and transfer into a low-binding microtube. Wash the well with 500 µL Tris buffer 1× and add the solution to the same microtube. Control under microscope that all cells have been transferred from the well (*see* **Note 10**).
7. Centrifuge the sample for 2 min at 640 × *g* to recover a pellet containing all intact cells. Remove the supernatant by gentle aspiration keeping the pellet intact.
8. Wash the pellet carefully with 1 mL buffer A (do not mix the sample or resuspend the pellet), centrifuge the sample for 2 min at 640 × *g* and remove the supernatant by gentle aspiration keeping the pellet intact. Place the sample on ice.
9. Add to the pellet of cells 150 µL of lysis solution A (when studying CPPs with no Cys) or of lysis solution B (when studying CPPs with Cys residues) and add the adequate and precise amount of ^{2}H-peptide (^{2}H-CPP or ^{2}H-Cargo-SH) (*see* **Note 11**). Immediately heat the sample for 15 min at 100 °C (*see* **Note 12**). A small precipitate is usually clearly visible at the end of this step.
10. Centrifuge the lysate for 5 min at 7080 × *g*. Transfer the supernatant into a new low-binding microtube.
11. Wash the pellet with 850 µL buffer A, centrifuge for 2 min at 7080 × *g* and recover the supernatant. Combine with the supernatant obtained **step 10**. For cargo quantification using

Cargo-SS-CPP disulfide conjugates, use 850 µL buffer D instead of buffer A.

12. For *n* samples studied, take $n \times 10$ µL of the commercial solution of streptavidin-coated magnetic beads Dynabeads® M-280 Streptavidin and place them into a microtube. Alternatively, use $n \times 5$ µL of the commercial solution of MyOne™ Streptavidin C1 beads. Place the microtube in a magnetic rack to immobilize the beads and wash the beads twice with $n \times 10$ µL buffer A. Remove the supernatant and add to the beads $n \times 10$ µL buffer A, briefly mix with a vortex.
13. To each sample of diluted cell lysate obtained **step 11**, add 10 µL of bead solution. Mix gently for 1 h with a vortex at room temperature to capture the biotinylated peptides.
14. Place the microtubes in the magnetic rack to immobilize beads and remove the supernatant with a micropipette. Wash beads twice with 200 µL buffer A, twice with 200 µL buffer B, twice with 200 µL buffer C and with H_2O (2×200 µL, 1×50 µL). Briefly mix with a vortex each time (*see* **Note 13**).
15. Incubate the beads for 1 min with 50 µL of 10 µM biotin solution.
16. Wash the beads with H_2O (1×50 µL) and acetonitrile/H_2O (1:1) (1×50 µL) (*see* **Note 14**).
17. Discard the supernatant and add 3 µL of the CHCA matrix solution. Remove the sample from the magnetic rack and mix with a micropipette. Incubate for 10 min at room temperature to elute the biotinylated peptides from the beads. Immobilize beads with the magnet and deposit the supernatant (0.5 or 1 µL) on the MALDI-TOF plate (*see* **Note 15**).
18. Analyze the sample by MALDI-TOF MS in positive ion reflector mode (*see* **Note 16**). Adjust the laser energy near the threshold of peptide ions production. Adjust the extraction delay time to get the highest resolution in the analyte mass range (focus mass range). Average mass spectra from several hundred laser shots recorded on different spots of the deposit (*see* **Note 17**).
19. Apply if necessary a baseline correction on the mass spectrum. Measure with the mass spectrometer data processing software the area of the $[M+H]^+$ signals (including all the isotopes) of the intact ^{1}H- and ^{2}H-peptide (Fig. 3). The quantity of intact internalized ^{1}H-peptide is calculated from the area ratio of both signals and from the amount of ^{2}H-peptide added (*see* **Notes 18** and **19**). Calculate the peptide intracellular concentration according to the number of cells used per sample.

4 Notes

1. ^{2}H-peptides can be synthesized on solid-phase using standard protocols by incorporating commercially available Boc-Gly-OH-2,2-d2 or Fmoc-Gly-OH-2,2-d2.
2. Peptide stock solutions should be stored in low-binding microtubes to limit the absorption of the peptide on the microtube walls. The relative ^{1}H- and ^{2}H-peptide solution concentrations should be controlled by MALDI-TOF MS before performing the first internalization experiment (this control should be repeated if solutions have been stored for long periods). For this, prepare a sample containing 100 μM ^{1}H- and ^{2}H-peptide in H_2O (add 3 equivalents TCEP when comparing the concentrations of the ^{1}H-Cargo-SS-CPP disulfide conjugate and ^{2}H-Cargo-SH solutions). Mix 1 μL of this peptide solution with 3 μL CHCA matrix solution, deposit 1 μL of the mixture on the MALDI plate and analyze by MALDI-TOF MS as described in **steps 18** and **19** in Subheading 3.2. This should give ^{1}H- and ^{2}H-peptide $[M+H]^{+}$ signals with the same intensity on the mass spectrum.
3. Tryspin only cleaves peptides after basic residues and is therefore not efficient to remove the membrane-bound CPP or cargo containing no Lys or Arg. For peptides with no basic residues use pronase which has no residue specificity. Trypsin is efficient at 37 °C but not at 4 °C. In contrast, pronase is efficient at both temperatures and is therefore used when measuring the entry of peptides at low temperature.
4. To prevent contamination of the cell culture, only use sterile reagents, media and consumables and work in a cell culture hood.
5. Before testing a new CPP or conjugate in an experiment of cellular uptake quantification, perform a cell viability assay using a range of peptide concentrations and incubation time. Use in the quantification experiments conditions that give no cytotoxicity.
6. The diluted solutions of ^{1}H and ^{2}H-peptide must be prepared freshly the day of the cellular uptake experiment. These solutions cannot be stored because over time peptide adsorption on the tube walls could significantly change their concentrations.
7. Cell washes are performed by gentle aspiration of the supernatant and gentle addition of new medium or buffer to prevent cell detachment and subsequent loss. Use cold buffers (4 °C) when testing the entry of the peptides at 4 °C and buffers pre-warmed at room temperature for experiment at 37 °C.

8. Detached or abnormal aspect of cells could reflect a cytotoxicity of the CPP (or conjugate). If some cells are lost after incubation with the peptide, count remaining cells after **step 8** in Subheading 3.2. Calculate the peptide intracellular concentration according to the number of remaining cells.
9. We have found that peptides containing Cys residues can form disulfide bonds with cell-surface proteins by thiol-disulfide exchange reactions [11]. These species conjugated to membrane proteins are resistant to proteases and can only be digested by proteases after disulfide reduction with TCEP. The step of TCEP reduction is therefore crucial to avoid the overestimation of the efficiency of internalization of peptides or conjugates containing Cys residues.
10. If the well still contains cells, wash the well with 1 mL buffer A, and use this suspension to wash the cell pellet in **step 8** of Subheading 3.2.
11. Quantification by MALDI-TOF MS is accurate and reliable for ratios between ^{1}H- and ^{2}H-peptide ranging between 0.2 and 5. When a peptide is tested for the first time and its efficiency of internalization is not known, different amounts of internal standard (^{2}H-peptide) are added to three different samples. Typically 1, 10 and 25 pmol of ^{2}H-peptide are added to the samples using volumes ranging from 1 to 10 μL. The amount of internalized ^{1}H-peptide is calculated after MALDI-TOF MS analysis from the area ratio of the ^{1}H and ^{2}H-peptide $[M+H]^{+}$ signals as described in **steps 18** and **19** in Subheading 3.2. The experiment is then repeated adjusting if necessary the amount of ^{2}H-peptide added to obtain a ratio close to 1.
12. Conditions of cell lysis are critical and have been optimized to avoid any artifacts. The heating step at 100 °C allows the fast and complete inhibition of proteases released during cell lysis preventing degradation of the ^{1}H and ^{2}H-peptides. Importantly, the internal standard (^{2}H-peptide) must be introduced before lysis to further provide a control of degradation. The experiment is only valid if no deuterated digest is observed on the mass spectrum. The heating step also enables both ^{1}H and ^{2}H-peptides to be exposed to the same interactions with lysate components. Both peptides are then captured on the streptavidin-coated beads with the same efficiency (**step 13** in Subheading 3.2) ensuring a reliable quantification.
13. We have found when studying CPP–cargo disulfide conjugates (Fig. 1b) that some CPPs can strongly bind to beads even if not biotinylated [8]. The CPP species is then also detected in the mass spectrum, sometimes hampering the detection of the species of interest (the biotinylated cargo). However, most non-biotinylated species can be removed from beads by replacing

in **step 14** (Subheading 3.2) washings with buffer B by 10 min incubation of the beads at 55 °C with diluted Laemmli buffer (1 % SDS, 6 % glycerol, 1 % β-mercaptoethanol, 0.025 % bromophenol blue, 25 mM Tris–HCl, pH 6.8).

14. If necessary, samples can be safely stored at this point overnight at 4 °C keeping the beads immersed in water.
15. The deposits can be stored up to 1 week at room temperature before MALDI-TOF MS analysis.
16. The positive ion reflector mode is used to analyze peptides with $m/z < 4000$. If proteins are studied then use the linear mode.
17. Because of low laser shot-to-shot reproducibility with MALDI-TOF MS, mass spectra must be averaged from a large number of laser shots to achieve a good statistical sampling and counting. For this, laser shots are accumulated until both ^{1}H- and ^{2}H-peptide signals exhibit the theoretical isotopic distribution. The sensitivity of the quantification method depends on the sequence of the peptide studied and on the performance of the mass spectrometer used. For the CPP Penetratin, the lower limit of quantification was found to correspond to 0.1 pmol peptide internalized in one million cells when using a ABI Voyager DE-PRO MALDI-TOF mass spectrometer for the analysis.
18. A small fraction of the ^{2}H-peptide may contain less than eight deuteriums if the bi-deuterated glycine used in the peptide solid-phase synthesis is not 100 % deuterated. Because of this possible non-complete deuteration of the internal standard and fluctuation of isotope abundance, quantification must be based on the sum of the peak area of all isotopes for both ^{1}H- and ^{2}H-peptide including potential components containing less than eight deuteriums (Fig. 3).
19. Since the ^{1}H- and ^{2}H-peptide have the same sequence, both are protonated and cationized with Na^{+} and K^{+} to the same extent. In addition, cationization is usually negligible compared to protonation. Quantification can therefore be based only on the $[M+H]^{+}$ signals of both peptides, not taking into account the $[M+Na]^{+}$ and $[M+K]^{+}$ signals.

Acknowledgments

We thank Dr. G. Chassaing, Dr. G. Bolbach, Dr. C.-Y. Jiao, Dr. S. Aubry, Dr. B. Aussedat, Dr. D. Delaroche, S. Bode, and M. Amoura for their contribution to the development of the CPP quantification protocol.

References

1. Aebersold R, Mann M (2003) Mass spectrometry-based proteomics. Nature 422: 198–207
2. Gobom J, Kraeuter KO, Persson R et al (2000) Detection and quantification of neurotensin in human brain tissue by matrix-assisted laser desorption/ionization time-of-flight mass spectrometry. Anal Chem 72:3320–3326
3. Ong SE, Mann M (2005) Mass spectrometry-based proteomics turns quantitative. Nat Chem Biol 1:252–262
4. Burlina F, Sagan S, Bolbach G et al (2006) A direct approach to quantification of the cellular uptake of cell-penetrating peptides using MALDI-TOF mass spectrometry. Nat Protoc 1:200–205
5. Burlina F, Sagan S, Bolbach G et al (2005) Quantification of the cellular uptake of cell-penetrating peptides by MALDI-TOF mass spectrometry. Angew Chem Int Ed 44: 4244–4247
6. Moody P, Burlina F, Martin SR et al (2013) Evaluating the use of Apo-neocarzinostatin as a cell penetrating protein. Protein Eng Des Sel 26:277–281
7. Aussedat B, Sagan S, Chassaing G et al (2006) Quantification of the efficiency of cargo delivery by peptidic and pseudo-peptidic Trojan carriers using MALDI-TOF mass spectrometry. Biochim Biophys Acta 1758:375–383
8. Bode SA, Thevenin M, Bechara C et al (2012) Self-assembling mini cell-penetrating peptides enter by both direct translocation and glycosaminoglycan-dependent endocytosis. Chem Commun 48:7179–7181
9. Aussedat B, Dupont E, Sagan S et al (2008) Modifications in the chemical structure of Trojan carriers: impact on cargo delivery. Chem Commun 12:1398–1400
10. Jiao CY, Delaroche D, Burlina F et al (2009) Translocation and endocytosis for cell-penetrating peptide internalization. J Biol Chem 284:33957–33965
11. Aubry S, Burlina F, Dupont E et al (2009) Cell-surface thiols affect cell entry of disulfide-conjugated peptides. Faseb J 23:2956–2967
12. Aubry S, Aussedat B, Delaroche D et al (2010) MALDI-TOF mass spectrometry: a powerful tool to study the internalization of cell-penetrating peptides. Biochim Biophys Acta 1798:2182–2189
13. Balayssac S, Burlina F, Convert O et al (2006) Comparison of penetratin and other homeodomain-derived cell-penetrating peptides: interaction in a membrane-mimicking environment and cellular uptake efficiency. Biochemistry 45:1408–1420
14. Bechara C, Pallerla M, Zaltsman Y et al (2013) Tryptophan within basic peptide sequences triggers glycosaminoglycan-dependent endocytosis. FASEB J 27:738–749
15. Delaroche D, Aussedat B, Aubry S et al (2007) Tracking a new cell-penetrating (W/R) nonapeptide, through an enzyme-stable mass spectrometry reporter tag. Anal Chem 79: 1932–1938
16. Bechara C, Pallerla M, Burlina F et al (2015) Massive glycosaminoglycan-dependent entry of Trp-containing cell-penetrating peptides induced by exogenous sphingomyelinase or cholesterol depletion. Cell Mol Life Sci 72:809–820
17. Fischer R, Hufnagel H, Brock R (2010) A doubly labeled Penetratin analogue as a ratiometric sensor for intracellular proteolytic stability. Bioconjugate Chem 21:64–73
18. Abes S, Moulton HM, Clair P et al (2006) Vectorization of morpholino oligomers by the (R-Ahx-R)4 peptide allows efficient splicing correction in the absence of endosomolytic agents. J Control Release 116:304–313
19. Mäe M, Andaloussi S, Lundin P et al (2009) A stearylated CPP for delivery of splice correcting oligonucleotides using a non-covalent co-incubation strategy. J Control Release 134: 221–227
20. Wadia JS, Stan RV, Dowdy SF (2004) Transducible TAT-HA fusogenic peptide enhances escape of TAT-fusion proteins after lipid raft macropinocytosis. Nat Med 10: 310–315

Chapter 8

Methods to Study the Role of the Glycocalyx in the Uptake of Cell-Penetrating Peptides

Samuel Schmidt, Rike Wallbrecher, Toin H. van Kuppevelt, and Roland Brock

Abstract

Cells are covered by a layer of negatively charged oligo- and polysaccharides, the glycocalyx. Cell-penetrating peptides and other drug delivery vehicles first encounter these polyanions before contacting the lipid bilayer of the plasma membrane. While a large body of data supports the notion that interactions with the glycocalyx promote or even trigger uptake, in some cases, the glycocalyx compromises delivery. As a consequence there is a need to address the role of the glycocalyx in delivery for each specific delivery vehicle and for each particular type of cell. Here, we describe protocols to obtain information on the composition and dynamics of the glycocalyx, and the role of individual glycocalyx components in the uptake of drug delivery vehicles.

Key words Click chemistry, Glycosaminoglycans, Immunofluorescence, Metabolic labeling, Single-chain antibody fragments

1 Introduction

Molecules approaching a cell first encounter a layer of oligo- and polysaccharides, the glycocalyx. The major components of the glycocalyx are proteoglycans which carry highly negatively charged repeating disaccharide units, the glycosaminoglycans (GAGs) [1]. Heparan sulfates, chondroitin sulfates, dermatan sulfates, and hyaluronic acid are important constituents of the glycocalyx. However, in the context of cell-penetrating peptide (CPP) uptake heparan sulfates have been studied most intensively [2, 3]. Furthermore, the terminal structures of the glycan moieties of glycoproteins and glycolipids can contain the negatively charged sialic acids.

Even though CPPs do not interact with specific receptors, a current model for the induction of endocytic uptake comprises the binding to heparan sulfates, followed by cross-linking of the associated proteoglycans which then leads to activation of small GTPases and subsequent actin reorganization [4]. Nevertheless,

Ülo Langel (ed.), *Cell-Penetrating Peptides: Methods and Protocols*, Methods in Molecular Biology, vol. 1324,
DOI 10.1007/978-1-4939-2806-4_8,

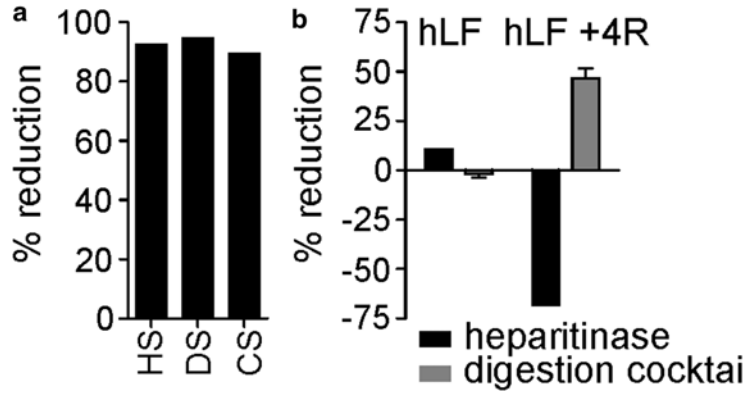

Fig. 1 Effect of enzymatic digestion of the glycocalyx on CPP uptake. (**a**) Assessment of enzymatic GAG removal by immunofluorescence. The percentage of reduction was calculated by comparing the signal as determined by flow cytometry before and after digestion. HS refers to median fluorescence obtained for the single-chain antibody HS4C3, CS to I03H10V and DS to LKN1V. Data of one single experiment are shown. (**b**) Degree of reduction in peptide uptake after heparitinase I treatment or glycocalyx removal by the enzyme cocktail. Heparitinase samples show a single experiment. For full digestion, $n=2$. Error bars show SEM. Peptides were N-terminally labeled with carboxyfluorescein (Fluo) and amidated at the C-terminus (hLF—Fluo-KCFQWQRNMRKVRGPPVSCIKR-NH_2, hLF + 4R—Fluo-KCFRWQRNRRKVRGRPVRCIKR-NH_2, where -NH_2 stands for the C-terminal amidation) [15]. A negative reduction indicates an increase in peptide uptake.

a number of observations do not fit into this concept (reviewed in Favretto et al. [2]). For example, using a cell line which is deficient in specific types of GAGs, it was found that the uptake of the Tat peptide was promoted [5].

Therefore, further analyses of the role of GAGs in uptake are urgently needed. In addition, a refinement of experimental protocols is required. Since cells defective in GAG synthesis [6–8] may potentially show long-term compensation, for the analysis of GAG involvement the use of protocols to analyze and manipulate GAG levels for a given cell type are desirable. At this point, most studies have only addressed heparan sulfates, even though this glycosaminoglycan may only comprise a minor part of the total GAG layer and thus removal of HS alone will also have only a minor effect on uptake, compared to total GAG removal (Fig. 1). We will provide protocols for a complete digestion of the glycosaminoglycans. In addition, we describe immunofluorescence protocols using a collection of single-chain antibody fragments to control for GAG chain removal and also compare cells with respect to GAG expression. Metabolic labeling is described as a means to label sialic acids which are hard to capture using immunofluorescence. The latter

Table 1
Overview of the presented methods

Method	Reagent	Aspect studied
Bioorthogonal labeling	Ac4ManNAz, BCN-biotin, Streptavidin-AF 488	Sialic acid distribution, GAG clustering, effectiveness of enzymatic removal
Immunofluorescence	HS4C3, EV3C3, A04B08	Heparan sulfate (relative expression level/distribution/completeness of digestion)
Immunofluorescence	I03H10	Chondroitin sulfate (relative expression level/distribution/completeness of digestion)
Immunofluorescence	GD3A12, LKN1	Dermatan sulfate (relative expression level/distribution/completeness of digestion)
Enzymatic removal	Heparitinase I, Chondroitinase ABC, Hyaluronidase, Neuraminidase	Involvement in CPP uptake

also provides the means to follow dynamics of the glycocalyx in living cells without the need to introduce genetically tagged fusion proteins. In combination, these methods provide detailed insights into the involvement of GAGs in uptake (Table 1).

2 Materials

For performing the protocols on GAG analysis described below no adjustments of tissue culture protocols are required. Cells can be propagated according to the requirements of each particular cell line. Therefore, no specifications for tissue culture reagents and protocols are provided.

2.1 Single-Chain Antibody Fragments and Reagents for Indirect Immunofluorescence

1. Anti-HS single-chain antibodies (HS4C3, A04B08, EV3C3) [9–11], anti-DS single-chain antibodies (LKN1, GD3A12) [12, 13], and the anti-CS single-chain antibody (I03H10) [14]. Except for cases in which purity is required, periplasmic fractions are used. All single-chain antibodies carry a VSV-tag for recognition by a secondary antibody.
2. Second mouse-anti VSV monoclonal antibody (P5D4) is from hybridoma culture supernatant. Cell line (P5D4) is available from American Type Culture Collection (ATCC). Alternatively, polyclonal rabbit anti-VSV-G (Sigma) can be used.
3. Goat-anti-mouse IgG Alexa Fluor 488-conjugated antibody (Invitrogen, Life Technologies, Carlsbad, USA).
4. Hepes-buffered saline (HBS; 10 mM HEPES, 135 mM NaCl, 5 mM KCl, 1 mM $MgCl_2$, 1.8 mM $CaCl_2$, pH 7.4).

2.2 Detection of GAG Chains and Sialic Acids on HeLa Cells Using Live Cell Confocal Microscopy

1. 8-well microscopy chambers (Nunc, Wiesbaden, Germany).
2. TCS SP5 confocal microscope (Leica Microsystems, Mannheim, Germany), equipped with an HCX PL APO 63×N.A. 1.2 water immersion lens with 37 °C incubation chamber.
3. Fiji ImageJ software (ImageJ, U. S. National Institutes of Health, Bethesda, USA) for image analysis.

2.3 Detection of GAG Chains and Sialic Acids on HeLa Cells Using Flow Cytometry

1. 2 mM EDTA (PAN Biotech, Aidenbach, Germany) in HBS.
2. Propidium iodide (Sigma-Aldrich, St. Louis, USA).
3. FACS tubes (Micronic, Lelystad, the Netherlands).
4. FACSCalibur flow cytometer (BD Biosciences, Erembodegem, Belgium).
5. DeNovo FCS 4.0 (De Novo Software, Glendale, USA) and Summit 4.3 (Dako, Fort Collins, USA).

2.4 GAG-Digesting Enzymes

1. Heparitinase I (Seikagaku, Tokyo, Japan).
2. Hyaluronidase (Sigma Aldrich, St. Louis, USA).
3. Chondroitinase ABC (*see* **Note 1**; Sigma Aldrich, St. Louis, USA).
4. Neuraminidase (Sigma Aldrich, St. Louis, USA).

2.5 Reagents for Metabolic Labeling

1. Peracetylated N-azidoethylmannosamine (Ac4ManNAz, 50 mM stock in milliQ, SynAffix, Nijmegen, the Netherlands). Store at −20 °C.
2. Biotin-conjugated Bicyclo [6.1.0] nonyne (BCN, 10 mM stock in MillQ, SynAffix, Nijmegen, the Netherlands). Store at −20 °C.
3. Alexa Fluor 647-conjugated streptavidin (Invitrogen, Life Technologies, Carlsbad, USA). Store at −20 °C.
4. HBS.

3 Methods

3.1 Detection of Cell Surface GAG Chains on Live Cells

1. Grow HeLa cells (ATCC) in Roswell Park Memorial Institute medium (RPMI 1640) supplemented with 10 % FCS and 2 mM L-glutamine.
2. One day before the experiment seed 40,000 HeLa cells in 8-well microscopy chambers yielding a confluency of approximately 80 %.
3. Remove medium and wash adherent cells gently once with HBS.
4. Prepare the antibody solutions in HBS (dilution of antibodies against HS epitopes 20 times, of antibodies against DS and CS 5 times) (*see* **Note 2**). Transfer the solution gently on top of the adherent cells (*see* **Note 3**). Prepare 150 µL per well.

5. Incubate cells for 45 min at 20 °C.
6. Remove the incubation solution and wash the adherent cells three times with HBS.
7. Dilute the second antibody, mouse-anti VSV (P5D4), ten times in HBS. Use HBS as a control.
8. Incubate cells for 30 min at 4 °C (*see* **Note 4**).
9. Remove the antibody solution and wash cells three times with HBS.
10. Prepare the third antibody, goat-anti-mouse IgG Alexa Fluor 488 in HBS at a final concentration of 10 μg/mL (or HBS as control). Conjugates with other fluorophores can be used as desired/needed by the specific experimental condition.
11. Incubate cells for 30 min at 4 °C.
12. Remove the incubation solution.

For live cell confocal microscopy:

13. Wash the cells three times with pre-warmed culture medium.
14. Perform confocal microscopy using excitation at 488 nm and detection of fluorescence over 500–550 nm (*see* **Note 5**).

For flow cytometry:

13. Wash the cells three times with HBS.
14. Detach the cells using HBS-EDTA (*see* **Note 6**).
15. Transfer the cell suspension into FACS tubes.
16. Add propidium iodide at a final concentration of 2.5 μg/mL directly before the measurement. Measure fluorescence using flow cytometry. Measure Alexa Fluor 488 in the FL1 channel and propidium iodide in channel FL3 (*see* **Notes 5** and **7**).

3.2 Bioorthogonal Labeling of Cell Surface Sialic Acid Residues on Live Cells

1. Seed cells as in Subheading 3.1 (*see* **Note 8**).
2. Add peracetylated *N*-azidoacethylmannosamine at a final concentration of 50 μM to the cells. The sugar analog will enter the cells to be incorporated into the glycocalyx for direct monitoring of GAG clustering (Figs. 2 and 3).
3. Incubate cells overnight at 37 °C, 5 % CO_2.
4. Remove medium and wash cells gently with HBS three times.
5. Prepare a BCN-biotin solution in HBS with a final concentration of 60 μM (*see* **Note 9**). In control samples use MilliQ instead of BCN-biotin in HBS.
6. Incubate cells for 1 h at 20 °C.
7. Remove the incubation solution and wash cells three times with HBS.
8. Dilute Alexa Fluor 647-conjugated streptavidin to a final concentration of 5 μg/mL in HBS.

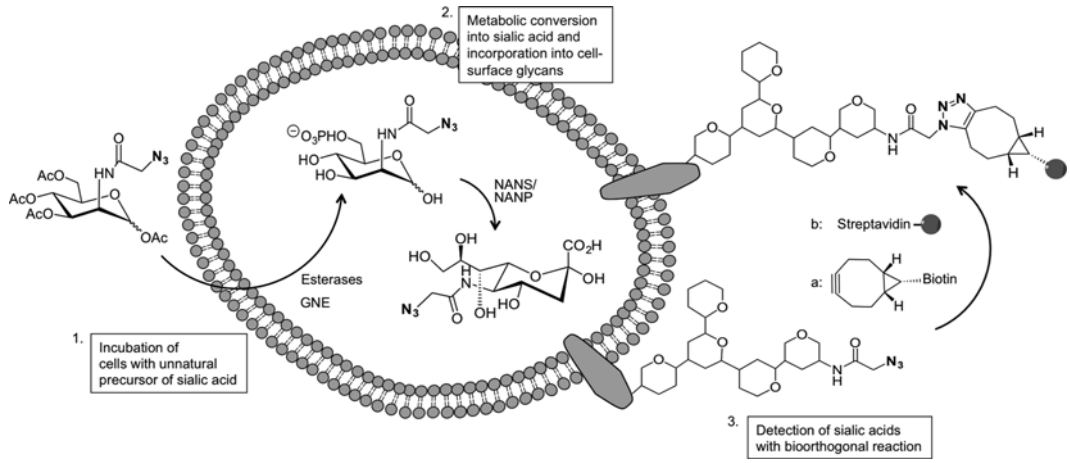

Fig. 2 Scheme of metabolic labeling. Exogenously added peracetylated *N*-azidoacethylmannosamine (Ac4ManNAz) can be taken up by cells and is deacetylated by intracellular esterases, and then enters into the salvage pathway, including UDP-GlcNAc 2-epimerase/ManNAc-6-kinase (GNE)-mediated phosphorylation of ManNAz and the generation of phosphorylated Neu5Ac (Neu5Ac-9-phosphate) by *N*-acetylneuraminic acid synthase (Neu5Ac-9-P synthetase/NANS) and dephosphorylation of Neu5Ac by *N*-acetylneuraminic-acid Phosphatase (Neu5Ac-9-P Phosphatase/NANP). After further modifications in the nucleus and the golgi apparatus, the azido-sialic acids appear as part of glycan moities of glycoproteins at the cell surface [16]. The detection of cell surface azido-sialic acids can be performed by using e.g. Bicyclo [6.1.0] nonyne (BCN) (*a*) in a metal-free strain promoted alkyne-azide cycloaddition (SPAAC) reaction, giving stable 1,2,3-triazoles. Finally, a fluorophore-conjugated streptavidin (*b*) can be used to visualize bioorthogonally labeled sialic acids using, e.g. confocal microscopy [17]

9. Incubate cells for 30 min at 4 °C.
10. Remove the incubation solution.
11. If peptide internalization is supposed to be measured, then the peptide solution should be added here.

For live cell confocal microscopy:

12. Wash the cells three times with pre-warmed culture medium.
13. Keep the cells for 1 h at 37 °C, 5 % CO_2 in culture medium before treatment with CPPs.
14. Perform confocal microscopy. Use the 633 nm laser line for excitation and collect the emission between 650 and 750 nm.

For flow cytometry:

15. Wash the adhered cells three times with HBS.
16. Detach the cells using HBS-EDTA.
17. Transfer the cell suspension to FACS tubes.
18. Measure the fluorescence using FACS-Calibur in the FL4 channel.

3.3 Enzymatic Removal of the Glycocalyx

1. In order to confirm the efficient removal of sialic acids, cells have to be fed with peracetylated *N-azidoacethylmannosamine* as described in Subheading 3.2 (bioorthogonal labeling)

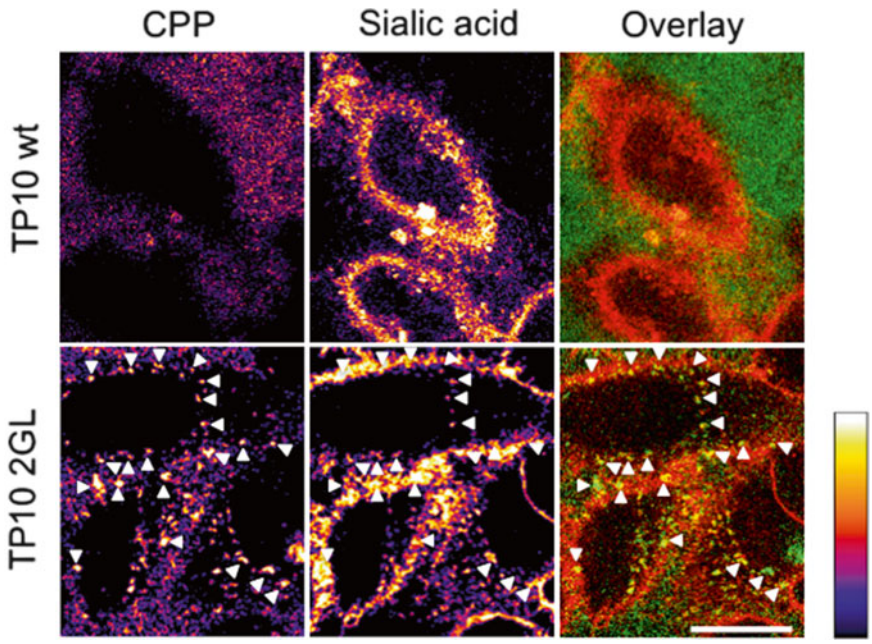

Fig. 3 Colocalization study of sialic acid with modified transportan peptides. Sialic acid moieties on HeLa cells were bioorthogonally labeled as described in Subheading 3.2. Subsequently, fluorescein-labeled TP10 wt or TP10 2GL (TP10 Gly2 → L-CF3-Bpg) was administered in a final concentration of 5 μM and confocal microscopy was performed after 30 min at 37 °C. Representative confocal images of cells are shown. For TP10 wt, no cluster formation was observed and no apparent changes in the cell surface distribution of sialic acids were visible (*upper panel*). In contrast, for TP10 Gly2 → L-CF3-Bpg, clusters are visible of cell surface sialic acid moieties which colocalizes with Gly2 → L-CF3-Bpg. Clusters are highlighted by *arrowheads* (*lower panel*). The false color look-up table ranges from *black* (low) to *white* (high) [18]. The scale bar corresponds to 20 μm

2. Seed cells as in Subheading 3.1
3. Prepare digestion cocktail containing all enzymes (Heparitinase I, Chondroitinase ABC, Neuraminidase, Hyaluronidase) or only some of the enzymes. When using hyaluronidase, weigh 2.75 mg hyaluronidase and add 5 mL RPMI + 1 % FCS yielding 275–550 U/mL.
4. If digestions of other GAGs are carried out in the presence of hyaluronidase take the required volume from the hyaluronidase mix (150 μL per sample) and add other enzymes. If hyaluronidase is not required add other enzymes to RPMI + 1 % FCS.
5. Add the other enzymes at the following concentrations: 10 mU/mL heparitinase I, 100 mU/mL chondroitinase ABC, 100 mU/mL neuraminidase.
6. Incubate cells for 1.5 h at 37 °C.
7. Wash cells with HBS twice.
8. Start peptide incubation as in Subheading 3.2 or stain glycocalyx as in Subheading 3.1.

4 Notes

1. Chondroitinase B is the dermatan sulfate-digesting enzyme.
2. No exact concentration of the scFvs can be measured as periplasmic fractions are used. Therefore, only dilution factors can be provided which may differ between batches.
3. In case of non-adherent or loose cells staining should be performed in suspension with EDTA-detached cells. Cells should be washed by centrifugation.
4. Incubation with the second antibody (P5D4) could also be performed at RT instead of 4 °C in order to reduce the stress for the cells.
5. If GAG labeling is to be performed concomitantly with uptake of fluorescein-labeled peptides, the third antibody comprising an alternative fluorophore such as Alexa Fluor 647 could be used.
6. Detachment of cells with 2 mM EDTA because protein cores of proteoglycans would be cleaved off if trypsin was used.
7. Text needs to be replaced by: Alexa Fluor 488 and fluorescein were detected in FL1 (530/30 BP), Propidium iodide in FL3 (< 670 LP) and excited with the 488 nm line of an argon ion laser. Alexa Fluor 647 was detected in FL4 (661/16 BP) and excited with the 647 nm line of a 635 nm-red diode laser.
8. For the analysis of sialic acid, it is important to cultivate the cells in RPMI and not in DMEM to prevent a strong competition between the *N*-azidoacethylmannosamine and the high glucose in DMEM.
9. Instead of using biotinylated BCN the bioorthogonal labeling can be performed using BCN which is directly conjugated to a fluorophore, e.g. BCN-Dy649 to prevent a possible crosslinking of the glycocalyx by streptavidin.

Acknowledgements

S. S. was supported by the Roche postdoc programme (ID 272).

References

1. Couchman JR (2010) Transmembrane signaling proteoglycans. Annu Rev Cell Dev Biol 26:89–114
2. Favretto ME, Wallbrecher R, Schmidt S, van de Putte R, Brock R (2014) Glycosaminoglycans in the cellular uptake of drug delivery vectors - bystanders or active players? J Control Release 180C:81–90
3. Christianson HC, Belting M (2014) Heparan sulfate proteoglycan as a cell-surface endocytosis receptor. Matrix Biol 35:51–55

4. Gerbal-Chaloin S, Gondeau C, Aldrian-Herrada G, Heitz F, Gauthier-Rouviere C, Divita G (2007) First step of the cell-penetrating peptide mechanism involves Rac1 GTPase-dependent actin-network remodelling. Biol Cell 99:223–238
5. Subrizi A, Tuominen E, Bunker A, Rog T, Antopolsky M, Urtti A (2012) Tat(48-60) peptide amino acid sequence is not unique in its cell penetrating properties and cell-surface glycosaminoglycans inhibit its cellular uptake. J Control Release 158:277–285
6. Esko JD, Stewart TE, Taylor WH (1985) Animal cell mutants defective in glycosaminoglycan biosynthesis. Proc Natl Acad Sci U S A 82:3197–3201
7. Esko JD, Weinke JL, Taylor WH, Ekborg G, Roden L, Anantharamaiah G, Gawish A (1987) Inhibition of chondroitin and heparan sulfate biosynthesis in Chinese hamster ovary cell mutants defective in galactosyltransferase I. J Biol Chem 262:12189–12195
8. Lidholt K, Weinke JL, Kiser CS, Lugemwa FN, Bame KJ, Cheifetz S, Massague J, Lindahl U, Esko JD (1992) A single mutation affects both N-acetylglucosaminyltransferase and glucuronosyltransferase activities in a Chinese hamster ovary cell mutant defective in heparan sulfate biosynthesis. Proc Natl Acad Sci U S A 89: 2267–2271
9. van Kuppevelt TH, Dennissen MA, van Venrooij WJ, Hoet RM, Veerkamp JH (1998) Generation and application of type-specific anti-heparan sulfate antibodies using phage display technology. Further evidence for heparan sulfate heterogeneity in the kidney. J Biol Chem 273:12960–12966
10. Jenniskens GJ, Oosterhof A, Brandwijk R, Veerkamp JH, van Kuppevelt TH (2000) Heparan sulfate heterogeneity in skeletal muscle basal lamina: demonstration by phage display-derived antibodies. J Neurosci 20:4099–4111
11. Smits NC, Robbesom AA, Versteeg EM, van de Westerlo EM, Dekhuijzen PN, van Kuppevelt TH (2004) Heterogeneity of heparan sulfates in human lung. Am J Respir Cell Mol Biol 30:166–173
12. Ten Dam GB, Yamada S, Kobayashi F, Purushothaman A, van de Westerlo EM, Bulten J, Malmstrom A, Sugahara K, Massuger LF, van Kuppevelt TH (2009) Dermatan sulfate domains defined by the novel antibody GD3A12, in normal tissues and ovarian adenocarcinomas. Histochem Cell Biol 132: 117–127
13. Lensen JF, Wijnhoven TJ, Kuik LH, Versteeg EM, Hafmans T, Rops AL, Pavao MS, van der Vlag J, van den Heuvel LP, Berden JH, van Kuppevelt TH (2006) Selection and characterization of a unique phage display-derived antibody against dermatan sulfate. Matrix Biol 25:457–461
14. Smetsers TF, van de Westerlo EM, ten Dam GB, Overes IM, Schalkwijk J, van Muijen GN, van Kuppevelt TH (2004) Human single-chain antibodies reactive with native chondroitin sulfate detect chondroitin sulfate alterations in melanoma and psoriasis. J Invest Dermatol 122:707–716
15. Wallbrecher R, Verdurmen WP, Schmidt S, Bovee-Geurts PH, Broecker F, Reinhardt A, van Kuppevelt TH, Seeberger PH, Brock R (2014) The stoichiometry of peptide-heparan sulfate binding as a determinant of uptake efficiency of cell-penetrating peptides. Cell Mol Life Sci 71:2717–2729
16. Munster-Kuhnel AK, Tiralongo J, Krapp S, Weinhold B, Ritz-Sedlacek V, Jacob U, Gerardy-Schahn R (2004) Structure and function of vertebrate CMP-sialic acid synthetases. Glycobiology 14:43R–51R
17. Dommerholt J, Schmidt S, Temming R, Hendriks LJ, Rutjes FP, van Hest JC, Lefeber DJ, Friedl P, van Delft FL (2010) Readily accessible bicyclononynes for bioorthogonal labeling and three-dimensional imaging of living cells. Angew Chem Int Ed Engl 49:9422–9425
18. Verdurmen WP, Wallbrecher R, Schmidt S, Eilander J, Bovee-Geurts P, Fanghanel S, Burck J, Wadhwani P, Ulrich AS, Brock R (2013) Cell surface clustering of heparan sulfate proteoglycans by amphipathic cell-penetrating peptides does not contribute to uptake. J Control Release 170:83–91

Chapter 9

Toxicity, Immunogenicity, Uptake, and Kinetics Methods for CPPs

Julia Uusna, Kent Langel, and Ülo Langel

Abstract

Cell-penetrating peptides (CPPs) have been utilized as delivery vectors for various payloads, both in vitro and in vivo. Similar issues as for any other drug delivery systems: cytotoxicity and the tendency to induce innate immune response may limit their applications in clinics. Therefore, assessment of cytotoxicity and immunogenicity is an important step toward characterization of applicability of these delivery vehicles. Studying internalization mechanisms and kinetics of CPPs provides important information for the development of novel and more efficient cellular delivery vectors. This chapter describes methods and protocols for investigation of cytotoxicity and immunogenic activities of CPPs in vitro and in vivo as well as methods for studying cellular uptake and internalization kinetics of CPPs. In the first section we describe methods for in vitro cell viability studies and ELISA assay, which allows to measure cytokine release in cell culture media and in blood serum in response to different CPP applications. This chapter also provides a protocol for assessing caspase-1 activity essential for inflammation. In the second section of this chapter, we describe a comprehensive method and protocol for determining the endocytosis mechanisms utilized in CPP uptake by using luciferin-CPP conjugates and endocytosis inhibitors.

Key words CPP, Toxicity, Immunogenicity, ELISA enzyme-linked immunosorbent assay, Kinetic uptake studies

1 Introduction

Efficient uptake of active molecules into target cells is essential to achieve the desired therapeutic effect. Since the cellular membrane limits internalization of several therapeutic agents including nucleic acids and proteins, several techniques such as electroporation, liposomes and viral delivery systems have been suggested to overcome this problem. The bottleneck of these approaches is cytotoxicity and undesired immunogenicity especially when applied in vivo. Cell-penetrating peptides (CPPs) are efficient transporters of various drug molecules, nucleic acids, and proteins not only in cultured cells but also in animal models. Although CPPs are generally considered to be non-toxic [1–3], anti-therapeutic protein antibodies can develop during the treatment compromising clinical

Ülo Langel (ed.), *Cell-Penetrating Peptides: Methods and Protocols*, Methods in Molecular Biology, vol. 1324,
DOI 10.1007/978-1-4939-2806-4_9,

effect [4]. Therefore, development of a suitable delivery system depends not only on the ability of delivery vectors to transport therapeutic agents through the biological barriers, but also on their risk of producing side effects: toxicity and undesired immunogenicity. Generation of cytotoxic and immunogenic profiles of CPPs is very essential for fully understanding their activity and desired effect modulation. In peptide-cargo conjugates the presence and origin of cargo molecule also influences the toxicity and may differ from that exerted by the peptide alone. Several independent studies have elucidated the effects derived from conjugation of different cargos to CPPs. Jones et al., compared the toxicities of rhodamine-labeled and unlabeled pAntp (43–58), pTAT (48–60), TP10, and Arg_{11}, and their conjugates with NBD peptide cargo in A549 cells [5]. The CPP-NBD or its scrambled sequence increased the toxicity of TP10 and pTAT (48–60), decreased the toxicity of Arg_{11} and had no effect on pAntp (43–58) response. Several reports demonstrated that the conjugation of the carboxyfluorescein to CPP increases the cytotoxicity of the peptide [6, 7]. Similarly, Cardozo et al. showed that the cytotoxicity of TAT (48–57) and penetratin was higher for CPP conjugates with larger cargo peptides than for those unlabelled or with smaller cargo [8].

The administration of almost any foreign macromolecule to an animal can elicit the immune response. Several in vitro assays have evaluated the effect that nanomaterials can produce on immune cell uptake, viability, and cytokine expression. Shukla et al. demonstrated that 3–8 nm gold nanoparticles (AuNP-s) at a certain concentration and of a certain size do not reduce viability and do not stimulate inflammatory cytokines such as TNF-α and IL-1 β. Yen et al. evaluated AuNP effect on J774 A1 macrophages testing different size ranges: 2–4 nm, 5–7 nm, and 20–40 nm [9, 10]. They showed that AuNP triggered the inflammatory response, producing higher levels of IL-1 β, IL-6, and TNF-α cytokines within 6 h compared to controls.

Moreover, several independent studies report that amphipathic CPPs are more toxic than cationic ones, demonstrating that even 5 μM of transportan 10 affects cellular metabolism [11], whereas the cationic peptides such as TAT are not cytotoxic in vitro even at concentrations up to 0.4 mM [12]. Still, in vivo studies of the same peptide indicated some mild cytotoxicity on a rabbit's eyelid after 7 days of application. These data show that in vivo studies that characterize the immunological response to the drug delivery agents are very important.

As it has been shown, CPPs are different in their properties and, therefore, might not utilize similar internalization pathways. Development of more efficient transporters for specific purposes requires the investigation of uptake mechanisms, uptake kinetics, and biological activities of different origin CPPs. Examples of CPP kinetic studies utilize fluorescein-tags [13–15], radiolabels [16],

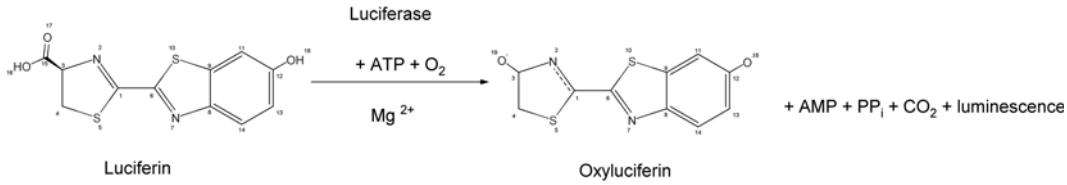

Fig. 1 Cell viability assay based on luciferase reaction. Stable luciferase enzyme catalyzes mono-oxidation of luciferin in the presence of magnesium, molecular oxygen and ATP released from the cells. The amount of ATP is directly proportional to the number of cells in culture

and more recently, biomarkers [17–19]. Uptake studies utilizing fluorescent labels may not distinguish between endosomally trapped and released peptides and can lead to misinterpretations. Moreover, kinetic assays provide many advantages over single-endpoint using methods, as different CPPs can have different internalization kinetic profiles often not reflected in endpoint analysis. Experiments with biomarker-CPP conjugates revealed that CPPs can be divided into fast and slow internalization groups based on their cellular uptake. Therefore, it is imperative, for further delivery vector development, to determine the exact employed internalization route as it likely dictates the intracellular fate and subsequent trafficking of the internalized ligands.

Based on these findings we suggest to analyze cytoplasmic uptake by using bioluminescence-based kinetic assays utilizing endocytosis inhibitors.

1.1 Luminescent Cell Viability Assay

Luminescent cell viability assay provides a fast and relatively simple method for evaluation of cellular viability in the presence of CPPs. The assay allows to determine the number of viable cells in culture based on quantification of ATP, which signals the presence of metabolically active cells. Luminescent cell viability assay results in cell lysis and generation of a luminescent signal proportional to the amount of ATP present. The amount of ATP is directly proportional to the number of cells in culture (Fig. 1). The luminescent cell viability assay is more sensitive [20–22] and less complicated than other commonly used methods such as MTT or MTS (*see* **Note 1**).

1.2 Luminescent Cytotoxicity Assays

The luminescent cytotoxicity assay comprises addition of a single homogeneous reagent that allows detection of dead cells in cell population by measuring a distinct protease activity [23]. The assay is based on luminogenic peptide substrate (alanyl-alanylphenylalanyl-aminoluciferin or AAF), which is cleaved by proteases released from damaged cells (Fig. 2). The substrate cannot penetrate the intact membrane and therefore, does not generate signal from the viable cell population. The assay is very precise as it allows calculating the total number of cells in each well detecting by sequential luminescent measures both viable and unviable cells (*see* **Note 2**). Data are collected as relative light units (RLU).

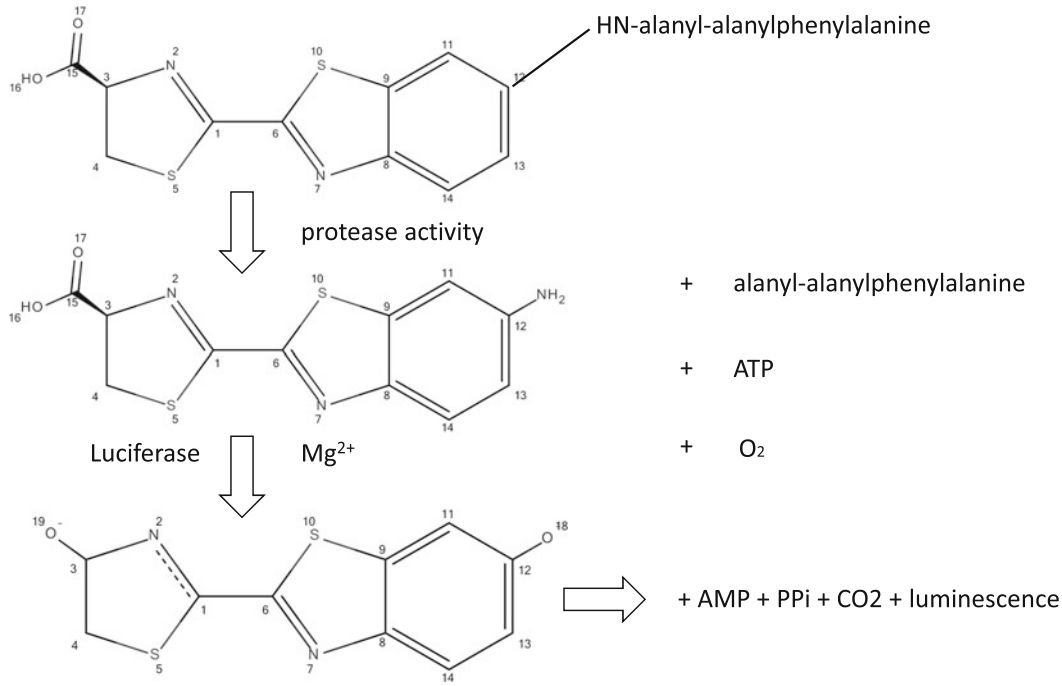

Fig. 2 Cytotoxicity assay based on proteolytic reaction. Dead cells release proteases, which cleave the luminogenic substrate. Active luciferin is converted into oxyluciferin by luciferase and luminescence is emitted

1.3 Cytokine Detection In Vitro Using ELISA Immunoassay

Enzyme-linked immunosorbent assay (ELISA) is a plate-based immunoassay for detection and quantification of substances such as peptides, proteins, antibodies, and hormones. The main principle of the assay is the immobilization of the antigen of interest that can be accomplished by direct adsorption to the assay plate or indirectly via a capture antibody which has been attached to the plate. The antigen is detected either directly (labeled primary antibody) or indirectly (labeled secondary antibody). The most powerful ELISA assay format is the sandwich assay where the antigen is bound between two primary antibodies—the capture antibody and the detection antibody. A monoclonal primary antibody specific for human IL-1β has been immobilized on a microplate. IL-1β present in standards and samples binds to immobilized antibody. After washing away any unbound substances, horseradish peroxidase-linked polyclonal antibody capture IL-1β present in standards and samples forming the so-called sandwich structure. Horseradish peroxidase catalyses conversion of chromogenic substrate TMB (3,3′,5,5′-tetramethylbenzidine) resulting in diimine that causes color change of the solution (blue) that can be read on a spectrophotometer at a wavelength of 650 nm. The reaction can be stopped by addition of sulfuric acid turning TMB into yellow [24, 25]. The signal can be read at 450 nm. The sandwich format has high selectivity and sensitivity as the key element of the

detection strategy is a highly specific antibody–antigen interaction. ELISA assay can be used for the analysis of the influence of novel CPPs and peptide/nucleic acid complexes on innate immune response by measuring IL-1β cytokine release in cell culture supernatants and mouse serum (*see* **Note 3**).

1.4 Caspase Activity Assay

Caspases are cysteine proteases, which use a cysteine residue for the cleavage of their substrate proteins at the aspartic acid residue. The generic name for all members is caspase with the "c" denoting a cysteine protease and "aspase" referring to the aspartate-specific cleaving ability of these enzymes. Caspases play important role in cells death and inflammation [26]. Among them, caspase-3 and 7 are a frequently activated proteases, catalyzing the specific cleavage of many key cellular proteins, initiating cellular death [27]. Caspase-1 or ICE (interleukin-1β-converting enzyme) is an essential regulator of inflammatory responses through its capacity to process and activate proIL-1β, proIL-18, and proIL-33 [28, 29]. Therefore, caspase-1 is considered as "inflammatory" caspase.

Here, the CPP's possible immunogenic effects were analyzed by measuring caspase-1 and caspase 3/7 activities in vitro [1]. Caspase-specific peptides conjugated to fluorescent reporter molecules were used as a cleavage substrate for caspase-1 and caspase 3/7. The cleavage of this caspase-specific molecules by the caspases releases the fluorochrome that, when excited by light at 400 nm wavelength, emits fluorescence at 505 nm [30–32]. Level of caspase enzymatic activity in the cell lysate is directly proportional to the fluorescence signal detected with a fluorimeter or a fluorescent microplate reader (*see* **Note 4**).

2 Materials

2.1 Luminescent Cell Viability and Cytotoxicity Assays

1. 96 multiwell plate.
2. Multichannel pipette or automated pipetting station for reagent delivery.
3. Plate shaker for mixing multiwell plates.
4. Assay buffer.
5. Luminogenic peptide substrate (AAF).
6. Digitonin.
7. Luminometer.

2.2 Preparation of the Reagents

1. Thaw assay buffer, and keep at room temperature before use or up to 48 h.
2. Equilibrate the lyophilized assay substrate to room temperature prior to use.

3. Transfer 10 ml of assay buffer into the lyophilized assay substrate to reconstitute the substrate or enzyme/substrate mixture resulting in cell viability assay reagent or cytotoxicity assay reagent.
4. For cytotoxicity assay prepare lysis reagent by adding 33 μl of digitonin to the assay buffer.
5. Mix gently to obtain a homogeneous solution and let it sit for 1 min.

2.3 ELISA Immunoassay

1. Microplate reader capable of measuring absorbance at 450 nm, with the correction wavelength set at 540 or 570 nm.
2. Pipettes and pipette tips.
3. Deionized or distilled water.
4. Squirt bottle, manifold dispenser or automated microplate washer.
5. 500 ml graduated cylinder.
6. 25× washing solution containing 10 mM phosphate buffer pH 7.4, 150 mM NaCl, 0.05 % Tween 20.
7. Polyclonal antibody specific for human IL-1β conjugated to horseradish peroxidase.
8. Substrate solution containing color reagent A (stabilized hydrogen peroxide).
9. Substrate solution containing color reagent B (stabilized chromogen (tetramethylbenzidine)).
10. Stop solution (2N sulfuric acid).
11. Human IL-1β standard (recombinant human IL-1β).
12. 96-well polystyrene microplate coated with a monoclonal antibody specific for human IL-1β.
13. Adhesive strips for plate sealing.

2.4 Preparation of the Reagents

1. Pre-warm all reagents at room temperature before use.
2. Add 20 ml of wash buffer concentrate to deionized or distilled water to prepare 500 ml of 1× wash buffer.
3. Prepare substrate solution by mixing color reagents A and B in equal volumes within 15 min of application. Keep the mixture away from light.
4. Prepare human IL-1β standard stock solution with concentration 250 pg/ml. For that reconstitute the pellet with 5.0 ml of buffered solution (for cell culture supernatant samples cell culture media can be used) or standard animal serum (for blood serum samples). Allow the standard to sit for 15 min.
5. Pipette 500 μl of buffered solution or standard animal serum into each tube.

6. Prepare human IL-1β standard dilution series using 250 pg/ml stock solution: 125, 62.5, 31.25, 15.6, 7.8, 3.9, 0 pg/ml. Mix each tube thoroughly before the next transfer.

2.5 Caspase Activity Assay

1. Pipettes and pipette tips.
2. Black 96-well flat bottom microplate.
3. 4 mM WEHD substrate, a peptide conjugated to 7-amino-4-trifluoromethyl coumarin (AFC) for caspase-1 and substrate rhodamine 110, bis-(*N*-CBZL-aspartyl-L-glutamyl-L-valyl-l-aspartic acid amide); Z-DEVD-R110 for caspase 3/7 detection.
4. 1 M solution of dithiothreitol (DTT).
5. Lysis buffer, a non-denaturing buffered solution with surfactant.
6. 2× reaction buffer containing 100 mmol/l HEPES (pH 7.5), 20 % (v:v) glycerol, 5 mmol/l DTT, and 0.5 mmol/l EDTA.
7. Centrifuge with microplate rotor.
8. Fluorimeter or a fluorescent microplate reader.

2.6 Preparation of the Reagents

1. Prepare 2× reaction buffer by adding 10 µl of fresh DTT stock per 1 ml of 2× reaction buffer.
2. Chill lysis buffer on ice. Use it pre-cooled for determination of caspase activity.

2.7 Internalization and Uptake Mechanisms of CPPs

1. Cell lines and cell culture media required for the corresponding cell line.
2. 6-well cell culturing plates.
3. 96-well clear-bottom plates.
4. Media without phenol red.
5. Luminometer.

2.8 Bioluminescence Assay Incorporating Endocytosis Inhibitors

1. Luciferin-CPP conjugates in 100 µM stock solution and free luciferin for control experiments.
2. Cells stably expressing luciferase or cells that can be transfected with a luciferase-encoding plasmid.
3. Stock solutions of endocytosis inhibitors at their effective concentration (*see* **Note 5**).

3 Methods

3.1 Cell Viability and Cytotoxicity Assays

1. Human breast cancer cell lines MDA-MB-231 and MCF-7 are commonly used for cytotoxic analyses. Seed 2×10^4 cells into 96-well plate, 100 µl per well. Multiwell plates must be compatible with the luminometer used.

2. Prepare control wells containing medium without cells to obtain a value for background luminescence.
3. Add the CPP for example here p53 C′ analogs peptide 4 and peptide 5 or at the concentration range 1–40 μM to experimental wells, and incubate for 24 and 48 h in complete medium.
4. Equilibrate the plate and its contents at room temperature for approximately 30 min.
5. In order to estimate cellular viability, add 100 μl of luminescent cell viability assay reagent equal to the volume of cell culture medium present in each well.
6. Mix contents for 2 min on an orbital shaker.
7. Allow the plate to incubate at room temperature for 10 min in order to stabilize luminescent signal.
8. Measure the luminescence using luminometer.
9. In case of cytotoxic assay proceed as described above till **step 4**.
10. In order to estimate cytotoxicity, add 50 μl of cytotoxicity assay to each well and mix briefly by shaking.
11. Incubate for 15 min at room temperature.
12. Measure the luminescence using luminometer.
13. Add 50 μl of lysis reagent containing digitonin to all wells. Mix, and incubate the plate at room temperature for 15 min.
14. Measure the luminescence again using luminometer.
15. Calculate the luminescent contribution of previously viable cells (after lysis) by subtracting the luminescent signal resulting from experimental cell death (first luminescence measurement) from total luminescence death (second luminescent measurement):
16. Viable cell luminescence = Total cell luminescence – Experimental dead cell luminescence.
17. Untreated cells were defined as 100 % viable. The results are the means of three independent experiment performed in duplicate. An example of the results is shown in Fig. 3 [33].

3.2 ELISA Immunoassay

1. For peptide immunogenic studies use THP-1, human acute monocytic leukemia cells and PBMC human peripheral blood mononuclear cells, isolated from healthy donor by standard density gradient centrifugation.
2. Stimulate THP-1 or PBMC cells with 15 ng/ml PMA (phorbol 12-myristate 13-acetate) 1 day before the experiment.
3. Seed 1×10^6 cells per well into 24-well plates on the day of the experiment.
4. Treat the cells with CPP at the concentration of 5 μM. In parallel, treat the cells with plasmid/CPP at different charge ratios, for instance, CR 1:1 and 1:5 and siRNA/CPP com-

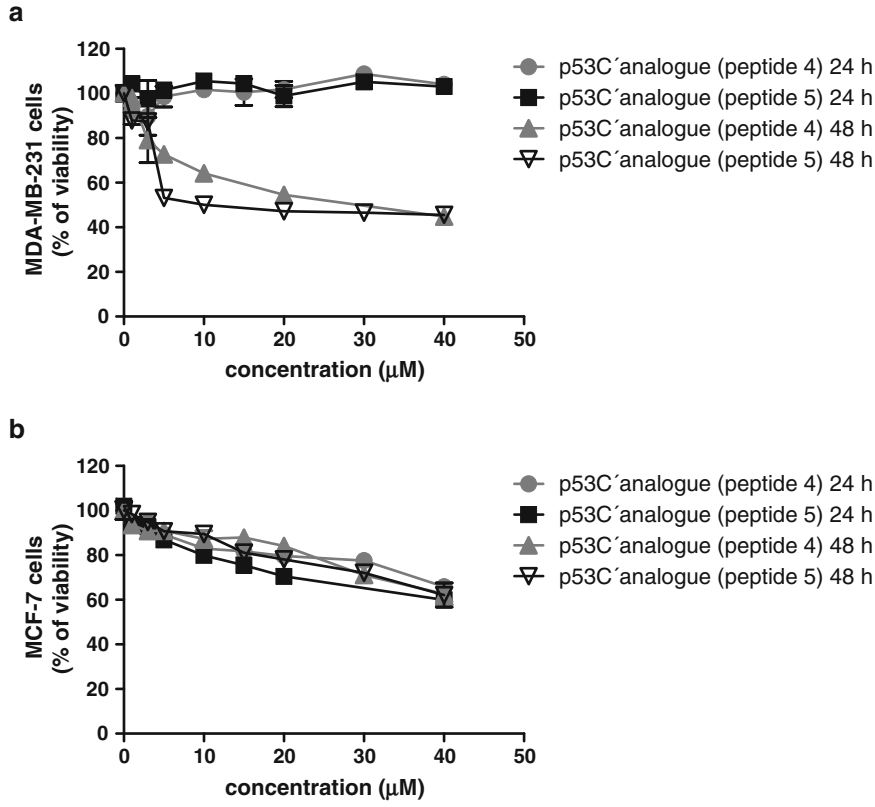

Fig. 3 p53C′ analog's activities in different breast cancer cell lines. The viability was measured in MDA-MB-231 (**a**) and MCF-7 (**b**) cells after 24 and 48 h of incubation

plexes at different molar ratios, here MR 40, 50 nM siRNA. Incubate for 4 h in serum-free medium followed by addition of 1 ml complete medium. Use 10 μg/ml LPS as positive control.

5. Collect 200 μl of supernatants after 24 and 48 h of incubation and apply on 96-well microplate coated with a monoclonal antibody specific for human IL-1β. In case of blood samples add additional 50 μl of standard serum to each sample for minor dilution.
6. Seal the plate with the adhesive strip. Incubate the plate for 2 h at room temperature.
7. Aspirate and wash by pipetting 400 μl of wash buffer in each well or use the automatic plate washer. Remove the liquid from the wells completely and repeat washing for two times. Invert the plate and blot it against the paper towels in order to discard all residues.
8. Add 200 μl of IL-1β conjugate to each well, place a new adhesive strip and incubate for 1 h at room temperature. If blood serum samples were used, prolong the incubation for 2 h.

9. Repeat the aspiration/wash as in **step 7**.
10. Add to each well 200 μl of substrate solution prepared as described previously. Incubate in dark place for 20 min at room temperature.
11. Add 50 μl of stop solution to each well and resuspend to ensure the solution is uniform.
12. Measure the optical density of each well within 30 min, using a microplate reader set to 450 nm. For more accurate results correct optical imperfections in the plate by subtracting readings at 540 nm or 570 nm from the readings at 450 nm. An example of the result is presented in Fig. 4a [1].

3.3 In Vivo Toxicology Assay

1. Analyze possible toxic and immunogenic effects of CPPs in vivo using ELISA immunoassay for blood serum samples. Perform immunoassay as described above using blood serum extracted from mice as described in Subheading 3.2.
2. Utilize immunocompetent C57BL/6 male and female mice, at least two mice per group.
3. Perform i.v. injection of 1 and 5 mg/kg of TP10, PF3, PF4, and PF6 and their equimolar doses of 0.01 and 0.06 μmol per animal respectively. For positive control inject some animals with 10 μg/ml LPS.
4. Analyze cytokine levels in serum 24 and 48 h post injection using ELISA immunoassay following the protocol described above.
5. Collect blood samples via heart puncture and separate serum using serum gel-separation tubes.
6. For anesthesia, prepare 75 mg/kg ketamine and 1.0 mg/kg dexmedetomidine in saline solution and perform i.p. injection to mice.
7. Dissert and collect liver, kidney, lung, and spleen immediately after blood sample extraction and frozen in 2-methylbutan at −60 °C.
8. Fix cryosections in formalin, stained with hematoxylin and eosin and use for histopathological analysis.
9. For better statistics analyze three independent experiments. An example of the result is presented in Fig. 4b [1].

3.4 Caspase Activity Assay

1. Stimulate THP-1 or PBMC cells with 15 ng/ml of PMA (phorbol 12-myristate 13-acetate) 1 day before the experiment.
2. Seed 1×10^6 cells per well into 24-well plates on the day of the experiment.
3. Treat the cells with CPPs: PF3, PF4, and PF6 peptides at the concentration of 5 μM. Incubate for 4 h in serum-free medium

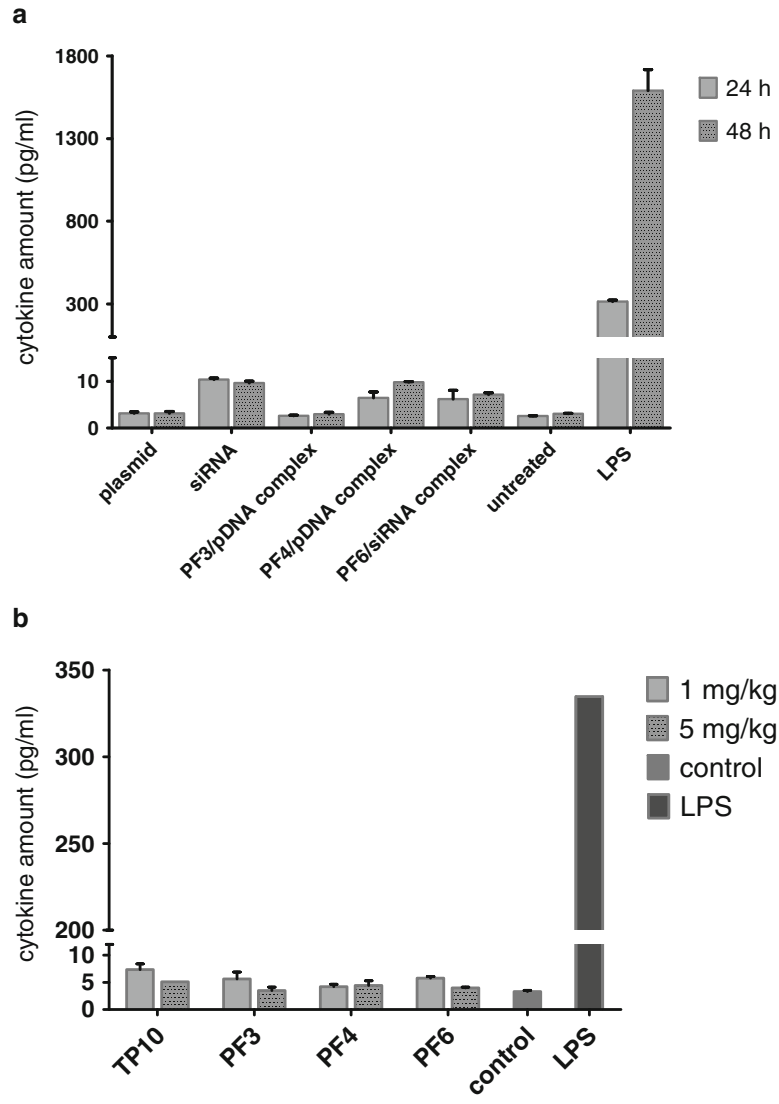

Fig. 4 IL-1β release in THP-1 cell's culture media and blood serum. IL-1β release (pg/ml) was measured in cell culture media after treatment with peptides or peptide/nucleic acids complexes (plasmid/PF3 at CR2 and plasmid/PF4 at CR4, and siRNA/PF6 MR40, 50 nM HPRT siRNA) (**a**). IL-1β amount (pg/ml) was measured in blood serum on the next day after injection with different peptides (**b**)

followed by addition of 1 ml complete medium. Use 10 μg/ml LPS as positive control.

4. After 48 h of incubation count the cells in each well and centrifuge the plate at 500 × *g* for 10 min.
5. Discard the supernatants and resuspend the pellet in cold lysis buffer. Calculate the amount of lysis buffer needed per each well,

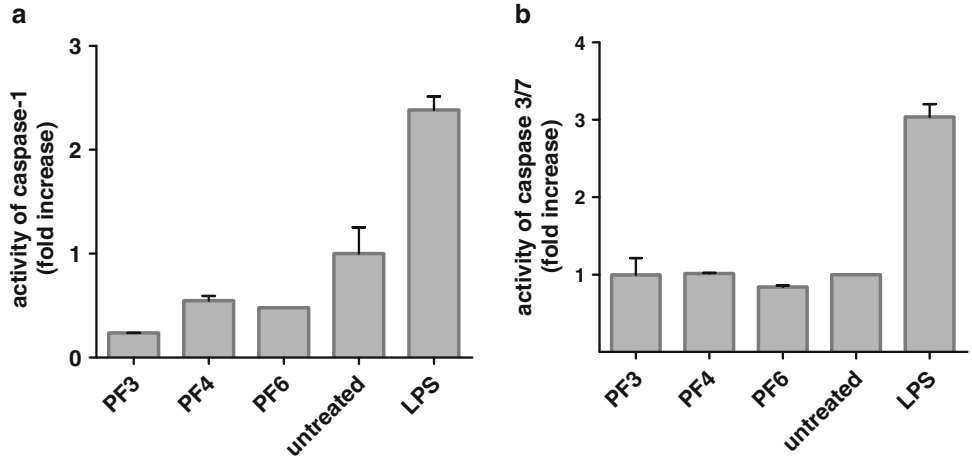

Fig. 5 Caspase activity measured in THP-1 cell line. Caspase-1 (**a**) and caspase-3/7 (**b**) activities were measured in cells incubated with PF3, PF4, and PF6 peptides for 48 h, as described previously. The results are expressed as fold increase in caspase activity of dead cells over untreated cells. Values represent the mean of at least three independent experiments performed in duplicate (mean ± SEM)

considering that 25 μl of reagent is required in order to lyse 1×10^6 cells.

6. Incubate on ice for 40 min and then centrifuge at $10{,}000 \times g$ for 1 min. The supernatant or cell lysate contains certain amount of protein that can be estimated by protein determination assay.
7. Transfer 50 μl of supernatant into a black 96-well flat bottom microplate that can be read with a microplate reader. Keep the plate on ice.
8. Add 50 μl of 2× reaction buffer to each well, mix thoroughly.
9. Add 5 μl of caspase fluorogenic substrate (WEHED-AFC) and incubate for 2 h at 37 °C.
10. Read the plate by fluorimeter using a set for excitation at 400 nm and emission at 505 nm (*see* **Note 4**). An example of caspase activity results are presented in Fig. 5 [1].

3.5 CPP Internalization and Uptake Mechanisms

1. Propagate the cells (e.g. HeLa pLuc 705 cells) in standard conditions at 37 °C and 5 % CO_2 concentration in standard cell culture dishes.
2. Seed a higher amount of cells for transfection to ensure cell viability for the assay, e.g. 2×10^5.
3. Complete medium without phenol red should be used to reduce possible cross-talk during uptake kinetics measurements.

3.6 Bioluminescence Assay Incorporating Endocytosis Inhibitors

1. Seed 2×10^5 HeLa pLuc 705 cells into a 6-well cell culture plate (Day 1).
2. After 24 h, transfect the cells with a luciferase-encoding plasmid (*see* **Note 6**) (Day 2).
3. After another 24 h, seed 9×10^3 cells into 96-well clear-bottom plate (Day 3).
4. 24 h after the second seeding, treat the cells with luciferin-CPP conjugates (Day 4). For this, prepare the conjugates in full cell culture media at the desired concentrations and wash the cells once with 100 µl complete cell culture media.
5. Before adding the conjugates pre-incubate the cells with endocytosis inhibitors. For this, dissolve the inhibitors at the required concentrations (*see* **Note 5**) in complete media without phenol red and carry out the pre-treatment for 30 min in a humidified 5 % CO_2 environment at 37 °C.
6. After pre-treating the cells with endocytosis inhibitors, replace the incubation media with the desired concentration of 120 µl luciferin-CPP solution in complete medium without phenol red. Also, endocytosis inhibitors have to remain present during luciferin-CPP treatment.
7. Measure the luminescence at 1.5 min time intervals for 2 h in complete medium in atmospheric CO_2 at room temperature (25 °C). For control experiments, use free luciferin at the same concentration as the luciferin-CPP conjugates.
8. In order to analyze how the used endocytosis inhibitors affect the overall luciferin-CPP uptake, calculate the area-under-the-curve (AUC) of the registered kinetics curves at desired time points. For normalizing, use the AUC of the no inhibitor treated sample at the same time points (Fig. 6) [34].

4 Notes

1. Maximal sensitivity of the assay will be achieved within 15 min. The signal intensity will remain largely unchanged for approximately 1 h. The signal half-life is 5 h.
2. Uneven luminescent signal within standard plates can be caused by temperature gradients, uneven seeding of cells or edge effects in multiwell plates.
3. IL 1 plays a central role in immune and inflammatory responses and it is not produced by unstimulated cells with the exception of skin keratinocytes, some epithelial cells, and certain cells of the central nervous system. Only in response to inflammatory agents, infections, microbial endotoxins, and peptides, a dramatic

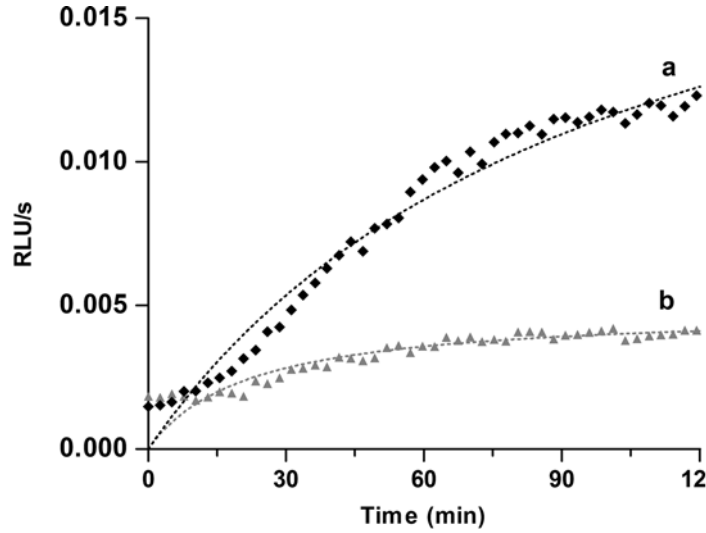

Fig. 6 Example of results from the bioluminescence assay incorporating endocytosis inhibitors. Cells were incubated with 10 μM luciferin-linker-M918 conjugate. The luminescence was recorded over a period of 2 h without (**a**) and in the presence of endocytosis inhibitors (**b**). The area-under-the-curve (AUC, in RLU units) for each sample was calculated at every time point and normalized to no inhibitor treated sample at the same time points

increase in the production of IL-1 by macrophages (PBMC), lymphocytes (THP-1), and various other cell types is observed [35–38]. Therefore, IL-1 is a good marker for immunogenic studies.

4. For caspase activity assay, normalize the results by the cell count in each well and express as fold increase in caspase activity of peptide-treated cells over untreated cells. The results are the mean values of three independent experiments performed in duplicates. Additional controls with no cell lysate and no substrate can be included in this assay. For that distilled water can be used to substitute the volume of cell lysate or substrate reagent.
5. Various endocytosis inhibitors can be used in order to inhibit endocytosis. For example, utilize 10 μM chlorpromazine in order to inhibit clathrin-mediated endocytosis, 4 μM cytochalasinD (CyD) to inhibit macropinocytosis, and 50 μM nystatin to inhibit caveolae/lipid raft-dependent endocytosis. Also 100 μM chloroquine can be used to study endosomal release and vesicle recycling.
6. For transient transfection, 4 μg luciferase encoding pGL3 plasmid was complexed with 10 μl Lipofectamine™ 2000 reagent and the cells were transfected according to the manufacturer's

instructions in 2.5 ml complete medium for 4 h. After that the transfection medium was replaced with fresh complete medium and the cells were grown for further 20 h.

Acknowledgements

The work was supported by the Swedish Research Council (VR-NT); by the Center for Biomembrane Research, Stockholm; by Knut and Alice Wallenberg's Foundation; by the EU through the European Regional Development Fund through the Center of Excellence in Chemical Biology, Estonia; by the targeted financing SF0180027s08 from the Estonian Government; by the DoRa Program of The European Social Fund; by the Archimedes Foundation; by SSF (Sweden Japan); by the funds from the targeted financing IUT20-26 from the Estonian Ministry of Education and Research; by the Estonian Science Foundation (ETF9438); by project HCV-Tech (3.2.0701.11-0015) and by Tumor-Tech: 3.2.1001.11-0008.

References

1. Suhorutšenko J, Oskolkov N, Arukuusk P et al (2011) Cell-penetrating peptides, PepFects, show no evidence of toxicity and immunogenicity in vitro and in vivo. Bioconjug Chem 22:2255–2262
2. el Khafagy S, Kamei N, Nielsen EJ et al (2013) One-month subchronic toxicity study of cell-penetrating peptides for insulin nasal delivery in rats. Eur J Pharm Biopharm 85:736–743
3. Lim S, Kim WJ, Kim YH et al (2012) Identification of a novel cell-penetrating peptide from human phosphatidate phosphatase LPIN3. Mol Cells 34:577–582
4. Trehin R, Merkle HP (2004) Chances and pitfalls of cell penetrating peptides for cellular drug delivery. Eur J Pharm Biopharm 58: 209–223
5. Jones SW, Christison R, Bundell K et al (2005) Characterisation of cell-penetrating peptide-mediated peptide delivery. Br J Pharmacol 145:1093–1102
6. El-Andaloussi S, Järver P, Johansson HJ et al (2007) Cargo-dependent cytotoxicity and delivery efficacy of cell-penetrating peptides: a comparative study. Biochem J 407:285–292
7. Dupont E, Prochiantz A, Joliot A (2007) Identification of a signal peptide for unconventional secretion. J Biol Chem 282:8994–9000
8. Cardozo AK, Buchillier V, Mathieu M et al (2007) Cell-permeable peptides induce dose- and length-dependent cytotoxic effects. Biochim Biophys Acta 1768:2222–2234
9. Shukla R, Bansal V, Chaudhary M et al (2005) Biocompatibility of gold nanoparticles and their endocytotic fate inside the cellular compartment: a microscopic overview. Langmuir 21:10644–10654
10. Yen HJ, Hsu SH, Tsai CL (2009) Cytotoxicity and immunological response of gold and silver nanoparticles of different sizes. Small 5:1553–1561
11. Kilk K, Mahlapuu R, Soomets U et al (2009) Analysis of in vitro toxicity of five cell-penetrating peptides by metabolic profiling. Toxicology 265:87–95
12. Akkarawongsa R, Cullinan AE, Zinkel A et al (2006) Corneal toxicity of cell-penetrating peptides that inhibit Herpes simplex virus entry. J Ocul Pharmacol Ther 22:279–289
13. Richard JP, Melikov K, Vives E et al (2003) Cell-penetrating peptides. A reevaluation of the mechanism of cellular uptake. J Biol Chem 278:585–590
14. Suzuki T, Futaki S, Niwa M et al (2002) Possible existence of common internalization mechanisms among arginine-rich peptides. J Biol Chem 277:2437–2443
15. Drin G, Mazel M, Clair P et al (2001) Physico-chemical requirements for cellular uptake of pAntp peptide. Role of lipid-binding affinity. Eur J Biochem 268:1304–1314
16. Polyakov V, Sharma V, Dahlheimer JL et al (2000) Novel Tat-peptide chelates for direct transduction of technetium-99 m and rhenium

into human cells for imaging and radiotherapy. Bioconjug Chem 11:762–771

17. Jones LR, Goun EA, Shinde R et al (2006) Releasable luciferin-transporter conjugates: tools for the real-time analysis of cellular uptake and release. J Am Chem Soc 128:6526–6527
18. Wender PA, Goun EA, Jones LR et al (2007) Real-time analysis of uptake and bioactivatable cleavage of luciferin-transporter conjugates in transgenic reporter mice. Proc Natl Acad Sci U S A 104:10340–10345
19. Eiriksdottir E, Mäger I, Lehto T et al (2010) Cellular internalization kinetics of (luciferin-) cell-penetrating peptide conjugates. Bioconjug Chem 21:1662–1672
20. Petty RD, Sutherland LA, Hunter EM et al (1995) Comparison of MTT and ATP-based assays for the measurement of viable cell number. J Biolumin Chemilumin 10:29–34
21. Cree IA, Pazzagli M, Mini E et al (1995) Methotrexate chemosensitivity by ATP luminescence in human leukemia cell lines and in breast cancer primary cultures: comparison of the TCA-100 assay with a clonogenic assay. Anticancer Drugs 6:398–404
22. Maehara Y, Anai H, Tamada R et al (1987) The ATP assay is more sensitive than the succinate dehydrogenase inhibition test for predicting cell viability. Eur J Cancer Clin Oncol 23:273–276
23. Niles AL, Moravec RA, Eric HP et al (2007) A homogeneous assay to measure live and dead cells in the same sample by detecting different protease markers. Anal Biochem 366:197–206
24. Martin TL, Mufson EJ, Mesulam MM (1984) The light side of horseradish peroxidase histochemistry. J Histochem Cytochem 32:793
25. Veitch NC (2004) Horseradish peroxidase: a modern view of a classic enzyme. Phytochemistry 65:249–259
26. Danial NN, Korsmeyer SJ (2004) Cell death: critical control points. Cell 116:205–219
27. Porter AG, Janicke RU (1999) Emerging roles of caspase-3 in apoptosis. Cell Death Differ 6:99–104
28. Dinarello CA (2002) The IL-1 family and inflammatory diseases. Clin Exp Rheumatol 20:S1–S13
29. Ogura Y, Sutterwala FS, Flavell RA (2006) The inflammasome: first line of the immune response to cell stress. Cell 126:659–662
30. Garcia-Calvo M, Peterson EP, Leiting B et al (1998) Inhibition of human caspases by peptide-based and macromolecular inhibitors. J Biol Chem 273:32608–32613
31. Nicholson DW, Ali A, Thornberry NA et al (1995) Identification and inhibition of the ICE/CED-3 protease necessary for mammalian apoptosis. Nature 376:37–43
32. Alnemri ES, Livingston DJ, Nicholson DW et al (1996) Human ICE/CED-3 protease nomenclature. Cell 87:171
33. Suhorutšenko J, Eriste E, Copolovici DM et al (2012) Human protein 53-derived cell-penetrating peptides. Int J Pept Res Ther 18(4):291–297
34. Mäger I, Langel K, Lehto T et al (2012) The role of endocytosis on the uptake kinetics of luciferin-conjugated cell-penetrating peptides. Biochim Biophys Acta 1818:502–511
35. Martinon F, Tschopp J (2007) Inflammatory caspases and inflammasomes: master switches of inflammation. Cell Death Differ 14:10–22
36. Isoda K, Ohsuzu F (2006) The effect of interleukin-1 receptor antagonist on arteries and cholesterol metabolism. J Atheroscler Thromb 13:21–30
37. Allan SM, Tyrrell PJ, Rothwell NJ (2005) Interleukin-1 and neuronal injury. Nat Rev Immunol 5:629–640
38. Kornman KS (2006) Interleukin 1 genetics, inflammatory mechanisms, and nutrigenetic opportunities to modulate diseases of aging. Am J Clin Nutr 83:475S–483S

Chapter 10

Unraveling the Mechanisms of Peptide-Mediated Delivery of Nucleic Acids Using Electron Microscopy

Helerin Margus, Carmen Juks, and Margus Pooga

Abstract

Cell-penetrating peptides (CPPs) are efficient non-viral delivery vectors for bioactive cargos, both in vitro and in vivo. Cargo molecules can be attached to CPPs either via covalent conjugation or by complex formation using co-incubation, which is typically used for charged molecules such as nucleic acids. The latter technique is efficiently used in case of CADY, MPG, Pep peptides, NickFects and PepFects that condense oligonucleotides (ONs) into nanoparticles, which efficiently enter cells and induce biological effects. Despite being highly promising candidates for developing new-generation medicines, CPPs' internalization mechanisms and intracellular trafficking are still far from being well-understood, and obtained data are often controversial. Transmission electron microscopy (TEM) is an informative and valuable tool for examining the mechanisms of CPP-ON nanoparticles. TEM enables to visualize nanoparticles or single molecules labeled with Nanogold™ tag, and follow their association with cells and intracellular localization. In this chapter, we present methods for preparation of CPP-ON nanoparticles for TEM analysis and for examination of their interactions with the plasma membrane, and subsequent cellular uptake either by direct translocation or endocytosis. In case of endocytosis, ONs have to be released from endosomes and reach their target site in nucleus or cytoplasm to reveal their activity. TEM enables to estimate when the endosomal escape begins, from which type of endosomal vesicles it occurs, whether the vesicles are broken, or nanocomplexes translocate across the membrane into cytosol. Since single ONs could be followed, the time-frame that is necessary for the splice-switching nucleotides to translocate into cell nucleus can be analyzed by TEM.

Key words Cell-penetrating peptides, Transmission electron microscopy, Nanogold-labeled oligonucleotides, Oligonucleotide delivery, Intracellular trafficking

1 Introduction

Various experimental techniques have been harnessed to study the cellular uptake and intracellular trafficking of CPPs and their payloads. CPPs exploit different endocytic routes for delivering the coupled cargo molecules into cells. Co-localization analysis of CPP/cargo with markers of endosomal pathways by fluorescence microscopy is the most frequently used approach in these studies. Indeed, fluorescence microscopy is an indispensable tool to study

Ülo Langel (ed.), *Cell-Penetrating Peptides: Methods and Protocols*, Methods in Molecular Biology, vol. 1324,
DOI 10.1007/978-1-4939-2806-4_10,

the biology of living cells; however, it has several limitations. Most importantly, the resolution of fluorescence microscope is about 200 nm (super-resolution 10–20 nm) and this limits the ability to distinguish close compartments as separate from each another. Thus, separate molecules or compartments can be erroneously considered co-localized. Moreover, fluorescence microscopy does not enable the visualization of morphology and cell surface interactions of individual molecules; hence, complementary techniques should be applied to enable correct interpretation of experimental data.

One option to gain additional knowledge about the cellular uptake mechanism of CPPs and their cargos is to use transmission electron microscopy. Due to a high resolution (1–5 nm in thin sections of cells), TEM visualizes cell membranes, organelles and even macromolecules, thus, enabling to detect labeled molecules in relation to cell structures. Therefore, TEM is a powerful method for imaging and tracking individual molecules or nanocomplexes, and it provides detailed information about their interactions with plasma membrane and intracellular localization.

TEM has been employed to examine the cell entry mechanisms and intracellular trafficking of various macromolecules and particles, for example gold nanoparticles [1–3], lipid nanoparticles [4], CPP-protein constructs [5], CPPs alone [6, 7], etc. Among these, a few studies have focused on the delivery of nucleic acids. For example, Choi et al. showed that spherical nucleic acids interact with the plasma membrane at lipid raft microdomains that appear electron dense areas in TEM, and are engulfed by cells via caveolin-mediated endocytosis [2]. Another example, perhaps one of the most detailed studies in this field analyzed the cellular uptake and intracellular trafficking of lipid nanoparticles (LNPs) with traceable short silencing RNA (siRNA). Comprehensive and quantitative data of TEM analysis helped authors to unravel the cellular uptake kinetics and provided detailed information about the biogenesis and maturation of LNP-containing organelles. They demonstrated that LNPs that contain siRNA accumulate into vesicles that resemble both early and late endosomes by their biochemical and morphological characteristics. These LNP-containing endosomes mature slowly, delaying the transport to lysosomes. Additionally the study showed only a low rate (about 1.5 %) of endosomal escape, emphasizing that the endosomal release of LNPs is the limiting factor of siRNA bioavailability. Interestingly, the siRNA release from endosomes occurred from the early endocytic compartments rather than acidic lysosomes [4].

TEM has been used to examine nucleic acid delivery by novel modified CPPs in a limited number of works. Our group has employed TEM analysis to characterize the cellular uptake of PepFect and NickFect nanocomplexes with splice-switching oligonucleotides (SCOs) [8, 9] and plasmid DNA (pDNA) [10, 11].

We demonstrated that CPP-nucleic acid nanocomplexes interact with the cell surface as nanoparticles and their accumulation on the plasma membrane induces cellular uptake and endocytosis. Remarkably, the plasma membrane interactions, cellular uptake, and intracellular trafficking may vary depending on the used CPP [8]. Additionally, we have employed TEM to explore the role of scavenger receptors in the uptake of CPP-nucleic acid complexes. We showed that the presence of class-A scavenger receptor (SCARA) inhibitor dextran sulfate almost entirely abolishes the association of PepFect14-SCO complexes with the cell surface [12].

In order to examine the cellular uptake mechanisms and intracellular trafficking of CPP-nucleic acid nanocomplexes by TEM, it is necessary to label nucleic acids with electron dense tag. The size of the applied tag can affect the properties of delivered cargo and thereby influence cellular uptake mode(s). In order to introduce minimal interference, we labeled ONs covalently by conjugating these to Nanogold™ (NG) cluster ($d = 1.4$ nm). The resulting well-defined conjugates where one gold label marks one ON molecule can then be non-covalently coupled to CPPs for cellular delivery. This strategy has been successfully used in several studies [8, 9, 13]. The conjugation of NG tag to pDNA is more complicated because plasmid does not have chemical groups that could be used for coupling of reactive NG-derivates to yield stable conjugates. One possibility to label pDNA is to first tag it with biotin and then associate the biotinylated pDNA with streptavidin or neutravidin molecules, which are labeled with colloidal gold particles or Quantum dots. This approach has been applied to characterize the intracellular distribution of lipoplexes [14] and CPP-nucleic acid nanocomplexes [10, 11].

In this chapter, we introduce a method for visualizing CPP-ON nanocomplexes at the plasma membrane, their cellular uptake, and intracellular trafficking by TEM. We present protocols for tagging splice-switching oligonucleotides with a Nanogold label and the embedding of cultured cells in a resin by flat-embedding technique that retains the correct orientation of cells.

2 Materials

2.1 Labeling of Oligonucleotides

2.1.1 Reagents and Solutions

1. ON with thiolinker (and protecting cleavable group) (*see* **Note 1**).
2. Monomaleimido Nanogold (Nanoprobes Inc., Yaphank, NY).
3. Oxygen-free water (MilliQ or similar quality). Remove air dissolved in water by vacuum, followed by bubbling argon through water for at least 15 min (*see* **Note 2**).
4. 0.1 M solution of dithiothreitol (DTT) in 50 mM sodium phosphate buffer, pH 6.0. (Prepared from 0.5 M stock of DTT

in oxygen-free water, and deaerated 0.2 M sodium phosphate buffer, pH 6.0.)

5. 50 % methanol (≥99.9 %) in oxygen-free water.

2.1.2 Materials and Equipment

6. Eppndorf tubes filled with argon.
7. Spectrophotometer (e.g. Nanodrop 1000, Thermo Fischer Scientific Inc.).
8. Thermostat-mixer (e.g. Thermomixer Comfort, Eppendorf AB).
9. Rotational vacuum concentrator (e.g. RVC 2-25, Christ GmbH, or Savant Speed-Vac SC110, Ramsey).
10. Chromatography system equipped with columns for ON purification by gel filtration (size exclusion), ion-exchange or reversed phase chromatography (*see* **Note 3**).

2.2 Materials and Solutions for TEM

11. Cell-penetrating peptides and ONs. CPP stocks (1 mM, in MilliQ water) are aliquoted into Eppendorf tubes and stored at −20 °C. We use 2′-O-Me PTO SCOs labeled with 1.4 nm Nanogold™ (Nanoprobes Inc., Yaphank, USA). ON stock solutions at 20 μM concentration (in MilliQ water) are stored at −20 °C.
12. Cell line: Human cervical carcinoma cell line HeLa pLuc 705 is cultured in Iscove's Modified Dulbecco's Medium (IMDM) supplemented with 100 IU/ml penicillin, 100 μg/ml streptomycin and 10 % fetal bovine serum (FBS). This protocol is also suitable for other cell lines.
13. Iscove's Modified Dulbecco's Medium (IMDM) for the incubation of cells with CPP-ON nanocomplexes. Depending on your assay and aim of experiment, incubation can be performed in serum-free IMDM.
14. Round coverslips (12 mm in diameter) for growing cells for TEM experiments. We recommend storage of coverslips in 70 % ethanol in 100 ml glass flask to avoid any dust on the glasses.
15. Cell culture dishes (35 × 10 mm).
16. Washing solutions and buffers. Sodium cacodylate buffer: prepare 0.4 M stock of sodium cacodylate (NaCac) buffer by dissolving 21.4 g of cacodylic acid sodium salt trihydrate ($[Na(CH_3)_2\ AsO_2{\cdot}3H_2O]$) in 250 ml of MilliQ water.

Adjust the pH of solution to 7.4 by adding 8 ml 0.2 M HCl to the 50 ml stock solution (0.4 M NaCac), and then add MilliQ water up to 200 ml to make 0.1 M NaCac working buffer. For preparing the osmium tetroxide solution, prepare also 0.2 M NaCac buffer [15].

17. Fixative: 2.5 % glutaraldehyde in 0.1 M NaCac buffer, pH 7.4. Fixative is prepared from 25 % glutaraldehyde (Electron Microscopy Sciences (EMS), Hatfield, PA), stored at −20 °C in 1 ml aliquotes.
18. Silver enhancement kit. We use HQ Silver Kit (Nanoprobes Inc., Yaphank, NY). The components of the silver enhancement kit can be aliquoted into amber Eppendorf tubes and stored at −20 °C. The components of the silver enhancement kit are light-sensitive; therefore all procedures (aliquoting and silver enhancement of Nanogold™ tag) must be performed in dark or under the safelight. Also other suitable enhancement kits can be used.
19. Gold toning solutions:
    (a) 2 % sodium acetate ($CH_3COOONa{\cdot}3H_2O$) in MilliQ water (always freshly made).
    (b) 0.3 % sodium thiosulfate pentahydrate ($Na_2S_2O_3{\cdot}5H_2O$) in MilliQ water (always freshly made).
    (c) 0.05 % gold chloride ($HAuCl_4{\cdot}H_2O$) in MilliQ water. This solution can be stored at 4 °C for several months.
20. Osmium tetroxide (OsO_4) solution for the staining and post-fixation of the specimens. Mix equal volumes of 2 % OsO_4 in MilliQ water and 0.2 M NaCac buffer with pH 7.4 to yield a 1 % OsO_4 in 0.1 M NaCac buffer (*see* **Note 4**). In order to gain better contrast, you may add to solution15 mg/ml $K_4[Fe(CN)_6]$ (*see* **Note 5**).
21. Water-free ethanol (100 %).
22. 70 % ethanol.
23. 96 % ethanol.
24. Acetone (≥99.5 %).
25. Embedding resin: we use TAAB Premix Embedding Kit resin (medium, TAAB Laboratories Equipment Ltd, UK), but you may use also other suitable resins. Embedding resin is stored in plastic syringes at −20° (*see* **Note 6**).
26. Solution of 2 % uranyl acetate in 50 % ethanol (*see* **Note 7**).
27. Lead citrate stain: dissolve 20 mg of the lead citrate in 10 ml of CO_2 free MilliQ water (boil water for 10 min to make it CO_2-free) (*see* **Note 8**). Add 0.1 ml of 10 N NaOH, seal the tube air-tightly and shake until the lead citrate is completely dissolved. Filter the solution through 0.2 μm filter before use.
28. Embedding capsules and capsule holder. We use BEEM embedding capsule (size 3) and BEEM capsule holders (available from EMS). Also other suitable capsules and holder can be used.
29. Round aluminum plates with diameter of 2 cm, used for mounting coverslips and resin capsules.

30. Oven adjusted to 60 °C.
31. Liquid nitrogen for removing glasses from resin blocks.
32. Copper grids.
33. Ultramicrotome for sectioning.
34. Tweezers, timer, 24-well plate, parafilm, glass bottle for wastes, ice box with ice, red safelight, single-use pipets.

3 Methods

3.1 Labeling of Oligonucleotides with Nanogold™

1. Dissolve lyophilized ON at 0.2 mM concentration in oxygen-free solution of 0.1 M DTT in 50 mM sodium phosphate buffer, pH 6.0, in order to remove the protecting group and activate the thiolinker on the ON. Calculate the volume of buffer necessary for dissolving ON batch based on its amount (in nanomoles or OD_{260}) (*see* **Note 9**).
2. Remove the protection group from ON by incubating the reaction mixture at 37 °C in dark with mild shaking (e.g. 300 rpm) for 90–120 min.
3. Purify the ON from removed protecting group by using gel filtration chromatography (*see* **Note 10**).
4. Concentrate the ON in rotational vacuum concentrator at 37 °C to ~1–1.5 ml volume and estimate its concentration by measuring OD_{260} (*see* **Note 11**).
5. Dissolve Monomaleimido Nanogold in 50 % methanol at 30 μM concentration (*see* **Note 12**).
6. Couple the Nanogold label to ON by adding the solution of active thiol group containing ON in small aliquots to NG solution upon stirring (*see* **Note 13**). Incubate the mixture for 60–90 min at 30 °C in dark under mild stirring.
7. Remove methanol and concentrate the solution of conjugate in rotational vacuum concentrator at 37 °C to volume of 0.6–0.8 ml (*see* **Note 11**).
8. Purify the ON-NG conjugate from removed unreacted label and ON by using gel filtration chromatography (*see* **Note 14**).
9. Concentrate the fractions of chromatographic purification by rotational vacuum concentrator (*see* **step 4**), pool if necessary.

Measure the absorbance of the resulting solution at 420 nm using suitable dilution and calculate the concentration of conjugate considering that 1 A_{420}/cm corresponds to ~1.3 μM (*see* **Note 15**) Nanogold concentration, and dilute to suitable concentration if necessary. Aliquot the conjugate and store in freezer. Store the working aliquot in fridge and use it within 1 month. Avoid the repeated freeze–thaw cycles.

3.2 Treatment of Cells with CPP-ON-NG Nanocomplexes

10. Take round glass coverslips from ethanol, dry and sterilize them in the flame of gas burner using tweezers until ethanol is burned/evaporated (couple of seconds).
11. Place sterilized coverslips to the bottom of cell culture dish (35 × 10 mm). We recommend to add at least two glasses (preferentially three) per one culture dish to get two parallels from each experimental point for silver-enhancement procedure. Maximally you can use four coverslips per one cell culture dish (35 × 10 mm).
12. Seed HeLa cells 2 days prior to experimental day onto round coverslips in cell culture dish and grow to reach 80–100 % of confluence.
13. Prepare the CPP nanocomplexes with SCOs labeled with 1.4 nm Nanogold™. Form complexes in MilliQ water in 1/10 of the final volume. The optimal volume for 35 × 10 mm cell culture dish is 1 ml, i.e. complexes are formed in 100 µl. The further complexation protocol is described for PepFect14 (PF14) and SCO. We form complexes at molar ratio 1:5, i.e. final concentrations in the medium on cells for SCO and PF14 are 200 nm and 1 µM, respectively (*see* **Note 16**).
14. First, dilute 20 µM SCO stock solution (stored at –20 °C) in MilliQ water to obtain 2 µM SCO solution, i.e. mix together 10 µl SCO and 80 µl MilliQ.
15. Dilute 1 mM PepFect14 stock (stored at –20 °C) in MilliQ water to obtain 100 µM PF14 solution.
16. Add 10 µl of the 100 µM PF14 into 90 µl of SCO-MilliQ solution and mix thoroughly.
17. The solution is further incubated for 30–45 min at room temperature (RT) to allow the spontaneous formation of complexes via electrostatic and hydrophobic interactions between positively charged CPPs and negatively charged ONs.
18. Take your cells from the incubator, remove the culture medium and wash twice with fresh medium to remove dead cells.
19. Before incubating cells with nanocomplexes, add 900 µl of fresh serum-containing cell culture medium to the 100 µl of preformed PF14-SCO-NG complex solution (depending on your experiment, you may also use serum-free medium). Incubate cells with PF14-SCO-NG nanocomplexes for different time intervals (in typical experiment for 30 min, 1 h, 2 h, and 4 h) at 37 °C in humidified atmosphere containing 5 % CO_2.
20. Wash cells twice with pre-warmed IMDM medium to remove unbound nanocomplexes.
21. Fix cells by adding 1 ml of the 2.5 % glutaraldehyde fixative in 0.1 M NaCac buffer (freshly made) into each dish, and fixate cells for 1 h at RT.

22. Remove the fixative and wash twice with 0.1 M NaCac buffer for 10 min. After the fixation, cells are sensitive to drying; all the washing and incubation solutions must be changed quickly. At this point you can leave your specimens in buffer for overnight at 4 °C.

3.3 Silver Enhancement

Silver enhancement is a commonly used technique to magnify small gold particle such as 1.4 nm Nanogold by silver deposition in order to make it detectable in cellular environment by TEM. Briefly, silver enhancement is a gold-label-catalyzed reaction, where silver ions are reduced to metallic silver that is deposited onto gold core, and resulting in particles with 2–10 nm diameter or larger, depending on the treatment time and temperature. The following silver enhancement procedure should be carried out at RT in the dark room or under the safelight.

23. Wash cells three times with MilliQ water for 3 min.
24. Meanwhile, fill the wells of the 24-well plate with MilliQ water, which is needed for stopping the enhancement procedure.
25. Prepare the silver enhancement solution by mixing initiator, moderator, and activator. Mix initiator solution and add equal volume of moderator solution and mix again. Add activator solution and mix again.
26. Pipette 40–60 μl drops of the silver enhancement solution on the piece of parafilm and place coverslips upside down onto the drops and incubate for 2–10 min. You may also use shorter or longer incubation times to find optimal time for your experiment (*see* **Note 17**). Always use timer to stop silver enhancement at the exact time.
27. Stop the enhancement by transferring glasses to MilliQ water (cells upside) in wells of cell culture dish.
28. Wash specimens three times with MilliQ water for 5 min.
29. Stabilize silver deposit by gold toning (*see* **Note 18**). First, wash cells three times with 2 % sodium acetate for 5 min at RT.
30. Incubate cells with 0.05 % gold chloride for 10 min on ice.
31. Wash specimens twice with 0.3 % sodium thiosulfate in MilliQ water for 10 min on ice.
32. Wash cells three times with MilliQ water for 3 min.

3.4 Embedding of Cells

33. After silver enhancement, cells are post-fixed and stained with 1 % OsO_4 (freshly prepared just before use). Add 0.5 ml of the 1 % OsO_4 solution in each well and incubate for 1 h at RT. Avoid direct daylight by covering the plate with aluminum foil during the osmification. Osmium tetroxide is highly toxic; please handle it with care (*see* **Note 19**).

34. After osmification, wash samples three times with 0.1 M NaCac buffer for 5 min.
35. Dehydrate cells with 70 % ethanol, with 96 % ethanol and two times with 100 % ethanol. Each washing step is for about 1 min.
36. Remove the caps from the embedding capsules, place the capsules in the holder and fill with embedding resin. If resin is stored at −20 °C, let it warm up to RT before use.
37. For final dehydration, dip glasses with cells into acetone for couple of seconds and then place onto aluminum plate (cells upside).
38. Immediately add a drop of the resin to cover the cell (cells are sensitive to drying).
39. Set resin-filled capsules upside down on the top of cells and let the resin to infiltrate into specimens at least 2 h at RT before transferring them to the oven.
40. Transfer samples to 60 °C oven and polymerize resin overnight or at least for 14 h.
41. After the polymerization take your samples from the oven and remove the coverslips mechanically or by dropping samples into liquid nitrogen. Make sure that no pieces of glass are left on the resin block; otherwise it may harm the diamond knife during the sectioning.
42. Before slicing, trim the resin block surface to a small trapezoid pyramid shape by using a razor (*see* **Note 20**). Cut ultrathin sections (50–70 nm) with ultramicrotome and diamond knife in parallel with the surface of resin blocks and then collect the sections on the copper grids.
43. Stain the sections on grids with 2 % uranyl acetate solution on parafilm in a 20 μl drop for 1 min at RT.
44. Wash the grids two times with 50 % ethanol and let specimens dry in the air for 15–20 min.
45. Stain the sections with lead citrate solution in 20 μl drop for 1–3 min, depending on the contrast you need to achieve.
46. Wash sections thoroughly three times by transferring grids from one drop of MilliQ water to another.
47. Let the grids to dry and transfer into box for grids for further analysis.
48. Analyze your specimens in TEM operated at 120 V and capture images.

4 Notes

1. The protocol is applicable for single- and double-stranded ONs with different backbone chemistry. ON should contain a thiol group at 5′ end for labeling with Monomaleimido Nanogold. The thiol group of synthesized ON is protected by forming a disulfide bond (e.g. Thiol Modifier C6 S-S), which has to be removed before coupling the NG tag. Thiol group of ON (ON-SH) could also be tagged with a smaller label (diameter 0.8 nm), Monomaleimido UndecaGold, but the magnification of this tag by silver enhancement in biological specimens is less reproducible than that with Nanogold label.

   ONs with amino linker (ON-NH_2) are tagged with Nanogold on the amino group using MonosulfoNHS Nanogold (NHS-NG), thereby avoiding deprotection and purification of ON-SH for labeling with NG (Steps 1-4 in Protocol). However, due to hydrolysis of NHS group in water, the labeling yield of ON-NH_2 by NHS-NG can be lower as compared to ON-SH labeling with Monomaleimido Nanogold.

2. All solutions used for removal of the protecting group from thiolinker of ON, and for coupling Monomaleimido Nanogold should be oxygen-free (made in oxygen-free water or deaerated after preparation).
3. In this work FPLC system (GE Healthcare/Pharmacia) equipped with absorbance detectors at 260, 280 and 210 nm, an automated fraction collector and the gel filtration chromatography columns Superdex-Peptide and Superdex 30 HR10/30 were used.
4. Osmium tetroxide is available as aqueous solution in glass ampoules (2 or 4 %) or as OsO_4 crystals stored in glass ampoules. Store the 2 % OsO_4 at 4 °C in a clean brown glass bottle and avoid the contamination with organic matter, and exposure to light. Osmium tetroxide solution evaporates from the bottle; therefore, the bottle has to be sealed tightly with parafilm.
5. Ferrocyanide in OsO_4 solution is used to enhance the contrast of cellular components such as glycogen. It also augments staining of cellular membranes.
6. Components of the embedding kit can be stored at 4 °C for 12 months. Ready-to-use embedding resin can be stored in plastic syringes without needle at –20 °C for up to 3 months. Caps for syringes are also available from EMS. Embedding resin is toxic and carcinogenic, use it with care. Used syringes and other material containing resin wastes, must be baked in the 60 °C oven for overnight. Polymerized resin is harmless and can be disposed with regular wastes.

7. Uranyl acetate (UA) enhances the contrast of specimen by interacting with lipid membranes, nucleic acids, and nucleic acid-rich structures as nucleus. UA solutions and wastes should be handled with care due to their chemical toxicity and low radioactivity. Before the usage, centrifuge UA solution (5 min at maximum speed) to make sure that no UA precipitates are in the solution, which might lead to artifacts and unwanted background staining.
8. Lead citrate enhances the contrast of specimen by interacting with proteins and glycogen.

Lead citrate precipitates easily in the presence of carbonate ions and may cause background staining; therefore, lead citrate has to be dissolved in CO_2-free MilliQ water. For the removal of CO_2, water is boiled for 10–15 min. Lead citrate staining solution should be fresh and used only once.

9. ON can be dissolved at any desired concentration but for optimal deprotection and coupling reaction we suggest 0.1–0.2 mM concentration.
10. Equilibrate the chromatography column (e.g. Superdex-Peptide HR10/30) with 3–4 column volumes of oxygen-free MilliQ water before chromatography in the same medium (preferentially in cold lab at 2–6 °C). Collect 0.5–1 ml fractions depending on the amount of ON into Eppendorf tubes filled with argon (in order to avoid oxidation of thiolinker and disulfide formation).

Collect the fractions of first peak (with the highest absorption at 260 nm), ON is usually diluted 3–4 times during chromatography.

11. Check regularly (every 30–60 min) the volume of concentrated ON solution in order to avoid evaporation of all water.
12. Dissolve Monomaleimido Nanogold in parallel with concentration of ON solution. Reconstitution of 30 nmol batch of Monomaleimido Nanogold with 1 ml deionized water will yield a 20 mM sodium phosphate buffer at pH 6.5 with 150 mM NaCl, i.e. suitable conditions for selective labeling of thiol group/linker of ON. Methanol (or acetonitrile) facilitates dissolution of the labeling reagent. However, Monomaleimido Nanogold can be reconstituted in a smaller or a larger volume of solvent if necessary.
13. Perform the coupling reaction in a tube filled with argon to maximize the yield of coupling by excluding oxidation of thiols. Use a 1.2- to1.5-fold molar excess of ON over the Monomaleimido Nanogold to assure that most of the label reacts with the ON. Typically >90 % of Nanogold is coupled to ON under the used reaction conditions.

14. Equilibrate the chromatography column (e.g. Superdex 30 HR10/30) with 3–4 column volumes of MilliQ water before chromatography in the same medium (preferentially in cold lab at 2–6 °C). Collect 0.5–1 ml fractions depending on the amount of conjugate.

The ON-NG conjugate can also be purified by reversed phase or ionic exchange chromatography. However, if the conjugate is further associated with PepFect or NickFect-type transfection agents to form non-covalent nanocomplexes, the purification by gel filtration in water is preferred.

The purification of the conjugate to homogeneity is sometimes not necessary since the unlabeled ON remains invisible in TEM and does not interfere with the analysis of the ON-NG conjugates localization.

15. The absorption of Nanogold from different lots can vary and the concentration should be calculated using the absorption coefficient of a particular lot of reagent.
16. Concentrations for CPPs and ONs are chosen in accordance with the biological activity. For SCOs, the optimal concentration is reported to be 200 nM, in some cases also 100 nM. For TEM, we use maximal concentration, of labeled ONs in order to facilitate its detection in specimens. CPP is added to nanocomplexes at optimal molar ratio or charge ratio that has been determined earlier in assays on the biological activity [15].
17. The growth of particles upon silver enhancement is faster during the first minutes, but is further slowed down in time as the surface area of the nanocomplexes increases. After the certain time period, silver may start self-nucleate and yield an unwanted background staining; therefore, very long incubation times should be avoided. Silver enhancement is also a temperature-dependent reaction; at 20–22 °C the enhancement solution is stable for at least 15–20 min. At higher temperatures the silver enhancement solution is less stable, silver ions/atoms might easily self-nucleate and cause background staining. The components of the silver enhancement kit are stored at –20 °C, and must be brought to RT before use to ensure uniform and reproducible results.
18. Gold toning is necessary to stabilize the silver layer on gold nanoparticles since in the presence of strong oxidizing reagents like osmium tetroxide the silver atoms are oxidized to soluble silver ions, which may cause loss of the silver deposit. During the gold toning with 0.05 % gold chloride, a thin layer of gold is deposited on the surface of the silver deposit, which makes particles more resistant against further treatments with oxidizing reagents, like osmium tetroxide and UA.

19. Osmium tetroxide is very hazardous and may damage eyes and skin. All work with osmium tetroxide must be performed under the vented hood. Osmium tetroxide wastes are collected into bottle that contains vegetable oil and is stored in the fume hood. According to suggestions by manufacturers, 2 % osmium tetroxide solution can be neutralized by mixing with two volumes of corn oil (for 10 ml osmium tetroxide 20 ml of the oil is needed). The most suitable is corn oil since it contains high percentage of fatty acids with unsaturated bonds. All the other materials, containing osmium tetroxide wastes, should be collected separately into plastic bag and disposed in accordance with local environmental safety regulations.
20. Before trimming, let the resin blocks to cool down to RT for 2 h. Small block surface (trapezoid shape) facilitates the parallel alignment of block surface and knife edge.

Acknowledgements

The authors were supported by grants from the Estonian Science Foundation (ESF 8705), the Estonian Ministry of Education and Research (0180019s11), and the European Union Regional Development Fund (grant EU30020) through the Competence Centre on Reproductive Medicine and Biology.

References

1. Tiwari PM, Eroglu E, Bawage SS, Vig K, Miller ME, Pillai S, Dennis VA, Singh SR (2014) Enhanced intracellular translocation and biodistribution of gold nanoparticles functionalized with a cell-penetrating peptide (vg-21) from vesicular stomatitis virus. Biomaterials 35:9484–9494
2. Choi CH, Hao L, Narayan SP, Auyeung E, Mirkin CA (2013) Mechanism for the endocytosis of spherical nucleic acid nanoparticle conjugates. Proc Natl Acad Sci U S A 110: 7625–7630
3. Yang C, Uertz J, Yohan D, Chithrani BD (2014) Peptide modified gold nanoparticles for improved cellular uptake, nuclear transport, and intracellular retention. Nanoscale 6:12026–12033
4. Gilleron J, Querbes W, Zeigerer A, Borodovsky A, Marsico G, Schubert U, Manygoats K, Seifert S, Andree C, Stoter M, Epstein-Barash H, Zhang L, Koteliansky V, Fitzgerald K, Fava E, Bickle M, Kalaidzidis Y, Akinc A, Maier M, Zerial M (2013) Image-based analysis of lipid nanoparticle-mediated sirna delivery, intracellular trafficking and endosomal escape. Nat Biotechnol 31:638–646
5. Säälik P, Padari K, Niinep A, Lorents A, Hansen M, Jokitalo E, Langel Ü, Pooga M (2009) Protein delivery with transportans is mediated by caveolae rather than flotillin-dependent pathways. Bioconjug Chem 20:877–888
6. Padari K, Koppel K, Lorents A, Hällbrink M, Mano M, Pedroso de Lima MC, Pooga M (2010) S4(13)-pv cell-penetrating peptide forms nanoparticle-like structures to gain entry into cells. Bioconjug Chem 21:774–783
7. Cardoso AM, Trabulo S, Cardoso AL, Lorents A, Morais CM, Gomes P, Nunes C, Lucio M, Reis S, Padari K, Pooga M, Pedroso de Lima MC, Jurado AS (2012) S4(13)-pv cell-penetrating peptide induces physical and morphological changes in membrane-mimetic lipid systems and cell membranes: Implications for cell internalization. Biochim Biophys Acta 1818:877–888
8. Oskolkov N, Arukuusk P, Copolovici DM, Lindberg S, Margus H, Padari K, Pooga M,

Langel Ü (2011) Nickfects, phosphorylated derivatives of transportan 10 for cellular delivery of oligonucleotides. Int J Pept Res Ther 17:147–157

9. Arukuusk P, Pärnaste L, Oskolkov N, Copolovici DM, Margus H, Padari K, Moll K, Maslovskaja J, Tegova R, Kivi G, Tover A, Pooga M, Ustav M, Langel Ü (2013) New generation of efficient peptide-based vectors, NickFects, for the delivery of nucleic acids. Biochim Biophys Acta 1828:1365–1373
10. Veiman KL, Mäger I, Ezzat K, Margus H, Lehto T, Langel K, Kurrikoff K, Arukuusk P, Suhorutsenko J, Padari K, Pooga M, Lehto T, Langel Ü (2013) Pepfect14 peptide vector for efficient gene delivery in cell cultures. Mol Pharm 10:199–210
11. Arukuusk P, Pärnaste L, Margus H, Eriksson NK, Vasconcelos L, Padari K, Pooga M, Langel Ü (2013) Differential endosomal pathways for radically modified peptide vectors. Bioconjug Chem 24:1721–1732
12. Ezzat K, Helmfors H, Tudoran O, Juks C, Lindberg S, Padari K, El-Andaloussi S, Pooga M, Langel Ü (2012) Scavenger receptor-mediated uptake of cell-penetrating peptide nanocomplexes with oligonucleotides. FASEB J 26:1172–1180
13. Rydstrom A, Deshayes S, Konate K, Crombez L, Padari K, Boukhaddaoui H, Aldrian G, Pooga M, Divita G (2011) Direct translocation as major cellular uptake for cady self-assembling peptide-based nanoparticles. PLoS One 6, e25924
14. Pitard B, Oudrhiri N, Vigneron JP, Hauchecorne M, Aguerre O, Toury R, Airiau M, Ramasawmy R, Scherman D, Crouzet J, Lehn JM, Lehn P (1999) Structural characteristics of supramolecular assemblies formed by guanidinium-cholesterol reagents for gene transfection. Proc Natl Acad Sci U S A 96:2621–2626
15. Ezzat K, Andaloussi SE, Zaghloul EM, Lehto T, Lindberg S, Moreno PM, Viola JR, Magdy T, Abdo R, Guterstam P, Sillard R, Hammond SM, Wood MJ, Arzumanov AA, Gait MJ, Smith CI, Hällbrink M, Langel Ü (2011) Pepfect 14, a novel cell-penetrating peptide for oligonucleotide delivery in solution and as solid formulation. Nucleic Acids Res 39:5284–5298

Chapter 11

SCARA Involvement in the Uptake of Nanoparticles Formed by Cell-Penetrating Peptides

Henrik Helmfors, Staffan Lindberg, and Ülo Langel

Abstract

The investigation of uptake mechanisms for cell-penetrating peptides (CPPs) is and has been an ongoing project for as long as the peptides have been known, a time period that now spans over two decades. The ultimate answer is yet to be revealed and the current understanding is that no "one" mechanism will ever be found. The reason for this is that the uptake mechanism seems to be dependent on a multitude of factors that include which CPP, what cells are used, whether or not there is cargo and what the cargo is. CPPs are capable of delivering a variety of bio-macromolecules that are by themselves unable to enter into cells. Our group has reported on many different peptides in recent years, many aimed at delivering various oligonucleotide-based cargoes. These peptides have utilized the inherent positive charge of the peptides and some rationally designed modifications to non-covalently complex oligonucleotides and bring them into cells. In this chapter, we present a brief overview of the current proposals for the uptake mechanisms of CPPs and describe methods for detecting and evaluating the role of scavenger receptor class A receptors in the uptake of non-covalent cell-penetrating peptide:oligonucleotide complexes.

Key words Cell-penetrating peptides, CPPs, Splice-correction, Scavenger receptors, siRNA, Transfection, SCARA3, SCARA5, Uptake mechanism

1 Introduction

Cell-penetrating peptides (CPPs) have been an active area of research for over 20 years and have been on the list of potentially exploitable vectors for gene therapy almost the entire time. CPPs possess the ability to cross the cellular membrane and bring in cargo that would otherwise be unable to enter into the cytosol. The type of cargo carried into cells by CPPs now includes almost every kind of bio-macromolecule, from plasmids [1], siRNA [2] and other oligonucleotides [3, 4] to proteins [5], peptides [6] and peptide nucleic acids [7]. None of the types of cargo mentioned above are normally taken up into cells in any significant quantities. Versatile carriers like CPPs are rare and interesting from a purely scientific point of view where understanding both the mechanism

Ülo Langel (ed.), *Cell-Penetrating Peptides: Methods and Protocols*, Methods in Molecular Biology, vol. 1324,
DOI 10.1007/978-1-4939-2806-4_11,

and perhaps also the (evolutionary) reason they work can be a worthwhile pursuit in itself. Additionally, it is not difficult to imagine an application-centric view of CPPs where delivering a molecule in order to treat disease is the ultimate goal. In the years since the CPPs were discovered most of the research focus has been on the last part, developing new CPPs and developing new applications for them, so much so that currently (December 2014) the online repository for CPPs [8] lists over 800 members.

Publications related to new CPPs, and applications for them, greatly outnumber the publications that attempt to determine the characteristics of CPPs, i.e. where and how they are taken up. Attempts to reach such conclusions are currently being made by our group and others; so far these experiments have been focused on determining the mechanisms of uptake for CPPs. In this chapter, we give a brief overview of the proposed mechanisms and describe the methods for recognizing the involvement of scavenger receptors.

1.1 Receptors in the Uptake of CPPs

In the early days of CPP research the uptake mechanisms of CPPs were thought to be mostly independent of any endocytosis pathway and rely on direct penetration of the cellular membrane. However, about 10 years ago a reevaluation of the methodology used to determine the uptake mechanism dispelled much of the previous gospel. The earlier results were found to likely be caused by artifacts related to fixation of cells [9]. In the following decade, reports indicating one or another kind of endocytotic mechanism as responsible for the uptake of CPPs have steadily increased in number.

It had been known since before the artifacts due to cell fixation came to light that internalization of the most famous and well-studied of CPPs, the cationic TAT-peptide requires cell surface heparan sulfate (HS) proteoglycans [10]. Unfortunately, there are reports that state the opposite, i.e. HS interaction inhibits the uptake of TAT [11].

The ambiguity extends to other arginine-rich peptides as well, there are reports indicating that this interaction is required for uptake [12], as well as that HS interaction is not necessary [13].

On the other hand, when it comes to the other major class of CPPs, the amphipathic ones, cell surface clustering of HS-proteoglycans does not contribute to nor inhibit the uptake [14]. The endocytotic mechanism by which the TAT peptide is taken up after the initial interaction with cell surface proteoglycans has been reported to be either: macropinocytotis [12], lipid raft caveolar endocytosis [15], clathrin-mediated endocytosis [16], and actually all three mechanisms simultaneously [17]. More recently a report detailing the ways which the TAT peptide can interact with, and be internalized in to, cells, added some clarity to this apparent lack of agreement. The TAT peptide can bind to HS-proteoglycans

and become internalized by endocytosis, it can also interact with the membrane and generate saddle-splay curvature and in this way induce pore-like structures in the membrane. If the cargo is sufficiently small the peptide can be internalized directly, larger cargo is anchored to the membrane via the peptide and a strong interaction between TAT and actin can remodel the cytoskeleton and promote other pathways like macropinocytosis [18].

Direct translocation for arginine-rich CPPs is likely related to the ability of the guanidinium moieties on arginines to form hydrogen bonds with membrane lipids [19]. Each cationic guanidinium head group has a rigid planar array of hydrogen bond donors that allows for highly effective bidentate hydrogen bond formation with negatively charged carboxylates, phosphates, and sulfates [20]. The possibility of direct translocation is further underscored by the ability of the arginine-rich TAT peptide to induce pores in artificial membranes [21].

Verdurmen et al. reported that uptake of cationic CPPs, especially at higher concentration, induces rapid formation of ceramide via hydrolysis of sphingomylin by the enzyme acid sphingomyelinase [22]. This in turn changes the composition of the plasma membrane allowing for entry into the cytosol, the mechanism of enzyme activation is not yet clear.

In 2012, Tanaka et al. [23] reported that CXCR4 chemokine receptor acts to stimulate the uptake of a dodecamer of arginine. Stimulation of CXCR4 with the intrinsic ligand SDF-1α induces macropinocytosis. Additionally, they showed that siRNA knockdown of the receptor prevents the formation of lamellipodia, further indicating that for oligo-arginine macropinocytosis is one uptake route.

There is also a report about peptides binding to the neurophilin-1 receptor (NRP-1) and then being quickly internalized. These peptides had c-terminal consensus sequence of R/KXXR/K which is similar to sequences found in many CPPs [24]. This is the same consensus sequence as found in the C-terminal end of VEGF-A165 and some semaphorins that are known to bind to NRP-1.

We have reported that our most recent generation of CPPs, peptides that have been modified using both a N-terminal stearylation, phosphorylated tyrosine or a side chain extension of the peptide chain were also taken up through differing endocytotic routes. Inhibitors for the different pathways revealed that NickFect1 is endocytosed via both the clathrin-mediated pathway and through macropinocytosis, whereas NickFect51 is internalized mainly through macropionocytosis [25].

1.2 Scavenger Receptors

Scavenger receptors are a family of cell surface glycoproteins first recognized to bind modified low-density lipoproteins (LDL) such as acetylated and oxidized LDLs.

After their discovery of the LDL receptor, Nobel laureates Brown and Goldstein went on to discover the scavenger receptors in patients who lack LDL receptors [26]. Initially, these receptors were thought to only scavenge acetylated LDL into macrophages [27]. This first definition has since grown to encompass receptors that can bind a diverse set of ligands, from modified endogenous proteins and lipoproteins, i.e. danger-associated molecular patterns (DAMP). Additionally, exogenous molecules like bacterial lipopolysaccharides (LPS) [28], microorganisms like *Staphylococcus aureus* bacteria [29], $PrP_{106–126}$ prion protein [30], and viral RNA [31], HCV virus [32], i.e. pathogen-associated molecular patterns (PAMP) [33] and foreign particles like silver nanoparticles [34] are recognized by these receptors. As they recognize so many PAMPS it is not surprising that the receptors are highly expressed on macrophages, where they were also initially identified. Later they were found in many different cell types, where subtypes were identified in different cells such as smooth muscle cells, epithelial and endothelial cells, splenic dendritic cells, and fibroblasts.

The number of cell surface receptors classified as scavenger receptors is continually growing from the first suggestion of classes A-F in 1997 [35] to now include 19 receptors that divided into class A through I [33]. The receptors share the ability to bind polyanionic ligands with low specificity. The term Scavenger receptor is defined as: an extracellular glycoprotein (either soluble or membrane-bound) involved in the recognition and/or endocytosis of negatively charged molecules [36]. Today many more functions for the receptors have been reported and they are generally considered a subclass of the membrane bound pattern recognition receptors [33], another emerging role is cellular adhesion [37].

Taken together, all of these properties make scavenger receptors a candidate for CPP:ON complexes. In several papers, we have demonstrated scavenger receptor class A 3 and 5(SCARA3 and SCARA5) as at least partially responsible for the uptake using both a number of pharmacological inhibitors and by knocking down the receptor using siRNA [4, 38–40].

2 Materials

Any number of different cell lines can be used to carry out these experiments; however, in this chapter, only protocols for HeLa, HeLa pLuc 705, and U2OS-SAMP1/YFP cells are given, for more detail on the cells used here *see* **Note 1**.

2.1 Cell Culture and Preparation

1. Cell culture medium for Hela and Hela pLuc 705: Dulbecco's Modified Eagle's Medium with l-glutamine (0.1 mg/mL) (DMEM) supplemented with GlutaMax and 10 % (w/v) fetal

bovine serum (FBS), penicillin (100 U/mL), and streptomycin (100 mg/mL) (*see* **Note 1**).

2. Cell culture medium for U2OS SAMP1-YFP: DMEM supplemented with GlutaMax and 10 % (v/v) FBS, and 1 % penicillin-streptomycin and 200 μg/mL of G418 (*see* **Note 1**).
3. Trypsin/EDTA: 0.5 g/l porcine trypsin and 0.2 g/l EDTA.
4. Sterile T75 cm^2 vented flasks.
5. Laminar Flow Class II tissue culture fume hood.
6. Water-jacketed CO_2 incubator.
7. Sterile syringes.
8. Sterile filters.
9. Sterile Eppendorf tubes.
10. Purified and lyophilized peptides (*see* **Note 2**).
11. Sterile 24-well TC-treated cell culture plates.
12. 96-well solid white plates.
13. Phosphate buffered saline (PBS).
14. Ultrapure water (18.2 MΩ).

2.2 Gene Up-Regulation

1. Cell culture materials as above.
2. Sterile 24-well plates.
3. SCARA3 and SCARA5 plasmid (*see* **Note 3**).
4. Firefly luciferase plasmid.
5. Liposome-based transfection reagent.
6. CPPs (*see* **Note 2**).

2.3 Gene Knockdown

1. Cell culture materials as above.
2. Sterile 24-well plates.
3. SCARA3 and SCARA5 siRNA (*see* **Note 3**).
4. 2 % paraformaldehyde (PFA) in PBS.
5. GFP siRNA (*see* **Note 3**).
6. CPPs.

2.4 Inhibitory Experiments

1. Cell culture materials as above.
2. Poly Inosinc acid (Poly I) solution (*see* **Note 4**).
3. Poly Cytidylic acid (Poly C) solution (*see* **Note 4**).
4. Dextran sulfate solution (*see* **Note 4**).
5. Chondroitin sulfate solution (*see* **Note 4**).
6. Fucoidin solution (*see* **Note 4**).
7. Galactose solution (*see* **Note 4**).

8. CPPs (*see* **Note 2**).
9. Splice-correcting oligonucleotides (SCOs) (*see* **Note 3**).
10. White 96-well plates.
11. Luciferase assay reagent.

3 Methods

3.1 SCARA Gene Up-Regulation

This assay is based on overexpressing the SCARA3 and SCARA5, the reasoning is fairly straightforward, more scavenger receptors should result in increase of uptake of a reporter gene, and higher expression of the same; a situation that is easily quantifiable (*see* **Note 5**).

1. Culture HeLa cells at 37 °C and 5 % CO_2 in DMEM containing GlutaMAX, 1 mM sodium pyruvate and 10 % FBS (v/v), 100 U/mL penicillin and 100 μg/mL streptomycin.
2. On the day before the experiments, trypsinate and seed 25,000 cells/well into 24-well plates, use 500 μL of media per well.
3. 24 h after seeding change media and treat the cells with plasmid expressing SCARA3 + 5 using a liposome-based transfection reagent (*see* **Note 6**), use the manufacturer's protocols.
4. 24 h after transfecting the SCARA plasmids, change media once again and treat cells with luciferase plasmid, this time use CPPs as transfection reagents. Examples of plasmid transfection using CPPs can be found in Arukuusk et al. [38] and Veiman et al. [1].
5. 24 h after transfecting, measure luciferase expression. Remove the media and lyse the cells (*see* **Note 7**), take 20 μL of each lysate and transfer to a well in a white 96-well plate, add 80 μL of luciferase assay reagent, measure luminescence immediately using a plate reader (*see* **Note 9**).

3.2 SCARA Gene Silencing

This assay is based on the opposite of the assay above, by knocking down the scavenger receptor and thus removing some of the receptors available for mediating cargo uptake, the delivery of a reporter gene is diminished and the signal is lowered (*see* **Notes 1** and **9**).

1. Culture U2OS SAMP1-YFP cells in DMEM supplemented with GlutaMax and 10 % (v/v) FBS, and 1 % penicillin-streptomycin and 200 μg/mL of G418 (*see* **Note 1**).
2. On the day before the experiments, trypsinate and seed 25,000 cells into 24-well plates, use 500 μL of media per well.
3. 24 h after seeding cells, change media and treat with siRNA against SCARA3 and SCARA5 receptors. Use liposome-based transfection reagents like, for example lipofectamine RNAiMax (*see* **Note 5**).

4. 48 h (72 h after seeding) after the down-regulation of SCARA receptors using siRNA, perform peptide:siRNA transfection against YFP. For siRNA transfection using peptides see for example Chapters 24 and 25 of cell-penetrating peptides: Methods and Protocols [41].
5. 48 h after peptide:siRNA treatment, trypsinate, wash the cells by spinning down cells at 800–1000 g, remove the supernatant, re-suspend the cells in PBS and repeat washing step three times, fix the cells using 200–300 μL of 2 % paraformaldehyde (PFA) in PBS, re-suspend carefully, and shake gently for 15 min at room temperature, add PBS to a final volume of about 1 mL refrigerate, this fixates the cells for FACS (*see* **Note 9**).

3.3 SCARA Inhibition

This assay does not alter the expression of the scavenger receptor genes like the two assays above instead it relies on depleting the cells of available receptors by first using ligands for them, thus preventing uptake of additional peptide nano-complexes via the same pathway (*see* **Note 4**).

1. Culture HeLa pLuc 705 cells at 37 °C and 5 % CO_2 in DMEM containing GlutaMAX, 1 mM sodium pyruvate and 10 % FBS (v/v), 100 U/mL penicillin and 100 μg/mL streptomycin (*see* **Note 1**).
2. On the day before the experiments, trypsinate and seed 25,000 cells/well into 24-well plates, use 500 μL of media per well.
3. 24 h after seeding change media and treat the cells with the inhibitors and their controls, the concentrations for the inhibitors need to be optimized for each new peptide, in our experience concentrations of Poly I/Poly C at 1–30 μg/mL, fuciodin/galactose and dextran-sulfate/chondroitin-sulfate at 0.1–10 μg/mL are sufficient to inhibit uptake of CPP:ON complexes.
4. 1 h after addition of the inhibitors, treat the cells with CPP:SCO complexes.
5. 24 h after transfecting, measure luciferase expression. Remove the media and lyse the cells (*see* **Note 7**), take 20 μL of each lysate and transfer to a well in a white 96-well plate, add 80 μL of luciferase assay reagent, measure immediately using a luminescence plate reader (*see* **Note 9**).

4 Notes

1. One of the most useful cell lines for assaying short oligonucleotide delivery vectors is the HeLa pLuc 705 cell line developed by Kole [42]. This cell line expresses a luciferase-encoding plasmid that has been interrupted by a mutated human β-globin

intron 2, the mutation causes aberrant splicing from luciferase pre-mRNA. Delivery of a SCO, with the correct sequence, masks the aberrant splice site and correct splicing is restored and functional luciferase is expressed. A detailed method for assessing delivery efficacy of CPPs using this cell line has been described [43]. We have also employed a U2OS cell line expressing Samp1-YFP [44], a fusion protein between yellow fluorescent protein (YFP) and a inner nuclear membrane protein; spindle-associated membrane protein 1 (SAMP1) [45]. Knocking down YFP in this cell line results in a lower fluorescent signal and is useful for assessing the delivery efficacy of down-regulating oligonucleotides such as siRNA.

2. Peptides are synthesized as described previously [4]. Briefly, peptides are synthesized on automated synthesizers using standard Fmoc/tBu-protected amino acid monomers, using polyethylene glycol (PEG)-based resins and standard coupling protocols. After synthesis the peptides are cleaved from resin, precipitated in ether, lyophilized and then purified using HPLC. Peptides are lyophilized again after HPLC. 1 mM stock solutions of the peptides are made based on accurately weighted substances, and stored in −20 °C. In our experience peptides will keep for several months when stored in this way.
3. For the splice-correcting assay, the sequence of the 2′ o-methyl phosphorothioate (2′OMe-PS) oligonucleotide targeting the cryptic splice site is CCTCTTACCTCAGTTACA. It is in our experience important that the chemistry is phosphorothioate and not phosphodiester.

The siRNA against YFP is the same as siRNA against GFP, the duplex siRNA has the sequence:

5′-P-GCAAGCUGACCCUGAAGUUCAU
GCCGUUCGACUGGGACUUCAAG-P-5′.

The siRNAs against SCARA3 have the following target sequences:

(a) GGAGAUGCCUUGUGCGUUA
(b) CGAAAGCCCUGAACAACUG
(c) GAGAGGCGGUCAAGAACAU
(d) GAGCAUGCACGACCUGGUA

The siRNAs against SCARA5 have the following target sequences:

(a) GAACAAAGCUAUGUACCUA
(b) GAACAUCUCCCUCGCGAAA
(c) GGGAGGAUCUGGAUGGAUG
(d) GAACAUGUGCUCCGAAGUA

4. There are ligands that have been described for the scavenger receptors, by treating cells with these molecules uptake of other molecules through them is inhibited. All the ligands have the common property that they are poly-anionic molecules. As controls there are molecules with similar molecular structure, which are similarly poly-anionic but have no effect on and do not inactivate the scavenger receptors.

Poly I is one such poly-anionic ligand that interacts inhibitory on the SCARA receptor, whereas the Poly C despite being a polymer of anions like Poly I does not. Dextran and chondroitin sulfate are another pair of molecules that have similar structural properties. They are also poly-anionic polymers where one molecule of the pair acts as a ligand and the other has no effect on the activity of the receptor. Other poly-anions that acts as inhibitors include: fucoidan and acetylated low-density lipoprotein; additional compounds that are not known to inhibit scavenger receptors include polyadenosinic acid (Poly A) and galactose [32, 46–48]. To aid the solubility of Poly C solution can be repeatedly pushed through a narrow syringe.

5. When performing up- or down-regulation of the SCARA receptors, it is advisable to always quantify the levels of SCARA protein using either Western blot or ELISA.

6. The transfection reagent should be different from a peptide-based transfection reagent. Any commercially available liposome-based transfection reagent can be used instead of Lipofectamine (2000/RNAiMAX). The purpose is to use another method that is different from CPP-based transfection. The manufacturer's protocols should always be used, however be aware that sometimes there may be some effects related to toxicity of the transfection reagent.

7. Cell lysis can be performed in many ways, we have in the past successfully utilized a variety of different methods, both commercial ready-to-use materials and home-made variants. The following methods are all for 24-well plates; 100 μL/well of the commercially supplied Promega lysis buffer, 100 μL/well a home-made version of the same, 100 μL/well of 1 % Triton x-100 in HKR buffer, or freezing (−70 °C) and then thawing dry plates for one cycle, after the cells reach room temperature add 100 μL of HKR buffer.

8. After fixing cells for FACS the sample can be kept in the refrigerator for several days, however if it is necessary to store the samples for longer before being able to perform the measurement sodium azide can be added, the cells will then keep for several weeks. FACS is a good way to measure differences in cell that are stably expressing a fluorescent protein, like the YFP-SAMP1 fusion protein described above. The cell sorting

method gives very robust data with small experimental errors. CPPs that transfect almost all of the treated cells give very clear population shifts in FACS. In the cells where the functionality or the expression levels of SCARAs have been altered the ability to transfect the siRNA is greatly diminished.

9. A luciferase-based luminescent readout is convenient to use and microplate readers capable of measuring luminescence are ubiquitous, even modest labs can perform experiments. A stably expressing cell line, like the HeLa pLuc 705, can be used to determine if inhibiting or knocking down the SCARAs results in lowered luminescence signal, compared to controls using oligonucleotides that are supposed to increase luciferase expression.

Acknowledgements

This work was supported by The Swedish Research Council.

References

1. Veiman K-L, Mäger I, Ezzat K et al (2013) PepFect14 peptide vector for efficient gene delivery in cell cultures. Mol Pharm 10: 199–210
2. El Andaloussi S, Lehto T, Mäger I et al (2011) Design of a peptide-based vector, PepFect6, for efficient delivery of siRNA in cell culture and systemically in vivo. Nucleic Acids Res 39:3972–3987
3. Ezzat K, El Andaloussi S, Zaghloul EM et al (2011) PepFect 14, a novel cell-penetrating peptide for oligonucleotide delivery in solution and as solid formulation. Nucleic Acids Res 39:5284–5298
4. Lindberg S, Muñoz-Alarcón A, Helmfors H et al (2013) PepFect15, a novel endosomolytic cell-penetrating peptide for oligonucleotide delivery via scavenger receptors. Int J Pharm 441:242–247
5. Myrberg HH, Lindgren M, Langel Ü (2006) Protein delivery by the cell-penetrating peptide YTA2. Bioconjug Chem 18:170–174
6. Jones SW, Christison R, Bundell K et al (2005) Characterisation of cell-penetrating peptide-mediated peptide delivery. Br J Pharmacol 145:1093–1102
7. El Andaloussi S, Johansson H, Holm T et al (2007) A novel cell-penetrating peptide, M918, for efficient delivery of proteins and peptide nucleic acids. Mol Ther 15: 1820–1826
8. Gautam A, Singh H, Tyagi A et al (2012) CPPsite: a curated database of cell penetrating peptides. Database 2012:bas015
9. Richard JP, Melikov K, Vivès E et al (2003) Cell-penetrating peptides. A reevaluation of the mechanism of cellular uptake. J Biol Chem 278:585–590
10. Tyagi M, Rusnati M, Presta M et al (2001) Internalization of HIV-1 tat requires cell surface heparan sulfate proteoglycans. J Biol Chem 276:3254–3261
11. Subrizi A, Tuominen E, Bunker A et al (2011) Tat(48-60) peptide amino acid sequence is not unique in its cell penetrating properties and cell-surface glycosaminoglycans inhibit its cellular uptake. J Control Release 158(2):277–285
12. Nakase I, Tadokoro A, Kawabata N et al (2007) Interaction of arginine-rich peptides with membrane-associated proteoglycans is crucial for induction of actin organization and macropinocytosis. Biochemistry 46:492–501
13. Lundin P, Johansson H, Guterstam P et al (2008) Distinct uptake routes of cell-penetrating peptide conjugates. Bioconjug Chem 19:2535–2542
14. Verdurmen WPR, Wallbrecher R, Schmidt S et al (2013) Cell surface clustering of heparan sulfate proteoglycans by amphipathic cell-penetrating peptides does not contribute to uptake. J Control Release 170:83–91

15. Fittipaldi A, Ferrari A, Zoppé M et al (2003) Cell membrane lipid rafts mediate caveolar endocytosis of HIV-1 Tat fusion proteins. J Biol Chem 278:34141–34149
16. Richard JP, Melikov K, Brooks H et al (2005) Cellular uptake of unconjugated TAT peptide involves clathrin-dependent endocytosis and heparan sulfate receptors. J Biol Chem 280:15300–15306
17. Duchardt F, Fotin-Mleczek M, Schwarz H et al (2007) A comprehensive model for the cellular uptake of cationic cell-penetrating peptides. Traffic 8:848–866
18. Mishra A, Lai GH, Schmidt NW et al (2011) Translocation of HIV TAT peptide and analogues induced by multiplexed membrane and cytoskeletal interactions. Proc Natl Acad Sci U S A 108:16883–16888
19. Rothbard JB, Jessop TC, Lewis RS et al (2004) Role of membrane potential and hydrogen bonding in the mechanism of translocation of guanidinium-rich peptides into cells. J Am Chem Soc 126:9506–9507
20. Wender PA, Galliher WC, Goun EA et al (2008) The design of guanidinium-rich transporters and their internalization mechanisms. Adv Drug Deliv Rev 60:452–472
21. Mishra A, Gordon VD, Yang L et al (2008) HIV TAT forms pores in membranes by inducing saddle-splay curvature: potential role of bidentate hydrogen bonding. Angew Chem Int Ed Engl 47:2986–2989
22. Verdurmen WPR, Thanos M, Ruttekolk IR et al (2010) Cationic cell-penetrating peptides induce ceramide formation via acid sphingomyelinase: implications for uptake. J Control Release 147:171–179
23. Tanaka G, Nakase I, Fukuda Y et al (2012) CXCR4 stimulates macropinocytosis: implications for cellular uptake of arginine-rich cell-penetrating peptides and HIV. Chem Biol 19:1437–1446
24. Teesalu T, Sugahara KN, Kotamraju VR et al (2009) C-end rule peptides mediate neuropilin-1-dependent cell, vascular, and tissue penetration. Proc Natl Acad Sci U S A 106: 16157–16162
25. Arukuusk P, Pärnaste L, Margus H et al (2013) Differential endosomal pathways for radically modified peptide vectors. Bioconjug Chem 24:1721–1732
26. Brown MS, Goldstein JL (1983) Lipoprotein metabolism in the macrophage: implications for cholesterol deposition in atherosclerosis. Annu Rev Biochem 52:223–261
27. Greaves DR, Gordon S (2009) The macrophage scavenger receptor at 30 years of age: current knowledge and future challenges. J Lipid Res 50(Suppl):S282–S286
28. Fenton MJ, Golenbock DT (1998) LPS-binding proteins and receptors. J Leukoc Biol 64:25–32
29. Dunne DW, Resnick D, Greenberg J et al (1994) The type I macrophage scavenger receptor binds to gram-positive bacteria and recognizes lipoteichoic acid. Proc Natl Acad Sci U S A 91:1863–1867
30. Kouadir M, Yang L, Tan R et al (2012) CD36 participates in PrP(106-126)-induced activation of microglia. PLoS One 7, e30756
31. DeWitte-Orr SJ, Collins SE, Bauer CMT et al (2010) An accessory to the "Trinity": SR-As are essential pathogen sensors of extracellular dsRNA, mediating entry and leading to subsequent type I IFN responses. PLoS Pathog 6, e1000829
32. Barth H, Schnober EK, Neumann-Haefelin C et al (2008) Scavenger receptor class B is required for hepatitis C virus uptake and cross-presentation by human dendritic cells. J Virol 82:3466–3479
33. Canton J, Neculai D, Grinstein S (2013) Scavenger receptors in homeostasis and immunity. Nat Rev Immunol 13:621–634
34. Wang H, Wu L, Reinhard BM (2012) Scavenger receptor mediated endocytosis of silver nanoparticles into J774A.1 macrophages is heterogeneous. ACS Nano 6:7122–7132
35. Krieger M (1997) The other side of scavenger receptors: pattern recognition for host defense. Curr Opin Lipidol 8:275–280
36. Sarrias MR, Grønlund J, Padilla O et al (2004) The Scavenger Receptor Cysteine-Rich (SRCR) domain: an ancient and highly conserved protein module of the innate immune system. Crit Rev Immunol 24:1–37
37. Santiago-García J, Kodama T, Pitas RE (2003) The class A scavenger receptor binds to proteoglycans and mediates adhesion of macrophages to the extracellular matrix. J Biol Chem 278: 6942–6946
38. Arukuusk P, Pärnaste L, Oskolkov N et al (2013) New generation of efficient peptide-based vectors, NickFects, for the delivery of nucleic acids. Biochim Biophys Acta 1828:1–9
39. Ezzat K, Helmfors H, Tudoran O et al (2012) Scavenger receptor-mediated uptake of cell-penetrating peptide nanocomplexes with oligonucleotides. FASEB J 26:1172–1180
40. Lindberg S, Regberg J, Eriksson J, Helmfors H, Muñoz-Alarcón A, Srimanee A, et al (2015) A convergent uptake route for peptide- and polymer-based nucleotide delivery systems,

J Control Release. doi:10.1016/j.jconrel.2015.03.009
41. Langel Ü (2011) Cell-penetrating peptides: methods and protocols. Springer, New York
42. Kang SH, Cho MJ, Kole R (1998) Up-regulation of luciferase gene expression with antisense oligonucleotides: implications and applications in functional assay development. Biochemistry 37:6235–6239
43. Andaloussi SEL, Guterstam P, Langel Ü (2007) Assessing the delivery efficacy and internalization route of cell-penetrating peptides. Nat Protoc 2:2043–2047
44. Jafferali MH, Vijayaraghavan B, Figueroa RA et al (2014) MCLIP, an effective method to detect interactions of transmembrane proteins of the nuclear envelope in live cells. Biochim Biophys Acta 1838:2399–2403
45. Buch C, Lindberg R, Figueroa R et al (2009) An integral protein of the inner nuclear membrane localizes to the mitotic spindle in mammalian cells. J Cell Sci 122:2100–2107
46. Patel PC, Giljohann DA, Daniel WL et al (2010) Scavenger receptors mediate cellular uptake of polyvalent oligonucleotide-functionalized gold nanoparticles. Bioconjug Chem 21:2250–2256
47. Terpstra V, van Berkel TJ (2000) Scavenger receptors on liver Kupffer cells mediate the in vivo uptake of oxidatively damaged red blood cells in mice. Blood 95:2157–2163
48. Suzuki K, Doi T, Imanishi T et al (1999) Oligonucleotide aggregates bind to the macrophage scavenger receptor. Eur J Biochem 260:855–860

Part III

Applications of Cpps In Vitro and In Vivo

Chapter 12

Protein Mimicry and the Design of Bioactive Cell-Penetrating Peptides

John Howl and Sarah Jones

Abstract

The multi-domain architecture of many human proteins provides a structural basis for the physical maintenance of interactomes, or networks of protein–protein interactions (PPIs), that are so obviously crucial to cellular functions. Moreover, the structural and electrostatic complementarity provided by PPI interfaces, predominantly located on protein surfaces, is a fundamental component of signal transduction events that are known to be compromised in human diseases including many cancers.

The pharmacokinetic advantages provided by cell-penetrating peptides (CPPs) are entirely compatible with the development of intrinsically permeable agents capable of modulating intracellular PPIs. Thus, the term bioportide is a useful descriptor of numerous bioactive CPPs that are distinct from the more usual inert CPP vectors. Herein we illustrate a generic strategy, predominantly centered upon the identification of cationic peptides derived from helical protein domains, which offers a reliable platform to identify bioportides capable of modulating intracellular signal transduction events. In addition, we describe robust methodologies to determine the precise intracellular distribution of fluorescent bioportides and present assays routinely employed to screen for the detrimental pharmacodynamic properties often exhibited by both CPPs and bioportides; namely adverse cytotoxicity and the receptor-independent stimulation of mast cell secretion.

Key words Alpha helix, Bioportide, Cell viability, Confocal microscopy, Fluorescence, Mast cell, Protein–protein interaction, Secretion

1 Introduction

An overwhelming majority of CPP vectors are polycationic sequences. Some of these, including the common delivery vectors Tat [1] and penetratin [2], derive from known helical domains of transcription factor that facilitate membrane translocation. Other CPP sequences, including the transportans [3], can be modeled, at least in part, as an amphipathic helix. Polyarginine-containing CPP sequences have since been identified in a range of other human proteins [4] and it is tempting to speculate that one or multiple polycationic sequences may enable other *supercharged* proteins [5] to traverse biological membranes and so fulfill their biological

Ülo Langel (ed.), *Cell-Penetrating Peptides: Methods and Protocols*, Methods in Molecular Biology, vol. 1324,
DOI 10.1007/978-1-4939-2806-4_12,

function(s). Polycationic α-helices are also a quantitatively dominant secondary structure within the extended surfaces that constitute PPI interfaces [6] where the amino acid arginine is commonly enriched [7]. Thus, PPIs are ubiquitous modulators of all major signaling pathways that often utilize common *promiscuous* domains [8] and so it is highly probable that aberrant PPI function is a causative factor of many human disease states [9].

Considering the aforementioned structural similarities between many protein-derived CPPs and common helical elements within PPIs, it is perhaps not surprising that some cell permeable polycationic sequences display intrinsic bioactivities. Indeed, it is certain that even common CPPs, usually perceived as inert vectors, may display unpredictable and undesirable influences upon cellular function at concentrations in the low micro molar range that are usually employed for effective cargo delivery [10]. Moreover, since human proteins are an abundant source of arginine-enriched cryptic CPP sequences [4], there is tremendous scope to develop CPPs capable of protein mimicry. For example [11], polycationic sequences within the intracellular domains of G-protein-coupled receptors can mimic the function of agonist-activated proteins. Moreover, it is most likely that CPPs which mimic cationic helices within PPI interfaces achieve a biological function through a dominant-negative mechanism [12, 13]. The question arises, of course, of how to select appropriate polycationic sequences for synthesis. It is entirely feasible to identify putative CPPs simply by selecting polycationic segments of human proteins [4]. Moreover, we often prefer to employ a QSAR prediction algorithm that compares the bulk properties of amino acids within a defined sequence and so enables the positive identification of CPPs [14, 15].

As recently elaborated upon [12, 16], the term bioportide was introduced as a simple descriptor to distinguish a bioactive CPP from the more usual pharmacokinetic modifier or deliver vector [17]. Furthermore, it is exceedingly probable that the protein mimicry afforded by bioportides will be exploited in a clinical setting. The purpose of his chapter is, therefore, to provide generic guidelines for the identification of putative bioportides within human proteins. Presented herein are detailed protocols to enable investigators to screen for bioportides capable of accessing discrete intracellular compartments in the absence of adverse influences upon cellular viability and mast cell stability. Of course, considering the widespread predicted utility of bioportide technologies, target-specific bioassays will also be required to positively identify polycationic peptide sequences with appropriate biological activities. Unfortunately, details of these numerous and exceedingly variable biological assays are beyond the scope of this chapter.

2 Materials

2.1 Peptide Synthesis Reagents

1. *N*-α-Fluorenylmethyloxycarbonyl (Fmoc)-protected amino acids, 5,6-carboxy-tetramethylrhodamine (TAMRA) and Rink amide methylbenzhydrylamine (MBHA) resin.
2. Rink amide MBHA resins pre-loaded with the first amino acid.
3. Dimethylformamide (DMF) and 20 % vol/vol piperidine/DMF.
4. Diisopropylethylamine (DIPEA).
5. The coupling reagent O-(6-Chloro-1-hydrocibenzotriazol-1-yl)-1,1,3,3-tetramethyluronium hexafluorophosphate (HCTU; AGTC Bioproducts, Hessle, UK) and the racemization suppressor hydroxybenzotriazole HOBt (*see* **Note 1**).
6. Trifluoroacetic acid (TFA).
7. Triisopropylsilane (TIS) and ethanedithiol (EDT) from Sigma-Aldrich.

2.2 Confocal Microscopy Reagents and Fluorescent Markers

1. Laminar Flow Class II tissue culture fume hood (Clean Air).
2. CO_2 incubator (Jencons, Millennium).
3. TAMRA-labeled purified and lyophilized peptides.
4. Distilled H_2O (dH_2O).
5. Sterile syringes, filters, and Eppendorf tubes.
6. 35 mm sterile petri dishes with 12 mm glass bases (IWAKI, purchased from Barloworld Scientific Ltd, Stone, UK).
7. Cell culture medium without phenol red, pre-warmed to 37 °C.
8. MitoTracker® and ER Tracker® (*see* **Note 2**).
9. Carl Zeiss LSM 510 Meta confocal microscope with live cell imaging chamber and quantitative co-localization analysis software, incorporating an interactive scatter plot and data table linked to the images.

2.3 MTT Assays

1. Laminar Flow Class II tissue culture fume hood (Clean Air).
2. CO_2 incubator (Jencons, Millennium).
3. Sterile 96-well plates.
4. Cell culture medium pre-warmed to 37 °C.
5. Hanks Balanced Salt Solution (HBSS).
6. 3-(4,5-Dimethylthiazol-2-yl)-2,5-diphenyltetrazolium bromide (MTT) solution (0.5 mg/ml): Prepare a 5 mg/ml stock solution of MTT (Sigma) in pre-warmed cell culture medium. 0.02 g MTT in 4 ml of medium should be sufficient for two 96-well plates. This preparation may require sonification to fully dissolve the MTT. Further dilute the MTT stock solution

by 1:10 in cell culture medium (3 ml of the above stock solution in 30 ml medium is sufficient for two 96-well plates).

7. Dimethylsulfoxide (DMSO).
8. 96-well plate reader.

2.4 Secretion of β-hexosaminidase

1. Cell culture medium (growing medium): Dulbecco's Modified Eagle's Medium with L-glutamine (0.1 mg/ml) (DMEM, Sigma) supplemented with 10 % wt/vol fetal bovine serum (FBS), penicillin (100 U/ml) and streptomycin (100 μg/ml).
2. Sterile T75 cm^2 vented flasks.
3. Sterile cell scrapers (Sarstedt).
4. Laminar Flow Class II tissue culture fume hood (Clean Air).
5. CO_2 incubator (Jencons, Millennium).
6. Sterile 24-well plates.
7. Cell culture medium (stimulation medium): Nutrient Mixture F-12 with L-glutamine and sodium bicarbonate (Hams-F12, Sigma) supplemented with 10 mM HEPES. Adjust pH to 7.4 and pre-warm to 37 °C.
8. Eppendorf tubes.
9. Lysis buffer: 0.1 % vol/vol Triton X-100 in dH_2O.
10. 96-well plates.
11. Substrate solution: 0.3423 mg/ml *p*-nitrophenyl-*N*-acetyl-β-D-glucosaminide in 0.1 M sodium citrate buffer, pH 4.5.
12. 0.1 M Na_2CO_3/0.1 M $NaHCO_3$ buffer (pH 10.5).
13. 96-well plate reader.

3 Methods

3.1 Identification of Putative CPP Sequences Within Human Proteins

As previously described [4], polycationic sequences derived from the primary sequences of human proteins, particularly those containing an abundance of Arg residues, are often efficient CPPs. It is also possible to employ a QSAR prediction algorithm that compares the bulk properties of amino acids within a defined sequence of amino acids [14, 15]. In our hands this latter approach has proven particularly attractive for the identification of protein-mimicking CPPs within the size range of 12–24 AA. For example, QSAR prediction enabled the identification of CPPs and bioportides within Cytochrome *c* [16] and also identified nosangiotide (Fig. 1), a 16 AA fragment of a regulatory loop of endothelial nitric oxide synthase ($eNOS^{492–507}$; [17]). When considering larger multifunctional proteins, QSAR analysis can be logically restricted to appropriate functional domains.

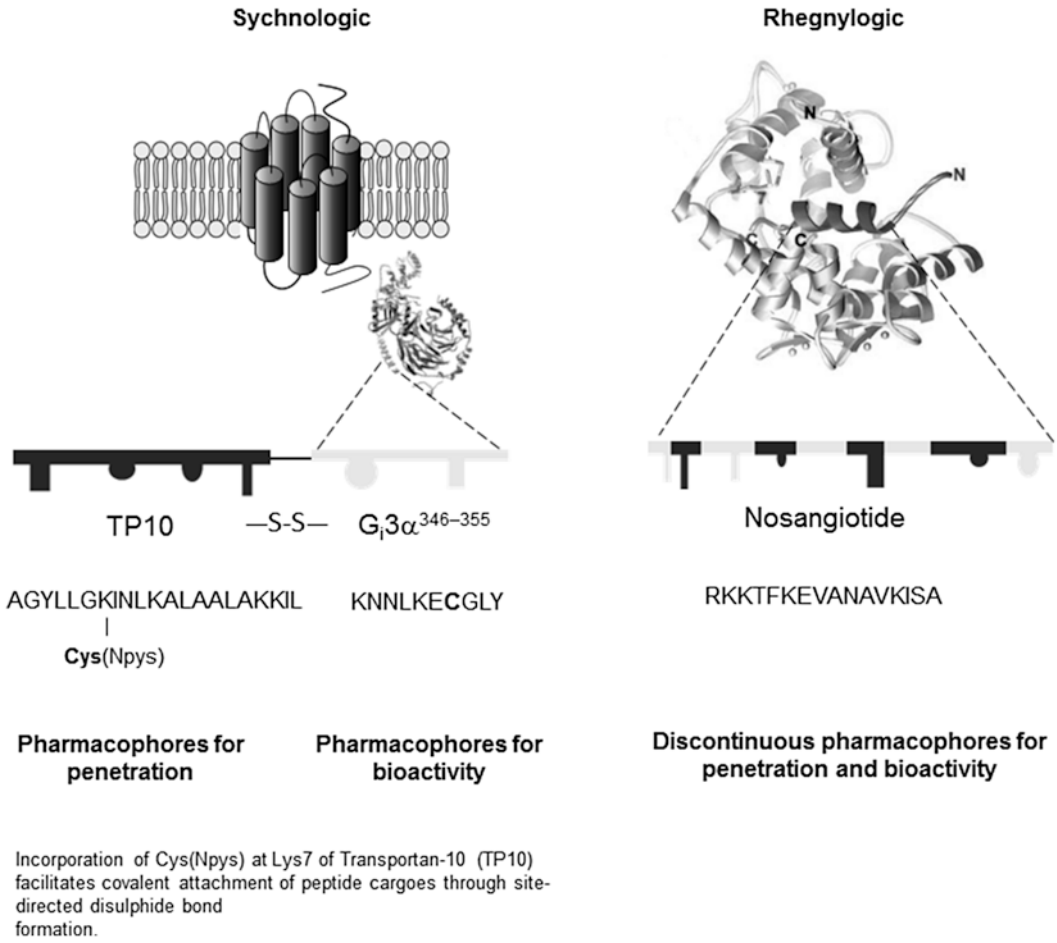

Fig. 1 Two structurally distinct types of organization can be observed in either sychnologic (*left panel*) or rhegnylogic (*right panel*) bioportides. If potential bioactive peptides are relatively impermeable then the modular nature of peptides enables such sequences to be readily conjugated in a tandem linkage to a CPP such as TP10. Moreover, many other polycationic CPPs, particularly those that mimic alpha-helical domains of protein, may possess intrinsic bioactivities. Theoretically at least, rhegnylogic bioportides, exemplified by nosangiotide (*right panel*), can be further modified by extension with homing peptides and other functional moieties

3.2 Bioportide Design Strategies

As previously described [12, 17, 18], two general patterns of organization can be distinguished in the design of bioportides (Fig. 1). A putative bioactive peptide that is essentially impermeable can be readily linked (*see* **Note 3**) to a CPP vector to achieve effective internalization. As an example, the sequence $G_i\alpha3^{346–355}$ (*H*-KNNLKECGLY-NH_2), which mimics the extreme carboxyl terminal of the $G_i\alpha3$ subunit of heterotrimeric G proteins, is a selective activator of p42/p44 mitogen-activated protein kinases when delivered into cells as a TP10-chimera [19]. By analogy to Schwyzer's message and address hypothesis [20], later expanded by Portoghese [21], this type of structural organization can be

described as sychnologic (Fig. 1) where the pharmacophores that enable effective cellular penetration (address) are structurally distinct from those responsible for biological activity (message). In contrast, it is also possible and usually desirable to identify rhegnylogically organized bioportides such as nosangiotide (eNOS$^{492\text{-}507}$; *H*-RKKTFKEVANAVKISA-NH_2). In this class of bioportide, the message and address pharmacophores are discontinuously organized within a single peptide (Fig. 1). Moreover, it is likely that side chains of amino acids in nosangiotide, particularly Arg and Lys, serve a dual purpose in enabling both cellular entry and a potent anti-angiogenic action [17].

3.3 Microwave-Enhanced Synthesis of Polycationic Peptide Sequences

Microwave-assisted solid phase peptide syntheses are performed using a Discover SPS Microwave Peptide Synthesizer (CEM Microwave Technology Ltd, Buckingham, UK) with fiber optic temperature control. Peptides are routinely synthesized (0.1 mmol scale) using an *N*-α-Fmoc protection strategy with HCTU activation. All coupling reagents and amino acids are dissolved in DMF. After each coupling and deprotection step, all resins are washed with DMF (~5 ml) and thoroughly drained three times. Crude peptides are purified to apparent homogeneity using reversed-phase semi-preparative scale high-performance liquid chromatography [12, 18, 19]. A qualitative test to detect the presence of free amines on resin beads (Kaiser test) can be routinely employed to confirm either coupling or deprotection [22].

1. Prior to the start of synthesis, swell the resin in DMF and then deprotect with 7 ml of 20 % vol/vol piperidine for 3 min at 50 W/75 °C. The same protocol method is routinely used after each AA coupling until Asp is introduced (see below).
2. A majority of amino acid (AA) coupling reactions are accomplished with a fourfold molar excess of Fmoc-protected AA with HCTU and diisopropylethylamine (DIPEA), molar ratio of 1:1:2 (AA/HCTU/DIPEA), in 4 ml for 10 min at 25 W/75 °C. Since HCTU can cap peptide chains, we routinely dissolve 0.45 mmol of each amino acid in 4 ml of 0.1 M HCTU before adding DIPEA (170 μl). After dissolution of the AA, the entire mixture is introduced to the resin and stirred in the microwave reaction vessel. Due to the restricted conformational space accessible to α-aminoisobutyric acid (Aib), a known helix promoter that can be successfully incorporated in the design of bioportides that mimic helical protein domains, Aib and the vicinal AA are routinely double-coupled.
3. The coupling of Arg is performed in two stages: 30 min 0 W/~25 °C followed by 5 min at 17 W/75 °C (*see* **Note 1**). We routinely double couple each Arg residue to ensure 100 % coupling efficiency.

4. To reduce the potential racemization of both Cys and His, coupling conditions are 5 min at 0 W/~25 °C followed by 6 min at 17 W/50 °C with the hindered base collidine at a molar ratio of 1:1:2 (AA/HCTU/collidine; [23]).
5. After Asp is incorporated into a peptide sequence, aspartimide formation is reduced by the employment of 5 % wt/vol piperazine in 0.1 M 1-hydroxybenzotriazole hydrate (HOBt; *see* **Note 1**) as the deprotection solution under similar condition described above in **step 1** [23].
6. Following synthesis approximately 25 % of the peptide (~0.025 mmol) is N-terminally acylated on resin with TAMRA to yield the fluorescent analog. We routinely perform this reaction using a twofold molar excess of TAMRA with HCTU as a coupling reagent at room temperature for 2–3 h.
7. To cleave peptides from the resin and remove blocking groups, resin is transferred to a glass reaction vessel and 4 ml of TFA/TIS/H_2O (95/2.5/2.5 % vol/vol) added and gently mixed for 2–3 h. If the sequence contains Cys and/or Met then ethanedithiol (EDT) is also included to scavenge additional blocking groups TFA/TIS/H_2O/EDT (94/1/2.5/2.5 % vol/vol).

3.4 Live Cell Confocal Imaging and Quantitative Co-localization Studies with Organelle-Specific Markers

As described (*see* **Note 2**), there is a bewildering variety and number of fluorescent markers that can be employed to illuminate intracellular organelles in living cells. These, in combination with a fluorescent bioportide or CPP, enable co-localization studies to determine the intracellular fate of exogenously added peptides. Furthermore, to avoid fixation artifacts, specifically those that promote a redistribution of fluorescent peptides, we always perform confocal microscopy upon living cells.

1. Purified and lyophilized peptides, as with all the protocols to follow, are dissolved in dH_2O to a final concentration of 1 mM, filter sterilized and stored in sterile Eppendorf tubes at −20 °C. Avoid repeated freeze–thaw cycles.
2. Grow cells to sub-confluence in 35 mm Petri Dishes with 12 mm glass bases in their recommended culture medium.
3. Wash cells with phenol red free medium and incubate with an appropriate fluorescent intracellular organelle probe and TAMRA-labeled bioportide/CPP (5 μM, to a maximum volume of 2 ml) at 37 °C in a humidified atmosphere of 5 % CO_2 (*see* **Note 4**).
4. Ensure that the live cell imaging chamber has stabilized at 37 °C and contains a humidified atmosphere of 5 % CO_2.
5. Immediately prior to observation, wash cells (eight times) in culture medium without phenol red and analyze intracellular distributions using a confocal microscope equipped with quantitative co-localization analysis software (Fig. 2; *see* **Note 5**).

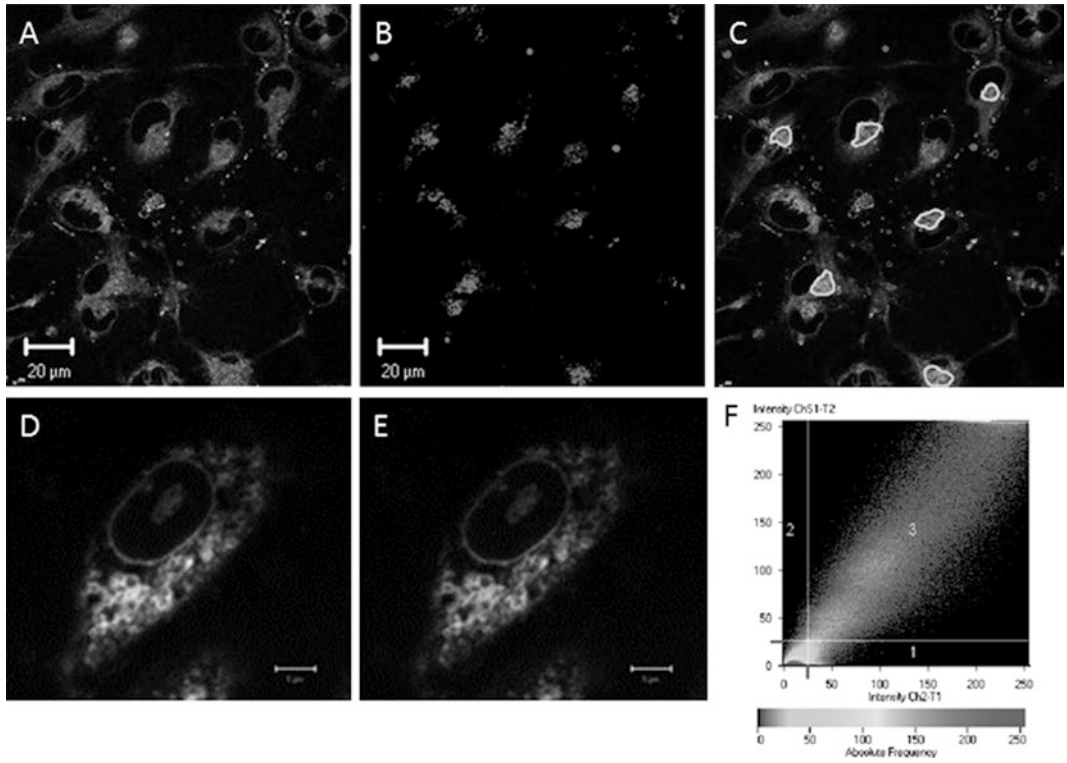

Fig. 2 Using a Carl Zeiss LSM 510Meta confocal microscope equipped with quantitative co-localization analysis software, incorporating an interactive scatter plot (**f**) and data table linked to the images, it is possible to quantify the degree of co-localization of your TAMRA-labeled bioportide/CPP with fluorescently (fluorescein or Cy5 for example)-labeled organelles. Analysis can either be taken from multiple regions of interest (**c**) or multiple whole images (**d**, **e**). We tend to opt for two coefficients which are commonly employed to estimate the degree of co-localization, the overlap coefficient after Manders (*R*) and co-localization coefficients, both of which are unaffected by signal intensities and therefore avoid complications associated with potential variance of signal strength between the two fluorophores (*see* **Note 5**). The cytochrome *c*-derived bioportide Cyt $c^{77–101}$ co-localizes with the endoplasmic reticulum. U373MG cells were treated with 1 μM ER Tracker® Green FM (**a**) and 5 μM TAMRA-labeled Cyt $c^{77–101}$ (**b**). The composite image (**c**) highlights multiple regions of interest selected for analysis. The bioportide Z-Gly-RGDf-mitP co-localizes with mitochondria. ECV304 cells were treated with 500 nM Mitotracker® Deep Red FM (**d**) and 5 μM fluorescein-labeled Z-Gly-RGDf-mitP (**e**) and viewed by confocal live cell imaging

3.5 MTT Assays of Cellular Viability

Many different lines can be utilized to determine the influence of exogenously added CPPs and bioportides on the viability of eukaryotic cells in culture. The MTT assay measures the oxidative capacity of mitochondria and is thus an index of cellular viability [24, 25]. MTT is reduced, by metabolically active cells only, to a colored water-insoluble formazan salt. Following solubilization and colorimetric measurement, only viable cells are therefore detected. Many similar methods using the reduction of tetrazolium salts are also available.

To ensure sterility, the procedure below should be carried out in a Class II laminar flow hood using aseptic tissue culture techniques. From **step 6** onwards, however, the procedure can be carried out on an open bench.

1. Grow cell lines in their specified medium to sub-confluence in 96-well plates in a humidified atmosphere of 5 % CO_2 at 37 °C (CO_2 incubator; *see* **Note 6**).
2. Treat cells with 200 μl medium/well containing CPP/bioportide or vehicle medium alone. An initial concentration range of 0.1–30 μM is a useful starting point for a majority of permeable peptides. Return cells to the CO_2 incubator for the designated time period (*see* **Note 7**).
3. Ensure to add 200 μl of stimulation medium alone to six empty well so as to detect any background absorbance readings.
4. To terminate the reaction, remove the stimulation medium.
5. Add the prepared MTT solution (0.5 mg/ml; 200 μl/well) and incubate for 3 h at 37 °C (*see* **Note 8**).
6. Gently aspirate medium taking care not to disturb the cell monolayer and insoluble colored product.
7. Solubilize in warm DMSO at 200 μl/well.
8. Incubate for a further 15 min at 37 °C.
9. Gently agitate and read absorbance at 540 nm on a 96-well plate reader.
10. Cell viability is expressed as a percentage of cells treated with vehicle (medium) alone. An average value for the background readings is calculated and subtracted from all values prior to the determination of % cell viability. Results are expressed as mean ± S.E.M.

3.6 Peptide-Stimulated Secretion of β-hexosaminidase from RBL-2H3 cells

The rat basophilic leukemia cell line RBL-2H3 (*see* **Note 9**) is a widely utilized model of mucosal mast cells. Moreover, RBL-2H3 is often employed to determine the influence of CPPs and bioportides on the regulated secretion of β-hexosaminidase, a secretory lysosome marker. The wasp venom-derived peptide secretegogue mastoparan (Bachem) can be used as a positive control in these assays [25]. During this procedure, both secreted and intracellular fractions are collected and assayed so as to establish the percentage of intracellular β-hexoseaminidase that is exocytosed

1. RBL-2H3 cells are routinely maintained in cell culture medium (growing medium) in a humidified atmosphere of 5 % CO_2 at 37 °C (CO_2 incubator).
2. RBL-2H3 cells grow as an adherent monolayer and are passaged, usually 1:3, by cell scraping. Do not use trypsin to detach cells.

3. To ensure sterility, cell culture maintenance should be carried out in a Class II fume hood, whilst wearing gloves throughout.
4. Plate out cells into 24-well plates and ensure that cells are confluent prior to assays.
5. Wash cells two times in pre-warmed stimulation medium.
6. Treat cells with 250 μl stimulation medium/well containing CPP/bioportide for 15 min at 37 °C. Include samples for basal levels of secretion (stimulation medium alone). An initial peptide concentration range of 0.1–30 μM is recommended.
7. To measure exocytosed (secreted) β-hexosaminidase, transfer medium from all wells to Eppendorf tubes and centrifuge at 14,000 RPM (~22,000 RCF) for 5 min.
8. To measure intracellular β-hexosaminidase, add 250 μl lysis buffer to all wells and leave for 5 min on ice.
9. Scrape wells and transfer cell lysates to Eppendorf tubes.
10. Collected samples, both secreted and intracellular fractions, should be placed on ice, particularly when assaying multiple plates.
11. Transfer 5 μl of collected samples (for secreted fraction, use the supernatant) to a 96-well plate.
12. Include 6 wells of 5 μl stimulation medium as a background control.
13. Add 20 μl of substrate to all wells.
14. Ensure that samples and substrate mix by placing on a shaker for 1 min.
15. Incubate for 60 min at 37 °C.
16. Add 250 μl/well 0.1 M Na_2CO_3/0.1 M $NaHCO_3$ buffer (pH 10.5) and read absorbance at 405 nm on a 96-well plate reader.
17. Results can be expressed as fold secretion of β-hexosaminidase. An average value for the background absorbance readings (stimulation media) is calculated and subtracted from all other values. Determine the mean basal value and express results as fold/basal ± S.E.M.
18. Alternatively, results can be expressed as % β-hexosaminidase secretion minus basal. Subtract the average background value from all other values. Calculate total β-hexosaminidase content by adding together the secreted and intracellular values for each well. Determine the % secretion (secreted/total) × 100. Calculate the basal mean % secretion and subtract from all other percentage values.

4 Notes

1. We routinely employ HCTU in microwave-enhanced coupling reactions but, in the case of Arg, this leads to formation of γ-lactam when the internal nitrogen of the guanidine attacks the active ester. The employment of *N*,*N*′-diisopropylcarbodiimide (DIC) with the additive ethyl 2-Cyano-2-(hydroxyimino)acetate (Oxyma) has been more recently described [26] as a very effective coupling strategy that can overcome problems with Arg and γ-lactam formation. Oxyma is also a safer alternative to HOBt that is now difficult to transport due to the potential of explosion [27].
2. Molecular Probes, part of Invitrogen, market a very wide variety of fluorescent cell markers that can be used to visualize intracellular organelles in living cells using confocal microscopy. Manufacturer's guidelines, particularly with regards to concentration, should be followed accordingly.
3. The quantitatively dominant method employed to join a CPP (address) and bioactive sequence (message) is a covalent peptide bond. Thus, sychnologically organized chimera can be synthesized as a linear sequence by routine SPPS methodologies. In such cases there are no general guidelines to direct the choice of molecular architecture, message-address or address-message, though in practical terms the two peptides are likely to display different properties. As exemplified by studies with TP10 analogs [19, 28], it may be advantageous to join bioactive cargoes to a CPP using a disulfide bond (usually cystine) that is reduced upon cellular penetration. Of course many other chemical methods for the orthogonal conjugation of peptides could be utilized to ligate CPP and peptide cargo [29]. Unfortunately, we currently lack a detailed comparative evaluation of the relative merits of such approaches within the CPP/bioportide field.
4. An initial concentration of 5 μM is recommended for the visualization of TAMRA-labeled bioportides/CPPs. An application concentration of higher than 5 μM may elicit non-specific membrane perturbations. It is strongly recommended that a time course is performed to identify possible temporal variations in the intracellular localization of any bioportide/CPP.
5. Using integrated co-localization analysis software, it is possible to quantify the degree of co-localization of any TAMRA-labeled bioportide/CPP with fluorescently labeled organelles. We tend to opt for two coefficients which are unaffected by signal intensities. Besides being insensitive to variances in signal strength, the overlap coefficients after Manders (R) are also resistant to photo-bleaching and amplifier settings. Coefficients

generate values between 0 and 1. A value of 0 indicates no co-localization, whereas a value of 1 indicates that all pixels are co-localized. Co-localization (coloc) coefficients can also be calculated for two different fluorophores using the following equations:

$$C1 = \frac{\text{pixels Ch1.}_{\text{coloc}}}{\text{pixels Ch1.}_{\text{total}}}, \qquad C2 = \frac{\text{pixels Ch2.}_{\text{coloc}}}{\text{pixels Ch2.}_{\text{total}}}$$

These define the relative number of co-localizing pixels in channel 1 (designated as TAMRA for example) and channel 2 (designate as fluorescein for example) as compared to the total number of pixels above threshold. Co-localization coefficients generate values from 0 to 1.0 whereby, a value of 1.0 for channel 1 and a value of 0.5 for channel 2 would indicate that 100 % TAMRA pixels co-localize with fluorescein and 50 % fluorescein pixels co-localize with TAMRA.

6. It is strongly advised to distribute cells into 96-well plates the day before the assay and not to "grow up" cells in 96-well plates over a period of days. Growth rates will necessarily depend upon the cell type being used. Do not use the outer wells of the 96-well plates, but fill them with 200 μl/well sterile HBSS.
7. Temporal analysis. You may wish to carry out your own temporal analysis of the potential detrimental cytotoxic effects of your designated CPP/bioportide. However, these membrane perturbatory effects, commonly associated with polycationic peptides, are usually evident within 4 h.
8. After 3 h a purple monolayer should be evident on the bottom of the wells containing viable cells. Incubating the MTT solution for longer than 4 h can lead to "clumping" and "loose" formazan salts, which carry the risk of being removed alongside the removal of the culture medium, thus greatly affecting your results.
9. There is some debate regarding the utility of RBL-2H3 as a mast cell model [30], not least because of its genesis from a rodent basophilic leukemia [31]. However, the cell line is widely utilized to investigate peptide-stimulated regulated secretion and can be further sensitized to polycationic peptides by the addition of quercetin [32]. In an ideal situation, we would choose to employ a human mast cell line for these studies. However, the choice of stable human mast cell lines is limited in both number and by the fact that maintenance of available lines usually requires the addition of prohibitively expensive culture supplements such as scatter factor.

References

1. Vivès E, Brodin P, Lebleu B (1997) A truncated HIV-1 Tat protein basic domain rapidly translocates through the plasma membrane and accumulates in the cell nucleus. J Biol Chem 272:16010–16017
2. Derossi D, Joliot AH, Chassaing G, Prochiantz A (1994) The third helix of the Antennapedia homeodomain translocates through biological membranes. J Biol Chem 269:10444–10450
3. Soomets U, Lindgrena M, Galletb X, Hällbrink M, Elmquist A, Balaspiri L, Zorko M, Pooga M, Brasseur R, Langel Ü (2000) Deletion analogues of transportan. Biochim Biophys Acta 1467:165–176
4. Futaki S, Suzuki T, Ohashi W, Yagami T, Tanaka S, Ueda K, Sugiura Y (2001) Arginine-rich peptides. An abundant source of membrane-permeable peptides having potential as carriers for intracellular protein delivery. J Biol Chem 276:5836–5840
5. Cronican J, Beir KT, Davis TN, Tseng J-C, Li W, Thompson DB, Shih AF, May EM, Cepko CL, Kung AL, Zhou Q, Liu DR (2011) A class of human proteins that deliver functional proteins into mammalian cells in vitro and in vivo. Chem Biol 18:833–838
6. Jochim AL, Arora PS (2009) Assessment of helical interfaces in protein-protein interactions. Mol Biosyst 5:924–926
7. Crowley PB, Golovin A (2005) Cation-π interactions in protein-protein interfaces. Proteins 59:231–239
8. Pawson T, Nash P (2000) Protein-protein interactions define specificity in signal transduction. Genes Dev 14:1027–1047
9. Vidal M, Cusick ME, Barabási A-L (2011) Interactome networks and human disease. Cell 144:986–998
10. Verdurmen WPR, Brock R (2010) Biological responses towards cationic peptides and drug carriers. Trends Pharmcol Sci 32:116–124
11. Östlund P, Kilk K, Lindgren M, Hällbrink M, Jiang Y, Budihna M, Cerne K, Bavec A, Östenson C-G, Zorko M, Langel Ü (2005) Cell-penetrating mimics of agonist-activated G-protein coupled receptors. Int J Pept Res Ther 11:237–247
12. Lukanowska M, Howl J, Jones S (2013) Bioportides: bioactive cell penetrating peptides that modulate cellular dynamics. Biotechnol J 8:918–930
13. Kiosses WB, Hood J, Gerritsen ME, Cheresh DA, Alderson N, Schwartz MA (2002) A dominant negative p65 PAK peptide inhibits angiogenesis. Circ Res 90:697–702
14. Hansen M, Kilk K, Langel Ü (2008) Predicting cell-penetrating peptides. Adv Drug Deliv Rev 60:572–579
15. Hällbrink M, Kilk K, Elmquist A, Lundberg P, Lindgren M, Jiang Y, Pooga M, Soomets U, Langel Ü (2005) Prediction of cell-penetrating peptides. Int J Pept Res Ther 11:249–259
16. Jones S, Holm T, Mäger I, Langel Ü, Howl J (2010) Characterisation of bioactive cell penetrating peptides from cytochrome c: protein mimicry and the development of a novel apoptogenic agent. Chem Biol 17: 735–744
17. Howl J, Matou-Nasri S, West DC, Farquhar M, Slaninová J, Östenson C-G, Zorko M, Östlund P, Kumar S, Langel Ü, McKeating J, Jones S (2012) Bioportide: an emergent concept of bioactive cell penetrating peptide. Cell Mol Life Sci 69:2951–2966
18. Howl J, Jones S (2008) Proteomimetic cell penetrating peptides. Int J Pept Res Ther 14:359–366
19. Jones S, Farquhar M, Martin A, Howl J (2005) Intracellular translocation of the decapeptide carboxyl terminal of $G_i3\alpha$ induces the dual phosphorylation of p42/p44 MAP kinases. Biochim Biophys Acta 1745:207–214
20. Portoghese P (1989) Bivalent ligands and the message-address concept in the design of selective opioid receptor antagonists. Trends Pharmacol Sci 10:230–235
21. Schwyzer R (1977) ACTH: a short introductory review. Ann N Y Acad Sci 297:3–26
22. Chan WD, White PD (2000) Basic Procedures. In: Chan WD, White PD (eds) Fmoc solid phase peptide synthesis: a practical approach. Oxford University Press, Oxford, UK, pp 41–76
23. Palasek SA, Cox ZJ, Collins JM (2007) Limiting racemization and aspartimide formation in microwave-enhanced Fmoc solid phase peptide synthesis. J Pept Sci 13:143–148
24. Carmichael J, DeGraff WG, Gazdar AF, Minna JD, Mitchell JB (1987) Evaluation of a tetrazolium-based semiautomated colorimetric assay: assessment of chemosensitivity testing. Cancer Res 47:936–942
25. Jones S, Howl J (2004) Charge delocalisation and the design of novel mastoparan analogues: enhanced cytotoxicity and secretory efficacy of [Lys^5, Lys^8, Aib^{10}]MP. Regul Pept 121: 121–128
26. Collins JM, Porter KA, Singh SK, Vanier GS (2014) High-efficiency solid phase peptide synthesis (*HE*-SPPS). Org Lett 16:940–943

27. Subirós-Funosas R, Probens R, Barbas R, El-Faham A, Albericio F (2009) Oxyma: an efficient additive for peptide synthesis to replace the benzotriazole-based HOBt and HOAt with a lower risk of explosion. Chem Eur J 15:9394–9403
28. Howl J, Jones S, Farquhar M (2003) Intracellular delivery of bioactive peptides to RBL-2H3 cells induces ß-hexoseaminidase secretion and phospholipase D activation. ChemBioChem 4:1312–1316
29. Tam JP, Yu Q, Miao Z (1999) Orthogonal ligation strategies for peptide and protein. Biopoly 51:311–332
30. Passante E, Frankish N (2009) The RBL-2H3 cell line: its provenance and suitability as a model for the mast cell. Inflamm Res 58:737–745
31. Barsumian EL, Isersky C, Petrino MG, Siraganian RP (1981) IgE-induced histamine release from rat basophilic leukemia cell lines: isolation of releasing and nonreleasing clones. Eur J Immunol 11:317–323
32. Senyshyn J, Baumgartner RA, Beaven MA (1998) Quercetin sensitizes RBL-2H3 cells to polybasic mast cell secretagogues through increased expression of Gi GTP-binding proteins linked to a phospholipase C signaling pathway. J Immunol 160:5136–5144

Chapter 13

Pepducins and Other Lipidated Peptides as Mechanistic Probes and Therapeutics

Ping Zhang, Lidija Covic, and Athan Kuliopulos

Abstract

Lipopeptides based on the intracellular loops of cell-surface receptors, known as "Pepducins," represent a promising new class of compounds used for the study of membrane proteins and as potential therapeutics in a variety of diseases. Detailed knowledge of the three-dimensional structure of G-protein-coupled receptors (GPCRs) and delineation of the mechanisms of pepducin activation and biased G-protein signaling has facilitated the development of even more potent pepducin allosteric modulators.

Key words Pepducins, Lipopeptides, GPCRs, PAR1, PAR2, PAR4, CXCR1, CXCR2, CXCR4

1 Introduction

G-protein-coupled receptors (GPCRs) are integral membrane proteins that are involved in a broad range of normal and pathological processes. GPCRs generally share high sequence conservation within their seven-transmembrane-domain (TM) core but have high diversity in their cytoplasmic loops (i1, i2, and i3) and C-terminal i4 domain. These intracellular surfaces play a critical role in the binding, selectivity, and activation of specific G proteins and non-G protein effectors [1, 2]. Pepducins are a new technology that selectively targets the intracellular receptor–effector interface [3]. Pepducins are derived from the intracellular i1–i4 domains of their cognate GPCR and gain the ability to readily penetrate cell membranes by the attachment of a lipid group such as a palmitate or steroid [2, 4, 5]. The rapid and efficient cell membrane flipping and membrane-tethering of pepducins [5–9] makes them well-suited for interrogation of the role of intracellular regions of receptors in G-protein coupling, cell signaling, and as potential therapeutics. The imbalance of GPCR signaling contributes to many diseases, and over 30 % of the U.S. Food and Drug Administration-approved therapeutics target GPCRs [10, 11].

Ülo Langel (ed.), *Cell-Penetrating Peptides: Methods and Protocols*, Methods in Molecular Biology, vol. 1324,
DOI 10.1007/978-1-4939-2806-4_13,

Since 2007, the determination of new GPCR structures and the detection of previously unseen conformational states [11–14] have spurred new research and development efforts to identify drugs with fewer side effects and more favorable pharmacological properties. However, most drug discovery efforts have focused on the design and discovery of ligands that bind at the orthosteric site located near the extracellular surface of the GPCR. Pepducins or other lipidated peptides target intracellular regions or transmembrane domains [15] of GPCRs in an allosteric manner and are now being investigated as a potential treatment strategy for cardiovascular diseases [16–19], cancer [20–24], inflammation and sepsis [25–27], asthma [28], and bone marrow transplant [29]. In this chapter, we summarize the current status of pepducins as mechanistic probes and as novel therapeutics (*see* Table 1).

Table 1
Pepducin applications and outcomes in diverse human diseases

Pepducin	Sequence	Target	Outcome	Ref.
PZ128 (P1pal-7)	pal-KKSRALF	PAR1	Inhibits platelet aggregation in humans and arterial thrombosis in primate models, suppresses tumor growth, metastasis and angiogenesis in mice	[16–18, 23, 44–46]
P1pal-12	pal-RCLSSSAVANRS	PAR1	Inhibits platelet aggregation, decreases thrombin-induced relaxation in rat aortic rings and limits pulmonary fibrosis	[18, 63, 64]
P1pal-12S	pal-RSLSSSAVANRS	PAR1	Temporally modulates sepsis survival, vascular leakage, and DIC	[33]
P1pal-13	pal-AVANRSKKSRALF	PAR1	Temporally modulates sepsis survival, vascular leakage, and DIC	[33]
P2pal-18S	pal-RSSAMDENSEKKRKSAIK	PAR2	Reduces acute inflammation and edema in skin inflammation models and reduces the severity of experimental biliary pancreatitis	[27, 54]
P4pal-10	pal-SGRRYGHALR	PAR4	Inhibits platelet aggregation and platelet deposition in guinea pig and baboon thrombosis models	[5]

(continued)

Table 1
(continued)

Pepducin	Sequence	Target	Outcome	Ref.
P4pal-i1	pal-ATGAPRLPST	PAR4	Inhibits platelet aggregation and prolongs the occlusion time in guinea pig arterial thrombosis	[16]
x1/2pal-i3	pal-RTLFKAHMGQKHR	CXCR1 CXCR2	Inhibits neutrophil migration toward interleukin-8, decreases transmigration of neutrophils into the peritoneal cavity, reverses the lethal sequelae of sepsis and improves survival in mice	[26]
x4pal-i3	pal-HSKGHQKRKALK	CXCR4	Completely inhibits the response of neutrophils toward SDF-1α	[26]
x4pal-i1	pal-MGYQKKLRSMTD	CXCR4	Completely inhibits the response of neutrophils toward SDF-1α, mobilizes leukocytes from the bone marrow	[26]
ATI-2341	pal-MGYQKKLRSMTDKYRL	CXCR4	Mediates release of granulocyte/macrophage progenitor cells from the bone marrow	[29, 34]
KRX-7	myristoyl-GMRPYDANKR	S1P3	Induces vasorelaxation and fibroblast proliferation	[58]
Compd 16	myristoyl-GRPYDAN	S1P3	Blocks KRX-725 activity	[58]
F2pal-16	pal-KIHKKGMIKSSRPLRV	FRP2	Activates neutrophils to produce superoxide	[65]
F2Pal-10	pal-KIHKKGMIKS	FRP2	Activates neutrophils to produce superoxide	[65]
F2pal-12	pal-KIHKKGMIKSSR	FRP2	Inhibits neutrophil chemotaxis and superoxide production	[61]

2 Pepducins as Mechanistic Probes of G-Protein-Coupled and Other Cell-Surface Receptors

In the simplified orthosteric activation mechanism of a GPCR, an agonist typically binds to the orthosteric binding pocket localized inside the receptor transmembrane bundle near the extracellular surface. This induces a conformational change in the receptor including a large outward movement of the lower part of TM6 and rotation of TM7 with disruption of the DRY-ionic lock between TM3 and TM6. In this agonist-stabilized on-state, the intracellular portion of the receptor will present a large hydrophobic cavity for

engagement of the Galpha protein C-terminal helix and exchange of GDP for GTP [12, 30, 31].

By comparison, pepducin agonists must first translocate across the plasma membrane in order to activate the receptor at an allosteric site(s) on the intracellular surface of the receptor–G protein interface [2, 5]. Attachment of a sufficiently hydrophobic lipid tether, typically a myristate, palmitate or lithocholic moiety to the peptide, confers the ability to partition to the outside leaflet of the lipid bilayer and then rapidly flip across the membrane to the inner leaflet, where it remains tethered [5–9]. Pepducins activate receptor–G protein signaling in the presence of their cognate receptor and are usually highly selective for receptor type [2, 4, 5]. For instance, the PAR1 i3-loop pepducin, P1pal-19, loses all ability to stimulate Gq-PLC-β-induced inositol phosphate production in the absence of PAR1 [4]. The i1-pepducin ATI-2766 bound to both the full-length native CXCR4 as well to mutants with truncations of the receptor N-terminus, which harbors an essential extracellular chemokine agonist docking site [8]. The CXCR4 i1 pepducin did not interact with the closely related chemokine receptor CCR5. The pepducin, ICL3-9, based on the β2AR receptor i3-loop promoted receptor interactions with Gs and increased Gs signaling, consistent with previous findings that pepducin activity requires the presence of its cognate receptor [28]. ICL3-9 induced an increase in the BRET signal between β2AR and Gs, in striking contrast to the decreased BRET signal observed with the orthosteric agonist isoproterenol. This result clearly demonstrated that the β2AR-Gs active conformation induced by the pepducin is different from that stabilized by isoproterenol. However, a more N-terminally based i3-loop pepducin, ICL3-8, induced receptor-independent Gs signaling [28]. The mechanism of this Gs direct activator pepducin remains unclear, however, this N-terminal region of the i3 loop of the β2AR is a critical interaction site with the Gs α5-β4 loop [12].

The i3 loop region is likewise critical for fine tuning G-protein-specific responses at the molecular level. For example, the i3 loop sequences of the formyl peptide receptors FPR1 and FPR2 differ by only two amino acids and differ in their response to orthotopic ligands [32]. A pepducin with the FPR2-specific K231 replaced by the FPR1-specific Q231 lost all activity to FPR2. However, the FPR2 pepducin F2Pal-10 triggered a response in cells expressing wild-type or FPR2 chimeras containing the i3 loop of FPR1, but not to wild-type FPR1 [32]. These data are consistent with the notion that i3 loop pepducins are not simply replacing the intracellular loops but utilize the specific receptor–G protein interactions encoded in the native receptor loops [4].

Pepducin agonists can also favor receptor–G protein engagement of one class of G proteins over others. The PAR1 i3 loop agonist pepducin, P1pal-13, preferentially activates PAR1

G12/13-Rho signaling in quiescent endothelial cells, rather than Gi pathways [33]. However, when co-expressed with PAR2, P1pal-13 was able to transactivate PAR2-Gi signaling as a PAR1–PAR2 heterodimer, and lost the ability to activate PAR1-G12/13 signaling [33]. The CXCR4 pepducin ATI-2431 corresponding to the i1 intracellular loop of CXCR4 [29] selectively triggered coupling to Gαi, not Gα12/13 with a negative bias toward the β-arrestins [34]. This negative bias toward β-arrestin was due to the inability to strongly stimulate GPCR-kinase (GRK) phosphorylation of the receptor. Likewise, the Gs-biased pepducin agonist of the β2 adrenergic receptor, ICL3-9, did not induce interaction with GRKs and β-arrestins [28]. Similar to the case with i3 agonist pepducins, an i3 antagonist pepducin, P2pal-18S, was strongly biased toward blocking PAR2-Gq and PAR-Gi signaling pathways including MAPK activation, but had no effect on triggering PAR2-ligand-activated endocytosis [27]. As PAR2 endocytosis is dependent on β-arrestin engagement, it was not surprising that P2pal-18S was unable to inhibit β-arrestin interactions with PAR2 [35].

Recently, an array of 389 pepducins and pepducin-like 12mer lipopeptides were screened for agonist activity against the apelin APJ receptor [15]. Their approach was to synthesize lipopeptides each containing 12 contiguous amino acids of the entire amino acid sequence of the APJ receptor from the N-terminus to the C-terminus with 1 amino acid residue increments. Lipopeptides derived from the C-terminal portion of TM2 were found to be robust agonists of APJ activity with EC50 values as low as 34 nM. Subsequent alanine point mutations resulted in a APJ pepducin-like compound (Palm-VTLPLWATYTAR) with 2.7 nM agonist activity [15]. Although the mechanism of activation of the APJ receptor by this pepducin-like compound is not understood, this TM2 segment is known to comprise part of the binding site for many hydrated orthosteric ligands within the transmembrane core of GPCRs [36]. Shield's group earlier employed a more sophisticated bioinformatics/high-throughput screening technique to identify pepducin and lipopeptide modulators of platelet function targeted to signaling-rich juxtamembrane regions of GPCRs and other transmembrane receptors [37]. Palmitoylated peptides derived from the insulin-like growth factor-1 (IGF-1) receptor juxtamembrane region were identified to be specific inhibitors of IGF-1-mediated Akt activation and breast cancer growth [37].

In addition to GPCRs, the pepducin approach has been successfully used as a mechanistic probe of other membrane proteins including ion channels such as M (Kv7) potassium channels and transient receptor potential vanilloid channels (TRPV). Cell-penetrating lipidated peptides were found to be selective antagonists of the TRPV1 channel by targeting the intracellular C-terminal TRP domain that was predicted to interact with the highly

conserved receptor internal gate [38]. G proteins were also directly targeted by synthesizing palmitoylated peptides corresponding to the C terminus of Gq/11 with the intent to inhibit the muscarinic acetylcholine receptor (mAChR) [39]. Selectivity was demonstrated between Gq/11- and Go-targeted palmitoylated peptides. Du's group [40] used a myristoylated C-terminal peptide fragment of G13 [41] to inhibit signaling from the platelet receptor αIIbβ3 to associated G13.

Given the large number of GPCRs and non-GPCRs and membrane-associated proteins, it is likely that the pepducin approach will continue to serve as a unique mechanistic probe of these critical juxtamembrane and transmembrane regions in the context of cell signaling and pharmacology.

3 Pepducin-Based Therapeutics

PAR1—The serine protease thrombin is one of the most potent activators of platelet aggregation, endothelial cell activation, and other responses in many cell types [42]. There are three known thrombin receptors, PAR1, PAR3 and PAR4, which share the same proteolytic mechanism of activation. Human platelets express PAR1 and PAR4 on their surface. PAR1 has recently emerged as a promising new target for therapeutic intervention in patients with thrombotic diseases and acute coronary syndromes [43]. PZ-128 (P1pal-7) is a first-in-class cell-penetrating pepducin inhibitor of PAR1 that targets the receptor–G-protein interface on the inside cell including platelets [16–18]. PZ-128 (P1pal-7) is a cell-penetrating lipopeptide derived from the juxtamembrane region of the i3 loop/N-terminus of TM6 of PAR1. This region has been shown to be essential for coupling of PAR1 with associated G proteins [4]. The NMR structure of PZ-128 revealed a well-defined α-helix extending from the palmitate lipid, which is highly similar with the structure of the corresponding region of PAR1 (residues 307–313) in the off-state with an RMSD of 1.4 Å [17].

PZ-128 is a highly efficacious inhibitor of PAR1-dependent platelet aggregation [17]. PZ-128 also inhibited collagen-MMP1-induced platelet aggregation of PAR1, blocked G12/13-Rho and p38 MAPK activation, and significantly reduced the propagation of platelet–platelet thrombi in human whole blood, under arterial flow conditions [18]. The onset of action of PZ-128 occurred within 15 min after intravenous administration and suppressed PAR1 aggregation and arterial thrombosis in guinea pigs and baboons and strongly synergized with the oral P2Y12 inhibitor clopidogrel [16–18]. Importantly, PZ128 had no effect on bleeding or coagulation parameters in primates or in blood from patients undergoing percutaneous coronary intervention (PCI) [17]. PZ-128 has successfully completed a Phase I clinical trial in 31

subjects with coronary artery disease risk factors with assessments for safety, tolerability, pharmacokinetics, and pharmacodynamics (anti-platelet efficacy). A large Phase II study in patients undergoing PCI is planned to be initiated in 2015.

In addition to its well-recognized roles in platelet and vascular biology, PAR1 has been shown to be involved in the invasive and metastasis process of cancer [44]. The i3 loop pepducin PZ-128 and i1 loop inhibitor P1pal-i1 PAR1 showed significant inhibition of cell migration in both primary and established lung cancer cell lines similar to silencing of PAR1 expression with short hairpin RNA (shRNA). Unlike the i1 loop P1pal-i1, PZ-128 was an effective inhibitor of PAR1-mediated ERK activation and tumor growth. Comparable in efficacy with Bevacizumab, PZ-128 monotherapy provided significant 75 % inhibition of lung tumor growth in nude mice [45].

Matrix metalloprotease-1 (MMP-1) robustly activates the PAR1-Akt survival pathway in breast carcinoma cells [23, 44]. Blockade of Matrix metalloprotease-1 (MMP-1)/PAR1 signaling by PZ-128 or MMP-1 inhibitor significantly promote apoptosis in breast tumor xenografts and inhibit metastasis to the lungs by up to 88 % [23]. Dual therapy with PZ-128 and taxotere inhibited the growth of MDA-MB-231 xenografts by 95 % [23]. Together, these findings indicate that blockade of MMP1-PAR1 signaling may provide a benefit beyond treatment with Taxotere alone in advanced, metastatic breast cancer [23, 44]. PZ-128 significantly reduced the peritoneal dissemination of OVCAR4 ovarian cancer cell line through inhibition of MMP1-PAR1-induced paracrine communication between ovarian carcinoma cells and endothelial cells [46]. PZ-128 almost completely blocked angiogenesis of peritoneal ovarian [46] and breast cancer [44] suggesting that the pepducin approach may prove useful as an anticancer strategy.

PAR4—The binding and subsequent activation of PAR1 and PAR4 by thrombin are mechanistically different [47, 48] and PAR4 may be an additional therapeutic target to prevent platelet-dependent thrombosis [3, 5, 49–52]. PAR1 and PAR4 also form a heterodimer on human platelets [16] which presents the opportunity to design pepducins that inhibit both receptors at the dimer interface or interaction site(s). PAR1-mediated platelet aggregation is transient and reversible unless strengthened by additional signaling inputs from $P2Y_{12}$-ADP receptors or from the PAR4 receptor [47, 52, 53]. To tease out mechanistic differences between PAR1 and PAR4 thrombin receptors, the i1 loop pepducin P4pal-i1 and the i3 loop P4pal-10 were designed [16]. P4pal-i1 specifically inhibited the PAR4 but not the PAR1 signal during platelet aggregation. Dual PAR1/PAR4 inhibition with the addition of P4pal-i1 to small-molecule PAR1 antagonist RWJ-56110 effectively suppressed aggregation of human platelets to even high concentrations of thrombin [16]. The i3 loop pepducin P4pal-10 was found to be

a dual PAR1/PAR4 [5] inhibitory pepducin. P4pal-10 inhibited 85 % of human platelet aggregation in response to 20 nM thrombin conditions where normally both PAR1 and PAR4 would be fully activated by thrombin [5]. P4pal-10 at a dose of 0.37 mg/kg afforded 50 % less platelet deposition in Dacron vascular graft segments in a femoral arterio-venous shunt-bearing baboon [16]. Inhibition of PAR1 with RWJ-56110 conferred partial protection against arterial thrombosis. Likewise, inhibition of PAR4 with P4pal-i1 gave partial blockade of arterial occlusion. However, combination inhibition of PAR1 and PAR4 gave significant protection against occlusive thrombus formation [16]. These data indicate that inhibiting PAR1 and PAR4 or the PAR1/PAR4 complex might offer alternative routes to suppressing pathophysiological activation of platelets during PCI and stenting.

PAR2—Protease-activated receptor-2 is a receptor for trypsin-like proteases such as tryptase and factors VIIa/Xa, and plays a key role in a number of acute and chronic inflammatory and fibrotic diseases of the skin, lungs, liver and gastrointestinal tract, joints, and vascular systems. As PAR2 exhibits significant constitutive activity, many inhibitors based on the extracellular ligand have partial agonist activity, potentially by stabilizing the latent on-state [27]. The constitutive activity of PAR2 could be ablated or enhanced by mutation of critical i3 loop pharmacophores in the intact receptor. Incorporation of these mutation led us to the discovery of PAR2 pepducin antagonists that lost residual agonist activity [27]. The P2pal-18S i3 loop pepducin, with a mutation of a critical Arg for Ser residue, was found to be a full antagonist of PAR2-dependent calcium signaling (Gq) and neutrophil (Gi) chemotaxis. P2pal-18S significantly attenuated mast cell tryptase-dependent neutrophil migration and paw edema in mice in models of acute skin inflammation [27]. P2pal-18S was also found to protect pancreatic acinar cells against bile acid-induced injury/death but did not affect bile acid-induced intracellular zymogen activation [54]. P2pal-18S significantly reduced the severity of experimental biliary pancreatitis induced by retrograde intraductal bile acid infusion, which mimics injury induced by endoscopic retrograde cholangiopancreatography [54].

3.1 Chemokine Receptors

Chemokines comprise a large family of small secreted proteins that regulate nearly all aspects of innate and acquired immunity. In particular, CXCR1 and CXCR2 are important chemokine receptors for IL-8 responsible for the activation of neutrophils, endothelium, epithelium, macrophages and other cells, and can contribute to adverse outcomes in systemic inflammatory response syndrome/sepsis. Opposing the action of CXCR1 and CXCR2, CXCR4 directs the removal of senescent neutrophils and retains immature leukocytes in the bone marrow [26, 55]. Pepducins derived from either the i1 (x1/2LCA-i1) or i3 (x1/2pal-i3) intracellular loops

of CXCR1 and CXCR2 prevent the IL-8 response of both receptors and reverse the lethal sequelae of sepsis, including disseminated intravascular coagulation (DIC) and multi-organ failure in mice [26]. Conversely, pepducin antagonists selective for CXCR4 i1 (x4pal-i1) and i3 (x4pal-i3) blocked SDF-1-dependent neutrophil chemotaxis and caused a massive leukocytosis that did not affect survival of mice in sepsis models [26].

The CXCR4 i1-loop pepducin agonist ATI-2341 induced CXCR4-G protein-dependent signaling, receptor internalization, and chemotaxis in CXCR4-expressing cells [29]. ATI-2341 also induced dose-dependent peritoneal recruitment of polymorphonuclear neutrophils (PMNs) when administered i.p. to mice. When administered systemically by i.v. bolus, ATI-2341 acted as a functional antagonist and dose-dependently mediated release of PMNs from the bone marrow of both mice and cynomolgus monkeys. ATI-2341 also mediated release of granulocyte/macrophage progenitor cells from the bone marrow. ATI-2341 may hold promise as a new therapeutic approach for the recruitment of hematopoietic stem and progenitor cells (HSPCs) before autologous bone marrow transplantation [29].

Inflammation, angiogenesis, and tumorigenesis are intimately linked [56]. CXCR2 is a key driver of tumor development and angiogenesis. CXCR2 deficiency profoundly suppressed inflammation-driven tumorigenesis in skin and intestine as well as spontaneous adenocarcinoma formation in a model of invasive intestinal adenocarcinoma [56]. The x1/2pal-i3 pepducin reduced CXCR2-driven tumorigenesis in *ApcMin/+* mice [56]. CXCR1/2 pepducins also blocked IL-8 angiogenesis in ovarian cancer and be beneficial in the setting of advanced ovarian disease where other treatment options are limited [24]. CXCR4 pepducin x4pal-i1 completely abrogated CXCL12-mediated cell migration of lymphocytic leukemias and lymphomas [57]. Combination treatment with CXCR4 pepducins and the CD20-targeted antibody rituximab significantly increased the apoptotic effect of rituximab which can be impacted by stromal-cell interactions. Furthermore, treatment of mice bearing disseminated lymphoma xenografts with pepducins alone or in combination with rituximab significantly increased survival [57] representing a potential new treatment strategy for lymphoid malignancies.

3.2 Sphingosine-1-Phosphate Receptor

Sphingosine-1-phosphate (S1P) is a bioactive lipid that plays key functions in the immune, inflammatory, and cardiovascular systems. S1P exerts its action through the interaction with a family of five GPCRs, named $S1P_{1-5}$. Among them, $S1P_3$ has been implicated in the pathological processes of a number of diseases, including sepsis and cancer. KRX-725 is a pepducin agonist derived from the i2 intracellular loop, which mimics the effects of S1P by specifically activating $S1P_3$ [58]. KRX-725 derivatives with deletions of

two amino acids from both N- and C-termini have the ability to inhibit both KRX-725-induced vasorelaxation and fibroblast proliferation [58].

3.3 Formyl Peptide Receptors

The formyl peptide receptors (FPR) are Gi-coupled receptors involved in chemotaxis and inflammation. These receptors were originally identified by their ability to bind *N*-formyl peptides such as *N*-formylmethionine produced by the degradation of bacterial pathogens. Human neutrophils express FPR1 and FPR2 that are important regulators of inflammation as well as innate defense reactions [59, 60]. FPR-based pepducins have been shown to possess potent immune regulatory functions. F2Pal-16, containing 16 amino acids of the i3 loop of FPR2, induced superoxide production in human neutrophils which was sensitive to FPR2 antagonists. A C-terminal six-amino acid deletion of Fpal-16 generated a more potent neutrophil activator, F2pal-10 [61]. Neutrophils desensitized with the FPR2-specific pepducin F2pal-10 displayed increased cellular responses to stimulation with the platelet-activating factor (PAF) or ATP by receptor cross-talk signals generated through PAF receptor and ATP receptor $P2Y_2R$ [61]. The pepducin F2pal-12 selectively inhibited FPR2 agonists MMK-1 and serum amyloid A-stimulated neutrophil chemotaxis and human umbilical vein endothelial cell (HUVECs) migration and tube formation [62]. Recent work has documented that FPR2 pepducins possess potent antibacterial activity against both gram-negative *E. coli* and gram-positive *S. aureus* in inhibition zone assays [61]. Both palmitoylated and myristoylated FPR2 pepducins were effective in killing clinical isolates for *Pseudomonas aeruginosa* from patients with cystic fibrosis and *Enterococcus faecalis* from septic patients. The mechanism of action required both the fatty acid and peptide portions acting together, which may facilitate specific interactions and perturbations of the bacterial membrane components [61]. The dual function of FPR2 pepducins warrants further exploration as a novel class of antibacterial agents with immunomodulatory properties.

References

1. Audet M, Bouvier M (2012) Restructuring G-protein- coupled receptor activation. Cell 151:14–23
2. O'Callaghan K, Kuliopulos A, Covic L (2012) Turning receptors on and off with intracellular pepducins: new insights into G-protein-coupled receptor drug development. J Biol Chem 287:12787–12796
3. Tressel SL, Koukos G, Tchernychev B, Jacques SL, Covic L, Kuliopulos A (2011) Pharmacology, biodistribution, and efficacy of GPCR-based pepducins in disease models. Methods Mol Biol 683:259–275
4. Covic L, Gresser AL, Talavera J, Swift S, Kuliopulos A (2002) Activation and inhibition of G protein-coupled receptors by cell-penetrating membrane-tethered peptides. Proc Natl Acad Sci U S A 99:643–648
5. Covic L, Misra M, Badar J, Singh C, Kuliopulos A (2002) Pepducin-based intervention of thrombin-receptor signaling and systemic platelet activation. Nat Med 8:1161–1165

6. Wielders SJ, Bennaghmouch A, Reutelingsperger CP, Bevers EM, Lindhout T (2007) Anticoagulant and antithrombotic properties of intracellular protease-activated receptor antagonists. J Thromb Haemost 5:571–576
7. Fontanini KB, Janz J, Looby R, Hamilton JA (2010) Rapid binding and transmembrane diffusion of pepducins in phospholipid bilayers. Biophys J 98:278a
8. Janz JM, Ren Y, Looby R, Kazmi MA, Sachdev P, Grunbeck A, Haggis L, Chinnapen D, Lin AY, Seibert C, McMurry T, Carlson KE, Muir TW, Hunt S 3rd, Sakmar TP (2011) Direct interaction between an allosteric agonist pepducin and the chemokine receptor CXCR4. J Am Chem Soc 133:15878–15881
9. Tsuji M, Ueda S, Hirayama T, Okuda K, Sakaguchi Y, Isono A, Nagasawa H (2013) FRET-based imaging of transbilayer movement of pepducin in living cells by novel intracellular bioreductively activatable fluorescent probes. Org Biomol Chem 11:3030–3037
10. Overington JP, Al-Lazikani B, Hopkins AL (2006) How many drug targets are there? Nat Rev Drug Discov 5:993–996
11. Rask-Andersen M, Almen MS, Schioth HB (2011) Trends in the exploitation of novel drug targets. Nat Rev Drug Discov 10:579–590
12. Rasmussen SG, DeVree BT, Zou Y, Kruse AC, Chung KY, Kobilka TS, Thian FS, Chae PS, Pardon E, Calinski D, Mathiesen JM, Shah ST, Lyons JA, Caffrey M, Gellman SH, Steyaert J, Skiniotis G, Weis WI, Sunahara RK, Kobilka BK (2011) Crystal structure of the beta2 adrenergic receptor-Gs protein complex. Nature 477:549–555
13. Standfuss J, Edwards PC, D'Antona A, Fransen M, Xie G, Oprian DD, Schertler GF (2011) The structural basis of agonist-induced activation in constitutively active rhodopsin. Nature 471:656–660
14. Chung KY, Rasmussen SG, Liu T, Li S, DeVree BT, Chae PS, Calinski D, Kobilka BK, Woods VL Jr, Sunahara RK (2011) Conformational changes in the G protein Gs induced by the beta2 adrenergic receptor. Nature 477: 611–615
15. McKeown SC, Zecri FJ, Fortier E, Taggart A, Sviridenko L, Adams CM, McAllister KH, Pin SS (2014) The design and implementation of a generic lipopeptide scanning platform to enable the identification of 'locally acting' agonists for the apelin receptor. Bioorg Med Chem Lett 24:4871–4875
16. Leger AJ, Jacques SL, Badar J, Kaneider NC, Derian CK, Andrade-Gordon P, Covic L, Kuliopulos A (2006) Blocking the protease-activated receptor 1-4 heterodimer in platelet-mediated thrombosis. Circulation 113:1244–1254
17. Zhang P, Gruber A, Kasuda S, Kimmelstiel C, O'Callaghan K, Cox DH, Bohm A, Baleja JD, Covic L, Kuliopulos A (2012) Suppression of arterial thrombosis without affecting hemostatic parameters with a cell-penetrating PAR1 pepducin. Circulation 126:83–91
18. Trivedi V, Boire A, Tchernychev B, Kaneider NC, Leger AJ, O'Callaghan K, Covic L, Kuliopulos A (2009) Platelet matrix metalloprotease-1 mediates thrombogenesis by activating PAR1 at a cryptic ligand site. Cell 137: 332–343
19. Kimmelstiel C, Zhang P, Kapur NK, Weintraub A, Krishnamurthy B, Castaneda V, Covic L, Kuliopulos A (2011) Bivalirudin is a dual inhibitor of thrombin and collagen-dependent platelet activation in patients undergoing percutaneous coronary intervention. Circ Cardiovasc Interv 4:171–179
20. Foley CJ, Fanjul-Fernandez M, Bohm A, Nguyen N, Agarwal A, Austin K, Koukos G, Covic L, Lopez-Otin C, Kuliopulos A (2014) Matrix metalloprotease 1a deficiency suppresses tumor growth and angiogenesis. Oncogene 33:2264
21. Foley CJ, Luo C, O'Callaghan K, Hinds PW, Covic L, Kuliopulos A (2012) Matrix metalloprotease-1a promotes tumorigenesis and metastasis. J Biol Chem 287:24330–24338
22. Kamath L, Meydani A, Foss F, Kuliopulos A (2001) Signaling from protease-activated receptor-1 inhibits migration and invasion of breast cancer cells. Cancer Res 61:5933–5940
23. Yang E, Boire A, Agarwal A, Nguyen N, O'Callaghan K, Tu P, Kuliopulos A, Covic L (2009) Blockade of PAR1 signaling with cell-penetrating pepducins inhibits Akt survival pathways in breast cancer cells and suppresses tumor survival and metastasis. Cancer Res 69:6223–6231
24. Agarwal A, Tressel SL, Kaimal R, Balla M, Lam FH, Covic L, Kuliopulos A (2010) Identification of a metalloprotease-chemokine signaling system in the ovarian cancer microenvironment: implications for antiangiogenic therapy. Cancer Res 70:5880–5890
25. Tressel SL, Kaneider NC, Kasuda S, Foley C, Koukos G, Austin K, Agarwal A, Covic L, Opal SM, Kuliopulos A (2011) A matrix metalloprotease-PAR1 system regulates vascular integrity, systemic inflammation and death in sepsis. EMBO Mol Med 3:370–384
26. Kaneider NC, Agarwal A, Leger AJ, Kuliopulos A (2005) Reversing systemic inflammatory

response syndrome with chemokine receptor pepducins. Nat Med 11:661–665

27. Sevigny LM, Zhang P, Bohm A, Lazarides K, Perides G, Covic L, Kuliopulos A (2011) Interdicting protease-activated receptor-2-driven inflammation with cell-penetrating pepducins. Proc Natl Acad Sci U S A 108:8491–8496
28. Carr R 3rd, Du Y, Quoyer J, Panettieri RA Jr, Janz JM, Bouvier M, Kobilka BK, Benovic JL (2014) Development and characterization of pepducins as Gs-biased allosteric agonists. J Biol Chem 289:35668
29. Tchernychev B, Ren Y, Sachdev P, Janz JM, Haggis L, O'Shea A, McBride E, Looby R, Deng Q, McMurry T, Kazmi MA, Sakmar TP, Hunt S 3rd, Carlson KE (2010) Discovery of a CXCR4 agonist pepducin that mobilizes bone marrow hematopoietic cells. Proc Natl Acad Sci U S A 107:22255–22259
30. Scheerer P, Park JH, Hildebrand PW, Kim YJ, Krauss N, Choe HW, Hofmann KP, Ernst OP (2008) Crystal structure of opsin in its G-protein-interacting conformation. Nature 455:497–502
31. Rasmussen SG, Choi HJ, Fung JJ, Pardon E, Casarosa P, Chae PS, Devree BT, Rosenbaum DM, Thian FS, Kobilka TS, Schnapp A, Konetzki I, Sunahara RK, Gellman SH, Pautsch A, Steyaert J, Weis WI, Kobilka BK (2011) Structure of a nanobody-stabilized active state of the beta(2) adrenoceptor. Nature 469:175–180
32. Forsman H, Bylund J, Oprea TI, Karlsson A, Boulay F, Rabiet MJ, Dahlgren C (2013) The leukocyte chemotactic receptor FPR2, but not the closely related FPR1, is sensitive to cell-penetrating pepducins with amino acid sequences descending from the third intracellular receptor loop. Biochim Biophys Acta 1833:1914–1923
33. Kaneider NC, Leger AJ, Agarwal A, Nguyen N, Perides G, Derian C, Covic L, Kuliopulos A (2007) 'Role reversal' for the receptor PAR1 in sepsis-induced vascular damage. Nat Immunol 8:1303–1312
34. Quoyer J, Janz JM, Luo J, Ren Y, Armando S, Lukashova V, Benovic JL, Carlson KE, Hunt SW 3rd, Bouvier M (2013) Pepducin targeting the C-X-C chemokine receptor type 4 acts as a biased agonist favoring activation of the inhibitory G protein. Proc Natl Acad Sci U S A 110:E5088–E5097
35. Hollenberg MD, Mihara K, Polley D, Suen JY, Han A, Fairlie DP, Ramachandran R (2014) Biased signalling and proteinase-activated receptors (PARs): targeting inflammatory disease. Br J Pharmacol 171:1180–1194
36. Tautermann CS (2014) GPCR structures in drug design, emerging opportunities with new structures. Bioorg Med Chem Lett 24: 4073–4079
37. Edwards RJ, Moran N, Devocelle M, Kiernan A, Meade G, Signac W, Foy M, Park SD, Dunne E, Kenny D, Shields DC (2007) Bioinformatic discovery of novel bioactive peptides. Nat Chem Biol 3:108–112
38. Valente P, Fernandez-Carvajal A, Camprubi-Robles M, Gomis A, Quirce S, Viana F, Fernandez-Ballester G, Gonzalez-Ros JM, Belmonte C, Planells-Cases R, Ferrer-Montiel A (2011) Membrane-tethered peptides patterned after the TRP domain (TRPducins) selectively inhibit TRPV1 channel activity. FASEB J 25:1628–1640
39. Robbins J, Marsh SJ, Brown DA (2006) Probing the regulation of M (Kv7) potassium channels in intact neurons with membrane-targeted peptides. J Neurosci 26:7950–7961
40. Gong H, Shen B, Flevaris P, Chow C, Lam SC, Voyno-Yasenetskaya TA, Kozasa T, Du X (2010) G protein subunit Galpha13 binds to integrin alphaIIbbeta3 and mediates integrin "outside-in" signaling. Science 327:340–343
41. Huang JS, Dong L, Kozasa T, Le Breton GC (2007) Signaling through G(alpha)13 switch region I is essential for protease-activated receptor 1-mediated human platelet shape change, aggregation, and secretion. J Biol Chem 282:10210–10222
42. Koukos G, Sevigny L, Zhang P, Covic L, Kuliopulos A (2011) Serine and metalloprotease signaling through PAR1 in arterial thrombosis and vascular injury. IUBMB Life 63: 412–418
43. Zhang P, Covic L, Kuliopulos A (2012) Protease-activated receptors. Platelets 31:249
44. Boire A, Covic L, Agarwal A, Jacques S, Sherifi S, Kuliopulos A (2005) PAR1 is a matrix metalloprotease-1 receptor that promotes invasion and tumorigenesis of breast cancer cells. Cell 120:303–313
45. Cisowski J, O'Callaghan K, Kuliopulos A, Yang J, Nguyen N, Deng Q, Yang E, Fogel M, Tressel S, Foley C, Agarwal A, Hunt SW 3rd, McMurry T, Brinckerhoff L, Covic L (2011) Targeting protease-activated receptor-1 with cell-penetrating pepducins in lung cancer. Am J Pathol 179:513–523
46. Agarwal A, Covic L, Sevigny LM, Kaneider NC, Lazarides K, Azabdaftari G, Sharifi S, Kuliopulos A (2008) Targeting a metalloprotease-PAR1 signaling system with cell-penetrating pepducins inhibits angiogenesis, ascites, and progression of ovarian cancer. Mol Cancer Ther 7:2746–2757

47. Covic L, Gresser AL, Kuliopulos A (2000) Biphasic kinetics of activation and signaling for PAR1 and PAR4 thrombin receptors in platelets. Biochemistry 39:5458–5467
48. Jacques SL, Kuliopulos A (2003) Protease-activated receptor-4 uses dual prolines and an anionic retention motif for thrombin recognition and cleavage. Biochem J 376:733–740
49. Kuliopulos A, Covic L (2003) Blocking receptors on the inside: pepducin-based intervention of PAR signaling and thrombosis. Life Sci 74:255–262
50. Leger AJ, Covic L, Kuliopulos A (2006) Protease-activated receptors in cardiovascular diseases. Circulation 114:1070–1077
51. Covic L, Tchernychev B, Jacques S, Kuliopulos A (2007) Pharmacology and in vivo efficacy of pepducins in hemostasis and arterial thrombosis. In: Langel U (ed) Handbook of cell-penetrating peptides. Taylor & Francis, New York, NY, pp 245–257
52. Covic L, Singh C, Smith H, Kuliopulos A (2002) Role of the PAR4 thrombin receptor in stabilizing platelet-platelet aggregates as revealed by a patient with Hermansky-Pudlak syndrome. Thromb Haemost 87:722–727
53. Trumel C, Payrastre B, Plantavid M, Hechler B, Viala C, Presek P, Martinson EA, Cazenave J-P, Chap H, Gachet C (1999) A key role of adenosine diphosphate in the irreversible platelet aggregation induced by the PAR1-activating peptide through the late activation of phosphoinositide 3-kinase. Blood 94:4156–4165
54. Michael ES, Kuliopulos A, Covic L, Steer ML, Perides G (2013) Pharmacological inhibition of PAR2 with the pepducin P2pal-18S protects mice against acute experimental biliary pancreatitis. Am J Physiol Gastrointest Liver Physiol 304:G516–G526
55. Allen CD, Ansel KM, Low C, Lesley R, Tamamura H, Fujii N, Cyster JG (2004) Germinal center dark and light zone organization is mediated by CXCR4 and CXCR5. Nat Immunol 5:943–952
56. Mantovani A, Allavena P, Sica A, Balkwill F (2008) Cancer-related inflammation. Nature 454:436–444
57. O'Callaghan K, Lee L, Nguyen N, Hsieh MY, Kaneider NC, Klein AK, Sprague K, Van Etten RA, Kuliopulos A, Covic L (2012) Targeting CXCR4 with cell-penetrating pepducins in lymphoma and lymphocytic leukemia. Blood 119:1717–1725
58. Severino B, Incisivo GM, Fiorino F, Bertolino A, Frecentese F, Barbato F, Manganelli S, Maggioni G, Capasso D, Caliendo G, Santagada V, Sorrentino R, Roviezzo F, Perissutti E (2013) Identification of a pepducin acting as S1P3 receptor antagonist. J Pept Sci 19:717–724
59. Fu H, Karlsson J, Bylund J, Movitz C, Karlsson A, Dahlgren C (2006) Ligand recognition and activation of formyl peptide receptors in neutrophils. J Leukoc Biol 79:247–256
60. Ye RD, Boulay F, Wang JM, Dahlgren C, Gerard C, Parmentier M, Serhan CN, Murphy PM (2009) International union of basic and clinical pharmacology. LXXIII. Nomenclature for the formyl peptide receptor (FPR) family. Pharmacol Rev 61:119–161
61. Winther M, Gabl M, Oprea TI, Jonsson B, Boulay F, Bylund J, Dahlgren C, Forsman H (2014) Antibacterial activity of pepducins, allosterical modulators of formyl peptide receptor signaling. Antimicrob Agents Chemother 58:2985–2988
62. Lee HY, Kim SD, Shim JW, Kim HJ, Kwon JY, Kim JM, Baek SH, Park JS, Bae YS (2010) Activation of human monocytes by a formyl peptide receptor 2-derived pepducin. FEBS Lett 584:4102–4108
63. Kubo S, Ishiki T, Doe I, Sekiguchi F, Nishikawa H, Kawai K, Matsui H, Kawabata A (2006) Distinct activity of peptide mimetic intracellular ligands (pepducins) for proteinase-activated receptor-1 in multiple cells/tissues. Ann N Y Acad Sci 1091:445–459
64. Lin C, Duitman J, Daalhuisen J, Ten Brink M, von der Thusen J, van der Poll T, Borensztajn K, Spek CA (2013) Targeting protease activated receptor-1 with P1pal-12 limits bleomycin-induced pulmonary fibrosis. Thorax 69:152–160
65. Gabl M, Winther M, Skovbakke SL, Bylund J, Dahlgren C, Forsman H (2014) A pepducin derived from the third intracellular loop of FPR2 is a partial agonist for direct activation of this receptor in neutrophils but a full agonist for cross-talk triggered reactivation of FPR2. PLoS One 9:e109516

Chapter 14

Identification and Characterization of Homing Peptides Using In Vivo Peptide Phage Display

Maija Hyvönen and Pirjo Laakkonen

Abstract

Each normal organ and pathological condition expresses a distinct set of molecules on their vasculature. These molecular signatures have been efficiently profiled using in vivo phage display. Several peptides homing to tumor blood vessels, lymphatic vessels, and/or tumor cells as well as to various normal organs have been isolated using this method. The in vivo screening of phage libraries has also revealed novel tissue-specific biomarkers of the normal and diseased vasculature. Tumor-homing peptides have been successfully used to target therapeutics and imaging agents to tumors. In vivo phage display has also been used in the identification of cell and/or tumor type-specific cell-penetrating peptides, which further facilitate the transmembrane delivery of various cargo molecules into cells. In this review we describe experimental setup for a combined ex vivo and in vivo screening procedure to select both conventional and cell-penetrating peptides homing to brain tumors.

Key words Phage display, T7, Cell-penetrating peptide, Tumor targeting, Vasculature, Nude mice, Ex vivo, In vivo, Brain tumor

1 Introduction

It has become evident that the vasculature in each individual normal organ as well as pathological condition, such as cancer, express different sets of molecules on its surface [1–3]. Also other cell types within tumor tissue express tumor-specific molecules. In vivo phage display technology is based on phage libraries, in which each individual phage expresses a unique peptide sequence or protein fragment on its surface [4]. This technique has been used to profile the distinct molecular signatures in normal [4–7] and tumor vasculature [8–11]. Previously, we have also shown that the vasculature of a premalignant lesion can be distinguished from that of a full-blown tumor and corresponding normal organ [12, 13]. In addition, the specific molecular signatures of

Ülo Langel (ed.), *Cell-Penetrating Peptides: Methods and Protocols*, Methods in Molecular Biology, vol. 1324,
DOI 10.1007/978-1-4939-2806-4_14, © Springer Science+Business Media New York 2015

tumor type- and tumor stage-specific lymphatic vessels have been identified (reviewed in [14]).

Due to their small size and therefore the ability to penetrate the blood-brain barrier (BBB), homing peptides can be specifically useful in therapeutic targeting of malignant brain tumors, such as gliomas. Recently, in vitro phage display was used to identify a glioma-targeting peptide sequence gHo, which was conjugated to a cell-penetrating peptide pVEC to develop tumor-targeting delivery vector [15]. In addition, a recent publication reported the use of a homing peptide conjugated to a proapoptotic peptide displayed on iron oxide nanoparticles in targeted treatment of glioblastomas in mice [16]. Furthermore, we recently identified a novel homing peptide, which enabled the targeted delivery of peptide-conjugated radioactive tracer and chemotherapeutic drug to intracranial gliomas in murine models of human glioma. These conjugates were used successfully to image and treat brain tumors in intracranial glioma-bearing mice [17]. Our glioma-homing peptide also significantly increased the accumulation of porous silicon nanoparticles to tumors [18].

Peptide display has also been used in identification of cell-penetrating peptides (CPP) [9, 11, 12, 19]. These peptides differ from the canonical CPPs in that their internalization is cell and/or tumor type specific while the canonical CPPs are able to enter all cells they encounter. CPPs aid the internalization of cargo molecules through cellular membranes. CPPs have been described to use various pathways for internalization, even though the exact penetration mechanisms appear to depend on the peptide and the cargo used [20, 21]; for example cationic CPPs utilize negatively charged glycosaminoglycans (GAGs) as cell surface receptors for their cellular uptake [22]. Internalization of many of the cell- and/or tumor type-specific peptides appear to follow the C-End rule (CendR) according to which the C-terminal arginine or lysine residues are crucial for the selective internalization of homing peptides. The CendR peptides bind to Neuropilin-1 on the target cells that facilitates their uptake by these cells. Importantly, the CendR peptides are also able to penetrate through the tissue [23, 24]. The prototype tumor-penetrating peptide, iRGD, was shown to increase vascular and tissue permeability. It also allowed co-administered drugs to penetrate into extravascular tumor tissues. This effect did not require the drugs to be chemically conjugated to the peptide [25]. Therefore, in order to improve the tissue-penetrating ability, homing peptides can be chemically modified [26] or conjugated into cell-penetrating peptides that improve their transport across the cell membrane [17].

This review describes a combined ex vivo and in vivo screening method using the lytic T7 phage-displayed peptide library to select both conventional and cell-penetrating tumor-homing peptides.

As a model we have used experimental murine models of human brain tumors. However, the method can be applied to identify peptides targeting any tumor type or normal organs.

2 Materials

2.1 Cell Culture (*See* Note 1)

1. Cancer cells: We have used Hif-1α-deficient murine astrocytes (HIFko, ref. 17). Alternatively, also tumorigenic human cell lines, such as U87MG, can be used.
2. Appropriate growth medium for the cells with the appropriate supplements: With the HIFko cells you need BME medium (GIBCO) supplemented with 5 % fetal bovine serum (FBS), 1 mM sodium pyruvate, 1 % HEPES (pH 7.35) 0.6 % glucose, and 1 % penicillin/streptomycin.
3. 1× Phosphate-buffered saline (PBS), pH 7.4.
4. Solution of 0.25 % (w/v) trypsin and 1 mM ethylenediaminetetraacetic acid (EDTA) in serum-free medium or PBS.
5. Cell culture plates or flasks.
6. Pipettes, Falcon tubes.
7. A hemocytometer for cell counting.

2.2 Intracranial Injection of Cancer Cells

1. Trypsinized cells in PBS ($1–7 \times 10^5$ cells/5 µl/injection).
2. Immunodeficient mice if non-murine cancer cells are used (*see* **Note 2**).
3. Sterile insulin syringes (e.g., BD Micro-Fine™+ insulin syringes, 0.30 mm (30G) × 8 mm).
4. Sterile needles (21G).
5. Hamilton syringe, Hamilton RN Needles (22S).
6. Stereotactic device.
7. Anesthetics (e.g., Rompun® vet, 20 mg/ml and Ketaminol® vet, 50 mg/ml).
8. Painkillers (Temgesic®, 0,3 mg/ml).
9. Eye drops (e.g., Viscotears, 2 mg/g).
10. 70 % EtOH, isopropanol, and distilled water (for needle cleaning).
11. NaCl (9 mg/ml).
12. Bone wax, scopula.
13. Warm water flasks.
14. Scalpel, scissors, suture with needle.
15. Ear marker.
16. Scale and timer.

2.3 Phage Display Using the Lytic T7 Bacteriophage

2.3.1 Ex Vivo Selection

1. At least one mouse carrying a xenograft tumor.
2. One set of surgical instruments containing a hemostat, a pair of scissors, a scalpel, and a pair of tweezers.
3. One insulin syringe per mouse.
4. Collagenase solution (50 ml of PBS, 0.5 g BSA, 50 μl of DNase, 0.125 g collagenase IV, 0.125 g collagenase II).
5. One clean plate per mouse (e.g., bacterial culture plates).
6. One 50 ml Falcon tube per mouse, tared Eppendorf tubes.
7. BLT5615 bacteria (Novagen) (*see* Subheading 2.3.3).
8. Spectrophotometer for measuring bacterial growth (optical density, OD).
9. Phage (phage-displayed peptide library, such as CX_7C library on the T7Select415-1-phage (Novagen), or a solution of selected bacteriophage and T7 control phage) (*see* **Note 9**).

2.3.2 In Vivo Selection

1. Mice carrying xenograft tumors.
2. One set of surgical instruments per mouse (*see* Subheading 2.3.1).
3. Two insulin syringes per mouse (one for anesthetic and the other for tail vein injection).
4. One 10 ml syringe and a needle (0.50 mm (25G) × 16 mm) per mouse.
5. Sterile 1× PBS, pH 7.4.
6. Collagenase solution (*see* Subheading 2.3.1).
7. One 50 ml Falcon tube per mouse.
8. One bacterial culture plate per mouse.
9. Tared Eppendorf tubes.
10. Phage.

2.3.3 Growth and Amplification of T7 Bacteriophage

1. BLT5615 bacteria (Novagen).
2. M9TB growth medium (5 ml of 20 × M9 salts, 2 ml 20 % glucose, 0.1 ml 1 M $MgSO_4$, 100 ml TB). 20 × M9 salts: 0.37 M NH_4Cl, 0.44 M KH_2PO_4, 0.45 M Na_2HPO_4.
3. Antibiotics (e.g., 25 mg/ml carbenicillin).
4. 0.6 % top agar (per 100 ml: 1 g Bacto tryptone, 0.5 g Yeast extract, 0.5 g NaCl, 0.6 g agarose, 100 ml deionized water).
5. Luria plates supplemented with antibiotics (e.g., 50 μg/ml carbenicillin).
6. Phage.

2.3.4 Identification of Individual Peptides

1. 1× TBS, pH 7.8.
2. Primers to amplify the multi-cloning site containing the insert encoding displayed peptide.
3. Sequencing facility.

2.4 Validation of the Specificity and Cell-Penetrating Ability of Displayed Peptides

1. Synthetic peptide conjugated to a fluorochrome or biotin.
2. Tumor-bearing mice.
3. One set of surgical instruments per mouse (*see* Subheading 2.3.1).
4. Two insulin syringes per mouse (one for anesthetic and the other for tail vein injection).
5. Two 10 ml syringes and needles (0.50 mm (25G)×16 mm) per mouse.
6. Sterile 1× PBS, pH 7.4.
7. HEPES Krebs Ringer (HKR) buffer.
8. NaOH (0.1 mol/l).
9. 4 % paraformaldehyde (PFA) in PBS.
10. One 50 ml Falcon tube per mouse.
11. One bacterial culture plate per mouse.
12. Tared Eppendorf tubes.
13. O.C.T. mounting compound (Tissue-Tek).
14. Cold 30 % sucrose in PBS.
15. Cryostat.
16. Cover slips and objective glasses.
17. Tumor cells of interest.
18. DAPI mounting medium (Vectashield, Vector Laboratories).
19. Fluorescence and confocal microscope.
20. Fluorescence microplate reader.

3 Methods

Homing peptides can be selected for any tumor type grown either subcutaneously (s.c) or orthotopically. If tumor cells are not of murine origin immunodeficient mouse strains are necessary for tumor implantation. The number of cells to be implanted and the requirement of a supporting matrix (e.g., Matrigel) depend on the tumor model to be used. In the in vivo phage screen, also called biopanning, the phage library is injected into the tail vein of tumor-bearing mice and allowed to circulate for 15 min. Excision of the tumor tissue is followed by preparation of a tumor-derived cell suspension. Bound phage is rescued and amplified by addition of the

bacterial culture. The amplified phage pool is then used for the next round of selection. Typically, the phage pool preferentially homes to the target tissue after 3–5 rounds of panning.

There are two major phage systems that have been used for the in vivo phage display: the fd-tet-derived FUSE5 vector system based on the M13 bacteriophage [27] and the T7 phage system (T7Select® system, Novagen). The two phage differ in size, shape, and life cycle; M13 is a 900 nm long filamentous phage and has a temperate life cycle while T7 is an icosahedral phage with diameter of about 60 nm and has a lytic life cycle. M13 system displays peptides up to five copies as an N-terminal fusion of the minor coat protein P3. This system has also been widely used to display antibody libraries [28]. T7 vectors display 1–415 copies of the peptide as a C-terminal fusion of the phage capsid protein. In this review we focus on the use of T7 phage system in the in vivo phage display application. This technology can be used for the identification of both conventional and cell-penetrating peptides.

3.1 Propagation of Cancer Cells (*See* Note 3)

1. Harvest cells with trypsin-EDTA solution when 80–90 % confluent. For a 10 cm cell culture dish an appropriate amount of trypsin-EDTA solution is 1–2 ml. You may need multiple plates of cells to acquire enough of them for implantation.
2. Add 8 ml of serum-containing growth medium to the cell after detachment to inactive the trypsin and split the suspension 1:2. Add medium to the final volume: 10 ml for 10 cm plates and 20 ml for 15 cm plates. Let the cells adhere and grow them o/n in a cell incubator.
3. Next day harvest the cells with trypsin (*see* **Note 3**). After detachment suspend the cells into growth medium and take a sample for cell counting (e.g., 100 μl). If you have several plates, combine the cell suspensions before taking the sample. Collect the rest of the cells to a Falcon tube for centrifugation (300–500 g/2–5 min).
4. While centrifuging, count the cells in your sample with a hemocytometer. After centrifugation, resuspend the cells in an appropriate volume of 1× PBS so that the final solution contains 0.7×10^6 cells/5 μl (*see* **Note 4**). Store the cells on ice. You are now ready for inoculation of the tumors.

3.2 Intracranial Injections

1. Clean Hamilton syringe before the operation. Wash first with isopropanol, 70 % EtOH, and distilled water. Finally, wash the needle with NaCl (9 mg/ml). (Perform the washes in opposite direction after the operation.)
2. Scale and anesthetize mice using a mixture of Rombun and Ketalar according to the manufacturer's recommendations. Test the deepness of the anesthesia by pressing the footpad of the hind limb. Keep the mouse warm during operation, e.g., by using warm water bottles.

3. Dilute painkillers (e.g., Temgesic 3 μg/ml) into NaCl (9 mg/ml) and administer s.c. to the back of the neck (100 μl/animal). Administer eye drops.
4. Mark the mouse with earmarks and clean the top of the head with 70 % EtOH.
5. Make a careful cut to the skin (1–1.5 cm is enough). Try to avoid cutting of blood vessels of the skull.
6. Use the 21G needle to carefully drill a hole into the skull, approx. 3 mm right from the bregma. Do not use excess force.
7. Set cleaned and loaded Hamilton syringe on the clamp of stereotactic. Slowly direct the tip of the needle into the skull (after reaching 3 mm depth, pull the needle upwards 0.5 mm). Try to penetrate the skull in an angle of 90°. After penetration wait for 1–2 min before proceeding.
8. Inject the cells slowly into the skull (5 μl/ 2 min) (*see* **Note 5**).
9. Wait for 1 min before removing Hamilton.
10. Spread warmed bone wax on top of the hole (warming can be done using hands). Suture the wound with 1–2 stitches.
11. Administer 0.3 ml of warm saline i.p. Also new eye drops can be administered.
12. Put the mouse back into the cage and keep it warm by wrapping it in paper tissue and laying it on top of the warm water bottle. Check that the mouse wakes up.
13. Administer painkillers once a day for 2 days after the operation.

3.3 Phage Display

The combination of an ex vivo/in vivo screen appears to be more efficient in identification of homing peptides than an in vivo screen by itself. We use the term ex vivo phage display to describe the addition of phage solutions to primary cell suspensions of organs and tumors. The screen is initiated with 1–3 ex vivo selection rounds followed by 3–5 in vivo selection rounds. During the ex vivo selections you select for peptides/phage that are able to bind to all tumor-derived cells while during the in vivo selections you select for the peptides/phage that are able to home and bind to the tumor tissue after systemic administration via the tail vein.

3.3.1 Ex Vivo Selection

1. Inoculate an overnight culture from a single BLT5615 colony (V = 5 ml, supplied with 10 μl of 25 mg/ml carbenicillin) 1 day prior to the experiment.
2. Dilute overnight culture 1:100 and grow to $OD_{600} \sim 1.0$ (*see* **Note 6**). During the incubation you should accomplish **steps 3–12**.
3. Anesthetize a mouse carrying a xenograft tumor (*see* **Note 7**).
4. To expose the heart for perfusion, use your scissors to make a wide cut in the abdomen directly under the rib cage. Move the

liver aside and cut the diaphragm from side to side to reveal the lungs. Then cut both sides of the rib cage. Clasp the apex of xiphoid process (xiphisternum) with a hemostat and bend the rib cage back to expose the heart. Be careful not to puncture the heart.

5. Make a cut on the right atrium or the main vein (superior vena cava).
6. Perfuse the mouse with 10 ml of PBS to remove the blood. The needle should penetrate only the wall of the left ventricle (i.e., insert the needle 2–3 mm into the heart). Perfusion is successful when the skin and the liver of the mouse become pale.
7. Cut off the head of the mouse and carefully remove the skull by using scissors and tweezers. Slide a spatula under the brain and remove them. Excise the tumor. Remove the surrounding brain tissue as much as possible. In case you use an infiltrative model of brain tumors excise the whole brain.
8. Weight the tumor/brain and mince it to small pieces using a scalpel.
9. Digest the tumor with the collagenase solution by incubating at +37 °C for 30–45 min. Vortex few times during the incubation. The collagenase solution should become more turbid while the digestion of the tumor proceeds. An appropriate volume of the collagenase solution is 10–15 ml/g of tumor.
10. Following the digestion add 15 ml of DMEM supplied with 5 % FBS to inactivate the collagenases. Filter the suspension using a cell strainer (pore size 100 μm) and collect the cells by centrifugation (250 g, 10 min, +4 °C). Discard the supernatant and resuspend the cells in 5 ml of 1 % BSA in DMEM. Collect the cells by centrifugation (250 g, 10 min, +4 °C). Discard the supernatant and weight the pellet. Resuspend the cells in 1 ml of 1 % BSA in DMEM. Divide the suspension in aliquots. One aliquot containing 0.05–0.10 g or ~10^6 of tumor cells is enough for an ex vivo experiment.
11. Add 100–500 μl of the phage library (*see* **Note 8**) or an amplified phage pool/individual phage (the titer should be 10^6–10^{10} pfu/μl) to tumor cells and fill the total volume to 1 ml with 1 % BSA in DMEM. Prepare an identical suspension using a control phage (*see* **Note 9**). Incubate the phage/tumor cell suspensions at +4 °C in a rotator. The incubation time may require optimization, but it usually varies between 2 and 24 h. *See also* **Note 10**.
12. In order to remove the unbound phage collect the tumor cells and phage bound to them by centrifugation (600×*g*, 3 min, RT). Resuspend the pellet into 0.5 ml of 1 % BSA in DMEM, and transfer the suspension to a fresh tube (*see* **Note 11**). Repeat the wash step four times. After the final wash transfer the suspension again to a fresh tube and collect the cells with

centrifugation. Discard the supernatant and add 50 µl of sterile PBS on top of the pellet to prevent drying. Keep the tube on ice.

13. Add 1.0 ml of BLT5615 culture (OD_{600} ~ 1.0) (from **steps 1–2**) to the tube containing tumor cell/phage mixture and suspend well. Incubate for 10 min at RT to allow phage to infect the bacteria.
14. To define the number of bound phage (*phage output*) add 0.1, 1, and 10 µl of the suspension from **step 13** to 350 µl of BLT5615 culture (OD_{600} ~ 1.0) and 3 ml of melted (50 °C) top agar. Mix and pour the top agar containing the phage and bacteria onto LB agar plates containing 50 µg/ml carbenicillin. Incubate the titer plates for 1.5–3 h at 37 °C or overnight at room temperature.
15. Save the rest of the suspensions for amplification (*see* Subheading 3.3.4). They can be stored o/n at +4 °C (*see* **Note 12**). Since the infection efficiency of the T7 phage solution may differ between different bacterial cultures, the most reliable results in defining the selection output are obtained by simultaneous determination of the output and input (=the number of phage particles added to the tumor cell suspension).

3.3.2 In Vivo Selection

1. Anesthetize a mouse carrying a xenograft tumor.
2. Warm the mouse's tail in warm water to dilate the tail veins and facilitate the injection. Inject slowly 150–200 µl of phage solution (the titer should be around 10^6–10^{10} pfu/µl) into the tail vein. Too fast injection rate may cause failure in cardiac function and be fatal for the mouse. Usually a rate of 20 µl/10 s is appropriate. Allow the phage circulate for 15 min.
3. Open the chest and expose the heart as described in Subheading 3.3.1.
4. Perfuse the mouse with 10 ml of PBS to remove the unbound phage.
5. Excise the tumor and separate it from the surrounding brain tissue as well as possible. Weight the tumor. In case you use an infiltrative model of brain tumors excise the whole brain and weight it.
6. Digest the tumor with collagenase solution and prepare the cell suspension as described above **steps 9** and **10** in Subheading 3.3.1.
7. Wash the cell suspension and add bacteria as described in **steps 12** and **13** in Subheading 3.3.1.
8. For titration of the phage output, add 0.1, 1, and 10 µl of the suspension to 350 µl of BLT5615 culture (OD_{600} ~ 1.0) and 3 ml of top agar. Save the rest of the suspensions for amplification (*see* Subheading 3.3.4). They can be stored o/n at +4 °C (*see* **Note 12**). Prepare also titer plates to determine the phage input if not determined earlier.

3.3.3 Analysis of Selection Output (Number of Bound Phage)

1. Count the plaques from the titer plates (*see* **Note 13**). Define titer/μl by multiplying plaque count with the dilution factor and dividing it by the volume of phage solution plated (*see* **Note 14**).
2. Calculate phage input by multiplying titer/μl with volume of phage solution used for selection (*see* **Note 14**).
3. Phage output is calculated by multiplying titer/μl with the total volume of suspension containing tumor cells, phage, and bacteria. Since the tumors vary in size the tumor mass must also be taken into account for analysis of the in vivo selection output. Divide the relative output value with the mass of the tumor cells to accomplish this (*see* **Note 14**).
4. Divide the output value with the input value and you will have a relative value that can be compared between different phage and screening rounds. Increase in this value by each round indicates *enrichment* and a successful selection of the homing phage. Decrease in this value, in turn, indicates that the homing capability of the phage pool to the tumor tissue is reduced (*see* **Note 15**).

3.3.4 Amplification of Phage After Ex Vivo or In Vivo Selection

1. Inoculate an overnight culture from a single BLT5615 colony ($V = 5$ ml, supplied with 10 μl of 25 mg/ml carbenicillin).
2. Dilute the overnight culture 1:100, $V = 10$ ml and grow to $OD_{600} \sim 0.5$.
3. Induce the expression of phage capsid in bacteria by adding isopropyl thiogalactoside (IPTG) to the bacterial growth medium (*see* **Note 6**). Add IPTG to a final concentration of 10 μM 45–60 min after inoculation of the diluted culture.

4.1 Amplification of a phage pool

Add phage and tumor cell mixture to an IPTG-induced BLT5615 bacterial culture grown to $OD_{600} \sim 0.5$.

4.2. Amplification of a single phage

Pick a plaque from a phage plate to a tube or 96-well plate containing 20 μl of 1× TBS, pH 7.8 and add 5 μl of phage solution to an IPTG-induced culture grown to $OD_{600} \sim 0.5$.

5. Incubate the culture at 37 °C for 3–5 h, or until the culture is clarified (phage lyses the bacteria). Sometimes, because of the tumor cell material, the clarification of the culture might not be complete and the lysis may appear only as reduced turbidity.
6. Remove the cell debris by centrifugation (7670 × *g*, 10 min, at +4 °C). Carefully, transfer the supernatant by decanting or pipetting to a new sterile Falcon tube.
7. Filter the supernatant through a 0.45 μm filter followed by filtration through a 0.2 μm filter (e.g., by using a syringe tipped with an appropriate filter). Now you have a phage solution ready to be used for the experiments.

3.3.5 Identification of Peptides Displayed by the Phage

1. Isolate individual phage from the bacterial plates by picking randomly selected plaques with a tip of a pipette to tubes or 96-well plates containing 20 μl of 1× TBS, pH 7.8.
2. Amplify the cloning site by PCR. A PCR reaction example is provided in **Note 16**. Presence of the leftover primers after PCR reaction may disturb sequencing reaction and require an additional purification step.
3. Check PCR products in a 2 % agarose gel.
4. Prepare sequencing samples (*see* **Note 17**).

3.3.6 Validation of the Specificity of Tumor Targeting

Once tumor-targeting phage are enriched, it is important to verify their specificity. This is performed as normal in vivo phage display (Subheading 3.3.2), but with a single phage instead of a library or a phage pool. This step is necessary to validate how well any individual phage homes to the target tissue compared to the control phage and whether it also homes to other organs (*see* **Note 18**).

1. Anesthetize a mouse carrying a xenograft tumor.
2. Place the mouse's tail in warm water to dilate the tail veins.
3. Inject 150–200 μl of phage solution into the tail vein and allow it to circulate for 15 min.
4. Open the chest and expose the heart as described in Subheading 3.3.1.
5. Perfuse the mouse with 10 ml of PBS.
6. Excise tumor and other necessary control organs (e.g., liver, kidney, spleen, and lungs). Selection of control organs will depend on your target organ.
7. Titer the phage from the organs as described in Subheading 3.3.3. The specificity of the phage can be estimated by comparing the output of the phage of interest to that of the control phage (*see* **Note 14**).

3.3.7 Validation of the Specificity of Displayed Peptides

To ensure that your selected peptide is responsible for the specific homing you should test the homing efficiency and specificity of a synthetic peptide conjugated to a fluorochrome or biotin. For example, we conjugated our brain tumor-specific homing peptide to isothiocyanate-activated fluorescein (FITC) via an additional N-terminal lysine [17]. *See also* **Note 19**. We usually inject 100 μl of 1 mM peptide solution into the tail vein of tumor-bearing mouse and allow it to circulate for 15–120 min. In order to study the homing of the peptide, tumor and the control organs are excised and prepared for histological examination.

1. Inject the peptide into the tail vein of tumor-bearing mouse and let it circulate for 15–120 min.
2. Perfuse the mice through the heart with 10 ml of PBS followed by 10 ml of 4 % (PFA) in PBS to remove the unbound peptide and fix the tissue.

3. Excise tumor and control organs.
4. Fix the tissues further by incubating them in 4 % PFA for 1 h at 4 °C.
5. Wash twice with PBS and add 30 % sucrose in PBS. Incubate o/n at 4 °C.
6. Dry the extra sucrose and mount in O.C.T. Mounting Compound (Tissue-Tek).
7. Cut cryo-sections (5–10 μm) and prepare them for microscopy (*see* **Note 20**).

3.3.8 Validation of Cell-Penetrating Ability of the Homing Peptide

To characterize whether the homing peptide is capable of cell penetration, you can use fluorochrome-conjugated peptides in conventional confocal microscopy experiments or quantitate the cellular uptake. Examples of these validations are described by El-Andaloussi et al. [29].

Confocal microscopy

1. Split the tumor/tissue-specific cells on cell culture dishes with glass cover slips (for example Ø 13 mm) on the bottom and incubate them o/n +37 °C.
2. Incubate the cells (now attached to cover slips) together with various concentrations (e.g., 1–5 μM) of the purified, fluorochrome-conjugated peptide for 30 min. The incubation time and peptide concentration might need optimization. *See also* **Note 20**.
3. Wash the cells three times with HEPES Krebs Ringer (HKR) buffer, to get rid of the unbound peptides.
4. Fix the cells with 4 % PFA-PBS for 20 min, RT.
5. Mount the cells with DAPI-containing mounting medium (such as Vectashield, Vector Laboratories) or alternatively counterstain the nuclei with Hoechst (1 mg/ml in PBS) for 10 min RT and mount the cells with aqueous mounting medium (such as Aquamount, Fisher Scientific). Protect your samples from light.
6. Analyze the localization of peptides with confocal microscopy.

Quantitative cellular uptake

1. Seed 2 × 10e5 cells 24 h before the experiment in 12-well plates to reach a 70 % confluence.
2. Treat the cells with 5 μmol/l of fluoresceinyl-labeled peptides in 500 μl of serum-free DMEM for 60–90 min
3. Wash cell twice with HKR buffer and trypsinate for 10 min in 0.25 % trypsin.
4. Centrifuge the cells at 1000 × *g* for 5 min at 4 °C.

5. Lyse the cell pellets with 300 μl 0.1 mol/l NaOH for 30 min.
6. Transfer 250 μl of the cell lysate to a black 96-well plate and measure fluorescence at 494/518 nm.

4 Notes

1. All equipment and solutions used in cell culture must be sterile. Cell culture room should be equipped with a table-top centrifuge, a microscope, a flow chamber suitable for cell cultivation, and a cell incubator that can be adjusted to 5.0 % CO_2, +37 °C.
2. In immunocompetent animals the immune response prevents tumor growth or results in regression of tumors after initial growth. Therefore, if cancer cells are of non-murine origin immunodeficient mouse strain has to be used for the formation of tumors. It is also recommended to use young, approximately 4–6-week-old animals in the experiments.
3. Cells should be checked frequently for possible contaminations. It is extremely important that only clean cells are used for the inoculation of xenograft tumors. Cells should be in the exponential growth phase when implanted into mice. In addition, to increase the cell viability, the cells should not be kept in trypsin too long. The detachment time using trypsin or other reagents is cell line dependent.
4. The number of cells to be implanted depends on the cell type. According to our experience, $1–7 \times 10^5$ HIFkos or U87MG-cells is sufficient.
5. Before the injection, make sure that there are no air bubbles inside the needle. In order to ensure that the cells are appropriately placed deep in the brain and not spurted outside, it is extremely important to make the injection slowly. It is also very important avoid injection of the cells too deep into the brain.
6. Some vector systems (T7Select1-1 and T7Select10-3 that display an average of 0.1–1 and 10 copies of peptides/phage particle, respectively) and the bacterial strains BL21 or BLT5403 require the induction of the expression of wild-type capsid protein in bacteria to allow the assembly of the phage. This is done by addition of IPTG to the bacterial growth medium. Add IPTG to a final concentration of 10 μM 45–60 min after inoculation of the diluted culture. We often amplify also the T7Select415-1b vector in the BLT5615 bacterial strain in the presence of IPTG to prepare mosaic phage to facilitate the phage assembly.

7. One tumor can be divided into several aliquots after preparation of the cell suspension for the ex vivo experiments.
8. The volume of the library used for the first round of selection depends on the diversity and titer of the library. The first round should contain at least ten copies of each individual phage particles (i.e., ten times the diversity of the phage).
9. As a control phage we use a non-recombinant phage T7Select 415-1 (T7 negative control from Novagen), which displays the stuffer-encoded SSVD peptide.
10. Alternatively, if you wish to identify cell-penetrating peptides in an early stage of the experiment, you can first culture the cell line of interest, such as HIFko or U87MG, on cell culture dishes and apply the amplified phage pool directly to the cultured cells. After incubation, cell surface-bound phages are removed by trypsin. Internalized ones are rescued by cell lysis, purified, and subjected again to the ex vivo selection. A detailed description for this approach can be found elsewhere [30].
11. Since phage binds to different surfaces you will get rid of all the phage that has bound to the walls of the tubes by transferring the cell suspension with bound phage to a new tube.
12. The number of plaques should be 20–100/plate in order to accurately quantify the results. If the number of plaques is too low or too high the phage/tumor cell suspension can be re-titrated the next day. Since the phage might slightly amplify during the o/n incubation even at 4 °C prepare new titration for all the phage simultaneously for comparable results.
13. T7 is a lytic phage, which means that following the infection phage lyses the infected bacterial cells that results in release of new phage particles to the culture medium (about 200 phage particles/infected cell). Top agar is used to prevent the escape of the released phage. Therefore, the phage will stay next to the lysed bacteria and infect the bacterial cells next to the dead cell resulting in a hole = plaque in the bacterial culture.
14. Example of the calculation of the selection outputs.
Phage titer (number of infective phage particles in the solution):

Input			**Plaque count**			
Phage	**Dilution**	**Plated (µl)**	**Plate #1**	**Plate #2**	**Average**	**Titer/µl (in)**
T7 control	$1{:}10^6$	10	54	57	55.5	5.55×10^6
	$1{:}10^6$	1	4	5	4.5	4.50×10^6
Phage of interest	$1{:}10^6$	10	45	40	42.5	4.25×10^6
	$1{:}10^6$	1	3	5	4.0	4.00×10^6

Phage input (number of infective phage particles added to the experiment):
The total input of the phage is calculated by multiplying titer/μl with the volume of the phage solution added to the selection.

Phage	Titer/μl (in) average	Input vol. μl	Input
T7 control	5.03×10^6	200	1.01×10^9
Phage of interest	4.13×10^6	200	8.25×10^8

Phage output (number of infective phage particles bound to the target):
Titer/μl is calculated by dividing average of the plaque count with the volumes of the diluted phage added to plates. Value for titer/ml is calculated by multiplying titer/μl with 1000.

Output			Plaque count				
Phage	Dilution	Plated (μl)	Plate #1	Plate #2	Avg.	Titer/μl (out)	Titer/ml (out)
T7 control	1:100	10	13	15	14	140	1.40×10^5
Phage of interest	1:100	10	167	173	170.0	1700	1.70×10^6

Relative value for output is calculated by dividing the "titer/ml" of the output with the value of "phage input." This relative value is comparable between different phage and different experiments.

Phage	Titer/ml (out)	Out/in	vs. control
T7 control	1.40×10^5	1.39×10^{-4}	1
Phage of interest	1.70×10^6	2.06×10^{-3}	14.79

In this example the phage of interest binds almost 15-fold better to the tumor than the control phage
Phage output for the in vivo experiment:
In an in vivo experiment the mass of tumor cells must be taken into account. Titer/ml is divided by the weight of tumor cells to obtain value "output/g of tissue." Then this value is divided by the input to obtain a relative value "output/input/ g of tissue." This value is a comparable selection output of different phage and can be used to compare different selection rounds with each other. In an ex vivo selection this is not necessary, because the tumor cells used in the experiment are divided equally between different samples.

Phage	Titer/ml (out)	Weight (g)	Out/gram of tissue	Out/in/gram of tissue	vs. control
T7 control	1.40×10^5	0.109	1.28×10^6	1.28×10^{-3}	1
Phage of interest	1.70×10^6	0.097	1.75×10^7	2.12×10^{-2}	16.62

In this example the phage of interest homes and binds almost 17-fold better to the tumor than the control phage.

15. An individual phage can enrich in a phage pool due to selection or amplification. Enrichment by selection means that more phage will specifically home and bind to the tumor tissue each round and the phage that reside in the tumor at the time of tumor excision will be amplified. Enrichment by amplification means that empty phage or a phage displaying truncated peptide sequences amplifies more rapidly and takes over the phage pool. The enrichment of phage carrying truncated peptides may develop, for instance, from a random mutation in DNA encoding the displayed peptide.
16. An example of a PCR reaction to amplify the DNA sequence encoding the displayed peptide from the phage genome performed using Dynazyme II polymerase (Finnzymes) and appropriate forward and reverse primers.

Reagent	1× reaction (μl)
Phage solution[a]	2.0
10× buffer	2.5
dNTPs	0.5
Forward primer (10 μM)	0.3
Reverse primer (10 μM)	0.3
dH_2O	19.4
Dynazyme II	1.0

[a]1× TBS containing a picked phage from **step 3.2** of Subheading 3.2.5.

17. Procedure for preparing sequencing samples depends greatly on the equipment and services of your local sequencing facility. Therefore, no instructions are provided here. Sequencing can be performed, e.g., using the forward primer (*see* **Note 16**).
18. Phage binds nonspecifically to any surface to a certain extent and therefore it is necessary to always assess the background of the binding or homing in your system using a control phage. Note that the more phage you put into your system the more

phage you will get out (this implies also for the control phage). The background in different organs will vary and therefore you will need to compare the homing of your phage to that of the control phage in different organs.

19. Peptide synthesis is not in the scope of this review and is not described here in detail. In addition to the specificity, it is equally important to characterize the stability of your peptide in vitro as well as its plasma half-life.
20. If the peptide is conjugated to a fluorochrome it might be visible in the tissue without further staining. If not, enhance the staining using antibodies against the fluorochrome (such as an anti-FITC antibody). Tumor cells, blood, and/or lymphatic vasculature can be stained to localize the peptide within the tissue using the standard procedures. Note that systemically administered peptide will be secreted through the kidneys to the urine. Therefore, the peptide should always be visible in the kidney tubules. This will also serve as a control organ for a successful injection.

Acknowledgements

This study was financially supported by the Finnish Cancer Organizations and Sigrid Juselius Foundation. Maija Hyvönen has been supported by the Doctoral Program in Biomedicine (DPBM).

References

1. Oh P, Li Y, Yu J, Durr E, Krasinska KM, Carver LA, Testa JE, Schnitzer JE (2004) Subtractive proteomic mapping of the endothelial surface in lung and solid tumours for tissue-specific therapy. Nature 429:629–635
2. Ruoslahti E (2002) Specialization of tumour vasculature. Nat Rev Cancer 2:83–90
3. St Croix B, Rago C, Velculescu V, Traverso G, Romans KE, Montgomery E, Lal A, Riggins GJ, Lengauer C, Vogelstein B, Kinzler KW (2000) Genes expressed in human tumor endothelium. Science 289:1197–1202
4. Pasqualini R, Ruoslahti E (1996) Organ targeting in vivo using phage display peptide libraries. Nature 380:364–366
5. Arap W, Haedicke W, Bernasconi M, Kain R, Rajotte D, Krajewski S, Ellerby HM, Bredesen DE, Pasqualini R, Ruoslahti E (2002) Targeting the prostate for destruction through a vascular address. Proc Natl Acad Sci U S A 99:1527–1531
6. Rajotte D, Arap W, Hagedorn M, Koivunen E, Pasqualini R, Ruoslahti E (1998) Molecular heterogeneity of the vascular endothelium revealed by in vivo phage display. J Clin Invest 102:430–437
7. Zhang L, Hoffman JA, Ruoslahti E (2005) Molecular profiling of heart endothelial cells. Circulation 112:1601–1611
8. Burg MA, Pasqualini R, Arap W, Ruoslahti E, Stallcup WB (1999) NG2 proteoglycan-binding peptides target tumor neovasculature. Cancer Res 59:2869–2874
9. Laakkonen P, Porkka K, Hoffman JA, Ruoslahti E (2002) A tumor-homing peptide with a targeting specificity related to lymphatic vessels. Nat Med 8:751–755
10. Pasqualini R, Koivunen E, Ruoslahti E (1997) Alpha v integrins as receptors for tumor targeting by circulating ligands. Nat Biotechnol 15: 542–546
11. Porkka K, Laakkonen P, Hoffman JA, Bernasconi M, Ruoslahti E (2002) A fragment of the HMGN2 protein homes to the nuclei of tumor cells and tumor endothelial cells in vivo. Proc Natl Acad Sci U S A 99:7444–7449

12. Hoffman JA, Giraudo E, Singh M, Zhang L, Inoue M, Porkka K, Hanahan D, Ruoslahti E (2003) Progressive vascular changes in a transgenic mouse model of squamous cell carcinoma. Cancer Cell 4:383–391
13. Joyce JA, Laakkonen P, Bernasconi M, Bergers G, Ruoslahti E, Hanahan D (2003) Stage-specific vascular markers revealed by phage display in a mouse model of pancreatic islet tumorigenesis. Cancer Cell 4:393–403
14. Laakkonen P, Zhang L, Ruoslahti E (2008) Peptide targeting of lymph vessels. Annu N Y Acad Sci 1131:37–43
15. Eriste E, Kurrikoff K, Suhorutsenko J, Oskolkov N, Copolovici DM, Jones S, Laakkonen P, Howl J, Langel U (2013) Peptide-based glioma-targeted drug delivery vector gHoPe2. Bioconjug Chem 24:305–313
16. Agemy L, Friedmann-Morvinski D, Kotamraju VR, Roth L, Sugahara KN, Girard OM, Mattrey RF, Verma IM, Ruoslahti E (2011) Targeted nanoparticle enhanced proapoptotic peptide as potential therapy for glioblastoma. Proc Natl Acad Sci U S A 108:17450–17455
17. Hyvonen M, Enback J, Huhtala T, Lammi J, Sihto H, Weisell J, Joensuu H, Rosenthal-Aizman K, El-Andaloussi S, Langel U, Narvanen A, Bergers G, Laakkonen P (2014) Novel target for peptide-based imaging and treatment of brain tumors. Mol Cancer Ther 13:996–1007
18. Kinnari PJ, Hyvonen ML, Makila EM, Kaasalainen MH, Rivinoja A, Salonen JJ, Hirvonen JT, Laakkonen PM, Santos HA (2013) Tumour homing peptide-functionalized porous silicon nanovectors for cancer therapy. Biomaterials 34:9134–9141
19. Zahid M, Phillips BE, Albers SM, Giannoukakis N, Watkins SC, Robbins PD (2010) Identification of a cardiac specific protein transduction domain by in vivo biopanning using a M13 phage peptide display library in mice. PLoS One 5, e12252
20. Lundin P, Johansson H, Guterstam P, Holm T, Hansen M, Langel U, EL Andaloussi S (2008) Distinct uptake routes of cell-penetrating peptide conjugates. Bioconjug Chem 19: 2535–2542
21. El Andaloussi S, Guterstam P, Langel U (2007) Assessing the delivery efficacy and internalization route of cell-penetrating peptides. Nat Protoc 2:2043–2047
22. Gump JM, Dowdy SF (2007) TAT transduction: the molecular mechanism and therapeutic prospects. Trends Mol Med 13:443–448
23. Sugahara KN, Teesalu T, Karmali PP, Kotamraju VR, Agemy L, Girard OM, Hanahan D, Mattrey RF, Ruoslahti E (2009) Tissue-penetrating delivery of compounds and nanoparticles into tumors. Cancer Cell 16:510–520
24. Teesalu T, Sugahara KN, Kotamraju VR, Ruoslahti E (2009) C-end rule peptides mediate neuropilin-1-dependent cell, vascular, and tissue penetration. Proc Natl Acad Sci U S A 106:16157–16162
25. Sugahara KN, Teesalu T, Karmali PP, Kotamraju VR, Agemy L, Greenwald DR, Ruoslahti E (2010) Coadministration of a tumor-penetrating peptide enhances the efficacy of cancer drugs. Science 328:1031–1035
26. Pang HB, Braun GB, She ZG, Kotamraju VR, Sugahara KN, Teesalu T, Ruoslahti E (2014) A free cysteine prolongs the half-life of a homing peptide and improves its tumor-penetrating activity. J Control Release 175:48–53
27. Smith GP (1985) Filamentous fusion phage: novel expression vectors that display cloned antigens on the virion surface. Science 228: 1315–1317
28. Hoogenboom HR (2002) Overview of antibody phage-display technology and its applications. Methods Mol Biol 178:1–37
29. El-Andaloussi S, Johansson HJ, Holm T, Langel U (2007) A novel cell-penetrating peptide, M918, for efficient delivery of proteins and peptide nucleic acids. Mol Ther 15:1820–1826
30. Zahid M, Robbins PD (2011) Identification and characterization of tissue-specific protein transduction domains using peptide phage display. Methods Mol Biol 683:277–289

Chapter 15

The Antimicrobial and Antiviral Applications of Cell-Penetrating Peptides

Kalle Pärn, Elo Eriste, and Ülo Langel

Abstract

Over the past two decades, cell-penetrating peptides (CPPs) have become increasingly popular both in research and in application. There have been numerous studies on the physiochemical characteristics and behavior of CPPs in various environments; likewise, the mechanisms of entry and delivery capabilities of these peptides have also been extensively researched. Besides the fundamental issues, there is an enormous interest in the delivery capabilities of the peptides as the family of CPPs is a promising and mostly non-toxic delivery vector candidate for numerous medical applications such as gene silencing, transgene delivery, and splice correction. Lately, however, there has been an emerging field of study besides the high-profile gene therapy applications—the use of peptides and CPPs to combat various infections caused by harmful bacteria, fungi, and viruses.

In this chapter, we aim to provide a short overview of the history and properties of CPPs which is followed by more thorough descriptions of antimicrobial and antiviral peptides. To achieve this, we analyze the origin of such peptides, give an overview of the mechanisms of action and discuss the various practical applications which are ongoing or have been suggested based on research.

Key words CPP, cell-penetrating peptide, AMP, antimicrobial peptide, Tat, HIV, HCV

1 Introduction

CPPs are a class of diverse peptides, typically 5–30 amino acids in length, and unlike most peptides, they can cross the cellular plasma membrane. CPPs are a family of peptides that are structurally diverse but share the ability to translocate a wide range of different bioactive molecules into living cells [1]. The list of available CPPs has grown rapidly and CPPs have been employed for a variety of applications. CPPs serving as vectors can successfully facilitate the intracellular transport of cargoes, such as small-molecule therapeutic agents [2], proteins, quantum dots [3], and MRI contrast agents [4], both in vitro and in vivo [5]. In addition, this efficient transport system has lower cytotoxicity in a variety of cell lines compared with other delivery methods [6].

Ülo Langel (ed.), *Cell-Penetrating Peptides: Methods and Protocols*, Methods in Molecular Biology, vol. 1324,
DOI 10.1007/978-1-4939-2806-4_15,

The mechanism of the internalization of CPPs and their cargo is not well understood and has recently been the subject of controversy. CPPs can interact with multiple cell surface molecules, including membrane lipids and membrane-associated proteoglycans [7]. CPPs can be taken up by cells via multiple pathways, such as direct translocation through the membrane bilayer or endocytosis-mediated uptake. Although molecules entering cells prefer the direct membrane translocation pathway, endocytosis, composed of two steps, endocytotic entry and endosomal escape, is the major cellular uptake pathway for most CPPs as most reports have pointed out [8]. Endocytosis occurs by various formats, which can be classified into caveolae and/or lipid raft-mediated endocytosis [9], micropinocytosis [10], through clathrin-mediated endocytosis [11] or via a cholesterol-dependent clathrin-mediated endocytosis [12]. The endocytosis pathway is proposed based on the fact that CPP uptake in cells was found to adopt an energy-dependent mechanism [13]. However, cellular uptake is not completely prohibited at low temperatures or in the presence of endocytosis inhibitors [13], suggesting a non-energy consuming route. Recently, the finding of strong peptide–lipid interactions supports direct translocation of the peptides across the membrane [14]. In addition, many studies also propose cellular uptake can follow multiple routes depending on experimental conditions, specific CPP sequence, and the cargo structure [15].

Besides CPPs, another important category of cationic membrane peptides are antimicrobial peptides (AMPs). Antimicrobial peptides, a major class of antibacterial agents, share amphiphilicity and cationic structural properties with cell-penetrating peptides. All AMPs known by the late-1990s are cationic. However, the concept that AMPs need to be cationic was changed later with the discovery of negatively charged AMPs in 1997 [16]. For example, maximin-H5 [17] discovered from frog skin and dermicidin [18] secreted from human sweat gland tissues are both anionic peptides. They also have a positive net charge, normally in the range of +4 to +6, which is due to the frequent presence of lysines and arginines in the amino acid sequence [19]. Additionally, nearly 50 % of their structure often consists of hydrophobic residues. They kill a broad spectrum of microbes including bacteria and fungi by destroying their cell membranes and are important components of the innate immune system of many animals and plants [20].

2 CPPs and AMPs: How Different Are They?

CPPs and AMPs share common characteristics. CPPs and AMPs are similar in the structural motif of amino acid composition, but differ in biological activities within the lipid membrane. Common to both groups are interactions of cell membrane components with

the charged amino acid residues of the peptides. This is probably the first step in cell association that leads to cellular uptake. Anionic phospholipids or phosphate groups of lipopolysaccharides (for gram-negative bacteria) or acidic polysaccharides, teichoic acids, and lipoteichoic acids (for gram-positive bacteria) are the membrane components at the cell surface responsible for generating an overall negative net charge, making the binding of positively charged or amphipathic peptides possible [21]. Furthermore, the lipid bilayer of bacterial membrane contains mainly lipids with negatively charged phospholipid headgroups, while fungi, in contrast, exhibit a zwitterionic lipid bilayer composition, upon which the uptake is driven by hydrophobic N- or C-terminus or particular amino acids of the peptide sequence, resulting in the accumulation of the peptide, which finally induces strong hydrophobic interaction to the membrane.

Charge interactions between cationic residues and lipids are essential to the biological function of many membrane peptides and proteins, for example, cellular translocation of CPPs, and membrane disruption of AMPs. The ratio between the cationic lysine (Lys) and arginine (Arg) residues influences membrane selectivity since the guanidino functionalities of arginines promote a more efficient interaction with eukaryotic membranes as compared to lysine. This is, however, most often at the expense of increased cytotoxicity. A high Lys content has been correlated with selectivity toward bacterial cells over eukaryotic cells [22]. Furthermore, the ability of CPPs to permeate cell membranes appears to be directly linked to their propensity to fold into a well-defined secondary structure (α-helix or β-sheet) while interacting with biological membranes [23]. Likewise, the antimicrobial activity of α-helical AMPs depends on their propensity to form an α-helix [24]. The highly basic Arg guanidinium and Lys ammonium groups remain protonated under physiological pH conditions and thus can function as hydrogen bond (H-bond) donors in various protein–protein and protein–lipid interactions. In lipid membranes, the guanidinium group in protein side chain can form a branched moiety by interacting with water and lipid molecules. In the past few years, many CPPs and AMPs have been extensively investigated to elucidate the structural basis of how these cationic macromolecules interact with membrane lipids and water [25].

Two examples of AMPs in the recent studies include protegrin-1 (PG-1) [26] and human neutrophil peptide-1 (HNP-1) [27]. PG-1 is representative of many β-sheet AMPs in its disulfide-linked structure and has an Arg-rich sequence. HNP-1 belongs to the α-defensin family of antimicrobial peptides and is the mediator of the host innate immune response. Most AMPs adopt rigid amphipathic secondary structures, either α-helical or β-sheet [28]. The two CPPs, TAT and penetratin, are the first two discovered and also most frequently applied CPPs [25]. They display a

turn-rich conformation and random coil structure in lipid bilayers, respectively, suggesting that the absence of intra- or intermolecular H-bonded conformation and high molecular mobility may be the hallmarks of CPPs which differentiates them from AMPs. Due to the similar Arg-rich structural motif, CPPs and AMPs have strong Arg-lipid and Arg-water interactions, which stabilize these hydrophobic peptides by membrane neutralization and water solvation and thus facilitate the insertion. However, CPPs interact with the cellular membrane in a non-invasive manner, while AMPs function by disrupting the lipid membrane. In addition, CPPs also experience charge–charge interaction from the distal phosphate layer and the guanidinium–phosphate interactions stabilize the CPP peptides in lipids and facilitate the insertion, while the plastic conformation and high mobility further promote the translocation.

For AMPs that preferentially attack internal cellular targets, similar translocation mechanisms have been reported: for buforin 2, which translocates efficiently, but with little membrane activity [29], the structure and orientation in the bilayer have been observed to be very similar to those of magainin 2 [30]. From these results a model was proposed whereby buforin 2 molecules would form a toroidal pore, just as magainin 2 does, but less stable; this would result in shorter pore lifetimes—with a concomitant decrease in permeabilization—at the same time that the translocation rate would increase because pore disintegration, which is the actual translocation step, would become more frequent [29, 30]. This model is supported by results that show that the presence of bilayer components that prevent the formation of toroidal pores (such as dioleyl phosphatidylethanolamine [31]) inhibit buforin 2 translocation, whereas anionic phospholipids, which decrease the charge repulsions between the cationic peptide molecules, stabilize the pore to a point that significant leakage and flip-flop is observed [30]. Buforin 2 translocation has also been shown to withstand cargo addition, as demonstrated by the attachment of green fluorescent protein [32], which makes this peptide a promising candidate for its development into a CPP. A "membrane-thinning" effect was proposed for the AMP magainin 2 [33], in which the peptide aggregates on the surface of the membrane and the decreased local surface tension allows the peptide to intercalate the membrane.

3 Antimicrobial Peptides

Antimicrobial peptides are gene-encoded, ribosomally synthesized polypeptides. They usually have common characteristics: small peptide with a varying number (from five to over a hundred) of amino acids, strongly cationic (pI 8.9–10.7), heat-stable (100 °C, 15 min), no drug fastness and no effect on eukaryotic cells [34]. In total, more than 5000 AMPs have been discovered, predicted or

synthesized up to date [35]. The natural AMPs have been isolated and characterized and produced from practically all living organisms, ranging from prokaryotes (e.g. bacteria) to eukaryotes (e.g. protozoan, fungi, plants, insects, and animals) [36, 37]. In animals, AMPs are mostly found in the tissues and organs that are exposed to airborne pathogens and are believed to be the first line of the innate immune defense [38] against viruses, bacteria, and fungi [37]. Several types of eukaryotic cells are involved in AMP production such as lymphs, epithelial cells in gastrointestinal and genitourinary systems [39], phagocytes [40], and lymphocytes of the immune system [37]. In addition to direct involvement in innate immunity, AMPs have also been found to influence inflammatory responses during an infection [41].

In short, AMPs have the ability to kill pathogenic microorganisms, including gram-positive and gram-negative bacteria, viruses, protozoa, and fungi. In contrast to conventional antibiotics, AMPs appear to be bactericidal (kills bacteria) instead of bacteriostatic (inhibits growth). They can destroy bacteria within minutes with the rate being faster than the bacteria growth rate [42].

3.1 Origins and Classification of AMPs

3.1.1 Origin of AMPs

AMPs can be commonly classified into four groups according to their origins. They can originate from insects, other animals, synthesis, and genetically engineered microorganisms. It is possible to make fully synthetic peptides by chemical synthesis [43] or by using recombinant expression systems [44]. These artificial sources of AMPs are useful for the modification of existing AMPs and for designing new synthetic AMPs. Such modifications have potential to change the targets of AMPs and improve the stability of AMPs against proteases [45]. Despite these advantageous features of AMPs, there are still some challenges to their applications, such as potential toxicity to humans [46], sensitivity to harsh environmental conditions (susceptibility to proteases and extreme pH) [47], lack of selectivity against specific strains [48], high production costs [49], folding issues of some large AMPs [50], reduced activity when used for surface coating, and bacterial resistance to some AMPs [51].

Historically, AMPs have also been referred to as cationic host defense peptides [52], anionic antimicrobial peptides/proteins [53], cationic amphipathic peptides [54], cationic AMPs [55], host defense peptides [56], and α-helical antimicrobial peptides [57]. The discovery of AMPs dates back to 1939, when Dubos extracted an antimicrobial agent from a soil Bacillus strain. This extract was demonstrated to protect mice from pneumococci infection. In the following year, Hotchkiss and Dubos fractionated this extract and identified an AMP which was named gramicidin [58]. In 1941, another AMP, tyrocidine, was discovered and found to be effective against both gram-negative and gram-positive bacteria. However, tyrocidine exhibited toxicity to human blood cells. In the same year, another AMP was isolated from a plant

Triticumaestivum, which was later named purothionin and found effective against fungi and some pathogenic bacteria [58]. The first reported animal-originated AMP is defensin, which was isolated from rabbit leukocytes in 1956. In the following years, bombinin from epithelia and lactoferrin from cow milk were both described. During the same time, it was also proven that human leukocytes contain AMPs in their lysosomes [58].

3.1.2 How Do AMPs Get Inside Cells?

There is no common molecular entry route for AMPs—it depends on the nature of the peptide, the membrane lipid composition and the peptide/lipid ratio. The mechanism comprises several stages which are not yet fully understood, despite extensive studies. The necessary step is peptide's association with membrane lipids which results in long-range defects. The different molecular mechanisms postulated (such as barrel-stave or toroidal/wormhole pore formation, aggregate channel formation or surfactant-like interactions [59]) assume that aggregation/oligomerization of AMP in the cytoplasmic membrane is the necessary step leading to the membrane lysis.

3.1.3 Classification

Most AMPs reported to date can be classified based on one of the following four types based on their secondary structural features: such as cathelicidins (with a linear α-helical structure), defensins (with a β-strand structure), and bactenecins (with a loop structure) [60], and extended helices with a predominance of one or more amino acids. Among these structural groups, α-helix and β-sheet structures are more common [61] and α-helical peptides are the most studied AMPs to date. The best known examples of such AMPs are protegrin, magainin, cyclic indolicin, and coiled indolicin [57] and α-helical peptides without the presence of cysteines in the sequence, such as melittin [62]. β-Sheet peptides are composed of at least two β-strands with disulfide bonds between these strands [63], such as the protegrins [64]. And the AMPs with intermolecular disulfide bonds exhibiting loop/hairpin-like structures, such as bactenecin [65], belong to the third group. The final groups are peptides with predominance of one or more distinct amino acids, such as the proline/arginine-rich peptide Bac7 [66].

3.1.4 AMP Design

The design of novel AMPs requires consideration of several factors, including secondary structure, amphipathicity, and the presence of positively charged residues. It is believed that an amphipathic secondary structure is required in order for AMPs to function, although the exact mechanism of action is still unclear. As pointed out by Tossi et al. [67], the design of AMPs is generally based on: (a) amino acid residue analogues of natural peptides (e.g. congeners) that differ at one or more residue positions, are shortened or contain deletions, as well as hybrid AMPs composed of fragments of two different natural peptides; (b) amino acid residues that

maximize the amphipathic nature of AMPs; (c) amino acid sequences from combinatorial libraries; and (d) amino acid sequences that are patterned from known, naturally occurring, α-helical peptide domains.

Important factors to consider when designing AMPs are the length of the peptide [68], net charge [69, 57], amphipathicity [70], and possible modifications such as phosphorylation [71], addition of D-amino acids [72], methylation [19], amidation [73], glycosylation [74], formation of disulfide linkage [75], and proteolytic cleavage [76].

3.2 Mechanisms of Action of AMPs

It is generally accepted that positively charged peptides interact directly with the negatively charged cellular membranes of bacterial cells, resulting in the increase of membrane permeability, which leads to a rapid cell death [77]. The groups of AMPs can be divided as: (a) antibacterials; (b) antivirals; (c) antifungals; (d) antiparasitics; and (e) anticancer peptides. AMPs kill bacteria by inhibiting some important pathways inside the cell such as DNA replication and protein synthesis [78]. Antiviral AMPs neutralize viruses by integrating in either the viral envelope or the host cell membrane. AMPs can integrate into viral envelopes and cause membrane instability, rendering the viruses unable to infect host cells [79]. AMPs can also reduce the binding of viruses to host cells [80]. Some of antifungal peptides are capable of binding to chitin. Such binding ability helps AMPs to target fungal cells efficiently. Cell wall-targeting antifungal AMPs kill the target cells by disrupting the integrity of fungal membranes by increasing permeabilization of the plasma membrane [81], or by forming pores directly [82]. An example of antiparasitic peptide is cathelicidin, which is able to kill *Caernohabditis elegans* by forming pores in the cell membrane [83]. Even though some parasitic microorganisms are multicellular, the mode of action of antiparasitic peptides is the same as other AMPs. They kill cells by directly interacting with cell membrane [83]. Anticancer peptides are also known as host defense peptides. They unction by targeting the cell membrane, as to date, more than 100 host defense peptides are known.

3.3 Applications of AMPs

Antimicrobial peptides represent a novel class of therapeutic agents that may be useful in the treatment of a range of infectious diseases. However, in order to develop antimicrobial peptides for therapeutic use, there are a number of technological hurdles to address, including optimizing peptide stability and antimicrobial activity. Most pharmaceutical efforts has been devoted to the development of topically applied agents, such as magainin analog pexiganan, largely because of the relatively safety of topical therapy and the uncertainty surrounding the long-term toxicology of any new class of *systemically* administrated drug. Diverse applications have been demonstrated for antimicrobial peptides as anti-infective

agents. The broad antimicrobial spectrum of antimicrobial peptides positions them for consideration as "chemical condoms" to limit the spread of sexually transmitted diseases, including *Neisseria*, *Chlamydia*, human immunodeficiency virus (HIV), and Herpes simplex virus (HSV).

3.3.1 AMP-Based Drug Development

In addition to the previously mentioned applications of AMPs, there are much broader uses for the peptides. This is a subject that has been previously thoroughly reviewed by several authors [84–86], therefore only the select few approaches that the authors regarded to be of interest will be discussed in the section at hand.

One noteworthy example entails the CPP-PMO conjugate developed in cooperation with AVI Biopharma. The AVI-6002 and AVI-6003 molecules developed by them show promising results against the mRNA translation process of Ebola virus and Marburg virus, which becomes increasingly important in the light of the recent Ebola outbreak. Various in vivo studies have been conducted with these drug candidates, including mice, guinea pigs and primates [87, 88]. Recently, they have been conducting preliminary clinical trials as well and have obtained positive results from phase 1 trials [88].

Another molecule of interest is a cationic peptide-based drug targeting fungal infections on toenails, is showing promise and has recently entered clinical studies. Novabiotics has created a cyclic hepta-arginine antimicrobial peptide that shows potency in inhibiting fungal growth by disrupting cellular membranes, leading to the loss of viability in affected fungal cells. The cyclic form that was introduced to the molecule is claimed to enhance the antifungal capabilities of the peptide and to increase its stability [89].

3.3.2 CPPs with AMP Properties

In recent years it has been discovered that the Tat peptide shows potent antibacterial activity (MIC 2–8 μM) against a broad spectrum of pathogens including gram-positive and gram-negative bacteria such as *S. aureus* and also fungi such as *Saccharomyces cerevisiae* and *Candida albicans* [90, 91]. The peptide internalizes without any damage to the cell membrane, thus being cytotoxic inside the cells, leading for example to a fast accumulation in the nucleus in fungi, where it causes cell cycle arrest in G1 phase. The uptake of the Tat peptide seems to be sequence-dependent and not induced by its secondary structure [92]. Nearly 20 years after its discovery, it was observed that the CPP penetratin is a potent antimicrobic against gram-negative and gram-positive bacteria such as *Bacillus megaterium*. An MIC of 0.5–4 μM was measured, and the peptide showed no cytotoxicity against mammalian cells.

In the 18-amino-acid peptide pVEC, uptake takes place by a non-endocytotic mechanism of translocation without alteration of plasma membrane permeability or cell morphology. After the internalization process, it is mainly localized in nuclear structures and

was used as a carrier for peptide nucleic acids (PNAs) and proteins [93]. It can enter mammalian and microbial cells and preferentially permeates and kills microbes; for example, it was described to kill *Mycobacterium smegmatis* at low micromolar doses at which normal human cells were not damaged [94].

Pep-1 has a hydrophobic tryptophan-rich domain, a spacer domain, and a hydrophilic lysine-rich domain and is characterized by an amphipathic α-helical structure [95]. Pep-1 has a broad antimicrobial spectrum against gram-negative and gram-positive bacterial strains but weak antibacterial activity [96]. A bacteria-selective variant could be designed by replacing several glutamic acids with lysines. The modified peptide showed high activity (MIC 1–2 μM) against strains of gram-positive and gram-negative bacteria as well as against clinical isolates of multidrug-resistant *Pseudomonas aeruginosa* (MDRPA) and methicillin-resistant *S. aureus* (MIC 1–8 μM) [96]. Certain chimeric peptides, such as Pep-1, may even be considered a "blend" between AMPs and CPPs. Although reported as a CPP, Pep-1 is a strongly amphipathic cationic peptide, rich in basic amino acids and tryptophan, having a proline residue in its sequence. These are the classical characteristics attributed to AMPs. The ability to cysteine-bridge monomers, which greatly improves translocation efficiency, further increases the similarities to AMPs. Not surprisingly, Pep-1 uses mainly physical routes to translocate membranes. However, this route is not always operative [95] and endocytic pathways are alternatives.

Transportan (TP) is a 27 amino acid chimeric peptide composed of the neuropeptide galanin and mastoparan-X linked by a lysine. It exhibits rapid and non-endocytotic uptake and was used for delivery of peptides, PNA oligomers or even intact proteins [97]. TP 10 is a 21-amino-acid deletion analog of the chimeric CPP transportan that contains the mastoparan sequence but lacks the toxicity of its parent compound. It can enter mammalian and microbial cells and preferably permeate and kill microbes such as *S. aureus* at low micromolar doses but does not damage human cells [98].

The cationic and amphipathic model peptide (MAP) is another CPP with antimicrobial properties. The uptake of the peptide again seems to be a combination of energy-dependent and energy-independent mechanisms, whereas the amphipathicity of the peptide is crucial for uptake [99]. It exhibits an antimicrobial effect against gram-positive bacteria such as *B. megaterium* and gram-negative bacteria such as *E. coli* in a low micromolar range. However, no antifungal activity against yeast *S. cerevisiae* has been observed [94]. A pore-formation mechanism was proposed for MPG (a 27-residue amphipathic peptide) and Pep-1 [100], which is also a common mechanism used by antimicrobial peptides (Table 1).

Increasing evidence indicates that membrane-interacting peptides, in fact, may exhibit cross-functionality, e.g. some AMPs possess the ability to cross mammalian cell membranes by non-damaging

Table 1
Selected examples of peptides with AMP-CPP properties

Name	Sequence	Source	Target	Reference
Tat	GRKKRRQRRRPPQ	HIV-1 Tat protein	Gram+ and gram– bacteria, fungi, HIV-1	Zhu and Shin [90], Jung et al. [91], Keogan et al. [105]
pVec	LLIILRRRIRKQAHAHSK	Murine sequence of the cell adhesion molecule vascular endothelial cadherin	Gram+ and gram– bacteria	Palm et al. [94], Nekhotiaeva et al. [98]
Pep-1	KETWWETWWTEWSQPKKKRKV	Simian virus 40 large T antigen and reverse transcriptase of human immunodeficiency virus	Gram+ and gram– bacteria	Zhu et al. [96]
Pep-1-K	KKTWWKTWWTKWSQPKKKRKV	Modified Pep-1	Gram+ and gram– bacteria	Zhu et al. [96]
TP10	AGYLLGKINLKALAALAKKIL	Deletion analog of Transportan-neuropeptide galanin and mastoparan-X linked by a lysine	Gram+ bacteria, fungi	Nekhotiaeva et al. [98]
MAP	KLALKLALKALKAALKLA	Artificial peptide	Gram+ and gram– bacteria	Palm et al. [94]
NYAD	ITFXDLLXYYGP	Page display, hydrocarbon stapled	HIV-1	Zhang et al.[106]
LK-3	LKKLCKLLKKLCKLAG	Artificial peptide (dimer)	HIV-1	Jang et al. [109]
	LKKLCKLLKKLCKLAG			
Deca-(Arg)8	Deca-WRRRRRRRRG	Synthetic analog of Tat-1 with additional fatty acid domain	Duck-HBV	Abdul et al. [111]
G1, G2	LRSRTKIIRIRH, MPRRRRIRRRQK	Phage display	HSV-1	Tiwari et al. [112]
Pyrrhocoricin	VDKGSYLPRPTPPRPIYNRN	*Pyrrhocoris apterus*	Gram– bacteria	Otvos [114]
Bactenecin 7	RRIRPRPPRLPRPRPRP-$(LPFPRPGPRPIPRP)_3$	Large granules of bovine neutrophils	Gram– bacteria	Tani et al. [120], Frank et al. [121]

processes, while several CPPs display significant antimicrobial activity. For example, Tat48–60 from the HIV-1 transactivating protein has been shown to inhibit growth of both gram-positive and gram-negative bacteria as well as of fungi [90, 91, 101]. Similarly, Pep-1 derived from simian virus has been modified (Glu → Lys) into an antimicrobial analog, Pep-1-K that possesses activity toward gram-positive and gram-negative bacteria [102]. Also, pVEC derived from cadherin exhibits activity toward both gram-negative and gram-positive bacteria [94, 98], while TP10, a deletion analog of the chimeric CPP transportan, possesses potency against gram-positive bacteria and fungi [98]. Furthermore, the designed model amphipathic peptide (MAP) shows antibacterial activity, whereas it does not exhibit antifungal activity [94].

4 Antiviral Peptides

Antiviral peptides form a distinct subcategory of antimicrobial peptides. While they share many common features with other antimicrobial peptides targeted against bacteria, fungi, and other microorganisms, these peptides, which are capable of inhibiting viruses, should be discussed separately. Unlike other microorganisms, that can be classified as living, viruses fall somewhere between living and non-living categories. Although they possess the capability to replicate, viruses do not have a metabolism and they lack the means to produce energy like living things do with the help of mitochondria. Instead, they recognize host cells, after which the execution of gene expression, genome replication, and virion formation will take place [103]. This is the main reason why antiviral substances can be considered a class of their own—as viruses are so varied, the drug which might show great promise against one type of virus is, with great probability, completely inefficient against some other virus, in some cases this lack of effect can even be observed against a different subtype of the same virus (a common example is HIV-1 with its various strains) [104, 105]. Furthermore, when the main focus of antibacterial, antifungal or even antitumor peptides is to neutralize the organism/cell that they have come to interact with, antiviral peptides must be capable of disabling the viral infection in such a way that the host cell would remain intact and operational, otherwise the host might be weakened by a great extent and, in worst cases, even suffer terminal organ failures.

4.1 CPPs with AVP Properties

While the main antiviral approach has been the use of a CPP-drug conjugate, some CPPs have demonstrated to possess antiviral properties by themselves. One of the viruses against which the antiviral effect of CPPs is evident is HIV-1. It has been described by Keogan et al. that a HIV-1-derived CPP, the Tat-peptide, interacts with CXCR4 and subsequently inhibits the replication efficiency of the

virus strains that use CXCR4 as their co-receptor [105]. Another successful approach is to modify the antiviral molecule to achieve cell-penetrating capabilities, like a direction taken by Zhang et al., in the case of which they used hydrocarbon stapling to create a more stable secondary structure and enhance the a-helicity of the peptide [106]. Following the success of the first hydrocarbon-stapled peptide, the research group has produced a wide range of such antiviral CPPs known as NYAD peptides [107, 108].

Antiviral CPPs can also be created by a synthetic approach, which is best illustrated by the creation of synthetic LK peptides [109]. The reason for such naming is that they are composed either only or mainly of leucine (L) and lysine (K) residues. The key elements in achieving the enhanced antiviral efficiency were once again the increased a-helicity and the amphipathic characteristics of the molecules, which further stresses the importance of these traits when developing antiviral CPPs. Some synthetic antiviral CPPs can also be a result of a lucky accident. While trying to improve the efficiency of their CPP-PNA conjugate [110] by adding a fatty acid domain, they created a CPP, which was an efficient antiviral agent even without the conjugated PNA. The infected cells treated with the peptide also demonstrated the tendency to release naked viral nucleocapsids that are extremely immunogenic, which could be used for vaccine-like immune system stimulation in the infected organism [111].

Screening of phage display libraries is also a possibility when looking for antiviral agents with penetrating properties. The use of this approach by Tiwari et al. has yielded peptide groups G1 (possesses alternating charges) and G2 (possesses repetitive charges) that bind heparin sulfate and inhibit viral entry by attaching themselves to cell surface and blocking the virus–cell interactions and membrane fusions [112]. While the main approach of the study was the prophylactic treatment against HSV-1 on the surface of the cell, it was noted that the particle is possibly internalized, in which case it can be classified as a CPP. This is further confirmed by additional study, where G2 has been conjugated to acyclovir in order to increase its antiviral efficiency [113]. And while the cell penetration might not prove to be especially relevant in the antiviral content of this study, it shows that the screening methodology contains in itself the capability to identify other peptides that possess cell-penetrating features.

5 Therapeutic and Scientific Applications of CPPs in the Field of Microbes and Viruses

5.1 Application of AMPs as Drug Delivery Vectors

As previously mentioned, AMPs have been described to show CPP properties as well, therefore they can be used as delivery vectors for several therapeutic and diagnostic molecules in the treatment

of cancer, genetic, cardiovascular, inflammatory, and infectious diseases. For example, pyrrhocoricin consists of 20 amino acids and is an antimicrobial peptide isolated from insects, being effective against gram-negative bacteria but almost inactive against gram-positive strains [114]. Furthermore, pyrrhocoricin itself has been used as a drug delivery system. Otvos et al. investigated a modified pyrrhocoricin dimer that could successfully deliver peptide antigens into dendritic cells and human fibroblasts [115]. Another example is the antimicrobial protein lactoferrin (hLF), the human milk protein, which is a very important protein in immune defense due to its antifungal, antimicrobial, and antiviral activities [116]. The truncated version of this peptide consists of 49 amino acids and exhibits antimicrobial, antiviral, antitumor, and immunological activity [117] and was described to enter different cells efficiently (e.g. Hela or rat IEC-6). The uptake mechanism of the hLF peptide seems to be concentration-dependent and for concentration higher than 10 μM, rapid delivery into the cytoplasm and nucleus is observed. Furthermore, the uptake pathway was determined to be sensitive to rottlerin, a protein kinase inhibitor with specificity for protein kinase C (PKC). This was also observed for the uptake of arginine-rich CPPs such as Tat and R9 [118]. The uptake efficiency is supposed to be conformation-dependent, because the cyclic structure is required for binding to heparin sulfate and correlates with lipid-induced conformational changes. Several examples of efficient cargo delivery have been described for the hLF peptide; especially proteins and high-molecular-weight complexes have been successfully transported [119].

Another peptide which combines cell-permeation and antimicrobial properties is Bactenecin 7 (Bac7) [120]. This is a linear 59-residue protein that was isolated from large granules of bovine neutrophils. Bac7 belongs to the bactenecin family and consists of four 14-residue repeats. It also belongs to the Pro/Arg-rich family and was described to be antimicrobially active against gram-negative bacteria in a micromolar range but not against gram-positive strains [121]. The antimicrobial effect is caused by inhibition of the intracellular protein synthesis machinery in a two-step mechanism, where the first is entry of the peptide into the cytoplasm and the second is intracellular inhibition of its target [120]. Generally, the longer segments of Bac-7, containing antibacterial and intracellular delivery regions, have antibacterial and cell-permeating activity. Also, SynB vectors from the antimicrobial peptide protegrin-1 (PG-1) can be used for cargo delivery purposes. It shows potent activity against fungi, bacteria, and several enveloped viruses. Like other AMPs, it interacts with the lipid matrix of bacterial membranes and forms pores [75].

The replacement of four cysteines and two valines of PG-1 led to linear peptides (SynB1) still able to penetrate cells efficiently but without being cytolytic to them. With the help of this, peptide

transport of covalently coupled doxorubicin to the brain has been reported. The blood–brain barrier was crossed with high efficiency and without any compromise to its integrity [122]. Another example is buforin II, a 21-amino-acid antimicrobial peptide that was discovered in stomach tissue of Asian toad. It penetrates through the cell membrane without destroying it and kills bacteria by binding to nucleic acids. BF2d, which is a modified analog of buforin II, exhibits cell-penetrating properties and is able to deliver the GFP protein to HeLa cells [32]. Recently, a cathelicidin-derived carrier peptide, sC18, has been developed. This peptide originates from the 18-kDa cationic antimicrobial protein (CAP18) that was first isolated from rabbit leukocytes. Like the hLF protein, CAP18 is a lipopolysaccharide binding protein with an α-helical structure [123]. CAP18 itself and also shortened variants exhibit antimicrobial properties in the lower micromolar range [124].

5.2 CPPs as Antiviral Drug Delivery Vectors

The delivery of antiviral drugs into eukaryotic cells has become increasingly popular over the years. While the specific therapeutic strategies to inhibit viruses might vary, it can be claimed that nearly all CPP-drug combinations, with a select few exceptions, make use of covalent bonding, effectively creating a single molecule which is efficient both in cellular penetration and in its antiviral activity with the advantage of being non-cytotoxic in a wide selection of cell lines and in vivo environments (w6). Here, we present a short overview of the studies that have successfully applied such fusion peptides in their research.

A common approach for antiviral treatment is the use of PNA-CPP conjugates. This strategy has been described to target such high-profile viruses such as HIV-1 and HCV with efficiency up to 99 % [125, 126]. The CPPs commonly used as a backbone for such molecules are Tat, Transportan, and Penetratin [127, 126, 128]. While the main target of the research has been virus inhibition in the cell culture environment, Ganguly et al. have demonstrated efficient uptake and slow clearance levels in Balb/C mice, suggesting a potential therapeutic application for their conjugate [127]. Another interesting result was produced by Chaubey et al., who described that a Transportan-PNA molecule, which had previously been shown to display significant antiviral efficiency (14a), is also a potent virucidal agent, rendering HIV-1 virions pre-treated with the conjugate noninfectious, suggesting a probable prophylactic medical application for their molecule [129]. PNA-CPPs such as the Tat-FS can also be used to block the frameshift process required for the replication of such viruses as SARS-Coronavirus, making them a viable tool against any viruses that require frameshifting to take place during their replication [130]. A successful Tat-based application of PNAs has been shown to lead to Japanese encephalitis virus inhibition by competing with RdRp through interactions with its binding sites at 3′ regions of the RNA [131].

An interesting anti-HIV-1 development has been published by Zhuang et al. Their approach was to combine an antibody fragment with the Tat-peptide, suppressing the reverse transcriptase activity of CCR5-topic HIV-1 isolates in primary blood mononuclear cells. What makes this development especially interesting is the fact that the anti-Rev antibody fragment did not have any antiviral activity on its own and only obtained the capability for strong inhibition after being conjugated to the Tat-peptide [104]. Penetratin has also been used to deliver antibody-derived antiviral agents known as humanized-VH/VHH, which displayed strong helicase binding affinity in order to inhibit HCV replication [132]. Furthermore, single-chain variable fragment antibodies have been attached to cytoplasmic transduction peptide in order to target the HBV core protein and to inhibit the nucleocapsid assembly and replication processes of the virus [133].

Mino et al. have reported the creation of cell-permeable artificial zinc-finger proteins in order to reduce HPV replication levels. Their approach entailed fusing their protein to the polyarginine CPP R9, allowing to block Rep binding to its replication origin sequence [134]. Proteins such as Mx-1 have been used to inhibit VSV virus in combination with Tat peptide through the suppression of replication and capability to cure ongoing infections [135]. Hexa-arginine with a synthetic peptide mimicking a β-sheet/loop motif commonly found in the C-terminal domain of the Chandipura virus P protein binds the positive-sense leader RNA to inhibit virus replication [136]. Heat shock protein gp96 has been fused to Tat-peptide in an attempt to enhance T-cell-based immune responses. This led to increased antiviral and antitumor potency and to the inhibition of HBV in mice [137]. Protease-inhibiting peptides have been developed against HCV infection. These molecules were conjugated to a selection of CPPs and the fusion with Antennapedia was regarded as the approach with the highest efficiency [138]. Peptide-targeting HIV-1 capsid formation has been successfully applied using a commercial CPP-based transfection reagent, Chariot. What makes this development especially interesting is that this is one of the rare occasions upon which the molecule of interest is not conjugated to the transfection peptide covalently but employs non-covalent bonding strategy instead [139]. The approach to target the capsid of the virus has also been used in HCV inhibition—the capsid has been targeted by R7 in fusion with nucleocapsid binding subunits. In addition to its inhibition of envelopment, the peptide conjugate also blocks the subsequent viral particle release [140].

A less common approach is to conjugate a siRNA molecule to a CPP, as it was done by Meng et al. using Tat-1 as a peptide backbone. Their siRNA designed against the 5′ UTR of HCV managed to efficiently enter the cells and inhibit the replication of viral RNA [141]. PMOs have been utilized in an approach against murine

hepatitis virus, which is a member of coronavirus family which holds such other, better known members, such as SARS. Various arginine-rich PPMO combinations were compared and it resulted in the selection of (R-Ahx-R)$_4$AhxB–PPMO over R9F2C–PPMO and Tat-PPMO based on their delivery efficiency in a splice-correcting model system [142] and antiviral efficiencies targeted against 5′-terminal nucleotides of the viral genome [143]. The P007 CPP-conjugated PMO targeting the 3′ region of the internal ribosomal entry site was shown to hold great potency against the coxsackievirus B3, a known cause for viral myocarditis, both in cell culture and in mice, showing a perspective for further therapeutic research [144]. PMOs in combination with arginine-rich CPPs, such as AVI-6002 and AVI-6003 have also been reported to be capable of inhibiting Ebola and Marburg viruses respectively. The main mechanism of action for these molecules is the inhibition of viral mRNA translation, which leads to the inhibition of the whole replication process [88].

5.3 Use of CPPs in Antiviral Research

While there are a large number of possibilities present to use CPPs to combat viral infections, some applications for such peptides can, instead, help the researchers to understand the virus more thoroughly. While it may not be apparent at first, there are possible applications present for almost any type of CPP when it comes to fundamental research. If to consider, for example, a CPP delivery vector that has been proven to have no effect whatsoever in regards to viral infection-replication cycle and also shows no considerable cytotoxic effects against the host cell, such as the CPP PepFect6 when combined with Semliki Forest Virus [145], a member of alphavirus family, it opens up numerous possibilities to gain insight into the properties of the virus and about its behavior when some molecule of interest has been introduced into the environment. This lack of interference becomes especially important when taking into account the fact that other widely used transfection methods, such as electroporation [146] or lipofection [147] either damage the cells to a great extent or inhibit the infection and replication capabilities of viruses [145], resulting in data about the virus that can be considered as unreliable.

But the research applications of CPPs are not limited to the experimental set-ups where the virus is left undisturbed. As mentioned before, there are numerous occasions where CPP-based vector has been used to deliver an antiviral substance into the cells. This approach, combined with the fact that some CPPs do not affect viruses, allows the conduction of research related to viral replication. If to introduce a CPP-drug conjugate into the cellular environment that completely inhibits late-stage virion formation, it could create a setting in which it is easier to observe viral replication without the need to create replicon models of the original virus, the downside of which is that while they do carry out the replication in a similar way

to the virus of interest, they are still, in essence, a shortened version of the original genome, resulting in a possible change of replication speeds and cellular immune response [148]. In the case of highly mutagenic viruses, such as HIV-1, it would also open up the possibility to efficiently research the abilities of the viruses to overcome some obstacle in their life cycle—for example which beneficial mutations is the virus capable of obtaining if a certain replication stage or pathway is blocked. Similar capability has been observed by Zhang et al., where they observed mutations in viral proteins to overcome the antiviral effect of their CPP molecules [107].

Another interesting research topic is the intracellular detection of viruses. CPP vectors have successfully been used to transport small molecular beacons into eukaryotic cells with the goal to observe the behavior of viruses in real-time. A good example is the experiment by Yeh et al. in which they describe using the widely used Tat-peptide to transport nuclease-resistant molecular beacons to detect coxsackievirus B6 replication [149]. They used this approach to verify the presence of viral RNA in cells and were able to observe the spreading of replication from one cell to another with great accuracy. Small molecule transport can be used to identify the various interactions that certain virus regions might have with the host cell. Caignard et al. used a Tat-conjugated peptide version of the measles virus V protein to characterize in which way do the intracellular interactions between the virus and IFN-α/β signaling pathway take place [150].

6 Conclusion

Antimicrobial peptides prove themselves to be highly efficient and versatile therapeutic systems that allow the inhibition of various pathogens. With the advent of CPPs, the two fields are evolving closely, resulting in various combinations, adoptions of antimicrobial strategies and novel approaches. As demonstrated, the line between AMPs and CPPs can be very thin at times, with several molecules displaying characteristics common to both groups. In addition, CPPs can be made to serve antimicrobial or fundamental research purposes either by themselves or in conjugation with various inhibitory molecules, further increasing the spectrum of this field.

Acknowledgements

This work was supported by the EU through the European Regional Development Fund through the project Tumor-Tech (3.2.1001.11-0008) and Centre of Excellence of Chemical Biology, and by the Estonian Ministry of Education and Research through IUT20–26.

References

1. Järver P, Mäger I, Langel Ü (2010) In vivo biodistribution and efficacy of peptide mediated delivery. Trends Pharmacol Sci 31:528–535
2. Lindgren M, Rosenthal-Aizman K, Saar K et al (2006) Overcoming methotrexate resistance in breast cancer tumour cells by the use of a new cell-penetrating peptide. Biochem Pharmacol 71:416–425
3. Santra S, Yang H, Stanley JT et al (2005) Rapid and effective labeling of brain tissue using TAT-conjugated CdS:Mn/ZnS quantum dots. Chem Commun (Camb) 3144–3146
4. Lewin M, Carlesso N, Tung CH et al (2000) Tat peptide-derivatized magnetic nanoparticles allow in vivo tracking and recovery of progenitor cells. Nat Biotechnol 18:410–414
5. Vasconcelos L, Pärn K, Langel Ü (2013) Therapeutic potential of cell-penetrating peptides. Ther Deliv 4:573–591
6. Vives E, Schmidt J, Pelegrin A (2008) Cell-penetrating and cell-targeting peptides in drug delivery. Biochim Biophys Acta 1786: 126–138
7. Nakase I, Akita H, Kogure K et al (2011) Efficient intracellular delivery of nucleic acid pharmaceuticals using cell-penetrating peptides. Acc Chem Res 45:1132–1139
8. Koren E, Torchilin VP (2012) Cell-penetrating peptides: breaking through to the other side. Trends Mol Med 18:385–393
9. Mayor S, Pagano RE (2007) Pathways of clathrin-independent endocytosis. Nat Rev Mol Cell Biol 8:603–612
10. Futaki S, Nakase I, Tadokoro A et al (2007) Arginine-rich peptides and their internalization mechanisms. Biochem Soc Trans 35:784–787
11. Richard JP, Melikov K, Brooks H et al (2005) Cellular uptake of unconjugated TAT peptide involves clathrin-dependent endocytosis and heparan sulfate receptors. J Biol Chem 280: 15300–15306
12. Vandenbroucke RE, De Smedt SC, Demeester J et al (2007) Cellular entry pathway and gene transfer capacity of TAT-modified lipoplexes. Biochim Biophys Acta 1768:571–579
13. Richard JP, Melikov K, Vives E et al (2003) Cell-penetrating peptides. A reevaluation of the mechanism of cellular uptake. J Biol Chem 278:585–590
14. Su Y, Waring AJ, Ruchala P et al (2010) Membrane-bound dynamic structure of an arginine-rich cell-penetrating peptide, the protein transduction domain of HIV TAT, from solid-state NMR. Biochemistry 49:6009–6020
15. von Heijne G (2006) Membrane-protein topology. Nat Rev Mol Cell Biol 7:909–918
16. Brogden KA, Ackermann M, Huttner KM (1997) Small, anionic, and charge-neutralizing propeptide fragments of zymogens are antimicrobial. Antimicrob Agents Chemother 41:1615–1617
17. Lai R, Liu H, Hui Lee W et al (2002) An anionic antimicrobial peptide from toad Bombina maxima. Biochem Biophys Res Commun 295:796–799
18. Steffen H, Rieg S, Wiedemann I et al (2006) Naturally processed dermcidin-derived peptides do not permeabilize bacterial membranes and kill microorganisms irrespective of their charge. Antimicrob Agents Chemother 50:2608–2620
19. Hancock RE, Chapple DS (1999) Peptide antibiotics. Antimicrob Agents Chemother 43:1317–1323
20. Zasloff M (2002) Antimicrobial peptides of multicellular organisms. Nature 415:389–395
21. Tossi A, Sandri L, Giangaspero A (2000) Amphipathic, alpha-helical antimicrobial peptides. Biopolymers 55:4–30
22. Park KH, Nan YH, Park Y et al (2009) Cell specificity, anti-inflammatory activity, and plausible bactericidal mechanism of designed Trp-rich model antimicrobial peptides. Biochim Biophys Acta 1788:1193–1203
23. Caesar CE, Esbjorner EK, Lincoln P et al (2006) Membrane interactions of cell-penetrating peptides probed by tryptophan fluorescence and dichroism techniques: correlations of structure to cellular uptake. Biochemistry 45:7682–7692
24. Adao R, Nazmi K, Bolscher JG et al (2011) C- and N-truncated antimicrobial peptides from LFampin 265–284: biophysical versus microbiology results. J Pharm Bioallied Sci 3:60–69
25. Hong M, Su Y (2011) Structure and dynamics of cationic membrane peptides and proteins: insights from solid-state NMR. Protein Sci 20:641–655
26. Tang M, Hong M (2009) Structure and mechanism of beta-hairpin antimicrobial peptides in lipid bilayers from solid-state NMR spectroscopy. Mol Biosyst 5:317–322
27. Zhang Y, Doherty T, Li J et al (2010) Resonance assignment and three-dimensional structure determination of a human alpha-defensin, HNP-1, by solid-state NMR. J Mol Biol 397:408–422
28. Ulmschneider MB, Ulmschneider JP (2008) Membrane adsorption, folding, insertion and translocation of synthetic trans-membrane peptides. Mol Membr Biol 25:245–257

29. Kobayashi S, Takeshima K, Park CB et al (2000) Interactions of the novel antimicrobial peptide buforin 2 with lipid bilayers: proline as a translocation promoting factor. Biochemistry 39:8648–8654
30. Kobayashi S, Chikushi A, Tougu S et al (2004) Membrane translocation mechanism of the antimicrobial peptide buforin 2. Biochemistry 43:15610–15616
31. Matsuzaki K, Murase O, Fujii N et al (1995) Translocation of a channel-forming antimicrobial peptide, magainin 2, across lipid bilayers by forming a pore. Biochemistry 34: 6521–6526
32. Takeshima K, Chikushi A, Lee KK et al (2003) Translocation of analogues of the antimicrobial peptides magainin and buforin across human cell membranes. J Biol Chem 278:1310–1315
33. Ludtke S, He K, Huang H (1995) Membrane thinning caused by magainin 2. Biochemistry 34:16764–16769
34. Li Y, Xiang Q, Zhang Q et al (2012) Overview on the recent study of antimicrobial peptides: origins, functions, relative mechanisms and application. Peptides 37:207–215
35. Zhao X, Wu H, Lu H et al (2013) LAMP: a database linking antimicrobial peptides. PLoS One 8:e66557
36. Conlon JM, Sonnevend A (2010) Antimicrobial peptides in frog skin secretions. Methods Mol Biol 618:3–14
37. Radek K, Gallo R (2007) Antimicrobial peptides: natural effectors of the innate immune system. Semin Immunopathol 29:27–43
38. Schauber J, Gallo RL (2008) Antimicrobial peptides and the skin immune defense system. J Allergy Clin Immunol 122:261–266
39. Ganz T (2003) The role of antimicrobial peptides in innate immunity. Integr Comp Biol 43:300–304
40. Hancock RE, Scott MG (2000) The role of antimicrobial peptides in animal defenses. Proc Natl Acad Sci U S A 97:8856–8861
41. Kindrachuk J, Jenssen H, Elliott M et al (2013) Manipulation of innate immunity by a bacterial secreted peptide: lantibiotic nisin Z is selectively immunomodulatory. Innate Immun 19:315–327
42. Lohner K (2009) New strategies for novel antibiotics: peptides targeting bacterial cell membranes. Gen Physiol Biophys 28: 105–116
43. Wade JD, Lin F, Hossain MA et al (2012) Chemical synthesis and biological evaluation of an antimicrobial peptide gonococcal growth inhibitor. Amino Acids 43:2279–2283
44. Ramos R, Moreira S, Rodrigues A et al (2013) Recombinant expression and purification of the antimicrobial peptide magainin-2. Biotechnol Prog 29:17–22
45. Papo N, Oren Z, Pag U et al (2002) The consequence of sequence alteration of an amphipathic alpha-helical antimicrobial peptide and its diastereomers. J Biol Chem 277: 33913–33921
46. Matsuzaki K (2009) Control of cell selectivity of antimicrobial peptides. Biochim Biophys Acta 1788:1687–1692
47. Svenson J, Stensen W, Brandsdal BO et al (2008) Antimicrobial peptides with stability toward tryptic degradation. Biochemistry 47:3777–3788
48. Eckert R, Qi F, Yarbrough DK et al (2006) Adding selectivity to antimicrobial peptides: rational design of a multidomain peptide against Pseudomonas spp. Antimicrob Agents Chemother 50:1480–1488
49. Bommarius B, Jenssen H, Elliott M et al (2010) Cost-effective expression and purification of antimicrobial and host defense peptides in Escherichia coli. Peptides 31: 1957–1965
50. Duquesne S, Destoumieux-Garzon D, Zirah S et al (2009) Post-translational modification and folding of a lasso-type gene-encoded antimicrobial peptide require two enzymes only in Escherichia coli. Adv Exp Med Biol 611:35–36
51. Marr AK, Gooderham WJ, Hancock RE (2006) Antibacterial peptides for therapeutic use: obstacles and realistic outlook. Curr Opin Pharmacol 6:468–472
52. Brown KL, Hancock RE (2006) Cationic host defense (antimicrobial) peptides. Curr Opin Immunol 18:24–30
53. Harris F, Dennison SR, Phoenix DA (2009) Anionic antimicrobial peptides from eukaryotic organisms. Curr Protein Pept Sci 10:585–606
54. Groenink J, Walgreen-Weterings E, van't Hof W et al (1999) Cationic amphipathic peptides, derived from bovine and human lactoferrins, with antimicrobial activity against oral pathogens. FEMS Microbiol Lett 179: 217–222
55. Bradshaw J (2003) Cationic antimicrobial peptides : issues for potential clinical use. BioDrugs 17:233–240
56. Riedl S, Zweytick D, Lohner K (2011) Membrane-active host defense peptides–challenges and perspectives for the development of novel anticancer drugs. Chem Phys Lipids 164:766–781

57. Huang Y, Huang J, Chen Y (2010) Alpha-helical cationic antimicrobial peptides: relationships of structure and function. Protein Cell 1:143–152
58. Bahar AA, Ren D (2013) Antimicrobial peptides. Pharmaceuticals (Basel) 6:1543–1575
59. Barzyk W, Rogalska E, Wieclaw-Czapla K (2013) Penetration of milk-derived antimicrobial peptides into phospholipid monolayers as model biomembranes. Biochem Res Int 2013:914540
60. Boman HG (2003) Antibacterial peptides: basic facts and emerging concepts. J Intern Med 254:197–215
61. Powers JP, Hancock RE (2003) The relationship between peptide structure and antibacterial activity. Peptides 24:1681–1691
62. Steiner H, Hultmark D, Engstrom A et al (1981) Sequence and specificity of two antibacterial proteins involved in insect immunity. Nature 292:246–248
63. Bulet P, Stocklin R, Menin L (2004) Antimicrobial peptides: from invertebrates to vertebrates. Immunol Rev 198:169–184
64. Steinberg DA, Hurst MA, Fujii CA et al (1997) Protegrin-1: a broad-spectrum, rapidly microbicidal peptide with in vivo activity. Antimicrob Agents Chemother 41:1738–1742
65. Romeo D, Skerlavaj B, Bolognesi M et al (1988) Structure and bactericidal activity of an antibiotic dodecapeptide purified from bovine neutrophils. J Biol Chem 263:9573–9575
66. Gennaro R, Skerlavaj B, Romeo D (1989) Purification, composition, and activity of two bactenecins, antibacterial peptides of bovine neutrophils. Infect Immun 57:3142–3146
67. Tossi A, Tarantino C, Romeo D (1997) Design of synthetic antimicrobial peptides based on sequence analogy and amphipathicity. Eur J Biochem 250:549–558
68. Westerhoff HV, Juretic D, Hendler RW et al (1989) Magainins and the disruption of membrane-linked free-energy transduction. Proc Natl Acad Sci U S A 86:6597–6601
69. Jiang Z, Vasil AI, Hale JD et al (2008) Effects of net charge and the number of positively charged residues on the biological activity of amphipathic alpha-helical cationic antimicrobial peptides. Biopolymers 90:369–383
70. Fernandez-Vidal M, Jayasinghe S, Ladokhin AS et al (2007) Folding amphipathic helices into membranes: amphiphilicity trumps hydrophobicity. J Mol Biol 370:459–470
71. Goumon Y, Strub JM, Moniatte M et al (1996) The C-terminal bisphosphorylated proenkephalin-A-(209-237)-peptide from adrenal medullary chromaffin granules possesses antibacterial activity. Eur J Biochem 235:516–525
72. Kreil G (1997) D-amino acids in animal peptides. Annu Rev Biochem 66:337–345
73. Rifflet A, Gavalda S, Tene N et al (2012) Identification and characterization of a novel antimicrobial peptide from the venom of the ant Tetramorium bicarinatum. Peptides 38: 363–370
74. Oman TJ, Boettcher JM, Wang H et al (2011) Sublancin is not a lantibiotic but an S-linked glycopeptide. Nat Chem Biol 7:78–80
75. Mangoni ME, Aumelas A, Charnet P et al (1996) Change in membrane permeability induced by protegrin 1: implication of disulphide bridges for pore formation. FEBS Lett 383:93–98
76. Shinnar AE, Butler KL, Park HJ (2003) Cathelicidin family of antimicrobial peptides: proteolytic processing and protease resistance. Bioorg Chem 31:425–436
77. Zhu S, Gao B (2009) A fossil antibacterial peptide gives clues to structural diversity of cathelicidin-derived host defense peptides. FASEB J 23:13–20
78. Brogden KA (2005) Antimicrobial peptides: pore formers or metabolic inhibitors in bacteria? Nat Rev Microbiol 3:238–250
79. Sitaram N, Nagaraj R (1999) Interaction of antimicrobial peptides with biological and model membranes: structural and charge requirements for activity. Biochim Biophys Acta 1462:29–54
80. Belaid A, Aouni M, Khelifa R et al (2002) In vitro antiviral activity of dermaseptins against herpes simplex virus type 1. J Med Virol 66:229–234
81. van der Weerden NL, Hancock RE, Anderson MA (2010) Permeabilization of fungal hyphae by the plant defensin NaD1 occurs through a cell wall-dependent process. J Biol Chem 285:37513–37520
82. Moerman L, Bosteels S, Noppe W et al (2002) Antibacterial and antifungal properties of alpha-helical, cationic peptides in the venom of scorpions from southern Africa. Eur J Biochem 269:4799–4810
83. Park Y, Jang SH, Lee DG et al (2004) Antinematodal effect of antimicrobial peptide, PMAP-23, isolated from porcine myeloid against Caenorhabditis elegans. J Pept Sci 10:304–311
84. Gordon YJ, Romanowski EG, McDermott AM (2005) A review of antimicrobial peptides and their therapeutic potential as anti-infective drugs. Curr Eye Res 30:505–515
85. Fjell CD, Hiss JA, Hancock RE et al (2012) Designing antimicrobial peptides: form follows function. Nat Rev Drug Discov 11: 37–51

86. Fox JL (2013) Antimicrobial peptides stage a comeback. Nat Biotechnol 31:379–382
87. Warren TK, Warfield KL, Wells J et al (2010) Advanced antisense therapies for postexposure protection against lethal filovirus infections. Nat Med 16:991–994
88. Iversen PL, Warren TK, Wells JB et al (2012) Discovery and early development of AVI-7537 and AVI-7288 for the treatment of Ebola virus and Marburg virus infections. Viruses 4:2806–2830
89. Breaker RR, Li S (2013) Antimicrobial compositions and methods. Google Patents
90. Zhu WL, Shin SY (2009) Effects of dimerization of the cell-penetrating peptide Tat analog on antimicrobial activity and mechanism of bactericidal action. J Pept Sci 15:345–352
91. Jung HJ, Jeong KS, Lee DG (2008) Effective antibacterial action of tat (47-58) by increased uptake into bacterial cells in the presence of trypsin. J Microbiol Biotechnol 18:990–996
92. Vives E, Brodin P, Lebleu B (1997) A truncated HIV-1 Tat protein basic domain rapidly translocates through the plasma membrane and accumulates in the cell nucleus. J Biol Chem 272:16010–16017
93. Elmquist A, Lindgren M, Bartfai T et al (2001) VE-cadherin-derived cell-penetrating peptide, pVEC, with carrier functions. Exp Cell Res 269:237–244
94. Palm C, Netzereab S, Hallbrink M (2006) Quantitatively determined uptake of cell-penetrating peptides in non-mammalian cells with an evaluation of degradation and antimicrobial effects. Peptides 27:1710–1716
95. Henriques ST, Costa J, Castanho MA (2005) Translocation of beta-galactosidase mediated by the cell-penetrating peptide pep-1 into lipid vesicles and human HeLa cells is driven by membrane electrostatic potential. Biochemistry 44:10189–10198
96. Zhu WL, Lan H, Park IS et al (2006) Design and mechanism of action of a novel bacteria-selective antimicrobial peptide from the cell-penetrating peptide Pep-1. Biochem Biophys Res Commun 349:769–774
97. Pooga M, Kut C, Kihlmark M et al (2001) Cellular translocation of proteins by transportan. FASEB J 15:1451–1453
98. Nekhotiaeva N, Elmquist A, Rajarao GK et al (2004) Cell entry and antimicrobial properties of eukaryotic cell-penetrating peptides. FASEB J 18:394–396
99. Scheller A, Oehlke J, Wiesner B et al (1999) Structural requirements for cellular uptake of alpha-helical amphipathic peptides. J Pept Sci 5:185–194
100. Deshayes S, Gerbal-Chaloin S, Morris MC et al (2004) On the mechanism of non-endosomial peptide-mediated cellular delivery of nucleic acids. Biochim Biophys Acta 1667:141–147
101. Jung HJ, Park Y, Hahm KS et al (2006) Biological activity of Tat (47-58) peptide on human pathogenic fungi. Biochem Biophys Res Commun 345:222–228
102. Zhu WL, Hahm KS, Shin SY (2009) Cell selectivity and mechanism of action of short antimicrobial peptides designed from the cell-penetrating peptide Pep-1. J Pept Sci 15: 569–575
103. Viru L, Heller G, Lehto T et al (2011) Novel viral vectors utilizing intron splice-switching to activate genome rescue, expression and replication in targeted cells. Virol J 8:243
104. Zhuang X, Stahl SJ, Watts NR et al (2014) A cell-penetrating antibody fragment against HIV-1 Rev has high antiviral activity: characterization of the paratope. J Biol Chem 289:20222–20233
105. Keogan S, Passic S, Krebs FC (2012) Infection by CXCR4-Tropic Human Immunodeficiency Virus Type 1 Is Inhibited by the Cationic Cell-Penetrating Peptide Derived from HIV-1 Tat. Int J Pept 2012:349427
106. Zhang H, Zhao Q, Bhattacharya S et al (2008) A cell-penetrating helical peptide as a potential HIV-1 inhibitor. J Mol Biol 378:565–580
107. Zhang H, Curreli F, Waheed AA et al (2013) Dual-acting stapled peptides target both HIV-1 entry and assembly. Retrovirology 10:136
108. Zhang H, Curreli F, Zhang X et al (2011) Antiviral activity of alpha-helical stapled peptides designed from the HIV-1 capsid dimerization domain. Retrovirology 8:28
109. Jang S, Hyun S, Kim S et al (2014) Cell-penetrating, dimeric alpha-helical peptides: nanomolar inhibitors of HIV-1 transcription. Angew Chem Int Ed Engl 53:10086–10089
110. Robaczewska M, Narayan R, Seigneres B et al (2005) Sequence-specific inhibition of duck hepatitis B virus reverse transcription by peptide nucleic acids (PNA). J Hepatol 42: 180–187
111. Abdul F, Ndeboko B, Buronfosse T et al (2012) Potent inhibition of late stages of hepadnavirus replication by a modified cell penetrating peptide. PLoS One 7:e48721
112. Tiwari V, Liu J, Valyi-Nagy T et al (2011) Anti-heparan sulfate peptides that block herpes simplex virus infection in vivo. J Biol Chem 286:25406–25415

113. Park PJ, Antoine TE, Farooq AV et al (2013) An investigative peptide-acyclovir combination to control herpes simplex virus type 1 ocular infection. Invest Ophthalmol Vis Sci 54:6373–6381
114. Otvos L Jr (2000) Antibacterial peptides isolated from insects. J Pept Sci 6:497–511
115. Otvos L Jr, Cudic M, Chua BY et al (2004) An insect antibacterial peptide-based drug delivery system. Mol Pharm 1:220–232
116. Gonzalez-Chavez SA, Arevalo-Gallegos S, Rascon-Cruz Q (2009) Lactoferrin: structure, function and applications. Int J Antimicrob Agents 33(301):e301–e308
117. Gifford JL, Hunter HN, Vogel HJ (2005) Lactoferricin: a lactoferrin-derived peptide with antimicrobial, antiviral, antitumor and immunological properties. Cell Mol Life Sci 62:2588–2598
118. Duchardt F, Fotin-Mleczek M, Schwarz H et al (2007) A comprehensive model for the cellular uptake of cationic cell-penetrating peptides. Traffic 8:848–866
119. Duchardt F, Ruttekolk IR, Verdurmen WP et al (2009) A cell-penetrating peptide derived from human lactoferrin with conformation-dependent uptake efficiency. J Biol Chem 284:36099–36108
120. Tani A, Lee S, Oishi O et al (1995) Interaction of the fragments characteristic of bactenecin 7 with phospholipid bilayers and their antimicrobial activity. J Biochem 117:560–565
121. Frank RW, Gennaro R, Schneider K et al (1990) Amino acid sequences of two proline-rich bactenecins. Antimicrobial peptides of bovine neutrophils. J Biol Chem 265:18871–18874
122. Rousselle C, Smirnova M, Clair P et al (2001) Enhanced delivery of doxorubicin into the brain via a peptide-vector-mediated strategy: saturation kinetics and specificity. J Pharmacol Exp Ther 296:124–131
123. Chen C, Brock R, Luh F et al (1995) The solution structure of the active domain of CAP18–a lipopolysaccharide binding protein from rabbit leukocytes. FEBS Lett 370:46–52
124. Larrick JW, Hirata M, Shimomoura Y et al (1993) Antimicrobial activity of rabbit CAP18-derived peptides. Antimicrob Agents Chemother 37:2534–2539
125. Kaushik N, Basu A, Palumbo P et al (2002) Anti-TAR polyamide nucleotide analog conjugated with a membrane-permeating peptide inhibits human immunodeficiency virus type 1 production. J Virol 76:3881–3891
126. Ahn DG, Shim SB, Moon JE et al (2011) Interference of hepatitis C virus replication in cell culture by antisense peptide nucleic acids targeting the X-RNA. J Viral Hepat 18: e298–e306
127. Ganguly S, Chaubey B, Tripathi S et al (2008) Pharmacokinetic analysis of polyamide nucleic-acid-cell penetrating peptide conjugates targeted against HIV-1 transactivation response element. Oligonucleotides 18:277–286
128. Turner JJ, Ivanova GD, Verbeure B et al (2005) Cell-penetrating peptide conjugates of peptide nucleic acids (PNA) as inhibitors of HIV-1 Tat-dependent trans-activation in cells. Nucleic Acids Res 33:6837–6849
129. Chaubey B, Tripathi S, Ganguly S et al (2005) A PNA-transportan conjugate targeted to the TAR region of the HIV-1 genome exhibits both antiviral and virucidal properties. Virology 331:418–428
130. Ahn DG, Lee W, Choi JK et al (2011) Interference of ribosomal frameshifting by antisense peptide nucleic acids suppresses SARS coronavirus replication. Antiviral Res 91:1–10
131. Yoo JS, Kim CM, Kim JH et al (2009) Inhibition of Japanese encephalitis virus replication by peptide nucleic acids targeting cis-acting elements on the plus- and minus-strands of viral RNA. Antiviral Res 82:122–133
132. Phalaphol A, Thueng-In K, Thanongsaksrikul J et al (2013) Humanized-VH/VHH that inhibit HCV replication by interfering with the virus helicase activity. J Virol Methods 194:289–299
133. Xun Y, Pan Q, Tang Z et al (2012) Intracellular-delivery of a single-chain antibody against hepatitis B core protein via cell-penetrating peptide inhibits hepatitis B virus replication in vitro. Int J Mol Med 31:369–376
134. Mino T, Mori T, Aoyama Y et al (2008) Cell-permeable artificial zinc-finger proteins as potent antiviral drugs for human papillomaviruses. Arch Virol 153:1291–1298
135. Zhang XM, He DN, Zhou B et al (2013) In vitro inhibition of vesicular stomatitis virus replication by purified porcine Mx1 protein fused to HIV-1 Tat protein transduction domain (PTD). Antiviral Res 99:149–157
136. Roy A, Chakraborty P, Polley S et al (2013) A peptide targeted against phosphoprotein and leader RNA interaction inhibits growth of Chandipura virus – an emerging rhabdovirus. Antiviral Res 100:346–355
137. Zhao B, Wang Y, Zhang Y et al (2012) TAT-mediated gp96 transduction to APCs enhances gp96-induced antiviral and antitumor T cell responses. Vaccine 31:545–552
138. Kugler J, Schmelz S, Gentzsch J et al (2012) High affinity peptide inhibitors of the hepatitis

C virus NS3-4A protease refractory to common resistant mutants. J Biol Chem 287: 39224–39232

139. Bocanegra R, Nevot M, Domenech R et al (2011) Rationally designed interfacial peptides are efficient in vitro inhibitors of HIV-1 capsid assembly with antiviral activity. PLoS One 6:e23877
140. Pan XB, Wei L, Han JC et al (2010) Artificial recombinant cell-penetrating peptides interfere with envelopment of hepatitis B virus nucleocapsid and viral production. Antiviral Res 89:109–114
141. Meng S, Wei B, Xu R et al (2009) TAT peptides mediated small interfering RNA delivery to Huh-7 cells and efficiently inhibited hepatitis C virus RNA replication. Intervirology 52:135–140
142. Abes S, Moulton HM, Clair P et al (2006) Vectorization of morpholino oligomers by the (R-Ahx-R)4 peptide allows efficient splicing correction in the absence of endosomolytic agents. J Control Release 116:304–313
143. Moulton HM, Fletcher S, Neuman BW et al (2007) Cell-penetrating peptide-morpholino conjugates alter pre-mRNA splicing of DMD (Duchenne muscular dystrophy) and inhibit murine coronavirus replication in vivo. Biochem Soc Trans 35:826–828
144. Yuan J, Stein DA, Lim T et al (2006) Inhibition of coxsackievirus B3 in cell cultures and in mice by peptide-conjugated morpholino oligomers targeting the internal ribosome entry site. J Virol 80:11510–11519
145. Pärn K, Viru L, Lehto T et al (2013) Transfection of infectious RNA and DNA/RNA layered vectors of semliki forest virus by the cell-penetrating peptide based reagent PepFect6. PLoS One 8:e69659
146. Gehl J (2003) Electroporation: theory and methods, perspectives for drug delivery, gene therapy and research. Acta Physiol Scand 177:437–447
147. Dalby B, Cates S, Harris A et al (2004) Advanced transfection with Lipofectamine 2000 reagent: primary neurons, siRNA, and high-throughput applications. Methods 33:95–103
148. Kato T, Date T, Miyamoto M et al (2003) Efficient replication of the genotype 2a hepatitis C virus subgenomic replicon. Gastroenterology 125:1808–1817
149. Yeh HY, Yates MV, Mulchandani A et al (2008) Visualizing the dynamics of viral replication in living cells via Tat peptide delivery of nuclease-resistant molecular beacons. Proc Natl Acad Sci U S A 105:17522–17525
150. Caignard G, Bourai M, Jacob Y et al (2009) Inhibition of IFN-alpha/beta signaling by two discrete peptides within measles virus V protein that specifically bind STAT1 and STAT2. Virology 383:112–120

Chapter 16

Visualizing Actin Architectures in Cells Incubated with Cell-Penetrating Peptides

Lin He, Peter D. Watson, and Arwyn T. Jones

Abstract

Defining the exact role of the actin cytoskeleton in mediating endocytosis through different pathways is a significant challenge. The general consensus is that actin has an important role in organizing the early stages of endocytosis but there is still much to learn. Actin has also been implicated in cell internalization of cell-penetrating peptides (CPPs). It is suggested that CPP variants such as octaarginine (R8) and the HIV Tat peptide induce actin-dependent plasma membrane perturbation and enter via macropinocytosis. Here, we describe confocal microscopy techniques that allow for high-resolution spatial characterization of the actin cytoskeleton in untreated mammalian cells and those incubated with actin-disrupting agents and CPPs. By performing *X*–*Y*–*Z* projection images through different regions of cells to show basal and apical profiles, we initially highlight how these techniques can be used to reveal major differences in cortical and filamentous actin organization between different cell lines. Using these techniques, we demonstrate that the actin-disrupting agent cytochalasin D rapidly changes this framework at concentrations significantly lower than is normally used. Experiments are also performed to highlight that serum starvation significantly sensitizes cells to the effects of R8 on actin-induced ruffling and lamellapodia formation. The techniques described here can be used to gain a higher level of knowledge of the organization of the actin network in individual model cell systems, how this is perturbed using commonly used actin inhibitors, and how plasma membrane reorganization can be induced by the addition of drug delivery vectors such as CPPs.

Key words Actin cytoskeleton, Cell-penetrating peptides, Cytochalasin D, Filapodia, Lamellapodia, Macropinocytosis

1 Introduction

The health of all eukaryotic cells is absolutely dependent on a functional cytoskeleton as numerous cellular events rely on the duties of actin, microtubules, and intermediate filaments. Membrane traffic involves the packaging of materials into vesicular-like compartments that bud from and fuse with each other and travel along defined pathways to a variety of cellular destinations. These vesicles associate with the cytoskeleton that provide the necessary directionality to allow them to reach their final destination. The starting

Ülo Langel (ed.), *Cell-Penetrating Peptides: Methods and Protocols*, Methods in Molecular Biology, vol. 1324,
DOI 10.1007/978-1-4939-2806-4_16,

point for endocytosis is the plasma membrane that undergoes reorganization to form invaginations or protrusions that eventually results in the formation of a vesicular compartment containing a portion of the plasma membrane and accompanying extracellular medium. Endocytosis can be broadly categorized into clathrin-mediated and clathrin-independent processes; the latter can be further broken up into other less well defined pathways such as those involving caveolae and also macropinocytosis [1, 2]. The role of the cell cytoskeleton, particularly actin, has been widely studied within the endocytosis remit but there is, to date, little consensus as to exactly how, spatially and temporally actin filaments control endocytic processes [3–5]. Microtubules, often working in association with actin, are most often thought to regulate downstream traffic from the very early stages of endocytosis [6], and comparatively little is known about the role of intermediate filaments.

Cell-penetrating peptides (CPPs) have been widely studied as potential vectors for delivering small molecular entities and macromolecular structures into cells. For relatively small molecular cargo such as fluorophores there is clear evidence that entry may occur directly across the plasma membrane or via endocytosis [7, 8]. Direct penetration through the plasma membrane gives immediate cytosolic delivery, but if endocytosis is utilized for initial entry into the cytoplasm an additional endosome escape step is required if the cargo target lies beyond the confines of the endolysosomal system.

Two independent studies published 10 years ago brought attention to the actin cytoskeleton in the uptake of cationic CPPs, and the possibility that they may in fact be promoting their own uptake by influencing the actin cytoskeleton [9, 10]. One endocytic pathway that is absolutely reliant on actin is macropinocytosis that has the capacity to form large (>1 μM) intracellular vesicles termed macropinosomes [11–14]. Classically this process is induced in response to growth factor activation such as epidermal growth factor (EGF) binding to the EGF receptor, initially leading to extensive actin-dependent ruffling on the plasma membrane. This induces a “gulping effect” manifest as an increased uptake of extracellular fluid [15]. To what extent this occurs in the absence of growth factor activation—constitutive macropinocytosis—or indeed upon the addition of artificial entities such as CPPs remains to be determined. Of interest are observations that some CPPs may induce plasma membrane effects similar to that seen upon growth factor activation [9, 16] and that they also promote the uptake of 70 kDa Rhodamine-labeled dextran, a marker of fluid phase endocytosis [10, 17, 18].

For these types of studies it is of value to gain an insight into how actin is arranged within cell models under different conditions. This could for example provide much needed supporting information on the effects of actin-modifying agents on cell uptake of CPPs using both microscopy and flow cytometry

analysis. Here, we initially describe confocal microscopy methods to study in detail how actin is distributed in cells with and without the actin disruptor cytochalasin D. This agent is widely used to study the requirement for a functional actin cytoskeleton in the uptake of CPPs and other drug delivery systems. The second section highlights how these methods can be used to analyze the influence of CPPs on actin distribution under different experimental conditions.

2 Materials

2.1 Cell Culture

1. HeLa (cervical carcinoma, epithelial) cells ATCC Code CCL-2.
2. A431 (skin epidermal) cells ATCC Code CRL-1555.
3. Growth Media: Dulbecco's Modified Eagle's medium supplemented with Fetal Bovine Serum (FBS, 10 % final volume) and penicillin/streptomycin (100 units/ml and 100 μg/ml respectively).
4. 5 % CO_2 incubator.
5. Phosphate-buffered saline (PBS) pH 7.4.
6. Trypsin-EDTA: 0.05 %.

2.2 Reagents for Visualization of the Actin-Cytoskeleton

1. Glass Cover slips: 16 mm diameter, 0.16–0.19 mm thickness.
2. Microscope slides.
3. Six-well tissue culture plates.
4. Paraformaldehyde (PFA) fixative solution 12 % w/v.
5. 0.2 % w/v Triton-X 100: 100 mg Triton X-100 in 50 ml PBS.
6. Hoescht 33342 (Life Technologies): 10 mg/ml in distilled water. Protect from light, aliquot and store at −20 °C.
7. Rhodamine-conjugated phalloidin (Rh-P, Sigma-Aldrich): 0.5 mg/ml in filter sterilized DMSO. Protect from light, aliquot and store at −20 °C (*see* **Note 1**).
8. DAKO fluorescent mounting medium (Agilent technologies, Stockport, UK).
9. Confocal Microscope: Leica SP5.
10. Microscopy immersion oil: Type F (Leica).

2.3 Reagents for Inducing Actin Rearrangement

1. Cytochalasin D (Cyt D): 10 mM stock in filter-sterilized DMSO. Protect from light, aliquot and store at −20 °C.
2. Octaarginine: Peptide R8 with sequence Ac-RRRRRRRR-NH_2 was from EZBiolab, Carmel, IN, USA. 5.0 mM stock solution in sterile water, aliquot and store at −80 °C.
3. Human Epidermal growth factor (EGF, Sigma Aldrich): 400 μg/ml stock solution in PBS. Aliquot and store at −80 °C.

3 Methods

3.1 Cell Culture for Confocal Microscopy

1. Cells were maintained in Dulbecco's Modified Eagle's medium supplemented with Fetal Bovine Serum (FBS, 10 % final volume) and penicillin/streptomycin (100 units/ml and 100 μg/ml respectively).
2. Place three autoclaved cover slips into each well of 6-well tissue culture plate (Corning life Sciences, Amsterdam).
3. Seed HeLa (0.5×10^6 cells/well) or A431 (1.0×10^6 cells/well) cells in 2.5 ml DMEM containing 10 % FBS.
4. Allow cells to adhere for 24 h in a 37 °C, 5 % CO_2 incubator. They should reach a confluence of ~80–90 %.

3.2 Preparation of Fixative Solution

1. Weigh 12.0 g PFA powder in a fume hood, and dissolve in 85 ml distilled water heated to 65 °C in the fume hood. While it is dissolving, add drops of 5 M NaOH until pH reaches 7.0–7.5. An initially cloudy suspension will then turn clear.
2. Add distilled water to give 100 ml final volume to yield a 12 % w/v stock solution.
3. Cool down to room temperature, aliquot and store at −20 °C.
4. For the working solution dilute the thawed stock to 3 % w/v solution in PBS.

3.3 Labeling the Actin Cytoskeleton in Tissue Culture Cells

1. Prepare cells on coverslips as described in Subheading 3.1.
2. Remove medium, wash three times with PBS.
3. Fix cells with 3 % PFA in PBS at room temperature for 15 min.
4. Wash three times with PBS and permeabilize with 0.2 % Triton-X 100 at room temperature for 5 min.
5. Wash cells three times with PBS. Stain for cell nuclei and polymerized actin with 1.0 ml PBS containing both 1.0 μg/ml Hoescht 33342 and 1.0 μg/ml Rh-P from stock solutions (Subheading 2.2). Incubate at room temperature for 15 min.
6. Wash the cells three times with PBS and once with distilled water (to remove salt from the coverslip), mount coverslip onto a clean glass microscope slide containing 12 μl of mounting medium.

3.4 Actin Visualization by Confocal Microscopy

1. Confocal microscopy: Here we use a Leica SP5 confocal laser scanning microscope equipped with laser lines 405 Blue Diode (Excitation wavelength 405 nm) and Helium Neon (Excitation wavelength 543 nm) for visualization of Hoechst 33342 and Rh-P respectively.
2. All images presented here were obtained using a HCX PL APO 63× 1.4 NA oil immersion objective with Leica Type F immersion oil.

3. For multi-channel image acquisition, scan the channels in a sequential recording mode (two channels separately). This avoids spectral cross-talk caused by overlapping excitation and/or emission spectra of fluorophores. Although the scan time increases twofold, this ensures spectral separation of the two cell stains.
4. Initially set the percentage laser output quite low to avoid bleaching and saturation of the fluorescent signal. Assess the signal to noise level based on the image acquired, and adjust the laser output intensity accordingly.
5. Selected emission (capture) bands ~420–500 nm (Hoechst 33342) and ~560–680 nm (Rh-P) are used here.
6. Parameters "Gain" and "Off-set" of the individual photomultiplier tubes need to be adjusted in order to obtain optimal image acquisition avoiding saturation.
7. Select "XYZ" as the acquisition mode with image resolution (pixels/image) of 512×512. Set pinhole size to 1 Airy Unit, scan speed 200 Hz. For both single sections and multiple projection images, the same optical section is scanned three times to generate a frame average image.
8. To obtain a three-dimensional actin distribution (Z-stack) initiate the scanning at the glass–cell interface.
9. Image through the cell body with a step size of 0.3 μm ensuring coverage of the whole cell volume. In HeLa cells this requires approximately 25–30 sections (*see* **Note 2**).
10. Captured images are then analyzed using Fiji, the open source platform for biological image analysis [19]. Classically, images are shown as a maximum intensity projection through the entire stack and highlight the location of the nucleus (Fig. 1 Max Proj). However, depth information regarding the localization of the actin cytoskeleton is lost. Here, we present the data in an alternative format to highlight differences in the actin cytoskeleton across the entire depth of the cell. The images shown in Fig. 1 represent: *Max Proj*, maximum intensity projections through the entire cell volume of both Hoechst (blue) and Rh-P (red); *Basal*, the three sections closest to the cover slip as a maximum intensity projection of Rh-P corresponding to the lower surface of the cell approximately 1.0 μm from the glass surface; *Cell Body and Apex* (*CBA*), Maximum *Z*-projection through the rest of the cell; *Merge*, false color merge of basal and CBA images highlighting in a single image the different actin structures found at the different sections of the cell.
11. HeLa cells display classical filamentous actin (stress fibers) that are very apparent in the basal sections (Fig. 1), whereas the CBA image displays a more granulated appearance highlighting actin structures near the top surface of the cells.

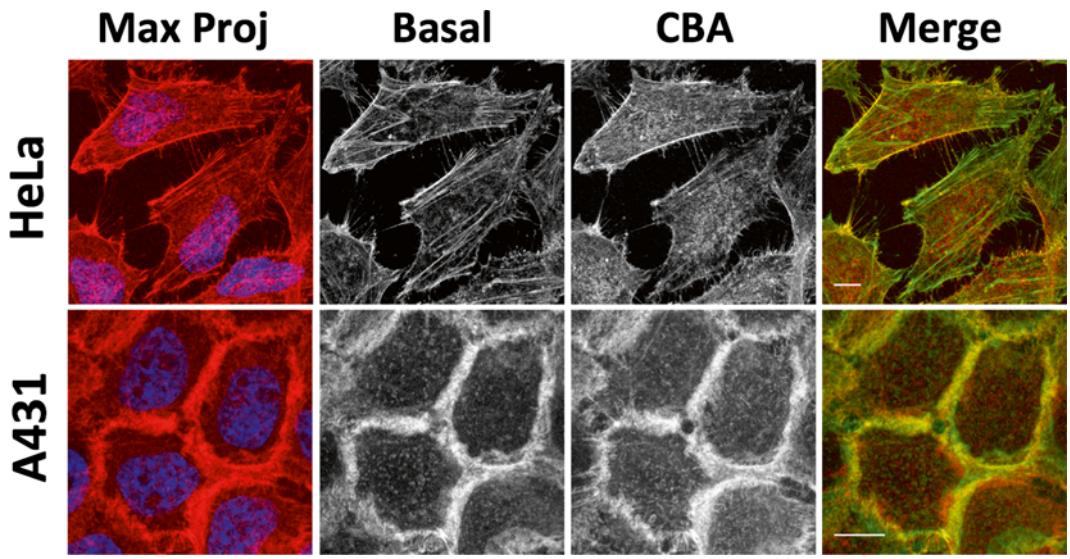

Fig. 1 HeLa and A431 cells fixed and stained with Rh-P and Hoechst 33342 were imaged by confocal microscopy. The images shown represent: Maximum intensity projection (Max Proj), Basal, Cell Body and Apex (CBA) and Merge images as defined in Subheading 3.4. Scale bars: 10 μm

12. In A431 cells generally very few stress fibers are observed (Fig. 1) and the fluorescence is concentrated at the cell periphery especially at cell–cell contacts. This is where cortical actin is found and it remains to be determined what role it has, whether positive or negative, on endocytosis [17, 20, 21] (*see* **Note 3**).

3.5 Analyzing the Actin Cytoskeleton in Cyt D-Treated Cells

1. Seed Hela cells on coverslips as described in Subheading 3.1 and culture for 24 h.
2. Wash the cells three times with PBS before addition of diluent control or Cyt D (1, 10 μM) for 15 min in serum-free DMEM under tissue culture conditions.
3. Fix cells and label the actin cytoskeleton and nucleus as described in Subheading 3.3 (*see* **Note 4**).
4. Cells are then imaged on the confocal microscope as previously described in Subheading 3.4.
5. The selected control cells in Fig. 2 have very well defined stress fibers but also long fillapodia that are commonly observed in this cell line at <100 % confluency. Actin labeling this way shows the dramatic effect that a short Cyt D treatment has on the cells. Basal sections show that actin stress fibers are almost completely disassembled with 1.0 μM Cyt D; less effect is observed on fillapodia. In these cells, actin aggregates especially at cell periphery and apical surface sections; this is particularly apparent at 10 μM Cyt D concentration (*see* **Note 5**).

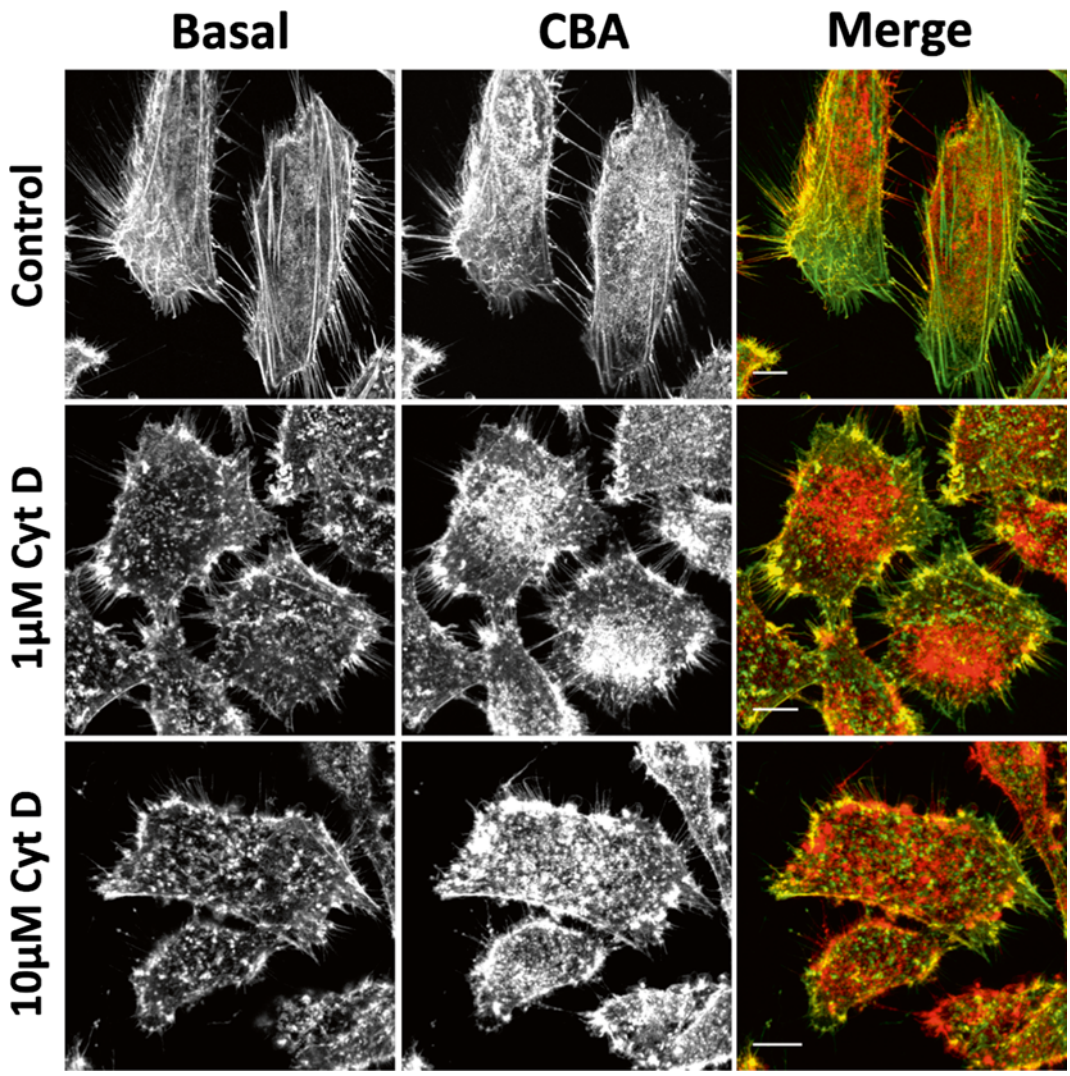

Fig. 2 HeLa cells on cover slips were treated either with diluent control, 1.0 or 10 μM Cyt D for 15 min before fixing and staining with Rh-P and Hoechst. Images were acquired as described in Subheading 3.4. Scale bars: 10 μm

3.6 Analyzing Plasma Membrane Dynamics in Control or Serum-Starved Cells Treated with R8 or EGF

1. Seed HeLa and A431 cells at respective densities of 0.25×10^6 and 0.5×10^6 cells/well as described in Subheading 3.1, and culture for 24 h under tissue culture conditions.
2. For serum starvation wash the cells three times with PBS and replace medium with fresh DMEM lacking serum. For control cells replace medium with fresh DMEM supplemented with 10 % FBS.
3. Culture cells under tissue culture conditions for 16 h (*see* **Note 6**).

4. Wash cells three times in PBS then add serum-free DMEM containing 10 or 20 μM R8 (HeLa) or 20 μM R8 or 50 nM EGF (A431). Incubate under tissue culture conditions for 2.5 min only.
5. Quickly wash then fix the cells, label the nucleus and actin and image by confocal microscopy as described in Subheadings 3.3 and 3.4.
6. Analysis of these cells demonstrate that there is no clear effects on actin staining in cells treated with 10 μM R8. Membrane ruffling is, however, apparent in some cells treated with 20 μM R8 (Fig. 3). The arrow denotes the thin sheet-like lamellapodium at the leading edge of the cell that is clearly defined in the basal image. As lamellapodia are linked with cell motility it would be interesting to determine whether incubation with R8 influences cell migration. This concentration of R8 is much higher than is usually used to demonstrate endocytic uptake of a fluorescent R8 conjugate and at these levels the peptide freely diffuses through the plasma membrane and into the cytosol [8]. When the same experiment is performed in serum-starved cells (Fig. 3 bottom half), there is a dramatic effect at both concentrations with single cells displaying very prominent splayed membrane sheets often covering several micrometers and also long filopodia emanating from them (*see* **Note 7**). At 20 μM the cells have severely altered morphologies, are spiculated and quite possibly in retraction. Incubating HeLa cells with 20 μM R8 in serum-containing medium is non-toxic but the data here suggest that adding the peptide at this concentration in serum-free medium to serum-starved cells may yield very different cytotoxicity results.
7. A431 cells express very high levels of EGF receptor and it is well documented that addition of EGF causes extensive membrane ruffling and macropinocytosis [12, 17, 22, 23]. Serum-starved A431 cells, prepared as previously described for HeLa experiments, were incubated for 2.5 min with EGF (50 nM) or R8 (20 μM). We observe extensive membrane reorganization at the cell edges in response to these short R8 incubations (Fig. 4, *see* **Note 8**) with clear display of lamellapodia (arrow). EGF treatment, compared with R8, however, had a much more pronounced effect and seen in this figure are confluent cells with interdigitated ruffles. This highlights the different effects on cell morphology, and thus actin organization, in R8 versus EGF-treated cells (*see* **Note 9**).

4 Notes

1. Phalloidin binds to polymeric and oligomeric but not monomeric actin (G-actin). Thus in contrast to observing total cellular actin, only organized structures will be visualized using

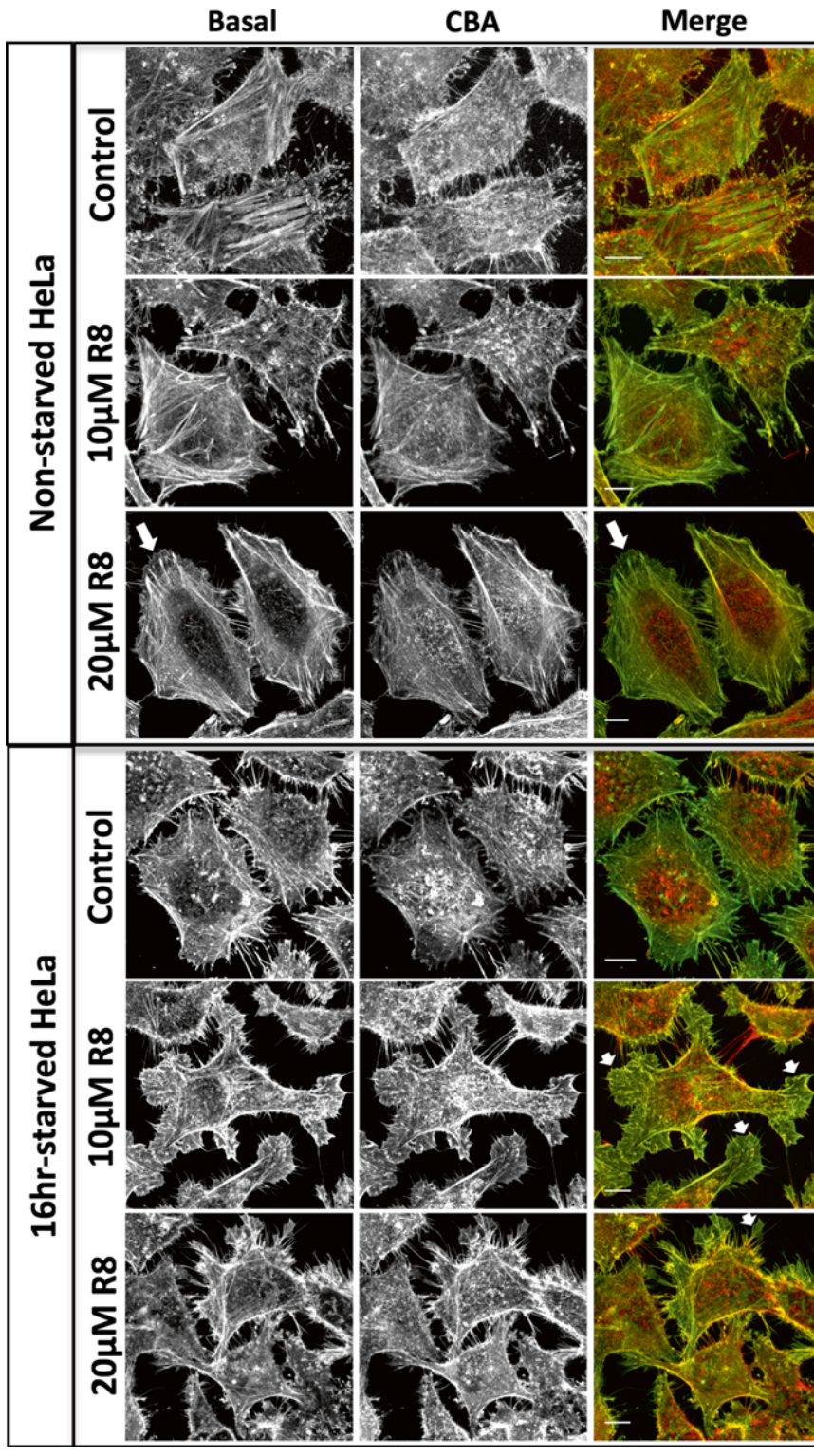

Fig. 3 Non-starved or starved HeLa cells incubated for 2.5 min with diluent control, 10 or 20 μM R8 before fixing and staining with Rh-P and Hoechst. Images were acquired as described in Subheading 3.4. *Large arrow* denotes R8-induced lamellapodia structure on the leading edge of the cell. *Small arrows* in Merge image show R8-induced membrane protrusions/extensions in serum-starved cells. Scale bars: 10 μm

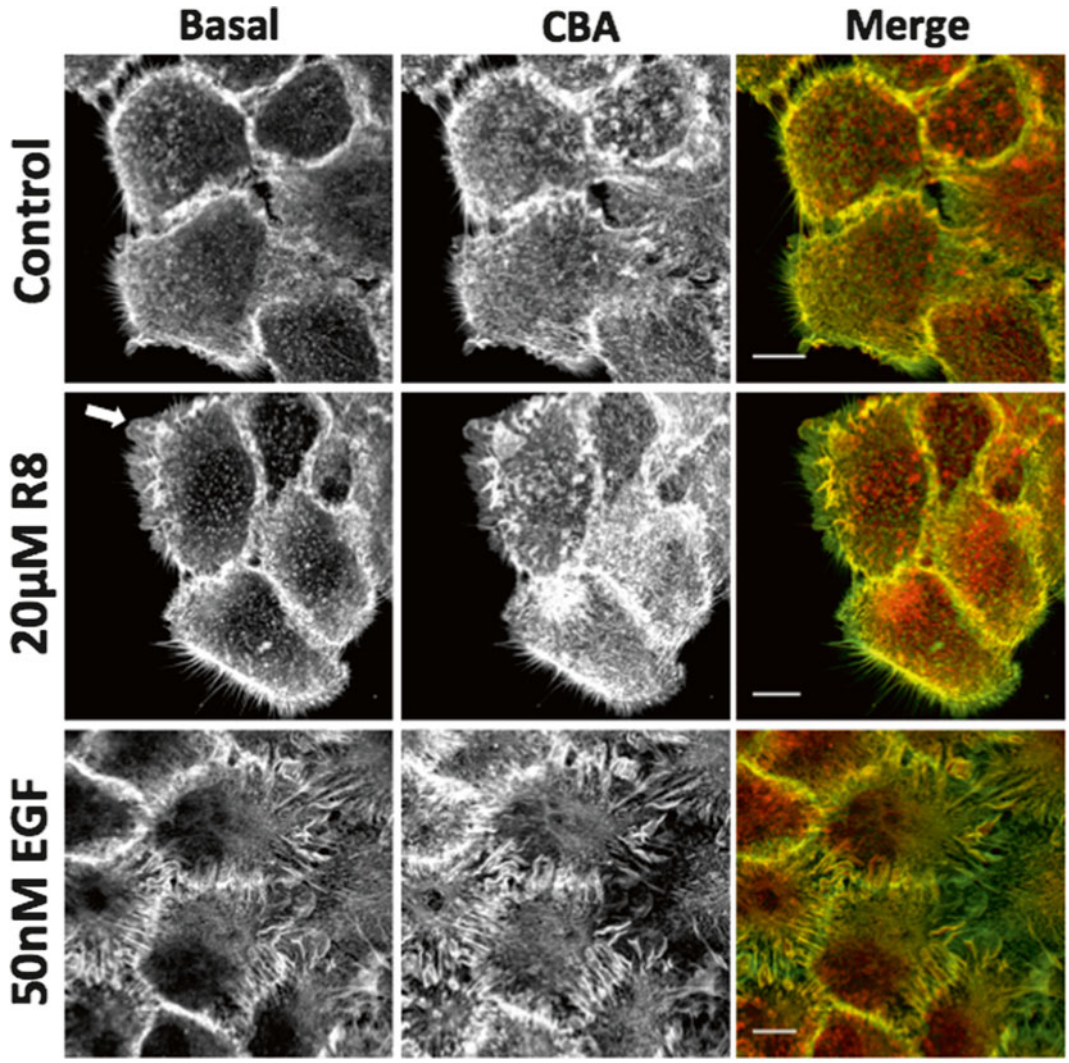

Fig. 4 Serum-starved A431 cells incubated for 2.5 min with diluent control, 20 μM R8 or 50 nM EGF before fixing and staining with Rh-P and Hoechst. Images were acquired as described in Subheading 3.4. *Arrow* denotes R8-induced lamellapodia structure on the cell periphery. Scale bars: 10 μm

fluorescent phalloidin. Commercially available are a range of fluorophores conjugated to phalloidin including Texas Red and Alexa dyes such as 488 and 647.

2. Fixing causes the cells to flatten thus reducing the *Z*-axis depth and the number of optical sections that need to be imaged. Step size must be calculated according to the axial resolution of the microscope. Actin protrusions such as filopodia may extend above the obvious cell outline so ensure the imaging volume extends beyond the cell surface to capture these structures.
3. We previously commented on this difference in actin organization between these two cells lines in attempts to explain

differences we obtained in analyzing the role of actin in cell uptake of CPPs R8 and HIV Tat, and especially the fluid phase marker dextran [17]. Extensive differences in organization of actin between different cell lines were previously noted in a review describing methods for imaging actin in live and fixed cells [24]. There are also differences between the way HeLa and A431 cells expand during tissue culture. A431 cells tend to grow in clusters and this is clearly reflected in the way the actin is organized especially at the cell periphery. These two cell lines also display very different endocytic characteristics when incubated with CPPs and endocytic probes [17].

4. Labeling the nucleus provides a well-defined organelle for cell orientation. To more clearly visualize actin distribution, we do not show the nucleus in the remaining figures but we strongly recommend that it is stained and visualized for a complete dataset.
5. Cyt D binds to actin filaments and prevents further filament assembly by monomeric actin. Other actin disrupters are available working directly or indirectly at different processes of assembly and disassembly. They can often provide supporting information to Cyt D experiments and may be used together as a cocktail [25]. If live cells are imaged then the effects of Cyt D on cell morphology can be clearly observed using bright field or Differential Interference Contrast microscopy [25]. Endocytosis studies, including those analyzing CPP uptake typically use Cyt D at 10 μM (5.1 μg/ml) for longer pre-incubation times, but data in Fig. 2 show that the actin cytoskeleton is completely destroyed at this concentration with the appearance of large actin aggregates becoming more pronounced. Using these microscopy methods, visible effects on the actin cytoskeleton can be visualized at a Cyt D concentration of only 200 nM.
6. Studies have shown that some CPPs cause membrane ruffling in cells akin to that observed upon growth factor stimulation. Noted in these studies is that the cells were previously starved of serum for periods 18–24 h [9, 16]. To investigate whether serum starvation is required to observe these effects, we incubated cells with the CPP R8 in untreated cells or those starved of serum for 16 h.
7. It is questionable as to whether these sheet-like structures are true lamellapodia or blebs or structures unique to cells incubated with this CPP. It is also unknown as to whether actin is actually required for them to form; they may simply be a product of the direct effects of the peptides on the membranes. Membrane blebs are formed when there is loss of actin interaction with the plasma membrane, often due to excess membrane, but that actin–membrane interaction is essential for lamellapodia to form [21].

8. These lamellapodia-like structures can only clearly be observed in cells that are not in contact with each other and it is documented that cell–cell contact inhibits the formation of these structures [21]. It remains to be determined exactly how much cell confluency influences the effects of CPPs on the plasma membrane of the cells studied here and others.
9. We observe very little actin rearrangement in non-starved A431 cells similarly treated with R8 but extensive ruffling of the type observed in Fig 4 when they were incubated with EGF. As little as 1 h serum starvation is sufficient for EGF to mediate macropinocytosis, measured as an increase in fluid phase endocytosis [17]. It remains to be determined as to whether this short starvation period also sensitizes the plasma membrane of the cells to CPPs.

5 Conclusions

Cellular actin can be microscopically visualized in tissue culture cells using a number of techniques and the discovery of Green Fluorescent Protein allowed for live cell imaging analysis of this protein as a monomer and in organized structures [26]. The reader is referred to this recent study revealing how microscopy development and new actin probes allows us to image actin action in live cells [27]. The future clearly lies in supporting fixed cell analysis highlighted in this chapter with the capacity to monitor actin in live cells. The advent of super-resolution technology and new probes for visualization of actin structures [28] will undoubtedly provide much needed new information on exactly why this protein is of such fundamental importance in cell physiology and how it impacts on the cellular uptake of CPPs.

Acknowledgements

This work was supported by a Cardiff University Studentship awarded to LH. This work was supported by a Cardiff University Studentship (LH) and an Engineering and Physical Sciences Research Council (EPSRC) award EP/J021334/1 (ATJ, PW).

References

1. Cleal K, He L, Watson PD, Jones AT (2013) Endocytosis, intracellular traffic and fate of cell penetrating peptide based conjugates and nanoparticles. Curr Pharm Des 19:2878–2894
2. Doherty GJ, McMahon HT (2009) Mechanisms of endocytosis. Annu Rev Biochem 78:857–902
3. Fujimoto LM, Roth R, Heuser JE, Schmid SL (2000) Actin assembly plays a variable, but not obligatory role in receptor-mediated endocytosis in mammalian cells. Traffic 1:161–171
4. Mooren OL, Galletta BJ, Cooper JA (2012) Roles for actin assembly in endocytosis. Annu Rev Biochem 81:661–686

5. Robertson AS, Smythe E, Ayscough KR (2009) Functions of actin in endocytosis. Cell Mol Life Sci 66:2049–2065
6. Anitei M, Hoflack B (2012) Bridging membrane and cytoskeleton dynamics in the secretory and endocytic pathways. Nat Cell Biol 14:11–19
7. Fretz MM, Penning NA, Al-Taei S, Futaki S, Takeuchi T, Nakase I, Storm G, Jones AT (2007) Temperature-, concentration- and cholesterol-dependent translocation of L- and D-octa-arginine across the plasma and nuclear membrane of CD34+ leukaemia cells. Biochem J 403:335–342
8. Watkins CL, Schmaljohann D, Futaki S, Jones AT (2009) Low concentration thresholds of plasma membranes for rapid energy-independent translocation of a cell-penetrating peptide. Biochem J 420:179–189
9. Nakase I, Niwa M, Takeuchi T, Sonomura K, Kawabata N, Koike Y, Takehashi M, Tanaka S, Ueda K, Simpson JC, Jones AT, Sugiura Y, Futaki S (2004) Cellular uptake of arginine-rich peptides: roles for macropinocytosis and actin rearrangement. Mol Ther 10:1011–1022
10. Wadia JS, Stan RV, Dowdy SF (2004) Transducible TAT-HA fusogenic peptide enhances escape of TAT-fusion proteins after lipid raft macropinocytosis. Nat Med 10:310–315
11. Falcone S, Cocucci E, Podini P, Kirchhausen T, Clementi E, Meldolesi J (2006) Macropinocytosis: regulated coordination of endocytic and exocytic membrane traffic events. J Cell Sci 119:4758–4769
12. Jones AT (2007) Macropinocytosis: searching for an endocytic identity and role in the uptake of cell penetrating peptides. J Cell Mol Med 11:670–684
13. Kerr MC, Teasdale RD (2009) Defining macropinocytosis. Traffic 10:364–371
14. Lim JP, Gleeson PA (2011) Macropinocytosis: an endocytic pathway for internalising large gulps. Immunol Cell Biol 89:836–843
15. Haigler HT, McKanna JA, Cohen S (1979) Rapid stimulation of pinocytosis in human carcinoma cells A-431 by epidermal growth factor. J Cell Biol 83:82–90
16. Nakase I, Tadokoro A, Kawabata N, Takeuchi T, Katoh H, Hiramoto K, Negishi M, Nomizu M, Sugiura Y, Futaki S (2007) Interaction of arginine-rich peptides with membrane-associated proteoglycans is crucial for induction of actin organization and macropinocytosis. Biochemistry 46:492–501
17. Al Soraj M, He L, Peynshaert K, Cousaert J, Vercauteren D, Braeckmans K, De Smedt SC, Jones AT (2012) siRNA and pharmacological inhibition of endocytic pathways to characterize the differential role of macropinocytosis and the actin cytoskeleton on cellular uptake of dextran and cationic cell penetrating peptides octaarginine (R8) and HIV-Tat. J Control Release 161:132–141
18. Amand HL, Fant K, Norden B, Esbjorner EK (2008) Stimulated endocytosis in penetratin uptake: effect of arginine and lysine. Biochem Biophys Res Commun 371:621–625
19. Schindelin J, Arganda-Carreras I, Frise E, Kaynig V, Longair M, Pietzsch T, Preibisch S, Rueden C, Saalfeld S, Schmid B, Tinevez JY, White DJ, Hartenstein V, Eliceiri K, Tomancak P, Cardona A (2012) Fiji: an open-source platform for biological-image analysis. Nat Methods 9:676–682
20. de Curtis I, Meldolesi J (2012) Cell surface dynamics - how Rho GTPases orchestrate the interplay between the plasma membrane and the cortical cytoskeleton. J Cell Sci 125:4435–4444
21. Ridley AJ (2011) Life at the leading edge. Cell 145:1012–1022
22. Hewlett LJ, Prescott AR, Watts C (1994) The coated pit and macropinocytic pathways serve distinct endosome populations. J Cell Biol 124:689–703
23. Swanson JA, Watts C (1995) Macropinocytosis. Trends Cell Biol 5:424–428
24. McKayed KK, Simpson JC (2013) Actin in action: imaging approaches to study cytoskeleton structure and function. Cells 2:715–731
25. Peng GE, Wilson SR, Weiner OD (2011) A pharmacological cocktail for arresting actin dynamics in living cells. Mol Biol Cell 22:3986–3994
26. Ballestrem C, Wehrle-Haller B, Imhof BA (1998) Actin dynamics in living mammalian cells. J Cell Sci 111(Pt 12):1649–1658
27. Chen BC, Legant WR, Wang K, Shao L, Milkie DE, Davidson MW, Janetopoulos C, Wu XS, Hammer JA 3rd, Liu Z, English BP, Mimori-Kiyosue Y, Romero DP, Ritter AT, Lippincott-Schwartz J, Fritz-Laylin L, Mullins RD, Mitchell DM, Bembenek JN, Reymann AC, Bohme R, Grill SW, Wang JT, Seydoux G, Tulu US, Kiehart DP, Betzig E (2014) Lattice light-sheet microscopy: imaging molecules to embryos at high spatiotemporal resolution. Science 346:1257998
28. Lukinavicius G, Reymond L, D'Este E, Masharina A, Gottfert F, Ta H, Guther A, Fournier M, Rizzo S, Waldmann H, Blaukopf C, Sommer C, Gerlich DW, Arndt HD, Hell SW, Johnsson K (2014) Fluorogenic probes for live-cell imaging of the cytoskeleton. Nat Methods 11:731–733

Chapter 17

Cell-Penetrating Peptides as Carriers for Transepithelial Drug Delivery In Vitro

Stine Rønholt, Mie Kristensen, and Hanne Mørck Nielsen

Abstract

There is a growing interest in the use of cell-penetrating peptides (CPPs) as carriers for transepithelial drug delivery. This chapter gives an introduction to and discussion of the commonly used production and characterization methods for CPP–cargo samples including high-throughput cell viability screening. Moreover, we describe methods for permeation and cell viability assessment in the Caco-2 cell culture model with and without implementation of biosimilar mucus. Last, a method to assess metabolic degradation in vitro is described.

Key words Caco-2, Cell viability, Cell-penetrating peptides as carriers, High-throughput screening, In vitroMucus, Metabolic degradation, Permeability, Transepithelial drug delivery

1 Introduction

Cell-penetrating peptides (CPPs) are commonly known to be efficient excipients for intracellular delivery of cargoes such as imaging agents [1], small-molecule drugs [2], nucleic acids [3], and proteins [4]. Nevertheless, they may also be suitable candidates as carriers for transepithelial drug delivery of, e.g. therapeutic peptides or proteins when these are either co-administered with [5–7] or directly conjugated to [8] the cell-penetrating peptide. In order to predict the CPP-mediated transepithelial permeation of a co-administered or conjugated cargo, various well-established epithelial cell culture models are available. The human colon adenocarcinoma cell culture model Caco-2 [9] is a widely accepted and commonly used model for the assessment of oral drug delivery. However, the Caco-2 model represents only the absorptive enterocytes and not the mucus-producing Goblet cells, which constitutes an additional physical and metabolic barrier to drug delivery via the intestine (Fig. 1).

Recent studies have addressed the importance of implementing a mucus barrier in studies of intestinal drug delivery in vitro, and for this purpose we have developed and characterized a

Ülo Langel (ed.), *Cell-Penetrating Peptides: Methods and Protocols*, Methods in Molecular Biology, vol. 1324,
DOI 10.1007/978-1-4939-2806-4_17,

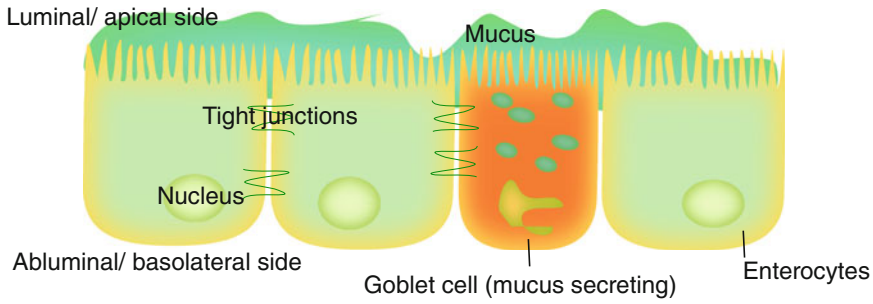

Fig. 1 A simplified illustration of the intestinal epithelial barrier with the individual cells tightly interconnected by tight junctions and the epithelium surface lined by a mucus layer composed of secretions from Goblet cells in the intestinal tissue

biosimilar mucus representative of the mucus otherwise secreted by the Goblet cells and studied its applicability together with monolayers of Caco-2 cells [10, 11]. Another commonly used strategy for implementation of the mucus barrier is based on more advanced cell co-culture models, in which the Caco-2 cells are co-cultured with human colonic HT29 cells (*see* **Note 1**), which differentiates into mucus-secreting cells [12]. As an alternative to the Caco-2 cell culture model, the Madin-Darby canine kidney (MDCK) cell co-culture model is often employed despite its non-intestinal and non-human origin. Despite comparable barrier properties between the MDCK and the Caco-2 cell culture models [13], it may be argued that the MDCK model has the advantage over the Caco-2 model [14] that it displays a more in vivo-like integrity of the epithelial cell layer [15] and faster differentiation [13]. Further relevant epithelial cell culture models commonly used to predict transepithelial drug delivery counts the human bronchial cell culture model Calu-3 [16] and the human buccal cell culture model TR146 [17]; the latter mimicking a stratified epithelium, whereas the Caco-2, the MDCK, and the Calu-3 models represent columnar-like absorptive epithelia. The Calu-3 model is commonly employed to predict delivery of inhaled drugs and facilitates the study of diffusion through the mucosa due to the presence of the mucus produced by these cells.

Epithelia do not only constitute a physical barrier made up by the tightly interconnected mucus-lined epithelial cells, but also a metabolic barrier represented by the presence of various enzymes [18]. Therefore, a major obstacle when employing peptide-based excipients, such as the CPPs, is their inherently chemical instability when presented to the metabolic enzymatic barrier of epithelia, thus limiting their use for transepithelial drug delivery. Multiple approaches have been pursued for increasing the metabolic stability of CPPs, including changing stereochemistry [19, 20] and modification of amino acid side chains [21]. Moreover, backbone stabilization [22] may also be a viable approach to hinder

degradation of CPPs when in contact with the metabolic barrier of epithelia. On the other hand, specific metabolic cleavage may also be a prerequisite for release of a biologically active compound conjugated to or complexed with the CPP. Finally, as for use of other types of excipients, the risk of undesired immune responses and cellular toxicity as well as any undesired effect of the physiological clearance as a result of using such CPP-stabilizing strategies must be carefully evaluated.

In this chapter, we introduce the use of the Caco-2 cell culture model for use to predict CPP-mediated transepithelial delivery of a co-administered cargo. This includes considerations for establishment of CPP–cargo sample preparation and protocols for high-throughput viability screening, permeation experiments with or without a biosimilar mucus barrier, as well as a protocol for the assessment of the metabolic stability of CPPs.

2 Materials

All solutions should be prepared at room temperature using analytical grade chemicals and ultrapure water unless otherwise stated. If using isotope-labeled components, one should pay particular attention of how to handle and dispose the components according to current national and internal guidelines.

2.1 Components for High-Throughput Cell Viability Screening

1. Cell culturing: Prior to the experiment, culture the Caco-2 cells in cell culturing medium (ex. DMEM supplemented with 10 % (v/v) fetal bovine serum (FBS), penicillin (100 U/mL), streptomycin (100 μg/mL), 1 % (v/v) L-glutamine and 1 % (v/v) non-essential amino acids). Keep the culturing flasks at 37 °C in a 5 % CO_2 humidified atmosphere and passage the cells weekly. Seed the cells 24 h before the experiment on the bottom of 96-well plates (Corning Costar, Tewksbury, MA, USA) using 100 μL supplemented DMEM per well aiming for a seeding concentration resulting in 80 % confluence after culturing for 24 h (*see* **Note 2**).
2. Cell compatible buffer (*see* **Note 3**): 10 mM (*see* **Note 4**) HEPES HBSS, pH 7.4. Weigh 1.191 g HEPES and add 450 mL Hanks' Balanced Salt solution (HBSS) (Sigma-Aldrich, St. Louis, MO, USA). Adjust pH to 7.4 and add HBSS to a final volume of 500 mL. Check the osmolality (300 ± 20 mOsmol/kg) and store at 4 °C until use (*see* **Note 5**).
3. MTS stock solution: Prepare stock solutions of 3-(4,5-dimethyl thiazol-2-yl)-5-(3-carboxymethoxyphenyl)-2-(4-sulfophenyl)-2H-tetrazolium (MTS) (CellTiter 96® AQ_{ueous} MTS Reagent Powder, Promega, Fitchburg, WI, USA) in a concentration of 2 mg/mL by transferring 10 mL HBSS to a light-protected

container. Add 21 mg MTS reagent powder and mix at moderate speed using magnetic stirring for 15 min. Adjust pH to 6.5 and filter the MTS solution through a 0.2 μm filter into a sterile, light-protected container. Divide the solution in 1.3 mL aliquots and store at −20 °C for up to 2 months.

4. PMS stock solution: Prepare the phenazine methosulfate (PMS) (Promega, Fitchburg, WI, USA) stock in a concentration of 1 mg/L by dissolving in HBSS and filter the solution through a 0.2 μm filter into a sterile, light-protected container. Divide the solution in aliquots of 0.1 mL and store at −20 °C for up to 1 month.

2.2 Components for Permeation and Cell Viability Assessment in the Caco-2 Cell Culture Model

1. Cell culturing: Prior to the experiment, culture the Caco-2 cells in cell culturing medium as described in Subheading 2.1. Seed 0.5 mL cell suspension on the apical side of polycarbonate filter inserts in a 12-well plate (Corning Costar, Tewksbury, MA, USA) (Fig. 2) 20–29 days prior to the experiment. To obtain a tight, well-differentiated epithelium within the culturing period, a standard seeding concentration for Caco-2 cells is around 8.9×10^{-4} cells/cm^2. Add 1 mL supplemented DMEM medium to the basolateral side. Replace the apical and the basolateral medium every other day and culture the cells for 20–29 consecutive days under the conditions previously described (*see* **Note 6**).
2. Radioactive components: ^{3}H-mannitol or ^{14}C-mannitol (PerkinElmer, Cleveland, OH, USA) are commonly used permeation markers [23]; a test solution with a concentration of 2.5 μCi/mL is used to allow for sufficient detectability in the samples generated from the permeation experiments [10]. For scintillation counting, a scintillation fluid such as Ultima Gold (PerkinElmer, Cleveland, OH, USA) is needed.

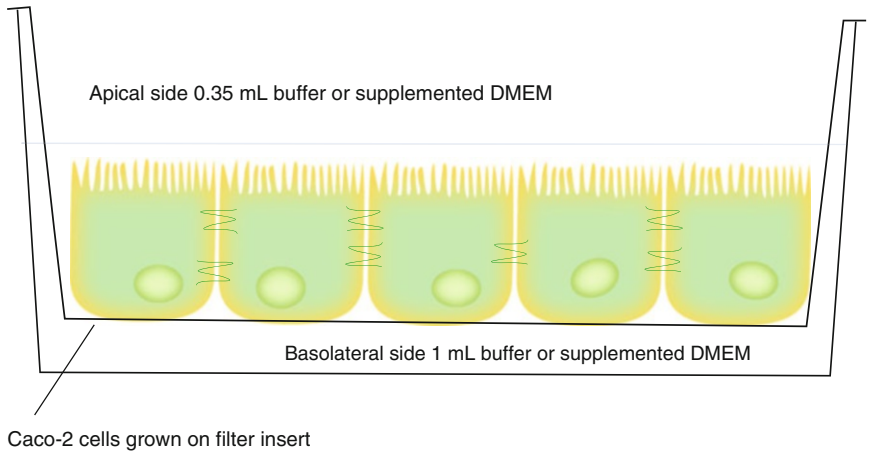

Fig. 2 Illustration of Caco-2 cells grown on filter inserts

3. Cell viability: Prepare MTS and PMS stock solutions as described in Subheading 2.1.
4. 10 mM HEPES HBSS buffer: Prepare buffer as described in Subheading 2.1.

2.3 Components for Biosimilar Mucus

1. 10 mM HEPES buffer: Weigh 1.191 g HEPES and dissolve in 450 mL ultrapure water. Adjust pH to 7.4 and add ultrapure water to a final volume of 500 mL.
2. Isotonic 10 mM HEPES buffer (*see* **Note 7**): Final concentrations are 137 mM NaCl, 1.3 mM $CaCl_2$, and 1 mM $MgSO_4$. Weigh 73.8 mg $MgSO_4 \cdot 7H_2O$, 43.2 mg $CaCl_2$ and 1.7 g NaCl and dissolve in 181.3 mL 10 mM HEPES buffer. Adjust pH to 7.4 with low amounts of 5 M NaOH. Check the osmolality (300 ± 20 mOsmol/kg).
3. 10 mM HEPES mucus buffer: Weigh off 7.2 mg $CaCl_2$ and 12.3 mg $MgSO_4 \cdot 7H_2O$ and dissolve in 30.5 mL 10 mM HEPES buffer. Adjust pH to 7.4 with low amounts of 5 M NaOH.
4. Mucus preparation (total 2 mL): Final concentrations are 9 mg/mL poly(acrylic acid) (PAA), 50 mg/mL mucin, and 6.5 mg/mL lipid (cholesterol and phosphatidylcholine (PC)). For the lipid solution, weigh off 5.4 mg PC and 10.8 mg cholesterol. Add 10 μL polysorbate 80 and 273.8 μL isotonic 10 mM HEPES buffer to the lipid solution and stir for a few minutes. In a separate container, weigh 18 mg PAA and dissolve in 1.8 mL 10 mM HEPES mucus buffer by stirring for 5–10 min. Add 100 mg mucin and continue stirring. Add bovine serum albumin (BSA) and stir gently until dissolved. Finally, add 200 μL of the lipid solution and mix by stirring gently. Adjust pH to 7.4 with low amounts of 5 M NaOH. Check the osmolality (300 ± 20 mOsmol/kg) and store in the fridge overnight.
5. 10 mM HEPES HBSS buffer: As described in Subheading 2.1.

2.4 Components for Metabolic Degradation

1. Cell culturing: Prior to the experiment, culture and seed the Caco-2 cells onto filter inserts as previously described in Subheading 2.1.
2. Buffer: Prepare the cell compatible buffer as previously described in Subheading 2.1.

3 Methods

3.1 Production and Characterization of CPP–Cargo Sample

For CPP-mediated transepithelial delivery of cargo, the CPPs are either co-administered with the cargo or directly conjugated to the cargo [6, 24]. In addition to the specific delivery strategy, the preparation of such carrier systems for evaluation in in vitro models

includes many aspects of the production process and the desired properties of the drug delivery system that needs to be taken into account such as the molar ratio between CPP and cargo, concentration, pH, osmolality, size, stability, charge, effect on cell viability and of course biological activity of the cargo and cell-penetrating propensity of the CPP. Conjugation between a CPP and a cargo requires methodological development outside the scope of this chapter. Complexation between cargo and CPP is based on electrostatic and/or hydrophobic interactions between the molecules, and isothermal titration calorimetry (ITC) is therefore a suitable method to evaluate at which ratio the desired interaction between the two components occurs. Preparation of the complexes is done in several ways, primarily using bulk mixing where the total volumes of cargo and CPP solutions are mixed in a one-step process at room temperature or the CPP solution is added dropwise to the drug solution; both methods using magnetic stirring in the range of 300 rpm. In this step, carefully monitoring the pH is essential to obtain the desired molecular interaction. Moreover, the effect of temperature during complex formation can be evaluated [25].

Once having prepared the CPP–cargo sample, the complex formation needs to be confirmed. This can be done in several ways. Native polyacrylamide gel electrophoresis (PAGE) is a simple and efficient method to confirm complex formation. Moreover, the zeta potential of complexes in solution can be used. Depending on the size of the formed complexes, changes in an X-ray diffraction pattern is a strong method to confirm complex formation. As previously described, it is important to continuously monitor pH. In this context, it is relevant to consider if the apparent pI of the drug molecule may be different once complexed. This can be assessed by a pH titration of the zeta potential from high to low pH and vice versa, with subsequent calculation of an average pI. Another important aspect is to quantify the size of the formed complex. If using dynamic light scattering for this purpose, size measurements can be very challenging due to the often high polydispersity observed in the samples. A first step to obtain more homogenous samples and good size distribution data is to filter the buffers before use, spin down the largest aggregates prior to measurements, and spend time on analytical method optimization by evaluation of whether backward or forward scattering is the most appropriate method. Also, the data fitting method and considerations regarding the use of number distribution for comparison instead of average size (both volume and intensity), which is often biased due to the high polydispersity in the sample, should be carefully evaluated. Last, high-throughput screening of the cell viability on proliferating cells cultured in 96-well plates is a useful method to indicate the relevant concentrations of the test solutions to be used for permeation and degradation studies (Subheadings 3.2 and 3.4) [26].

The MTS/PMS (*see* **Note 8**) assay (also described for cells grown on filter inserts in Subheading 3.2) could be as follows:

1. On the day of experiment, pre-warm buffer and test solutions to 37 °C.
2. Check pH and osmolality of test solutions (300 ± 20 mOsmol/kg).
3. Remove the cell culturing plates from the incubator. Note cell type, passage number (*see* **Notes 2** and **6**), seeding date and time.
4. Carefully remove growth medium from the wells by suction or inverting the plates.
5. Add relevant dilution series of the test substances in triplicate (*see* **Note 10**).
6. Add references (*see* **Notes 11** and **12**).
7. Incubate the cells at 37 °C with gentle shaking (50 rpm) with orbital movements (Fig. 3).
8. After incubation, wash the cells carefully twice using 200 µL 10 mM HEPES HBSS, pH 7.4.
9. Prepare the MTS/PMS solution immediately before use. For 96 wells: 1200 µL MTS, 24 µL PMS, and 8.776 µL 10 mM HEPES HBSS buffer.
10. Add 100 µL MTS/PMS solution to each well, incubate and protect from light until sufficient color development (1.5–3 h) (*see* **Note 8**).

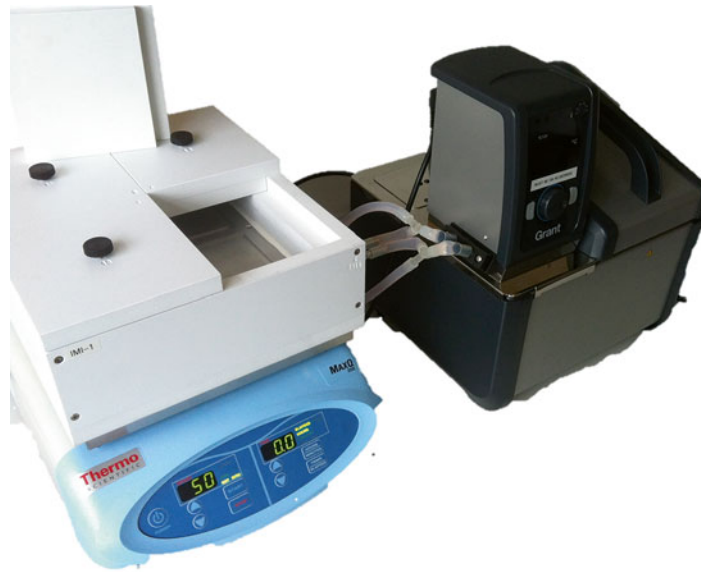

Fig. 3 On-site-constructed incubator on a temperated shaking board

11. To quantify the cell viability, measure the plates using absorbance (492 nm) on a plate reader.
12. Calculate the cell viability as follows: The dehydrogenase activity in untreated cells (A_{ref}) is set to 100 % and the relative cell viability (cytotoxicity) for cells incubated with test components (A_{test}) is calculated as a percentage hereof: %Viability = $(A_{test} - A_{0.2\%SDS})/(A_{ref} - A_{0.2\%SDS}) \times 100$ (*see* **Note 12**).

3.2 Permeation and Cell Viability Assessment in the Caco-2 Cell Culture Model

1. On the day prior to the experiment, prepare vials, buffer, etc. (*see* **Notes 11** and **13**).
2. On the day of the experiment, pre-warm 10 mM HEPES HBSS buffer, pH 7.4, and test solutions to 37 °C.
3. Check pH and osmolality of test solutions (300 ± 20 mOsmol/kg).
4. Remove cell culturing plates from the incubator. Note cell type, passage number (*see* **Notes 2** and **6**), and seeding date.
5. Carefully remove growth medium from the wells and filter inserts by suction; first from basolateral then from apical side of the filter insert (*see* **Note 14**).
6. Wash both sides of the monolayer twice in 37 °C warm buffer (500 μL apical and 1000 μL basolateral) and leave to equilibrate in 10 mM HEPES HBSS buffer for 15 min at room temperature.
7. In the meantime, prepare another set of 12-well plate(s) (without filter inserts) by adding 1100 μL buffer to each well (*see* **Note 15**) and equilibrate to 37 °C.
8. Measure the transepithelial electrical resistance $(TEER)_{before}$ (*see* **Note 16**) of the monolayer of each of the filter inserts (*see* **Note 17**) at room temperature (*see* **Note 18**) and note in a scheme along with the value of a cell-free filter insert.
9. Remove buffer solution from cell monolayers by suction; first from the basolateral side then from the apical side.
10. Add 370 μL test solution to the apical compartment. Immediately collect 20 μL donor test solution ($t = 0$ min) from the apical compartment in order to later calculate the initial donor concentration and determine the final mass balance (*see* **step 14**).
11. Add reference samples (*see* **Notes 9, 11, 12,** and **19**).
12. Start the experiment by transferring the filter inserts to the new 12-well plates (containing 1100 μL buffer). Place the cells in an incubator (37 °C) with mechanical shaking (50 rpm) (Fig. 3). Collect test samples of 100 μL from the basolateral side at timepoints 0, 15, 30, 45, 60, 90, 120, 150, 180, 210, and 240 min. Add 100 μL pre-warmed buffer to the basolateral side every time a sample has been collected (except the 0 min sample).

13. For scintillation measurements, add 2 mL Ultima Gold per sample vial and briefly vortex to obtain a clear sample before placing the vials in the scintillation counter.
14. At 240 min take 20 μL from the apical side (donor), in addition to the basolateral sample, to determine the mass balance after the experiment calculated as follows: $((C_{\text{final apical}} \times 0.35\ \text{mL} + C_{\text{final basolateral}} \times 1000\ \text{mL})/C_{\text{sample}} \times 0.35\ \text{mL}) \times 100\ \%$, where $C_{\text{final apical}}$ is the concentration (mg/mL) in the sample from the apical side after 240 min incubation, $C_{\text{final basolateral}}$ is the concentration in the sample from the basolateral side after 240 min incubation (mg/mL) and C_{sample} is the concentration of the applied sample. Remember to correct for the different volumes withdrawn when calculating the concentrations (C). All concentrations are corrected for the volume to obtain a total amount of drug permeated. The amount of test compound in the cells and filter insert can be determined and included in the mass balance calculation.
15. For scintillation measurements, use 3×100 μL buffer for background subtraction.
16. After collection of the last samples, wash both sides of the monolayer twice in 37 °C buffer (500 μL apical and 1000 μL basolateral) and leave to equilibrate in 10 mM HEPES HBSS buffer for 15 min at room temperature.
17. Measure $\text{TEER}_{\text{after}}$ for each well at room temperature. Note in scheme. Correct the measured value for the area of the filter insert by multiplying the measured value with the filter area and calculate the relative TEER as compared to control by: $((\text{TEER}_{\text{sample after}}/\text{TEER}_{\text{sample before}})/(\text{TEER}_{\text{buffer after}}/\text{TEER}_{\text{buffer before}})) \times 100$.
18. Prepare the MTS/PMS solution immediately before use (for 12 filter inserts: 600 μL MTS, 12 μL PMS, and 4388 μL 10 mM HEPES HBSS buffer).
13. Remove buffer. Add 320 μL MTS/PMS solution on the apical side of the cell monolayer and 1 mL 10 mM HEPES HBSS buffer on the basolateral side, incubate and protect from light until sufficient color development (1.5–3 h) (*see* **Note 8**).
19. When reaching sufficient color development, take 2×100 μL samples from the apical side of each well and transfer it to a 96-well plate (1 well per 100 μL).
20. Measure the absorbance (492 nm) using a plate reader.
21. From the permeation data, the flux ($\mathrm{d}Q/\mathrm{d}t$) of a test substance through a cell monolayer is determined under sink conditions, and can be used to calculate the apparent permeability coefficient (P_{app}). P_{app} is calculated as follows: $P_{\text{app}} = (\mathrm{d}Q/\mathrm{d}t)\ (1/AC_0)$ (cm/s), where A is the surface area of the monolayer (the filter insert area) and C_0 is the initial concentration on the

apical side of the monolayer given in amount/mL. Remember to include correction factors for, e.g. min to sec.

22. Cell viability is calculated as follows: The dehydrogenase activity in cells exposed to 10 mM HEPES HBSS, pH 7.4, used for the samples (A_{ref}) is set to 100 % and the relative cell viability (indicative of cytotoxicity) for cells incubated with test components in the same buffer (A_{test}) is calculated as a percentage hereof subtracting the value obtained for the positive control ($A_{0.2\%SDS}$): $\%Viability = (A_{test} - A_{0.2\%SDS})/(A_{ref} - A_{0.2\%SDS}) \times 100$ (*see* **Notes 11** and **12**).

3.3 Permeation Across the Caco-2 Cell Culture Epithelium Supplemented with Biosimilar Mucus

1. Prepare the biosimilar mucus a day in advance as described in Subheading 2.3.
2. Pre-warm buffers and test solutions to 37 °C.
3. Remove cell culturing plates from incubator. Note cell type, passage number (*see* **Note 21**), and seeding date.
4. Carefully remove growth medium from the wells and filter inserts (*see* **Note 15**).
5. Wash both sides of the monolayer twice in 37 °C warm buffer (500 μL apical and 1000 μL basolateral) and leave to equilibrate in 10 mM HEPES HBSS buffer for 15 min at room temperature.
6. Add 1100 μL 10 mM HEPES HBSS buffer to each well of new 12-well plates and equilibrate to 37 °C.
7. Measure $TEER_{before}$ (*see* **Notes 16–18**) for each of the filter inserts.
8. Remove the buffer on the apical side of the cell monolayer. Add 250 μL biosimilar mucus or 10 mM HEPES HBSS buffer (as a reference) to the apical compartment and equilibrate to 37 °C in the incubator (50 rpm) for 15 min (Fig. 3).
9. Add 120 μL of test solution to the apical side and immediately collect 20 μL donor test solution ($t = 0$ min) from the apical compartment in order to later calculate the initial donor concentration and determine the final mass balance (*see* **step 13**).
10. Add references (*see* **Notes 9, 11, 12** and **19**).
11. Start the experiments by transferring the filter inserts to the 12-well plates containing pre-warmed 10 mM HEPES HBSS buffer. Place them in the incubator (50 rpm, 37 °C).
12. Collect test samples of 100 μL from the basolateral side at timepoints 0, 15, 30, 45, 60, 90, 120, 150, 180, 210, and 240 min. Replenish with 100 μL pre-warmed 10 mM HEPES HBSS buffer every time a sample is collected (except for the 0 min sample).
13. When reaching time point 240 min withdraw 20 μL from the apical side (donor), in addition to the basolateral sample,

to determine the final mass balance calculated as follows: $((C_{\text{final apical}} \times 0.35 \text{ mL} + C_{\text{final basolateral}} \times 1000 \text{ mL})/C_{\text{sample}} \times 0.35 \text{ mL}) \times 100$ %, where $C_{\text{final apical}}$ is the concentration (mg/mL) in the sample from the apical side after 240 min incubation, $C_{\text{final basolateral}}$ is the concentration in the sample from the basolateral side after 240 min incubation (mg/mL) and C_{sample} is the concentration of the applied sample. All concentrations are corrected for the volume to obtain a total amount. Remember to correct for the different volumes withdrawn when calculating the concentrations (C). The amount of test compound in the cells and filter insert can be determined and included in the mass balance calculation.

14. For scintillation measurements, use 3×100 µL 10 mM HEPES HBSS buffer for background subtraction.
15. After collecting the last samples, wash both sides of the monolayer twice in 37 °C warm buffer (500 µL apical and 1000 µL basolateral) and leave to equilibrate in 10 mM HEPES HBSS buffer for 15 min at room temperature.
16. Measure $\text{TEER}_{\text{after}}$ for each filter insert at room temperature. Note in scheme. Calculate relative TEER as compared to control by: $((\text{TEER}_{\text{sample after}}/\text{TEER}_{\text{sample before}})/(\text{TEER}_{\text{buffer after}}/\text{TEER}_{\text{buffer before}})) \times 100$ (*see* **Notes 11** and **12**).
17. Prepare the MTS/PMS solution immediately before use (for 12 filter inserts: 600 µL MTS, 12 µL PMS, and 4388 µL 10 mM HEPES HBSS buffer).
18. Remove buffer. Add 320 µL MTS/PMS solution on the apical side of the cell monolayer and 1 mL 10 mM HEPES HBSS buffer on the basolateral side, incubate and protect from light until sufficient color development (1.5–3 h) (*see* **Note 8**).
19. Take 2×100 µL from the apical side of each well and transfer it to a 96-well plate (100 µL per well).
20. Measure the absorbance (492 nm) using a plate reader.
21. From the permeation data, the flux ($\mathrm{d}Q/\mathrm{d}t$) of a test substance through a cell monolayer is determined under sink conditions, and can be used to calculate the apparent permeability coefficient (P_{app}). P_{app} is calculated as follows: $P_{\text{app}} = (\mathrm{d}Q/\mathrm{d}t)(1/AC_0)$ (cm/s), where A is the surface area of the monolayer (the area of the filter insert) and C_0 is the initial concentration on the apical side of the monolayer (*see* **Note 20**).
22. Calculate cell viability as follows: The dehydrogenase activity in untreated cells (A_{ref}) is set to 100 % and the relative cell viability (cytotoxicity) for cells incubated with test components (A_{test}) is calculated as a percentage hereof subtracting the value obtained for the positive control ($A_{0.2\%\text{SDS}}$): $\%\text{Viability} = (A_{\text{test}} - A_{0.2\%\text{SDS}})/(A_{\text{ref}} - A_{0.2\%\text{SDS}}) \times 100$ (*see* **Notes 11** and **12**).

3.4 Metabolic Degradation

Several methodologies are available for studying the chemical stability of CPPs during in vitro experiments. These count incubation of the CPP in buffer with or without relevant enzymes or enzyme mixtures [27], incubation with biological or biosimilar fluids [20], or incubation with the CPPs exposed to the apical side of the epithelial cell culture model of interest. A protocol for the latter (adapted from Tréhin et al. [28]) follows:

1. Pre-warm buffer and test solutions to 37 °C.
2. Remove cells from the incubator. Note cell type, passage number (*see* **Note 6**), and seeding date.
3. Remove growth medium from the wells and filter inserts (*see* **Note 14**).
4. Wash both sides of the monolayer twice in 37 °C warm buffer (500 μL apical and 1000 μL basolateral) and leave to equilibrate in 10 mM HEPES HBSS buffer for 15 min at room temperature.
5. Measure TEER of each filter insert (*see* **Note 21**)[v, vi], and of an empty filter insert for background correction.
6. Equilibrate to 37 °C in the incubator (50 rpm) for 15 min (Fig. 3).
7. Place the inserts on the bottom of empty 6-well polystyrene plates (*see* **Note 22**).
8. Remove the buffer and start the experiment by adding up to 800 μL test solution.
9. 50 μL samples are drawn after 15 min followed by every 30 min for 4 h (0, 15, 30, 60, 90, 120, 150, 180, 210, and 240 min) in ice-cold HPLC vials added 5 μL 1 % (v/v) formic acid in methanol to stop further enzymatic reactions.
10. Evaluate the kinetics of the metabolic degradation of the test compounds by RP-HPLC (*see* **Note 23**) and analyze the data according to the relevant order kinetics. For first-order and pseudo-first-order kinetics, calculate the half-lives ($t_{1/2}$) as follows: $t_{1/2}$: $\ln(2)/[\mathrm{d}(\log C)/\mathrm{d}t]$.

4 Notes

1. For the cells to produce mucus, they must be stimulated to do so [29].
2. The seeding concentration varies with cell line, passage number, and growth medium used. For Caco-2 cells, a standard seeding concentration is in the range of 9000 cells/well.
3. The commonly used buffer for such experiments is 10 mM HEPES HBSS adjusted to pH 7.4. However, Tippin and

Thakker [30] evaluated a biorelevant refinement in which the HEPES buffer was exchanged with fasted-state simulated intestinal fluid (FaSSIF). Using FaSSIF compared to HEPES buffer will especially alter the permeation of amphiphilic drugs. Moreover, the increased lipid content caused by FaSSIF compared to HEPES is likely to, if applying lipid-based drug delivery systems or carriers, decrease the cell viability after 4 h of incubation (unpublished results).

4. 10 mM is recommended as the standard MES or HEPES buffer concentration. If increased buffer capacity is required, the concentration can be increased up to 25 mM. If doing so, it is, however, essential to test the effect on the cell viability and on the TEER prior to the experiment.
5. As it is a biocompatible buffer subjected to fluctuating temperatures, bacterial growth may occur. Therefore, always visually inspect the buffer prior to use.
6. The TEER across a cell monolayer is known to vary with cell passage number hence permeability, sucrase activity, alkaline phosphatase activity, and also growth behavior together with morphology may likely vary with passage number [31]. Thus, it is of outmost importance to monitor cell characteristics during growth and differentiation, and also repeat experiments over several passages.
7. Final concentrations of NaCl (137 mM), $CaCl_2$ (1.3 mM), and $MgSO_4$ (1 mM) are similar to those of the physiological HBSS buffer.
8. The aim of the MTS/PMS assay is to measure cell viability. In living cells, the MTS is reduced to a formazan product by mitochondrial reductase enzymes. Thus, as the colored formazan product is directly related to cell viability, viability is quantified by measuring the absorbance of this product.
9. Another barrier in the permeability model that needs to be considered upon designing the experiment is the barrier formed by the filter insert material. The barrier properties are mainly related to two parameters being the pore size of the filter insert and the material itself. Adsorption of drug and permeation enhancers to the filter insert and plastic ware (*see* **Note 24**) should be avoided if possible. To evaluate the influence on those parameters on the experiment, it is important to include the relevant controls such as diffusion of the permeation marker and carrier across filter inserts without cells, and cell monolayers incubated with buffer only.
10. The dilution series can either be prepared in 10 mM HEPES HBSS pH 7.4 or supplemented DMEM, depending on the incubation time. Once removed from the incubator, the

supplemented DMEM medium does not provide sufficient buffer capacity. It is therefore suggested that for incubation in a normal atmosphere for longer than 1 h, 10 mM HEPES HBSS buffer is used instead. Moreover, the supplemented DMEM medium is known to induce a lower solubility of various compounds due to high ion content and complexating compounds (HBSS also has this tendency, but to a less extent), hence facilitating unwanted precipitation of the test compounds.

11. Once overcoming the cell monolayer (and mucus), the permeated amount of drug or permeation marker needs to be quantified. CPPs are often used in low concentrations (hence low drug concentration) to reduce the risk of cytotoxicity, requiring sensitive quantification assays such as enzyme-linked immunosorbent assay (ELISA). Radioactive tracers such as ^{3}H or ^{14}C coupled to, e.g. mannitol or FITC-labeled proteins are also commonly used [10]. Fluorophore labeling is, however, likely to affect the cell-penetrating propensity of the CPP [32] due to changed physicochemical properties. Alternatively, both HPLC and LC-MS are useful quantification methods for detection of the drug; the latter especially to detect degradation products of the components used.
12. Sodium dodecyl sulfate (SDS) is a commonly used reference known to be toxic to proliferating cells when at a concentration of 0.2% (w/v). When working with biological material, e.g. cell viability assays, it is useful to always include an SDS dilution series as an internal standard to allow for comparison between experiments and cell passage numbers. In addition to the SDS, the potential variation caused by manual seeding of the cells must be considered. For this purpose, a row of cells incubated with buffer or supplemented DMEM medium must be included. Generally, all test solutions are tested in triplicate.
13. If suitable for analysis by e.g. HPLC, add 5 μL 1 % (v/v) formic acid in methanol to stop further enzymatic reactions.
14. To avoid the cells from being pushed off the filter insert by the liquid, it is important never to have liquid only on the basolateral side. Therefore, when removing the liquid, the medium on the basolateral side must be removed first followed by the apical side. When applying cell medium, always add to the apical side first followed by addition to the basolateral side.
15. The reason for using new plates is that the ones used during the 21-day growth period most likely are contaminated with proteins and other unwanted components from the cell culturing medium.
16. Be aware that TEER of the monolayers differs depending on supplier (e.g. ATCC vs. DSMZ), passage number, and general culturing and handling conditions.

17. It is observed in literature that some research groups measure TEER in the cell medium (DMEM) before transport. This approach is relevant if the purpose of TEER measurement is purely evaluation of the cell monolayer integrity prior to the experiment. When studying permeation, it is often relevant to measure TEER both before and after incubation with the test substance in order to evaluate to which extent the test substance affects the tight junctions, hence the potential permeation pathway for the test compound. To obtain the best possible comparison in this case, TEER should be measured in the buffer used for the experiment, e.g. 10 mM HEPES HBSS pH 7.4 both before and after incubation. Moreover, TEER of the filter insert is measured for background correction.
18. If the TEER is unstable upon measurement, the temperature of the medium is most likely not equilibrated. If so, allow the cells to equilibrate further before measuring.
19. Remember to include untreated cells as a reference for 100 % viability and also for relative TEER values. The cells are incubated with 10 mM HEPES HBSS buffer during the experiment, and subjected to the same number of washes, etc., in order to apply the same degree of stress to all cells.
20. As previously discussed, not only the cell monolayer constitutes a permeation barrier for the test substance, also the filter on which the cells are grown induces barrier properties. Thus, the permeability coefficient of the porous filter (P_f) can be derived from P_{app}. $1/P_{app}$ describes the apparent resistance to drug absorption (R_{app}) of the various barriers in the described experiment, as $R_{app} = 1/P_{app} = 1/P_f + 1/P_c + 1/P_{aq}$, where P_c equals the permeability coefficient of the cell monolayer and P_{aq} is combined permeability coefficients of the unstirred water layers in the model, which in some cases include the mucus layer.
21. The purpose of measuring TEER in the described experiment is solely to validate the integrity of the cell monolayer as opposed to when studying permeation (*see* **Note 6**).
22. Filter inserts are placed on the bottom of empty polystyrene 6-well plates in order to limit permeation across the monolayer, thus ensuring accumulation of the metabolites in the apical donor compartment.
23. Ensure the concentrations of the test solutions applied are within the limit of detection by running standard curves prior to experimental start.
24. 0.05 % (w/v) BSA can be added to the buffer to prevent adsorption to plastic ware.

Acknowledgements

María García-Díaz is acknowledged for supplying the protocols for the mucus preparation and the permeation study using Caco-2 cell monolayers supplemented with biosimilar mucus. The research leading to these results has received support from the Innovative Medicines Initiative Joint Undertaking under grant agreement no. 115363 resources which are composed of financial contribution from the European Union's Seventh Framework Programme (FP7/2007–2013) and EFPIA companies' in kind contribution. Additionally, the work was financially supported by the Drug Research Academy (University of Copenhagen), The Danish Agency for Science, Technology & Innovation, and the Novo Nordisk Foundation Center for Protein Research.

References

1. Stewart KM, Horton KL, Kelley SO (2008) Cell-penetrating peptides as delivery vehicles for biology and medicine. Org Biomol Chem 6:2242–2255
2. Lindgren M, Rosenthal-Aizman K, Saar K, Eiríksdóttir E, Jiang Y, Sassian M, Ostlund P, Hällbrink M, Langel U (2006) Overcoming methotrexate resistance in breast cancer tumour cells by the use of a new cell-penetrating peptide. Biochem Pharmacol 71:416–425
3. Margus H, Padari K, Pooga M (2012) Cell-penetrating peptides as versatile vehicles for oligonucleotide delivery. Mol Ther 20:525–533
4. Morris MC, Depollier J, Mery J, Heitz F, Divita G (2001) A peptide carrier for the delivery of biologically active proteins into mammalian cells. Nat Biotechnol 19:1173–1176
5. Khafagy E-S, Kamei N, Nielsen EJB, Nishio R, Takeda-Morishita M (2013) One-month subchronic toxicity study of cell-penetrating peptides for insulin nasal delivery in rats. Eur J Pharm Biopharm 85:736–743
6. Khafagy E-S, Morishita M (2012) Oral biodrug delivery using cell-penetrating peptide. Adv Drug Deliv Rev 64:531–539
7. Kamei N, Morishita M, Eda Y, Ida N, Nishio R, Takayama K (2008) Usefulness of cell-penetrating peptides to improve intestinal insulin absorption. J Control Release 132:21–25
8. Liang JF, Yang VC (2005) Insulin-cell penetrating peptide hybrids with improved intestinal absorption efficiency. Biochem Biophys Res Commun 335:734–738
9. Artursson P, Palm K, Luthman K (1996) Caco-2 monolayers in experimental and theoretical predictions of drug transport. Adv Drug Deliv Rev 22:67–84
10. Boegh M, Baldursdóttir SG, Müllertz A, Nielsen HM (2014) Property profiling of biosimilar mucus in a novel mucus-containing in vitro model for assessment of intestinal drug absorption. Eur J Pharm Biopharm 87:227–235
11. Boegh M, Baldursdottir SG, Nielsen MH, Müllertz A, Nielsen HM (2013) Development and rheological profiling of biosimilar mucus. Annu Trans Nord Rheol Soc 21:233–240
12. Hilgendorf C, Spahn-Langguth H, Regårdh CG, Lipka E, Amidon GL, Langguth P (2000) Caco-2 versus Caco-2/HT29-MTX co-cultured cell lines: permeabilities via diffusion, inside- and outside-directed carrier-mediated transport. J Pharm Sci 89:63–75
13. Hämäläinen MD, Frostell-Karlsson A (2004) Predicting the intestinal absorption potential of hits and leads. Drug Discov Today Technol 1:397–405
14. Antunes F, Andrade F, Ferreira D, Nielsen HM, Sarmento B (2013) Models to predict intestinal absorption of therapeutic peptides and proteins. Curr Drug Metab 14:4–20
15. Irvine JD, Takahashi L, Lockhardt K, Cheong J, Tolan JW, Selick HE, Grove JR (1999) MDCK (Madin – Darby Canine Kidney) cells: a tool for membrane permeability screening. J Pharm Sci 88:28–33
16. Forbes B (2000) Human airway epithelial cell lines for in vitro drug transport and metabolism studies. Pharm Sci Technol Today 3:18–27
17. Rupniak T, Rowlatt C, Lane EB, Steele JG, Trejdosiewicz LK, Laskiewicz B, Povey S, Hill BT (1985) Characteristics of four new human cell lines derived from squamous cell carcinomas of the head and neck. J Natl Cancer Inst 75:621–635

18. Prueksaritanont T, Gorham LM, Hochman JH, Tran LO, Vyas KP (1996) Comparative studies of drug-metabolizing enzymes in dog, monkey, and human small intestines, and in Caco-2 cells. Drug Metab Dispos 24:634–642
19. Elmquist A, Langel U (2003) In vitro uptake and stability study of pVEC and its all-D analog. Biol Chem 384:387–393
20. Nielsen EJB, Yoshida S, Kamei N, Iwamae R, Khafagy e-S, Olsen J, Rahbek UL, Pedersen BL, Takayama K, Takeda-Morishita M (2014) In vivo proof of concept of oral insulin delivery based on a co-administration strategy with the cell-penetrating peptide penetratin. J Control Release 189:19–24
21. Rennert R, Wespe C, Beck-Sickinger AG, Neundorf I (2006) Developing novel hCT derived cell-penetrating peptides with improved metabolic stability. Biochim Biophys Acta 1758:347–354
22. Horne WS, Gellman SH (2008) Foldamers with heterogeneous backbones. Acc Chem Res 41:1399–1408
23. Pantzar N, Lundin S, Wester L, Weström BR (1994) Bidirectional small-intestine permeability in the rat to some common marker molecules in vitro. Scan J Gastroenterol 8:703–709
24. Kristensen M, Foged C, Berthelsen J, Nielsen HM (2013) Peptide-enhanced oral delivery of therapeutic peptides and proteins. J Drug Del Sci Tech 23:365–373
25. Kasimova MR, Velázquez-Campoy A, Nielsen HM (2011) On the temperature dependence of complex formation between chitosan and proteins. Biomacromolecules 12:2534–2543
26. Eirheim HU, Bundgaard C, Nielsen HM (2004) Evaluation of different toxicity assays applied to proliferating cells and to stratified epithelium in relation to permeability enhancement with glycocholate. Toxicil In Vitro 18:649–657
27. Zhu X, Shan W, Zhang P, Jin Y, Guan S, Fan T, Yang Y, Zhou Z, Huang Y (2014) Penetratin derivative-based nanocomplexes for enhanced intestinal insulin delivery. Mol Pharm 11:317–328
28. Tréhin R, Nielsen HM, Jahnke H-G, Krauss U, Beck-Sickinger AG, Merkle HP (2004) Metabolic cleavage of cell-penetrating peptides in contact with epithelial models: human calcitonin (hCT)-derived peptides, Tat(47-57) and penetratin(43-58). Biochem J 382:945–956
29. Navabi N, McGuckin MA, Lindén SK (2013) Gastrointestinal cell lines form polarized epithelia with and adherent mucus layer when cultured in semi-wet interfaces with mechanical stimulation. PLoS One 8:e68761
30. Tippin TK, Thakker DR (2008) Biorelevant refinement of the Caco-2 cell culture model to assess efficacy of paracellular permeability enhancers. J Pharm Sci 97:1977–1993
31. Briske-Anderson MJ, Finley JW, Newman SM (1997) The influence of culture time and passage number on the morphological and physiological development of Caco-2 cells. Proc Soc for Exp Biol Med 214:248–257
32. Hirose H, Takeuchi T, Osakada H, Pujals S, Katayama S, Nakase I, Kobayashi S, Haraguchi T, Futaki S (2012) Transient focal membrane deformation induced by arginine-rich peptides leads to their direct penetration into cells. Mol Ther 20:1–10

Chapter 18

A Pathway Toward Tumor Cell-Selective CPPs?

Isabel D. Alves, Manon Carré, and Solange Lavielle

Abstract

Despite the great potential of CPPs in therapeutics and diagnosis, their application still suffers from a non-negligible drawback: a complete lack of cell-type specificity. In the innumerous routes proposed for CPP cell entry there is common agreement that electrostatic interactions between cationic CPPs and anionic components in membranes, including lipids and glycosaminoglycans, play a crucial role. Tumor cells have been shown to overexpress certain glycosaminoglycans at the cell membrane surface and to possess a higher amount of anionic lipids in their outer leaflet when compared with healthy cells. Such molecules confer tumor cell membranes an enhanced anionic character, a property that could be exploited by CPPs to preferentially target these cells. Herein, these aspects are discussed in an attempt to confer CPPs certain selectivity toward cancer cells.

Key words Tumor-homing CPP, Anticancer efficacy, Peptide/lipid interaction, Mitochondrial network organization, Mitochondrial membrane permeability, Electrostatic interaction

1 Introduction

CPPs have proven highly efficient molecules for the delivery of a large variety of cargos and thus present great potential in diagnosis and therapeutic applications. Although highly efficient in mediating cellular uptake of different molecules into several cell lines, the use of CPPs remains hampered by the lack of cell-type specificity.

In what concerns their uptake mechanism, both endocytotic pathways and membrane translocation mechanisms have been evoked as possible entry routes for CPPs and their transported cargoes. Despite the route(s) taken, there is common agreement regarding the importance of electrostatic interactions in cell membrane recognition by CPPs. Most CPPs share the property of being cationic including in their primary sequence residues such as lysine or arginine. As for the cell membranes, two classes of molecules should be considered as potential CPPs targets: lipids and carbohydrates, as CPPs do not act by specific membrane receptors.

Ülo Langel (ed.), *Cell-Penetrating Peptides: Methods and Protocols*, Methods in Molecular Biology, vol. 1324,
DOI 10.1007/978-1-4939-2806-4_18,

Cell surface carbohydrates, due to their carboxyl and sulfate moieties, strongly contribute to the cell membrane polyanionic character. They can act as recruiting platforms and have been called "electrostatic traps" for cationic molecules that are in close membrane vicinity. Indeed, glycosaminoglycans (GAGs) deletion from the cell membrane surface decreases and even abolishes CPPs cellular internalization [1–5]. Biophysical studies on model systems performed by Seelig and others also point to the importance of electrostatic interactions between GAGs and CPPs [6–8]. Heparan sulfate proteoglycan (HSPGs) expression is developmentally regulated and altered in various pathophysiological processes, including cancer. Recent studies have shown that tumor cells overexpress certain HSPGs such as glypicans and syndecans that are implicated in several tumorigenesis processes such as cell adhesion, growth, and motility [9–16].

As per the lipids, the eukaryotic plasma membrane is mainly composed of zwitterionic lipids (80–90 %) and the small amount of anionic lipids is mainly present (fourfold more) in the inner leaflet. During cancer development cellular membrane lipid composition is highly modified. Different types of cancer have been associated with particular and very unique lipid membrane composition, as described by lipidomic analysis [17]. One aspect that changes during cancer development, and ultimately during apoptosis, concerns the asymmetry of the lipid composition between external and internal leaflets. Indeed the asymmetry is lost due to the inhibition of aminophospholipid translocase and the activation of scramblase, responsible for the membrane flip-flop. This leads to an overall increase in phosphatidylserine (PS) at the membrane surface that can reach up to 9 % [18–23]. PS being anionic, contrarily to the major lipids in the membrane (zwitterionic), leads to a considerable increase in membrane surface charge. Lipid membranes of healthy and tumor cell membranes also differ in their fluidity that is substantially higher in tumor membranes due to the differences in the cholesterol to phospholipid ratio [24–26]. Yet another aspect that differs between tumor and healthy membranes is the larger surface area of tumor cell membranes by the microvillus. Overall, the greater surface and enhanced anionic character presented by tumor cell membranes relative to healthy ones may further favor the interaction of cationic CPPs with tumor membranes in spite of healthy ones. In addition, the higher fluidity of the tumor cell membrane may facilitate peptide action (perturbation, disorganization) on the membrane leading to its passage. Studies performed by our and other laboratories have shown that certain CPPs possess a stronger affinity and are more prone to interact and perturb model lipid membranes composed of anionic lipids than zwitterionic ones [27–36].

The approach described herein is to: (1) design CPPs with potential tumor cell selectivity, some successful sequences and hints

are provided based on reported studies; (2) to investigate whether peptides selectively affect tumor cell viability relative to healthy cells and to determine if they do so through perturbation of the mitochondrial network; (3) to determine if the enhanced anionic character of tumor cell outer leaflet could be among the factors contributing to their tumor cell selectivity.

The methods used to achieve the above-mentioned tasks are described below. First, attempts are made to provide some general clues that one may want to consider regarding CPP candidates possessing tumor cell targeting ability. Then, to establish whether the designed CPP has a selective activity on tumor cell lines, biological assays must be performed on both healthy and tumor cell lines. One of the first tests to be performed is the cytotoxic assay, to determine whether the peptide is effective to reduce the global cell population and to precise its spectrum of activity. In a second stage, the origin of this cytotoxicity related to the action mode of the peptide is investigated. They might exert their action by disrupting the cell plasma membrane (necrosis) or the mitochondrial membrane (apoptosis), by mechanisms of mediated immunity, through action of membrane receptors, by inhibition of DNA synthesis, by anti-angiogenic effects or any combination of those pathways (for a revue *see* [37]). Herein, we will treat how to investigate the membrane disruption (plasma and mitochondrial), by following the mitochondrial network organization and the mitochondrial membrane permeabilization with live fluorescence microscopy and flow cytometry, respectively, as well as by studying the properties of model lipid membranes using a biophysical approach.

2 Materials

2.1 Human Cells and Cell Culture Materials

1. Here is a non-exhaustive list of cancer cell lines that can be used: breast cancer cell lines MCF-7, SKBR3 and MDA-MB-231, glioblastoma cell lines U251 and U87-MG, neuroblastoma cell lines BE(2)-C, SHEP, SK-N-SH and IMR-32, colon cancer cell lines SW480 and HT29, non-small cell lung cancer cell line A549.
2. Non-cancer cells that can be used are, for example: embryonic kidney cells HEK-293t, keratinocytes HaCaT, microvascular endothelial cells HMEC-1, umbilical vein endothelial cells HUVECs, breast epithelial cell line HBL-100 or lung fibroblasts MRC-5.
3. Culture media (*see* **Note 1**): supplement with 10 % Fetal Calf Serum (FCS), 2 mM L-glutamine and 1 % penicillin streptomycin. Add also 1 μg/mL hydrocortisone and 10 ng/mL epithelial growth factor for HMEC-1 cells; 1 mM sodium pyruvate, 2 % sodium bicarbonate and 1 % non-essential amino acids for

MRC-5 cells; 1 % non-essential amino acids HEK-293t; 20 % heat-inactivated FCS, 2 mM glutamine, 1 % penicillin/streptomycin, 50 IU/mL sodium heparin, and 50 Ag/mL endothelial cell growth supplement for HUVECs. Store at 4 °C.

4. Sterile culture flasks (0.1 % gelatin-coated for HMEC-1) with vent caps that contain a 0.2 μm porous hydrophobic membrane.
5. Trypsine-EDTA 0.05 % ready to use solution (with or without phenol red).

2.2 Cytotoxicity Assays Components

1. Multi-well plates: transparent and opaque-walled sterile 96-well plates.
2. 3-(4,5-dimethylthiazol-2-yl)-2,5-diphenyltetrazolium bromide (MTT) solution: to be prepared from the (yellow) powder at 0.5 mg/mL in cell culture medium.
3. Alamar blue solution: 10× ready-to-use solution (from various commercial kits). You can also prepare it: weigh 75 mg resazurin, 12.5 mg methylene blue, 164.5 mg potassium hexacyanoferrate (III) and 253.2 mg potassium hexacyanoferrate (III) trihydrate. Dissolve them one by one in 500 mL of sterile PBS. Store aliquots of this stock solution in light-resistant plastic bottles at 4 °C.
4. High-quality, anhydrous dimethylsulfoxide (DMSO).

2.3 Components for the Live Fluorescent Microscopy of the Mitochondrial Network

1. Glass bottom culture dishes, such as LabTek Chambered Coverglass or MaTek glass bottom microwell dishes.
2. MitoTracker® Green FM or Red FM: store at −20 °C when in lyophilized solid form. Prepare the stock solution at 1 mM in DMSO, and store at −20 °C and protect from light. Dilute this stock solution to the final working concentration (50 mg/mL) in cell culture medium, and use it immediately after.
3. Phosphate buffered saline (PBS): dissolve one tablet in 200 or 500 mL (depending on the supplier) of deionized water to obtain 0.01 M phosphate buffer, 0.0027 M potassium chloride and 0.137 M sodium chloride, pH 7.4, at 25 °C.
4. Transparent sterile 6-well plates.
5. Lipofectamine 2000™ (Life Technologies).
6. Sterile geneticine solution at 100 mg/mL.
7. Plasmid encoding for mtDsRed or mtGFP.

2.4 Components for the Mitochondrial Membrane Potential Measure

1. 3,3′-Dihexyloxacarbocyanine Iodide (DIOC6(3)): store the powder at room temperature and protect from light. Prepare the stock solution at 10 μM in DMSO, and store at −20 °C.
2. Transparent sterile 6-well plates.
3. PBS: see above.

2.5 Studies with Lipid Model Systems

1. Lipids can be acquired from Avanti Lipids or Sigma.
2. Peptides can be synthesized by solid-phase peptide chemistry using either Fmoc or Boc strategy.
3. Tris–HCl buffer: 10 mM Tris–HCl, 0.1 M NaCl, 2 mM EDTA, pH 7.6.
4. Phosphate buffer: 10 mM, pH 7.6.
5. Calcein solution: 70 mM.
6. Size-exclusion chromatography columns (Sephadex G-75).
7. 10 % Triton X-100 solution.
8. D_2O.
9. Mini-extruder (Avanti, Alabaster, AL).
10. Nitrogen pressure-driven extruder (Lipex, Northern Lipids Inc, BC).
11. 100 nm polycarbonate membranes (Millipore).
12. Vortex.
13. Titanium rod-sonicator.
14. Jobin-Yvon CD6-SPEX.
15. Malvern SetaSizer Nano ZS.
16. Perkin Elmer LS55 spectrometer.
17. nano ITC (TA Instruments).
18. Differential Scanning Calorimeter (TA Instruments).
19. Nicolet 6700 FT6IR spectrometer.

3 Methods

3.1 The Choice of the CPP

There is no "recipe" provided here to turn a regular CPP into a tumor-selective one, rather some considerations are provided that could help in their design. The ideas arise from studies done by our own laboratory and from the scarce literature on this domain. Studies where CPPs are coupled to know tumor-homing peptides or protein cargoes will not be presented here. Considering the fact that CPPs and antimicrobial peptides (AMPs) share many properties namely cell penetrating ability [38], and that some AMPs have anticancer activity (for reviews *see* [37, 39]), some considerations are also taken from AMP sequences even though this book is dedicated to CPPs.

One may want to consider the use of a CPP alone, as it has been successfully done by Kondo and collaborators where they have used mRNA display technology to indentify a library of novel tumor-homing CPPs. They have synthesized 47 peptides and out of those 10 were shown to be preferentially uptaken by tumor cells in a lineage-dependent manner [40]. As seen in Table 1, all peptides are composed of 15 residues, all possess a positive net charge

Table 1
Examples of each class of peptides possessing anticancer activity: tumor lineage-homing CPP, CPP-apoptotic conjugate and AMPs

Peptide class	Peptide name	Amino acid sequence	Net charge	Secondary structure	Amphipathicity
Tumor lineage homing CPP	2	DSLKSYWYLQKFSWR	+2	nd	Partially[a]
	7	KLWMRWWSPTTRRYG	+3	nd	Partially[a]
	10	RLWMRWYSPWTRRWG	+4	nd	Partially[a]
	28	RLIMRIYAPTTRRYG	+4	nd	Partially[a]
	30	RLYMRYYSPTTRRYG	+4	nd	Partially[a]
	33	RLWMRWYSPRTRAYG	+4	nd	Partially[a]
	44	KRPTMRFRYTWNPMK	+5	nd	Partially[a]
	45	WKCRRQCFRVLHHWN	+6	nd	Partially[a]
	47	WKCRRQAFRVLHHWN	+6	nd	No[a]
	48	WKARRQCFRVLHHWN	+6	nd	Partially[a]
CPP-apoptotic cargo	Pen-KLA	$(KLAKLAK)_2$C-CRQIKIWFQNRRMKWKK	+13	α-helical[b]	Partially
AMP	BMAP-27	GRFKRFRKKFKKLFKKLSPVIPLLHL	+11	α-helical	Yes
	Cecropin A	KWKLFKKIEKVGQNIRDGIIKAGPAVAVVGQATQIAK	+6	α-helical	Yes
	LL37/hCAP-18	LLGDFFRKSKEKIGKEFKRIVQRIKDFLRNLVPRTES	+6	α-helical[b]	Yes
	Magainin 2	GIGKFLHSAKKFGKAFVGEIMNS	+4	α-helical	No
	HNPs-1	ACYCRIPACIAGERRYGTCIYQGRLWAFCC	+4	β-sheet	No
	Lactoferrin	FKCRRWQWRMKKLGAPSITCVRRAF	+8	β-sheet	Yes
	PR-39	RRRPRPPYLPRPRPPPFFPPRLPPRIPPGFPPRFPPRFP	+10	random	No

Note: this table is not exhaustive, just provides some examples from the literature
[a]When projected in a helical wheel, so assuming major α-helical structure
[b]α-helical under certain conditions such as higher concentrations or presence of ions or anionic lipids

(mostly +4) and contain hydrophobic residues (mostly Trp and Tyr). When projected in a helical wheel they all show partially amphipathic character.

One may also render a non-tumor-selective CPP, such as penetratin, selective toward tumor cell lines by coupling it to a proapoptotic peptide. Penetratin coupling to KLA (acetyl-$(KLAKLAK)_2$-NH_2) by a disulfide bond formed between two cysteine residues added to each peptide resulted in a conjugate that selectively reduced the cell growth of several tumor cell lines, even those resistant to conventional chemotherapy agents (Table 1) [41]. Once internalized, either the conjugate or KLA alone (as the disulfide bond might have been reduced once the conjugate is internalized, this point still needs to be clarified) act on the tumor target cell by disrupting the mitochondria network organization (formation of aggregates) in a rather fast manner (few minutes) starting at low μM concentrations.

As mentioned above, certain AMPs have reported anticancer activity and thus can be interesting anticancer candidates, especially for those that are totally non-cytotoxic. They can adopt a variety of secondary structures: α-helical like cecropin, magainin and melittin; β-sheet like defensins, lactoferrin; linear or hybrid and synthetic (Table 1) (*see* [42] for a revue) for a revue. Besides their variety in secondary structure profiles, their length, net charge and amphipathic character are properties that vary considerably among their sequence.

In terms of the general properties of the tumor-homing peptides discussed above, their highly cationic nature is probably the only remarkable common property observed among all sequences.

3.2 Cytotoxicity Assays

Cell-based assays are often used for high-throughput screening to determine if they have in vitro cytotoxic effects, via the inhibition of cell proliferation and/or induction of cell death. These assays can be used to investigate the cytotoxic activity of CPPs, CPP-proapoptotic peptide conjugates or AMPs in human cancer and non-cancer cells to determine their spectrum of activity. The promising peptides should be highly active in various tumor cells while safe for healthy ones, as shown for the Pen-KLA conjugate and tumor-homing CPPs developed by Kondo [40, 41]. The most common methods, developed for multi-well plates, use colorimetric tetrazolium or fluorescent resazurin reagents. They are all based on the difference between viable cells, which convert the substrate to product, and dying cells that have lost this ability. The signal produced is proportional to the number of viable cells.

The MTT colorimetric cell viability assay is carried out as follows:

1. Human cancer and non-cancer cells are seeded in transparent 96-well plates and allowed to adhere for 24 h in a cell incubator (37 °C and 5 % CO_2). For all cell lines, the number of cells in

wells has to be first optimized to ensure sustained exponential growth for 4–6 days. It generally ranges from 2000 to 10,000 cells per well, depending on the cell line, in 150 μL of culture medium per well.

2. Cells are then exposed to peptides for a desired period of time ranging from some hours to several days. We recommend to use three wells for each treatment condition (same peptide concentration and same time exposure), and run at least three experiments to obtain statistically representative values.
3. At the end of the treatment period, the peptide-containing solutions should be removed and replaced by 100 μL MTT solution, for 1–4 h depending on the cell type. MTT is positively charged and readily penetrates human cells. The optimal incubation time for MTT needs to be determined for each cell type, such that viable cells generate a sufficient amount of product that can be detected above background and in the linear range the data.
4. Viable cells, with active metabolism, convert MTT into a purple colored formazan product that accumulates as crystals inside cells and next to their surface. Formazan products must be solubilized by 100–150 μL of DMSO per well (mix to ensure complete solubilization) prior to recording changes in absorbance at 570 nm using a plate-reading spectrophotometer.
5. Ultimately, cell survival is expressed as a percentage of control (vehicle-treated) cells. Sample signals should be corrected for background signal measured in wells containing only cell culture medium. IC_{50} value, i.e. concentration that inhibits 50 % of cell survival, can be determined by a curve-fitting software (such as GraphPad Prism® or SigmaPlot®).

The resazurin-based Alamar blue assay can also be used to quantitatively monitor viable cell number (see the MTT assay two first steps for more details):

1. Human cancer and non-cancer cells are seeded in opaque-walled 96-well plates.
2. Cells are incubated with peptides at various concentrations and for various time exposures.
3. 15 μL of Alamar blue reagent can be added directly to cells in culture, and incubated for 4–6 h at 37 °C protected from direct light (i.e. in the cell incubator). For samples with less than 5000 cells per well, use longer incubation times of up to 24 h. Assay plates can be stored at 4 °C and read within 1–3 days without affecting the fluorescence or absorbance values (protect from light).
4. Upon entering cells, resazurin is reduced to resorufin, a highly fluorescent compound that can be quantified using a microplate

fluorometer, with a 560 nm excitation/590 nm emission filter set (*see* **Note 2**). Finally, results are analyzed, as those from the MTT assay, by plotting fluorescence intensity versus compound concentration.

In some specific conditions, for instance if the time course of peptide activity is difficult to define or if treatment interferes with these two metabolic indicators, a real-time label-free cell investigation should be considered (*see* **Note 3**).

3.3 Live Fluorescent Microscopy of the Mitochondrial Network

In mammalian cells, mitochondria form physically interconnected networks (Fig. 1) that often change shape and subcellular distribution (*see* **Note 4**). A fragmentation of the network, i.e. decrease in connectivity and formation of short, round mitochondria, occurs during the early stages of apoptotic cell death (Fig. 2). Provided that a mitochondrial toxin can be conjugated to a CPP, which is likely to target preferentially mitochondrial membranes through its cationic properties (as discussed in Subheadings 3.1 and 3.5), one can easily consider that this strategy may result in dramatic alterations in mitochondrial morphology. For instance, disintegration of the tubular mitochondrial network has been observed, after only a few minutes, in tumor cells of various tissue origins subjected to the KLA-penetratin conjugate (Fig. 2 and [41]).

Study of the mitochondrial network organization over time has been made possible in living human cells by the use of fluorescent dyes specifically targeting the mitochondrial network matrix. One "easy" way to label mitochondria is to:

1. Seed human cancer (or non-cancer) cells in glass bottom culture dishes that are amenable to fluorescence imaging techniques (*see* **Note 5**). The optimal number of cells per cm^2 should be in line with those determined in 96-well plates (*see* Subheading 3.2).

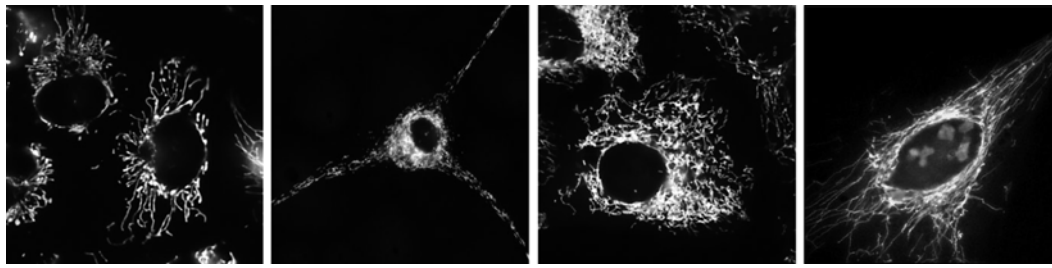

Fig. 1 Different shapes of the mitochondrial network in human cancer and non-cancer cells. Images are representative of a population (from *left* to *right*) of A549 lung adenocarcinoma cells, U87-MG glioblastoma cells, HaCaT keratinocytes, HUVEC endothelial cells. Cells were transfected with mtDsRed and imaged by fluorescence microscopy

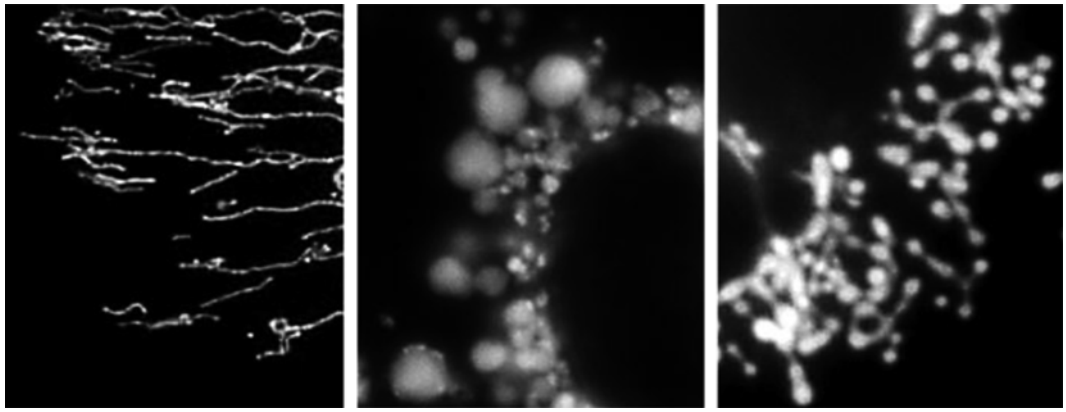

Fig. 2 Mitochondrial fragmentation during apoptosis. Fluorescence microscopy observation of the mitochondrial network in lung cancer A549 cells grown in control culture medium (*left* picture), incubated with 10 μM KLA-Pen for 10 min (*middle* picture), or incubated with 50 nM Taxol® for 6 h (*right* picture)

2. Expose cells to peptides for a desired period of time, generally ranging from a few minutes to hours. Once again, the most promising concentrations to be tested should have been identified by the cytotoxic assay (described in Subheading 3.2).
3. Incubate cells with the cell-permeant carbocyanine-based dyes (MitoTracker® Green FM or Red FM), which accumulate in active mitochondria (*see* **Note 6**), under growth conditions appropriate to the particular cell types. Efficiency of the mitochondrial labeling will vary depending on the cell type, but a 20-min incubation at 37 °C with the probe at 50 mg/mL generally results in a good signal/noise fluorescence ratio within living cells.
4. After two washes of the cell layer with PBS, the impact of peptides on the mitochondrial network organization can be analyzed by live microscopy. Use a fluorescence-inverted microscope (coupled to a digital camera) with a 490 nm excitation/516 nm emission filter set for the MitoTracker® Green FM and 581 nm excitation/644 nm emission filter set for the MitoTracker® Red FM.

To bypass some limitations of such stains (*see* **Note 7**) and stably label mitochondria in living cells with mitochondrial matrix-targeted (mt) DsRed or GFP (i.e. Discosoma sp. red and green fluorescent protein, respectively), the following method can be followed:

1. Human cancer cells are seeded in 6-well plates, so that they will be 80–90 % confluent at the time of transfection (that is generally 24 h after plating).

2. At least 2 h before cell transfection, the culture medium should be removed from wells and replaced by 2 mL of a FCS and antibiotics-free medium (non-supplemented) per well. Alternative media can be used to skip this step (*see* **Note 8**).
3. Per well of cells to be transfected, dilute 10 μL of the Lipofectamine® 2000 cationic lipid transfection reagent in 250 μL of non-supplemented medium. In a distinct tube, proceed to the same step with 4 μg of the plasmid encoding for the mtDsRed or mtGFP. Then, mix the two and incubate for 20 min at room temperature to allow DNA and lipids to form complexes.
4. Directly add the suspension of DNA–lipid complexes (500 μL/well) to the 2 mL of cell culture medium per well, gently mix, and place the plate in the cell incubator for 24 h.
5. To obtain stable transfectants, a selection with high concentrations of antibiotics must be performed (*see* **Note 9**). To do so, cells from each well have to be collected according to standard procedures and seeded in 2T75 flasks in the conventional supplemented culture medium. Then, cells should be exposed to geneticin (G418 sulfate), with a concentration usually ranging from 500 to 1000 μg/mL to be highly selective within 3 weeks.
6. A good fluorescence quality must be ensured by fluorescence-activated cell sorting (FACS) of live cell populations (*see* **Note 10**). As a general requirement, all samples should be prepared in a single-cell suspension form, at a concentration of ≈2 million/mL (up to 10 million/mL). Aspirate up and down through a pipet several times to help disaggregate clumps. Use the 557 nm excitation/592 nm emission or the 488 nm excitation/510 nm emission set of filters to sort the mtDsRed- and mtGFP-expressing cells, respectively. Immediately after cell sorting, cells are placed back in incubators.
7. Then, to examine the mitochondrial network, the stably mt-DsRed- or mt-GFP-expressing cells are plated in glass bottom culture dishes and exposed to peptides for a desired period of time (*see* **steps 1** and **2** of the previous method). Cells can be thus directly imaged, with an inverted fluorescence microscope, and replaced in the incubator. This allows performing a real-time analysis of the peptide-mediated mitochondrial fragmentation.

3.4 Mitochondrial Membrane Potential Measurements

The effects of the CPPs, or their conjugated forms with pro-apoptotic peptides, can also be characterized by their impact on the mitochondria transmembrane potential ($\Delta\psi m$). The $\Delta\psi m$ is maintained by charge differences between the two faces of the inner mitochondrial membrane, due to a higher concentration of protons in the membrane interspace, which is crucial for cell survival

(*see* **Note 11**). Thus, the fluorescent detection of the mitochondrial Δψm collapse is conventionally used to quantify treatment-induced mitochondrial toxicity.

Probes that detect mitochondrial membrane potential are lipophilic cations, causing them to accumulate in the electronegative interior of active mitochondria, in proportion to Δψm. Among the fluorescent probes available (*see* **Note 12**), 3,3′-dihexyloxacarbocyanine iodide (DIOC6) is a cell-permeant green-fluorescent dye that can be used to measure mitochondrial membrane depolarization as followed:

1. Seed human cancer (or non-cancer) cells in 6-well plates for 24 h. The optimal number of cells per cm^2 should be in line with those determined in 96-well plates (*see* Subheading 3.3).
2. Expose cells to peptides for a desired period of time, generally ranging from a few hours to 48 h (*see* **Note 13**). Once again, the most promising concentrations to be tested should have been identified by the cytotoxic assay (described in Subheading 3.3).
3. At the end of treatment, collect cells in conical tubes according to standard methods, and incubate in a DIOC6 solution at 25 nM (in standard culture medium) for 30 min in the dark.
4. After two washes with PBS, cells must be immediately analyzed by flow cytometry (482 nm excitation/504 nm emission). The loss of fluorescence will indicate the Δψm collapse.

3.5 Interaction and Induced Perturbation of the CPP in Lipid Model Systems

Several biophysical methods can be used to follow the interaction and perturbation of the membrane of lipid model systems (liposomes, planar lipid membranes, etc.) by CPPs both kinetically and thermodynamically. Herein, some of the many approaches (mostly used in our laboratory) will be presented. Concerning the lipids chosen for the experiments, ideally one should use a mixture that best mimics the outer leaflet of a cell membrane (a healthy and a tumoral one). The tumoral membrane model is different from the healthy one by the presence of anionic lipids like PS (up to 9 %) in their outer leaflet. Depending on the variety and type of approaches used to follow the P/L interaction it might not be possible to use complex lipid mixtures (that best mimic the cellular membrane), in that case one may opt for single lipid component model membranes, such as zwitterionic lipid (like phosphatidylcholine, PC) to represent the healthy cell membrane and an anionic lipid (such as phosphatidylglycerol, PG or ideally PS) to represent the tumor cell membrane. *See* **Notes 14–16** for general considerations about experiments regarding P/L interactions.

3.5.1 Preparation of MLVs, LUVs, SUVs, and Solid-Supported Lipid Bilayers

Below, methods are presented for the preparation of model membranes that will be employed in the biophysical studies described below.

1. Lipid films are made by dissolving the appropriate amount of lipid in chloroform and methanol, 2/1 (v/v), followed by solvent evaporation under nitrogen to deposit the lipid as a film on the wall of a test tube. Final traces of solvent are removed under *vacuum* for 2 h.
2. Films are hydrated with Tris–HCl buffer (for differential scanning calorimetry (DSC), isothermal titration calorimetry (ITC)) or with phosphate buffer (for CD, Turbidity, and DLS experiments) and vortexed extensively above the melting temperature (T_m) of lipids to obtain multilamellar vesicles (MLVs). Other buffer systems might be used except for CD measurements (*see* **Note 17**).
3. To form large unilamellar vesicles (LUVs), the MLVs are subjected to five freeze/thawing cycles. For low concentration of lipids (~1 mg/mL), the homogeneous lipid suspension is passed 19 times trough a mini-extruder (Avanti Alabaster, AL) equipped with two stacked 100 nm polycarbonate membranes at a temperature above T_m. For higher lipid concentrations (>1 mg/mL), the homogeneous lipid suspension is passed ten times through a nitrogen pressure-driven extruder (LIPEX, Northern Lipids Inc., BC) equipped with a 100 nm polycarbonate membrane at a temperature above T_m.
4. Small unilamellar vesicles (SUVs) are obtained by MLV sonication using a titanium rod sonicator in an ice-water bath to avoid lipid thermal degradation. Titanium traces are removed by centrifugation (5600 × *g*, 2 min).
5. In all experiments performed the peptides are added to the lipid model systems after their formation, which is ideal because it better resembles what occurs in nature. This is possible because the peptides are water-soluble which is the case for most CPPs (*see* **Note 14**).

3.5.2 Measurements of Liposome Turbidity and Distribution

Such measurements can provide information about the peptide effect in general supramolecular liposome organization, whether they induce aggregation. Information about the hydrodynamic radius and distribution of the objects is also obtained.

1. To measure liposome turbidity, one should use LUVs and monitor their absorbance at 436 nm following peptide addition. Aliquots of peptide stock solutions are added to 250 μL suspensions of LUV (lipid concentration, 1250 μM) in sodium phosphate buffer.
2. The absorbance was measured using a Jobin-Yvon CD6-SPEX before and after addition of peptide. The temperature of the measurement depends on the T_m of the lipids under study; one may test both below and above T_m to check the role of membrane fluidity in the process.

3. Liposome size distribution can be monitored by DLS. The peptide is added to LUVs to obtain the desired P/L ratio. Measurements are performed on a Malvern ZetaSizer Nano ZS instrument with a detection angle at 173°. Mean hydrodynamic diameters are determined by fitting the normalized time auto-correlation function of the electric field of the scattered light with the cumulant method and applying the Stokes–Einstein equation.

3.5.3 Calcein Leakage

The experiment objective is to investigate if the peptide perturbs lipid membrane integrity.

1. Calcein-containing LUVs are made using the same protocol used to make regular LUVs (described above), except for the hydration step that is performed in presence of 70 mM calcein. At this concentration calcein is self-quenched.
2. Free calcein is separated from the calcein-containing LUVs using size-exclusion column chromatography (Sephadex G-75) with Tris–HCl as elution buffer. The first colored band in the column corresponds to LUVs encapsulating calcein and after this band-free calcein comes out. Several aliquots should be collected to ensure good separation.
3. The concentration of lipids in the above collected samples is estimated using the Rouser protocol (not described here, please find description here [43]).
4. The peptide is then added to the lipid at the P/L ratios chosen. Fluorescence is measured to follow leakage from the liposomes due to peptide perturbation of the membrane. Absence of fluorescence indicates no membrane perturbation. Measurements are performed with a Perkin Elmer LS55 spectrometer (Burckinghamshire, UK). Data are collected every 1 s at room temperature using a λ_{exc} at 485 nm and λ_{em} at 515 nm. Measurements can also be performed in a 96-well plate to use smaller amounts of material. The fluorescence from calcein at 70 mM concentration is low due to self-quenching, but increases considerably upon dilution. The fluorescence intensity at the equilibrium is measured after 2.5 h.
5. At the end of the assay (after equilibrium has been reached), complete calcein leakage is provoked by adding 100 μL of 10 % Triton X-100 which dissolves the lipid membrane without interfering with the fluorescence signal.
6. The percentage of calcein release is calculated according to the following equation:

$$\%\text{Calcein leakage} = \left(\text{Ft} - \text{Fo}\right) / \left(\text{Ff} - \text{Fo}\right) \times 100 \qquad (1)$$

where the percent of calcein leakage is the fraction of dye released (normalized membrane leakage), Ft is the measured fluorescence intensity at time t, and Fo and Ff are the fluorescence intensities at times $t = 0$, and after final addition of Triton X-100, respectively. A dilution correction is applied on the fluorescence intensity after injection of the Triton X-100.

3.5.4 Isothermal Titration Calorimetry (ITC)

These experiments can provide information about the thermodynamics of P/L interaction, namely allow one to obtain an affinity constant for the process.

1. To avoid air bubbles, peptide and LUV solutions are degassed *under vacuum* before use. The concentrations of peptide and lipid solutions to be used depend on the affinity between the two (property that is to be determined by these experiments). Therefore, often more than one measurement needs to be done to find the ideal concentration range. Estimative can be performed by simulation using a software option provided. Otherwise, a general rule is to approximate the concentration needed in the cell to about 10× the expected K_D value. For very tight binders, the concentration should be on the low side of this value and for weak binders, it should be on the high side of this value. Multiply the cell concentration by the stoichiometry (n) and by 10–15 for the syringe concentration. Again, the value, for very tight binders, should be on the low side and for weak binders it should be on the high side.
2. The lower concentration sample is placed in the cell (the peptide) and the highest concentration is placed in the syringe (lipid LUVs). Keep in mind that LUVs must be used so that all the lipids in the sample are available for peptide contact (no inner inaccessible shells as with MLVs). It is best to keep the peptide as the lower concentration partner as often peptides have tendency to aggregate at high concentration.
3. After loading samples, titrations are performed by injecting aliquots of LUVs (10 mg/mL) into the calorimeter cell containing the peptide solution (0.1 mM), with 5 min waiting between injections (20–50 injections of 5 μL). The conditions were ideal for low μM affinity.
4. The instrument used for measurements is a nano ITC from TA Instruments. Data analysis is performed using the program NanoAnalyze provided by TA Instruments.

3.5.5 Differential Scanning Calorimetry (DSC)

In order to obtain information about the effect of the peptide on the lipid phase transition, differential scanning calorimetry (DSC) can be used. By following the effect of the peptide on the temperature and the shape of the lipid (MLVs or LUVs can be used) transition peak information about the perturbation of the fatty acid

chain packing by the peptides and thus on their insertion mode can be obtained.

1. For pure lipid mixtures, 1 mg/mL of lipid is enough to get a good signal while for more complex mixtures concentrations should be increased to obtain a good signal (*see* **Note 18**). A buffer with constant thermal behavior over the temperature range should be used, Tris-HCl buffer was used. The instrument possesses two cells: the sample and the reference, the sample to be measured is loaded in the sample cell and the same buffer used to prepare this sample is loaded in the reference cell. A blank measurement is made where buffer is loaded in the two samples; these data are needed to calculate the thermodynamic parameters of the lipid in absence and presence of the peptide. A control should also be performed to ensure that the peptide alone has no observable thermal transitions in the temperature range investigated. For that the peptide alone (at concentrations similar to those used in the lipid + peptide experiment) is placed in the sample cell and buffer alone in the reference cell. The signal of the lipid alone is registered first, then the peptide is added to get the desired P/L ratios and the signal is recorded again.
2. Several heating and cooling scans are acquired at 1 °C/min with a delay of 10 min between sequential scans in a series that allows for thermal equilibration. The temperature range used needs to be adapted to the lipid studied; ideally, it should start and finish about 10 °C before and after the observed lipid phase transition. Data are acquired on a high-sensitivity Differential Scanning Calorimeter (Calorimetry Sciences Corporation).
3. Data analysis is performed with the fitting program CPCALC provided by CSC and plotted with Igor. The data of buffer alone are used as baseline in the calculations of thermodynamic parameters of the lipid and lipid + peptide samples.

3.5.6 Circular Dichroism (CD) Spectroscopy

CD is used to follow the peptide secondary structure in solution and upon lipid contact.

1. In terms of buffer, 10 mM phosphate or water alone is used as many buffers absorb considerably around 180 nm and interfere with measurements. For the measurements, spectra are recorded between 185 and 260 nm with 0.5 nm step with a Jobin-Yvon CD6-SPEX dichrograph linked to a PC. The instrument is prior calibrated with D(+)-10-camphorsulphonic acid. Eight scans are accumulated and averaged after buffer (or LUV) spectra subtraction and baseline correction.
2. Spectra of peptide in solution is acquired at a concentration not much lower than around 20 μM as the intensity of the signal becomes quite low below this value.

3. For the study in presence of lipids, LUVs must be used (freshly extruded) to avoid scattering problems that will completely mask the CD signal. Usually ratios from 1/100 to 1/10 of P/L with 1250 μM of lipid (constant) and variable peptide concentrations are used.
4. Look out for precipitation problems (some might be anticipated by the turbidity and DLS measurements described previously) as this will decrease the amount of secondary structure due to decreased amount of peptide in solution and can lead to data misinterpretation.
5. The data are then normalized to express the molar ellipticity θ per residue, this is performed using the following equation: $[\theta] = (\theta \times 10^{-3})/(c \times l \times N_R \times 10^{-9})$, where θ is the ellipticity expressed in millidegrees, c represents the peptide concentration in micromolar, l is the path of the cuvette in centimeter, and N_R is the number of amide bonds in the peptide.
6. Data are deconvoluted by programs like CDpro and CDNN (available online) or CD friend developed by S. Buchoux in the laboratory (non-published) (*see* **Note 18**).

3.5.7 ATR-FTIR Spectroscopy

Polarized ATR-FTIR spectroscopy is also a useful method to follow not only the peptide secondary structure in contact with a planar lipid membrane but also the peptide orientation and the effect of the peptide in the lipid organization (water accessibility, chain orientation and ordering). The use of deuterated buffer is ideal for the visualization of the amide I and amide II regions necessary for peptide secondary structure determination since the water band is shifted from its position (that overlaps with the amide I and amide II region) while the use of non-deuterated samples is better to observe lipids absorption region. If both types of information are sought, independent measurements with deuterated and non-deuterated samples should be performed or experiments should be performed with deuterated sample and then wait for D/H exchange before acquisition in absence of D_2O. *See* **Note 19** for some precautions to be taken regarding the peptide investigated.

1. The first stage consists in preparing the lipid membrane, this is done by the fusion of SUVs onto the ATR germanium crystal. Briefly, 20 μL of 1.5 mg/mL SUVs solution is deposited on the crystal containing the Teflon cell. After 10–15 min, the non-adsorbed lipids are rinsed several times with buffer, following addition of 20 μL of Tris-HCl buffer before spectra acquisition. The experiment must be performed above T_m of the lipids used so they are in the fluid phase otherwise the lipid bilayer cannot be formed.
2. Spectra are acquired, with both p- and s-polarized light on a Nicolet 6700 FT-IR spectrometer equipped with a liquid

nitrogen 190 cooled mercury-cadmium-telluride detector on a germanium crystal. 800 scans are co-added at a resolution of 8 cm^{-1}.

3. For an oriented bilayer, the dichroic ratio ($R_{ATR} = Ap/As$, where Ap and As represent the absorption bands obtained with p- and s-polarized light, respectively) should be around 1.4 and the intensity in p-polarization of 1.3×10^{-3} (single bilayer of about 40 Å is deposited).
4. The peptides are added to the bilayer (final concentration of about 1 mM). Spectra are recorded over time for both polarizations both before and after rinsing the cell with buffer to remove unbound peptide.
5. After data acquisition, spectra are corrected for the baseline, to remove water vapor (using a water vapor spectra previously collected) or D_2O using the software Omnics.
6. Spectra deconvolution for secondary structure determination is performed using the software Grams. The amide I frequencies are attributed as follow: 1615–1625 cm^{-1} and 1685–1695 cm^{-1} antiparallel beta sheet, 1630–1635 cm^{-1} parallel beta sheet, 1640–1650 cm^{-1} random coil, 1650–1662 cm^{-1} alpha helix, 1662–1680 cm^{-1} beta turn.

4 Notes

1. The following culture media should be used:
   - DMEM for MCF-7, U251, BE(2)-C, SHEP, SW480, HT29, HEK-293t, and HaCaT cells.
   - RPMI-1640 for MDA-MB-231, A549, HUVECs, SK-N-SH, and IMR-32 cells.
   - McCoy'5A for SKBR3 cells.
   - MEM for HBL-100, U87-MG, and MRC-5 cells.
   - MCDB-131 for HMEC-1.
2. If a fluorescence reader is not available, absorbance measurement can be done with a microplate spectrophotometer (at 570 nm), since the cell culture medium changes from deep blue to pink when cells are alive. However, it is far less sensitive than fluorescence.
3. The major advantages of the MTT and Alamar blue methods are that: (1) they are adapted for a wide-set range of conditions in multi-well plates; (2) commercial powders are relatively inexpensive and are available from several chemical vendors; (3) they only require standard plate readers. The main disadvantage is the fact that acquiring the signal must be

considered as an endpoint. To circumvent this methodological limitation, technologies that monitor cellular events without the incorporation of labels are of great interest. For instance, the xCELLigence System (from ACEA Biosciences) is a real-time analyzer allowing label-free cell investigation. It captures data throughout the entire time course of the experiment, by measuring electrical impedance across interdigitated micro-electrodes integrated in 96-well plates (which stay in the cell incubator). However, conversely to the two methods described herein, the impedance-based technology is expensive since it requires high-tech equipment and specific multi-well plates for cell culture.

4. This dynamics relies on the fact that mitochondria can elongate, shorten and branch, conduct fission and fusion processes and make vivid movements between cell center and periphery. The mitochondrial behavior is closely related to the broad spectrum of their functions, ranging from providing metabolic energy and regulation of calcium homeostasis to reactive oxygen species generation and control of apoptosis. As a sustained interruption of these processes results in cell death, targeting mitochondria is now largely accepted as a strategy of choice to suppress cancer cells.
5. Plastic bottom dishes do not work because they are too thick to image through; plastic coverslips are not recommended for their inherent fluorescence.
6. To avoid the potential stain of other structures and mitochondrial toxicity from overloading, keep the concentration of dye as low as possible.
7. The carbocyanine-based stains are relatively stable once the mitochondria experience a loss in membrane potential. However, the fluorescence intensity usually rapidly decreases during image acquisition of the mitochondrial network.
8. This step can be bypassed by using an OptiMEM® reduced serum medium or its equivalent throughout the transfection protocol.
9. Plasmid constructs used to express fluorescent proteins in human cells generally also encode for the neomycin resistance gene that confer to cells that have successfully integrated the plasmid a high insensitivity to geneticin (G418 sulfate). Others will die in a few days.
10. It is possible to sort under aseptic conditions to isolate the most fluorescent cell population of transfected cells for expansion in culture. An unstained control is used to detect autofluorescence or background staining innate to the cells of interest. The controls must undergo the same preparation as all the tubes in the FACS experiment.

11. The higher concentration of protons in the mitochondrial membrane interspace is a requisite for the ultimate ATP synthesis. While the exact time schedule of apoptotic events is still discussed, depolarization of the mitochondrial membranes is largely accepted to be linked to loss of energy supply and release of apoptogenic factors that ultimately result in cell death.
12. Rhodamine-based probes such as TMRM (tetramethylrhodamine, methyl ester) or TMRE (tetramethylrhodamine, ethyl ester) are other cell-permeant red-orange fluorescent dyes widely used to measure the mitochondrial potential in a quite similar manner to DIOC6 staining. Alternatively, the JC-1 dye (5,5′,6,6′-tetrachloro-1,1′,3,3′-tetraethylbenzimidazol carbocyanine iodide) exhibits a potential-dependent accumulation in mitochondria indicated by a fluorescence emission shift from green (~529 nm) to red (~590 nm). Consequently, mitochondrial depolarization is indicated by a decrease in the red/green fluorescence intensity ratio. The potential-sensitive color shift is due to concentration-dependent formation of red fluorescent J-aggregates.
13. DIOC6 is selective for the mitochondria of live cells when used at low concentrations. Nevertheless, to ensure the mitochondrial uptake, we also recommend to treat cells with 50 μM of carbonyl cyanide *m*-chlorophenylhydrazone (CCCP), which is a protonophore that dissipates the mitochondrial $\Delta\psi m$.
14. In all experiments performed to follow peptide interaction with lipids, the peptides are added to the lipid model systems after their formation. This is the ideal case because it resembles what occurs in nature best. This is possible when the peptides are water-soluble, which is generally the case for CPPs. In case the peptides are not water-soluble, one should co-dissolve them with the lipids in the organic solvent (chloroform or methanol) before the formation of a lipid film.
15. To compare experiment results among the different techniques, lipids should be in the same phase, ideally fluid phase such as found in mammalian cell membranes. This can be controlled by the choice of the temperature set in the measurement.
16. In terms of the P/L ratio chosen for the studies, one should be aware of the inherent sensibility of the technique used and adapt as needed. Here, P/L ratios of 1/100, 1/50, 1/25, and 1/10 were used. When comparing results attention should be paid to the P/L ratios used as this property strongly affects the mode of the interaction.
17. For CD studies, MLVs and SUVs are not compatible because they diffract. Most buffer systems are not compatible either due to absorbance; ideally, CD studies should be performed with phosphate buffer 10 mM or in water. For data deconvolution, one needs to take into account that most softwares

available for have been developed mostly for proteins and are not very appropriate for small peptides such as CPPs that often are quite malleable in their structure. Thus data from deconvolution need to be considered with caution.

18. For DSC experiments, care must be taken in the choice of the lipids to be used. One needs to choose a lipid whose phase transition temperature is above 0 °C (the instrument cannot record below that unless a special solvent is used that does not freeze at this temperature). Also, one cannot use complex lipid mixtures as each one of the lipid components will have a different phase transition and the final result is a very shallow and broad transition. Indeed, the best is to use a single lipid component to obtain a very sharp phase transition.
19. For ATR-FTIR measurements, certain points need to be taken into account: (1) one cannot form bilayers by SUV fusion using 100 % anionic lipids, indeed 30 % is the highest one can use of anionic lipids in the mixture; (2) special attention must be given to the amino acid content of the peptide to be investigated as certain amino acids such as arginines, glutamine and asparagine have side chains that absorb in the amide I and II region and thus hamper secondary structure attribution; (3) counterions such as TFA have a strong absorption band in the amide region and thus need to be exchanged with other counterion such as HCl that is inoffensive.

References

1. Nakase I et al (2007) Interaction of arginine-rich peptides with membrane-associated proteoglycans is crucial for induction of actin organization and macropinocytosis. Biochemistry 46(2):492–501
2. Jiao CY et al (2009) Translocation and endocytosis for cell-penetrating peptide internalization. J Biol Chem 284(49):33957–33965
3. Ziegler A, Seelig J (2008) Binding and clustering of glycosaminoglycans: a common property of mono- and multivalent cell-penetrating compounds. Biophys J 94(6):2142–2149
4. Bechara C et al (2015) Massive glycosaminoglycan-dependent entry of Trp-containing cell-penetrating peptides induced by exogenous sphingomyelinase or cholesterol depletion. Cell Mol Life Sci 72:809
5. Favretto ME et al (2014) Glycosaminoglycans in the cellular uptake of drug delivery vectors - bystanders or active players? J Control Release 180:81–90
6. Ziegler A, Seelig J (2011) Contributions of glycosaminoglycan binding and clustering to the biological uptake of the nonamphipathic cell-penetrating peptide WR9. Biochemistry 50(21):4650–4664
7. Binder H, Lindblom G (2003) Charge-dependent translocation of the Trojan peptide penetratin across lipid membranes. Biophys J 85(2):982–995
8. Lecorche P et al (2012) Cellular uptake and biophysical properties of galactose and/or tryptophan containing cell-penetrating peptides. Biochim Biophys Acta 1818(3):448–457
9. Matsuda K et al (2001) Glypican-1 is overexpressed in human breast cancer and modulates the mitogenic effects of multiple heparin-binding growth factors in breast cancer cells. Cancer Res 61(14):5562–5569
10. Lee JH et al (2009) Syndecan-2 regulates the migratory potential of melanoma cells. J Biol Chem 284(40):27167–27175
11. Sanderson RD (2001) Heparan sulfate proteoglycans in invasion and metastasis. Semin Cell Dev Biol 12(2):89–98

12. Vlodavsky I et al (2002) Mammalian heparanase: involvement in cancer metastasis, angiogenesis and normal development. Semin Cancer Biol 12(2):121–129
13. Yoon WH et al (1996) Effect of O-glycosylated mucin on invasion and metastasis of HM7 human colon cancer cells. Biochem Biophys Res Commun 222(3):694–699
14. Kufe DW (2009) Mucins in cancer: function, prognosis and therapy. Nat Rev Cancer 9(12): 874–885
15. Lopez PH, Schnaar RL (2009) Gangliosides in cell recognition and membrane protein regulation. Curr Opin Struct Biol 19(5):549–557
16. Vynios DH et al (2001) The interactions of cartilage proteoglycans with collagens are determined by their structures. Biochimie 83(9):899–906
17. Hendrich AB, Michalak K (2003) Lipids as a target for drugs modulating multidrug resistance of cancer cells. Curr Drug Targets 4(1): 23–30
18. Martin SJ et al (1995) Early redistribution of plasma membrane phosphatidylserine is a general feature of apoptosis regardless of the initiating stimulus: inhibition by overexpression of Bcl-2 and Abl. J Exp Med 182(5):1545–1556
19. Ran S, Downes A, Thorpe PE (2002) Increased exposure of anionic phospholipids on the surface of tumor blood vessels. Cancer Res 62(21):6132–6140
20. Utsugi T et al (1991) Elevated expression of phosphatidylserine in the outer membrane leaflet of human tumor cells and recognition by activated human blood monocytes. Cancer Res 51(11):3062–3066
21. Rao LV, Tait JF, Hoang AD (1992) Binding of annexin V to a human ovarian carcinoma cell line (OC-2008). Contrasting effects on cell surface factor VIIa/tissue factor activity and prothrombinase activity. Thromb Res 67(5):517–531
22. Schroder-Borm H, Bakalova R, Andra J (2005) The NK-lysin derived peptide NK-2 preferentially kills cancer cells with increased surface levels of negatively charged phosphatidylserine. FEBS Lett 579(27):6128–6134
23. Kirszberg C et al (2009) Simultaneous tissue factor expression and phosphatidylserine exposure account for the highly procoagulant pattern of melanoma cell lines. Melanoma Res 19(5):301–308
24. Sok M, Sentjurc M, Schara M (1999) Membrane fluidity characteristics of human lung cancer. Cancer Lett 139(2):215–220
25. Nakazawa I, Iwaizumi M (1989) A role of the cancer cell membrane fluidity in the cancer metastases: an ESR study. Tohoku J Exp Med 157(3):193–198
26. Schroeder F, Gardiner JM (1984) Membrane lipids and enzymes of cultured high- and low-metastatic B16 melanoma variants. Cancer Res 44(8):3262–3269
27. Ziegler A et al (2003) Protein transduction domains of HIV-1 and SIV TAT interact with charged lipid vesicles. Binding mechanism and thermodynamic analysis. Biochemistry 42(30): 9185–9194
28. Goncalves E, Kitas E, Seelig J (2005) Binding of oligoarginine to membrane lipids and heparan sulfate: structural and thermodynamic characterization of a cell-penetrating peptide. Biochemistry 44(7):2692–2702
29. Walrant A et al (2011) Different membrane behaviour and cellular uptake of three basic arginine-rich peptides. Biochim Biophys Acta 1808(1):382–393
30. Takechi Y et al (2011) Physicochemical mechanism for the enhanced ability of lipid membrane penetration of polyarginine. Langmuir 27(11):7099–7107
31. Jobin ML et al (2013) The enhanced membrane interaction and perturbation of a cell penetrating peptide in the presence of anionic lipids: toward an understanding of its selectivity for cancer cells. Biochim Biophys Acta 1828(6):1457–1470
32. Alves ID et al (2011) Relationships between membrane binding, affinity and cell internalization efficacy of a cell-penetrating peptide: penetratin as a case study. PLoS One 6(9): e24096
33. Schwieger C, Blume A (2009) Interaction of poly(L-arginine) with negatively charged DPPG membranes: calorimetric and monolayer studies. Biomacromolecules 10(8):2152–2161
34. Persson D et al (2003) Application of a novel analysis to measure the binding of the membrane-translocating peptide penetratin to negatively charged liposomes. Biochemistry 42(2):421–429
35. Drin G et al (2001) Translocation of the pAntp peptide and its amphipathic analogue AP-2AL. Biochemistry 40(6):1824–1834
36. Christiaens B et al (2002) Tryptophan fluorescence study of the interaction of penetratin peptides with model membranes. Eur J Biochem 269(12):2918–2926
37. Gaspar D, Veiga AS, Castanho MA (2013) From antimicrobial to anticancer peptides. A review. Front Microbiol 4:294
38. Henriques ST, Melo MN, Castanho MA (2006) Cell-penetrating peptides and antimi-

crobial peptides: how different are they? Biochem J 399(1):1–7

39. Hoskin DW, Ramamoorthy A (2008) Studies on anticancer activities of antimicrobial peptides. Biochim Biophys Acta 1778(2): 357–375
40. Kondo E et al (2012) Tumour lineage-homing cell-penetrating peptides as anticancer molecular delivery systems. Nat Commun 3:951
41. Alves ID et al (2014) A proapoptotic peptide conjugated to penetratin selectively inhibits tumor cell growth. Biochim Biophys Acta 1838(8):2087–2098
42. Mader JS, Hoskin DW (2006) Cationic antimicrobial peptides as novel cytotoxic agents for cancer treatment. Exp Opin Investig Drugs 15:933
43. Rouser G, Fkeischer S, Yamamoto A (1970) Two dimensional then layer chromatographic separation of polar lipids and determination of phospholipids by phosphorus analysis of spots. Lipids 5(5):494–496

Chapter 19

PepFects and NickFects for the Intracellular Delivery of Nucleic Acids

Piret Arukuusk, Ly Pärnaste, Mattias Hällbrink, and Ülo Langel

Abstract

Nucleic acids can be utilized in gene therapy to restore, alter, or silence gene functions. In order to reveal the biological activity nucleic acids have to reach their intracellular targets by passing through the plasma membrane, which is impermeable for these large and negatively charged molecules. Cell-penetrating peptides (CPPs) condense nucleic acids into nanoparticles using non-covalent complexation strategy and mediate their delivery into the cell, whereas the physicochemical parameters of the nanoparticles determine the interactions with the membranes, uptake mechanism, and subsequent intracellular fate. The nanoparticles are mostly internalized by endocytosis that leads to the entrapment of them in endosomal vesicles. Therefore design of new CPPs that are applicable for non-covalent complex formation strategy and harness endosomolytic properties is highly vital. Here we demonstrate that PepFects and NickFects are efficient vectors for the intracellular delivery of various nucleic acids.

This chapter describes how to form CPP/pDNA nanoparticles, evaluate stable nanoparticles formation, and assess gene delivery efficacy.

Key words Cell-penetrating peptide, Co-incubation, Nanoparticle formation, Oligonucleotide delivery, PepFect, NickFect

1 Introduction

Genetic disorders, inherited or gained through genetic mutations, can be treated or alleviated by altering gene expression. Gene therapy approaches can be roughly classified according to their pharmacological effect. One possibility is to incorporate genetic material into plasmid DNA (pDNA) and by delivering pDNA restore the normal protein expression level. The second option is modification of gene function by interfering with the splicing machinery by delivering splice-correcting oligonucleotides (SCO) to block undesirable aberrant splice site and redirect splicing to normally functioning splice site. The third alternative is silencing disease-causing genes by RNA interference (RNAi) approaches by delivering microRNA (miRNA) or small interfering RNA (siRNA) to knock down the gene of interest.

Ülo Langel (ed.), *Cell-Penetrating Peptides: Methods and Protocols*, Methods in Molecular Biology, vol. 1324,
DOI 10.1007/978-1-4939-2806-4_19,

All these approaches are based on nucleic acids, negatively charged large molecules that by nature cannot permeate the plasma membrane. In order to reveal the biological activity, nucleic acids have to reach the target site inside the cells, either in the nucleus or in the cytoplasm. A promising approach for the intracellular delivery of various bioactive molecules, including nucleic acids, is using peptides with membrane permeation activity. The peptides, named cell-penetrating peptides (CPPs) or peptide transduction domains (PTDs), have been used to transport nucleic acids into cells both in vitro and in vivo [1].

Oligonucleotide (ON) can be linked to CPP either covalently or non-covalently. Covalent conjugation results in a well-defined chemical compound that can be easily verified by mass-spectrometry analysis and the structure-activity relationships are straightforward to interpret [2, 3]. Still, covalent conjugation is often complicated and laborious chemical synthesis where several critical factors have to be considered. Effective dose ratio between the CPP and cargo, steric hindrance, suitable linker, and conjugation site in the backbone of the CPP are just some of them [2]. Furthermore, this strategy is not suitable for large nucleic acids, e.g., pDNA.

The non-covalent approach that relies on complex formation between the CPP and cargo due to electrostatic and hydrophobic interactions was first demonstrated by the group of Divita for linking pDNA [4]. This strategy is easy to perform and cost efficient and low concentrations of compounds can be utilized. The main drawback of non-covalent strategy is the difficulty in generating and characterizing homogenous nanoparticles. As physicochemical properties of the nanoparticles significantly affect pharmacokinetics and biological activity of the cargo, it is highly important to study conditions for the complex formation and parameters of the formed nanoparticles.

CPPs condense nucleic acids into smaller nanostructures than naked ON; for example CPP/pDNA nanoparticle size is often 30–100 nm, while naked DNA is up to 1000 nm. The size of the nanoparticles plays an important role regarding in vivo and in vitro applications. It can influence not only the mechanisms and specificity of uptake by different cells and organs, but also passive accumulation into tumors [3, 5]. The successful transfection of cells in culture relies on the careful tuning of the particle size. Particles smaller than 100 nm are often taken up to a higher degree than larger particles, whereas micrometer-sized particles sediment and by this increase the local concentration at the bottom of the cell culture. Therefore for the adherent cultures the optimal particle size is likely around 1 μm to achieve the highest transfection level.

Nanoparticle size or flocculation tendency can be influenced by many factors, including medium composition. However, it is well known that colloids are stabilized by the surface charge and zeta potential of the particles. The salt concentration, that can

screen electrostatic repulsion, is of primary importance. Divalent ions such as calcium and magnesium can possibly cross-link particles into larger flocculates. Numerous publications have shown that the pK_a of polyelectrolytes may be different from the theoretical value predicted from the incorporated monomers. Thus small shifts in the pH around the pK_a may have large effects on the surface charge, and hence the stability, of the colloidal particles.

Besides the size, optimal stability of the nanoparticles is also crucial for the successful delivery. During circulation in the bloodstream or infiltration into the tissues, nanoparticles interact with serum proteins and encounter polyanions, e.g., heparan sulfates on the cell surface. These interactions may result in premature cargo release from the nanoparticle [6]. On the other hand, after reaching the target, cargo should be released from the complex for subsequent functions. The interactions between the cargo and the delivery agent have to be balanced in order to provide stability as well as to enable dissociation of the nucleic acid to exert its activity [7, 8]. Various strategies have been applied to fine-tune the stability of nanoparticles, like stearylation [9], replacement of lysine with ornithine [10], or changing the hydrophobicity of the peptide [11].

The surface charge, characterized by zeta potential, may determine the mode of interaction of the nanoparticle with the cell surface. The positive surface charge is commonly believed to allow interaction with polyanionic glycosaminoglycans on the cell surface [6]. Recently, we showed that PF/ON and NF/ON nanoparticles obtain negative surface charge in the presence of serum proteins and their uptake is mediated by scavenger receptors [12, 13]. Acquisition of negative zeta potential in serum-containing media was also measured for arginine-rich peptides and a linear correlation between the zeta potential and the sensitivity to serum was observed. Still it remained unclear whether the highly negative surface charge protects the nanoparticles from the interactions with serum components, or alternatively induces the formation of a protective layer of serum proteins that protects the nanoparticles from degradation [6].

CPP/ON nanoparticles utilize mainly endocytic pathways to gain access into the cells and this leads to the entrapment of the nanoparticles in endosomal vesicles. The endosomal escape of the therapeutic macromolecules is critical for obtaining the desired biological effects. Without reaching the target in cytosol or in nucleus delivered cargo cannot exert its function and prolonged stay in the endosomes increases the risk of degradation by lysosomal enzymes [14]. This has led to intense investigations to overcome this limitation and a large number of novel CPPs with endosomolytic properties have been developed for non-covalent complexation strategy.

We have shown that N-terminal stearylation of chimeric peptide TP10 leads to a novel vector PepFect3 (PF3) that was applicable for non-covalent complexation strategy. PF3 efficiently condensed SCO into nanoparticles that facilitated splice correction at low SCO concentrations [9]. Furthermore, PF3 proved to be efficient vector for pDNA not only in vitro, but also in vivo [15]. These findings paved the way to the development of PepFect (PF) and NickFect (NF) families of peptides in our group. PFs and NFs described in the current chapter are listed in Table 1.

In PF6 a successive endosomolytic modification was accomplished: a lysine tree with pH titratable trifluoromethyl-quinoline derivatives was coupled to the lysine sidechain of PF3. PF6 evidenced high delivery capability for siRNA, resulting in efficient knockdown of HPRT1 mRNA levels in different cell lines, including hard-to-transfect cell lines such as HUVEC, Jurkat, and embryonic stem cells. Comparison with the parental peptide PF3 proved that PF6 has obtained pH-dependent endosomolytic properties. Furthermore, after intravenous injection PF6/luc-siRNA complexes mediated knockdown in liver without inflammatory side effects and showed the applicability of PF6 for in vivo settings [16].

In PF14, all lysines in the backbone were replaced with ornithines and the sequence modification was inspired by leucine zippers to enhance ON binding. PF14 efficiently delivered SCOs to reporter HeLa pLuc705 cells and Duchenne's muscular dystrophy cell culture model, mdx mouse myotubes [17]. In addition PF14 formed non-covalent nanoparticles with siRNA that evoke efficient RNA-interference response in different cell lines [18]. Furthermore, we demonstrated the feasibility to incorporate PF14/SCO and PF14/siRNA nanoparticles into solid formulation for successive therapeutic applications [17, 18]. Subsequent studies proved the applicability of PF14 not only for shorter ONs, but also for the delivery of pDNA. Efficient gene delivery and expression was acquired even in difficult-to-transfect primary cells [19].

Combining the superior properties of PF6 and PF14, we created a novel peptide PF15 and utilized it for the delivery of anti-microRNA [20].

NickFects are the second family of CPPs derived from stearylated TP10. In order to enhance the interactions of the peptide with cellular membranes and induce endosomal release, we incorporated the phosphoryl-group to the backbone of the original peptide obtaining NF1, pH-dependent vector with reduced net positive charge and hydrophilicity. Intracellular delivery of SCO by NF1 demonstrated significant improvement of splice correction in Hela pLuc705 cells compared to PF3. Furthermore, co-transfection of NF1/SCO complexes with chloroquine demonstrated that the improvement in transfection efficacy was achieved due to the escape of the complexes from endosomal compartments [11].

Table 1
Sequences of the peptides and physicochemical parameters of PF;NF/ON complexes

CPP	Sequence	Charge	Cargo	CPP/cargo	Particle size, nm	ζ Potential, mV	Ref.
PF6	Stearyl-AGYLLK*INLKALAALAKKIL-NH_2	+3	siRNA	MR30	127[b]	−7[b]	[16]
PF14	Stearyl-AGYLLGKLLOOLAAAALOOLL-NH_2	+5	SCO pDNA siRNA	MR10 CR3	285[b] 148[b] 119[b]	−9.84[b] −24[b] −8.54[b]	[12] [17] [18]
PF15	Stearyl-AGYLLGK*LLOOLAAAALOOLL-NH_2	+4	SCO miRNA	MR12 MR5	365.6[a] 504.2[a]	−7.9[a] −11.2[a]	 [19]
NF1	Stearyl-AGY(PO3)LLKTNLKALAALAKKIL-NH_2	+3	SCO pDNA	MR7 CR3	449[a] 165[b]	−15.8[a] −9.6[b]	[11] [13]
NF51	(Stearyl-AGYLLG)-δ-OINLKALAALAKKIL-NH_2	+4	SCO pDNA siRNA	MR10 CR3 MR10	168[b] 121.4[b] 94.4[b]	−11.1[b] −11.5[b] −11.8[b]	 [10]

a measured in OptiMem
b measured in OptiMem supplemented with 10 % of fetal bovine serum K*-Lysine with lysine tree and chloroquine analogues attached.

NF51 is a kinked peptide, where neuropeptide galanin motif and mastoparan residue in PF3 sequence are linked via the side chain of ornithine. NF51 proved to be versatile delivery vector that mediated not only gene delivery, but also siRNA and SCO transfection in different cell lines [10]. Importantly, variety of experiments evidenced the endosomolytic properties of NF51 [10, 13]. Furthermore, we demonstrated that NF51 as a transfection agent is applicable in QMCF technology for the expression and production of recombinant proteins in hard-to-transfect suspension cell lines [10].

All PepFects and NickFects described in this chapter condensed different types of nucleic acids, e.g., pDNA, SCO, and siRNA into stable and small nanoparticles in water. The size of the formed nanoparticles enlarged in the presence of serum, but mostly remained less than 150 nm (Table 1). Importantly all NF;PF/ON complexes exhibited negative Zeta-potential in the presence of serum. For PF14/SCO complexes we demonstrated for the first time the engagement of scavenger receptors in the uptake of CPP/ON nanoparticles [12]. Thereafter the involvement of scavenger receptors, more precisely subtypes 3 and 5 from class A (SCARA) was verified for the uptake of other PFs, NFs and different types of nucleic acids [13, 18–20].

In this chapter we introduce a protocol to screen CPPs for the delivery of pDNA. We demonstrate in details how to form CPP/pDNA complexes, validate complex formation, and assess gene delivery in HeLa cells.

2 Materials

This chapter focuses on the delivery of the plasmid DNA. We have evaluated our NickFects and PepFects for the delivery of the pDNA by measuring the expression of the reporter gene. The described assay is based on luciferase-encoding plasmid. In order to express luciferase the plasmid has to reach the cell nucleus and the expressed luciferase can be measured. The protocol is also applicable for other types of plasmids.

2.1 Peptides, Oligonucleotides, and Complex Formation

1. Plasmid DNA stock (*see* **Note 1**).
2. 1 mM peptide solutions of in MQ water. Store peptide solution at −20 °C as 20 μl stocks. (For obtaining 1 mM stock solution *see* **Note 2**.)
3. MQ water.
4. Lipofectamine™ 2000 (*see* **Note 3**).
5. OptiMem (for Lipofectamine™ 2000) and full growth media.
6. 1.5 ml tubes.

2.2 Ethidium Bromide Gel Assay

1. Reagents described above.
2. 10 μM Ethidium bromide stock solution dissolved in MQ water (*see* **Note 4**).
3. Agarose powder.
4. 0.5× TAE buffer in MQ water.
5. Loading dye.
6. 1 kbp ladder.

2.3 PicoGreen Assay

1. Reagents described in complex formation.
2. Black 96-well plate.
3. PicoGreen™ (*see* **Note 5**) or other fluorescent dye compatible for DNA quantification.

2.4 Cell Culturing and Lysis of Cells

1. HeLa cells maintained in Dulbecco's modified Eagle's medium (DMEM) supplemented with Glutamax, 0.1 mM nonessential amino acids, 1.0 mM sodium pyruvate, 10 % fetal bovine serum, 100 U/ml penicillin, 100 mg/ml streptomycin.
2. 100 mm cell culture dishes.
3. 0.25 % Trypsin and 1 mM ethylenediamine tetraacetic acid (EDTA) (*see* **Note 6**).
4. 24-Well culture plates.
5. Phosphate-buffered saline (PBS): 137 mM NaCl, 10 mM Na_2HPO_4, 2.7 mM KCl, pH 7.4.
6. 0.1 % Triton X-100 in PBS water for the lysis of the cells.

2.5 Luciferase Assay and Protein Determination

1. White 96-well plates or black 96-well plates with white wells (*see* **Note 7**).
2. Cell lysate (*see* **Note 8**).
3. Luciferase substrate mix: Mix substrate with the buffer solution and store as 5 ml aliquots at −20 °C for a maximum of 1 month.
4. Transparent 96-well plates.
5. Detergent compatible with Lowry protein determination.

3 Methods

3.1 Complex Formation

CPP and pDNA particles are formed using non-covalent complexation strategy, based on the negative charges in the nucleic acid backbone and positive charges in the peptide sequence.

1. Thaw 20 μl of 1 mM peptide stock by adding 180 μl of MQ water to obtain a 100 μM final concentration (*see* **Note 9**).
2. Thaw 1 mg/ml pDNA stock by diluting it 20× in PBS to obtain 0.05 mg/ml pDNA solution.

3. Prepare NF/pDNA complexes at different charge ratios (*see* **Note 10**).
4. The protocol below describes formation of complexes of pDNA size 5.2 kbp and CPP NF51 with a total charge of +4 (*see* **Note 11**). Form complexes in triplicates with an excess, using different charge ratios (*see* **Note 12**). For this calculate the MQ needed if the final volume is 160 µl. Start by mixing MQ and pDNA (0.5 µg per well). Lastly add 100 µM dilution peptide solution depending on the charge ratio.
5. Pipette gently the pDNA/MQ/CPP mixture and allow complexes to form by incubating the solution at room temperature for 45 min.
6. In parallel, prepare positive control (e.g., Lipofectamine™ 2000/pDNA complexes according to the manufacturer's protocol).

3.2 Ethidium Bromide Assay to Determine the Efficacy of Complex Formation on Agarose Gel

The principle of the assay is that formed complexes are too large to efficiently migrate from gel tooth into the gel, whereas pDNA that is not incorporated into the complex moves freely. The assay demonstrates at which peptide/pDNA charge ratios stable nanoparticles are formed (Fig. 1).

1. Form complexes as described above.
2. Prepare 50 ml of 1 % agarose gel in 0.5× TAE buffer with 5 µg of ethidium bromide solution (EtBr) to obtain 150 × 100 mm gel (*see* **Note 13**).

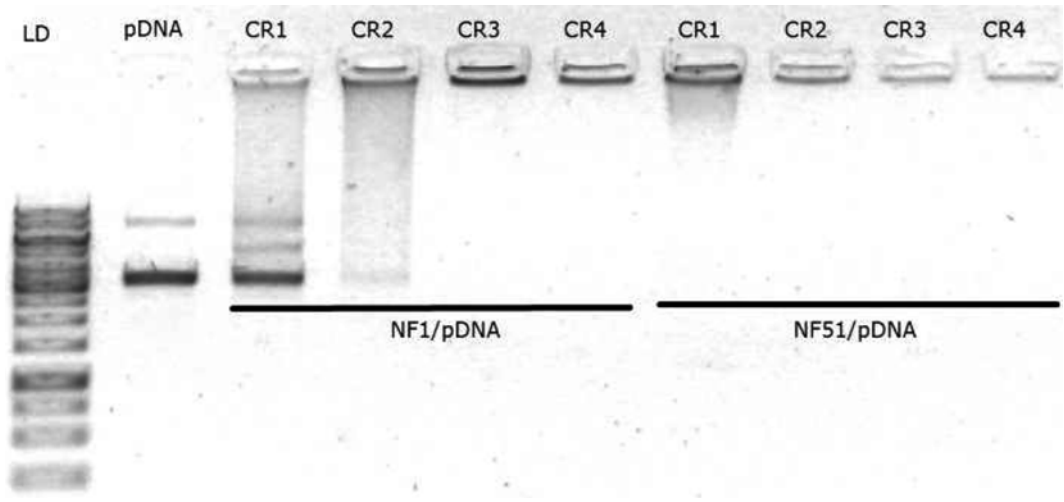

Fig. 1 Ethidium bromide assay to determine CPP/pDNA complex formation. The formed complexes stay in the gel tooth, whereas pDNA that is not incorporated into complex is transferred into gel during electrophoresis. On the gel as follows: LD—ladder, pDNA in the same concentration as in the complexes, NF1/pDNA and NF51/pDNA complexes at different charge ratios

3. Mix 10–15 μl of complex solution with 2 μl of loading dye and transfer 10 μl of mixture to the gel tooth.
4. Allow gel electrophoresis at max 60 mA per gel until bands have migrated halfway.
5. Detect bands under UV ($\lambda_{ex} = 518$ nm, $\lambda_{em} = 605$ nm).

3.3 PicoGreen Assay to Determine Complex Formation

The principle of the assay is that PicoGreen is able to reach pDNA that is not condensed into the complex, giving fluorescence. The advantage of the dye is higher specificity to DNA, lower toxicity, and longer period of stable fluorescence.

1. Prepare complexes as described above.
2. Thaw PicoGreen reagent and make 150–200× dilution in MQ water (*see* **Note 14**).
3. Add 10 μl of complex solution, 110 μl of MQ water, and 30 μl of PicoGreen dilution to 96-well plate to each well. Make at least triplicates of each complex. Incubate for 15–30 min at room temperature protected from light.
4. Detect fluorescence on a compatible fluorimeter at $\lambda_{ex} = 485$ nm and $\lambda_{em} = 528$ nm.

3.4 Cell Culturing and Lysis of Cells

1. HeLa cells are passaged when approaching full confluence with trypsin/EDTA. In general, cells are passaged every third day when using a 1:10 splitting ratio.
2. On the day before experiment, typsinate the cells and seed 50,000 cells (*see* **Note 15**) in 1 ml media on a 24-well plate to each well.
3. After 24 h, remove the old media and add 450 μl of fresh full growth media (*see* **Note 16**) at least 20 min before adding complexes. For cells that are treated with Lipofectamine™ 2000, replace media with 400 μl of full growth media. For negative controls just add 500 μl of full growth media.
4. Gently pipette the complex solution few times before adding 50 μl of preformed complexes per well. To the wells used for a positive control add 100 μl of Lipofectamine™ 2000/pDNA.
5. Gently mix the plates to distribute evenly complexes in wells.
6. Incubate cells at 37 °C for 4 h and add 1 ml of full growth media to each well.
7. Incubate for an additional 20 h to allow expression from plasmid.

3.5 Luciferase Assay

Luciferase assay enables to detect the biological expression from pDNA that has reached its destination in the cell nucleus (Fig. 2).

1. Remove old media from cells and add PBS for washing. Aspirate PBS and add 100 μl of cold lysis buffer to each well. For this, 0.1 % Triton-X 100 in PBS is suitable.

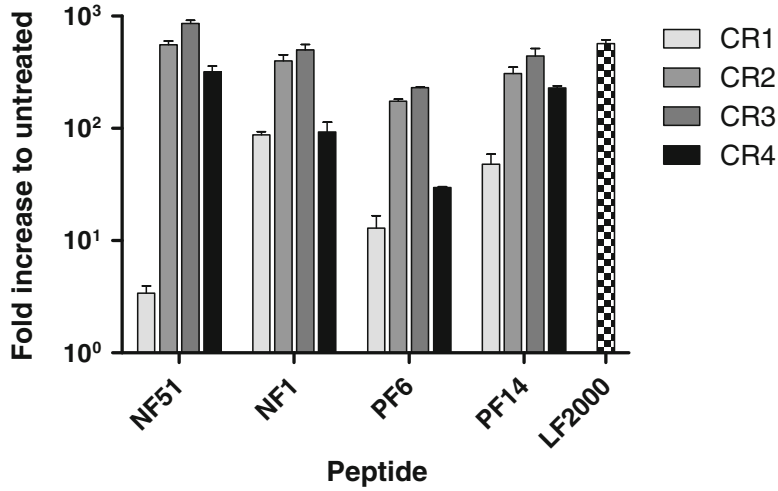

Fig. 2 Luciferase gene expression in HeLa cells at serum-containing conditions. CPP/pDNA complexes were formed at different charge ratios. Luciferase was measured 24 h after transfection. Results are expressed in relative luminescence units per mg protein and normalized as a fold increase to untreated cells. Lipofectamine™ 2000 is used as positive control

2. Incubate cells at 4 °C for 30 min; thereafter incubate for 15 min at room temperature on a shaker to detach cells from plate (*see* **Note 17**).
3. Transfer lysed cells to 1.5 ml tube and vortex.
4. From each sample transfer 20 μl to a corresponding well on a white 96-well plate.
5. To each sample add 80 μl luciferase substrate and mix gently, avoiding bubbles in the sample (*see* **Note 18**).
6. Measure luminescence on luminometer (*see* **Note 19**).

3.6 Protein Determination

Determination of protein in the samples enables normalization of luminescence values to protein contents, excluding errors arrived from different amount of protein per well.

1. Follow **steps 1–3** from "Luciferase assay."
2. Transfer 5 μl of cell lysate to transparent 96-well plate.
3. Add 25 μl of reagent A′ (20 μl reagent S per 1 ml reagent A) and 200 μl of reagent B to each well.
4. Mix gently to avoid bubbles.
5. Incubate at room temperature for 15 min and measure absorbance at $\lambda = 690$ nm (*see* **Note 20**).
6. Calculate protein concentrations in each well and normalize the relative luminescence (RLU) by dividing RLU values with protein content expressed in milligram, obtaining values RLU per mg (*see* **Note 21**).

4 Notes

1. Luc-gene-encoding plasmids are available in 1 mg/ml stocks. It is advisable to store the plasmid at high concentrations and for experimental use make 20 μl aliquots and store at −20 °C.
2. For peptides containing tyrosine (Y) or phosphotyrosine adsorption measurement can be done to verify the concentration of the peptide solution. Dilute peptide powder in smaller amount of MQ water than needed to make 1 mM solution. Make 100 μM dilution and measure absorbance at 276 nm/266 nm respectively. Divide results by coefficient $\varepsilon = 1.450$. Add needed amount of MQ water to the stock to obtain 1 mM solution. Make 20 μl aliquots, as repeated freeze-thaw cycles could lower efficacy of the peptide.
3. Lipofectamine™ 2000 could be substituted with other known transfection reagents suitable for nucleic acid delivery. As a positive control Lipofectamine™ 2000 is most commonly used, but Lipofectamine™ 3000 and other transfection reagents are also possible.
4. Store ethidium bromide in the fridge protected from light and separately from other reagents, as it is highly carcinogenic. Always use gloves when handling EtBr.
5. Store PicoGreen stocks as aliquots of 20 μl at −20 °C. Make dilutions in MQ only before measurement under the hood to avoid foreign DNA contamination. Keep solution away from light or wrapped in foil.
6. Lower trypsin concentration reagents could be used when dealing with sensitive cell lines. When needed, increase the incubation time with trypsin and track changes in cell shape under the microscope. When cells turn into ball-shaped formations, add media and wash cells off the plate.
7. Use black 96-well plates with white wells if dealing with high luciferase expression to avoid luminescence deviations into neighboring wells. If possible, leave empty wells between samples.
8. When lysing the cells, always check the solution for large aggregates. Remove them by pipetting or vortex. Lysate should be homogenous. If dealing with highly aggregating cells, transfer solute into 1.5 ml tube and mix for 1 min on vortex.
9. Stocks should be kept at higher concentrations, whereas working solution should be diluted enough for workable volumes. For each experiment, the use of freshly mixed dilution is advisable.

10. When other plasmids are used, the size of the pDNA should be considered while calculating peptide concentrations for each charge ratio. The optimal charge ratios of PFs and NFs for plasmid delivery are 2 and 3 with CPP in excess. The calculation of ratios is as follows: The theoretical number of negative charges in pDNA phosphate backbone is divided to the theoretical positive charges in peptide sequence to obtain the number of peptides per plasmid to cover all negative charges. This ratio is 1. For 24-well plate the pDNA quantity should be 0.5 μg per well.
11. The theoretical positive charges for the peptides are shown in Table 1 and correspond to the number of functional lysines (K) and ornithines (O) in the sequence.
12. For each well on 24-well plate 50 μl of complex in final volume of 500 μl is optimal.
13. Avoid having bubbles in the gel by mixing it gently. If you have air bubbles in the gel, use pipette tip to remove or move the bubble to the corners of the gel. Especially try to avoid bubbles near the gel teeth.
14. Always use freshly diluted PicoGreen for experiment. You can optimize the dilution for your pDNA, but lower concentration dilutions are advised.
15. The number of seeded cells depends on the time of cell cycle. On the day of transfection, the confluence should be 70–80 %. Although the transfection efficacy is not highly dependent on cell number, avoid having overgrown cells before the lysis.
16. We use full media in experiments, as this is more relevant to the conditions for in vivo experiments, although transfection efficacy could be lower.
17. You can see under light, if cells are still attached to the plate (white haze vs. shiny clean). If unable to remove cells completely or have aggregates, use pipette to wash cells off and homogenize lysate.
18. Bubbles interfere with the measurement. To remove bubbles, use pipette or short shaking.
19. Measure luminescence after lysing, as longer periods and freeze-thawing may result in loss of activity.
20. Establish a protein concentration curve using solutions with known protein concentrations. For example, use a known amount of bovine serum albumin (BSA) and make serial dilutions to obtain the standard curve. When possible, always include standards on the protein measurement plate.
21. Presentation of results as a fold increase to untreated enables better comparison between different experimental sets.

Acknowledgements

This work was supported by EU through the European Regional Development Fund through the project Tumor-Tech (3.2.1001.11-0008) and Centre of Excellence of Chemical Biology, by the Estonian Ministry of Education and Research through IUT20–26 and Estonian Science Foundation Grant ETF9438.

References

1. Brasseur R, Divita G (2010) Happy birthday cell penetrating peptides: already 20 years. Biochim Biophys Acta 1798:2177–2181
2. Lee SH, Castagner B, Leroux JC (2013) Is there a future for cell-penetrating peptides in oligonucleotide delivery? Eur J Pharm Biopharm 85:5–11
3. Lehto T, Kurrikoff K, Langel Ü (2012) Cell-penetrating peptides for the delivery of nucleic acids. Expert Opin Drug Deliv 9:823–836
4. Morris MC, Vidal P, Chaloin L et al (1997) A new peptide vector for efficient delivery of oligonucleotides into mammalian cells. Nucleic Acids Res 25:2730–2736
5. Scholz C, Wagner E (2011) Therapeutic plasmid DNA versus siRNA delivery: common and different tasks for synthetic carriers. J Control Release 161:554–565
6. van Asbeck AH, Beyerle A, McNeill H et al (2013) Molecular parameters of siRNA–cell penetrating peptide nanocomplexes for efficient cellular delivery. ACS Nano 7:3797–3807
7. Viola JR, El-Andaloussi S, Oprea II et al (2010) Non-viral nanovectors for gene delivery: factors that govern successful therapeutics. Expert Opin Drug Deliv 7:721–735
8. Kwok A, Hart SL (2010) Comparative structural and functional studies of nanoparticle formulations for DNA and siRNA delivery. Nanomedicine 7:210–219
9. Mäe M, El Andaloussi S, Lundin P et al (2009) A stearylated CPP for delivery of splice correcting oligonucleotides using a non-covalent co-incubation strategy. J Control Release 134:221–227
10. Arukuusk P, Pärnaste L, Oskolkov N et al (2013) New generation of efficient peptide-based vectors, NickFects, for the delivery of nucleic acids. Biochim Biophys Acta 1828:1365–1373
11. Oskolkov N, Arukuusk P, Copolovici DM et al (2011) NickFects, phosphorylated derivatives of Transportan 10 for cellular delivery of oligonucleotides. Int J Pept Res Ther 17:147–157
12. Ezzat K, Helmfors H, Tudoran O et al (2012) Scavenger receptor-mediated uptake of cell-penetrating peptide nanocomplexes with oligonucleotides. FASEB J 26:1172–1180
13. Arukuusk P, Pärnaste L, Margus H et al (2013) Differential endosomal pathways for radically modified peptide vectors. Bioconjug Chem 24:1721–1732
14. Lundin P, Johansson H, Guterstam P et al (2008) Distinct uptake routes of cell-penetrating peptide conjugates. Bioconjug Chem 19:2535–2542
15. Lehto T, Simonson OE, Mäger I et al (2011) A peptide-based vector for efficient gene transfer in vitro and in vivo. Mol Ther 19:1457–1467
16. El Andaloussi S, Lehto T, Mäger I et al (2011) Design of a peptide-based vector, PepFect6, for efficient delivery of siRNA in cell culture and systemically in vivo. Nucleic Acids Res 39:3972–3987
17. Ezzat K, El Andaloussi S, Zaghloul EM et al (2011) PepFect 14, a novel cell-penetrating peptide for oligonucleotide delivery in solution and as solid formulation. Nucleic Acids Res 39:5284–5298
18. Ezzat K, Zaghloul EM, El Andaloussi S et al (2013) Solid formulation of cell-penetrating peptide nanocomplexes with siRNA and their stability in simulated gastric conditions. J Control Release 162:1–8
19. Veiman KL, Mäger I, Ezzat K et al (2012) PepFect14 peptide vector for efficient gene delivery in cell cultures. Mol Pharm 10: 199–210
20. Lindberg S, Munoz-Alarcon A, Helmfors H et al (2012) PepFect15, a novel endosomolytic cell-penetrating peptide for oligonucleotide delivery via scavenger receptors. Int J Pharm 441:242–247

Chapter 20

In Vitro Assays to Assess Exon Skipping in Duchenne Muscular Dystrophy

Prisca Boisguerin, Liz O'Donovan, Michael J. Gait, and Bernard Lebleu

Abstract

Cell-penetrating peptide (CPP)-mediated delivery of phosphorodiamidate morpholino oligomers (PMO) results in efficient exon skipping and has shown great promise as a potential therapy for Duchenne muscular dystrophy (DMD). However, large differences in efficiency have been observed between CPPs and in delivery to different tissues. Cellular trafficking has appeared to be an important determinant of activity. This chapter provides details of experimental procedures to monitor exon skipping efficiency and cellular trafficking of Pip6a-PMO, a recently developed and particularly efficient conjugate, in skeletal H2k cells and in primary cardiomyocytes from *mdx* mice. Similar procedures may be used in principle to evaluate any free or vector-associated oligonucleotide for exon skipping.

Key words Exon skipping, Oligonucleotides, Cell-penetrating peptides, Cell trafficking, PMO

1 Introduction

An exon skipping strategy capitalizing on splice switching oligonucleotides (SSOs) to bypass the mutated exons of dystrophin gene has shown great promise for the treatment of Duchenne muscular dystrophy (DMD) both in vitro, in animal models (mainly *mdx* mice) and in small scale clinical trials [1–3]. However, large concentrations of free SSOs are required to achieve dystrophin expression upon systemic administration in skeletal muscles and no restoration has been observed in the cardiac muscle unless extremely high doses are used [4, 5].

Charge-neutral PMOs bind to RNA with high affinity and have been used as SSO and covalently linked to cell-penetrating peptides (CPP) to enhance delivery. Such conjugates are called P-PMOs [6, 7]. Extensive in vitro and in vivo studies have been conducted using the arginine-rich B peptide ($(RXRRBR)_2$ where X stands for aminohexanoic acid and B for beta-alanine) [8, 9]. These P-PMO conjugates promote dystrophin rescue at lower doses than free PMO SSOs in skeletal muscles but remain poorly active in the

Ülo Langel (ed.), *Cell-Penetrating Peptides: Methods and Protocols*, Methods in Molecular Biology, vol. 1324,
DOI 10.1007/978-1-4939-2806-4_20,

heart [10]. Our group has proposed an R_6-penetratin (R_6-Pen) PMO conjugate [11] which has served as a lead compound for the engineering of a series of peptides called Pips, the most recent paradigm being Pip6a [6]. This Pip6a turned out to be the most efficient PMO delivery CPP so far achieved in both in vitro [12] and *mdx* mice experiments [6] and such P-PMO is now undergoing extensive preclinical studies.

Since cellular uptake (mostly by endocytosis) and release from endocytic vesicles are key determinants of the biological activity of CPP-transported cargoes [13], we felt it important to set up easy-to-implement tools to monitor PPMO trafficking in relevant cells. We describe here tools to follow the uptake mechanism and the intracellular distribution of the Pip6a-PMO conjugate in skeletal and cardiac muscle cells isolated from *mdx* mice. These same tools will be easily adaptable to other CPP-cargo conjugates in various cell types.

2 Materials

2.1 Synthesis of Peptide-PMO Conjugates (Fig. 1)

1. CPP sequence Pip6a is Ac-R-X-R-R-B-R-R-X-R-Y-Q-F-L-I-R-X-R-B-R-X-R-B-COOH (X = aminohexanoic acid and B = beta-alanine purchased from a number of suppliers, such as Cambridge Research Biochemicals).
2. PMO (Gene Tools LLC).
3. 2-(1H-benzotriazole-1-yl)-1,1,3,3-tetramethyluronium hexafluorophosphate (HBTU).
4. Hydroxyazabenzotriazole (HOAt).
5. Diisopropylethylamine (DIPEA, >99 %).

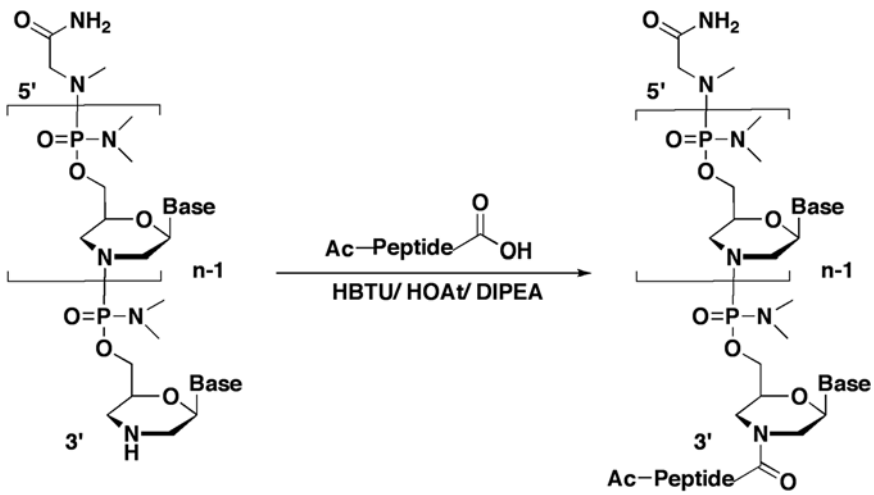

Fig. 1 Scheme of the conjugation reaction of an *N*-acetylated peptide to PMO

6. *N*-methyl-2-pyrrolidone (NMP).
7. Dimethyl sulfoxide (DMSO)
8. 2 ml Spin-X 0.22 μm cellulose acetate filtration units.
9. Reversed-phase analytical HPLC, use a C-18 Jupiter reversed phase (250 × 10 mm, 10 μm pore size) analytical column (Phenomenex). Buffer A: 0.1 % trifluoroacetic acid (TFA), buffer B: 90 % acetonitrile/0.1 % TFA.

2.2 Animals

1. C57BL/10ScSn-Dmd^{mdx}/J mice (common name *mdx*) have a loss-of-function mutation in the dystrophin gene [13].

2.3 Culture and Differentiation of mdx H2k Skeletal Muscle Cells

1. *Full growth medium*: D-MEM (with high glucose and glutamax) supplemented with 10 % (v/v) fetal bovine serum Gold (FBS), 2 % Chicken Embryo Extract (Seralab, UK), 1 % penicillin-streptomycin (100×, PS) antibiotic mixture.
2. Recombinant murine Interferon-γ (IFNγ, PeproTech, France).
3. *Differentiation medium*: D-MEM (with high glucose and glutamax) supplemented with 5 % (v/v) horse serum (HS), 1 % penicillin-streptomycin (PS) antibiotic mixture (100×).
4. 175 cm^2 cell culture flasks.
5. Phosphate-buffered saline (D-PBS).
6. Trypsin/EDTA 0.05 % for cell dissociation.
7. Gelatin from porcine skin, Type A.
8. Two CO_2 incubators: 33 °C and 10 % CO_2 for cell maintenance; 37 °C and 5 % CO_2 for cell differentiation.
9. Thoma cell for cell counting.

2.4 Isolation and Culture of Primary mdx Cardiomyocytes

1. Collagenase IV (Serlabo, UK) and Collagenase II (Life Technologies, France).
2. *Plating medium*: 42 % D-MEM (with high glucose and glutamax), 42 % M199 supplemented with 10 % horse serum (HS), 5 % fetal bovine serum (FBS), 1 % penicillin-streptomycin (PS) antibiotic mixture.
3. 25 cm^2 cell culture flasks.
4. *ADS buffer*: 3.4 g NaCl, 2.38 g 4-(2-hydroxyethyl)-1-piperazine-ethanesulfonic acid (HEPES), 0.06 g NaH_2PO_4, 0.5 g glucose, 0.2 g KCl, 0.05 g $MgSO_4$; ad. 500 ml; pH 7.35 (sterile filtered).
5. Trypsin/EDTA 0.05 % for cell dissociation.
6. Gelatin from porcine skin, Type A.
7. Laminine (Life Technologies).

8. Stop buffers (SB1): 1 ml ADS+ 10 % FBS+ 12.5 μM $CaCl_2$ (SB2)-(SB6): 1 ml ADS+ 5 % FBS+ 62 μM; 112 μM; 212 μM; 500 μM; 1,000 μM $CaCl_2$, respectively.
9. CO_2 incubator: 37 °C and 5 % CO_2.
10. Thoma cell for cell counting.

2.5 Cell Transfection

1. Unlabeled or Cy5-labeled Pip6a-PMO.
2. Opti-MEM medium for serum-free incubations.
3. Phosphate-buffered saline (D-PBS).
4. 24-Well cell culture plates.

2.6 Fluorescence Spectroscopic Analysis of PMO Conjugates (Cellular Uptake)

1. Trypsin/EDTA 0.05 %.
2. Trypsin inhibitor from soya bean.
3. Phosphate-buffered saline (D-PBS).
4. Glo Lysis Buffer.
5. BCA Protein Assay Kit.
6. POLARstar Omega (BMG Labtech).

2.7 RNA Extraction

1. NucleoSpin RNA II.
2. TRI reagent.
3. Chloroform.
4. Isopropanol.
5. Ethanol.
6. Water, nuclease free.
7. NanoDrop 1000.

2.8 RT PCR Analysis of Exon Skipping

1. Primers:
   Exon26Ro—5'-TTC TTC AGC TTG TGT CAT CC-3'.
   Exon20Fo—5'-CAG AAT TCT GCC AAT TGC TGAG-3'.
   Exon20Fi—5'-CCC AGT CTA CCA CCC TAT CAG AGC-3'.
   Exon26Ri—5'-CCT GCC TTT AAG GCT TCC TT-3'.
2. GeneAmp® Gold RNA PCR Core Kit.
3. GeneAmp RNA PCR Core Kit.
4. Gel Loading Dye, Blue (6×).
5. 100 bp DNA Ladder.
6. Ethidium bromide.
7. 10× Tris/borate/EDTA (TBE): 540 g Tris base, 275 g boric acid, 38 g ethylenediaminetetraacetic acid, ad. 5 l.
8. Agarose.

9. T Personal Thermocycler.
10. InGenius LHR Gel Imaging System (Syngene, UK).

2.9 Fluorescence Microscopy of PMO Conjugates (Intracellular Distribution)

1. Glass-bottom dish.
2. Hoechst 33342.
3. Inverse Microscope DMIRE2.

2.10 Endocytosis Inhibition Assays

1. 2-Deoxy-D-glucose.
2. Sodium acid.
3. 5-(*N*-Ethyl-*N*-isopropyl)-amiloride (EIPA).
4. Chlorpromazine (CPZ).
5. Chloroquine (CQN).
6. Nystatin (NYS).

3 Methods

3.1 Synthesis of Peptide-PMO Conjugates (2 μmol Scale)

1. Place 20 μL of a 0.1 M solution of Pip6a or other peptide IS in NMP in a 1.5 ml centrifuge tube.
2. Add 15.3 μL of a 0.3 M solution of HBTU in NMP and 13.3 μL of a 0.3 M solution of HOAt and mix the solution briefly.
3. Add DIPEA (0.8 μL) and PMO (100 μL of a 10 mM solution in DMSO) and mix briefly.
4. Heat the solution at 40 °C for 2 h and stop the reaction by the addition of water (500 μL).
5. Purify the conjugate on a (HR)-16 cation-exchange column in one injection using a gradient elution with a sodium phosphate buffer (25 mM, pH 7.2) containing 25 % acetonitrile (HPLC grade) as buffer A and a sodium phosphate buffer (25 mM, pH 7.2) containing 25 % acetonitrile and 1 M NaCl as buffer B and a flow rate of 6 ml min^{-1}. Set the detector to record at 218 nm for detection of peaks.
6. Collect purified product and desalt using an Amicon® Ultra-15 3 K centrifugal filter device as per the manufacturer's instructions.
7. Lyophilize the desalted product.
8. For qualitative analysis, dissolve peptide-PMO conjugate product in sterile water and filter through a Spin-X 0.22 μm cellulose acetate filtration unit.

9. Analyze the product by reversed-phase HPLC using a gradient elution at a flow rate of 1 ml min^{-1} and monitoring at 218 nm as well as by MALDI-TOF mass spectrometry.
10. Perform quantification by measuring the UV absorbance at 265 nm in 0.1 M HCl (*see* **Note 1**).

3.2 Culture and Differentiation of H2k Skeletal Muscle Cells

1. Cultivate H2k *mdx* cells at 33 °C with 10 % CO_2 in full growth medium supplemented with 0.1 μg/μl IFNγ on 0.01 % gelatine-coated dishes.
2. Change cell culture medium every 2–3 days and grow until 80–90 % confluence.
3. Wash cells twice and detach them from the bottom of the cell culture dish using trypsin/EDTA for 5 min at 37 °C, 5 % CO_2. Stop trypsin/EDTA activity by adding supplemented cell culture medium.
4. Transfer 1/10th of the cell suspension into new cell culture dishes and add fresh cell culture medium. Use the remaining part for the experiments.
5. For performing assays, seed 4×10^4 cells/ml/well in gelatine pre-coated 24-well plates, grow them for 2 days at 33 °C, 10 % CO_2, and replace growth medium by differentiation medium. After starting of the differentiation, change differentiation medium daily and culture cells for 5–6 days at 37 °C, 5 % CO_2 (*see* **Note 2**).

3.3 Isolation and Culture of Primary mdx Cardiomyocytes

1. Sacrifice neonatal mice (C57BL/10ScSn-Dmd^{mdx}/J) aged between 1 and 2 days by head abscission, excise the hearts, cut it into small pieces, and collect them in ADS buffer.
2. Pre-warm the collected hearts in the ADS buffer at 37 °C for 15 min.
3. Replace the buffer by 1 ml of enzyme solution consisting of Collagenase II and Collagenase IV (each 4 mg/ml), 12.5 μM $CaCl_2$ in ADS buffer.
4. Shake the tube at 37 °C, 800 rpm, for 15 min.
5. Leave the undigested heart pieces for sedimentation in the tube for some seconds.
6. Transfer the supernatant to a 2 ml tube and add 1 ml of stop buffer (SB1).
7. Add again 1 ml of enzyme solution to the hearts and pipet up and down with a glass pipette (Fig. 2) for manual dissociation (*see* **Note 3**). Repeat all steps three times.
8. Centrifuge all tubes at $250 \times g$ for 2 min.
9. Discard the supernatant and resuspend the dissociated cardiomyocytes in 1 ml SB2 solution.

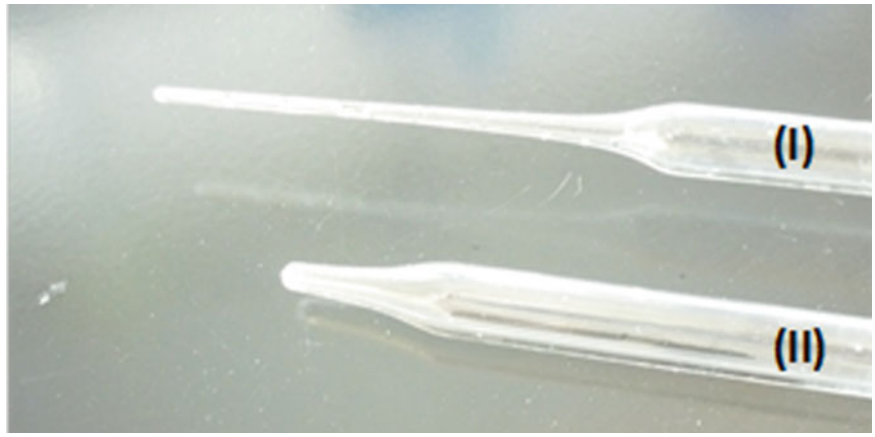

Fig. 2 Example of glass pipets with different diameters and ground ends

10. Centrifuge the cells again and replace the SB2 buffer by SB3, which contains a higher $CaCl_2$ concentration. Repeat this procedure six times (till the use of SB6) (*see* **Note 3**).
11. After the last addition of calcium-containing buffer, centrifuge the cells and replace the buffer SB6 by 1 ml of plating medium.
12. Pass the cell suspension through a cell strainer, add 9–15 ml plating medium, and transfer into a 25 cm^2 flask.
13. Incubate the cells at 37 °C, 5 % CO_2 for 45 min. The fibroblasts should have attached to the flask bottom during this time and the cardiomyocytes will remain in suspension, so that they could be transferred to a tube for counting.
14. After counting, put 1×10^5 cells/ml/well into 24-well plates and incubate cells overnight at 37 °C, 5 % CO_2.
15. Change medium after washing twice with ADS buffer to remove dead cells. Then change medium every day without washing until performing the desired assay (*see* **Note 4**).

3.4 Fluorescence Spectroscopy (Cellular Uptake)

1. Wash the cells twice with PBS.
2. Add the desired PMO or Pip6a-PMO concentration either in OptiMEM or in serum-containing medium (500 µl incubation volume) to the cells for 4 h at 37 °C, 5 % CO_2 (Fig. 3).
3. After the incubation time, wash the cells twice with PBS and incubate them with 100 µl trypsin (10 min, at 37 °C, 5 % CO_2) to detach the cells from the wells and to remove cell-membrane-bound P-PMO (*see* **Note 5**).
4. Stop the reaction by adding 100 µl trypsin inhibitor and 400 µl PBS and transfer the cell suspensions in tubes and centrifuge them (5 min, $900 \times g$).

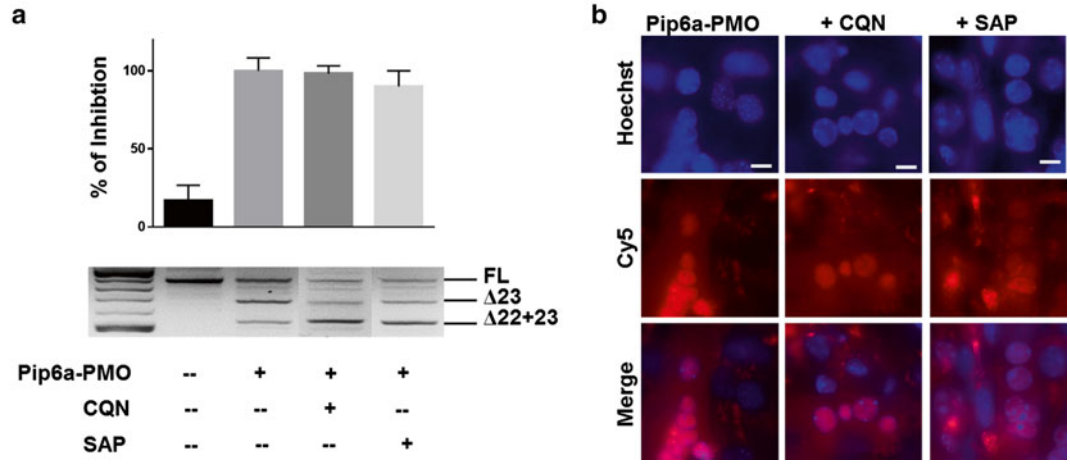

Fig. 3 Example of Pip6a-PMO cellular trafficking in mdx H2k myotubes. (**a**) Effect of endosomolytic (chloroquine = CQN) and membrane-permeating (saponin = SAP) reagents on the uptake of Pip6a-PMO (at 250 nM) in H2k *mdx* myotubes at 4 h post-treatment as measured by fluorescence spectroscopy (*upper panel*, $n \geq 4$). Exon skipping within the sample samples as above was analysed by RT-PCR (*lower panel*). Treatment with the reagents was started 30 min prior to Pip6a-PMO addition. The following reagents were used at indicated concentrations: CQN (100 μM) and SA (10 μM). Percentage of exon skipping (%ES) was calculated on the densitometric value of the Δ23 band related to the other bands (full length + Δ23 + Δ23 + 22). (**b**) Representative images of H2K *mdx* myotubes incubated for 4 h with Cy5-labeled Pip6a-PMO alone or in the presence of CQN or SAP. Cell nuclei were labeled with Hoechst dye. Untreated cells are shown as controls. Pip6a-PMO distribution in live unfixed cells was evaluated by fluorescence microscopy with a Zeiss Axiovert 200 M. *White bar* = 10 μm

5. Remove the supernatants and perform the cell lysis using 300 μl Glo Lysis buffer (1-h incubation at 4 °C on a rotating wheel).
6. Take 100 μl samples for fluorescence measurement on POLARStar plate reader.
7. Measure the protein concentration using the BCA Protein Assay Kit according to the manufacturer's instruction.
8. Calculate the RFL (relative fluorescence) per mg protein to get representative results for the Pip6a-PMO uptake.
9. Use the remaining sample amount for RNA isolation with the TRI Reagent Protocol (*see* Section 3.5.1).

3.5 Exon Skipping Evaluation

3.5.1 RNA Isolation Using TRI Reagent Protocol

1. After determination of Pip6a-PMO uptake, add 0.5 ml TRI Reagent to each sample (200 μl remaining lysate), mix the samples and freeze them overnight.
2. Thaw samples and centrifuge them for 10 min to remove fat, polysaccharides and proteins. Carry all centrifugation steps at 4 °C and 12,000 × *g*.
3. Transfer the supernatant to a fresh tube and add 0.2 ml chloroform to separate RNAs from proteins and DNA.
4. Shake and incubate the samples for 10 min at room temperature. Afterwards centrifuge the tubes 15 min.

5. Transfer the colorless upper phase, containing RNA, to a fresh tube and add 0.5 ml isopropanol.
6. Mix and incubate the samples 10 min at room temperature.
7. Following a centrifugation step for 10 min, remove the supernatant and wash the pellet by adding of 75 % cold ethanol.
8. Keep the samples 1 h at −20 °C. Afterwards, centrifuge all samples for 5 min and repeat the ethanol washing procedure.
9. Discard the washing solution and dry the RNA pellet at room temperature for 10 min following by a drying step at 33 °C for about 8 min.
10. Dissolve the RNAs in 30 µl nuclease-free water and measure the RNA concentration at the NanoDrop (*see* **Note 6**).

3.5.2 RNA Isolation Using NucleoSpin Extraction

1. Perform RNA isolation following the manufacturer's instructions of the NucleoSpin Kit II, if uptake measurement was not required.

3.5.3 Reverse Transcription

1. Perform the reverse transcription in two steps by using the GeneAmp RNA PCR Core Kit following the manufacturer's instructions. *See* Table 1 for the protocol and the cycler program for the first step.
2. Use 350 ng of RNA as template.
3. Perform the second step of the reverse transcription using the mastermix composition shown in Table 2.
4. Add 35 µl of the mastermix directly to the PCR tube of the first step RT and start the program for the second part immediately.

Table 1
First step of reverse transcription

Protocol		**Cycler program**		
Components	Vol (µl/1 rxn)	Temperature	Time	# of cycles
MgCl2 (25 mM)	2.00	42 °C	30 min	1
PCR buffer II (10×)	1.50	94 °C	5 min	1
dNTP's mix (10 mM)	4.00	5 °C	5 min	1
RNAse inhibitor (20 U/µl)	0.50	5 °C	Hold	∞
Exon26 Ro (10 µM) MuLV RT (50 U/µl) Water RNA (350 ng) *Final volume*	0.75 0.50 *Varies* *Varies* *15*			

Table 2
Second step of reverse transcription

Protocol		**Cycler program**		
Components	Vol (µl/rxn)	Temperature	Time	# of cycles
MgCl2 (25 mM)	2.00	95 °C	2 min	1
PCR Buffer II (10×) Exon26 Fo (10 µM) Amplitaq (5 U/µl)	3.50 0.75 0.25	95 °C 58 °C 72 °C	30 s 60 s 2 min	30
Water	28.50	72 °C	10 min	1
Final volume	*35*	5 °C	Hold	∞

Table 3
Nested polymerase protocol

Protocol		**Cycler program**		
Components	Vol (µl/rxn)	Temperature	Time	# of cycles
PCR Gold Buffer (10×)	5.00	95	10 min	1
$MgCl_2$ (25 mM) dNTP mix (10 mM) Exon20 Fi (10 µM)	4.00 1.00 2.50	95 58 73	30 s 60 s 2 min	22
Exon26 Ri (10 µM)	2.50	72	10 min	1
Amplitaq Gold	0.25	5	Hold	∞
Water RT-PCR template *Final volume*	32.75 2.00 *50.00*			

3.5.4 Nested Polymerase Chain Reaction

1. Perform a nested PCR using the GeneAmp® Gold RNA PCR Core Kit following the manufacturer's instructions, after the RT-PCR.
2. Use the protocol described in Table 3.

3.5.5 Agarose Gel Electrophoresis and Evaluation

1. Prepare 2 % w/v agarose melted in 1× TBE buffer for exon skipping visualization by agarose gel electrophoresis.
2. Dilute the samples in 6× DNA gel loading buffer and visualize them by ethidium bromide staining.
3. Use a 100 bp DNA ladder (2.5 µl) as standard.
4. Perform the electrophoresis in 1× TBE buffer at 100 V for approximately 1 h.

5. Quantify the band intensities for calculation of exon skipping (%ES) by densitometric analysis with ImageJ (http://rsbweb.nih.gov/ij/).
6. Calculate ES% using the densitometric value of the Δ23 band related to the other bands [ES% = (full-length + Δ23 + Δ22)/Δ23 × 100].

3.6 Fluorescence Microscopy of PMO Conjugates (Cellular Distribution)

1. Seed 4×10^4 H2k *mdx* cells/compartment on gelatin (0.01 %)-coated four-compartment dishes and treat them as described in Section 2.2.
2. Seed 4×10^5 cardiomyocytes/compartment on Laminin (1 ng/ml)-coated four-compartment dishes and keep them as described in Section 2.3.
3. Transfect the cells with Pip6a-Cy5-PMO (1 μM in OptiMEM) for 4 h at 37 °C, 5 % CO_2.
4. Add 2 μl Hoechst 33342 on cells 30 min before the end of the incubation to visualize nuclei.
5. Eliminate the excess of conjugate or dye by washing twice with PBS.
6. Add new OptiMEM and image immediately using a DMIRE2 inverted microscope.

3.7 Evaluation of the Internalization Mechanism

1. Pre-treat the cells for 30 min with the following inhibitors/reagents: 10 mM NaN_3 and 6 mM 2 deoxy-D-glucose (DDG) for ATP depletion (-ATP); 7.5 μM, 15 μM or 30 μM chlorpromazine (CPZ) for clathrin-mediated endocytosis inhibition; 50 μM or 25 μM nystatin (Nys) for caveolae-mediated endocytosis inhibition; 10 μM 5-(*N*-ethyl-*N*-isopropyl) amilorid (EIPA) for macropinocytosis inhibition, 100 μM chloroquine (CQN) as endosomlytic reagent; and 10 μM saponin (SAP) as membrane-permeating reagent (*see* **Note 7**).
2. Add PMO or Pip6a-PMO at the desired concentration for a 4-h incubation.
3. After the incubation time, treat the cells as mentioned above for uptake measurement (Section 3.2) and for exon skipping evaluation (Section 3.3).

4 Notes

1. This protocol should result in a yield of around 20–30 % and may be scaled up as required.
2. The differentiation of H2k *mdx* cells can be monitored by a Western blot assay for troponin T level or by observation under the microscope. Myotubes can easily be distinguished by morphology and contractile movements.

3. During cardiomyocytes isolation, it is important to use a grinded (over a flame) glass pipet to dissociate the cells; and also during the procedure of $CaCl_2$ reintroduction. Do not use conventional 1,000 µl pipets since the tip will disrupt cardiomyocyte membrane integrity.
4. The differentiation of *mdx* cardiomyocytes can be monitored by their contractile movements.
5. For uptake measurement, trypsinization of the cells is crucial to remove P-PMOs sticking on the cell surface, which could otherwise result in an overestimation of P-PMO internalization.
6. To obtain good yields of RNA with high-quality purity during TRI reagent protocol, it is important: (1) to use ice-cold 75 % ethanol for RNA precipitation, (2) to put the samples at least 1 h at −20 °C, and (3) to include a second washing step with 75 % ethanol.
7. Concentration of endocytosis inhibitors should be carefully adapted to the used cell by performing dose-responses to prevent toxic side effects.

Acknowledgments

MJG and BL are members of the MDEX consortium. Liz O'Donovan was supported by a grant from the French muscular dystrophy association AFM (programme number 14784). Work in the laboratory of MJG was supported by the Medical Research Council (MRC programme number U105178803). We thank Matthew Wood and his team at Oxford University for continuing collaboration on design and use of CPP-PMO to treat various neuromuscular diseases.

PB thanks Dr Stéphanie Barrère-Lemaire (IGF, Montpellier, France) for introduction in cardiomyocyte isolation.

References

1. Wilton SD et al (1999) Specific removal of the nonsense mutation from the mdx dystrophin mRNA using antisense oligonucleotides. Neuromuscul Disord 9:330–338
2. Goemans NM et al (2011) Systemic administration of PRO051 in Duchenne's muscular dystrophy. N Engl J Med 364:1513–1522
3. Cirak S et al (2011) Exon skipping and dystrophin restoration in patients with Duchenne muscular dystrophy after systemic phosphorodiamidate morpholino oligomer treatment: an open-label, phase 2, dose-escalation study. Lancet 378:595–605
4. Lu QL et al (2005) Systemic delivery of antisense oligoribonucleotide restores dystrophin expression in body-wide skeletal muscles. Proc Natl Acad Sci U S A 102:198–203
5. Malerba A et al (2011) Chronic systemic therapy with low-dose morpholino oligomers ameliorates the pathology and normalizes locomotor behavior in mdx mice. Mol Ther 19:345–354
6. Betts CA, Wood MJA (2013) Cell penetrating peptide delivery of splice directing oligonucleotides as a treatment for Duchenne muscular dystrophy. Curr Pharm Des 19:2948–2962

7. El Andaloussi SA, Hammond SM, Mäger I, Wood MJA (2012) Use of cell-penetrating-peptides in oligonucleotide splice switching therapy. Curr Gene Ther 12:161–178
8. Moulton HM et al (2007) Cell-penetrating peptide-morpholino conjugates alter pre-mRNA splicing of DMD (Duchenne muscular dystrophy) and inhibit murine coronavirus replication in vivo. Biochem Soc Trans 35: 826–828
9. Jearawiriyapaisarn N et al (2008) Sustained dystrophin expression induced by peptide-conjugated morpholino oligomers in the muscles of mdx mice. Mol Ther 16:1624–1629
10. Wu B et al (2008) Effective rescue of dystrophin improves cardiac function in dystrophin-deficient mice by a modified morpholino oligomer. Proc Natl Acad Sci U S A 105: 14814–14819
11. Abes S et al (2007) Efficient splicing correction by PNA conjugation to an R6-Penetratin delivery peptide. Nucleic Acids Res 35: 4495–4502
12. Lehto T et al (2014) Cellular trafficking determines the exon skipping activity of Pip6a-PMO in mdx skeletal and cardiac muscle cells. Nucleic Acids Res 42:3207–3217
13. Schertzer JD et al (2008) Muscle-specific overexpression of IGF-I improves E-C coupling in skeletal muscle fibers from dystrophic mdx mice. Am J Physiol Cell Physiol 294: C161–C168

Chapter 21

Applications of ApoB LDLR-Binding Domain Approach for the Development of CNS-Penetrating Peptides for Alzheimer's Disease

Eliezer Masliah and Brian Spencer

Abstract

Delivery of protein therapeutics to the CNS has proven to be a challenge to due to the presence of the blood-brain barrier (BBB), which prevents the passage of most proteins and large molecules from invading the neuronal space. Recently, we, and others, have developed technologies to circumvent this barrier by targeting receptors on the surface of the endothelial cells of the BBB to facilitate transport of therapeutic proteins. We describe here one such approach for targeting the LDLR by fusion of 38 amino acids from the ApoB protein to a therapeutic protein.

Key words Blood-brain barrier, Transcytosis, LDLR, ApoB, ApoE, Protein transport, CNS delivery, Therapeutics

1 Introduction

The blood-brain barrier (BBB) controls the passage of substances from the blood into the central nervous system. Thus, a major challenge for the delivery of protein therapeutics following intravenous delivery is the transport of these large proteins to the CNS. The BBB is composed of tight junction forming endothelial cells, pericytes, and astrocytes. This combination functions to allow only small molecules and directed transport by receptor-mediated transcytosis from the blood to the CNS.

The receptors expressed on the endothelial cells of the BBB function to capture proteins in the blood, endocytose the protein/receptor complex, and transcytose the complex to the neuronal side of the cells where the protein is released. Starzyk et al. were the first to show that targeting a receptor on the blood-brain barrier could transport a "cargo" protein to the neuronal side of the BBB [1]. An antibody developed against the transferrin receptor

Ülo Langel (ed.), *Cell-Penetrating Peptides: Methods and Protocols*, Methods in Molecular Biology, vol. 1324,
DOI 10.1007/978-1-4939-2806-4_21,

expressed on the blood-brain barrier was able to transport methotrexate to the CNS. This same approach has been used to target the transport of proteins and peptides across the BBB efficiently [2, 3]. Other well-characterized BBB receptors include low-density lipoprotein receptor, insulin receptor, and insulin growth factor receptor [4].

The low-density lipoprotein receptor family is a group of cell surface receptors that bind lipoprotein complexes for internalization to the lysosomes. The family comprises approximately ten different receptors with the most common examples being -ow-density lipoprotein receptor (LDLR), low-density lipoprotein-related receptor (LRP), very-low density lipoprotein receptor (VLDL), megalin, and apolipoprotein E receptor. The receptors are expressed in a tissue-specific manner and primarily bind apolipoprotein complexes. The apolipoprotein, of which the two most prominent members are apolipoprotein B (ApoB) and apolipoprotein E (ApoE), function to bind lipids in the blood stream and target them for lysosomal degradation. Binding of the apolipoproteins to the receptor results in endocytosis and transport to the lysosome where the low pH compartment facilitates the release of the protein complex. The LDL receptor is then recycled to the cell surface. At the blood brain barrier, the LDL receptor binds lipoproteins resulting in endocytosis. Following endocytosis by the endothelial cells, a portion of the LDL receptor is shuttled to the apical side of the BBB where presumably, the apolipoprotein is released to be taken up by neurons and/ or astrocytes (reviewed in Refs. [5, 6]).

We and others have identified receptor binding domains from apolipoprotein B (38 amino acids) [7] and apolipoprotein E (19 amino acids) [7, 8] that can be readily fused to target proteins including antibodies. Addition of the LDLR-binding domain significantly increased brain penetration of the cargo protein but also presented an unique cellular uptake and clearance mechanism in the brain for antibodies targeted to the CNS [9].

The ApoB sequence facilitates binding to and transport with the LDL receptor at the blood-brain barrier [7]. The LDLR receptor is also highly expressed in the liver and the spleen as well as blood circulating macrophages [5]. Single-dose administration of the ApoB-cargo protein results in significant accumulation in the liver as would be expected [7]. Previous investigation of LDLR targeted recombinant proteins has shown uptake in spleen and muscle [7]. In contrast, the lung does not express the LDLR, and we have not observed recombinant protein accumulation in this organ.

In this chapter we describe the methods for cloning the ApoB LDLR-binding domain to a cargo protein for transport to the CNS across the blood-brain barrier. The recombinant protein can

then be expressed by a viral vector from a depot organ such as the liver [7, 9, 10] or as be delivered by i.v. or i.p. injection as a recombinant protein [11].

2 Materials

2.1 Oligonucleotides

1. Oligonucleotides (Fig. 1) can be ordered from any local vendor that is capable of synthesizing long oligonucleotides.
2. Order both complementary strands of the oligonucleotide including the necessary overhangs for your cloning restriction site (*see* **Note 1**), stop codon (*see* **Note 2**), and epitope tag (*see* **Note 3**).
3. To reduce the incorporation of errors in the long synthesis of the oligonucleotides, specify PAGE purification.
4. Specify 5' phosphorylation on the oligonucleotide order. Alternatively, you can phosphorylate the oligonucleotides prior to the annealing step with T4 Kinase.

2.2 Transfection Reagents

1. *500 ml 2× BBS*
   (a) 50 ml 2.8 M NaCl (Sigma, St. Louis, MO, USA).
   (b) 50 ml 500 mM BES (Calbiochem, Darmstadt, Germany).
   (c) 5 ml 150 mM Na_2HPO_4 (Sigma, St. Louis, MO, USA).
   (d) Adjust pH 6.95 with 1 M NaOH.
   (e) Filter sterilize through 0.22 μm filter.
   (f) Store at 4 °C for 3–4 days prior to validation.
2. *10× CaCl2*
   (a) 2.5 M $CaCl_2$ (Calbiochem, Darmstadt, Germany) dissolved in H_2O.
   (b) Filter sterilize through a 0.22 μm filter (*see* **Note 4**).
   (c) Store at −20 °C in 1.4 ml aliquots (will not freeze).
   (d) Working solution (*see* **Note 5**) will be diluted to 1× with sterile water immediately before use.

```
 S  S  V  I  D  A  L  Q  Y  K  L  E  G  T  T  R  L
TCA TCT GTC ATT GAT GCA CTG CAG TAC AAA TTA GAG GGC ACC ACA AGA TTG
 T  R  K  R  G  L  K  L  A  T  A  L  S  L  S  N  K
ACA AGA AAA AGG GGA TTG AAG TTA GCC ACA GCT CTG TCT CTG AGC AAC AAA
 F  V  E  G  S
TTT GTG GAG GGT AGT
```

Fig. 1 ApoB LDLR-binding domain oligonucleotides and amino acid sequence

3 Methods

3.1 Annealing Oligonucleotides

1. Dilute oligonucleotides to 40 μM in H_2O.
2. Set up the following reaction in a thin-wall PCR tube.
   (a) 1 μl each oligonucleotide.
   (b) 2 μl T4 ligase buffer (NEB Biolabs, Ipswich, MA, USA).
   (c) 16 μl H_2O.
3. Place in 95 °C water bath (3 l) for 2 min.
4. Turn off water bath and allow to cool to room temperature.

3.2 Cloning ApoB Oligonucleotide

1. Dilute annealing reaction from above 1:2 with 20 μl H_2O.
2. Digest the expression plasmid containing your cargo gene with the appropriate restriction enzymes.
3. Run the restriction reaction on an agarose gel and isolate the vector. Clean the vector from the agarose before proceeding with the next step (Wizard SV Gel and PCR Clean Up, Promega, WI USA).
4. Set up the following reaction in 0.5 ml tube.
   (a) 50 ng linearized vector.
   (b) 2 μl phosphorylated annealed oligonucleotides from the above reaction.
   (c) 1 μl T4 ligase buffer.
   (d) QS 9 μl H_2O.
   (e) 1 μl T4 ligase (NEB Biolabs, Ipswich, MA, USA).
5. Incubate 16 °C overnight.
6. Transform full ligation mix into chemically competent bacterial cells such as Top10.
   (a) Plate bacteria onto LB agar plates containing selection media.
   (b) Be sure to include vector-only control.
7. The next day pick 3–5 colonies and grow up in LB broth containing selection media overnight.
   (a) Isolate the DNA from the clones.
   (b) Sequence the DNA with an appropriate primer to verify the insertion of the ApoB oligonucleotide sequence.

3.3 Transfecting

1. Fibroblast cells such as 293 (human embryonic kidney) or CHO (Chinese hamster ovary) have previously served to produce good quantities of protein.

2. Add 10 μg of the final expression plasmid with the cloned ApoB LDLR-binding domain along with H_2O so the final volume including the $CaCl_2$ of the next step equals 0.5 ml for each 10 cm dish of cells at 80 % confluency.
3. Add $CaCl_2$ at the dilution you established during validation (*see* **Note 5**).
4. Add 2× BBS to the solution (0.5 ml for each 10 cm dish).
5. Mix gently by inverting ~3–5 times, and incubate for 15 min at room temperature.
6. Add the DNA/$CaCl_2$ mix dropwise to the dish (1.0 ml per 10 cm dish). Spread DNA by carefully rocking the plate.
7. Place the cells at 3 % CO_2 at 37 °C.
8. Change medium next morning, and incubate at 10 % CO_2.
9. Use complete media with serum or alternatively, use OptiMem (Life Technologies).
10. At predetermined time the medium is collected and filtered through a 0.22 μm filter.

3.4 Protein Purification

1. Proceed with protein purification with previously established protocols for the cargo protein (*see* **Note 6**).
2. Alternatively, utilize an epitope or His tag inserted with the ApoB sequence for purification (*see* **Note 7**).

3.5 Virus Vector Production

1. For virus vector production, see one of the previously published protocols for details on packaging the vector construct [12].

4 Notes

1. Addition of unique restriction sites in the cargo gene will aid in cloning the ApoB peptide. Site-directed mutagenesis could be achieved with the QuickChange Lightning Site-Directed Mutagenesis Kit (Stratagene, Santa Clara, CA, USA).
2. Care should be taken to ensure that the ApoB LDLR-binding domain remains in the same reading frame as the target protein. Additionally, a stop codon should be added at the end of the sequence if it is placed at the 3' of the target protein.
3. Addition of an epitope tag is often desirable to differentiate endogenous protein from the targeted protein or to identify proteins with poor commercial antibodies. Addition of an epitope tag should be placed between the ApoB LDLR and the targeted protein so that the ApoB LDLR-binding domain is always at the terminus of the protein.

4. Pre-wet the filter prior to filtering the $CaCl_2$ solution to allow the high-salt solution to pass through the membrane easier.
5. Check $CaCl_2$ diluted 1:8, 1:10, and 1:12 in combination with 2× BBS in a transfection experiment with a GFP reporter such as pcDNA3-GFP (Addgene, Cambridge, MA, USA). Usually 293 Ts in 10 cm dishes are used for this. Using the combination that gives the best transfection results are recommended, which will also be useful for large-scale protein production later. Transfect a 10 cm dish of 293 T cell (70–80 % confluent) with 20 μg GFP reporter plasmid and check transfection efficiency the next day. Should be at least 90–95 % GFP^+ cells. Aliquot 2XBBS and store at 4 °C.
6. A functional assay for the targeted protein is desirable to determine if addition of the ApoB LDLR targeting sequence alters or abolishes normal protein function.
7. The 38 amino acid ApoB LDLR-binding domain is highly hydrophobic and could affect protein purification protocols. It may be advisable to consider this when designing the protein and to add a poly-histidine tag for purification purposes.

Acknowledgments

This work supported by NIH grants AG18440 and AG10435.

References

1. Friden PM, Walus LR, Musso GF, Taylor MA, Malfroy B, Starzyk RM (1991) Anti-transferrin receptor antibody and antibody-drug conjugates cross the blood-brain barrier. Proc Natl Acad Sci U S A 88(11):4771–4775
2. Shin SU, Friden P, Moran M, Olson T, Kang YS, Pardridge WM, Morrison SL (1995) Transferrin-antibody fusion proteins are effective in brain targeting. Proc Natl Acad Sci U S A 92(7):2820–2824
3. Boado RJ, Zhang Y, Zhang Y, Pardridge WM (2007) Genetic engineering, expression, and activity of a fusion protein of a human neurotrophin and a molecular Trojan horse for delivery across the human blood-brain barrier. Biotechnol Bioeng 97(6):1376–1386. doi:10.1002/bit.21369
4. Pardridge WM (2005) Molecular biology of the blood-brain barrier. Mol Biotechnol 30(1): 57–70
5. Hussain MM, Strickland DK, Bakillah A (1999) The mammalian low-density lipoprotein receptor family. Annu Rev Nutr 19: 141–172
6. Bickel U, Yoshikawa T, Pardridge WM (2001) Delivery of peptides and proteins through the blood-brain barrier. Adv Drug Deliv Rev 46(1–3):247–279
7. Spencer BJ, Verma IM (2007) Targeted delivery of proteins across the blood-brain barrier. Proc Natl Acad Sci U S A 104:7594–7599
8. Bockenhoff A, Cramer S, Wolte P, Knieling S, Wohlenberg C, Gieselmann V, Galla HJ, Matzner U (2014) Comparison of five peptide vectors for improved brain delivery of the lysosomal enzyme arylsulfatase A. J Neurosci 34(9):3122–3129. doi:10.1523/JNEUROSCI.4785-13.2014
9. Spencer B, Emadi S, Desplats P, Eleuteri S, Michael S, Kosberg K, Shen J, Rockenstein E, Patrick C, Adame A, Gonzalez T, Sierks M, Masliah E (2014) ESCRT-mediated uptake and degradation of brain-targeted alpha-synuclein single chain antibody attenuates neuronal degeneration

in vivo. Mol Ther 22(10):1753–1767. doi:10.1038/mt.2014.129

10. Spencer B, Marr RA, Gindi R, Potkar R, Michael S, Adame A, Rockenstein E, Verma IM, Masliah E (2011) Peripheral delivery of a CNS targeted, metalo-protease reduces abeta toxicity in a mouse model of Alzheimer's disease. PLoS One 6(1):e16575. doi:10.1371/journal.pone.0016575
11. Spencer B, Verma I, Desplats P, Morvinski D, Rockenstein E, Adame A, Masliah E (2014) A neuroprotective brain penetrating endopeptidase fusion protein ameliorates Alzheimer's disease pathology and restores neurogenesis. J Biol Chem. doi:10.1074/jbc.M114.557439
12. Tiscornia G, Singer O, Verma IM (2006) Production and purification of lentiviral vectors. Nat Protoc 1(1):241–245

Chapter 22

CPP-Based Delivery System for In Vivo Gene Delivery

Kaido Kurrikoff, Kadi-Liis Veiman, and Ülo Langel

Abstract

The method presents most important steps in estimating a CPP-mediated reporter gene delivery in a mouse model. The method is applicable for administrating noncovalent CPP/pDNA complexes via i.v. injection and for analysis of luciferase levels in tissue homogenates. This method could be extended to analyze the delivery of different nucleic acid cargos with other types of delivery vectors. First, a simple method is presented for assessing the stability of complexes in blood after i.v. administration, based on quantitation of a fluorescently labeled nucleic acid. Secondly, a protocol is presented for assessing and analyzing luciferase levels in mouse organs.

Key words CPP, pDNA, Noncovalent complexes, Gene delivery, In vivo reporter gene induction

1 Introduction

Gene delivery using pDNA expression systems represents a most potential way of achieving diverse gene expression modulation in target cell, organ, tissue, or whole organism. Accordingly, an exogenous gene along with its expression regulating elements, such as promoters and enhancers, can be inserted into a pDNA expression vector. Transfection of pDNA into cells allows induction of therapeutic gene and subsequently alter disease progression. Alternatively, pDNA can be designed to produce different gene expression regulating elements, such as shRNA, which allows to silence aberrant target gene levels. Depending on the pDNA design, the expression of its gene of interest can vary in expression levels and expression time (short- or long-term expression), and these can in turn depend on tissue type, such as when using tissue-specific promoters and enhancers.

DNA transfection requires effective delivery mediators. This is especially important in vivo settings, where most of the cell transfection reagents are ineffective, and toxicity aspects should be assessed profoundly. This chapter focuses on using cell-penetrating peptides (CPP) for the delivery of nucleic acids, especially pDNA, in vivo.

Ülo Langel (ed.), *Cell-Penetrating Peptides: Methods and Protocols*, Methods in Molecular Biology, vol. 1324,
DOI 10.1007/978-1-4939-2806-4_22,

Most CPP-based transfection systems utilize noncovalent complexation strategy [1] for nucleic acid and the peptide, and thus, the following protocol is only applicable to such methodology. Furthermore, this chapter describes administration of pDNA-based expression system via i.v. route, although other methods may also be beneficial in certain disease models. While there are only scarce few reports on using CPPs as sole mediators for in vivo gene induction [2, 3], this approach is nevertheless important as an emerging method from the clinical perspective. CPPs are more frequently applied as a functionalization moiety for lipoplex or polyplex systems to enhance their uptake potential to cells [4]. Nevertheless, currently achieved lipoplex- and polyplex-mediated gene transfer efficacies are not even nearly satisfactory, as only certain organs and tissues can be targeted. The gene delivery potency of CPPs is mostly unknown from in vivo perspective, and therefore this protocol serves the purpose of enhancing their use in this context.

The most obvious challenge that the CPP/nucleic acid complexes have to face in vivo is blood environment and before starting to assess the potential gene delivery efficacy of a CPP in vivo, it is recommended to consider this important aspect. First, one should thoroughly assess transfection efficacy in vitro in the presence of serum [5]. Although there are no assays or tests that allow prediction of in vivo efficacy, in our experience, only the CPPs that have high efficacy in vitro, in the presence of serum, are able to show any activity in vivo. Next, we recommend assessment of complex stability in the presence of serum or in whole blood. One possible method is to assess the clearance of the CPP and/or its nucleic acid cargo from the blood after i.v. administration of the complexes. That can be easily achieved by using a fluorescently labeled DNA and assessing its recovery from the blood circulation. Compared to injection of naked pDNA, the complexes should persist much longer in the circulation. Concomitantly, the same methodology could be used to assess the uptake of CPP/pDNA complexes in all organs, either by quantitative assessment of whole organs or by histological follow-up. This protocol, however, focuses on quantitation of labeled nucleic acids in blood. The organ uptake values can subsequently be compared to actual gene induction levels. Accordingly, in the second part of the chapter, we present a protocol to assess reporter gene induction levels in organs.

2 Materials

2.1 Peptides, Plasmids, and Complex Formation

In routine studies for luciferase expression we have used CMV-driven Fluc2 expression cassette, mixed with CPP at different CRs. pDNA aliquots in MQ water are stored at −20 °C. Our standard pDNA injection dose is 1–2.5 mg/kg.

1. pDNA solution (1 mg/ml).
2. Cy5 labelling kit (Mirus, USA) for plasmid DNA labelling.

3. PepFect14 [5] peptide solution (1 mM).
4. MQ water.
5. 1.5 ml Eppendorf tubes.
6. D-Glucose powder.

2.2 Intravenous Administration of Complexes

1. I.v. injection equipment and accessories (depending on the injection method that is used): tail warming method, mouse restrainer, syringes.
2. Syringes and filter for filtering glucose.
3. 70 % ethanol.

2.3 Collecting Blood

1. Shaver, clipper, or scissors for hair removal.
2. 27-G needle.
3. Vaseline.
4. Sodium-heparinized (80 iu/ml ± 30 %) capillaries (Marienfeld, Germany).
5. Heparinized blood-collecting tubes (Sarstedt, Germany).

2.4 Collecting Tissues

1. Surgical instruments—Scissors, forceps.
2. Dry ice.
3. Eppendorf tubes or glass slides.

2.5 Sample Homogenization

1. Mortar and pestle or other physical homogenization or grinding equipment, such as Precellys®24-Dual homogenization system (Bertin Technologies, France).
2. 1 × Promega lysis buffer (Promega, Sweden).
3. Temperature-controlled centrifuge.

2.6 Fluorescence Measurements from Blood and Tissue Lysates

1. Black 96-well plate.
2. Fluorometer plate reader, such as Synergy Mx Multi-Mode Reader (Biotek, USA).

2.7 Luciferase Assay and Protein Determination

1. Luciferase assay substrate (Promega, Sweden).
2. Black 96-well plate with white wells.
3. Transparent 96-well plates.
4. DC™ Protein Assay reagents (BioRad).
5. Microplate luminometer, such as GLOMAX 96 (Promega, Sweden).
6. Tecan Sunrise Spectrophotometer (Tecan, Switzerland).

3 Methods

The ability of CPPs to deliver Cy5-labeled pDNA or luciferase encoding pDNA in vivo conditions is assessed using Balb/c mice. The luciferase assay is based on Promega's luciferase reporter system, where gene expression levels induced by CPP-mediated pLuc delivery from different tissues are measured. Raw light units are normalized against protein content from the sample, further normalized against respective pDNA-treated tissue. This strategy enables to identify the potential of CPP of interest to deliver genes to organs.

There are several possibilities to study the stability of pDNA/peptide complexes. One of the most common assay is incubation of complexes in the presence of serum components. However this assay does not allow to assess the impact of the washout by the organism or the removal of complexes by immune system components in blood. For that the most straightforward assay is to measure complex stability in blood and for that Cy5-labeled pDNA (Mirus, USA) was used, where 1 mg/kg of labeled pDNA was mixed with the peptides and injected i.v. via tail vein.

Luciferase-based reporter systems have an advantage over different fluorescence-based systems especially for in vivo applications. Firstly, it is very sensitive and already picograms of luciferase give reasonable signal. Secondly, compared to fluorescence-based methods, it has lower signal-to-noise ratio and when using it with live imaging it enables to measure already small gene expression values from deep tissues, such as lungs, liver or even intracranial disease models such as tumors. Although live imaging has a great potential to evaluate gene expression changes over time, and the expression dynamics can be followed in the same animal, it is not as sensitive a method as direct luciferase measurements from tissue homogenates. Moreover, live imaging is a means of screening the behavior of the gene delivery vector at a whole body level, but the exact organ quantitation should be performed separately. Therefore, we mainly use live imaging in parallel with luciferase measurements from tissue homogenates to evaluate the potential of CPP-mediated gene delivery.

3.1 Complex Formation for In Vivo Applications

1. Mix Cy5-labeled pDNA (for complex stability from blood) or luciferase encoding pDNA (1 mg/ml) into fresh MQ water and thereafter add peptide (1 mM) to obtain desired charge ratio. Obtained volume for complexes is 100 μl.
2. Incubate the complexes for 40 min at room temperature.
3. Prepare 10 % glucose solution in MQ water and filtrate it through 0.2 μm filter.

4. After the incubation time stated in Subheading 3.1, **step 2**, add 100 μl of 10 % of glucose solution to complexes and mix with a pipette. Final injection volume is 200 μl in 5 % glucose.
5. Immediately proceed with the injection procedure (either Subheading 3.2 or 3.4).

3.2 Blood Collection

1. At different time points after injection (15 min–24 h) collect blood samples from mouse saphenous vein. For that remove hair locally using animal hair clipper or scissors (*see* **Note 1**). Recommended time points that should be included are 30 min, 1 h, 3 h, 6 h, 12 h, and 24 h (*see* **Note 2**).
2. Place the mouse into restrainer tube and grab hold of the leg tightly. Apply vaseline at the thigh area.
3. Punctuate the vein with a sterile 27G syringe needle at 90° angle.
4. Collect about 40 μl of blood into sodium-heparinized (80 iu/ml ± 30 %) capillary collection tubes. Stop the bleeding by applying gentle pressure to the puncture area.
5. Transfer blood from the capillary into heparinized blood collection tube and (optional) store samples at –20 °C, and proceed with the fluorescence measurements.

3.3 Fluorescence Measurements from Blood

1. Transfer 20 μl of blood to black 96-well plate, and if possible duplicate or triplicate the sample.
2. Add 80 μl MQ water.
3. Measure Cy5-labeled pDNA fluorescence on a fluorometer plate reader (at $\lambda_{ex} = 650$ nm and $\lambda_{em} = 670$ nm). Fluorescence from an untreated blood sample should be measured as a negative control.
4. Subtract untreated sample values from Cy5-pDNA-containing samples. Normalize the acquired values to pDNA concentration. For that, construct naked labeled-pDNA and peptide/labeled-pDNA complex spike-in fluorescence calibration curves (according to the pDNA concentration) and calculate pDNA amount in blood sample at different time points (*see* **Note 3**).
5. An example graph is represented in Fig. 1.

3.4 Tissue Collection and Homogenization for the Quantitation of Luciferase Levels from Tissue Homogenates

1. 24 h after administration of complexes sacrifice mice using cervical dislocation.
2. Proceed immediately with harvesting the tissues of interest (lungs, liver, spleen, kidney, etc.) and snap-freeze on dry ice. Work quickly, without unnecessary pauses until the tissues have been frozen.

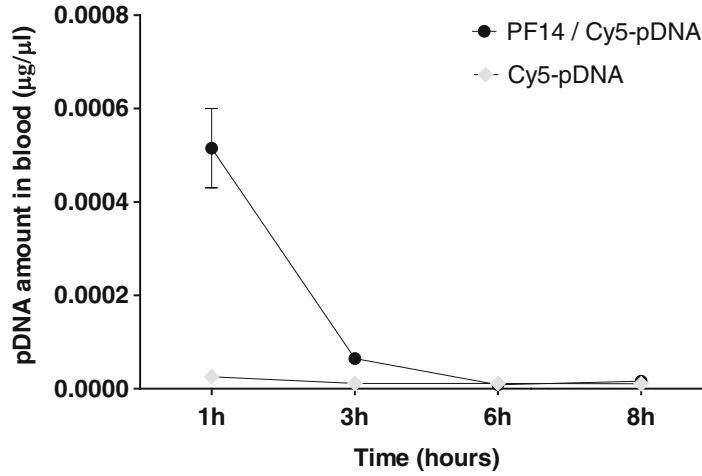

Fig. 1 Estimation of complex stability in blood. For the normalization, naked Cy5-pDNA or peptide/Cy5-pDNA calibration curves were constructed. Fluorescence levels are quantified, using small amount of blood sample at indicated time points. Note that CPP-bound pDNA levels persist longer in blood circulation, compared to free pDNA

3.5 Tissue Homogenization

1. Homogenize the tissues using Precellys®24-Dual homogenization system or mortar and pestle (*see* **Note 4**).

3.6 Quantitation of the Luciferase Content

1. Lyse the homogenized tissues using 500 μl of Promega Reporter lysis 1 × buffer.
2. Vortex the samples for 15 min.
3. Perform three consecutive freeze-thaw cycles (liquid nitrogen and 37 °C water bath).
4. Centrifuge for 3 min at 10,000 × *g*, 4 °C.
5. Remove the supernatant and place it in a new 1.5 ml tube.
6. Add another 500 μl of lysis buffer to the pellet.
7. Repeat the extraction process (without freeze-thaw cycles).
8. Combine the second supernatant with the first one.
9. Measure the luciferase activity using Promega luciferase assay system, in combination with GLOMAX 96 microplate luminometer. For that, transfer 20 μl of the supernatant to the white 96-well plate and add 80 μl of luciferase substrate to each sample. The obtained LU values will be analyzed in the subsequent step, after measuring the protein content.

3.7 Quantitation of Protein Content

1. For measuring protein content from homogenized and lysed tissues DC™ Protein Assay (Bio-Rad, USA) was used according to the manufacturer's protocol. For that dilute sample 10–20 times in MQ water. Transfer 5 μl of sample into transparent 96-well plate.

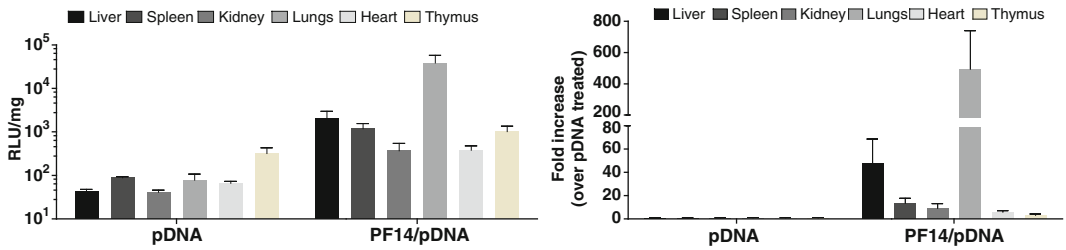

Fig. 2 Luciferase gene induction in different organs in BALB/c mice, using an i.v. injection of PF14/pLuc complexes, 50 μg of naked pDNA or in complex with PF14 at CR2. Raw RLU values are first normalized to protein content (*Left*). Next, luciferase levels are represented as fold increase over the respective pDNA-treated tissue

2. Prepare sufficient amount of A' solution in new 1.5 tube. For that add 20 μl of DC Reagent S to each 1 ml of DC Reagent A.
3. Add 25 μl of Reagent A' to each sample.
4. Add 200 μl Reagent B to each sample and mix by gentle pipetting. Incubate samples for 15 min at room temperature.
5. Measure the absorbance at 700 nm (*see* **Note 5**).

3.8 Data Analysis

1. Calculate an average protein absorbance value out of three technical replicates from Subheading 3.7. Calculate protein content of 1 ml of sample, taking into account the dilutions.
2. Calculate an average LU (light unit) out of three technical replicates from Subheading 3.6 for subsequent data analysis.
3. Normalize the average LU values within each sample against protein content obtained from Subheading 3.7. An example graph is represented in Fig. 2 (left).
4. Normalize the resultant RLU/mg against the corresponding tissue of the animals that received naked pDNA injection (sham treatment) (*see* **Note 6**).
5. An example graph is represented in Fig. 2 (right).

4 Notes

1. This can be done prior to the experiment (recommended) or immediately before the blood collection procedure (for experienced experimentators). *See* also **Note 2**, for planning the experiment timetable.
2. Note that more than one experimentator may be needed, where one person is performing injections and the other is collecting blood samples. Alternatively, if only one person is available, the number of animals has to be small, because the

injections have to be finished before the first blood collection time point occurs. The blood collection timing should be carefully followed. The early time points (i.e., within the first hour postinjection) are most informative (and hence the most important) in terms of changes in blood levels.

3. Using labeled pDNA (or any other kind of nucleic acid) requires verification that the modified DNA forms similar complexes as normal DNA. Comparative gel shift assay and heparin displacement assay should be carried out [5]. Furthermore, it should be taken into account that quantitative fluorescence levels may depend on the state of the DNA, and it may vary considerably when comparing DNA in solution and the same amount of DNA in complex with CPPs, where the compacted fluorophores often quench the fluorescence excitation signal. Therefore, DNA quantitation should be carried out using normalization curves for each CPP/pDNA complex.
4. If using mortar and pestle for tissue homogenization, the process should be carried out on dry ice to avoid thawing of homogenized tissue powder. Transfer the tissue powder to cold Eppendorf tubes (for that keep tubes on dry ice for at least 5 min) and proceed with luciferase content quantification.
5. To establish protein concentration of sample, the absorbance of known amounts of BSA solution is measured and calibration curves are constructed.
6. It should be noted that in all such experiments, use of proper controls should be followed. Therefore, the gene induction should be analyzed relative to (naked) pDNA treatment or relative to other pDNA induction method. It is important that the expression levels should not be compared to untreated tissues, because of the sensitivity of the luciferase reporter gene method, where even naked pDNA often induces measurable expression, especially in some organs or in case of some disease models.

Acknowledgements

This work was supported by the EU through the European Regional Development Fund through the project Tumor-Tech (3.2.1001.11-0008) and Centre of Excellence of Chemical Biology, and by the Estonian Ministry of Education and Research through IUT20–26.

References

1. Lehto T, Kurrikoff K, Langel U (2012) Cell-penetrating peptides for the delivery of nucleic acids. Expert Opin Drug Deliv 9(7):823–836. doi:10.1517/17425247.2012.689285
2. Rittner K, Benavente A, Bompard-Sorlet A, Heitz F, Divita G, Brasseur R, Jacobs E (2002) New basic membrane-destabilizing peptides for plasmid-based gene delivery in vitro and in vivo. Mol Ther 5(2):104–114. doi:10.1006/mthe.2002.0523
3. Read SP, Cashman SM, Kumar-Singh R (2010) A poly(ethylene) glycolylated peptide for ocular delivery compacts DNA into nanoparticles for gene delivery to post-mitotic tissues in vivo. J Gene Med 12(1):86–96. doi:10.1002/jgm.1415
4. Torchilin VP (2014) Multifunctional, stimuli-sensitive nanoparticulate systems for drug delivery. Nat Rev Drug Discov 13(11):813–827. doi:10.1038/nrd4333
5. Veiman K-L, Mäger I, Ezzat K, Margus H, Lehto T, Langel K, Kurrikoff K, Arukuusk P, Suhorutšenko J, Padari K, Pooga M, Lehto T, Langel Ü (2013) PepFect14 peptide vector for efficient gene delivery in cell cultures. Mol Pharm 10(1):199–210. doi:10.1021/mp3003557

Chapter 23

Application of CPPs for Brain Delivery

Artita Srimanee, Jakob Regberg, and Ülo Langel

Abstract

Cell-penetrating peptides provide a promising strategy for delivery of drugs across the blood–brain barrier. Here, we present an overview of CPP and peptide-mediated delivery to the central nervous system as well as a Transwell in vitro model to evaluate passage across an endothelial cell layer mimic of the blood–brain barrier.

Key words Blood–brain barrier, Transwell, Brain delivery, Glioblastoma, Cell-penetrating peptide

1 Introduction

Transport across the blood–brain barrier (BBB) is the limiting issue for most therapies directed to the CNS since most drugs are not able to pass the barrier on their own. The only exceptions are certain small molecular drugs and hydrophobic molecules. However, passage of larger molecules including "biologics" such as protein, nucleic acid, or antibody-based drugs is virtually completely restricted by the blood–brain barrier. Physiologically, the BBB is formed by tight junctions between the brain endothelial cells with supportive functions from astrocytes and pericytes. The tight junctions between endothelial cells are formed by integral membrane proteins claudin, occludin, and specific junction adhesion molecules [1, 2]. Cell-penetrating peptides provide a potential strategy for transport of large molecules across the blood–brain barrier. CPPs have been used as vectors in the delivery of proteins and peptides, nucleic acids, and small molecular drugs, and in the nanoparticles both in vitro and in vivo [3]. Chimeric peptide-mediated delivery across the BBB was reported by Pardridge and colleagues in 1987 [4]. TAT was the first CPP used in delivery of β-galactosidase in vivo study. A conjugation of TAT and β-galactosidase was found to reach the brain after i.p. administration in mice [5]. Furthermore, modified TAT with 10 histidine

Ülo Langel (ed.), *Cell-Penetrating Peptides: Methods and Protocols*, Methods in Molecular Biology, vol. 1324,
DOI 10.1007/978-1-4939-2806-4_23,

residues (TAT-10H) showed an improvement of plasmid transfection efficiency in both human and rat glioma cell lines [6].

RNA interference (RNAi) is a gene-silencing process which has been used in the treatment of CNS diseases such as brain tumors, neurotrauma, neuromuscular diseases [3], and neurodegenerative diseases, including Alzheimer's disease, Huntington's disease, and Parkinson's disease [7]. A peptide derived from rabies virus glycoprotein (RVG) was successful in siRNA delivery through the binding to nicotinic acetylcholine receptor (nAChR) across the BBB to target the neuronal cells [8]. In addition, the chimeric peptide of RVG and nonaarginines (RVG-9R) was synthesized and able to deliver siRNA to neuronal cells in vitro and also in mice, leading to specific gene knockdown in the brain [9]. Another study, penetratin linked to caspase and SOD siRNA enhanced the transfection in primary mammalian hippocampal and sympathetic neurons [10]. The peptide-based vector for delivery of small molecular drugs such as doxorubicin, paclitaxel, and benzylpenicillin has also been developed. Pegelin peptides, including SynB1 and SynB3, are amphipathic peptides derived from protegrins. They showed an ability to deliver doxorubicin to the brain using an in situ mouse brain perfusion method. This study also indicated that the peptides mediated doxorubicin uptake via an adsorptive endocytotic pathway [11, 12]. Additionally, SynB1 also has potential to transport conjugated benzylpenicillin across the BBB [13]. Recently, brain-targeting peptides have been used for modification of delivery systems, including peptide-based vectors, liposomes, polymers, and nanoparticles [14].

Glioblastoma is one of the most common targets of interest for brain-targeted therapies due to the high mortality of the disease and the relative ease of targeting cancer tumors compared to other types of tissue targeting for other neurological diseases. The targeting properties can be obtained by coupling a targeting moiety such as a receptor ligand, an antibody or antibody fragment or a targeting peptide sequence. Upon using CPPs for delivery, targeting peptides can be added to the cell-penetrating sequence in order to combine two functional parts for targeting and uptake enhancement. Homing peptides are cheaper to produce than antibodies and peptides are also less immunogenic. Several receptors, such as transferrin receptor (TfR), insulin receptor (IR), low-density lipoprotein receptor-related protein (LRP-1 and LRP-2) [15], and scavenger receptor class A and B (SR-AI and SR-BI) [16], are expressed on the BBB and targeted to facilitate the transport of drug-carrying particles via receptor-mediated transcytosis (RMT). In the past few years, a family of peptides, named Angiopeps, which were derived from Kunitz protease inhibitor domain of aprotinin [17]. Angiopep-2 (ANG) is a potentially specific ligand to LRP-1 which is highly expressed on the BBB and over-expressed on glioma cells [18]. In order to exhibit higher transcytosis and

accumulation in parenchyma than original aprotinin [19], ANG has been used for dual purposes as a peptide-based carrier and a targeting moiety. Therefore, ANG was either conjugated with anticancer drugs or modified on the nanoparticles. Treatment with covalently coupled angiopep-paclitaxel causes a reduction of metastases in the patients with advanced solid tumors and brain metastases [20, 21]. In addition, ANG has been widely used on nanoparticles [18, 22–24], cationic liposomes [25], and dendrimers [26, 27]. Recently, an activatable CPP, octaarginine (R8) linked to octaglutamate (E8) with MMP2 cleavable linker, was conjugated with ANG on the modified nanoparticles in order to develop the delivery for glioma dual targeting and glioma penetrating [28]. Moreover, ANG coupled to the CPP PepFect 32 was found to efficiently deliver plasmids in glioma cells and had ability to cross an in vitro model of the BBB [29]. Lastly, brain tumor-homing peptide named CooP was discovered from in vivo phage display which specifically targets to invasive tumor satellites and the vessels of malignant glioblastomas. The conjugation of CooP-CPP-chlorambucil significantly reduced tumor satellites in the brain, showing that CooP is another potential targeting peptide [30].

Many peptides have been designed for optimal endosomal escape, in the case of delivery across an endothelial layer those peptides are likely to remain in the endothelial cells rather than pass into the underlying tissue. CPPs have generally not been specifically designed for transcytosis, and modifications aimed at increasing the endosomal escape of peptides, this might prove contra-productive when transport across an endothelial cell layer is desired. Delivery across the blood brain barrier might require a different set of chemical properties compared to simple delivery across the cell membrane. In the case of the BBB, the peptide and cargo have to reach the CNS and must therefore not only cross the membrane once but twice, and in the process avoid to be entrapped in the cell. Taking advantage of the endogenous intracellular transport routes to deliver the cargo into the CNS is a potential strategy to overcome the difficulties.

In vitro systems are widely used to study transport across endothelial cell layers, including systems mimicking the BBB. This is commonly done by growing endothelial cells to confluence on a semi-permeable membrane, such as the Transwell system. The cell layer can either be a monoculture of endothelial cells or contain several different cell BBB-relevant cell types such as astrocytes in addition to the endothelial cells [31]. The trans-endothelial electrical resistance (TEER) of the intact blood–brain barrier is high due to the tight junctions preventing the passage of charged molecules. Thus, measurements of this resistance can be used to assess the integrity of the BBB on a BBB model system. However, the TEER of the BBB in vivo is much higher than the values obtained for measurements from in vitro models.

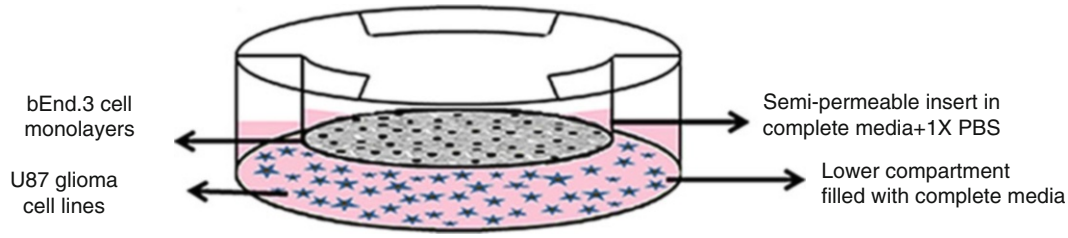

Fig. 1 An in vitro BBB model using Transwell™ apparatus. The bEnd.3 brain endothelial cell monolayers cultured on the upper chamber represents apical part of the blood side. The U87 glioma cells cultured on the bottom chamber refers to a basolateral part of the brain side

In this chapter, the study of peptide-based delivery of oligonucleotides is demonstrated in particular of the setup in vitro model of the BBB using Transwell™ apparatus and the passage evaluation of the peptide-pDNA complex. The setup BBB model is composed of two compartments, apical and basolateral parts (Fig. 1). The upper chamber is a semi-permeable membrane representing the blood side and cultured with mouse brain endothelial cells, bEnd.3. The bEnd.3 cell line has been used as a model of the BBB due to their rapid growth and maintenance of BBB characteristics with the expression of the tight junction proteins over repeated passages [32]. Another lower chamber corresponds to the brain side which is cultured with U87 glioblastoma cells. They are seeded separately from bEnd.3 due to chemokine secretion promoting permeability of brain endothelial cells [33].

2 Materials

2.1 Cell Culturing

1. Mouse brain endothelial cell line, bEnd.3 cells.
2. Glioblastoma cell line, U87 cells.
3. Cell culture medium for bEnd.3 cells: Dulbecco's modified Eagle medium (DMEM) with glutamax, 10 % fetal bovine serum (FBS), 3 mM l-glutamine, 100 U/ml penicillin, and 100 μg/ml streptomycin.
4. Cell culture medium for U87 cells: Dulbecco's modified Eagle medium (DMEM) with glutamax, 10 % fetal bovine serum (FBS), 100 U/ml penicillin, and 100 μg/ml streptomycin.

2.2 Peptide/pDNA Complex Formation

1. Stock solution of peptide in MilliQ water (MQ water) (*see* **Note 1**).
2. Luciferase-encoding plasmid (pGL3) 4.7 kbp, MW 3.10×10^6 g/mol in concentration 1 mg/ml.

2.3 Transwell

1. Transwell™ 24-well plates, clear inserts with 0.4 μm pore size of polyester (PET) membrane, 6.5 mm diameter with 0.33 cm^2 area.
2. bEnd.3 cell medium with 1× PBS (*see* **Note 2**).
3. Epithelial voltohmmeter, EVOM^2 (*see* **Note 3**).

2.4 Luminescence Assay

1. Glomax™ 96 microplate luminometer.
2. Promega's luciferase assay.
3. Protein assay.

3 Methods

3.1 Transwell™ Apparatus

1. Seed 2.5×10^4 of bEnd.3 cells in semipermeable inserts 10–14 days prior to the experiment.
2. Change cell culture media in both upper and lower chambers 100 and 600 μl, respectively, in every 2–3 days (*see* **Note 4**).
3. Measure TEER values 1–2 times a week using EVOM^2.
4. Seed 2.5×10^4 of U87 cells in each well separately with bEnd.3, 3–4 days prior to the experiment (*see* **Note 5**).
5. Place the bEnd.3 cell monolayers on semipermeable inserts on the top of U87 wells.
6. Monitor the TEER values before and after adding the complexes at 15, 45, 75, and 105 min (*see* **Note 6**).
7. Remove all inserts from U87 wells and incubate bEnd.3 and U87 separately at 37 °C, 5 % CO_2 for another 22 h.

3.2 Peptide-pDNA Complex Formation

1. Mix 1 μg of pDNA in the media (+1X PBS).
2. Add peptide in various charge ratios for total volume 100 μl.
3. Incubate the complex at room temperature for an hour.
4. Mix the same amount of pDNA with Lipofectamine 2000 using as a positive control.
5. Mix only pDNA in the media using as a negative control.

3.3 Luciferase Analysis

1. Remove the media in each wells.
2. Lyse the cells with 100 μl of cell lysis buffer at room temperature for 30 min.
3. Measure the luciferase activity using luciferase substrate (luciferin) 80 μl in 20 μl of the lysed cells.
4. Measure the relative light unit (RLU) on a Glomax™ 96 microplate luminometer.
5. Determine the mg protein content using Lowry protein determination assay kit.

4 Notes

1. Peptide stock solution (1 mM in MQ water) is normally aliquoted in 20 μl in Eppendorf tube to avoid freeze-thaw cycle. Before making complexes, the stock solution is diluted with 180 μl MQ water to obtain 100 μM of peptide solution.
2. The serum-containing medium for bEnd.3 cells on the upper compartment where the peptide/pDNA complexes are added, it is mixed with 10X PBS to obtain 1X PBS in the medium in order to maintain the integrity of the cell monolayers throughout the experiment.
3. EVOM^2 is an instrument used to monitor the integrity of the cell monolayers by measurement the resistance (TEER values); the electrode has to be in the right position and switch off the charger of EVOM^2 during measurement; charging will cause the unstable values.
4. Upon changing the media in the inserts, the pipetting tip holds against the insert wall in order to avoid scratching bEnd.3 cell monolayers and to maintain the cell integrity.
5. bEnd.3 and U87 cells are cultured separately in the same plate but different wells since U87 cells secret chemokine in the culture media and promote the permeability of the brain endothelial cells [33]. There are 12 wells in a 24-well plate having the semipermeable inserts so that the rest of other 12 wells are cultured with U87.
6. It is important to keep the cells in 37 °C; therefore, after measuring the TEER values at each time point, the cultured cells are kept in the incubator. In addition, the electrode is rinsed in the media after measuring different samples in order to avoid the contamination. The electrode can cause the infection in the cell cultures then it has to be immersed in 70 % ethanol for 10 min before using and let it dry under the laminar airflow hood (LAF).

Acknowledgement

This work was supported by the Innovative Medicines Initiative Joint Undertaking under grant agreement n° 115363 resources of which are composed of financial contribution from the European Union's Seventh Framework Programme (FP7/2007-2013) (IMI), Swedish Cancer Foundation, Sweden. Thank Maria Arvanitidou for modification of Fig. 1.

References

1. Obermeier B, Daneman R, Ransohoff RM (2013) Development, maintenance and disruption of the blood-brain barrier. Nature Med 19:1584–1596
2. Daneman R (2012) The blood-brain barrier in health and disease. Ann Neurol 72:648–672
3. Zou LL, Ma JL, Wang T et al (2013) Cell-penetrating peptide-mediated therapeutic molecule delivery into the central nervous system. Curr Neuropharmacol 11:197–208
4. Kumagai AK, Eisenberg JB, Pardridge WM (1987) Absorptive-mediated endocytosis of cationized albumin and a P-endorphin-cationized albumin chimeric peptide by isolated brain capillaries. Biochem Biophys Res Commun 146: 307–313
5. Schwarze SR (1999) In vivo protein transduction: delivery of a biologically active protein into the mouse. Science 285:1569–1572
6. Lo SL, Wang S (2008) An endosomolytic Tat peptide produced by incorporation of histidine and cysteine residues as a nonviral vector for DNA transfection. Biomaterials 29: 2408–2414
7. Nielsen TT, Nielsen JE (2013) Antisense gene silencing: therapy for neurodegenerative disorders? Genes 4:457–484
8. Mathupala SP (2009) Delivery of small interfering RNA (siRNA) to the brain. Expert Opin Ther Pat 19:137–140
9. Kumar P, Wu H, McBride JL et al (2007) Transvascular delivery of small interfering RNA to the central nervous system. Nature 448: 39–43
10. Davidson TJ, Harel S, Arboleda VA et al (2004) Highly efficient small interfering RNA delivery to primary mammalian neurons induces MicroRNA-like effects before mRNA degradation. J Neurosci 24:10040–10046
11. Rousselle C, Clair P, Lefauconnier JM et al (2000) New advances in the transport of doxorubicin through the blood-brain barrier by a peptide vector-mediated strategy. Mol Pharmacol 57:679–686
12. Rousselle C, Smirnova M, Clair P et al (2001) Enhanced delivery of doxorubicin into the brain via a peptide-vector-mediated strategy: saturation kinetics and specificity. J Pharmacol Exp Ther 296:124–131
13. Rousselle C, Clair P, Temsamani J et al (2002) Improved brain delivery of benzylpenicillin with a peptide-vector-mediated strategy. J Drug Target 10:309–315
14. de Boer AG, Gaillard PJ (2007) Drug targeting to the brain. Annu Rev Pharmacol Toxicol 47:323–355
15. Jones AR, Shusta EV (2007) Blood-brain barrier transport of therapeutics via receptor-mediation. Pharm Res 24:1759–1771
16. de Boer AG, van der Sandt ICJ, Gaillard PJ (2003) The role of drug transporters at the blood-brain barrier. Annu Rev Pharmacol Toxicol 43:629–656
17. Demeule M, Currie JC, Bertrand Y et al (2008) Involvement of the low-density lipoprotein receptor-related protein in the transcytosis of the brain delivery vector angiopep-2. J Neurochem 106:1534–1544
18. Xin H, Jiang X, Gu J et al (2011) Angiopep-conjugated poly(ethylene glycol)-co-poly(ε-caprolactone) nanoparticles as dual-targeting drug delivery system for brain glioma. Biomaterials 32:4293–4305
19. Demeule M, Re A, Che C et al (2008) Identification and design of peptides as a new drug delivery system for the brain. J Pharmacol Exp Ther 324:1064–1072
20. Bertrand Y, Currie JC, Poirier J et al (2011) Influence of glioma tumour microenvironment on the transport of ANG1005 via low-density lipoprotein receptor-related protein 1. Br J Cancer 105:1697–1707
21. Kurzrock R, Gabrail N, Chandhasin C et al (2012) Safety, pharmacokinetics, and activity of GRN1005, a novel conjugate of angiopep-2, a peptide facilitating brain penetration, and paclitaxel, in patients with advanced solid tumors. Mol Cancer Ther 11:308–316
22. Ren J, Shen S, Wang D et al (2012) The targeted delivery of anticancer drugs to brain glioma by PEGylated oxidized multi-walled carbon nanotubes modified with angiopep-2. Biomaterials 33:3324–3333
23. Xin H, Sha X, Jiang X et al (2012) The brain targeting mechanism of Angiopep-conjugated poly(ethylene glycol)-co-poly(ε-caprolactone) nanoparticles. Biomaterials 33:1673–1681
24. Xin H, Sha X, Jiang X et al (2012) Anti-glioblastoma efficacy and safety of paclitaxel-loading Angiopep-conjugated dual targeting PEG-PCL nanoparticles. Biomaterials 33: 8167–8176

25. Sun X, Pang Z, Ye H et al (2012) Co-delivery of pEGFP-hTRAIL and paclitaxel to brain glioma mediated by an angiopep-conjugated liposome. Biomaterials 33:916–924
26. Ke W, Shao K, Huang R et al (2009) Gene delivery targeted to the brain using an Angiopep-conjugated polyethyleneglycol-modified polyamidoamine dendrimer. Biomaterials 30:6976–6985
27. Huang S, Li J, Han L et al (2011) Dual targeting effect of Angiopep-2-modified, DNA-loaded nanoparticles for glioma. Biomaterials 32:6832–6838
28. Gao H, Zhang S, Cao S et al (2014) Angiopep-2 and activatable cell-penetrating peptide dual-functionalized nanoparticles for systemic glioma-targeting delivery. Mol Pharm 11:2755–2763
29. Srimanee A, Regberg J, Hällbrink M et al (2013) Peptide-based delivery of oligonucleotides across blood–brain barrier model. Int J Pept Res Ther 20:169–178
30. Hyvönen M, Enbäck J, Huhtala T et al (2014) Novel target for peptide-based imaging and treatment of brain tumors. Mol Cancer Ther 13:996–1007
31. Xue Q, Liu Y, Qi H et al (2013) A novel brain neurovascular unit model with neurons, astrocytes and microvascular endothelial cells of rat. Int J Biol Sci 9:174–189
32. Brown RC, Morris AP, Neil RGO (2008) Tight junction protein expression and barrier properties of immortalized mouse brain microvessel endothelial cells. Brain Res 1130: 17–30
33. Dwyer J, Hebda JK, Le Guelte A et al (2012) Glioblastoma cell-secreted interleukin-8 induces brain endothelial cell permeability via CXCR2. PLoS One 7:e45562

Chapter 24

Intracellular Delivery of Nanoparticles with Cell Penetrating Peptides

Giuseppina Salzano and Vladimir P. Torchilin

Abstract

The functionalization of nanoparticles (NPs) with cell penetrating peptides (CPPs) constitutes a breakthrough for the intracellular delivery of therapeutic and diagnostic payloads. In late 1998, a significant cellular uptake of a small protein from the HIV-1 virus, namely TAT peptide (TATp), was observed. Thereafter, research began on design of similarly acting peptides, and the coupling of NPs with these novel CPPs. Here, we describe recent methods used to modify the surface of NPs with CPPs and the in vitro and in vivo effects of such functionalization on the intracellular delivery of various cargos. In particular, we highlight recent advances aimed at reducing the non-selectivity of CPPs and the prevention of their enzymatic cleavage en route to target tissues.

Key words CPPs, TATp, Liposomes, Polymeric micelles, Multifunctional nanocarriers, Stimulus-sensitive nanoparticles

1 Introduction

1.1 Cell Penetrating Peptides

The term CPPs refers to a wide variety of peptides, usually containing less than 30 amino acids with predominately basic residues, that readily breach the cell membrane and that can deliver a wide range of macromolecular cargos to the interior cells. In late 1988, Frankel and Pabo [1] first described significant cellular uptake of a small protein from the HIV-1 virus, the so-called TATp. Known CPPs currently include penetratin [2], synthetic polyarginines [3], transportan [4], and the widely studied TAT peptides [5]. These peptides facilitate the intracellular uptake of molecules including proteins, nucleic acids, chemotherapeutic drugs, and even nanoparticle-sized vesicles [6, 7]. Despite extensive study of their delivery of molecules into cells, the exact uptake mechanism of these CPP peptides remains under debate. Two main cellular uptake mechanisms of CPPs have been proposed: the non-endocytotic and the endocytotic pathways. The pathway used appears to depend on the size and type of the molecule carried,

Ülo Langel (ed.), *Cell-Penetrating Peptides: Methods and Protocols*, Methods in Molecular Biology, vol. 1324,
DOI 10.1007/978-1-4939-2806-4_24,

the cell type, and the membrane lipid composition [8]. The usefulness of CPPs stems from their lack of toxicity and the ease of synthesis of such peptides and attachment to various cargos, including NPs. The functionalization of NPs with CPPs has been accomplished by use of both covalent and non-covalent methods. In late 1999, Josephson L and colleagues [9] were the first to internalize NPs using CPPs. Dextran based-superparamagnetic iron oxide NPs were coated with TATp to improve intracellular magnetic labeling of different target cells [10]. A 100-fold greater cellular uptake of TATp-coated NPs by lymphocytes occurred compared to non-modified NPs. The next challenge was to modify the most popular nanocarriers (liposomes and micelles) with CPPs.

1.2 Liposomes

Liposomes are nanosized vesicles composed mainly of cholesterol (Chol) and phospholipids. Liposomes represent a very versatile system able to load a wide variety of molecules. The therapeutic efficacy and the superiority of drugs encapsulated in liposomes compared to free drugs have been well established [11]. The success of liposomes stems not only from the ease of synthesis but also from the possibility to modify the surface of such nanosystems with other compounds to change their pharmacokinetic and pharmacodynamic profile. For example, by simply introducing PEG to the surface of liposomes, their circulation time is markedly increased, facilitating the accumulation in pathological areas with a compromised vasculature, such as tumor tissues, by the enhanced permeability and retention effect (EPR effect) [12–14]. However, the presence of PEG chains on the surface of liposomes can hinder the interaction between the liposomes and cells, reducing the cell internalization of the payload. To address this problem, CPPs have been attached to liposomes. Multiple TATp molecules can be attached to PEGylated liposomes via a spacer, such as *p-nitrophenylcarbonyl-PEG*-phosphatidylethanolamine (pNP-PEG-PE) [15, 16]. Few hundred pNP-PEG-PE-TATp conjugates can be attached to a single liposome. The result is a highly increased internalization of the carrier into many different cell types, including ovarian carcinoma cells, Lewis lung carcinoma cells, breast BT20 cells, and rat cardiac myocytes (H9C2) [15]. With the same approach, polymeric micelles can be efficiently functionalized with CPPs.

1.3 Polymeric Micelles

Polymeric micelles are made of amphiphilic block copolymers which can self-assemble in aqueous solution as a core–shell structure with incorporated poorly soluble drugs. They are small (10–100 nm), with a high in vivo stability and low toxicity. The choice of a particular amphiphilic block copolymer can confer properties such as extended blood half-life and targeting the carrier to specific tissues. For example, micelles made of PEG-PE have relatively good longevity, stability in vivo, together with the capability to accumulate in areas with damaged or abnormal blood vessels (tumors, infarcts) [17, 18]. There are several good examples of

CPP-modified PEG-PE micelles [19–21]. The incorporation of a TATp-PEG-PE conjugate into self-assembling PEG-PE micelles confers complete protection of the TATp from proteolysis when the PEG chain of the PEG-PE is longer than the PEG chain of the TATp-PEG-PE conjugate [22].

1.4 Recent Achievements

Despite such extensive applications thus far, the main downside in the use of exogenous CPPs for delivery of cargos is the lack of selectivity of CPPs and their ability to induce an immune response against the delivered cargo, which compromises the therapeutic efficacy and the toxicity of the active agent. Several strategies have been proposed to overcome these problems and to generate effective CPP based NPs. In the next segment, we highlight the recent advances in developing "programmed" NPs that shield the CPPs while in blood circulation and "deshield" them when at a target site. The design of NPs able to efficiently incorporate active agents and selectively deliver them into target site has been a major focus of pharmaceutical research. Here, the term "multifunctional NPs" refers to vesicles which co-incorporate multiple broadly active agents and specific targeting ligands, such as antibodies and CPPs. One of the main efforts has been to build NPs where the nonspecific CPP moiety is shielded by a function conferring protection and/or tissue specific delivery while en route to the target site. When in the desired microenvironment, the protective function, such as long chain of PEG, detaches via a stimulus-sensitive impulse (such as a particular pH, temperature, protease) and allows the CPPs to generate the intracellular delivery of the carrier. Several "de-shielding" strategies have been proposed. For example, low pH, oxygen deficiency and overexpression of a proteinase, such as metallo-proteinase (MMP) 2 and 9 in tumoral cells can be exploited to couple a stimuli-sensitive bond on the protective function. Hydrazone bonds (Hz) are commonly used for this purpose because they can be cleaved in relative low pH conditions. With this in mind, doxorubicin based-multifunctional liposomes decorated with a CPP moiety and a nucleosome-specific monoclonal antibody (mAb), 2C5, were developed [23]. The 2C5 and the TATp were attached to the liposomal surface via a PEG 3400 spacer and a relatively shorter PEG1000-PE derivative, respectively. As stimulus-sensitive moiety, the Hz-pH-sensitive bond between the PEG2000 chain and PE moiety was added to the liposomes to further shield the TATp. With this approach, the CPPs based function is sterically shielded in the body circulation until arriving at a site with low pH (Fig. 1). This strategy has lead to very promising results both in vitro and in vivo. In particular, the multifunctional liposomes developed have shown a superior and significant anticancer activity in xenografted models of resistant ovarian cancer compared to the non-functionalized formulation [24]. Alternatively, MMP-2/9, overexpressed in the tumor microenvironment, represents another suitable substrate which may be

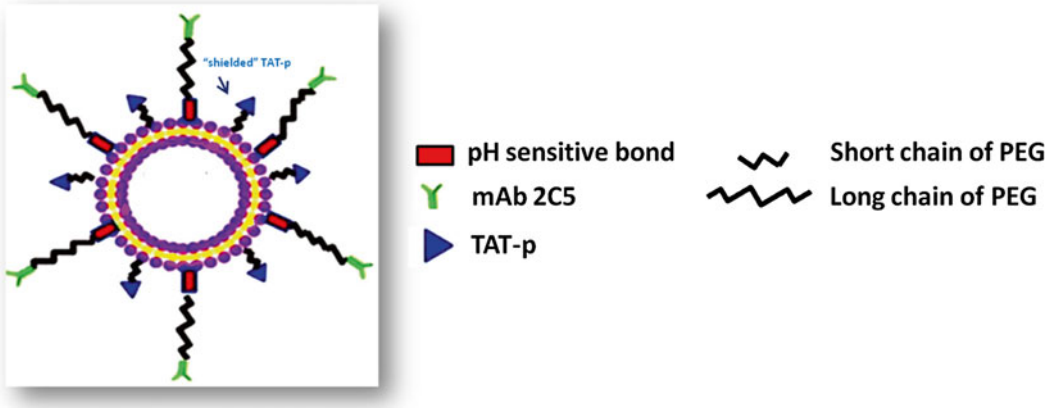

Fig. 1 Schematic of TAT-based pH sensitive immunoliposomes and the "de-shielded" effect of low pH

utilized as linker to construct a cleavable shield [25]. In the next section, we describe in detail the methods to prepare TATp-based-stimuli-sensitive nanocarriers and their applicability for the treatment of diseases such as cancer.

2 Materials

2.1 Synthesis of TATp-PEG1000-PE Conjugate

1. TAT cysteine peptide (TATp-Cys) (12-mer: CysTyrGlyArgLys-LysArgArgGlnArgArgArg) from Tufts University Core Facility (Boston, MA). Stored at −20 °C.
2. 1,2-dioleoyl-sn-glycero-3-phosphoethanolamine (DOPE) and maleimide-polyethyleneglycol1000-*N*-hydroxysuccinimide ester (NHS-PEG1000-maleimide) from Avanti Polar Lipids (Alabaster, AL). Stored at −80 °C.

2.2 Preparation of TATp-Based pH-Sensitive Immunoliposomes

1. Polyethylene-glycol (PEG), phosphoethanolamine-N-[carboxy(polyethylene glycol)-2000] (PEG2000-PE), phosphatidylcholine (PC) and 1,2-dioleoyl-sn-glycero-3-phosphoethanolamine-*N*-(lissamine rhodamine B sulfonyl) (ammonium salt) (Rh-PE) from Avanti Polar Lipids (Alabaster, AL).
2. PEG2000-Hz-PE and 2C5-PEG3400-PE synthesized in house. Stored at −80 °C.

2.3 Preparation of TATp-Based pH-Sensitive Polymeric Micelles

1. Polyethylene-glycol (PEG), phosphoethanolamine-N-[carboxy(polyethylene glycol)-750] (mPEG750-PE) from Avanti Polar Lipids (Alabaster, AL).
2. TATp-PEG1000-PE and PEG2000-Hz-PE synthesized in house. Stored at −80 °C.

2.4 Preparation of TATp-Based MMP2-Sensitive Immunoliposomes

1. MMP2 peptides (GPLGIAGQ) from Tufts University Core Facility (Boston, MA). Stored at –20 °C.
2. TATp-PEG(1000)-PE and MAL-PEG(3400)-MMP2-DOPE synthesized in house. Stored at –80 °C.

2.5 Preparation of TATp-Based MMP2-Sensitive Mixed Micelles

1. Polyethylene-glycol (PEG), phosphoethanolamine-N-[carboxy(polyethylene glycol)-1000] (PEG1000-PE) from Avanti Polar Lipids (Alabaster, AL).
2. PEG2000-MMP2-DOPE and TATp-PEG1000-PE synthesized in house. Stored at –80 °C.

2.6 In Vitro Studies

1. Cell lines from ATCC (Rockville, MD), cell culture media and fetal bovine serum from Cellgro (Kansas City, MO).
2. Human active MMP2 protein (MW 66,000 Da) from EMD Biosciences (La Jolla, CA).

3 Methods

Various approaches have been proposed to induce cell-selectivity with CPPs and to reduce their susceptibility against proteolysis cleavage in physiological conditions. Here, we describe protocols for the preparation of two TATp-based-multifunctional nanopreparations: pH-sensitive and MMP2-sensitive multifunctional nanocarriers. In both cases, the first step involves the conjugation of TATp to PEG-PE derivatives. The TATp conjugated can then be incorporated by the PE moiety in stimulus-sensitive liposome and micelle formulations.

3.1 Synthesis of TATp-PEG1000-PE Conjugate

A TATp-PEG1000-PE conjugate is synthesized as follows:

1. Add a 1.5-fold molar excess of NHS-PEG1000-maleimide to a DOPE solution in chloroform for 2 h, with stirring at room temperature in the presence of a threefold molar excess of triethylamine.
2. Add a twofold molar excess of TATp-Cys to the reaction mixture and stir overnight at room temperature.
3. Remove the organic solvent by rotary evaporation followed by overnight freeze-drying.
4. Remove the excess of TATp-Cys from the product by gel filtration chromatography. Collect fractions and monitor them by thin layer chromatography (TLC) using silica plates (use a mobile phase of chloroform/methanol 80:20 % v/v), and visualize the TATp-PEG-PE with phosphomolybdenic acid and Dragendorff spray reagents.

Alternatively, mix NHS-PEG1000-maleimide with DOPE (1:1.4, molar ratio) in DCM overnight, under stirring. Then, purify the DOPE-PEG1000-MAL conjugate by preparative TLC (use a mobile phase of chloroform/methanol 80:20 % v/v). Incubate DOPE-PEG1000-MAL and Cys-TATp (1:1.2, molar ratio) in a pH 7.2 HEPES buffer at 4 °C, under nitrogen protection overnight, followed by dialysis (MWCO 2000 Da) against distilled water to remove unreacted TATp.

3.2 Preparation of TATp-Based pH-Sensitive Immunoliposomes

The aim is to prepare liposomes where TATp is protected in the blood by long PEG chains while en route to target tissues. Here, a TAT-PEG1000-PE conjugate, prepared as above, a pH degradable PEG2000-Hz-PE [23] conjugate with longer PEG chain and a monoclonal antibody 2C5-PEG3400-PE [25] conjugate are incorporated into liposomes by the PE moiety. These conjugates can be incorporated into liposomes by the post-insertion method or the lipid-film hydration method [26]. Under normal tissue condition, the long pH-sensitive PEG chain shields and protects the TATp moieties. As liposomes accumulate at the target site, via the EPR effect and 2C5 initiates active targeting, the acidified environment cleaves the Hz bond and the TATp becomes free to interact with the cell surface.

1. Prepare a lipid film composed of a mixture of mPEG2000-PE, PC, Chol at a weight ratio of 1:3:1.
2. Remove the organic solvent by rotary evaporation under nitrogen and freeze-dry.
3. Hydrate the film in HEPES-buffed saline at pH 7.4.
4. Sonicate the liposomes with a probe-type sonicator at 11 W power for 30 min.
5. Incubate the liposomes with a micellar dispersion of TATp-PEG1000-PE (2.5 mol%), 2C5-PEG3400-PE (2.5 mol%), and PEG2000-Hz-PE (15 mol%) overnight at room temperature (*see* **Note 1**).
6. Dialyze the liposomes against water (MWCO 3500–5000) to remove unreacted reagents.

Alternatively, prepare a lipid film composed of a mixture of PC:Chol (7:3), TATp-PEG1000-PE, and PEG2000-Hz-PE at a molar ratio of 10:0.25:15. Then, hydrate the dry lipid film with a PBS buffer at pH 7.4 and extrude the lipid dispersion 20 times through polycarbonate membranes with 0.2 μm pore size.

To prepare fluorescent immunoliposomes for confocal microscopy, add Rh-PE (1 %mol) in the lipid mixtures and proceed as above.

3.3 Preparation of TATp-Based pH-Sensitive Polymeric Micelles

1. Prepare a film from a mixture of mPEG750-PE, TATp-PEG1000-PE, and PEG2000-Hz-PE at a molar ratio of 4:0.5:5.4 as described above.
2. Hydrate the dry film with pH 7.4 PBS and vortex vigorously for 2 min to form mixed micelles.

For confocal microscopy, add Rh-PE (1 %mol) in the organic mixtures and proceed as above.

3.4 Preparation of TATp-Based MMP2-Sensitive Immunoliposomes

The concept is to combine different active function in the same nanocarrier. This involves a TATp-PEG-PE moiety and a hydrophilic and flexible long PEG chain functionalized at the distal end with a mAb 2C5 and containing a MMP 2-sensitive bond between the PEG chain and the PE moiety. Ideally, after intravenous injection, the multifunctional nanocarrier accumulates at the tumor site via a combination of an EPR effect and active targeting effects of the anticancer mAb 2C5. In the tumor microenvironment, the upregulated levels of MMP2 cleave the MMP2-sensitive linker and "de-shield" the TATp from the protective long-chain PEG, resulting in an enhanced cellular internalization.

1. Prepare a lipid mixture of PC, Chol, TATp-PEG(1000)-PE, and MAL-PEG(3400)-MMP2-DOPE [25] at a 6:3.8:0.1:0.1 molar ratio in chloroform.
2. Evaporate the organic solvent by rotary evaporation followed by overnight freeze-drying.
3. Hydrate the lipid film with a pH 7.4 PBS buffer at room temperature for 20 min and extrude the dispersion 20 times through polycarbonate filters (pore size, 200 nm).
4. Incubate the liposomal dispersion with thiolated mAb2C5 at the molar ratio of 20 MAL groups per antibody at room temperature, in pH 7.4 PBS, at 4 °C overnight.
5. Purify the liposomal dispersion by dialysis with a floating dialysis device (MWCO 300,000 Da) against PBS to remove unreacted mAb2C5.

To follow the liposome–cell interactions, add Rh-PE (0.5 mol%) to the lipid mixture and proceed as above.

3.5 Preparation of TATp-Based MMP2-Sensitive Mixed Micelles

1. Prepare a film of PEG2000-MMP2-DOPE, PEG1000-PE, and TATp-PEG1000-PE at a 5:4:1 molar ratio in chloroform and dried in a freeze-dryer overnight.
2. Hydrate the film at room temperature with pH 7.4 PBS buffer.

In Fig. 2, a schematic representation of an MMP2 sensitive mixed micelles is shown.

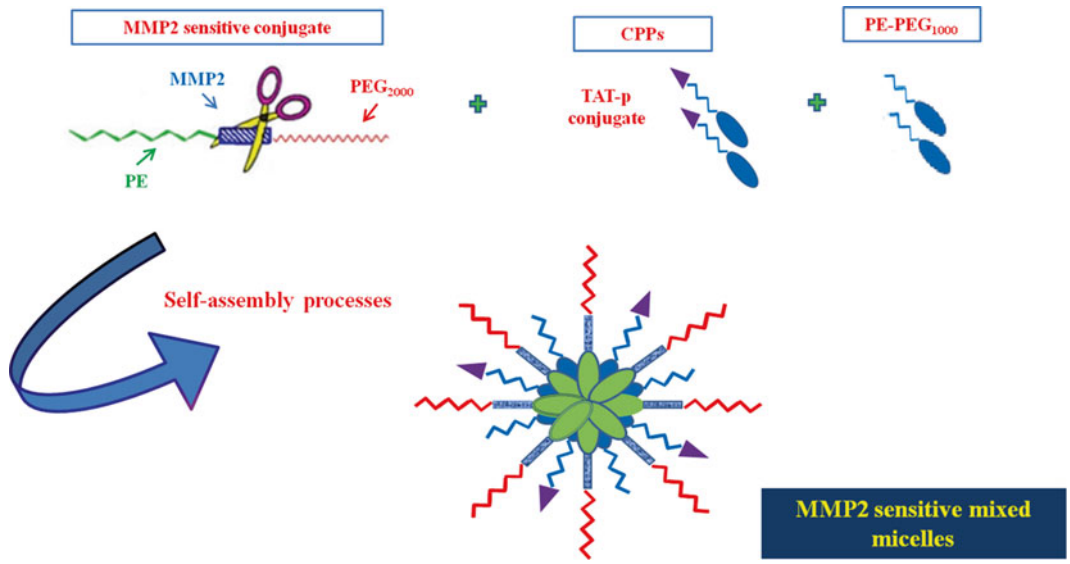

Fig. 2 Schematic of TAT-p modified MMP2 sensitive mixed micelles

3.6 Characterization

3.6.1 Size Distribution and Morphology of TATp-Modified Nanocarriers

The size measurements and the size distribution of the TATp NPs are usually determined by dynamic light scattering (DLS) using a Coulter® N4-Plus Submicron Particle Sizer (Coulter Corporation, Miami, FL). The size distribution of multifunctional liposomes and polymeric micelles is generally unimodal, in the range of 100–150 nm and 15–25 nm, respectively. Interestingly, the size of liposomes/micelles does not change significantly after decorating the surface with TATp conjugates. To confirm the results obtained from dynamic light scattering, evaluate the size distribution and the morphology by transmission electron microscopy (TEM) (Jeol, JEM-1010, Tokyo, Japan).

3.6.2 "Shielded" Efficiency of TATp-Modified Stimulus-Sensitive Nanocarriers

Since TATp is a charged peptide, the presence of the peptide on the surface of nanocarriers can be investigated by surface charge analysis performed using a Zeta Phase Analysis Light Scattering (PALS) UltraSensitive Zeta Potential Analyzer instrument (Brookhaven Instruments, Holtsville, NY). The zeta potential analysis of the different formulations can be used to determine the optimal concentration of the long and stimulus-sensitive PEG chain required to efficiently shield TATp at normal conditions. Usually a higher PEG shielding results in a less positive zeta potential value. It is dose-dependent and directly correlated to the lengths of the PEG chain (the longer the PEG chain used, the more negative the zeta potential) (*see* **Note 2**). In Fig. 3a is shown a schematic representation of the "shielding" effect of increasing mol% of PEG chain and the approximate zeta potential values (Fig. 3b).

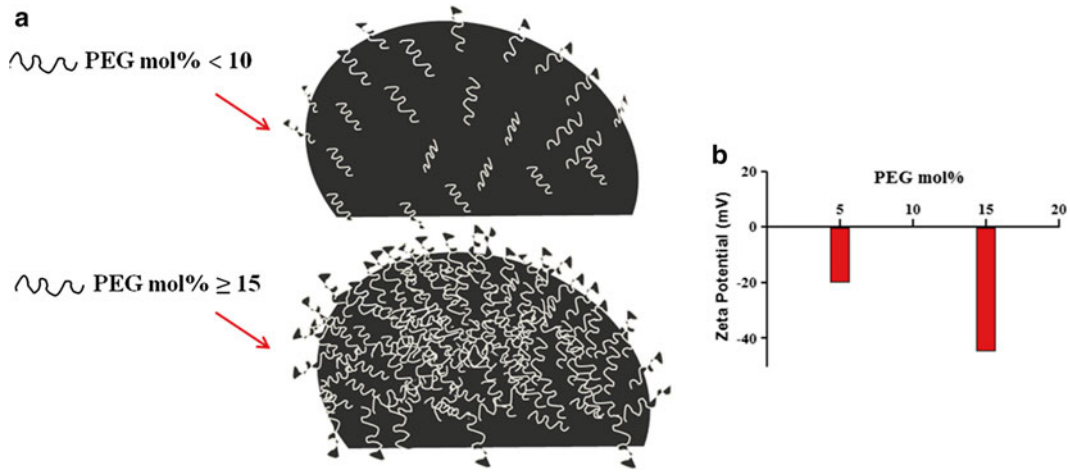

Fig. 3 (**a**) Shielding effect of increasing mol% of PEG blocks. (**b**) Approximate zeta potentials values of TATp-based NPs shielded with different mol% of PEG chain

3.6.3 Interaction of Multifunctional Nanocarriers with Cells and Spheroids, Confocal Microscopy

To evaluate the interaction of TATp modified stimuli-sensitive nanocarriers in monolayers of cells,

1. Grow the cells on cover slips in 24-well culture plates at the density of 1×10^5 cells/well.
2. When the cells reach 60–70 % of confluence, wash the cells twice with pH 7.4 PBS and treat the cells with various Rh-PE-labeled multifunctional formulations in free-serum media. For pH-sensitive nanopreparations, pre-incubate samples at pH 5.0 (*see* **Note 3**). In the case of MMP2-sensitive formulations, pre-incubate samples with 5 ng/μL of human MMP2 overnight, at 37 °C (*see* **Notes 4** and **5**).
3. After fixed incubation times, add Hoechst 33342 nuclear stain (2.5 μg/ml) for the last 30 min of incubation.
4. Remove the media and wash the cells three times with pH 7.4 PBS. Mount cover slips cell-side down on glass slides using fluorescence-free glycerol-based mounting medium (Fluoromount-G), visualize with a Zeiss LSM700 confocal microscope system and analyze using Zeiss Image Browser software.

To evaluate the interaction of TATp modified stimuli-sensitive nanocarriers in spheroids,

1. Transfer spheroids to eight-well glass Lab-Tek chamber slides (Thermo Scientific) and incubate with various Rh-PE-labeled formulations of 100 μL per well of serum-free media for 2 h.
2. Wash the spheroids with PBS and image them by confocal microscopy.

3. The spheroids can be sectioned with a HM550 Cryostat microtome (Thermo Scientific) and stained with Hoechst 33342. The spheroid sections are viewed with a Nikon Eclipse E400 microscope and a Spot Advanced software (Spot Imaging).

3.6.4 In Vivo Studies of TATp Modified Stimulus-Sensitive Nanocarriers

The enhancement of the therapeutic activity of different drugs incorporated in TATp modified nanosystems can be evaluated with mouse xenograft models. In a typical example, tumor cells are grown in immune-deficient mice by injecting a known number of cells subcutaneously into the left flank. When the tumors reach a size in the range of 100–200 mm^3, 100–200 μl of TATp formulations in PBS buffer are injected i.v. via the tail vein at different time points. At end points in the study, anesthetized mice are killed by cervical dislocation, tumors are excised to evaluate the tumor weight and cryofixed for further biological examinations. Interestingly, in this mouse model of cancer, the administration of a Rh-PE labeled TATp-based MMP2-sensitive nanopreparation leads to a significant and preferential accumulation of the formulation in tumors that are characterized by overexpressed levels of MMP2, while other tissues show a negligible presence of the stimuli-sensitive nanopreparation [27]. These data suggest the potential, for excellent tissue targetability, of formulated CPPs in multifunctional systems.

To evaluate the in vivo tumor internalization of TAT-based nanopreparations,

1. Inject Rh-labeled nanopreparations via the tail vein of tumor-bearing mice.
2. After 2 h, sacrifice the animals and collect tumors and organs.
3. Dissociate cells from fresh tissues and immediately analyze the single cells by FACS.

4 Notes

1. The TATp-PEG-PE conjugate is an easy and efficient way to attach TATp to the surface of both liposomes and micelles. An amount in the range of 2.5–10 mol% is enough to guarantee the presence of TATp in the surface of the developed nanocarriers without affecting the size distribution of the NPs.
2. Here we describe protocols for the incorporation of TATp in multifunctional nanocarriers. In particular, we focus on TATp-modified stimulus-sensitive liposomes/micelles as a potential platform to expose CPPs selectively in targeted tissues. In the development of a "smart" system, it is very important to optimize the amount of PEG-lipid and the length of the PEG chain in the preparation of both liposomes and micelles in order to properly shield the TATp while in bloodstream.

The PEG-shielding proprieties are dose-and chain length-dependent. From our study, the use of pH or MMP2-sensitive PEG conjugate at up to 15 % is considered optimal to obtain efficient shielding of the CPPs (Fig. 3b). Note the length of the PEG chain influences the shielding proprieties of PEG. The longer PEG chain used, i.e., PEG2000 compared to PEG3400, the more effective is the protection of the CPPs (Fig. 3b).

3. In cell penetration studies, since the presence of a long PEG chain in the nanopreparations decreases the cell association, to better mimic the in vivo conditions, the pre-incubation of TAT-based pH-sensitive nanocarriers at low pH is suggested. To completely cleave the Hz bond, the formulations should be incubated at acidic conditions for more than 30 min.
4. Before treating the spheroids with TAT-based MMP2-sensitive nanopreparations, incubate the formulation overnight, at 37 °C with human MMP2.
5. After the pre-incubation of liposomes/micelles at acidic pH and MMP2, before adding the formulations to the cells, readjust the pH to 7.4 and remove the MMP2 by dialysis, respectively.

Acknowledgments

The authors thank Dr. William C. Hartner for the help in the manuscript preparation.

References

1. Frankel AD, Pabo CO (1988) Cellular uptake of the tat protein from human immunodeficiency virus. Cell 55:1189–1193
2. Derossi D, Joliot AH, Chassaing G et al (1994) The third helix of the Antennapedia homeodomain translocates through biological membranes. J Biol Chem 269:10444–10450
3. Futaki S, Suzuki T, Ohashi W et al (2001) Arginine-rich peptides. An abundant source of membrane-permeable peptides having potential as carriers for intracellular protein delivery. J Biol Chem 276:5836–5840
4. Pooga M, Hällbrink M, Zorko M et al (1998) Cell penetration by transportan. FASEB J 12:67–77
5. Schwarze SR, Ho A, Vocero-Akbani A et al (1999) In vivo protein transduction: delivery of a biologically active protein into the mouse. Science 285:1569–1572
6. Fonseca SB, Pereira MP, Kelley SO (2009) Recent advances in the use of cell-penetrating peptides for medical and biological applications. Adv Drug Deliv Rev 61:953–964
7. Huang Y, Jiang Y, Wang H et al (2013) Curb challenges of the "Trojan Horse" approach: smart strategies in achieving effective yet safe cell-penetrating peptide-based drug delivery. Adv Drug Deliv Rev 65:1299–1315
8. Choi YS, David AE (2014) Cell penetrating peptides and the mechanisms for intracellular entry. Curr Pharm Biotechnol 15:192–199
9. Josephson L, Tung CH, Moore A et al (1999) High-efficiency intracellular magnetic labeling with novel superparamagnetic-Tat peptide conjugates. Bioconjug Chem 10:186–191
10. Wunderbaldinger P, Josephson L, Weissleder R (2002) Tat peptide directs enhanced clearance and hepatic permeability of magnetic nanoparticles. Bioconjug Chem 13:264–268
11. Torchilin VP (2005) Recent advances with liposomes as pharmaceutical carriers. Nat Rev Drug Discov 4:145–160

12. Lasic DD, Papahadjopoulos D (1995) Liposomes revisited. Science 267:1275–1276
13. Yuan F, Dellian M, Fukumura D et al (1995) Vascular permeability in a human tumor xenograft: molecular size dependence and cutoff size. Cancer Res 55:3752–3756
14. Maeda H, Bharate GY, Daruwalla J (2008) Polymeric drugs for efficient tumor-targeted drug delivery based on EPR-effect. Eur J Pharm Biopharm 71:409–419
15. Torchilin VP, Rammohan R, Weissig V et al (2001) TAT peptide on the surface of liposomes affords their efficient intracellular delivery even at low temperature and in the presence of metabolic inhibitors. Proc Natl Acad Sci U S A 98:8786–8791
16. Pappalardo JS, Langellotti CA, Di Giacomo S et al (2014) In vitro transfection of bone marrow-derived dendritic cells with TATp-liposomes. Int J Nanomedicine 9:963–973
17. Lukyanov AN, Gao Z, Mazzola L et al (2002) Polyethylene glycol-diacyllipid micelles demonstrate increased accumulation in subcutaneous tumors in mice. Pharm Res 19:1424–1429
18. Lukyanov AN, Hartner WC, Torchilin VP (2004) Increased accumulation of PEG-PE micelles in the area of experimental myocardial infarction in rabbits. J Control Release 94:187–193
19. Sawant RR, Torchilin VP (2009) Enhanced cytotoxicity of TATp-bearing paclitaxel-loaded micelles in vitro and in vivo. Int J Pharm 374:114–118
20. Sethuraman VA, Bae YH (2007) TAT peptide-based micelle system for potential active targeting of anti-cancer agents to acidic solid tumors. J Control Release 118:216–224
21. Sawant RR, Sawant RM, Kale AA et al (2008) The architecture of ligand attachment to nanocarriers controls their specific interaction with target cells. J Drug Target 16:596–600
22. Koren E, Apte A, Sawant RR et al (2011) Cell-penetrating TAT peptide in drug delivery systems: proteolytic stability requirements. Drug Deliv 18:377–384
23. Koren E, Apte A, Jani A et al (2012) Multifunctional PEGylated 2C5-immunoliposomes containing pH-sensitive bonds and TAT peptide for enhanced tumor cell internalization and cytotoxicity. J Control Release 160:264–273
24. Apte A, Koren E, Koshkaryev A, Torchilin VP (2014) Doxorubicin in TAT peptide-modified multifunctional immunoliposomes demonstrates increased activity against both drug-sensitive and drug-resistant ovarian cancer models. Cancer Biol Ther 15:69–80
25. Zhu L, Kate P, Torchilin VP (2012) Matrix metalloprotease 2-responsive multifunctional liposomal nanocarrier for enhanced tumor targeting. ACS Nano 6:3491–3498
26. Ishida T, Iden D, Allen TM (1999) A combinatorial approach to producing sterically stabilized (Stealth) immunoliposomal drugs. FEBS Lett 460:29–133
27. Zhu L, Wang T, Perche F et al (2013) Enhanced anticancer activity of nanopreparation containing an MMP2-sensitive PEG-drug conjugate and cell-penetrating moiety. Proc Natl Acad Sci U S A 110:17047–17052

Chapter 25

Multifunctional Oligoaminoamides for the Receptor-Specific Delivery of Therapeutic RNA

Judith Weber, Ulrich Lächelt, and Ernst Wagner

Abstract

Drugs with novel and versatile modes of action, such as therapeutic nucleic acids or proteins, open new possibilities for the precise therapy of different diseases. The most crucial limitation during the development of a therapeutic drug remains the safe and efficient intracellular delivery.

To overcome the hurdles and to realize the successful delivery of such new biopharmaceuticals, our laboratory has recently developed a sequence-defined, cationic oligomer platform based on solid-phase synthesis. These multifunctional oligomers have displayed efficient delivery of therapeutic RNA in vitro and in vivo. In this chapter, we provide a brief background on the special features and applications of these carrier systems as well as detailed protocols for the oligomer and polyplex synthesis and their evaluation.

Key words Drug delivery, Polymer conjugates, Polyplex, Endosomal escape, Tumor targeting

1 Introduction

Most contemporary drugs used for cancer pharmacotherapy do not have an exclusive antitumoral action and can cause adverse reactions in healthy tissue. This issue often leads to a narrow therapeutic window and therapy limitations. Therefore, the development of effective and safe antitumoral drugs is a major concern of cancer therapy research. Receptor-specific delivery represents one attractive approach to shift the biodistribution of a drug toward its target tissue. Moreover, the use of drugs with novel modes of action, such as therapeutic nucleic acids or proteins, opens new possibilities for the precise interference with the cellular pathway of the disease. But many of these drugs are limited by biodegradation, rapid elimination, unwanted off-target tissue toxicity as well as suboptimal intracellular uptake and drug resistance [1–3]. Hence there is a great demand to develop strategies to overcome these stints. The main challenges for this are:

Ülo Langel (ed.), *Cell-Penetrating Peptides: Methods and Protocols*, Methods in Molecular Biology, vol. 1324,
DOI 10.1007/978-1-4939-2806-4_25,

- Stability: Preventing biodegradation, interaction with serum constituents as well as rapid elimination to prolong biological half-life and reduce immunogenicity.
- Selectivity: Decreasing the drug's burden on healthy cells but increasing the burden of diseased cells to minimize off-target tissue toxicity.
- Intracellular delivery: Improving transport and effective uptake of the drug into diseased cells as well as the controlled release of the biologically active form into the correct intracellular compartment to achieve optimal therapeutic effect.

One way to realize these needs is to incorporate the drug into polymer therapeutics [1–3]. Our laboratory has recently developed a library of sequence-defined monodisperse peptide-like oligomers based on artificial oligoamino acids and the use of solid phase supported synthesis [4]. Various functionalized cationic polymer conjugates have been generated including potent, nontoxic carriers for nucleic acid and protein delivery [5–8]. Different precise oligomer topologies and the optional incorporation of shielding domains (to increase stability), targeting ligands (to increase selectivity), and/or endosomolytic entities (for intracellular delivery) offer the opportunity to alter pharmacokinetic characteristics and improve the therapeutic profile. Moreover, these delivery systems enable combination therapy by delivering several agents simultaneously [9].

Since cellular uptake and vesicular release are necessary hurdles for macromolecular compounds, many different strategies have been investigated aiming to overcome these [10]. For example, TAT, penetratin [11], acidic peptide analogues derived from the influenza virus hemagglutinin (HA-2) [12] or modified mellitin derivatives [13, 14] facilitate the uptake and/or release of the cargo into the cytoplasm. Not only sequence variations of naturally occurring peptides show these qualities, but also oligoaminoamide-based building blocks (e.g., Stp) feature endosomolytic properties [5, 10]. Due to the protonatable diaminoethane motif they enhance endosomal release by the hypothesized proton-sponge effect and destabilization of the lipid membrane.

These cationized diaminoethane amines derive an additional benefit when using negative charged cargos such as siRNA, dsRNA, and pDNA. In this case, polyplex formation is initiated by electrostatic interaction between the nitrogens of the polymers and the phosphates of the nucleic acid, which additionally protects the cargo in the extracellular environment. Introducing cysteines, hydrophobic or aromatic units into the polymer enables further stabilization of the polyplexes through disulfide bounds, hydrophobic or π–π interactions [5, 6, 10, 15]. In this chapter we describe the concept and synthesis of two sequence-defined, cationic polymers and their RNA polyplex formation.

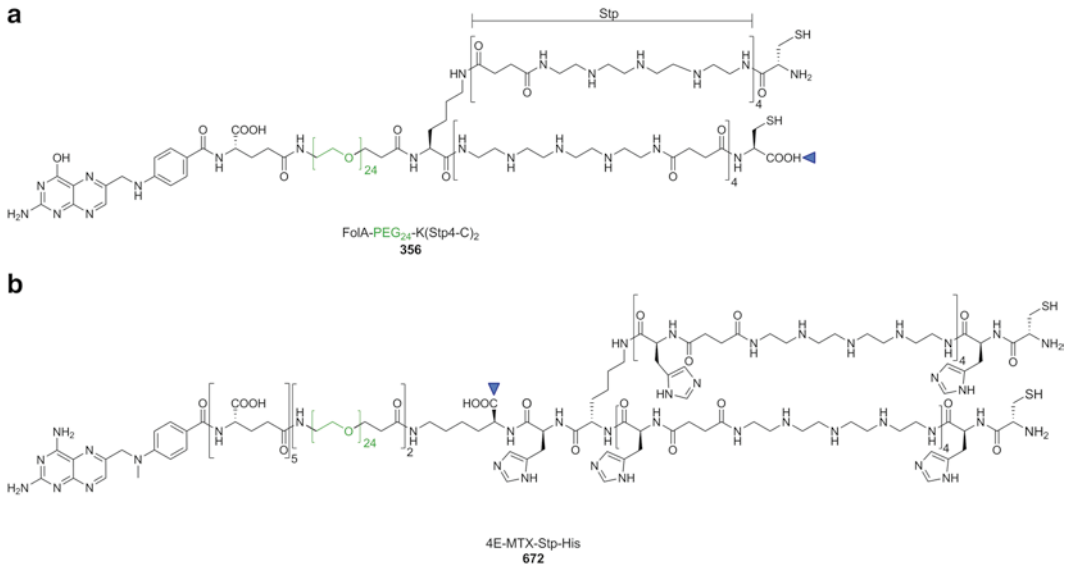

Fig. 1 Chemical structure of (**a**) the folic acid targeted, defined polycation *356* and (**b**) the MTX/oligo(ethanamino) amide conjugate *672*. The *blue triangle* marks the start of the SPS

The first oligomer *356* (Fig. 1a) forms multifunctional polyplexes for receptor-mediated siRNA delivery [16]. The monodisperse delivery system contains a cationic backbone composed of eight units of the building block Stp (succinoyl tetraethylene pentamine). This structural element forms complexes with siRNA and thus leads to polyplex formation. To increase siRNA polyplex stability, cysteines are inserted at both ends of the peptide-like backbone. During polyplex formation, the cysteines form intermolecular disulfide cross-links which increase the complex stability while maintaining the ability to biodegrade. At a central position of the carrier system a monodisperse polyethylene glycol (PEG) chain (24 ethylene glycol units) is located. PEG shields the oligomer/siRNA polyplex core and thus reduces interactions with serum constituents. As cell targeting ligand, folic acid terminates the PEG unit. The coupling of the endosomolytic peptide Inf7 to the 5′-end of the siRNA sense strand ensured the endosomal escape ability of the cargo. The size of the formed polyplexes with these PEGylated oligomers is dependent on the size and type of the nucleic acid. With siRNA, the resulting polyplexes contain only one siRNA molecule and possess a hydrodynamic diameter of 6 nm (Fig. 2a). This multifunctional carrier system showed in vivo tolerability, stability, receptor-specific cellular uptake, and effective gene silencing.

The second oligomer *672* (Fig. 1b) focuses on codelivery of the antifolate drug methotrexate (MTX) and the cytotoxic dsRNA polyinosinic-polycytidylic acid poly(I:C) [9]. MTX acts as a ligand of the folate receptor and mediates uptake into folate receptor

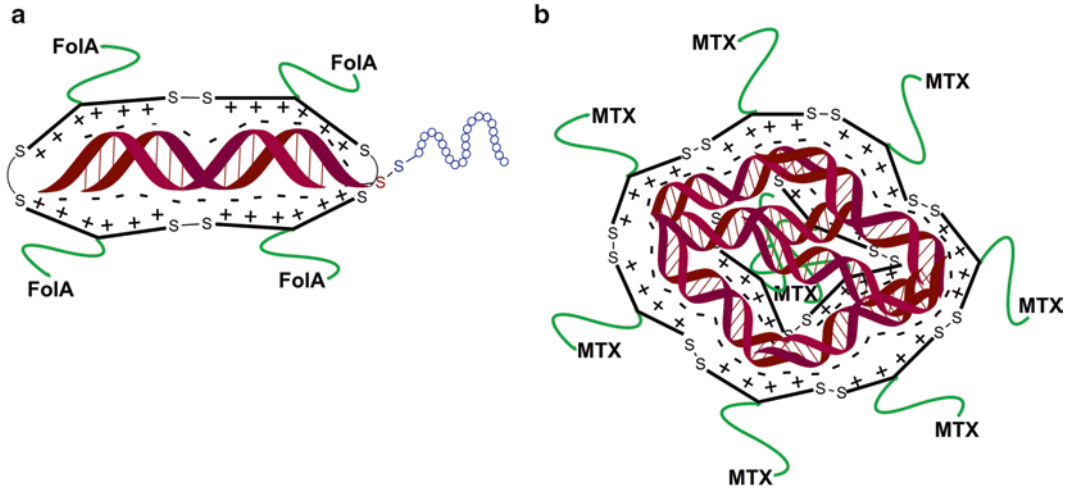

Fig. 2 Schematic illustration of (**a**) Inf7-siRNA/*356* polyplexes and (**b**) poly(I:C)/*672* polyplexes. PEG in *green color*, Inf7 peptide in *blue color*

expressing cells. Inside the cell, free MTX undergoes conversion to more potent poly-γ-glutamyl derivates, which inhibit dihydrofolate reductase and other target enzymes. Through the covalent incorporation of MTX into oligomers the natural conversion is hampered and the bioactivity of MTX affected. Hence, we conjugated MTX through a synthetic polyglutamate chain (composed of four glutamic acids) to the (ethanamino)amide oligomer. This a priori glutamylation had a major impact on the delivery on the final outcome of combined MTX/poly(I:C) cytotoxicity. Again, eight units of the Stp served as cationic core to form complexes with the cytotoxic dsRNA polyinosinic-polycytidylic acid poly(I:C). Additional alternating incorporation of histidine into this structural element (Fig. 1b, *672*/4E-MTX-Stp-His) enhances buffering in the endolysosomal pH range and thus improves endosomal escape [17]. As before, cysteines were attached at the ends of the cationic backbone for further stabilization of the polyplexes. Between the cationic backbone and the polyglutamate chain, monodisperse PEG units (two times 24 ethylene glycol units) are located as shielding domain. In contrast to the *356*/siRNA complexes, the larger poly(I:C) molecules (around 1000 bp) form complexes in the range of 500–600 nm with the oligomer *672* (*N*/*P* 10, Fig. 2b). The increased size is essential for the "histidine effect", since a critical amount of buffering units is required for the proton-sponge activity. The resulting polyplexes trigger folate receptor-specific cellular uptake and a combined antifolate/poly(I:C) toxicity.

Figure 3 shows the results of killing KB cells with cytotoxic double-stranded poly(I:C) and the above described oligomers.

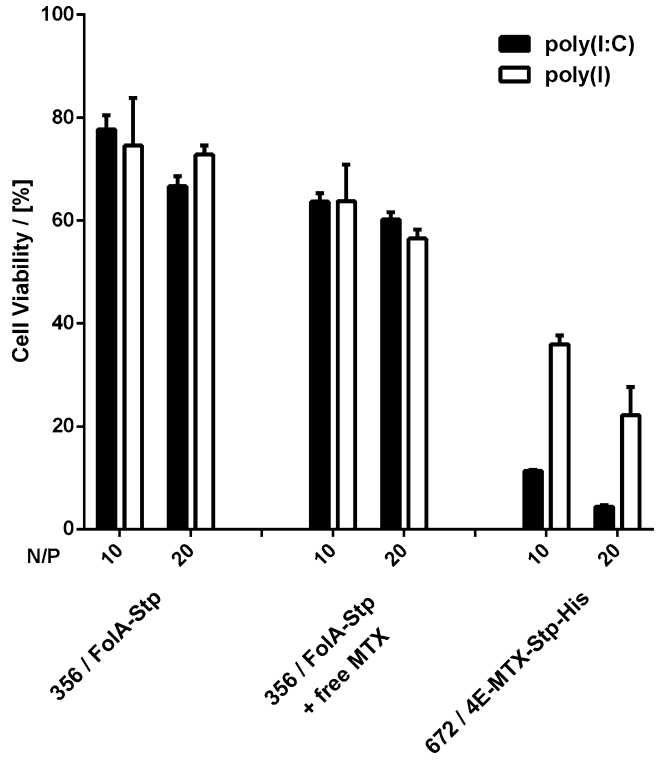

Fig. 3 Effect of poly(I:C) or poly(I) polyplexes (*N/P* = 10, 20) on cell viability of KB cells ($n = 3$). The concentration of free MTX was based on the concentration of *356* at the indicated *N/P* values

Single-stranded poly(I) served as a less toxic negative control, which allows to distinguish between the MTX and the combined MTX/poly(I:C) mediated cytotoxicity. The well biocompatible folic acid conjugate *356*, despite good uptake efficiency, showed very low poly(I:C) mediated toxicity. This is expected since endosomal escape is limited due to the lack of the endosomolytic peptide Inf7 [16]. The equimolar addition of free MTX to the *356* polyplexes showed only a moderate additional effect. In comparison to this, the polyplexes formed with *672* features an effective MTX and combined MTX/poly(I:C) mediated cytotoxicity. This highlights that the antifolate ligand MTX and poly(I:C) complement each other and that the incorporation of histidines improves the cytosolic delivery [9].

In the following method section we describe the synthesis and the characterization of the folic acid targeted polycation *356* and the antifolate/oligo(ethanamino)amide conjugate *672*. At first, we show how Fmoc solid-phase peptide synthesis conditions can be used to synthesize the sequence-defined conjugates. Secondly, we demonstrate the polyplex formations. Finally, the evaluation of the polyplexes is described.

2 Materials

2.1 Solid-Phase Synthesis (SPS)

Use solvents and reagents of high quality for all experiments (*see* **Note 1**). The SPS can be carried out manually on a laboratory vacuum manifold (Promega Corporation, Madison, WI, USA) using microreactors (*see* **Note 2**) with polyethylene filters (Multisyntech GmbH, Witten Germany) for vacuum filtration. As solid phase 2-chlorotrityl chloride resin (Iris Biotech, Marktredewitz, Germany) is used.

2.1.1 Amino Acids

1. Protected α-amino acids.
2. Fmoc-Stp(Boc_3)-OH synthesized as described in ref. 18.
3. Fmoc-*N*-amido-dPEG$_{24}$-OH (Quanta Biodesign, Powell, Ohio, USA).
4. N^{10}-(trifluoroacetyl)pteroic acid (Clauson-Kaas A/S, Farum, Denmark).
5. 4-[[(2,4-diamino-6-pteridinyl)methyl]methylamino]-benzoic acid (Clauson-Kass A/S, Farum, Denmark).

2.1.2 Reagents and Solutions

1. *N*,*N*-diisopropylethylamine (DIPEA).
2. 1-Hydroxybenzotriazole (HOBt).
3. Benzotriazol-1-yl-oxy tripyrrolidinophosphonium hexafluorophosphate (Pybop®).
4. Fmoc-deprotection solution: piperidine –*N*,*N*-dimethylformamide (DMF) (2/8, v/v).
5. Capping solution: dichloromethane (DCM)–methanol–DIPEA (80/15/5, v/v/v).
6. Kaiser test solutions: 80 % phenol–ethanol (w/v), 5 % ninhydrine–ethanol (w/v), KCN–pyridine (2 mL 0.001 M KCN in 98 mL pyridine).
7. Dde-deprotection solution: hydrazine monohydrate–DMF (2/98, v/v).
8. Tfa-deprotection solution: 25 % ammonium hydroxide–DMF (1/1, v/v).
9. Cleavage cocktail: Trifluoro acetic acid (TFA)–triisopropylsilane (TIS)–H_2O (95/2.5/2.5, v/v/v).
10. Precipitating solution: methyl *tert*-butyl ether (MTBE)–*n*-hexane (1/1, v/v).

2.2 siRNA-Inf7 Conjugate

1. siRNAs: C6-SS-C6-siGFP, C6-SS-C6-siCtrl (disulfide modification at the 5′-end of the passenger strand; *see* ref. 16 for sequences) (Axolabs GmbH, Kulmbach, Germany).
2. Tris(2-carboxyethyl)phosphine (TCEP).

3. Inf7: H_2N-GLFEAIEGFIENGWEGMIDGWYGC-amide (Biosyntan, Berlin, Germany).
4. 5,5′-Dithiobis(2-nitrobenzoic acid) (Ellman's reagent, DTNB).

2.3 Polyplex Formation

1. siRNA (unmodified from Axolabs GmbH, Kulmbach, Germany or siRNA-Inf7 conjugate synthesized as described in Subheading 3.2).
2. Poly(I:C) sodium salt (Sigma-Aldrich, Munich, Germany).
3. Poly(I) potassium salt (Sigma-Aldrich, Munich, Germany).

2.4 Biophysical Polyplex Characterization

1. Agarose powder.
2. GelRed.
3. Zetasizer Nano ZS with backscattering detection and folded capillary cells (DTS1061 or DTS1070) (Malvern Instruments, Worcestershire, UK).

2.5 Buffers

1. TBE Buffer: 89 mM TRIS, 89 mM boric acid, 2 mM ethylenediaminetetraacetic acid disodium salt (EDTA-Na_2) (pH 8.0).
2. HEPES buffer.
3. HBG: 20 mM HEPES, 5 % glucose (w/v) (pH 7.4).
4. Electrophoresis loading buffer: 6 mL glycerine, 1.2 mL 0.5 M EDTA-Na_2 solution (pH 8.0), 2.8 mL H_2O, 20 mg bromophenol blue.
5. IEX-Buffer A: 20 mM HEPES buffer (pH 6.5), acetonitrile (ACN) (7/3, v/v).
6. IEX-Buffer B: 20 mM HEPES, 1 M NaCl (pH 6.5), 30 % ACN.

3 Methods

3.1 Solid-Phase Synthesis (SPS)

Solid phase supported synthesis offers the opportunity to synthesize sequence-defined (ethanamino)amide oligomers with precise modification patterns and topology [4]. The oligomers *356* and *672* are generated by standard Fmoc-based solid phase supported peptide synthesis, which follows defined steps of a synthesis cycle (Fig. 4). As a solid support serves 2-chlorotrityl chloride resin. For coupling, the resin is incubated with a fourfold excess (related to free amines) of the protected amino acid, which is preactivated through equimolar amounts of HOBt, PyBOP and the two-molar amount of DIPEA. The Fmoc-deprotection is carried out in 20 % piperidine/*N*,*N*-dimethylformamide (DMF) (v/v). After each coupling and deprotection step the resin is washed three times with DMF followed by three times DCM (10 mL/g resin). To validate coupling and deprotection, the Kaiser test is used to determine free amino groups qualitatively [19]. The previous coupling

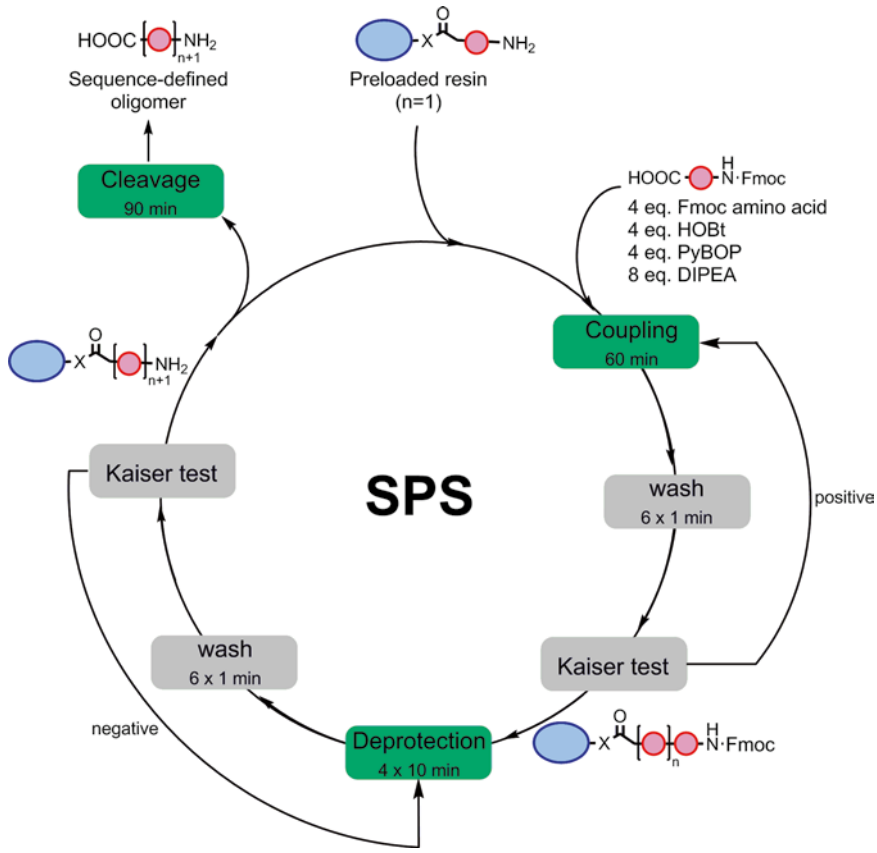

Fig. 4 Schematic illustration of the general process of solid-phase synthesis (SPS)

or deprotection step is repeated, if the results of the Kaiser test have been unsatisfying. Table 1 summarizes the general synthesis procedure.

3.1.1 *Resin Loading*

1. Place 0.5 g of 2-chlorotrityl chloride resin in a 10 mL syringe reactor (*see* **Note 2**).
2. Swell the resin in 5 mL dry DCM for 30 min in the closed reactor under shaking (*see* **Note 3**).
3. Discard the DCM.
4. Dissolve 0.23 mmol of the intended Fmoc-amino acid (Fmoc-Cys(Trt) in case of *356*, Fmoc-Lys(ivDde) in case of *672*) in 5 mL dry DCM and 89 μL DIPEA (0.45 mmol). Add the solution to the resin and incubate for 60 min in the closed reactor under shaking.
5. Discard the solution and add 5 mL of capping solution and incubate for additional 30 min to cap remaining reactive chloride groups.

Table 1
General steps of Fmoc-based solid-phase synthesis

Step	Description	Solvent	*V* [mL/g resin]	Time [min]
0	Resin swelling	DCM	10	30
1	Coupling	DCM–DMF (1:1, v/v)	5	60
2	Wash	3× DMF, 3× DCM	10	6×1
3	Kaiser test	–	–	4
4	Fmoc-deprotection	20 % piperidine–DMF (v/v)	10	4×10
5	Wash	3× DMF, 3× DCM	10	6×1
6	Kaiser test	–	–	4
7	Cleavage	TFA–TIS–H_2O (95:2.5:2.5, v/v/v)	10	90

Step 0 and **7** are only carried out once per synthesis. **Step 1–6** are repeated dependent on the oligomer sequence

6. Discard the mixture and wash five times with 5 mL of DCM.
7. For loading determination, separate and dry a small amount of resin (~30 mg) in vacuo. Accurately weigh samples of 5–10 mg dry resin (triplicates) into Eppendorf reaction tubes, add 1 mL Fmoc-deprotection solution to each sample and incubate for 1 h at room temperature (RT) under shaking. Take 25 µL of the supernatant and dilute with 975 µL DMF. Determine the absorption at 301 nm (A_{301}) against an equally diluted Fmoc-deprotection solution as blank solution. The resin load can then be calculated by the following formula:

$$\text{Loading}\left[\text{mmol} / \text{g}\right] = \frac{1000 \cdot A_{301}}{D \cdot 7800 \cdot m\left[\text{mg}\right]}$$

with D as dilution factor (0.025) and 7800 as molar extinction coefficient [$\text{Lmol}^{-1}\text{cm}^{-1}$]. Calculate the arithmetic mean of the triplicate values as final resin loading.

8. Incubate the remaining resin four times for 10 min with Fmoc-deprotection solution to remove the Fmoc-protection group.

3.1.2 Kaiser Test

1. Transfer a few resin beads of DCM washed resin into an Eppendorf reaction tube.
2. Add two drops of each Kaiser test solution.
3. Incubate at 100 °C for 4 min under shaking.

The presence of free amines is indicated by an intense blue color.

3.1.3 Synthesis of 356

1. Put the amount of L-Cys(Trt)-loaded 2-chlorotrityl resin corresponding to the intended synthesis scale size into a syringe reactor with adequate size (*see* **Note 2**).
2. Swell the resin in DCM for 30 min (10 mL/g resin).
3. Generate the polyamido backbone by sequential coupling of 4 Fmoc-Stp(Boc_3)-OH building blocks, followed by Dde-L-Lys(Fmoc)-OH as branching unit, 4 more Fmoc-Stp(Boc_3)-OH units and Boc-L-Cys(Trt)-OH (*see* **Note 4** and Table 1). No Fmoc deprotection is required after the coupling of the terminal Boc-protected amino acid.
4. Remove the Dde-protecting group with Dde-deprotection solution: incubate 10–30 times for 5 min until the supernatant does not show absorption at 290 nm, which confirms the completion of deprotection.
5. Continue with the synthesis at the free amine by coupling Fmoc-dPEG$_{24}$-OH, Fmoc-Glu-OtBu, and N^{10}-(trifluoroacetyl) pteroic acid under standard coupling conditions (*see* **Note 5** and Table 1).
6. Add tfa-deprotection solution four times for 30 min to remove the tfa-protecting group.
7. Dry the resin in vacuo.
8. Cleave the complete assembled oligomer from the solid phase by incubation with a cleavage cocktail (10 mL/g resin) for 90 min (*see* **Note 6**).
9. Wash the resin three times with TFA (10 mL/g resin) and combine the solutions.
10. Evaporate the solvent to a final volume of around 1 mL and add it dropwise to 50 mL of ice cold precipitating solution to precipitate the oligomer.
11. Centrifuge (20 min, 4000 rcf, 4 °C), discard the supernatant and dry the precipitate under nitrogen stream.
12. Dissolve the crude product in acetonitrile–H_2O (25/75, v/v), snap-freeze and lyophilize.
13. The product is obtained as a yellow TFA salt of the multiple protonatable amines of the oligomer (MW = 4075.1 + 2850.0 g/mol, *see* **Note 7**).
14. Store the hygroscopic and oxidation-sensitive compound at −20 °C in a sealed tube under nitrogen and with exclusion of air and moisture.

The oligomer can be analyzed by ^{1}H-NMR and RP-HPLC (*see* **Notes 8** and **9**).

3.1.4 Synthesis of 672

1. Put the amount of L-Lys(ivDde)-loaded 2-chlorotrityl resin corresponding to the intended synthesis scale size into a syringe reactor with adequate size (*see* **Note 2**).
2. Swell the resin in DCM for 30 min (10 mL/g resin).
3. Synthesize the polyamido backbone by sequential coupling of Fmoc-L-His(Trt)-OH, Fmoc-L-Lys(Fmoc)-OH (symmetrical branching point; after Fmoc-deprotection free amines are doubled), followed by alternating coupling of five times Fmoc-L-His(Trt)-OH and four times Fmoc-Stp(Boc_3)-OH. The synthesis of the backbone is terminated by the coupling of the terminal cysteines as Boc-L-Cys(Trt)-OH (*see* **Note 4** and Table 1).
4. Remove the Dde-protecting group with Dde-deprotection solution: incubate 10–30 times for 5 min until the supernatant does not show absorption at 290 nm, which confirms the completion of deprotection.
5. Continue with the synthesis at the free amine by coupling two times Fmoc-$dPEG_{24}$-OH, five times Fmoc-L-Glu-OtBu, and finally the pteroic acid derivate 4-[[(2,4-diamino-6-pteridinyl) methyl]methylamino]-benzoic acid under standard coupling conditions (*see* **Note 5** and Table 1).
6. Dry the resin in vacuo.
7. Cleave the complete assembled oligomer from the solid phase by incubation with a cleavage cocktail (10 mL/g resin) for 90 min (*see* **Note 6**).
8. Wash the resin three times with TFA (10 mL/g resin) and combine the solutions.
9. Evaporate the solvent to a final volume of around 1 mL and add it dropwise to 50 mL of ice cold precipitating solution to precipitate the oligomer.
10. Centrifuge (20 min, 4000 rcf, 4 °C), discard the supernatant and dry the precipitate under nitrogen stream.
11. Dissolve the crude product in acetonitrile–water (25/75, v/v), snap-freeze and lyophilize.
12. The product is obtained as a yellow TFA salt of the multiple protonatable amines of the oligomer (MW = 7369.6 + 4218 g/mol, *see* **Note 7**).
13. Store the solid hygroscopic and oxidation-sensitive compound at −20 °C in a sealed tube under nitrogen and with exclusion of air and moisture.

The oligomer can be analyzed by ^{1}H-NMR and RP-HPLC (*see* **Notes 8** and **9**).

3.2 Synthesis of Endosomolytic siRNA-Inf7 Conjugate

For therapies based on the cytosolic delivery of macromolecules it is important to ensure the endosomal escape of the cargo. Covalent binding of the lytic peptide Inf7 to the siRNA improves the co-localization of the drug and the lytic unit and thereby the efficiency of endosomal escape and the drug.

Inf7 is linked via a disulfide bridge to siRNA with thiol-modification at the 5′-end of the sense strand. Since disulfide bonds are cleaved under the reductive cytosolic conditions, the disulfide linkage prevents unwanted influence of Inf7 on the siRNA activity. Initially, the thiol group of the modified siRNA is protected as disulfide with hexane thiol to prevent oxidation.

The Inf7-siRNA conjugate synthesis consists of three reaction steps (Fig. 5).

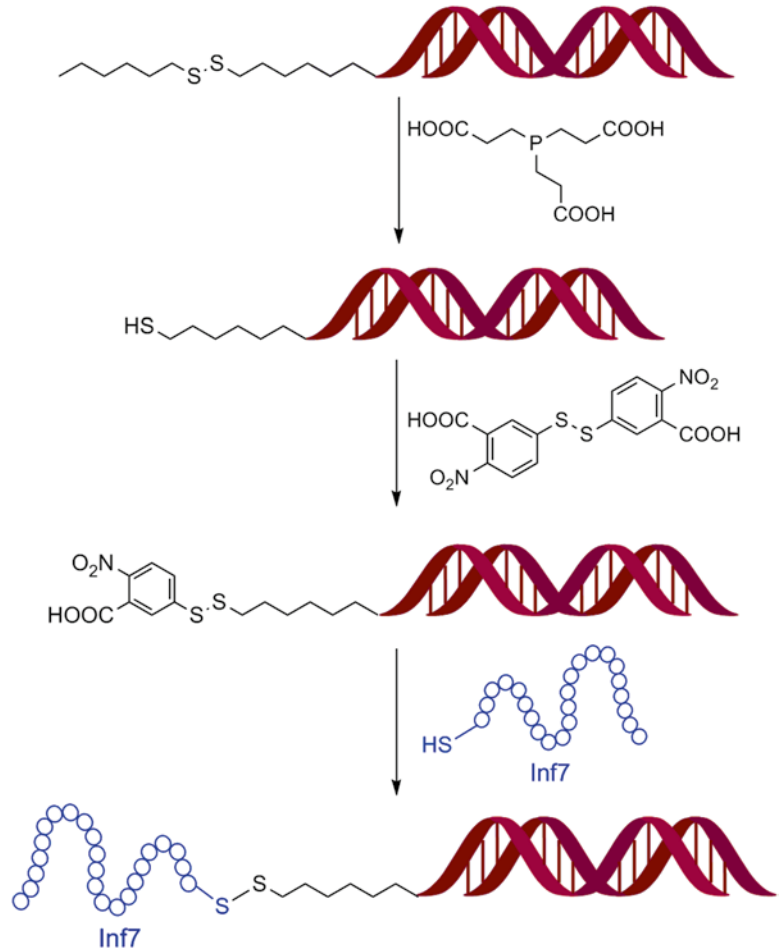

Fig. 5 Synthesis scheme of the siRNA-Inf7 conjugate

1. Dilute 0.5 μmol of C6-SS-C6 modified siRNA to a volume of 400 μl H_2O in an Eppendorf reaction tube.
2. Add 10 μL of a 0.5 M TCEP hydrochloride solution (5 μmol, 10 eq.) and incubate for 30 min at RT to get the free thiol groups.
3. Purify the deprotected siRNA by anion exchange chromatography using a 1 mL ResourceQ-column connected to an ÄKTApurifier 10 system (GE Healthcare Biosciences AB, Uppsala, Sweden) and photometrical detection at 260 nm. The column is equilibrated with a mixture of IEX-Buffer A and B 95/5 (v/v). Load the siRNA sample with the same buffer mixture. Subsequently, increase the amount of IEX-Buffer B to 20 % and wash the column until a stable baseline is observed. Start collection of fractions with a volume of 0.5 mL and elute the product with a gradient from 20 % IEX-Buffer B to 50 % in 30 min. Pool the fractions with absorption at 260 nm.
4. Activate the free thiol group of the siRNA by incubating with DTNB. Dissolve 2 mg of DTNB (5 μmol, 10 eq.) in 200 μL 20 mM HEPES (pH 8). Add the siRNA solution dropwise to the DTNB solution to avoid dimerization and incubate for 1 h at RT under shaking.
5. Add an equal volume of IEX-Buffer A to the reaction mixture to dilute the contained NaCl before anion exchange. Subsequently, purify the activated siRNA using the same conditions as described in **step 2**.
6. Dissolve 2.1 mg of Inf7 peptide (TFA salt, 0.75 μmol, 1.5 eq.) in 20 mM HEPES (pH 8.5) containing 30 % acetonitrile and incubate with the activated siRNA for 2 h at RT under shaking.
7. Add an equal volume of IEX-Buffer A to the reaction mixture to dilute the contained NaCl before anion exchange. Subsequently, purify the final siRNA-Inf7 conjugate based on the same ion exchange chromatography conditions as described in **step 2**. To identify the product, fractions with absorption at 260 nm are collected separately.
8. Remove the acetonitrile of the separate fractions in a vacuum concentrator and analyze them by agarose gel electrophoresis (2.5 % agarose gel, 100 min, 100 V). Unconjugated siRNA serves as a reference and the fractions with lower electrophoretic mobility are pooled.
9. Determine the concentration of the siRNA solution photometrically at 260 nm, aliquot, snap-freeze and store at −20 °C. Try to avoid multiple freezing and thawing.

3.3 Polyplex Formation

Polyplex formation arises from binding of positively charged oligomers to the negatively charged nucleic acids. The ratio between oligomer and nucleic acid is an important parameter for the formation

of stable ionic complexes. In case of basic oligomers with protonatable nitrogens, the *N/P* (protonatable nitrogens of the oligomer/phosphate groups of RNA) ratio is a common way to describe the oligomer and nucleic acid proportions in the polyplex formulation. To find optimal conditions for stable polyplex formation, it is necessary to examine polyplex formation at different *N/P* ratios (*see* **Note 10**).

3.3.1 siRNA Polyplexes

Polyplex formation is described for in vitro transfections; for other trials the polyplexes are prepared similarly with different amounts of RNA and oligomer.

1. Dilute 0.27 μg of siRNA (free or conjugated) in 10 μL HBG.
2. Dilute the calculated amount of oligomer at different *N/P* ratios (*see* **Note 11**) in 10 μL HBG.
3. Add the oligomer solution to the RNA solution and mix by pipetting up and down at least 5–10 times.
4. Incubate the mixture for 40 min at RT to allow the formation of polyplexes and disulfide bonds. Use the polyplexes immediately after preparation for your experiments.

3.3.2 Poly(I:C) and Poly(I) Polyplexes

Polyplex formation is described for in vitro transfections; for other trials the polyplexes are prepared similarly with different amounts of siRNA and oligomer.

1. Dilute 1 μg of nucleic acid in 10 μL HBG.
2. Dilute the calculated amount of oligomer at different *N/P* ratios (*see* **Note 11**) in 10 μL HBG.
3. Add the oligomer solution to the RNA solution and mix by pipetting up and down at least 5–10 times.
4. Incubate the mixture for 40 min at RT to allow the formation of polyplexes and disulfide bonds. Use the polyplexes immediately after preparation for your experiments.

3.4 Biophysical Polyplex Characterization

One way to screen polyplex formation is the agarose gel retardation assay. In the electrical field, free RNA migrates through the agarose matrix towards the anode. The complexation of the RNA by oligomers inhibits the electrophoretic mobility due to the loss of negative charge and the increased size. Thus, the difference in gel migration allows evaluating polyplex formation and the determination of the minimal *N/P* ratio required for complete binding (*see* **Notes 12** and **13**). Free RNA serves as control.

Another method to determine and characterize particle formation is to measure their size. A common method for size determination of particles in nanoscale is dynamic light scattering (DLS). However, for the characterization of the mono-siRNA-*356*

polyplexes (cf. Fig. 2a) with a size below 10 nm, fluorescence correlation spectroscopy (FCS) is a suitable method.

It is necessary to shield the charge of polyplexes to avoid unwanted interactions with serum compounds and untargeted cells. The zeta potential, which can be determined by electrophoretic light scattering, is a common parameter for the characterization of the surface charge of a particle or polyplex and thus the shielding efficiency.

FCS and further biophysical characterization techniques and their advantages and disadvantage are described in Troiber et al. [20].

3.4.1 Gel Migration Assay for siRNA Polyplexes

1. Fix a 15 × 15 cm UV-transparent gel tray in a gel casting unit.
2. For siRNA polyplexes weigh 3.0 g agarose (2.5 % gel, w/v), for poly(I:C) polyplexes 1.2 g agarose (1 % gel, w/v) into a beaker and add 120 mL TBE buffer.
3. Heat the mixture to boiling until all agarose is completely dissolved and a clear solution is formed (*see* **Note 14**).
4. Let the solution cool down to 50 °C and add 12 μL of GelRed (10,000× concentrate) for the subsequent nucleic acid staining.
5. Pour the solution into the gel casting unit, fix a well comb and let the gel solidify for at least 30 min (*see* **Note 15**).
6. Prepare polyplexes containing 0.5 μg siRNA or 0.8 μg poly(I:C) in different *N/P* ratios as described in Subheading 3.3. After incubation for 40 min add 4 μL loading buffer.
7. Remove the well comb of the hardened gel to expose the sample pockets and put the gel into an electrophoresis unit. Fill the chamber with TBE-Buffer until the gel is situated at least 0.5 cm below the surface and all sample pockets are filled.
8. Load the samples into the sample pockets and apply a voltage of 80 V for 60 min in case of siRNA polyplexes or 85 V for 90 min in case of poly(I:C) polyplexes.
9. Examine the gel on a UV-transilluminator (*see* **Note 16**).

3.4.2 Size Measurement via Dynamic Light Scattering and Measurement of Zeta Potential

1. Prepare polyplexes containing 10 μg nucleic acid and oligomer at intended *N/P* ratio in 50 μL HEPES (20 mM, pH 7.4) as described in Subheading 3.3.
2. After 40 min incubation, add 750 μL HEPES (20 mM, pH 7.4) and transfer the solution into a folded capillary cell.
3. For size measurement, measure each sample three times with 10 subruns of 10 s at 25 °C.
4. For determination of the zeta potential, measure each sample three times with 10–30 subruns of 10 s at 25 °C.

4 Notes

1. Since DMF can hydrolyze to formic acid and dimethylamine which interferes with the synthesis, we recommend anhydrous peptide grade DMF and storage with exclusion of air and moisture.
2. The syringe microreactors are available in different sizes (2–100 mL) and have to be chosen according to the resin amount.
3. DCM used for the loading of 2-chlorotrityl chloride resins have to be dry and should be kept over calcium chloride with exclusion of air and moisture.
4. The adequate volume of coupling solution depends on the solubility of the used building block, the resin amount and the scale size. In general the lowest possible volume (≥5 mL/g resin) with complete dissolution of the reagents is favorable.
5. Both pteroic acid derivatives are poorly soluble. The coupling solutions are prepared in the lowest possible volume (≥5 mL/g resin) for complete dissolution. The derivative for synthesis of *672* can be dissolved in a mixture of NMP/DMF/DMSO (1:1:1 v/v/v).
6. TFA is corrosive and volatile. Be sure to wear appropriate protective clothing (lab coat, goggles, gloves) and work under the fume hood, as always.
7. The salt form with the multiple protonatable amines has to be considered in the calculation of the molecular weight. The number n of protonatable amines is 25 in case of *356* and 37 in case of, *672*. The molecular weight of the TFA salts is calculated according to the following formula:

$$\mathrm{MW}\left(\mathrm{TFA\ salt}\right) = \mathrm{MW}\left(\mathrm{free\ base}\right) + n \cdot 114$$

   n represents the number of protonatable amines and 114 is the mass of TFA.
8. ^{1}H-NMR spectra of the compounds are complex with overlapping signals. Characteristic peaks are located in the chemical shifts ranges of δ (ppm) = 2.3–2.6 (4H per Stp, 2H per $dPEG_{24}$), 3.0–3.5 (16H per Stp, 2H per cysteine, histidine, lysine), 3.5–3.7 (98H per $dPEG_{24}$), 4.0–4.7 (1H per cysteine, glutamate, histidine, lysine), 6.7–6.9 (2H per FolA, MTX), 7.1–7.3 (1H per histidine), 7.5–7.7 (2H per FolA, MTX), 8.5–8.6 (1H per histidine), 8.6–8.8 (1H per FolA, MTX).
9. For the analysis by RP-HPLC the use of a C18 column and a water–acetonitrile gradient containing 0.1 % TFA (vol %) are recommended. The compounds can be detected photometrically at 214 and 280 nm.

10. If the N/P ratio is too low the occurring polyplexes are in general unstable; if the N/P ratio is too high agglomeration is likely.
11. The amount of oligomer (n_{oligomer}) for a given amount of RNA (n_{RNA}) is calculated via N/P (protonatable nitrogens of the oligomer (N)/phosphate groups of RNA (P)) ratio:

$$n_{\text{oligomer}}\left[\mu\text{mol}\right] = n_{\text{RNA}}\left[\mu\text{mol}\right] \cdot P \cdot \frac{N/P}{N}$$

    Histidine nitrogens are not considered in the calculation. We usually test N/P ratios from 3 to 20.
12. Weak smears during the gel migration assay can result from slight degradation of the polyplexes under electrophoresis conditions.
13. Gel migration assay with poly(I:C) containing polyplexes show broad bands due to the polydispersity of the poly(I:C).
14. We recommend heating in a microwave. However, the agarose can also be dissolved on a heating plate equipped with a magnetic stirrer. In both cases, watch the mixture carefully to avoid superheating.
15. Avoid bubbles since they can influence migration of the samples. In case of bubbles, push them away towards the sides/edges of the gel with a pipette tip.
16. UV light can cause serious eye damage. Avoid looking into the light source and wear protective goggles or a mask with appropriate UV filter.

Acknowledgements

This work was supported by the DFG Cluster "Nanosystems Initiative Munich". We thank Wolfgang Rödl and Miriam Höhn for technical support, and Olga Brück for skillful assistance.

References

1. Duncan R (2003) The drawing era of polymer therapeutics. Nat Rev Drug Discov 2(5): 347–360
2. Duncan R, Gaspar R (2011) Nanomedicine(s) under the microscope. Mol Pharm 8(6): 2101–2141
3. Haag R, Kratz F (2006) Polymer therapeutics: concepts and applications. Angew Chem Int Ed 45:1198–1215
4. Schaffert D et al (2011) Solid-phase synthesis of sequence-defined T-, i-, and U-shape polymers for pDNA and siRNA delivery. Angew Chem Int Ed Engl 50:8986–8989
5. Frohlich T et al (2012) Structure-activity relationships of siRNA carriers based on sequence-defined oligo (ethane amino) amides. J Control Release 160:532–541
6. Troiber C et al (2013) Stabilizing effect of tyrosine trimers on pDNA and siRNA polyplexes. Biomaterials 34:1624–1633
7. Edinger D et al (2014) Gene silencing and antitumoral effects of Eg5 or Ran siRNA

oligoaminoamide polyplexes. Drug Deliv Transl Res 4(1):84–95

8. Maier K, Wagner E (2012) Acid-labile traceless click linker for protein transduction. J Am Chem Soc 134(24):10169–10173
9. Lächelt U et al (2014) Synthetic polyglutamylation of dual-functional MTX ligands for enhanced combined cytotoxicity of poly(I:C) nanoplexes. Mol Pharm 11(8):2631–2639
10. Edinger D, Wagner E (2011) Bioresponsive polymers for the delivery of therapeutic nucleic acids. Wiley Interdiscip Rev Nanomed Nanobiotechnol 3:33–46
11. Copolovici DM, Langel K, Langel Ü (2014) Cell-penetrating peptides: design, synthesis, and applications. ACS Nano 8(3):1972–1994
12. Mechtler K, Wagner E (1997) Gene transfer mediated by influenza virus peptides: the role of peptide sequences. New J Chem 21: 105–111
13. Meyer M et al (2008) Breathing life into polycations: functionalization with pH-responsive endosomolytic peptides and polyethylene glycol enables siRNA delivery. J Am Chem Soc 130:3272–3273
14. Meyer M et al (2009) Synthesis and biological evaluation of bioresponsive and endosomolytic siRNA-polymer conjugate. Mol Pharm 6: 752–762
15. Wagner E (2012) Polymers for siRNA delivery: inspired by viruses to be targeted, dynamic, and precise. Acc Chem Res 45:1005–1013
16. Dohmen C et al (2012) Nanosized multifunctional polyplexes for receptor-mediated siRNA delivery. ACS Nano 6:5198–5208
17. Lächelt U et al (2014) Fine-tuning of proton sponges by precise diaminoethanes and histidines in pDNA polyplexes. Nanomedicine: NBM 10:35–44
18. Schaffert D, Badgujar N, Wagner E (2011) Novel Fmoc-polyamino acids for solid phase synthesis of defined polyamidoamines. Org Lett 13(7):1586–1589
19. Chan WC, White PD (2000) Fmoc solid phase peptide synthesis: a practical approach. Oxford University Press, Oxford
20. Troiber C et al (2013) Comparison of four different particle sizing methods for siRNA polyplex characterization. Eur J Pharm Biopharm 84:255–264

Chapter 26

Cell Penetrating Peptides for Chemical Biological Studies

Ikuhiko Nakase, Toshihide Takeuchi, and Shiroh Futaki

Abstract

Significant progress has been made in the development of chemical biology methods used to study the molecular behavior and interplay among live cells. These include the development of novel fluorescent molecules and photo-cross-linking agents that can be used to determine the cellular locations of biomacromolecules (including proteins and nucleic acids). Various biosensors utilizing the remarkable ligand-recognition abilities of biomacromolecules have also been developed. To allow such chemically functionalized molecules to interact with their partners, and to fully exploit the abilities and functions thereof, it is necessary to efficiently deliver such molecules into cells, specifically into the cytosol. Here, we illustrate intracellular delivery methods employing arginine-rich cell-penetrating peptides (CPPs) (e.g., octa-arginine) in the presence of a counteranion, pyrenebutyrate. This approach is especially suitable for intracellular delivery of small proteins and peptides. Approaches employing arginine-rich CPPs tagged with a penetration-accelerating sequence can also be used toward this end.

Key words Arginine-rich cell-penetrating peptide, Direct membrane penetration, Pyrenebutyrate, Counteranion, Penetration-accelerating sequence (PAS)

1 Introduction

Fluorescent protein technologies have been epochal in the field of cell biology [1, 2]. The use of fluorescent fusion proteins (e.g., green fluorescent protein, GFP) as visualization tags has allowed the locations and behaviors of cellular proteins to be studied in real time. Such technologies have also been applied in related research fields and have had enormous impacts in the area of chemical biology. Fluorescence has been used not only to visualize proteins within cells but also to sense protein–protein interactions in living cells [3, 4]. Two proteins of interest, each tagged with a single split (putatively fluorescent) fragment, fold into their native structures, and become fluorescent when the split fragments of interest are brought into close proximity via protein–protein interaction. However, fusion with a fluorescent protein is associated with steric hindrance (relative to the untagged protein), which can create artifacts when the cellular locations of such proteins are sought.

Ülo Langel (ed.), *Cell-Penetrating Peptides: Methods and Protocols*, Methods in Molecular Biology, vol. 1324,
DOI 10.1007/978-1-4939-2806-4_26,

Tagging with fluorescent proteins may affect protein–protein interactions and the behaviors/bioactivities of such proteins inside cells. In addition, it is difficult to control the expression levels of fusion proteins in cells transfected with the corresponding genes.

Alternatively, proteins chemically modified by attachment of fluorescent probes or via the actions of photo-cross-linking agents have been used to analyze protein interplay within cells [5, 6]. Such studies afford valuable information complementing that obtained using fluorescent protein technology. Over the last few years, many biosensors employing the abilities of natural proteins to recognize their specific ligands have been developed [7, 8]. For example, lectins have been chemically modified via attachment of fluorescent tags in the vicinities of sugar-recognition sites; binding to a specific sugar (a ligand) affects the environment of the fluorescent tag in a manner resulting in alteration of the fluorescence property [9]. Therefore, such chemically modified proteins can potentially serve as tailor-made sensors.

Chemically modified molecules cannot perform their required functions until they are internalized by cells. The cell-penetrating peptides (CPPs) described in this book are practical tools aiding the effective delivery of exogenous molecules into cells. Many reports on the use of CPPs to aid protein delivery have appeared [10]. Endocytosis plays a role in the cellular uptake thereof [11]. However, only limited amounts of endosome-entrapped proteins conjugated to CPPs escape from endosomal membranes to attain their target molecules in the cytosol (Fig. 1) [12]. Proteins trapped in endosomes not only are dysfunctional as sensing or photo-cross-linking molecules but may also send false signals when fluorescently labelled molecules are used to analyze the cellular locations of proteins. Therefore, it is necessary to develop a highly efficient

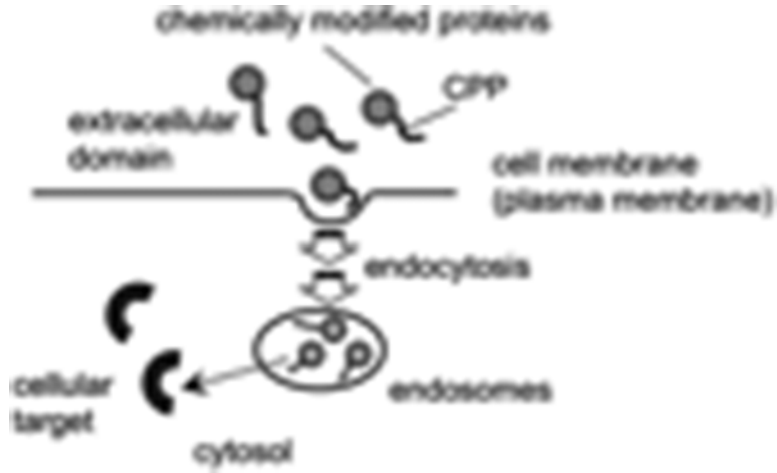

Fig. 1 Limited protein/peptide escape from endosomes hampers chemical biological studies of the cell

means whereby chemically modified proteins can be delivered to the cytosol to explore the activities thereof within live cells.

In the present chapter, we describe two approaches developed by our group for efficient protein delivery into cells. These approaches should aid studies in chemical biology. The first approach is the use of pyrenebutyrate as a counteranion promoting the translocation of arginine-rich CPPs through plasma membranes (*see* Subheading 3.1) [13–16]. The second approach is addition of a penetration-accelerating sequence (a PAS) to arginine-rich sequences (*see* Subheading 3.2) [17, 18].

Facile translocation of arginine-rich peptides, and conjugates thereof with peptides/small proteins, is possible when the cells are pretreated with pyrenebutyrate in phosphate-buffered saline (PBS). Alexa 488-labelled octa-arginine (R8) exhibited marked influx into almost all cells within 5 min (Fig. 2) [13, 14]. Such translocation

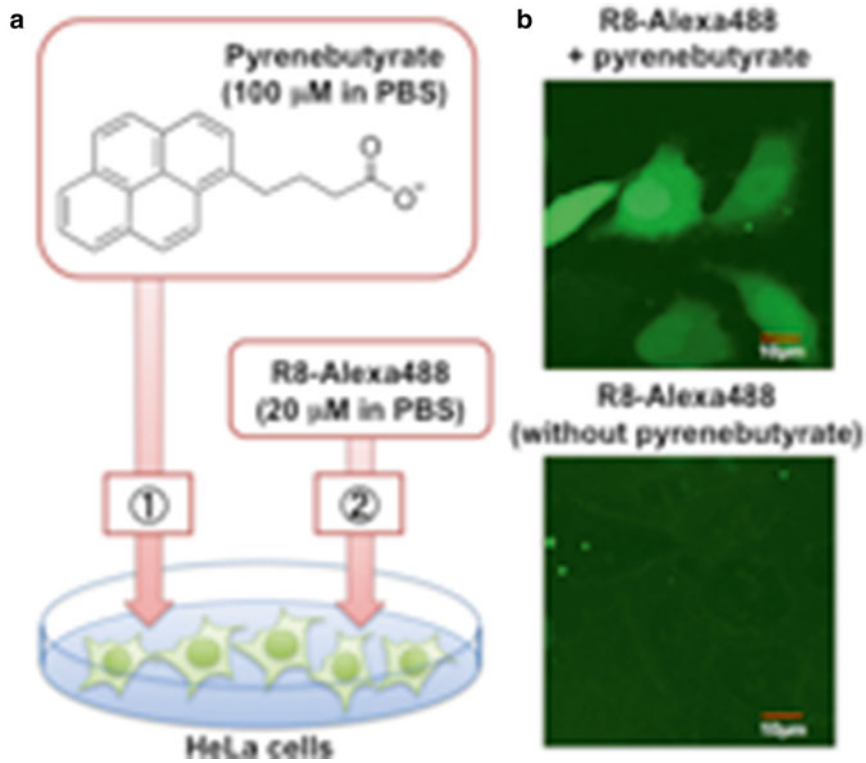

Fig. 2 Outline of the pyrenebutyrate-mediated intracellular delivery of Alexa 488-labelled octa-arginine (R8-Alexa 488). (**a**) Cells are treated with pyrenebutyrate in PBS, and next with R8-Alexa 488, without washout of pyrenebutyrate. Addition of equal amounts of pyrenebutyrate and R8-Alexa 488 solutions in PBS yields final concentrations of 50 and 10 μM, respectively (*see* Subheading 3.1). Simultaneous addition of pyrenebutyrate and R8-Alexa 488 may result in precipitation prior to cell interaction, which diminishes the internalization efficiency of R8-Alexa 488. The use of PBS rather than medium is important to ensure high-efficiency internalization. (**b**) Confocal micrographs of HeLa cells treated with R8-Alexa 488 in the presence or absence of pyrenebutyrate (Subheading 3.1)

was also observed at 4 °C even though endocytosis is not in play at this temperature [14]. Therefore, the translocation was energy-independent. Translocation was not accompanied by notable membrane perturbation, and no significant nuclear staining was observed when the cells were treated with propidium iodide (a membrane-impermeable nucleus-staining dye of low molecular weight) in the presence of Alexa 488-labelled R8 and pyrenebutyrate. Using this methodology, efficient delivery of GFP tagged with R8 into rat hippocampal primary cultured neurons was evident within a few minutes [14]. Successful delivery of stable isotope-labelled ubiquitin was also established using this methodology; subsequent NMR analysis of protein behavior within live cells was possible [15].

The guanidino function of the arginine side chain is a strong base (p*K*a ~12.5) and is thus highly cationized. The guanidino function forms hydrogen bonds with water molecules or solutes and would also be expected to engage in significant electrostatic interactions with electrolytes in water. On the other hand, a membrane is considered to be a hydrophobic barrier separating the cell interior from the outside. When guanidino functions enter membranes, such interactions must be cancelled; this is energetically unfavorable. When hydrophobic counteranions reside in membranes, these may form hydrogen bonds and engage in electrostatic interactions with the guanidino functions of arginines, reducing the energy barrier impeding the transfer of arginine-rich CPPs across the membranes. The counteranions thus work to catalyze translocation, driven by the membrane potential (i.e., the voltage gap between the inside and outside of the membrane).

Our second approach is the use of arginine-rich CPPs bearing PASs [17, 18]. We accidentally found that addition of an FFLIPKG segment to the N-terminus of R8 considerably accelerated cytosolic translocation [17]. Although significant cytosolic signals of Alexa 488-labelled FFLIPKG-R8 (PasR8) were observed in almost all cells, R8 alone did not diffuse markedly in the cytosol. A later study demonstrated the importance of the phenylalanine (Phe) residues in the PAS segment in terms of facilitating delivery. The FFFF sequence afforded an effect comparable to that of FFLIPKG [18]. Facilitated delivery of peptides 20–30 amino acids in length was achieved via attachment of the PAS or F4 segment to R8-tagged peptides. Addition of Phe-containing segments affords net hydrophobicity to R8 conjugates and thus adequately stimulates cytosolic delivery.

In the present chapter, we describe typical delivery procedures using R8 in combination with pyrenebutyrate or the PAS. Alexa 488 can be regarded as a model low-molecular-weight compound, and EGFP as a model protein to be delivered into cells.

2 Materials

2.1 Pyrenebutyrate-Mediated Intracellular Delivery of Alexa 488-Labelled Octa-Arginine (R8-Alexa 488) and Enhanced Green Fluorescent Protein Fused with R8 (R8-EGFP)

1. HeLa cells (human cervical cancer-derived cells) maintained in α-minimum essential medium (α-MEM) (Gibco, Life Technologies Corporation, Grand Island, NY) with 10 % (v/v) heat-inactivated bovine serum (BS) (Gibco).
2. Glass-bottomed dishes (35 mm in diameter) (Iwaki, Tokyo, Japan) for confocal microscopy.
3. Twenty-four-well microplates (Iwaki) for flow cytometric analysis.
4. A synthetic peptide of fluorescently labelled octa-arginine [amino acid sequence: RRRRRRRRGC(Alexa 488)-amide] (R8-Alexa 488) (*see* **Notes 1** and **2**).
5. R8-tagged enhanced green fluorescent protein (R8-EGFP) (*see* **Note 3**).
6. Pyrenebutyrate (1-pyrenebutyric acid) (Sigma-Aldrich, St. Louis, MO) dissolved in dimethyl sulfoxide (20 mM).
7. Heparin (Nacalai Tesque, Kyoto, Japan) dissolved in phosphate-buffered saline (PBS) (0.5 mg/mL).
8. $MgCl_2$ (0.5 mM) and $CaCl_2$ (1 mM) containing PBS (PBS (+)).

2.2 Facilitated Delivery of R8-Alexa 488 with the Aid of the PAS and Related Peptides

1. Cells, glass-bottomed dishes, microplates, and heparin (*see* Subheading 2.1., **items 1–3**, 7).
2. A synthetic peptide in which fluorescently labelled R8 is tagged with the PAS [amino acid sequence: FFLIPKG-RRRRRRRRGC(Alexa 488)-amide] (PasR8-Alexa 488), and tetraphenylalanine-attached octa-arginine [amino acid sequence: FFFFG-RRRRRRRRGC(Alexa 488)-amide] (F4R8-Alexa 488) (*see* **Notes 2** and **4**).

3 Methods

3.1 Pyrenebutyrate-Mediated Intracellular Delivery of Alexa 488-Labelled Octa-Arginine (R8-Alexa 488) and Enhanced Green Fluorescent Protein Fused with R8 (R8-EGFP) (Confocal Microscopy and Flow Cytometry Analyses)

1. Plate HeLa cells (2×10^5 cells/well) in glass-bottomed dishes, and culture in 2-mL amounts of 10 % (v/v) BS-containing α-MEM under 5 % (v/v) CO_2 at 37 °C for 24 h.
2. Remove the cell culture medium, and wash the cells twice with PBS (+) (1 mL PBS(+) each time).
3. Dilute pyrenebutyrate in DMSO (20 mM) with PBS (+) to yield a final concentration of 100 μM. Incubate the cells with this solution (100 μL/well) for 5 min at 37 °C under 5 % (v/v) CO_2 (*see* **Notes 5** and **6**).
4. Add R8-Alexa 488 or R8-EGFP (20 μM in PBS (+)) (100 μL/well) to the cells, without removing the pyrenebutyrate solution (*see* **Notes 5–7**).

5. Incubate the cells for 5 min at 37 °C under 5 % (v/v) CO_2.
6. Wash twice with 0.5 mg/mL heparin in PBS (1 mL) and add 10 % (v/v) BS-containing α-MEM (1 mL/well).
7. Analyze via confocal laser scanning microscopy (Fig. 2). (Quantification of the cellular uptakes of peptides and proteins via flow cytometry).
8. Plate HeLa cells (5×10^4 cells/well) in 24-well microplates, and culture in 1-mL amounts of α-MEM with 10 % (v/v) BS per well under 5 % (v/v) CO_2 at 37 °C for 24 h.
9. Remove the cell culture medium, and wash the cells twice with PBS (+) (500 μL each time).
10. Incubate the cells with pyrenebutyrate in PBS (+) (100 μM, 200 μL/well) for 5 min at 37 °C under 5 % (v/v) CO_2 (*see* **Notes 5** and **6**).
11. Add R8-Alexa 488 or R8-EGFP dissolved in PBS (+) (20 μM, 200 μL/well) to the cells, without removal of the pyrenebutyrate solution (*see* **Notes 5**–**7**).
12. Incubate the cells for 5 min at 37 °C under 5 % (v/v) CO_2.
13. Wash twice with 0.5 mg/mL heparin in PBS (200 μL) and add 0.01 % (w/v) trypsin in PBS (200 μL).
14. Incubate the cells for 10 min at 37 °C under 5 % (v/v) CO_2.
15. Collect the cells in a tube and centrifuge ($800 \times g$, 5 min, 4 °C).
16. After removal of the supernatant, wash the cells with PBS (400 μL) and centrifuge ($800 \times g$, 5 min, 4 °C).
17. Repeat this washing cycle and suspend the cells in PBS (400 μL).
18. Analyze via flow cytometry.

3.2 Facilitated Delivery of R8-Alexa 488 with the Aid of the PAS and Related Peptides

1. Plate HeLa cells and culture for 24 h as described in Subheading 3.1, **step 1**.
2. Remove the cell culture medium, and wash twice with 10 % (v/v) BS-containing α-MEM (1 mL).
3. Incubate the cells with PasR8-Alexa 488, or F4R8-Alexa 488, in 10 % (v/v) BS-containing α-MEM (10 μM, 200 μL/well) for 15 min at 37 °C under 5 % (v/v) CO_2 (*see* **Note 7**). **Notes 8** and **9** contain examples of conjugation of CPPs and cargoes with the BS^3 cross-linker.
4. Wash twice with 0.5 mg/mL heparin in PBS (1 mL) and add 10 % (v/v) BS-containing α-MEM (1 mL/well).
5. Analyze via confocal laser scanning microscopy.
6. To detect fluorescence from cell-internalized PasR8-Alexa 488 or F4R8-Alexa 488 using a flow cytometer, plate the HeLa cells for 24 h as described in Subheading 3.1, **step 8**.

7. Remove the cell culture medium, and wash twice with 10 % (v/v) BS-containing α-MEM (500 μL).
8. Incubate the cells with PasR8-Alexa 488 or F4R8-Alexa 488 in 10 % (v/v) BS-containing α-MEM (10 μM, 400 μL/well) for 15 min at 37 °C under 5 % (v/v) CO_2.
9. Wash and collect the cells as described in Subheading 3.1, **steps 13–18**.
10. Analyze via flow cytometry.

4 Notes

1. The peptide is prepared by Fmoc (9-fluorenylmethyloxycarbonyl) solid-phase peptide synthesis on a Rink amide resin using a standard peptide synthesizer protocol. A combination of 1-[bis(dimethylamino)methylene]-1H-benzotriazolium 3-oxide hexafluorophosphate (HBTU), 1-hydroxybenzotriazole (HOBt), and *N*-ethyldiisopropylamine (DIEA) serves as the coupling system. Fmoc-Arg (pbf)-OH (*Nα-9*-fluorenylmethoxycarbonyl-*N*g-2,2,4,6,7-pentamethyldihydrobenzofuran-5-sulfonyl-arginine), Fmoc-Gly-OH (9-fluorenylmethoxycarbonylglycine), and Fmoc-Cys(Trt)-OH (9-fluorenylmethoxycarbonyl-*S*-trityl-cysteine), serve as amino acid derivatives. To cleave the peptide from the resin, and to deprotect the peptide, the peptide-bearing resin is treated with trifluoroacetic acid (TFA)-ethanedithiol (EDT) (95:5 by volume) at room temperature for 3 h. Crude peptides are purified with the aid of reverse-phase high-performance liquid chromatography (RP-HPLC), followed by lyophilization to yield powders. The peptide structures are confirmed with the aid of matrix-assisted laser desorption ionization time-of-flight mass spectrometry (MALDI-TOFMS).
2. Fluorescently labelled peptides are prepared by modifying the sulfhydryl group of cysteine with a maleimide-activated fluorophore. Purified peptides with cysteine residues (**Notes 1** and **4**) are treated with 1.5 equivalents of Alexa Fluor 488 C5 maleimide (Invitrogen, Eugene, OR) in a *N*,*N*-dimethylformamide–methanol mixture (1:1 by volume) for 1.5 h at room temperature. The fluorescently labelled peptides are next purified using RP-HPLC and the peptide structures confirmed with the aid of MALDI-TOFMS.
3. The EGFP protein bearing an R8 segment and a thrombin cleavage site at the N-terminus (R8-EGFP) is prepared as previously described [14]. Briefly, a 720-bp fragment (nt 679–1398) of pEGFP-N1 (Clontech, Mountain View, CA) is amplified using a standard PCR method and combined with

fragment-encoded $(His)_6$ (H6) and R8 sequences. The fragment is digested with restriction enzymes (*Bam*HI and *Eco*RI) and inserted into pEV29b. The sequence is validated using a DNA sequencer. R8-EGFP is overexpressed in the *E. coli* strain BL21(DE3)pLysS and purified using Ni-NTA agarose (Qiagen, Valencia, CA) followed by gel filtration (Sephadex G-25).

4. The peptides are prepared by Fmoc-solid-phase peptide synthesis on a Rink amide resin in a manner similar to that described in **Note 1**. The amino acid derivatives, Fmoc-Phe-OH (9-fluorenylmethoxycarbonyl-phenylalanine), Fmoc-Leu-OH (9-fluorenylmethoxycarbonyl-leucine), Fmoc-Ile-OH (9-fluorenylmethoxycarbonyl-isoleucine), Fmoc-Pro-OH (9-fluorenylmethoxycarbonyl-proline), Fmoc-Lys(Boc)-OH z(*Nα*-9-fluorenylmethoxycarbonyl-*Nε*-*t*-butyloxycarbonyl-lysine), Fmoc-Gly-OH, and Fmoc-Arg(Pbf)-OH, are employed to this end.
5. PBS should be used when cells are treated with pyrenebutyrate and R8-Alexa 488. The use of cell culture medium (e.g., α-MEM) instead of PBS is associated with very low-efficiency cell membrane penetration by the peptide.
6. Optimization of the concentrations of both peptides and pyrenebutyrate is required to ensure high-efficiency membrane penetration.
7. Propidium iodide (PI, 5 μM) can be used to detect cell membrane disruption and cytotoxicity. Intact plasma membranes do not allow entry of PI to stain the nucleus. On the other hand, disruption of the cell membrane triggers PI staining.
8. Chemical conjugation with CPPs can also be employed to deliver bioactive molecules into cells. We have worked with oligo-arginines (R8 and R12) bearing sulfosuccinimidylsuberyl moieties, which allow of one-pot modification of the amino functions of the cargoes by mixing preactivated CPPs in an aqueous buffer [19]. A bis(sulfosuccinimidyl)suberate (BS^3) cross-linker (Thermo Scientific, Rockford, IL) is used to prepare preactivated CPPs (BS^3-CPPs). Similarly, R8 bearing a PAS can be preactivated using BS^3. As BS^3 can interact with the lysine side-chain of the PAS sequence, R8 bearing a PAS-related sequence lacking the lysine and proline of PasΔPKR8 (amino acid sequence: FFLIGRRRRRRRR) can be employed to this end.
9. Reference 19 contains an example of the conjugation of PasΔPKR8 with amino-PEG5000 (propylamine-functionalized polyethylene glycol, Sunbright PA series, NOF Corporation, Tokyo, Japan) as a model cargo. PasΔPKR8 was labelled with Alexa 488 to allow for microscopic observation,

and quantification via flow cytometry. To prepare BS^3-conjugated PasΔPKR8 (Alexa 488), the BS^3-cross-linker (1.1 μmol, 1.5 equiv.) in H_2O (400 μL) is added to an aqueous solution (600 μL) of PasΔPKR8 (Alexa 488) (0.7 μmol). After adjusting the pH to 7–8 with *N*-methylmorpholine (NMM), the mixture is stirred at room temperature for 20 min prior to RP-HPLC purification. The peptide structure is confirmed by MALDI-TOFMS. Amino-PEG5000 (0.65 μmol) dissolved in H_2O (400 μL) is then added to a solution of BS^3-PasΔR8 (Alexa 488) (0.7 μmol, 1.1 equiv.) in H_2O/CH_3CN (600 μL, volume ratio 7:5) with addition of NMM (0.2 μL). The mixture is stirred at room temperature for 2 h prior to RP-HPLC purification. The structure of the conjugate is confirmed by MALDI-TOFMS.

Acknowledgment

This work was supported in part by Grants-in-Aid for Scientific Research from the Ministry of Education, Culture, Sports, Science and Technology of Japan and Collaborative Research Program of Institute for Chemical Research, Kyoto University.

References

1. Tsien RY (2009) Constructing and exploiting the fluorescent protein paintbox. Angew Chem Int Ed Engl 48:5612–5626
2. Chalfie M (2009) GFP: lighting up life. Angew Chem Int Ed Engl 48:5603–5611
3. Jung D, Min K, Jung J, Jang W, Kwon Y (2013) Chemical biology-based approaches on fluorescent labeling of proteins in live cells. Mol Biosyst 9:862–872
4. Kanno A, Ozawa T, Umezawa Y (2011) Detection of protein-protein interactions in bacteria by GFP-fragment reconstitution. Methods Mol Biol 705:251–258
5. Lukinavičius G, Johnsson K (2011) Switchable fluorophores for protein labeling in living cells. Curr Opin Chem Biol 15:768–774
6. Lowder MA, Appelbaum JS, Hobert EM, Schepartz A (2011) Visualizing protein partnerships in living cells and organisms. Curr Opin Chem Biol 15:781–788
7. Tamura T, Hamachi I (2014) Recent progress in design of protein-based fluorescent biosensors and their cellular applications. ACS Chem Biol 9(12):2708–2717
8. Aoki K, Komatsu N, Hirata E, Kamioka Y, Matsuda M (2012) Stable expression of FRET biosensors: a new light in cancer research. Cancer Sci 103:614–619
9. Hayashi T, Sun Y, Tamura T, Kuwata K, Song Z, Takaoka Y, Hamachi I (2013) Semisynthetic lectin-4-dimethylaminopyridine conjugates for labeling and profiling glycoproteins on live cell surfaces. J Am Chem Soc 135:12252–12258
10. Vasconcelos L, Pärn K, Langel Ü (2013) Therapeutic potential of cell-penetrating peptides. Ther Deliv 4:573–591
11. Futaki S, Hirose H, Nakase I (2013) Arginine-rich peptides: methods of translocation through biological membranes. Curr Pharm Des 19:2863–2868
12. Tünnemann G, Martin RM, Haupt S, Patsch C, Edenhofer F, Cardoso MC (2006) Cargo-dependent mode of uptake and bioavailability of TAT-containing proteins and peptides in living cells. FASEB J 20:1775–1784
13. Perret F, Nishihara M, Takeuchi T, Futaki S, Lazar AN, Coleman AW, Sakai N, Matile S (2005) Anionic fullerenes, calixarenes, coronenes, and

pyrenes as activators of oligo/polyarginines in model membranes and live cells. J Am Chem Soc 127:1114–1115

14. Takeuchi T, Kosuge M, Tadokoro A, Sugiura Y, Nishi M, Kawata M, Sakai N, Matile S, Futaki S (2006) Direct and rapid cytosolic delivery using cell-penetrating peptides mediated by pyrenebutyrate. ACS Chem Biol 1:299–303
15. Inomata K, Ohno A, Tochio H, Isogai S, Tenno T, Nakase I, Takeuchi T, Futaki S, Ito Y, Hiroaki H, Shirakawa M (2009) High-resolution multi-dimensional NMR spectroscopy of proteins in human cells. Nature 458:106–109
16. Guterstam P, Madani F, Hirose H, Takeuchi T, Futaki S, El Andaloussi S, Gräslund A, Langel Ü (2009) Elucidating cell-penetrating peptide mechanisms of action for membrane interaction, cellular uptake, and translocation utilizing the hydrophobic counter-anion pyrenebutyrate. Biochim Biophys Acta 1788:2509–2517
17. Takayama K, Nakase I, Michiue H, Takeuchi T, Tomizawa K, Matsui H, Futaki S (2009) Enhanced intracellular delivery using arginine-rich peptides by the addition of penetration accelerating sequences (Pas). J Control Release 138:128–133
18. Takayama K, Hirose H, Tanaka G, Pujals S, Katayama S, Nakase I, Futaki S (2012) Effect of the attachment of a penetration accelerating sequence and the influence of hydrophobicity on octaarginine-mediated intracellular delivery. Mol Pharm 9:1222–1230
19. Takayama K, Tadokoro A, Pujals S, Nakase I, Giralt E, Futaki S (2009) Novel system to achieve one-pot modification of cargo molecules with oligoarginine vectors for intracellular delivery. Bioconjug Chem 20:249–257

Chapter 27

Experiences with CPP-Based Self Assembling Peptide Systems for Topical Delivery of Botulinum Toxin

Jane Lee, Phil Kennedy, and Jacob M. Waugh

Abstract

Considerations in rational designs of CPP-based transcutaneous delivery systems are described. Impact of design considerations of nonclinical and clinical results are presented in detail.

Key words Botulinum toxin, Lateral canthal lines, Hyperhidrosis, TAT, Ionic

1 Introduction

As will be apparent upon reading the other chapters in this book, there has been remarkable progress in our understanding of cell-penetrating peptides (CPPs). More continues to be elucidated about this powerful family of agents and their potential applications each day. Our group has primarily focused on translational applications for CPPs. Specifically, we have focused on attributes of CPPs useful for transcutaneous local delivery of botulinum toxin type A (BoNTA).

Our group typically employs a noncovalent means of initially screening CPPs with potential therapeutic payloads. This has allowed exploration of various CPPs alone and in combination without issues relating to activity, altered pharmacologic properties, or safety issues related to generation of new chemical entities (NCE). The focus of this chapter will be on the considerations in development of a CPP-enabled topical form of botulinum toxin for facial wrinkles and hyperhidrosis. Although our laboratories typically employ marker studies and in vitro work as an initial step, here we will focus on transcutaneous flux studies, in vivo nonclinical biologic effects and clinical outcomes primarily to illustrate the design principles and caveats in practice.

Ülo Langel (ed.), *Cell-Penetrating Peptides: Methods and Protocols*, Methods in Molecular Biology, vol. 1324,
DOI 10.1007/978-1-4939-2806-4_27,

1.1 Clinical Use and Characteristics of Botulinum Toxin

Revance Therapeutics, Inc. (Revance) is developing a topical product, RT001 (Botulinum Toxin Type A Topical Gel), an investigational drug containing the 150 kDa portion of Botulinum Toxin Type A (BoNTA) as the active moiety, for the treatment of moderate to severe lateral canthal lines (crow's feet wrinkles) and severe primary axillary hyperhidrosis. Injectable BoNTA has been successfully used in a range of medical disorders including strabismus, blepharospasm, focal dystonias, spasticity associated with juvenile cerebral palsy and adult stroke, and various cosmetic treatments [1–5]. Thus, the safety and effectiveness of BoNTA for treating these conditions has been well established for over 20 years.

Aesthetic medicine has been inundated with treatments for facial rhytids. BoNTA is the only Food and Drug Administration (FDA) approved treatment to temporarily relax the underlying facial muscle that wrinkles the skin resulting in hyperfunctional rhytids. Since 1992, botulinum toxin has been used to treat a variety of cosmetic conditions and medical indications. Following Carruthers' first description of treatment of glabellar rhytids ("frown line" wrinkles), botulinum toxins have revolutionized the practice of noninvasive aesthetic medicine [6]. In 2002, the US FDA approved the use of BOTOX® Cosmetic (Botulinum Toxin Type A Purified Toxin Complex; Allergan, Inc.) for the treatment of moderate-to-severe glabellar rhytids, associated with corrugator and/or procerus muscle activity in adult patients 65 years of age and younger. Patient satisfaction is above 80 % and BoNTA is considered to be effective and safe [7]. By 2005, BOTOX® Cosmetic injections were the most common noninvasive physician-administered cosmetic procedure with more than 3.2 million injections administered [8]. In addition, botulinum toxin was initially shown to be effective in reducing sweat production in healthy volunteers [9, 10] and subsequently for the treatment of primary axillary hyperhidrosis, excessive underarm sweating [11–13].

Lateral canthal lines (LCLs), commonly termed crow's feet, result from muscle activity in combination with photoaging. BoNTA has demonstrated safety and excellent efficacy in treatment of LCL via injection [14–16]. Limitations of injections, including those with BoNTA, include pain, erythema, swelling, needle marks, tenderness, and potential infection from needle use. The patient's medical regimen is potentially impacted by being advised to avoid aspirin, nonsteroidal anti-inflammatory drugs, and vitamin E prior to injection to reduce the risk of bleeding and bruising. Bruising is of particular concern in the crow's feet/lateral canthus/orbicularis oculi region, where the blood vessels are superficial and the skin is thin. Treatments for primary axillary hyperhidrosis typically require 10–15 injections per treatment area [17], thus injection site pain is a major concern for treatment of this condition.

All types of botulinum toxin block cholinergic neurotransmission by preventing acetylcholine (ACh) release at peripheral

neuromuscular junctions [4]. Botulinum toxin type A is produced by *Clostridium botulinum* (serotype A-Hall strain) as a single inactive polypeptide chain of 150 kDa, which subsequently undergoes proteolytic cleavage by proteases present in the fermentation culture to yield the fully active di-chain molecule comprised of a 100 kDa heavy chain and a 50 kDa light chain linked via both noncovalent interactions and a disulfide bond [18]. The heavy chain plays a role in cell binding, internalization, and translocation of botulinum toxin into nerve cells, while the light chain acts as a site-specific metalloprotease. Botulinum toxin acts on cholinergic nerve terminals of eccrine gland secretion and involuntary smooth muscle as well as striated muscle but does not appear to act on cardiac muscle. The ACh vesicles in target neurons are associated with a protein aggregate called the SNARE complex (soluble *N*-ethylmaleimide-sensitive fusion attachment protein receptor). In order to affect signal transmission across the neuromuscular junction, vesicles of ACh in the presynaptic neural bouton must be released into the synaptic cleft. In the case of striated muscle, the neurotransmitter binds to specific receptors on the muscle plate that trigger opening of sodium ion channels, resulting in depolarization and contraction in the adjacent striated muscle. This ACh release requires the participation of the SNARE proteins that mediate the fusion of synaptic vesicles with the neuronal plasma membrane [19]. It is generally accepted that the SNARE proteins form the core of the machinery for the intracellular membrane fusion necessary for ACh exocytosis. The SNARE complex consists of at least five proteins that play differing roles in the exocytosis process. For example, VAMP (vesicle associated membrane protein), also known as synaptobrevin, is associated with the synaptic vesicles, whereas SNAP-25 becomes associated with the synaptic membrane. Under the influence of an action potential in the neuron, calcium channels open and calcium binds to the SNARE proteins. This causes them to spontaneously assemble into a soluble ternary complex that moves to the neuronal plasma membrane where the SNARE complex enables the ACh vesicle to fuse with the cell membrane [20]. The fewer the number of vesicles released into the synaptic cleft, the lower the probability that an action potential will propagate and result in muscle fiber contraction. It is important to note that inhibition of ACh exocytosis by botulinum toxin is temporary and neurotransmission is eventually restored.

The RTT150 form of purified toxin (150 kDa) is different from the form of the toxin complex which is currently marketed as BOTOX® and BOTOX® Cosmetic (consisting of a 900 kDa complex comprised of the 150 kDa toxin with several bacterially derived accessory proteins). Unlike either marketed product [17], the RTT150 drug product is not formulated in human serum albumin, hemagglutinin, or other pooled human or animal derived components. The structure of RTT150 is important in development of a

CPP-based therapeutic, since any interference with selectivity, binding, or steps to generate a functional domain may render the product unusable. As a result, an ionic, rather than covalent, approach was taken. Essentially, a nonnative complex is self-assembled using a PTD-containing peptide and the RTT150 core. A similar approach can be taken using the larger 900 kDa complex as a core or variations thereupon, though the larger size and other physical characteristics render the self-assembled nonnative particle quite different in pharmacokinetics and pharmacodynamics.

2 RT001

The active pharmaceutical ingredient in RT001 is a purified 150 kDa BoNTA, derived from the Hall strain *Clostridium botulinum* supplied as lyophilized drug product referred to as RTT150. RT001 is composed of purified RTT150, formulated in a poloxamer gel containing a CPP-based permeation-enhancing peptide excipient, RTP004. The peptide excipient in this product ionically self-assembles with and enables the transcutaneous delivery of the toxin as detailed below. RTP004 is a single, straight-chain, synthetic peptide consisting of 35 L-amino acids. The theoretical molecular weight of RTP004 peptide is 4698 Da. The complete chemical sequence is:

Arg-Lys-Lys-Arg-Arg-Gln-Arg-Arg-Arg-Gly-**Lys-Lys-Lys-Lys-Lys-Lys-Lys-Lys-Lys-Lys-Lys-Lys-Lys-Lys-Lys**-Gly-*Arg-Lys-Lys-Arg-Arg-Gln-Arg-Arg-Arg*

As will be apparent from this sequence, RTP004 contains two distinct types of domains. The first type of domain, which is the core of RTP004, is a sequence of 15 consecutive lysines, each of which confers a full positive charge to the peptide [21]. The purpose of this charged domain is to form a noncovalent electrostatic interaction with anionic surface domains of the RTT150 (Botulinum Toxin Type A) protein.

Like most biologically active proteins, RTT150 is negatively charged to preserve its tertiary structure in aqueous environments and confer specificity of interactions in vivo. The positively charged core of RTP004 forms a noncovalent bond with the RTT150 molecule to form RT001, the proprietary Revance topical compound (Fig. 1). The selection of the length of the cationic core is a crucial design consideration and will be explored further in this chapter. The second type of domain in RTP004 is a Protein Transduction Domain (PTD) which is responsible for enabling transcutaneous flux of the peptide. The PTD employed in RTP004 is derived from residues 49–57 of the transactivator of transcription (TAT) protein. The rationale and empirical data supporting selection of this PTD for this application will be examined in detail.

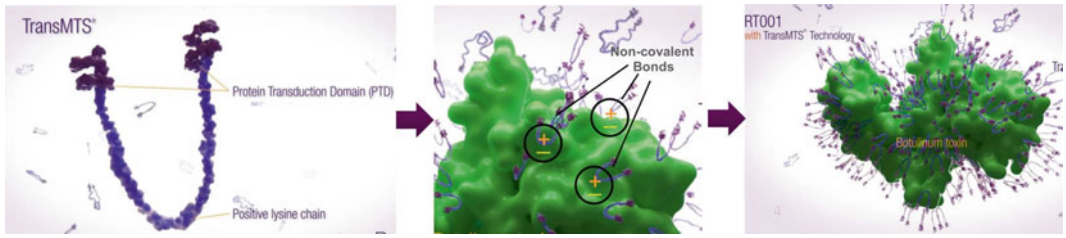

Fig. 1 RT001, an investigational drug. The positively charged core of RTP004 forms a noncovalent bond to associated CPPs with the RTT150 molecule to form RT001

2.1 Design Considerations Relating to the Cationic Core

To self-assemble a particle containing both a therapeutic active like botulinum toxin and a CPP-containing carrier, some form of noncovalent bond must be employed. For biologically active proteins, which often have a conserved motif of high densities of negatively charged amino acids on their surface, ionic bonding is particularly facile. With an ionic interaction holding the CPP to its payload, the strength of the ionic interaction is a first determinant of the assembled particle's characteristics. For a given CPP and payload, varying the number of positive charges on the CPP-based carrier was found to change the probabilistic depth of penetration. Longer runs of cationic amino acids flanking the CPP for example tended to provide deeper release of markers or payloads. Our initial work focused on in vitro and tagged in vivo studies as proxies. Based on those initial findings, an in vivo system reading penetration of functional botulinum toxin was developed to confirm the conclusions.

In order to confirm the impact of cationic core length on transcutaneous delivery of botulinum toxin, several peptidyl carriers were constructed. After screening several combinations of these in marker experiments a functional model of in vivo toxin function was employed after topical delivery. Polycations of varying lengths were conjugated to PTDs covalently (e.g., R9) and compared to controls of either polycation without PTD or toxin alone. For this experiment, a commercially available 900 kDa botulinum toxin complex (BOTOX®, Allergan, Inc., Irvine, CA) was employed as the active payload. BOTOX® was reconstituted according to the manufacturer's instructions. In each case, an excess of polycation was employed to assemble a final complex that has an excess of positive charge. Optimal ratios were selected based on pilot experiments (data not presented). BOTOX® dose was standardized across all groups as was total volume and final pH of the composition to be applied topically. Samples were prepared as detailed in Table 1.

All animal use was performed under IRB-approved protocols in compliance with all applicable laws and usage standards including NIH and institutional guidelines (Covance, Inc., Berkeley, CA). As with all our laboratories work, all observers were blinded

Table 1
Description of the prepared samples

Group	PTD	MW polycation	Toxin dose
K125PTD	Yes	125,000	2 U
K30PTD	Yes	30,000	2 U
K125	None	125,000	2 U
Control	None	None	2 U

Table 2
Digital abduction scores 30 min after single-time topical application of BOTOX® with the poly-L-lysine of MW 125,000 or 30,000 conjugated to a PTD (K125R or K30R respectively), BOTOX® with a control polycation K (K125) or Controls (BOTOX® alone and untreated)

Group	Mean	Std. Error
K125R	3.333	0.333
K30R	0.500	0.100
K125	0.333	0.333
Control	0.397	0.150

$P = 0.0351$ (Significant at 95 %)

to treatment group identities. Animals were anesthetized via inhalation of isoflurane during application of treatments. After being anesthetized, C57 black 6 mice ($N = 4$ per group) underwent topical application of metered 400 μL dose of the appropriate treatment applied uniformly from the toes to the mid-thigh. Both limbs were treated, and treatments were randomized to either side. Mice were evaluated for digital abduction capability according to published digital abduction scores for foot mobility after BOTOX® administration [22]. Mouse mobility was also subjectively assessed. Digital abduction scores (DAS) were tabulated independently by two blinded observers. Mean and standard error were subsequently determined for each group with analysis of significance at 95 % confidence in one way ANOVA repeated measures using StatView® software (Abacus Concepts, Inc., Berkeley, CA). Mean digital abduction scores after single-time topical administration are presented in Table 2. The Revance peptidyl carrier KNR affords statistically significant functional delivery of BOTOX® across skin relative to both controls, which were comparable to one another. Additional independent repetitions (total of three independent experiments all with identical conclusions in statistically significant paralysis from topical BOTOX® with KNR but not controls) of the

present experiment confirmed the present findings and revealed no significant differences between topical BOTOX® with or without K (i.e., both controls). Interestingly, mice consistently ambulate toward a paralyzed limb.

Since the relatively targets presented by cosmetic applications and hyperhidrosis are quite superficial, the refinement of the cationic core in design of RTP004 was biased toward more superficial delivery. Shorter cationic cores were thus chosen over the long ones employed by our group in other applications. Given the elective, non-life-threatening nature of these conditions, a superficial and hence safer delivery system was essentially required for viability.

The primary design bias was thus for safety above efficiency for the intended clinical applications of RT001. As a result, a degradable sequence was required. L-amino acids were thus employed for the sequence. Consistent with the density of dibasic L-amino acid sequences in the core, it was expected that the sequence would be trypsin- and serum-degradable. These effects were confirmed both in gel electrophoresis and HPLC with both time-course and dosing studies. A sequence that can be safely degraded by tissue trypsin activity or serum was selected for RTP004.

3 Confirmation of Intended Characteristics When RTP004 CPP-Containing Peptide Excipient Is Combined with Botulinum Toxin

RTP004 can be tuned to carry payloads to different depths of penetration based on the length of the peptide; the longer the peptide, the deeper the penetration. In the case of RT001, the RTP004 peptide is specifically formulated to deliver the toxin to a relatively superficial target in the mid-dermis as is necessary to treat lateral canthal lines or hyperhidrosis. The bias in development of this peptide was safety over efficiency, Pharmacology studies have focused on the transcutaneous flux of RTT150 mediated by the RTP004 peptide in vitro (using labeled RTT150) and in vivo using the murine DAS assay as well as murine muscle force testing. Additional studies underway include the effort to characterize the kinetics and degree of denervation and renervation upon repeat dosing of animals with RT001. It is intended that these studies will aid in the design and dosing frequency of longer term toxicity studies.

3.1 Transdermal Flux of Biotinylated-RTT150 with and Without RTP004 (RT001-RD004)

The purpose of this study was to examine transcutaneous flux patterns of RTT150 alone or mixed with RTP004 using a Franz Chamber. RTT150 (0.05 μg/in-line cell) was biotinylated and evaluated against biotinylated RTT150 (0.05 μg/in-line cell) mixed with RTP004 (0.055 μg). Freshly dermatomed living porcine skin was loaded into in-line cells, and 200 μL of the test article mixtures was added to each cell (N=4). The Franz Chamber was run for 4 h, with a shuttle change once per hour. Enzyme-linked

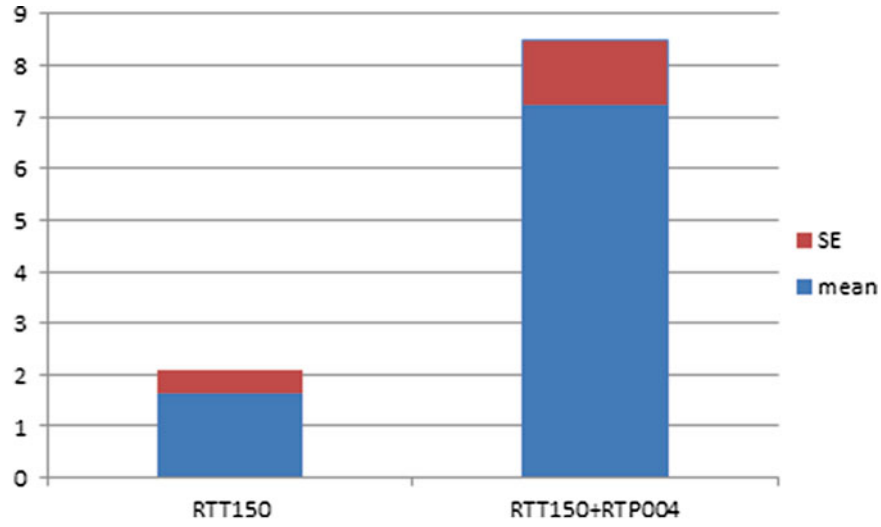

Fig. 2 ELISA transdermal flux measurements. Toxin delivery was measured by percentage of applied biotin-tag appearing in the flow through. Similar results were obtained in an identical repetition

immunosorbent assay (ELISA) analysis was performed on the resulting flow through samples. Toxin delivery was measured by percentage of applied load appearing in the flow through. The combination of RTT150 with RTP004 exhibited a statistically significant increase in the amount of fluxed RTT150 in the flow through as compared to RTT150 alone as shown in Fig. 2, suggesting that approximately 8–9 % of the dose applied to skin is able to cross into cell receptor fluid. Some toxin flux was noted in the absence of RTP004; however, this is attributed to the background signal of the assay.

3.2 Transdermal Flux of RT001

The purpose of this study was to examine transcutaneous flux patterns of RT001 using a Franz Chamber. Prior experiments (Subheading 3.2.1) relied on using biotin-tagged BoNTA; this type of experiment allows for facile detection but can lead to higher background levels and overestimation of degree of flux. As a result, a method for measuring untagged BoNTA directly was developed. Freshly dermatomed living porcine skin was loaded into in-line cells, and 190 μL of the test article mixtures was added to each cell ($N = 10$ cells per test article). RT001 was applied to in-line cells at a dose of (approximately 4 ng). In-line cells with RTD006 reconstituted in RTD800 served as controls. The Franz Chamber was run for 6 h, with a shuttle change once per hour.

Alpha-LISA using antibodies to BoNTA was performed on the resulting flow through samples to quantitate the amount of toxin present. Toxin flux was expressed as a percentage of applied load appearing in the flow through. Results obtained in repeat experiments with independent analysts yielded transcutaneous flux measurements of approximately 3–6 % of the applied dose during the 6 h time period as depicted in Fig. 3 for one such experiment.

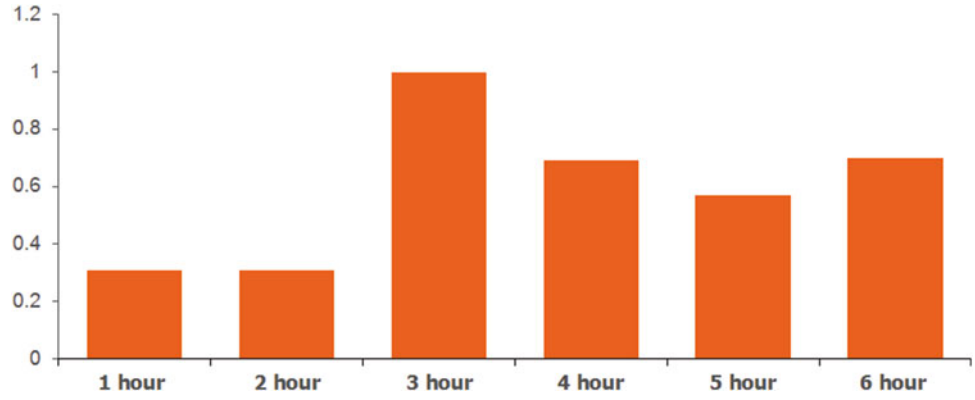

Fig. 3 Alpha-LISA transcutaneous flux measurements. Toxin flux was expressed as a percentage of applied RTT150 load appearing in the flow through. Control is not detectable at any time point

3.3 Design Considerations in Selection of the Delivery Vehicle for the CPP- BoNTA

3.3.1 Interaction Between the CPP and the Payload

As may seem obvious, the CPP-based carrier must associate with the payload in order for the CPP to enable delivery of the payload. The practical implications may be a bit subtler however. In the case of an ionic association, one must not only consider the total energy of interaction (i.e., length in this example), but also the relative p*K*a of each component of the formulation versus that of the payload. If other tighter-binding components are present, the binding of the payload can be reduced and transcutaneous flux diminished or abolished. A simple system can illustrate the point effectively. RTP004 was synthesized and ion paired with chloride (anion of hydrochloric acid, p*K*a –7), trifluoroacetate (anion of trifluoroacetic acid, p*K*a –0.3), and acetate (anion of acetic acid, p*K*a 4.7). The stronger the corresponding acid, the easier it will be to displace the counter anion of the weaker acid. As an illustration, each of these RTP004 salts was combined with a simple anion, salicylate (anion of salicylic acid, p*K*a 3.0), and compared with one another versus salicylate alone in transcutaneous flux across porcine skin as before, then analyzed for salicylic acid concentration via HRMS in the receptor flow through. The results are presented as Fig. 4.

Consistent with the predicted binding affinity to RTP004, chloride allows complete pairing of CPP-based carrier and payload. This pairing results full CPP-based delivery of payload resulting in a transcutaneous flux rate that is 90-fold higher than salicylate alone. In contrast, the tighter binding TFA was harder to displace with salicylate so only afforded an 18-fold increase of salicylate alone. Finally, acetate which would be predicted to bind better to RTP004 than salicylate does, exhibited the same rate of flux as salicylate alone—presumably because nearly all salicylate was unbound. Formulation components and buffers that can potentially interfere with self-assembly of the CPP to the payload thus must be avoided.

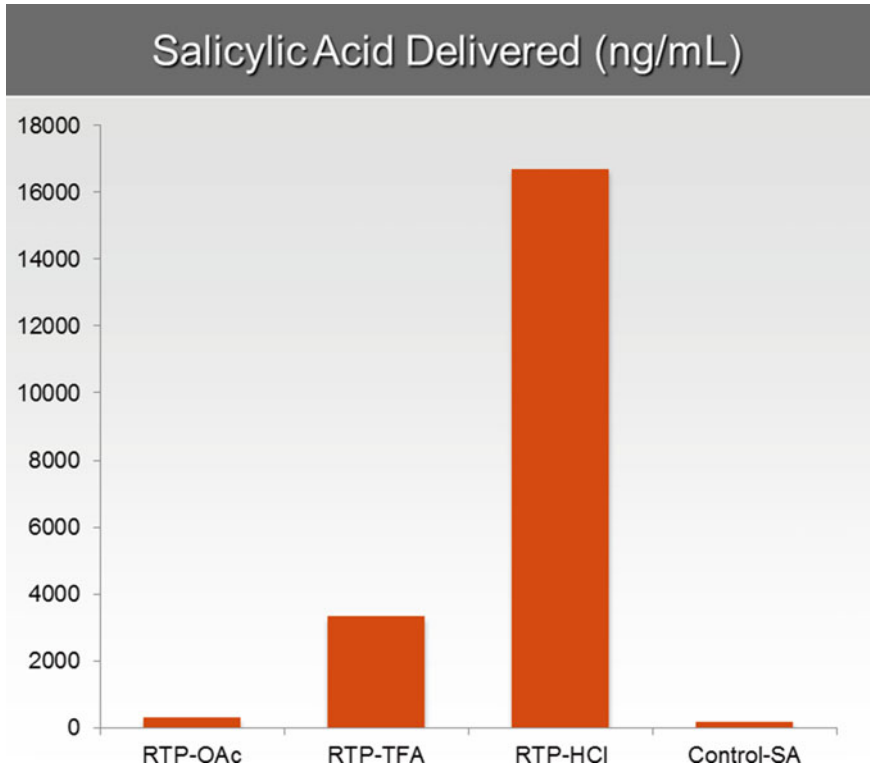

Fig. 4 Transcutaneous flux measurements of salicylate with varying counter-ions

3.3.2 Interaction Between the CPP and the Biologic Interface (Receptor Binding)

Formulation components can also interfere with the ability of the CPP to bind to either the cell surface or to stratum corneum. Although it is harder to predict a priori than those that interfere with the binding of CPP to payload, the impact of these agents can be confirmed empirically in model systems. Such a confirmation can become critically important as discussed below, and limitations of the model system must be considered as well. One example of such an agent is the antioxidant beta hydroxyl toluene (BHT) which is used in a wide variety of finished products and individual ingredients. Although it is relatively innocuous in many applications, BHT has been shown to exert a number of effects beyond those of a simple antioxidant. For example BHT alters the chemical composition of the stratum corneum without physical structural changes [23] and BHT can alter cellular lipid charge states which may impact binding of CPP carriers [24]. BHT also induces ornithine decarboxylase, and peroxides of BHT generate reactive electrophile species in the presence of keratinocytes [25]. BHT has been shown to directly alter flux of some compounds across skin [26] One or more of these effects may underlie the empirical evidence that BHT can interfere with binding and transcutaneous delivery of RT001. After addition on 0.01 % BHT to the diluent

Table 3
Percent change in transcutaneous flux after addition of BHT

	0.01 % BHT	0.03 % BHT
% of base flux	+21 %	−52 %

Flux of formulations of RT001 with 0.01 or 0.03 % was normalized to rates of flux for the base formulation for RT001 without BHT. Repetition exhibited similar patterns

for RT001, the transcutaneous flux assay was performed as above. There was no detectable decrease of flux across porcine skin in this model, so the revised product was employed clinically. All efficacy disappeared with RT001 after the change—across all time-points, endpoints, scales, and centers. The lack of a predictive indication in the transcutaneous flux assay was thus concerning. The assay was repeated at both 0.03 % BHT and 0.01 % BHT levels. The data is presented in Table 3.

Here, a dose-dependent decrease in transcutaneous flux was observed with 0.03 % BHT. Given that the literature shows that BHT can alter flux and the data that BHT does alter flux of RT001 in a dose-dependent way, the discrepancy between the porcine data and the clinical data in the threshold for BHT concentration was considered. In this model, a hair-bearing, viable porcine graft is used to model flux. While this approach models many clinical applications well, it truly only models skin with both follicle-mediated and direct flux across stratum corneum. For skin like LCL which lacks significant follicle-mediated transport, the limitations of a model with both follicle-mediated and cornified skin must be considered. Each pathway can, not surprisingly exhibit its own dose dependence so a model with both can prove misleading when used to predict a system with only one pathway. Nonetheless, the potential for BHT to chemically alter flux RT001 was confirmed clinically and in vitro. Fortunately, reversion to a diluent without BHT restored clinical efficacy. Potential impact of even generally innocuous formulation components should be carefully considered over a range of skin types and doses in vitro prior to use with a CPP-mediated transport system such as RT001.

4 Clinical Experience

Revance is developing a topical drug product, RT001 (Botulinum Toxin Type A Topical Gel) for the treatment of moderate to severe LCLs and severe primary axillary hyperhidrosis. The anticipated clinical benefits are the temporary improvement in the appearance of LCLs and a temporary reduction in sweating. The safety and efficacy of RT001 have been assessed in 18 clinical studies to date (14 studies in LCLs, two in hyperhidrosis, and one each in seasonal

allergies and migraine prophylaxis). Doses up to 25 ng/mL botulinum toxin with 50 ng total exposure have been studied with no significant safety issues.

4.1 RT001 for the Treatment of Lateral Canthal Lines: US Phase 1 Safety and Tolerability Study (RT001-CL004CF)

The objectives of the study were to evaluate the potential for irritation and sensitization, the topical and systemic safety of RT001, and the systemic immunogenicity of RT001. Each subject received both test articles, RT001 300 U (study drug) and RTD800 (placebo diluent) on the forearms; subjects were randomized as to which forearm received RT001 and which received RTD800. The study was conducted in three phases. During the Induction Phase (Days 0–28), treatments were applied to defined areas of the forearms on Days 0, 14, and 28. During the Rest Phase (Days 29–41), no treatments were applied. During the Challenge Phase (Days 42–56), the fourth and final treatment was applied on Day 42. Skin sensitization evaluations were performed on Days 2, 16, 30, 44, 45 (if required), and 56 (End of Study). All treatments were applied for 30 min with Tegaderm occlusion. Safety evaluations included skin irritation and sensitization evaluations, Clinical Signs/Symptoms Descriptors, AEs, clinical laboratory tests, ECG, serum BoNTA antibodies, and muscle grip strength. In addition to the per protocol laboratory tests, serum RTP004 antibodies were measured.

Overall, no study pause criteria were met and no SAEs were reported. There were only two transient, definitely related adverse events (papular rash and pruritus) experienced by one subject that were moderate in severity and resolved within 24 h, and two possibly related episodes of mild joint pain (occurring 2 weeks apart) each resolving within 24 h. There was no evidence to suggest any trend for skin sensitivity and neither test article caused cumulative irritation. In addition, there were no test article effects on muscle grip strength, prothrombin time, or ECG results. Finally, there were no systemic or local clinically significant abnormalities or findings, and no subject had positive BoNTA antibody results at any time or developed antibodies reacting with RTP004.

This Phase 1 study helped establish that a novel and potent CPP-containing peptide like RTP004 can be used safely and with low irritancy and sensitization potential. This study thus represents an early validation of design considerations at least in application to less sensitive skin and coarser musculature.

4.2 Phase 2 Study of RT001 with Various Concentrations of RTP004 for Lateral Canthal Lines (RT001-CL003CF)

The objective of this study was to evaluate the need for the CPP-containing peptide for transcutaneous delivery and evaluate safety of RT001 on sensitive target areas. A total of 77 subjects with moderate to severe LCLs were enrolled in two cohorts and randomized to receive RT001 300 U combined with RTD005 diluent concentrations of 0.5, 2.0, or 4.5 μg/0.5 mL, or RTD800 placebo control (Cohort 1) and RT001 300 U combined with RTD005 diluent concentrations of 6.0, 7.5, or 10.5 μg/0.5 mL,

or RTD800 placebo control (Cohort 2). Treatments were applied for 30 min to each lateral canthal area (LCA) with Tegaderm occlusion. Assessments included the Investigator Assessment Rating of Crow's Feet Facial Line Severity at maximum smile and at rest. Success was defined as a 1-point or greater improvement from Baseline. Safety assessments included AEs, skin irritation and sensitization, eye irritation, clinical laboratory tests, and evaluation of cranial nerves II–VII.

A total of 49 subjects (63.6 %) had one or more AEs considered related to study treatment (Cohort 1, 73.0 %, Cohort 2, 55.0 %). All related AEs were mild or moderate in severity. The most common related AEs were nervous system disorders (32.5 %; mostly involuntary muscle contraction); general disorders and administration site conditions (26.0 %; mostly erythema [23.3 %]); skin and tissue disorders (16.2 %; erythema, pain, and burning sensation); and eye disorders (13.0 %; typically eye irritation, eye pain, or foreign body sensation). The most common systemic reaction was headache (2.6 %). Most events of skin erythema were minimal. There were no notable changes in clinical laboratory variables and no subject had any abnormality in the Regional House–Brackmann System for cranial nerve VII. All changes were unrelated to test article.

For the active treatment groups, a 1-point or 2-point improvement was observed for a majority of LCAs at rest and a 1-point improvement was observed for a majority of LCAs at maximum smile. Compared to the placebo group, the response rate was significantly higher in the RT001 7.5 μg/0.5 mL group for 2-point improvement at rest and 1-point improvement at maximum smile, and in the RT001 6.0 μg/0.5 mL group for 1-point improvement at maximum smile. As illustrated in Fig. 5, this study established that not only was RTP004 required for function but it must be present in a target concentration threshold to achieve a desired effect with a given dose of a payload. This finding is consistent with the nonclinical data to date and external reality-macromolecules do

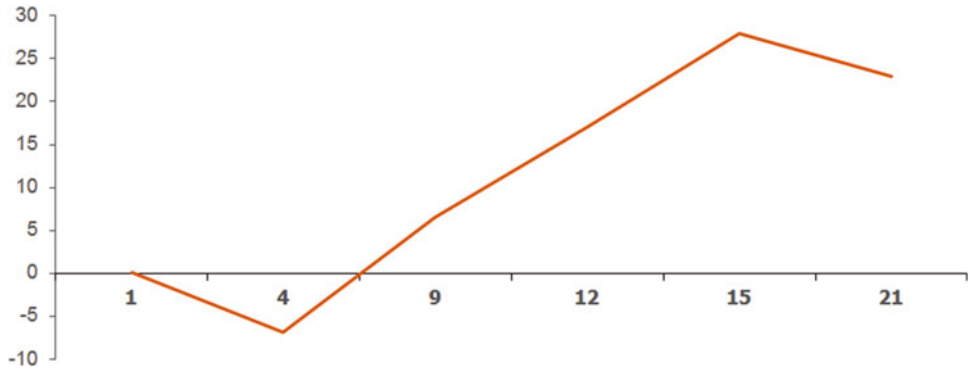

Fig. 5 US Phase 2 RT001-CL003CF results. RTP004 must be present at a threshold level or above in order to deliver functional toxin across skin

not readily cross skin. A CPP-containing peptide can enable topical delivery of a therapeutic amount of a macromolecule, however as shown here. That a threshold concentration of RTP004 appears necessary marks an interesting finding in this work as well. Here as in the Phase 1 study on less sensitive target areas, RT001 demonstrates a remarkable safety profile, particularly considering the powerful CPP employed in conjunction with the most potent toxin known to man. These results represent a validation of the previously discussed safety-biased design considerations for RTP004 even in application to fine musculature and sensitive skin around the eye.

4.3 Overview of the Safety Profile of RT001 Topical Gel

Overall, there were no significant differences in the incidence of any treatment-related AEs between the RT001 and control groups, or with escalation of RT001 dose. RT001 and individual components (RTT150 toxin and RTP004 peptide used as controls) were well tolerated.

A total of 1483 subjects have participated in the 14 studies for LCL treatment. A total of 1031 subjects have received RT001 at doses of 1.1–25 ng/mL (up to 1 mL per subject) of toxin (equivalent to 200–6250 U per subject) with cumulative exposures up to 50 ng, and peptide exposures up to 30 μg/mL per subject. Fifty four (54) subjects have received peptide diluent (RTD005 or RTD006) as control, 62 subjects have received BoNTA alone (RTT150) as control, and 336 subjects have received placebo diluent (RTD800) as control. In Study RT001-CL025LCL, a repeat dose at 28 days of 25 ng/mL RT001 in 40 subjects was well tolerated relative to controls and single dose administration of 25 ng/mL in other studies. In study RT001-CL004CF, 41 subjects received both RT001 (on one forearm) and RTD800 (on the opposite forearm) as control. These 41 subjects are included in the RT001 population (only) for the purposes of this summary of clinical safety. All subjects who were enrolled in a study and received at least one bilateral application of study treatment are included in this safety analyses.

Across the LCL clinical program, there have been: (1) No SAEs related to any study treatment; No subject discontinued a study due to an AE, (2) No systemic safety concerns or evidence of any systemic exposure based on clinical laboratory results (hematology, urinalysis, chemistry), serum antibodies for BoNTA and peptide RTP004, and ECGs, (3) No significant observations or evidence of regional spread of toxin based on assessments of cranial nerves II–VII and local muscle strength evaluations, including assessments of pupillary reaction to light, extraocular movements, local muscle strength and facial nerves, (4) No dermal or ocular safety concerns; skin or ocular irritation events were few, transient, and generally mild in severity, and are similar in frequency and severity to those observed in controls. Of note, these events

occurred at a decreased rate in later studies which encompassed the specific procedures, formulations, and the dose to be employed in future studies, and (5) No safety concerns with a repeat administration of RT001 at 2 week (RT001-CL011LCL) or 4 week intervals (RT001-CL015LCL and RT001-CL025LCL).

Across all 14 studies (1483 total subjects: 1031 RT001 subjects and 452 control subjects), there were 526 treatment-emergent AEs among 163 RT001-treated subjects and 202 treatment-emergent AEs 82 among control subjects. There were no withdrawals due to adverse events. There were no related serious adverse events (SAEs), and no deaths. Three SAE were unrelated to study treatment. Treatment-emergent AEs were generally mild and transient and occurred in RT001 subjects at rates similar to controls except where noted for brow elevation and ocular events that are related to the direct effects of RT001 on its target muscle, the orbicularis oculi. Overall, there was no increase in the frequency, severity or duration of adverse events observed with an increase in RT001 dose.

4.4 Investigator-Initiated Study of Botulinum Toxin Type A with Revance Diluent for Primary Axillary Hyperhidrosis

An investigator-initiated pilot study in primary axillary hyperhidrosis was conducted at a single center in the US using commercially available BOTOX® and the Revance peptide diluent [27]. Twelve adult subjects with a gravimetric measurement of sweat production of at least 50 mg over 5 min were enrolled. Each subject served as his or her own control with blinded, randomized assignment of each axilla to a treatment group. Study treatments were mixed with Cetaphil® cream, applied to the axillae, and remained in place for 60 min. Subjects returned for a follow-up evaluation at 4 weeks after treatment.

The mean reduction in sweat production at 4 weeks post-treatment was 65.3 % for BOTOX® treated axillae compared with a 25.3 % for the control axillae ($P < 0.05$). The ratio of mean sweat production for the BOTOX®-treated axillae relative to the control axillae was 1.3 at baseline and 0.8 at 4 weeks post-treatment. The results from the Minor's iodine starch test to visualize sweating were consistent with the gravimetric results. No systemic AEs were reported. Four local AEs were reported, all of which occurred in the control axillae. The AEs were folliculitus, tenderness, erythema, and eczema (2 cm inferior to the axilla on the lateral trunk). The results of this study indicate that topically applied BoNTA appears to be safe and may prove to be effective for the treatment of axillary hyperhidrosis.

Perhaps more importantly from a CPP perspective, safety and efficacy of this CPP-based peptide are not specific to facial skin and apply to skin with high density of hair follicles and sweat glands. Delivery in this environment is particularly noteworthy given high levels of skin hydration and the physical barriers presented by hyperhidrosis.

4.5 US Phase 2 Studies of RT001 with Escalating Doses of RT001 for Lateral Canthal Lines (RT001-CL006LCL, RT001-CL010LCL, and RT001-CL015LCL)

The objective of these studies was to evaluate the safety and efficacy of escalating toxin doses in RT001 in management of LCLs. Across three separate Phase 2 studies, three hundred six (306) adult subjects with moderate to severe LCLs were randomized to receive control diluent ($N=104$) or RT001 at the following doses of toxin (U) with 9.0 μg/mL RTP004: 3.3 ng/mL ($N=26$) or 5.5 ng/mL U ($N=22$); 11 ng/mL ($N=72$) or 22 ng/ml U ($N=82$). The studies were conducted at multiple sites in the US. Subjects received a single 30-min treatment of 0.5 mL with Saran Wrap occlusion to each LCA. Follow-up evaluations were conducted at Days 14 and 28 for all subjects and 7, 21, 60, and 90 in some studies. These evaluations included AEs, clinical laboratory tests, ECG, skin and ocular irritation evaluations, evaluation of cranial nerves II–VII, and Investigator Global Assessment (IGA)-LCL-Rest and IGA-LCL-Smile Severity Scales. Adverse events were typically mild, transient and local. The more common related events were administration site conditions and nervous system events. The nervous system events were burning sensation, facial paresis (two subjects in control), and headache. All events of skin or ocular irritation were mild. There were no clinically significant laboratory or ECG results. Complete detailed analysis of the AEs in this study is not currently available.

The primary efficacy endpoint for each of these studies was a 2-point improvement at rest in the IGA-LCL-Rest Scale. Preliminary results by dose group are presented as Fig. 6. Not only was statistically significant efficacy achieved, but also a dose

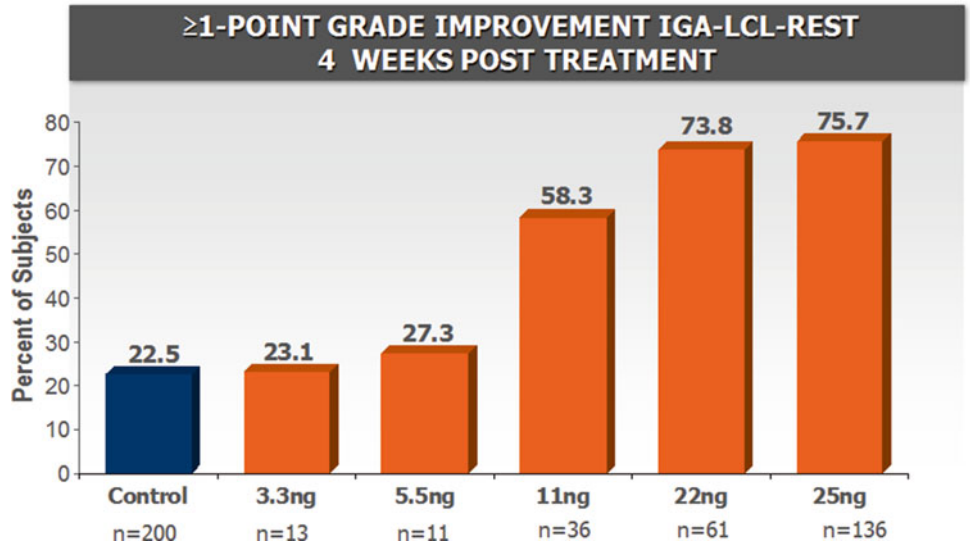

Fig. 6 US Phase 2 RT001-CL006LCL, RT001-CL010LCL, RT001-CL015LCL, and CL024. Preliminary results by dose group. Efficacy was defined as a 1-point bilateral improvement in the investigator crow's feet severity score (IGA-LCL) 28 days after single-time administration

response allowing dosage selection was observed. Duration data (not presented) demonstrates comparability to toxin results when injected and further supports dosage selection. Here as in prior phase 1 and 2 studies, RT001 demonstrates a remarkable safety profile, particularly considering the powerful CPP employed in conjunction with escalating doses of the most potent toxin known to man. Thus the design considerations for the CPP-based peptide excipient have been validated with escalation of active dose to therapeutic effect in application to the fine musculature and sensitive skin around the eye. Clinical validation of noncovalent PTD-based delivery of an active therapeutic across skin for a therapeutic benefit has thus been demonstrated here.

4.6 US Phase 2b Studies Demonstrating the Necessity of the CPP to Achieve Clinical Effect and Confirming Efficacy and Safety Signals (RT001-CL017LCL and RT001—CL024LCL)

Based upon the identification of a dose which achieved efficacy comparable to that reported for injectable toxins and appropriate safety, two randomized, controlled, double-blind, multicenter confirmatory phase 2b studies were performed. The first, and probably most interesting from a CPP perspective was designed to address the relative contribution of and necessity for the CPP-based carrier in RT001 (RT001-CL017-LCL). Otherwise identical formulations were prepared for RT001, placebo, placebo plus toxin (no CPP), and placebo plus RTP004 CPP-based carrier (no toxin). The results are presented in Fig. 7 on the right panel. Safety results were similar across all groups. AEs were generally mild, localized

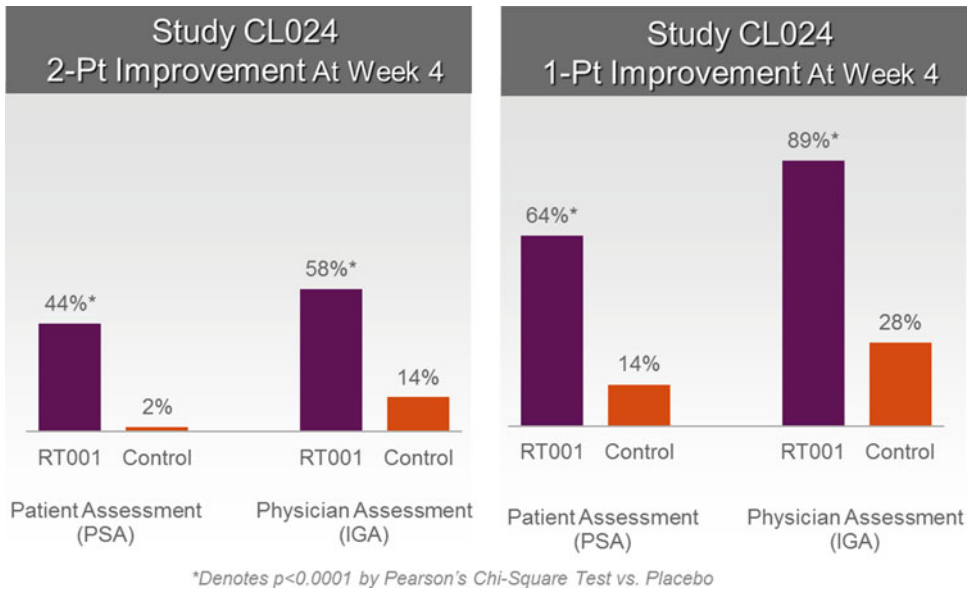

Fig. 7 US Phase 2b studies RT001-CL017LCL (*right*) and RT001-CL024LCL (*left*). Preliminary results by dose group. Primary efficacy was defined as a composite of both 2-point improvement in investigator assessment of crow's feet severity (IGA-LCL) Scale and the patient assessment of crow's feet severity (PSA) 28 days after single-time administration

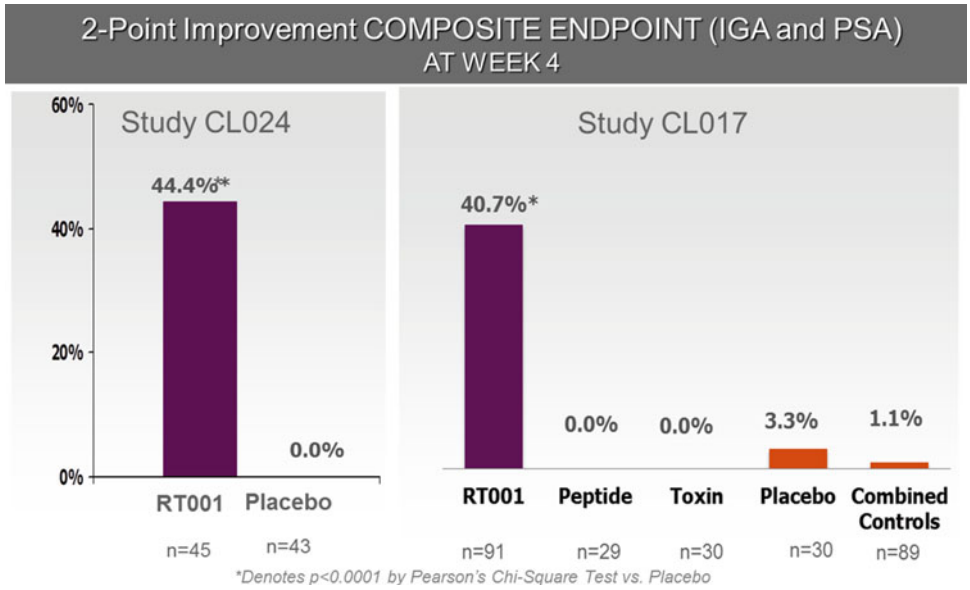

Fig. 8 US Phase 2b study ("mini phase 3 study") RT001-CL024LCL. Preliminary results of all efficacy endpoints by dose group

and transient. This study confirmed that the placebo, toxin alone, and carrier alone were all similar in efficacy and none achieved efficacy. Thus, 150 kDa botulinum toxin does not cross skin on its own—which is not surprising. RTP004 carrier does not paralyze muscle or improve wrinkles. However, when the two are combined to form RT001 at the same concentration levels, statistically significant efficacy is achieved on all endpoints versus each individual controls and versus all controls in aggregate. All endpoints were significant and exhibited the same pattern. This phase 2b study thus addresses the combination rule and confirms the requirement for the CPP in toxin-based transcutaneous delivery. An additional phase 2b study (RT001-CL024LCL) was conducted to support the power analysis for the phase 3 studies. The results are presented in Figs. 7 and 8. This study confirmed that RT001 at the phase 3 dose achieved all efficacy endpoints with an acceptable safety profile similar to prior studies. Response rates and AE rates were remarkably consistent between the two phase 2b studies. Thus, with the design considerations presented in this chapter, a CPP-based delivery of botulinum toxin has been achieved.

References

1. Scott AB (1981) Botulinum toxin injection of eye muscles to correct strabismus. Trauma Am Opthalmol Soc 79:734–770
2. Hallett M (1999) One man's poison-clinical applications of botulinum toxin. N Engl J Med 341:118–120
3. Spencer JM (2002) Botulinum toxin B. The new option in cosmetic injection. J Drugs Dermatol 1:17–22
4. Carruthers A, Carruthers J (2005) Botulinum toxin type A. J Am Acad Dermatol 53: 284–290

5. Carruthers J, Carruthers A (2007) The evolution of botulinum toxin type A for cosmetic applications. J Cosmet Laser Ther 9:186–192
6. Carruthers J, Carruthers A (1992) Treatment of glabellar frown lines with *C. botulinum-A* exotoxin. J Dermatol Surg Oncol 18:17–21
7. Carruthers J, Fagien S, Matarasso SL, BOTOX Consensus Group (2004) Consensus recommendations on the use of botulinum toxin type A in facial aesthetics. Plast Reconstr Surg 114:1S–22S
8. The American Society for Aesthetic Plastic Surgery, Cosmetic Surgery National Data Bank. 2006 statistics. www.surgery.org/download/2006stats.pdf. Accessed 30 March 2007.
9. Bushara KO, Park DM, Jones JC, Schutta HS (1996) Botulinum toxin-a possible new treatment for axillary hyperhidrosis. Clin Exp Dermatol 21:276–278
10. Schnider P, Binder M, Berger T, Auff E (1996) Botulinum A toxin injection in focal hyperhidrosis. Br J Dermatol 134:1160–1161
11. Naumann M, Hofmann U, Bergmann I, Hamm H, Tiyka KV, Reiners K (1998) Focal hyperhidrosis: effective treatment with intracutaneous botulinum toxin. Arch Dermatol 134:301–304
12. Heckmann M, Ceballos-Baumann AO, Plewig G (2001) Botulinum toxin A for axillary hyperhidrosis (excessive sweating). N Engl J Med 344:488–493
13. Naumann M, Lowe NJ (2001) Botulinum toxin type A in treatment of bilateral primary axillary hyperhidrosis: randomised, parallel group, double blind, placebo controlled trial. BMJ 323:596–599
14. Lowe NJ, Lask G, Yamauchi P, Moore D (2002) Bilateral, double-blind, randomized comparison of 3 doses of botulinum toxin type A and placebo in patients with crow's feet. J Am Acad Dermatol 47:834–840
15. Lowe NJ, Ascher B, Heckmann M, Kumar C, Fraczek S, Eadie N, BOTOX Facial Aesthetics Study Team (2005) Double-blind, randomized, placebo-controlled, dose-response study of the safety and efficacy of botulinum toxin type A in subjects with crow's feet. Dermatol Surg 31:257–262
16. Matarasso SL, Matarasso A (2001) Treatment guidelines for botulinum toxin type A for the periocular region and a report on partial upper lip ptosis following injections to the lateral canthal rhytids. Plast Reconstr Surg 108:208–214
17. Allergan, Inc. (2006) BOTOX cosmetic (botulinum toxin type A) prescribing information. Irvine, CA
18. Aoki KR, Guyer B (2001) Botulinum toxin type A and other botulinum toxin serotypes: a comparative review of biochemical and pharmacological actions. Eur J Neurol 8:21–29
19. Grumelli C, Verderio C, Pozzi D, Rossetto O, Montecucco C, Matteoli M (2005) Internalization and mechanism of action for clostridial toxins in neurons. Neurotoxicology 26:761–767
20. Dutton JJ, Fowler AM (2007) Botulinum toxin in ophthalmology. Surv Ophthalmol 52:13–31
21. Ford KG, Souberbielle BE, Darling D, Farzaneh F (2001) Protein transduction: an alternative to genetic intervention? Gene Ther 8:1–4
22. Aoki KR (2001) A comparison of the safety margins of botulinum toxin serotypes A, B, and F in mice. Toxicon 39:1815–1820
23. Koone MD, Black HS (1986) A mode of action for butylated hydroxytoluene-mediated photoprotection. J Invest Dermatol 87:343–347
24. Black HS (2002) Pro-oxidant and anti-oxidant mechanism(s) of BHT and beta-carotene in photocarcinogenesis. Front Biosci 7:d1044–d1055
25. Guyton KZ, Bhan P, Kuppusamy P, Zweier JL, Trush MA, Kensler TW (1991) Free radical-derived quinone methide mediates skin tumor promotion by butylated hydroxytoluene hydroperoxide: expanded role for electrophiles in multistage carcinogenesis. Proc Natl Acad Sci 88:946–950
26. Muhammad F, Brooks JD, Riviere JE (2004) Comparative mixture effects of JP-8(100) additives on the dermal absorption and disposition of jet fuel hydrocarbons in different membrane model systems. Toxicol Lett 150:351–365
27. Glogau RG (2007) Topically applied botulinum toxin type A for the treatment of primary axillary hyperhidrosis: results of a randomized, blinded, vehicle-controlled study. Dermatol Surg 33:S76–S80

Chapter 28

Applications of CPPs in Genome Modulation of Plants

Alicja Ziemienowicz, Jordan Pepper, and François Eudes

Abstract

Cell-penetrating peptides (CPPs) are a class of short peptides that are known to translocate inside living cells through the cell membrane. Many CPPs show an ability to bind and deliver macromolecular cargoes such as DNA, RNA and protein into living cells, making them excellent transfection and transduction agents with low cytotoxicity. While their use is well established in mammalian cell systems, they have also been explored in the last decade as transfection agents in plant cells. Their efficacy has been demonstrated in both monocot and dicot clades as well as a variety of tissues and cell cultures, from leaves to protoplasts. Factors affecting CPP and CPP–cargo uptake have been addressed with specific attention to the plant cell wall and classes of CPPs utilized in plant cell systems. It has been shown that internalization of most free peptides in plant cells has been dominated by direct translocation across the cell membrane, while CPP–macromolecular cargo complexes and conjugates were translocated via macropinocytosis. Moreover, functionalization of CPPs resulted in generation of peptides with specialized cargo delivery attributes, e.g., for specific subcellular targeting. Thus, the use of CPPs in plants presents a promising method for plant transgenesis as well as genome regulation and modification.

Key words Cell-penetrating peptides, Cell wall, Plant cells, Proteins, DNA, RNA, TAT, TAT_2, Transportan, *p*VEC, Exine, Microspore, Amphipathic

1 Introduction

The delivery and expression of exogenous genes in plant cells have been of particular interest for plant research and biotechnology [1]. Genetic transformation, or transgenesis, finds many applications in cell biology and gene function studies. It also allows for the generation of plants with improved agricultural traits. The arsenal of techniques for transgene delivery includes physical methods (electroporation, microinjection, bombardment), chemical methods (PEG-mediated DNA delivery), and biological methods (viral vectors and *Agrobacterium*-mediated DNA delivery). However, these methods have some limitations including low transformation efficiency, risk of gene damage, and limitation of transgene size, applicable plant species/tissues, random delivery and cytotoxicity [2]. Therefore, new gene delivery systems that are

Ülo Langel (ed.), *Cell-Penetrating Peptides: Methods and Protocols*, Methods in Molecular Biology, vol. 1324,
DOI 10.1007/978-1-4939-2806-4_28,

facile and widely applicable to all types of plants and genes are needed. CPP-based gene delivery seems not to have the limitations of other systems; thus, it has the potential to become the major transgenesis method in plant biotechnology.

Cell-penetrating peptides (CPPs), also known as protein transduction domains (PTDs) are short polypeptides (5–30 amino acids) that can transit across the phospholipid bilayer of living cells [3–5]. Based on their degree of amphipathicity CPPs are classified into three categories: non-amphipathic, secondary amphipathic and primary amphipathic. Most common CPPs, such as TAT, *p*VEC, R9 and Penetratin are characterized by a high number of basic residues, specifically arginine and lysine. It is the cationic nature of these residues which allows CPPs to form complexes (often called polyplexes) with anionic cargoes like DNA. This cationic character also seems to contribute to the cell membrane penetration ability of these peptides through electrostatic interaction with anionic phospholipid head groups. While DNA has been the most common cargo, CPPs have also demonstrated delivery of a number of other macromolecular cargoes including RNA, proteins and quantum dots, with potential for many other small molecule cargoes [3–5]. Detailed, up-to-date knowledge on various CPPs and mechanisms of cell penetration is reviewed in Chapters 1–3.

The first published evidence that peptides specifically may be used for macromolecular delivery into plant cells originated from studies which showed that core histone proteins had cellular penetration properties in petunia protoplasts and suspension cultured cells [6]. Core histone proteins (i.e., H2A, H2B, H3, and H4) share the primary characteristics of CPPs with high cationic character and DNA binding affinity, suggesting that CPPs may also be applied to plant cells. Despite the potential advantages of CPPs, plant cells have a number of morphological and chemical differences to that of mammalian cells which can render a portion of the knowledge obtained from mammalian cell studies of little benefit. These differences include, but are not limited to, membrane lipid composition (fatty acids, head groups, etc.), the cellulose cell wall, rates of endocytosis, membrane signalling systems and media conditions for tissue culture. Even with these several potentially confounding factors, common CPPs that have been successful in mammalian cell systems, like TAT, have also shown success in plant tissue culture systems. However, this success has been limited and there is a pressing need to build understanding of how CPPs interact specifically with plant cells and how to improve their efficacy. This review aims to detail the most crucial findings in the use of CPPs in plant cells, including genome modification, and shed some light on the mechanisms involved in CPP uptake and cargo delivery as they apply to planta.

2 CPP Uptake in Non-mammalian Cells

Since their discovery, the action of CPPs has been extensively investigated in various mammalian cells. These peptides can penetrate cell membrane in an energy independent fashion [7]. In addition, they can carry wide varieties of biologically active macromolecules in mammalian cells with high efficiency, specific targeting and absence of cytotoxicity [8, 9]. While most of the CPP uptake and cargo translocation studies have been done in mammalian cells, few studies have been executed in non-mammalian cells. Last decade brought several findings indicating that CPPs are able to overcome the barrier not only of plasma membrane but of the cell wall as well.

Cellular uptake of cell penetrating peptides into non-mammalian cells was first demonstrated in bacteria and fungi. Two CPPs, TP10 and *p*VEC, were found to enter a range of bacterial and fungal cells [10], and yeasts were also shown to internalize other peptides, like $(KFF)_3$ K and Penetratin [11]. Furthermore, comparison of 20 fluorescently labelled peptides showed that peptide uptake was easier in human cells than in yeast cells, as expected [12]. However, one peptide (TP10) efficiently entered both cells [12]. Moreover, *p*VEC, MAP and Penetratin peptides were internalized with various efficiencies in the cells of gram-positive bacteria (*Bacillus megaterium*), gram-negative bacteria (*E. coli*), yeast (*S. cerevisiae*), and insect cells (Sf9) [13].

Next studies in non-mammalian cells demonstrated that CPPs were able not only to enter cell wall containing cells but also to deliver macromolecules. Interestingly, first studies revealed that all species of prokaryotes tested, including cyanobacteria, bacteria, and archaea, as well as unicellular yeasts (*S. cerevisiae*) appeared to be capable of non-covalent GFP protein transduction mediated by arginine-rich intracellular delivery (AID) peptides R9 and SR9, whereas green algae (*Chlorella vulgaris*) and multicellular fungi (*Antrodia cinnamomea*) were impermeable to protein passage [14]. Moreover, it was stated that the CPPs could not translocate into algal cells of *Chlorella vulgaris*, but remained associated with the cells [14]. However, other studies demonstrated that several CPPs including *p*VEC, TAT, Penetratin, and Transportan were able to enter cells of another alga, *Chlamydomonas reinhardtii*, although the uptake was varied in all CPPs tested [15]. Another recent study showed the internalization of fluorescently labelled oligo-arginine peptides R8 and R9 into algal cells of *C. reinhardtii*, *Chlorella protophecoides*, *Neochloris oleoabundans*, and *Scenedesmus dimorphus* [16]. Additionally, these peptides were able to deliver small molecules (streptavidin, streptavidin–biotin) and proteins (horseradish peroxidase; HRP) into the *C. reinhardtii* cells and the cargoes retained their activity after delivery [16].

Discovery that CPPs can penetrate non-mammalian cells makes them a powerful tool for delivering macromolecules across cell walls and cell membranes in diverse cells for basic and applied research.

3 Uptake of CPPs in Plant Cells

Uptake of CPPs by many cell types is well documented, however the kinetics, mechanisms and physicochemistry of that uptake persists as a hotly debated issue, likely because CPPs tend to behave very differently from species to species and even from tissue to tissue [3, 17]. In plants, this is further compounded due to a number of biological and procedural differences between plant and animal tissue culture systems and model species. Thus, greater focus on plants may yield yet unseen answers to these mechanisms for other systems.

3.1 CPP Translocation into Plant Cells

Much like how it has been found in other non-mammalian cell types, CPPs in the absence of a bound cargo are often capable of energy independent translocation across the cell membrane of plant cells. In a study comparing Bowes human melanoma cells to tobacco SR-1 protoplasts it was found that Transportan displayed the highest translocation efficiency compared to *p*VEC, Penetratin and TP10 in the tobacco protoplasts. Despite a clear indication of translocation this efficiency was much lower than translocation of these same CPPs in the cultured melanoma cells [18]. The reasons for this large difference in efficiency are not yet clear, but are likely related to the chemical make-up of the plasma membrane of the protoplasts.

Further work in protoplasts was seen in triticale mesophyll protoplasts using TAT and TAT_2, a proprietary dimer of TAT [19]. Not only was translocation observed but accumulation in the nucleus was also found in both TAT and TAT_2, with TAT_2 displaying 1.6 times higher buildup. Interestingly, lowering of temperature of incubation to 4 °C was found to increase accumulation by nearly double what was found at 25 °C, indicating a favoritism towards an energy independent mechanism of uptake. Although penetration was much less than that in mammalian cell systems, it is interesting to note that CPP uptake has been observed in both monocot and dicot protoplasts with similar results [18–20].

However, delivery in protoplasts does not address a systemic layer of complexity intrinsic to plant cells, the plant cell wall. It must be recognized that the plant cell wall presents a unique challenge to CPP translocation due to its ubiquity in practical tissue culture systems (e.g., induced callus, cell suspension and microspores) and, of course, in mature plants. The plant cell wall consists primarily of polysaccharides, the principle one being cellulose in somatic tissue systems. The cell wall presents both a physical and chemical barrier to the use of CPP in plant cells. It acts as an adsorptive surface to highly cationic CPPs likely due to a slightly negative charge [21].

This adsorptive behavior can reduce the concentration of the solubilized CPPs and thereby reduce the amount that can make contact with the membrane and therefore translocate. It has also been shown that permeabilization of the cell wall increases uptake of CPPs in immature wheat embryos [22] indicating that the diameter of the cell wall pores and permeability of the cellulose matrix are, not surprisingly, factors in efficient uptake. Furthermore, CPPs derived from *Brome mosaic virus* (BMV) capsid protein (CPNT, CP9-22, and CP12-22) showed significant translocation and accumulation within cells of Arabidopsis and barley root hairs, but nearly ubiquitous accumulation at the cell wall, further reinforcing the issue of the cell wall [23].

In non-somatic tissue, particularly in isolated cereal microspores, the translocation of free peptide has also been verified. In the case of triticale microspores, translocation of free peptide was observed using fluoresceinated TAT, TAT_2, *p*VEC, and Transportan [24]. It was shown that Transportan translocated in the greatest amounts despite having little cationic character compared to the other peptides tested. This data seems to suggest that significant basic or cationic character alone is not sufficient for translocation of peptides across the plant cell membrane. Microspores themselves present a valuable model platform for these studies as they possess an immature exine, which is (by comparison to the cellulosic cell wall of somatic tissues) very impermeable, except for the micropore, a region of exposed membrane [24]. Additionally, the exine is composed of a chemically disparate polymer called sporopollenin, which is far more resilient and has more negative charge character than cellulose [25, 26]. These characteristics exacerbate the already present concerns of the cellulosic cell wall. Despite these exacerbations, translocation was still demonstrated in measurable quantities, strongly indicating the potential of CPPs in this tissue culture system as well. In order to increase the efficiency of CPP translocation, the plant cell wall remains a primary issue of interest.

3.2 Mechanisms of CPP Uptake

So far, CPP translocation studies in plant cells have directly addressed only differentiating between endocytotic and energy independent methods of entry. In most experiments with free peptides, many endocytosis inhibitors like chloroquine, EIPA, nocadazole, sodium azide, and cytochalasin D (CytD) as well as exocytosis inhibitor BFA have shown little effect [19, 20, 22, 23]. This strongly indicates an energy independent pathway being involved wherein direct translocation across the membrane is initiated.

Generally, the current data indicate that free peptides may translocate into plant cells with or without a cell wall. However, somatic tissues seem to demonstrate a different affinity than the microspore system, where non-amphipathic CPPs translocate more efficiently in somatic tissue (e.g., TAT_2 in wheat immature embryos) while accumulation in microspores was highest with Transportan,

a primary amphipathic CPP [19, 20, 23, 24]. This likely suggests that the exposed membrane of the microspore perhaps has significantly less anionic character, or adsorption to the microspore exine was more severe due to the TAT peptides higher cationic charge, or more likely, both factors contributed to translocation inhibition. A comparison of translocation efficiency in tobacco suspension cells using fluorescently labelled R4, R8, and R12, showed that R8 was the most efficient above R12 [21]. It was hypothesized that the higher cationic charge increased adsorption to the cell wall and reduced free peptides in the apoplastic space of the cells, while having too little cationic charge (i.e., R4) was not sufficient to adsorb to and translocate across the cell membrane [21]. Furthermore, work with polyguanidine "Trojan Peptoids" which have superficial similarity to polyarginine CPPs, showed favoritism towards accumulation in the apoplastic space before translocation to the cytoplasm [27]. This data suggests that the dynamics of CPP uptake in plant cells bearing a cell wall require a minimum of one extra step over protoplasts, as it has been suggested that cell wall adsorption and subsequent desorption, may need to occur before any direct translocation mechanism can be initiated.

Although direct translocation seems to be the most likely pattern of free CPP translocation into the plant cell, specific endocytotic pathways cannot be entirely excluded as contributors. In the same work on "Trojan Peptoids" [27], microtubule and actin filaments were seen to be associated with vesicular structures containing the fluorescently labelled peptoids. Moreover, a custom CPP, BP100, was found to be negatively impacted by latrunculin B (LatB) treatment of the tobacco suspension cells, reducing translocation by ~15 % [28], and similar results have been demonstrated for CPNT peptide in Arabidopsis root cells [23]. Lat B inhibits formation of actin filaments, which are required for macropinocytosis. F-actin polymerization inhibitor CytD also had a similar effect on internalization of Transportan and *p*VEC peptides [20]. Another macropinocytosis inhibitor, EIPA, showed modest effect on uptake of these two peptides [20] but significantly reduced internalization of CPNT peptide [23]. Intriguingly, disruption of microtubules by oryzalin increased BP100 translocation efficiency by ~50 % [28], whereas this inhibitor as well as other microtubule polymerization inhibitor, nocodazole, showed limited effect in internalization of other CPPs [19, 20, 23, 29]. Moreover, the fact that a less acidic pH reduced cytoplasmic accumulation of BP100 [28] point to a pH-dependent vesiculation, as has been noted in mammalian cells [30]. These studies implicate that CPP uptake may in part be contributed by an endocytotic pathway. Whatever the mechanism of uptake, it may be reasonable to conjecture that translocation of free CPPs in plant cells is largely dominated by a non-endocytic energy independent translocation process, with some contribution from cytoskeleton dependent macropinocytosis.

4 Applications of CPP-Mediated Delivery of Macromolecules into Plant Cells

Cell penetrating peptides have been widely used for the intracellular uptake and delivery of various macromolecules including proteins, nucleic acids, PNA oligomers, dyes, and therapeutic drugs into mammalian cells. Recent studies showed that several CPPs can also deliver protein and DNA macromolecules into plant cells (Fig. 1; [31, 32]).

4.1 Delivery of Proteins as CPP–Cargo Complex

First macromolecules delivered into plant cells with the help of CPPs were proteins. Chang and colleagues demonstrated cellular internalization of the CPP–GFP fusion proteins containing TAT or R9 peptides into tomato root cells, onion epidermal cells and onion root tip cells [33]. Time course analysis of protein internalization revealed that this process was very fast and reached a plateau after 5 min. Few years later, non-covalent protein transduction (NTP) in plant cells was reported [22, 24, 29, 34]. To investigate NTP in plant cells, corn and onion root tip cells were treated with various peptide–protein mixtures (TAT–GFP, R9–GFP, TAT–RFP, R9–RFP). Fluorescence microscopy analyses showed green or red fluorescence in the treated cells [34]. The process was as fast as in the case of peptide-protein fusion delivery. Moreover, the R9 AID peptide was shown to be able of rapid, efficient and simultaneous delivery of the GFP and RFP proteins into onion root tip cells in both covalent and non-covalent conjugates [29]. Covalent fusion of TAT

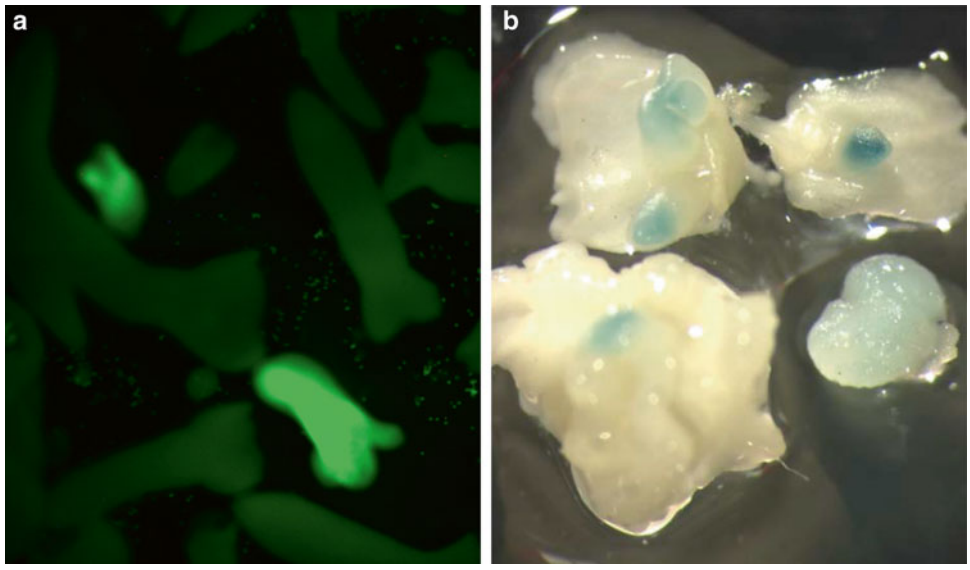

Fig. 1 Examples of CPP-mediated plant transgenesis. (**a**) GFP-positive embryos originating from *Brasica napus* microspores transfected with TAT_2-pGFP complexes. (**b**) β-glucuronidase activity detected in embryos developed from triticale microspores transfected with TAT_2-pGUS complexes

with a different bioluminescent protein (aequorin) was found to be rapidly and efficiently translocated into soybean suspension-cultured cell, and used to monitor intracellular Ca^{2+} concentrations [35].

In other studies non-somatic cells and tissues such as microspores and zygotic immature embryos were chosen as the systems for investigation of NTP in plants [22, 24]. TAT monomer and dimer peptides as well as commercially available Chariot kit for protein delivery in mammalian cells were shown to be able to deliver a large protein, β-glucuronidase enzyme (GUS) into wheat embryos [22]. However, the NPT was more efficient if embryos were permeabilized by treatment with toluene–ethanol mixture prior exposure to the peptide-GUS compound. The same CPPs were able to deliver large molecules like GUS protein into triticale microspores, despite a complex cell wall comprised of exine and intine that could impede the uptake of macromolecules [24]. Interestingly, TAT peptide was the least efficient in both cell types, whereas TAT_2 worked better than Chariot peptide (Pep1) in permeabilized embryos and Pep1 was the most efficient in GUS delivery in triticale microspores [22, 24].

CPPs applied in all the above reported studies in non-mammalian and plant cells were previously used in mammalian cells and they originated from mammalian proteins or mammalian cell-associated viral proteins, or were synthetic. Recently, an investigation of plants as potential source of natural CPPs demonstrated that the N-terminal region of a plant-infecting virus capsid protein (CaP) contained a 22-residue peptide (CPNT) with CPP properties [23]. The CPNT peptide from *Brome mosaic virus* (BMV) CaP carried the GFP protein into the mesophyll cells of barley and tobacco leaves both as covalent and non-covalent conjugates. Capsid proteins from other plant viruses, like *Barley yellow dwarf virus* (BYDV), *Tobacco curly shoot virus* (TCSV) and *Bean yellow dwarf virus* (BeYDV) also exhibited the cell penetrating properties in Arabidopsis roots and barley mesophyll cells [23], thus increasing the collection of plant CPPs.

An innovative approach to the use of CPPs for protein delivery into intact plant cells relays on conjugation of cell penetrating peptides with quantum dots which have far-reaching potential for the study of intracellular processes at the single-molecule level, high-resolution cellular imaging, long-term in vivo observation of cell trafficking, tumor targeting, and diagnostics. Combination of QDs with CPPs allows for precise examination of protein cargo delivery in cellular targeting and imaging in various organisms including plants [36].

The most recent report on use of CPPs in plants outlines the possibility of combining cell penetrating peptide effect with bio-encapsulation by modification of gamma-zein, a major storage protein in maize, to improve formation of protein bodies in seeds [37, 38]. This approach has a potential of generation of a new tool for delivery and stable storage of protein-derived pharmaceuticals in plants.

4.2 Gene Delivery into Plant Cell Nucleus Using CPPs

The utilization of CPPs in plant cell systems as gene delivery vectors is currently a burgeoning field compared to the extensive progress that has been made in animal, specifically mammalian, cell systems [39]. The first indication that cationic and basic agents may be used in plant cells as DNA delivery vectors was shown by Sawahel and colleagues in 2001. This short publication demonstrated the use of polybrene (a polycationic polymer) and spermidine (a polyamine) could successfully assist in delivery of DNA into callus derived cotton suspension cells merely by presence in the media along with naked DNA [40]. This study did not, however, rigorously analyze the mechanism of transfection and no further explorations resulted after the initial publication. It did, however, demonstrate the possibility of using polycations (like CPPs) in the transformation of plant cells.

CPP-mediated delivery of plasmid DNA (pDNA) into plant cells is a very new method: first report was published in year 2007. The group of Han-Jung Lee described transfer and expression of pDNA carrying the *gfp* reporter gene into the roots of mung bean and soybean plants via synthetic AID peptide SR9 [41]. This peptide-mediated DNA delivery presented several advantages, such as nuclear targeting, lack of toxicity, ease of preparation, and no need for protoplasts formulation. This finding encouraged other researches to apply CPP technology for DNA transfer into other cell types and tissues.

Two biotechnology important systems of immature embryos and microspore cells were tested for their ability to uptake plasmid DNA facilitated by TAT and TAT_2 peptides (Fig. 1; [22, 24]). TAT_2 peptide was found to be more efficient in delivering linear pDNA carrying the *uidA* (*GUS*) reporter gene into the cells of wheat permeabilized immature embryos and intact triticale microspores. Interestingly, addition of cationic transfecting agent Lipofectamine™ 2000 to the TAT_2-pDNA non-covalent complex resulted in increased *GUS* gene expression in the embryos [22]. Reporter plasmids were also delivered into plant cells via TAT conjugates with polyethylenimine and polyethylene glycol copolymer (PEI-PEG) which has been previously shown to be a promising gene delivery vehicle in mammals [42]. However, transfection efficiency of soybean suspension-cultured cells and protoplasts with pYFP as well as plasmids for cytoplasmic and nuclear expression of aequorin was not significantly improved by copolymer addition [35].

Triticale isolated microspores were also used to investigate the possibility of delivering nucleoprotein complexes into plant cells, because CPPs were shown to translocate separately proteins and nucleic acids. The first approach was based on *Agrobacterium* T-DNA complexes that were reconstructed in vitro by assembling single-stranded DNA (ssDNA) containing the *GUS* gene with the *Agrobacterium*-derived VirD2 protein and the ssDNA-binding RecA protein [43]. Such complexes were then mixed with TAT_2 peptide to form a nano-complex which was used subsequently to

transfect microspores. This approach allowed for single transgene copy integration events in the genome of a plant species and cell type that were difficult to transform by other methods. Moreover, this tactic led to the integration of intact copies of the transgene, because of protective role of the proteins accompanying DNA. The second approach in transferring nucleoprotein complexes into triticale microspores via CPPs relied on co-delivery of linear dsDNA and RecA protein using TAT_2 or Pep1 CPPs [44]. It resulted in generation of GUS-positive transgenic plants that showed reduced loss of transgene integrity. The protein–DNA–CPP nano-complex method can easily substitute the bombardment technique commonly used for monocots. It might also find applications in gene transfer to other plant cells and species, making it a highly valuable method for plant biology and biotechnology.

List of CPPs that can be used for nucleic acid delivery into plant cell is not limited to TAT, TAT_2, and Pep1. Peptides derived from capsid proteins of plant viruses were shown to be able to deliver viral genomic RNAs as well as target-specific dsRNA and ssRNA into barley leaf protoplasts [23]. In other studies, cell penetrating peptides Bp100 or TAT_2 were combined with a polycation, e.g., oligoarginine R9 [45]. The designed peptides demonstrated significantly higher efficacy of pGFP delivery into cells of Arabidopsis and tobacco leaves in comparison to the single peptides, indicating a synergistic effect of each peptide in the peptide fusion. This generates the opportunity to develop target-specific and efficient peptide-based gene delivery systems by combining peptides of various functions and specificities. Other modifications of CPPs generated to improve peptides for DNA delivery into plant cells included addition of histidine-rich region or Pas peptide to nona-arginine peptide, resulting in HR9 and PR9 fusion peptides. These peptides were shown to deliver proteins into human cells and DNA into paramecia, insect and plant cells [46]. Encouragingly, these CPPs alone or with their cargoes had no cytotoxicity at their working concentrations.

An innovative strategy in nonviral gene delivery was to employ linear polycations synthesized by the ring-opening polymerization between diglycidyl ethers and diamines. These polymers have the amino groups with various densities, thus mimicking peptides, and uniformly distributed hydroxyl groups which may benefit their biocompatibility. Like CPPs, they have also good DNA binding and condensation abilities and low cytotoxicity. Two of these polycations demonstrated sufficient ability to transfer luciferase reporter gene into mammalian cells [47]. If they prove to work in plant systems, it will widen the arsenal of carriers for gene delivery and genetic modification in plant biotechnology applications.

As in the case of protein delivery, CPPs and CPP–cargo complexes can be also combined with quantum dots (QDs) [36]. This strategy should allow for precise examination of DNA or RNA

cargo delivery during genetic modification of plants via transgene delivery or regulation of endogenous gene expression in gene silencing studies.

4.3 Gene Silencing in Plants Using dsRNA and CPPs

Gene silencing describes the epigenetic regulation of a gene, at the level of transcription or translation, to prevent gene expression [48]. Mechanisms include DNA methylation, histone modification and RNA interference (RNAi) [49]. Methods to silence genes are exploited by researchers to study gene function, and for the development of therapeutics for diseases including cancer, infectious diseases, and neurodegenerative disorders [50]. RNAi, also called posttranscriptional gene silencing (PTGS) in plants, is a process in which a short interfering RNA (siRNA) derived from dsRNA triggers the silencing of gene expression in a sequence-specific manner [51, 52]. In plants, manipulation of gene expression via RNAi can produce new quality traits, such as better protection against abiotic and biotic stresses, nutritional improvement, change in plant architecture, enhanced secondary metabolite synthesis, deletion of allergens and toxic compounds, prolongation of shelf life, modulation of flower color and scent, development of seedless fruits and male sterile plants [53, 54]. Another advantage of RNAi technology is its use as a natural defense mechanism against molecular parasites such as jumping genes and viral genetic elements that affect genome stability [53, 54].

Peptide-mediated siRNA delivery has been reported in mammalian and plant systems [55, 56] and received more attention [57, 58]. In plants, cationic oligopeptides such as polyarginine have been shown to deliver dsRNA to induce posttranscriptional gene silencing in tobacco suspension cells derived from shoots of transgenic tobacco plants [55]. When dsRNA for the *GUS* or *nptII* genes was delivered via POA peptide into cells carrying the same genes, the corresponding mRNA was degraded. The PTGS lasted for at least 3 weeks, and the occurrence of PTGS was confirmed by the presence of siRNA [55].

An example of RNA-induced silencing of an endogenous gene comes from studies on cell penetrating peptides derived from viral capsid proteins [23]. A silencing target was the well characterized phytoene desaturase (*PDS*) gene. The *PDS* RNA was reduced by 50 % in barley protoplasts transfected via CPNT peptide with dsRNA but not (+) or (−) ssRNA, which is in agreement with the requirement for dsRNA for the silencing of plant gene expression.

The most recent report on gene silencing achieved by delivery of dsRNA via CPPs combines the use of fusion peptides with targeting endogenous and exogenous genes [59]. BP100 CPP fused to histidine and lysine copolymer (KH_9) was shown to form a stable complex with synthesized dsRNA. Infiltration of the complex carrying *yfp* gene specific siRNA into the leaves of YFP expressing Arabidopsis and poplar plants resulted in significant reduction of

yellow fluorescence and production of YFP in infiltrated regions. Similar attempt but targeting the endogenous gene of chalcone synthase to silence anthocyanin biosynthesis pathway was also successful [59]. This approach enables fast delivery of siRNAs for local gene silencing in specific tissues and organs in plants.

Novel approaches for gene and genome modification via CPP-mediated delivery of sequence-specific nucleases, which were shown to be successful in mammalian cells [60–62] still await exploitation in plant systems for site-specific mutagenesis and genome editing.

4.4 Mechanisms of CPP–Cargo Delivery

With the general non-consensus regarding the mechanisms of cellular uptake of free CPPs, it should not be surprising that the picture becomes more convoluted when various macromolecular cargos are introduced. As with free peptides, two primary pathways have been suggested for CPP–cargo translocation into living cells, the endocytotic pathway and direct translocation mediated by amphipathicity [3]. In plant cells, once again, the presence of the cell wall introduces another layer of complexity to these mechanisms that is not yet fully unravelled.

Protein delivery in plant cells has been well evaluated, however with a very specific emphasis on small fluorescent proteins such as aequorin, GFP, and RFP. The favored mechanism of entry for protein cargoes has been nearly conclusively identified as macropinocytosis, wherein actin plays a major role in uptake. Similar to studies of free CPP uptake, macropinocytosis inhibitors that target actin polymerization (e.g., CytD, EIPA) showed marked decreases in protein cargo uptake in somatic and non-somatic cells [22, 24, 29, 34]. Unlike free peptide uptake, microtubule disruption with nocadazole and MβCD was reported to greatly decrease uptake of RFP and GFP covalently fused to CPPs in onion root tip cells [29]. Moreover, uptake of GFP and RFP complexed with R9 or TAT in the presence of NEM, valinomycin, nigericin, azide, and okadaic acid was unaffected in onion epidermal cell [34]. Also, differences were noted in one study as to whether the CPP was covalently or non-covalently associated with the protein. The non-covalent CPP associated GFP uptake was inhibited by addition of sodium chlorate, which neutralizes peripheral sulfates on the membrane, while the covalently conjugated RFP was unaffected [29]. Additionally, the β-glucuronidase enzyme has been delivered into both triticale microspores and wheat immature embryos via non-covalent association with the non-amphipathic peptides TAT and TAT_2. It was again shown that uptake was strongly inhibited by macropinocytosis inhibitors CytD and EIPA but not by endocytosis inhibitors nocodazole and sodium azide [22–24].

This collection of data seems to reinforce a macropinocytotic system, but also reveals that there is some dependency on the particular association between the protein and the CPP. Covalent conjugation or fusions of proteins to CPPs seem to avoid an apparent

issue found in non-covalent complexation, as they were shown to be unaffected by neutralization of negatively charged sulfates present on the membrane due to proteins. This may be a strong indicator that like animal cells, glycosaminoglycans (GAGs) or similar mucopolysaccharides or polyanions may play a role in CPP–protein uptake. It is thought that in animal cells non-amphipathic CPPs like those used in these studies must non-covalently and electrostatically associate with GAGs of the glycocalyx to initiate macropinocytosis and actin remodelling by clustering of the GAGs on the surface of the membrane [63, 64]. This implicates a similar process in plant cells, but it must be noted that the change in uptake efficiency was small, and cannot be construed as representative of plant cells generally. Still, the role of surface mucopolysaccharides in uptake in plant cells may warrant further investigation.

It is thought that the macropinocytosis also plays a major role in polynucleotide (i.e., DNA) delivery into cells using CPPs [3]. In plants, CPP-mediated plasmid DNA delivery was interfered with the treatment of macropinocytosis inhibitors CytD and EIPA and by 4 °C treatment. Among various endocytosis modulators, azide and NEM strongly suppressed pDNA uptake, whereas valinomycin, fusicoccin and nigericin did not interrupt this process [41]. Therefore, it was conjectured that uptake of CPP–DNA complexes into plant cells could be dependent of energy and macropinocytosis.

As noted, CPPs readily bind DNA due to electrostatic interactions between the negatively charged phosphate backbone and positively charged basic residues of the CPP. This electrostatic interaction acts to compress the DNA into a compact enough conformation, so that it can be taken-up by the cell. However, even the highest compaction of DNA by CPPs does not approach the small size of proteins, often being the size of 60 nm at best and 100–200 nm on average [65, 66]. Given that the functional pore diameter of many plant cell walls is around 5–20 nm [67], CPP–DNA complexes outstrip this size, but can still translocate. It also been noted that substantial aggregation of CPP–DNA complexes can occur over a 1 h incubation period, with TAT2-plasmid DNA aggregates as large as 6.5 μm, far too large for penetration through the cell wall [22, 24]. Improved transfection efficiency of pGFP into leaves was shown using a formulation that reduced aggregation and reduced the average size of the complexes to just over 100 nm [45]. Future investigations that actively reduce complex size using different formulations may assist in improving transfection efficiency [66] and unravelling the particulars of CPP–DNA complex uptake.

One should note with some trepidation regarding the studies so far, that they have exclusively utilized only non-amphipathic CPPs for delivery. Therefore, one cannot conclude at this point that the CPP mediated cargo delivery in plants is dominated by macropinocytosis, as primary and secondary CPP types have not been sufficiently investigated as potential transfection agents. This remains a point of further investigation in plant cell systems.

5 Emerging Applications for Mitochondria

The conventional plant nuclear transformation methods suffer from various limitations including variable transformation rates, random integration of transgenes, epigenetic instability, etc. Therefore, during the past few years, researchers have begun to evaluate application of organelle engineering (transformation) in plant biotechnology as a viable alternative to conventional technologies for transformation of the nuclear DNA. Organelle transformation is becoming popular alternative to nuclear genome transformation because of various advantages like site-targeted transgene integration via homologous recombination, the production of proteins at high levels, the feasibility of expressing multiple proteins from polycistronic mRNAs, the lack of epigenetic instability, and gene containment through the lack of pollen transmission. Particle bombardment (biolistcs), PEG treatment and electroporation are the primary gene delivery technologies used in both mitochondria and plastid transformation. They have been successfully employed to achieve stable plastid transformation in numerous dicot species and few monocot species [68]. Transformation of mitochondria was effective in mammalian cells but limited in non-mammalian species to algae and yeasts, except for transfection of isolated plant mitochondria [69]. Therefore, novel approaches to genetically manipulate the genomes of plant cell mitochondria and plastids are highly desired.

The first successful attempt in DNA delivery into plant organelles by using peptides was based on nanoparticles composed of dsDNA and POTCPPs, the plant organelle targeting cell penetrating peptides [70]. These peptides were selected from the N-terminal protein sorting signal sequences of the nuclear-encoded proteins which function in mitochondria or chloroplasts, resulting in five mTPs (mitochondria targeting peptides) and five cTPs (chloroplast targeting peptides). The peptides showed cell penetration, specific organelle targeting and DNA binding properties, and the ability to deliver dsDNA carrying the *aadA*::*gfp* fusion reporter gene into proper organelles of triticale monocot protoplasts and microspores. The POTCPP transfection method can be used for organelle gene targeting, gene expression studies and functional genomics, and in biotechnological applications [70].

Recently, another peptide-based carrier for delivery of genes into the mitochondria of plants was developed [71]. The group of Dr. Numata utilized peptide fusions to translocate plasmid DNA with the luciferase or *gfp* reporter gene into the cells of *Arabidopsis thaliana* leaves, similarly to their previous approaches to improve CPPs for nuclear delivery of pDNA and dsRNA [45, 59]. Plasmid DNA was first complexed with a mTP peptide composed of the first 12 amino acids of the pre-sequence from the yeast cytochrome

c oxidase subunit IV fused to the KH_9 copolymer, and the resulting particles were then combined with the BP100 peptide, with or without KH_9 [71]. The presence of BP100 CPP in the CPP– or CPP_{KH}–mTP_{KH}–pDNA complexes increased transfection levels by 2–3 folds, as compared to mTP_{KH}–pDNA complexes, thus indicating the advantage of the combination of the mitochondria targeting peptide with the cell penetrating peptide. The CPP improved intracellular penetration of the peptide-DNA complexes likely by enhanced condensation of DNA, since a change in the complex sizes from ~400 nm (mTP_{KH}-pDNA) to 160–280 nm (CPP– or CPP_{KH}–mTP_{KH}–pDNA) was observed. Interestingly, electrostatic interaction with the cell membrane was found not to be a critical factor for complex internalization.

It is highly anticipated that these two new approaches to peptide-mediated gene delivery into cell mitochondria, which have been developed in plant systems, may now be applied as alternative methods for genetic engineering of mammalian mitochondria.

6 Conclusions

The intrinsic property of cell penetrating peptides to deliver various molecules to cells and tissues in a nontoxic manner has indicated that they may be potential components of future agents for cell function studies and genetic modifications. These versatile peptides are simple to synthesize, functionalize, and characterize, and are able to deliver bioactive cargos inside cells, primarily via endocytosis, in order to obtain high levels of gene expression, gene silencing, or transgenesis. Typically, CPPs are often passive and nonselective. However, they can be functionalized or chemically modified to create effective delivery vectors that succeed in targeting the nucleus or the organelles. This possibility inspires synthetic biologists to generate a versatile platform consisting of building blocks that can be exchangeable and/or modifiable. These blocks include various cargoes (proteins, oligonucleotides, nucleic acids, drugs, imaging agents) and carriers (diverse CPPs) that are conjugated in a covalent and non-covalent manner. In addition, the carriers themselves can be functionalized to exhibit better cargo specificity and cargo-carrier complex characteristics, and to deliver their cargoes to specific subcellular destinations. Thus, CPPs are considered promising devices for biological and biotechnological developments.

Acknowledgements

We thank Dr. Fengying Jiang and Fan Liu for providing images illustrating CPP-mediated plant transgenesis.

References

1. Chilton MD (2005) Adding diversity to plant transformation. Nat Biotechnol 23(3):309–310
2. Miranda A, Janssen G, Hodges L, Peralta EG, Ream WJ (1992) Agrobacterium tumefaciens transfers extremely long T-DNAs by unidirectional mechanisms. J Bacteriol 174(7): 2288–2297
3. Brock R (2014) The uptake of arginine-rich cell-penetrating peptides: putting the puzzle together. Bioconjug Chem 25:863–868
4. Choi YS, David AE (2014) Cell penetrating peptides and the mechanisms for intracellular entry. Curr Pharm Biotechnol 15(3):192–199
5. Wang F, Wang Y, Zhang X, Zhang W, Guo S, Jin F (2014) Recent progress of cell-penetrating peptides as new carriers for intracellular cargo delivery. J Control Release 174:126–136
6. Rosenbluh J, Singh SK, Gafni Y, Graessmann A, Loyter A (2004) Non-endocytic penetration of core histones into petunia protoplasts and cultured cells: a novel mechanism for the introduction of macromolecules into plant cells. Biochim Biophys Acta 1664:230–240
7. Vives E, Brodin P, Lebleu B (1997) A truncated HIV-1 TAT protein basic domain rapidly translocates through the plasma membrane and accumulates in the cell nucleus. J Biol Chem 272:16010–16017
8. Fenton M, Bone N, Sinclair AJ (1998) The efficient and rapid import of a peptide into primary B and T lymphocytes and a lymphoblastoid cell line. J Immunol Methods 212:41–48
9. Snyder EL, Dowdy SF (2005) Recent advances in the use of protein transduction domains for the delivery of peptides proteins and nucleic acids in vivo. Expert Opin Drug Deliv 2:43–51
10. Nekhotieva N, Elmquist A, Rajarao GK, Hallbrink M, Langer U, Good L (2004) Cell entry and antimicrobial properties of eukaryotic cell-penetrating peptides. FASEB J 18(2):394–396
11. Holm T, Netzereab S, Hansen M, Langel U, Hällbrink M (2005) Uptake of cell-penetrating peptides in yeasts. FEBS Lett 579:5217–5222
12. Parenteau J, Klinck R, Good L, Langel U, Wellinger RJ, Elela SA (2005) Free uptake of cell penetrating peptides by fission yeast. FEBS Lett 579:4873–4878
13. Palm C, Netzereab S, Hällbrink M (2006) Quantitatively determined uptake of cell-penetrating peptides in non-mammalian cells with an evaluation of degradation and antimicrobial effects. Peptides 27:1710–1716
14. Liu BR, Chou J-C, Lee H-J (2008) Cell membrane diversity in noncovalent protein transduction. J Membr Biol 222:1–15
15. Suresh A, Kim Y-C (2013) Translocation of cell penetrating peptides on *Chlamydomonas reinhardtii*. Biotech Bioeng 110(10):2795–2801
16. Hyman JM, Geihe EI, Trantow BM, Parvin B, Wender PA (2012) A molecular method for the delivery of small molecules and proteins across the cell wall of algae using molecular transporters. Proc Natl Acad Sci U S A 109(33):13225–13230
17. Mäger I, Eiríksdóttir E, Langel K, El Andaloussi S, Langel Ü (2010) Assessing the uptake kinetics and internalization mechanisms of cell-penetrating peptides using a quenched fluorescence assay. Biochim Biophys Acta 1798:338–343
18. Mäe M, Myrberg H, Jiang Y, Paves H, Valkna A, Langer U (2005) Biochim Biophys Acta 1669:101–107
19. Chugh A, Eudes F (2007) Translocation and nuclear accumulation of monomer and dimer HIV-1 Tat basic domain in triticale mesophyll protoplasts. Biochim Biophys Acta 1768: 419–426
20. Chugh A, Eudes F (2008) Cellular uptake of cell-penetrating peptides *p*VEC and transportan in plants. J Pept Sci 14:477–481
21. Mizuno T, Miyashita M, Miyagawa H (2008) Cellular internalization of arginine-rich peptides into tobacco suspension cells: a structure-activity relationship study. J Pept Sci 15:259–263
22. Chugh A, Eudes F (2008) Study of uptake of cell penetrating peptides and their cargoes in permeabilized wheat immature embryos. FEBS J 275:2403–2414
23. Qi X, Droste T, Kao CC (2011) Cell-penetrating peptides derived from viral capsid proteins. Mol Plant Microbe Interact 24(1):25–36
24. Chugh A, Amundsen E, Eudes F (2009) Translocation of cell-penetrating peptides and delivery of their cargoes in triticale microspores. Plant Cell Rep 28:801–810
25. Lallemand B, Erhardt M, Heitz T, Legrand M (2013) Sporopollenin biosynthetic enzymes interact and constitute a metabolon localized to the endoplasmic reticulum of tapetum cells. Plant Physiol 162:616–625
26. Kim SS, Douglas CJ (2013) Sporopollenin monomer biosynthesis in Arabidopsis. J Plant Biol 56:1–6
27. Eggenberger K, Birtalan E, Schröder T, Bräse S, Nick P (2009) Passage of Trojan peptoids into plant cells. ChemBioChem 10:2504–2512
28. Eggenberger K, Mink C, Wadhwani P, Ulrich AS, Nick P (2011) Using the peptide Bp100 as a cell-penetrating tool for the chemical

engineering of actin filaments within living plant cells. ChemBioChem 12:132–137
29. Lu S-W, Hu J-W, Liu BR, Lee C-Y, Li J-F, Chou J-C, Lee H-J (2010) Arginine-rich delivery peptides synchronously deliver covalently and noncovalently linked proteins into plant cells. J Agric Food Chem 58:2288–2294
30. Ben-Dov N, Korenstein R (2012) Enhancement of cell membrane invaginations, vesiculation and uptake of macromolecules by protonation of the cell surface. PLoS One 7(4):e35204
31. Eudes F, Chugh A (2008) Cell penetrating peptides: from mammalian to plant cells. Plant Signal Behav 3(8):549–550
32. Chugh A, Eudes F, Shim Y-S (2010) Cell-penetration peptides: nanocarrier for macromolecule delivery in living cells. IUBMB Life 62(3):183–193
33. Chang M, Chou J-C, Chen C-P, Liu BR, Lee H-J (2005) Noncovalent protein transduction in plant cells by macropinocytosis. New Phytol 174:46–56
34. Chang M, Chou J-C, Lee H-J (2007) Cellular internalization of fluorescent proteins via arginine-rich intracellular delivery peptide in plant cells. Plant Cell Physiol 46(3):482–488
35. Zonin E, Moscatiello R, Miuzzo M, Cavallarin N, Di Paolo ML, Sandonà D, Marin O, Brini M, Negro A, Navazio L (2011) TAT-mediated aequorin transduction: an alternative approach for effective calcium measurements in plant cells. Plant Cell Physiol 52(12):2225–2235
36. Samuel J, Samboju NC, Yau KY, Lin G, Webb SR, Burroughs F (2012) Quantum dot carrier peptide conjugates suitable for imaging and delivery applications in plants, US 20120/244569 A1
37. Hofbauer A, Arcalis E, Stoger E (2014) Functionalized artificial protein bodies: bioencapsulation combined with a cell penetrating effect. Int Assoc Plant Biotechnol Abstract Book p 48
38. Hofbauer A, Peters J, Arcalis E, Rademacher T, Lampel J, Eudes F, Vitale A, Stoger E (2014) The induction of recombinant protein bodies in different subcellular compartments reveals a cryptic plastid-targeting signal in the 27-kDa γ-zein sequence. Front Bioeng Biotechnol 2:67
39. Järver P, Langel Ü (2006) Cell-penetrating peptides–a brief introduction. Biochim Biophys Acta 1758:260–263
40. Sawahel WA (2001) Stable genetic transformation of cotton plants using polybrene-spermidine treatment. Plant Mol Biol Rep 19:377a–377f
41. Chen C-P, Chou J-C, Liu BR, Chang M, Lee H-J (2007) Transfection and expression of plasmid DNA in plant cells by an arginine-rich intracellular delivery peptide without protoplast preparation. FEBS Lett 581:1891–1897
42. Kleemann E, Neu M, Jekel N, Fink L, Schmehl T, Gessler T, Seeger W, Kissel T (2005) Nanocarriers for DNA delivery to the lung based upon a TAT-derived peptide covalently coupled to PEG-PEI. J Control Release 109(1-3):299–316
43. Ziemienowicz A, Shim Y-S, Matsuoka A, Eudes F, Kovalchuk I (2012) A novel method of transgene delivery into triticale plants using the *Agrobacterium* transferred DNA-derived nano-complex. Plant Physiol 158:1503–1513
44. Shim Y-S, Eudes F, Kovalchuk I (2013) dsDNA and protein co-delivery in triticale microspores. In vitro Cell Dev Biol Plant 49:156–165
45. Lakshmann M, Kodama Y, Yoshizumi T, Sudesh K, Numata K (2013) Rapid and efficient gene delivery into plant cells using designed peptide carriers. Biomacromolecules 14:10–16
46. Liu M-J, Chou J-C, Lee H-J (2013) A gene delivery method mediated by three arginine-rich cell-penetrating peptides in plants. Adv Stud Biol 5(2):71–88
47. Zhang Q-F, Yi W-J, Wang B, Zhang J, Ren L, Chen Q-M, Guo L, Yu X-Q (2013) Linear polycations by ring-opening polymerization as non-viral gene delivery vectors. Biomaterials 34:5391–5401
48. Wilson RC, Doudna JA (2013) Molecular mechanisms of RNA interference. Annu Rev Biophys 42:217–239
49. Sioud M (2015) RNA interference: mechanisms, technical challenges, and therapeutic opportunities. Methods Mol Biol 1218:1–15. doi:10.1007/978-1-4939-1538-5_1
50. Kaur IP, Chopra K, Rishi P, Puri S, Sharma G (2014) Small RNAs: the qualified candidates for gene manipulation in diverse clinical pathologies. Crit Rev Ther Drug Carrier Syst 31(4):305–329
51. Baulcombe DC (1996) RNA as a target and an initiator of post-transcriptional gene silencing in transgenic plants. Plant Mol Biol 32: 79–88
52. Li L, Liu Y (2011) Diverse small non-coding RNAs in RNA interference pathways. Methods Mol Biol 764:169–182
53. Jagtap UB, Gurav RG, Bapat VA (2011) Role of RNA interference in plant improvement. Naturwissenschaften 98:473–492
54. Younis A, Siddique MI, Kim CK, Lim KB (2014) RNA interference (RNAi) induced gene

silencing: a promising approach of Hi-tech plant breeding. Int J Biol Sci 10(10):1150–1158

55. Unnamalai N, Kang BG, Lee WS (2004) Cationic oligopeptide-mediated delivery of dsRNA for post-transcriptional gene silencing in plant cells. FEBS Lett 566:307–310
56. Simeoni F, Morris MC, Heitz F, Divita G (2005) Peptide-based strategy for siRNA delivery into mammalian cells. Methods Mol Biol 309:251–260
57. Shukla RS, Qin B, Cheng K (2014) Peptides used in the delivery of small noncoding RNA. Mol Pharm 11(10):3395–3408
58. Draz MS, Fang BA, Zhang P, Hu Z, Gu S, Weng KC, Gray JW, Chen FF (2014) Nanoparticle-mediated systemic delivery of siRNA for treatment of cancers and viral infections. Theranostics 4(9):872–892
59. Numata K, Ohtani M, Yoshizumi T, Demura T, Kodama Y (2014) Local gene silencing in plants via synthetic dsRNA and carrier peptide. Plant Biotech J 12:1027–1034
60. Gaj T, Guo J, Kato Y, Sirk SJ, Barbas CF III (2012) Targeted gene knockout by direct delivery of zinc-finger nuclease proteins. Nat Methods 9:805–807
61. Liu J, Gaj T, Patterson JT, Sirk SJ, Barbas CF III (2014) Cell-penetrating peptide-mediated delivery of TALEN proteins via bioconjugation for genome engineering. PLoS One 9:e85755
62. Ramakrishna S, Kwaku Dad A-B, Beloor R, Lee S-K, Kim H (2014) Gene disruption by cell-penetrating peptide-mediated delivery of Cas9 protein and guide RNA. Genome Res 24(6):1020–1027
63. Favretto M, Wallbrecher R, Schmidt S, van de Putte R, Brock R (2014) Glycosaminoglycans in the cellular uptake of drug delivery vectors – bystanders or active players? J Control Release 180:81–90
64. Wallbrecher R, Verdurmen WPR, Schmidt S, Bovee-Geurts PH, Broecker F, Reinhardt A, van Kuppevelt TH, Seeberger PH, Brock R (2014) The stoichiometry of peptide-heparan sulfate binding as a determinant of uptake efficiency of cell-penetrating peptides. Cell Mol Life Sci 71:2717–2729
65. Yu J-H, Huang J, Jiang H-L, Quan J-S, Cho M-H, Cho C-S (2009) Guanidinylated poly(allyl amine) as a gene carrier. J Appl Polymer Sci 112:926–933
66. Khondee S, Baoum A, Siahaan TJ, Berkland C (2011) Calcium condensed LABL-TAT complexes effectively target gene delivery to ICAM-1 expressing cells. Mol Pharm 8:788–798
67. Sun D, Hussain HI, Yi Z, Siegele R, Cresswell T, Kong L, Cahill DM (2014) Uptake and cellular distribution, in four plant species of fluorescently labeled mesoporous silica nanoparticles. Plant Cell Rep 33:1389–1402
68. Wani SH, Haider N, Kumar H, Sigh N (2010) Plant plastid engineering. Curr Genomics 11(7):500–512
69. Larosa V, Remacle C (2013) Transformation of the mitochondrial genome. Int J Dev Biol 57:659–665
70. Eudes F, MacMillan T (2013) Organelle targeting nanocarriers. Patent # WO 2013016810 A1
71. Chuah J-A, Yoshizumi T, Kodama Y, Numata K (2015) Gene introduction into the mitochondria of *Arabidopsis thaliana* via peptide-based carriers. Sci Rep 5:7751

Chapter 29

DNA Transfer into Animal Cells Using Stearylated CPP Based Transfection Reagent

Kristiina Karro, Tiiu Männik, Andres Männik, and Mart Ustav

Abstract

The efficient transfection of cloned genes into cells has a critical role in nucleic acid-based therapeutic applications, molecular and cell biology studies, and the production of recombinant proteins in cultured cells. Using a stearylated cell-penetrating peptide (CPP) NickFect51, we have generated an effective, universal, and convenient method for the delivery of DNA vectors into animal cells derived from different origins (mammalian, avian, insect). The CPP-mediated transfection described in detail herein is efficient for many regular cell lines commonly used for research purposes and it is especially suitable for transfection of protein production cell lines adapted for growth in chemically defined serum-free medium.

Key words Transfection reagent, Cell-penetrating peptide, NickFect, Plasmid DNA, Cell culture, Recombinant protein production

1 Introduction

The delivery or transfection of cloned cDNA into the nuclei of eukaryotic cells is a well-established approach to express recombinant proteins in target cells. For animal cells, the transfection method can be virus-based, in which the cDNA of interest is inserted into the genome of a viral vector. Although usually very efficient, the preparation of viral vectors is rather complicated. For that reason, instrument-based (e.g., electroporation, microinjection etc.) and reagent-based transfection methods are also broadly used. Compared to instrument-based methods, the reagent-based approaches are usually easily scalable and do not need any special devices. Widely usable transfection reagents include calcium phosphate, cationic polymers such as polyethylenimine (PEI) and cationic lipids [1, 2].

Among the reagent-based transfection methods, cell-penetrating peptides (CPPs) have been extensively studied and developed as vehicles for the delivery of nucleic acids [3]. For example, hydrophobic stearyl moiety-containing amphipathic CPPs have been developed as improved transport vehicles for nucleic acids into animal cells [4, 5].

Ülo Langel (ed.), *Cell-Penetrating Peptides: Methods and Protocols*, Methods in Molecular Biology, vol. 1324,
DOI 10.1007/978-1-4939-2806-4_29,

One particular stearylated CPP, NickFect51 (NF51), is especially effective for the delivery of RNA and DNA species, including plasmid DNA into mammalian cells [6]. Based on this finding, we implemented NF51 as an efficient transfection reagent for recombinant protein production using QMCF technology (Icosagen, Estonia), which essentially stably replicates and maintains a plasmid DNA-based expression system [7] in modified human or rodent cell lines and preferably grows in chemically defined serum-free mediums.

Despite the quite high transfection efficiencies of NF51 in QMCF, which exceed the results obtained by commercially available transfection reagents [6], we decided to further optimize the reagent and protocol, including CPP synthesizing details, storage conditions, CPP–plasmid DNA charge ratio, CPP–DNA complex volume, incubation times, transfection mediums, etc. The main aim of this work was to generate a reliable and convenient method for using NF51 with QMCF technology in the production of different recombinant proteins [8] and pseudotyped virus-like particles [9]. As a result, we developed an NF51-based transfection reagent named Reagent 007 together with a convenient and scalable (from 96-well plates to liters) transfection protocol. Using CHO-based QMCF cells cultured in chemically defined serum-free medium, the method routinely ensures 85–90 % transfection efficiency that significantly exceeds the results obtained by other widely used commercial reagents (Fig. 1a, ref. 6). Using the reagent–DNA ratio described here, the transfection is also associated with low toxicity to cells, indicated by high post-transfection viability of the culture (Fig. 1b).

When we studied the reagent further to expand its usage by broadening the range of efficiently transfectable cell lines, we were surprised to find that the same charge ratio and protocol are fairly universally suitable and optimal for many different cell lines (*see* Table 1). The transfectable cell lines are not limited to mammalian cell lines but also include barely transfectable avian cells (chicken B cell line DT40) and insect cells (Sf9 cells commonly used for baculovirus vectors). Thus, the incubations and also complex formation conditions for NF51 seem to be universal, in contrast to several other commercial transfection reagents for which the reagent–DNA ratio must be adjusted for every new cell line transfected. We believe that these properties make the reagent and method attractive for many approaches related to research and protein production.

2 Materials

Ultrapure deionized sterile water is used for making all solutions. Prepare the CPP and DNA solutions at room temperature. To avoid contamination of cell cultures, perform all procedures under sterile conditions as these are commonly used for animal cell culture manipulations.

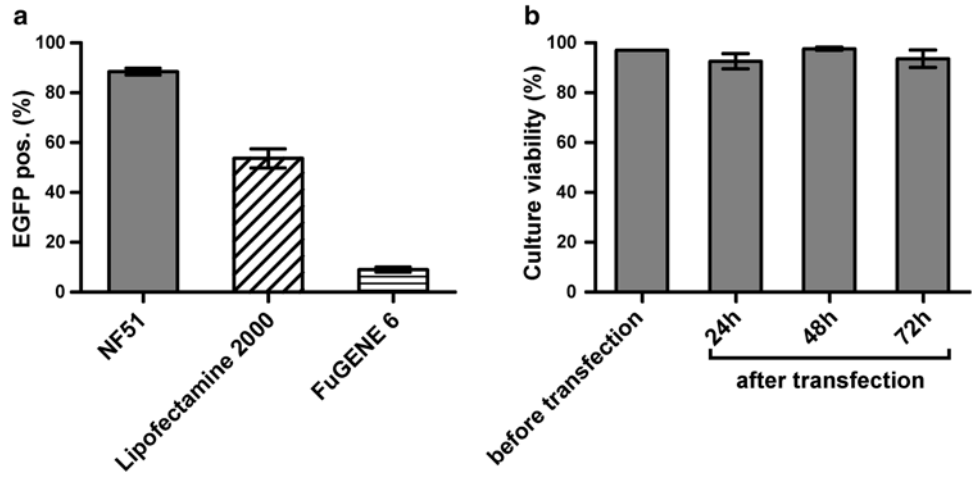

Fig. 1 Transfection efficiencies and post-transfection viability of CHOEBNALT85A (QMCF production cell line derived from CHO-S) protein production cultures growing as suspension cells in chemically defined serum-free medium. (**a**) Transfection efficiencies measured by FACS analysis 24 h after the transfection of 1.5×10^6 cells with 1 μg of EGFP expression plasmid (FreeStyle 293 Expression was used as Transfection medium) using NF51 (Reagent 007) and the protocol provided herein, Lipofectamine™ 2000 (Life Technologies, USA) or FuGENE 6 (Promega, USA). For Lipofectamine™ 2000 and FuGENE 6, the transfection conditions (reagent and DNA ratio) were pre-optimized accordingly to the manufacturer instructions. (**b**) The viabilities of the 20 ml scale cultures (1.5×10^7 cells) transfected with 10 μg of scFv-Fc antibody expression vector using NF51 (Reagent 007) and the protocol provided herein. The culture viability was measured before transfection as well as 24, 48, and 72 h post-transfection using trypan blue exclusion [11]

Table 1
Transfection efficiencies of different cell lines and cultures using NF51

Cell line	Origin	Culture type	Transfection efficiency[a] (%)
CHOEBNALT85A	Mammalian	Suspension, serum-free	90
FreeStyle™ CHO-S	Mammalian	Suspension, serum-free	75
		Adherent	70
HEK293T/17	Mammalian	Adherent	50
FreeStyle™ 293-F	Mammalian	Suspension, serum-free	75
		Adherent	60
U2OS	Mammalian	Adherent	70
U2OSEBNALTD3	Mammalian	Adherent	70
HeLa	Mammalian	Adherent	50
DT40	Avian	Suspension	15
Sf9	Insect	Adherent	40[b]

[a]Transfection efficiency was measured using FACS analysis 24 h after transfection with EGFP expressing plasmid (with exception of Sf9 cells, see below)
[b]Transfection efficiency was measured using FACS analysis 72 h after transfection with EGFP Bacmid

2.1 CPP NF51

1. CPP NF51 is synthesized using the Fmoc solid-phase peptide synthesis strategy (free of endotoxins, animal component free) with the water-soluble peptide Stearyl-AGYLLG(Orn) INLKALAALAKKIL-NH2 (stearyl moiety is CH_3–$(CH_2)_{16}$–CO–), MW = 2434.7 with 95–99 % purity. Acetate must be used as the counter-ion, and the final product obtained is a white or off-white powder. Store the powder at –20 °C.
2. NF51 **Stock Solution**: Dissolve the NF51 powder in water with a final concentration of 0.97 mg/ml = 400 μM (*see* **Note 1**). Store at 2–8 °C (*see* **Note 2**). The powder and stock solution of the NF51 are also commercially available as Reagent 007 (Icosagen, Estonia).

2.2 CPP–DNA Complex Formation Components

1. The plasmid DNA used for transfections should be of high purity (A_{260}/A_{280} of 1.7–1.9) and endotoxin free (*see* **Note 3**). After the final step of the purification, the DNA must be dissolved in sterile deionized *water containing no salts, buffering agents* etc. (*see* **Note 4**).
2. Sterile, pyrogen-free polypropylene vessels like non-binding surface V-bottom 96-well plates, microcentrifuge tubes, 15 ml centrifuge tubes or 50 ml tubes, depending on final volume of the complex.

2.3 Cell Culture Components

1. **Mammalian cells** currently tested as efficiently transfectable using the NF51 (*see* Table 1 and **Note 5**):

   HeLa (human adenocarcinoma, ATCC no. CCL-2)

   U2OS (human osteosarcoma, ATCC no. HB-96)

   U2OSEBNALTD3 (QMCF production cell line derived from U2OS, Icosagen, Estonia)

   HEK293T/17 (human embryonic kidney cells, ATCC no. CRL-11268)

   FreeStyle™ 293-F cells (Life Technologies, USA)

   FreeStyle™ CHO-S cells (Life Technologies, USA)

   CHOEBNALT85A (QMCF production cell line derived from CHO-S, Icosagen, Estonia).
2. **Avian cells** currently tested as efficiently transfectable using the NF51 (*see* **Note 5**):

   DT40 (*Gallus gallus* bursa lymphoma cells, ATCC no. CRL-2111).
3. **Insect cells** currently tested as efficiently transfectable using the NF51 (*see* **Note 5**):

   Sf9 (*Spodoptera frugiperda* cells, ATCC no. CRL-1711).
4. Animal cell culture vessels (multiwell plates, dishes, or flasks with suitable size).

5. Sterile pyrogen-free centrifuge tubes with conical bottoms suitable for the collection of cells.
6. The **Transfection Mediums** currently tested as suitable for incubation of the CPP–DNA complex with cells (*see* **Note 6**):

   RPMI-1640 Medium

   Ham's F12 Medium

   Dulbecco's Modified Eagle Medium (DMEM)

   Iscove's Modified Dulbecco's Medium (IMDM)

   FreeStyle™ 293 Expression Medium (Life Technologies, USA)

   Pro293s-CDM (Lonza, Switzerland)

   Expi293™ Expression Medium (Life Technologies, USA)

   FreeStyle™ CHO Expression Medium (Life Technologies, USA)

   CD FortiCHO™ Medium (Life Technologies, USA)

   UltraCHO (Lonza, Switzerland)

   PowerCHO-1 (Lonza, Switzerland)

   ExCell420 (for insect cells, Sigma-Aldrich, USA)

   The Transfection Medium must not contain serum or extra amounts of surfactants (like Pluronic® F-68) as they will decrease the transfection efficiency (see Note 7*).*

3 Methods

General workflow of transfection is illustrated in Fig. 2.

3.1 Preparation of Cells for Transfection

1. The cells for transfection must be viable and in active growth phase (*see* **Note 8**).
2. Pre-warm the **Transfection Medium** to culture temperature.
3. *For adherent cells,* remove the growth medium by aspiration and replace with the same amount of **Transfection Medium** (*see* **Note 9**)**.** Move directly to **step 7** in this section.
4. *For suspension cultures,* count the cells to determine the actual culture density (cells/ml) and calculate the amount of original culture needed for all transfections (*see* Table 2 for recommended cell numbers and **Note 9**).
5. Transfer the selected volume of cell suspension into 15 or 50 ml centrifuge tube(s) and precipitate the cells by centrifugation (200 × *g*, 5 min at room temperature) (*see* **Note 10**).
6. Remove the supernatant and resuspend the cells in a suitable amount of transfection medium (*see* **Note 11**) to obtain the desired density of cells (*see* Table 2 and **Note 12**).
7. Seed the cells into selected vessels (*see* Table 2 for recommended volumes).

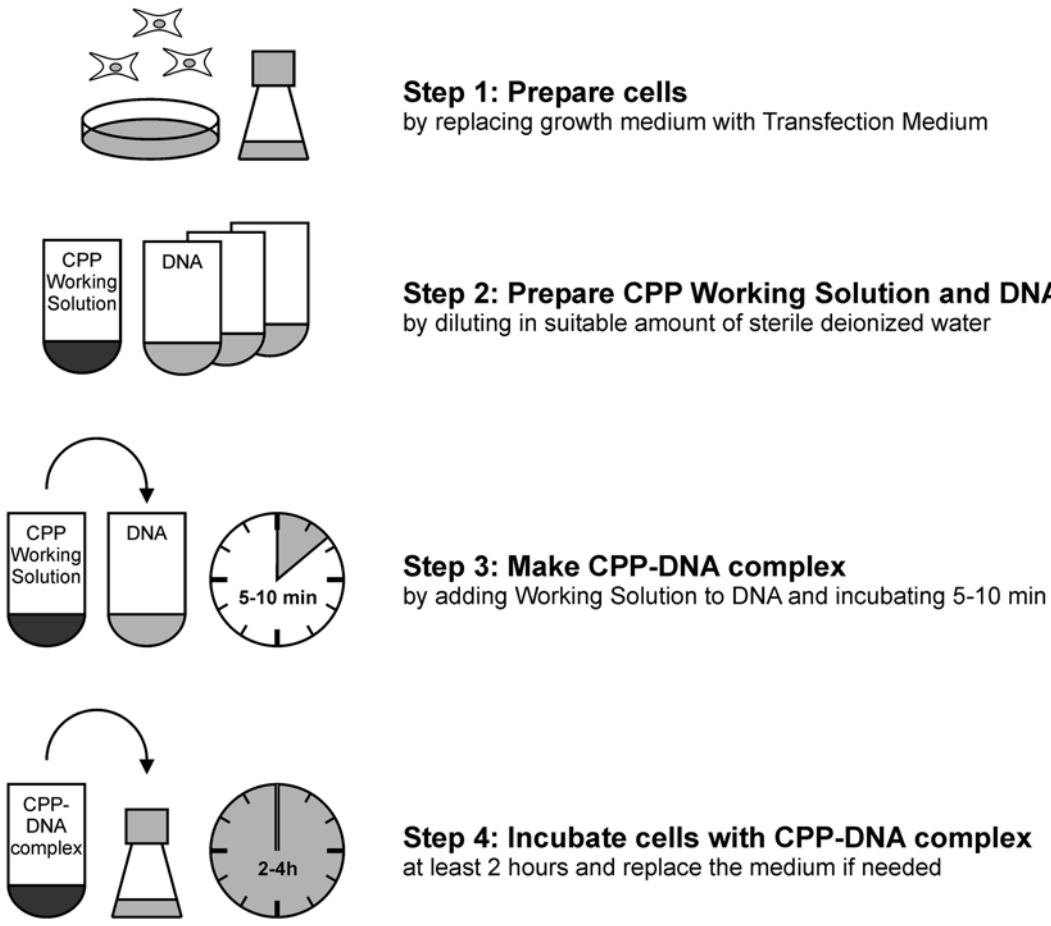

Fig. 2 General workflow of transfection procedure using the protocol provided herein

Table 2
Scaling of DNA and CPP Working Solution for suspension cells (*see* Notes 12 and 13)

Culture vessel	No. of cells collected per sample	Volume of transfection medium (ml)	Amount of DNA (μg)	Final volume of DNA sample (μl)	Volume of CPP Working Solution (μl)
96-well	1.5×10^5	0.1	0.5	5	10
6-well	1.5×10^6	2	2	60	40
60 mm dish	1.5×10^6	5	3	90	60
100 mm dish	7.5×10^6	10	5	150	100
125 ml flask	1.5×10^7	20	10	300	200
1 L flask	1.5×10^8	200	100	3000	2000

Table 3
Scaling of DNA and CPP Working Solution for adherent cells (*see* Note 13)

Culture vessel	Approximate no. of cells	Volume of medium (ml)	Amount of DNA (μg)	Volume of DNA sample (μl)	Volume of CPP Working Solution (μl)
96-well	2×10^4 to 4×10^4	0.1	0.5	5	10
24-well	1×10^5 to 2×10^5	0.5	1	30	20
6-well	4×10^5 to 8×10^5	2	2	60	40
60 mm dish	8×10^5 to 2×10^6	5	3	90	60
100 mm dish	2×10^6 to 5×10^6	10	5	150	100

8. Continue incubation in the incubator (using temperature and atmosphere suitable for the particular cells) until the CPP–DNA complexes are ready.

3.2 Preparation of DNA Samples

1. Use Tables 2 or 3 for suspension cultures and adherent cells, respectively, to find the recommended amounts of plasmid DNA as well as the final volume of the **DNA Samples** (*see* **Note 13**).
2. Prepare **DNA Samples** in water in appropriate tubes or wells by mixing the necessary amount of DNA with sterile water to reach the final volume.

3.3 Preparation of NF51 Working Solution

1. Use Tables 2 or 3 for suspension cultures and adherent cells, respectively, to calculate necessary amount of NF51 **Working Solution** sufficient for all transfections (*see* **Note 9**).
2. Prepare CPP **Working Solution** by diluting the NF51 **Stock Solution** four times in water (1 volume **Stock Solution** + 3 volumes water) (*see* **Note 14**).

3.4 Preparation of CPP–DNA Complex

1. Add the indicated amount (taken from Tables 2 or 3) of the **Working Solution** to the DNA solution and mix *immediately* by pipetting gently up and down 5–6 times. *Do not vortex the complex as it will decrease transfection efficiency!*
5. Incubate the mixture at room temperature for 5–10 min (see **Note 15**).

3.5 Incubation of the CPP–DNA Complex with Cells

1. Take the cells out from incubator.
2. Add CPP–DNA complex to the cells (drop-wise for larger amounts).
3. Carefully shake/rotate the plate, dish or flask (*see* **Note 16**).
4. Continue the incubation in the incubator (using temperature and atmosphere suitable for particular cells) for at least 2–4 h

(*see* **Note 17**). When the suspension cells are grown on a shaker platform, the shaking should also be maintained in this step.

5. If the **T**ransfection Medium *is also suitable as a growth medium* there is no need to replace the medium and incubation is continued until analysis or further manipulation. If necessary, just supplements (like serum) can be added in this step (*see* **Note 18**). The transfection procedure is complete here.
6. If the Transfection Medium *is not an optimal medium for culture growth*, replace the **Transfection Medium** with a suitable growth medium.
7. *For adherent cells,* remove the **Transfection Medium** by aspiration and replace with a suitable amount of appropriate growth medium.
8. *For suspension cultures,* collect the cells by centrifugation (200 × *g*, 5 min at room temperature) (*see* **Note 10**), remove the supernatant, resuspend the cells in a suitable amount of appropriate growth medium and re-seed into the selected vessel (*see* Table 2).
9. Continue the incubation in the incubator (using temperature and atmosphere suitable for particular cells) until analysis or further manipulation. The transfection procedure is complete here.

4 Notes

1. NF51 synthesized in this way has excellent water solubility and the Stock Solution remains clear.
2. The Stock Solution can be stored for at least 8 months. Avoid freezing/thawing the stock solution or long-term storage at room temperature as it may result in a decrease in transfection efficiencies. Sterile filtering through a 0.22-μm membrane is also not recommended as some amount of CPP binds even with low-binding PVDF membranes.
3. Suitable plasmid DNA preparation can be obtained using any appropriate method or kit, ensuring the pure supercoiled plasmid and involving a step for the removal of endotoxins (also known as lipopolysaccharides or LPS that are membrane components of gram-negative bacteria).
4. Once purified and dissolved in a solute other than water, the DNA can be precipitated using any conventional method for precipitation or desalting [10] and redissolved in sterile deionized water. However, our tests revealed that small amounts TE buffer (10 mM Tris–HCl, pH 8.0, 1 mM EDTA), which is commonly used for plasmid DNA storage, does not interfere with the CPP–DNA complex formation. In particular, the

TE-dissolved plasmid can be used for CPP–DNA complex formation and transfection without a decrease in efficiency if the volume of the TE-diluted DNA in the complex does not exceed 10 % of the complex final volume.

5. The NF51 transfection seems to be nearly universal for animal cell lines and many other cells are certainly efficiently transfectable using the protocol provided herein. Listed are just cells we have particularly tested in assays where the transfection efficiency was measured by FACS analysis as a percentage of EGFP expressing cells at 24 h after transfection (with pCMV-EGFP plasmid expression vector for vertebrate cells or 72 h after transfection with EGFP Bacmid for insect cells). The transfection was considered effective when the percentage of EGFP-positive cells was equal or greater compared to other routine methods (electroporation, lipofection, polyethyleneimine) and toxicity to cells (significant decrease of viability or growth inhibition) was not observed. For example, the 15 % efficiency for DT40 cells and 80–90 % efficiency for CHO suspension cells are both considered efficient because DT40 is well known as a difficult-to-transfect cell line.
6. Any other medium not listed here could be tested in comparison with any suitable Transfection Medium listed herein. The mediums we have already tested as certainly *not suitable* for incubation of the CPP–DNA complex with cells are: ExCell 302 CHO (Sigma-Aldrich, USA), PowerCHO-2 (Lonza, Switzerland), ExCell 293 Serum-Free Medium (Sigma-Aldrich, USA), and 293 SFM II (Life Technologies, USA) because these result in a significant decrease in transfection efficiency. CD CHO (Life Technologies, USA) had a moderate inhibiting effect, decreasing the efficiency from 80–90 % to 40–50 % in the case of CHO serum-free suspension culture. There are no complete chemical compositions available for these proprietary mediums and thus the reasons for the impaired efficiencies are not ultimately clear.
7. Adding 1 % of Gibco® Anti-Clumping Agent (Life Technologies, USA) to CD FortiCHO™ Medium (Life Technologies, USA) decreased the transfection efficiency from 90 to 2 %. If desired, the anti clumping agent can be added into the growth medium (after incubation of the CPP–DNA complex with cells).
8. The attached cells should be 70–85 % confluent and the viability of suspension cultures should be ≥95 % (measured by trypan blue exclusion [11], for example). It is always good practice to split the cultures the day before transfection, providing the fresh growth medium.
9. It is always recommended to prepare somewhat more cell suspension and Working Solution than it is exactly needed by

calculation: take number/volume of cells, and Working Solution enough for all transfections plus one additional.

10. The centrifugation conditions we are routinely using for cell lines listed herein. Of course, any other conditions can be used when appropriate for cells.
11. The change of medium to fresh one is recommended even in case when the growth medium is also suitable as the Transfection Medium for incubation of the CPP–DNA complex.
12. The recommended cell numbers per sample for suspension cultures are given by our experiments with CHO and 293 cells grown in chemically defined serum-free medium. Thus, using other cell types, these numbers can be subject to change depending on the discretion of the investigator.
13. Indicated DNA amounts are recommendations only (based on our experimental data with our vector system). Thus, the DNA amounts can be subject to change and be selected arbitrarily by the investigator depending on the analysis type, toxicity of the product, promoters used etc. Keep in mind that if you change the DNA amount, proportional changes must be made to the volume of DNA Sample and amount of Working Solution added to the DNA.
14. The remaining Working Solution can be stored for further use at 2–8 °C for up to 1 week.
15. Longer incubation is allowed, however the transfection efficiency starts to decrease slowly when incubation times are >15–20 min.
16. For 96-, 48- and 24-well plates, the rotating may not ensure proper mixing but careful tapping on the side of the plate works well. For larger amounts, rotate the vessel at the same time as adding complex (drop-wise).
17. The 2 h is a minimal incubation time in the case when the transfection medium is not suitable for optimal growth; changing of medium as soon as possible is beneficial. For some cell lines (e.g., for U2OS) longer incubation (4 h) moderately increase the transfection efficiency.
18. There is no preference between changing medium and just adding necessary supplements (e.g., serum). Select the way most convenient for you.

Acknowledgements

We warmly thank Ivar Ilves, Margit Ool, and Mart Toots for their assistance in experimental work. We also thank Anne Kalling, Andres Tover, Urve Toots, and Mart Ustav for their support.

References

1. Geisse S, Fux C (2009) Recombinant protein production by transient gene transfer into Mammalian cells. Methods Enzymol 463:223–238
2. Gao X, Kim KS, Liu D (2007) Nonviral gene delivery: what we know and what is next. AAPS J 9:E92–E104
3. Lehto T, Kurrikoff K, Langel Ü (2012) Cell-penetrating peptides for the delivery of nucleic acids. Expert Opin Drug Deliv 9:823–836
4. Mäe M, El Andaloussi S, Lundin P et al (2009) A stearylated CPP for delivery of splice correcting oligonucleotides using a non-covalent co-incubation strategy. J Control Release 134: 221–227
5. Lehto T, Simonson OE, Mäger I et al (2011) A peptide-based vector for efficient gene transfer in vitro and in vivo. Mol Ther 19:1457–1467
6. Arukuusk P, Pärnaste L, Oskolkov N et al (2013) New generation of efficient peptide-based vectors, NickFects, for the delivery of nucleic acids. Biochim Biophys Acta 1828: 1365–1373
7. Silla T, Hääl I, Geimanen J et al (2005) Episomal maintenance of plasmids with hybrid origins in mouse cells. J Virol 79:15277–15288
8. Chiou HC, Vasu S, Liu CY et al (2014) Scalable transient protein expression. Methods Mol Biol 1104:35–55
9. Kushnir N, Streatfield SJ, Yusibov V (2012) Virus-like particles as a highly efficient vaccine platform: diversity of targets and production systems and advances in clinical development. Vaccine 31:58–83
10. Green MR, Sambrook J (2012) Chapter 1: Isolation and quantification of DNA. In: Molecular cloning: a laboratory manual, 4th edn. Cold Spring Harbor Laboratory Press, New York, pp 11–78
11. Strober W (2001) Trypan blue exclusion test of cell viability. Curr Protoc Immunol 21:A.3B.1–A.3B.2

Chapter 30

Live Cell Genomics: Cell-Specific Transcriptome Capture in Live Tissues and Cells

Thomas J. Bell and James Eberwine

Abstract

The sensitivity of new transcriptomic techniques is rapidly improving to the point that single-cell molecular analysis is now becoming commonplace. However to obtain accurate transcriptome data, the initial experimental steps must strive to maintain the natural environment of cell and always get set in motion under in vivo conditions. Achieving these critical experimental parameters is technically challenging for investigators and currently the most frequently used molecular techniques experimentally commence with tissues or cells in artificial environments or under in vitro conditions. Here we review an innovative experimental approach that is called transcriptome in vivo analysis (TIVA) that was designed to overcome theses well-known limitations. The TIVA methods permit cell-specific transcriptome capture from viable intact heterogeneous tissues. Cell-penetrating peptides (CPPs) are used to deliver multifunctional transcriptome-capture tags (TIVA tags) to the cytoplasm of the cell under in vivo conditions. The TIVA capture tag enables investigators to target and isolate cell-specific transcriptomes in their natural microenvironments. The combination of maintaining in vivo conditions and selective cell-specific transcriptome capture provides investigators with the opportunity to yield the most biologically accurate and informative transcriptome data hitherto.

Key words Single-cell transcriptome, Cell-penetrating peptide, Alternatively spliced exons, Transcriptomics

1 Introduction

1.1 TIVA Technology Captures Cell-Specific Transcriptomes in Their Natural Environment

The cell's transcriptome is now studied at unparalleled detail due to emerging next-generation sequencing technologies such as RNA-seq [1, 2]. Our ability to isolate and collect uncorrupted single-cell transcriptomes must improve along with the experimental and analytical advances to yield more biologically accurate data. Currently, most methods for capturing RNA from live single cells are significantly hindered by unnatural experimental conditions or invasive collection practices. For example, the net effect on the transcriptome from dissociating, cell sorting, and/or culturing neurons in non-endogenous extracellular environment and removing their natural synaptic connections is beginning to be

Ülo Langel (ed.), *Cell-Penetrating Peptides: Methods and Protocols*, Methods in Molecular Biology, vol. 1324,
DOI 10.1007/978-1-4939-2806-4_30,

quantified and reported [3]. The transcriptome in vivo analysis (TIVA) technology overcomes this issue by in vivo capture of cell-specific transcriptomes from intact heterogeneous tissues. This technology will enable investigators to identify more accurate single-cell transcriptomes that will shed a better light on their true in vivo functions and biological importance.

1.2 How Does TIVA Technology Work?

TIVA technology was developed to permit in vivo capture of cell-specific transcriptomes. CPPs are used to deliver multifunctional transcriptome in vivo analysis (TIVA) capture tags into cytoplasm of the live cells. The capture molecule has four distinct components: (1) CCP to provide access to cytoplasm, (2) a caged TIVA tag, (3) a pair of fluorophores that provide fluorescence resonance energy transfer (FRET) to permit in vivo cell-specific uncaging of TIVA tag, and (4) a biotin-linked poly-U mRNA capture and recovery molecule. As CPPs can exhibit cellular specificity some CPPs are better at moving the TIVA tag into one cell type versus other cell types. Also some CPPs introduce the TIVA tag in endocytosed endosomes while others directly bring the TIVA tag into the cytoplasm. It is best to screen several CPPs to see which permits the most efficient vector for introduction of the TIVA tag into the cells of interest. Schematics of the TIVA capture molecule and procedure are provided in Figs. 1 and 2.

1.3 Cell-Specific mRNA Capture via the TIVA Molecule

Once inside the cell, the cytoplasmic environment drives the dissociation of the caged TIVA tag from the CCP. Next, laser-mediated photoactivation of the caged TIVA tag enables investigators to selectively activate and uncage the TIVA tags in individual target cells or subcellular regions of interest. Once the TIVA tag is uncaged, a poly-U mRNA capture molecule is free to bind the poly-A tails of mRNAs in the cytoplasm of the target cells. After the cellular mRNAs and the poly-U mRNA capture molecules of the TIVA tag anneal, the photolysed region containing both photolysed and non-photolysed cells is collected via glass pipette aspiration or another collection method.

1.4 Selective mRNA Recovery from Heterogeneous mRNA Populations

Once the cell collection is complete, a lysis buffer is used to release the mRNAs from the cytoplasm. Depending on the accuracy of the cell collection method, the mRNA population will be some mixture of TIVA-tagged mRNAs (annealed cellular mRNA-TIVA tag-poly-U complexes) and non-TIVA-tagged mRNAs. While the mRNAs from many cells are present in the mixture, the only mRNA annealed to the activated TIVA tag is that which was present in the cell that was photoactivated. The biotin moiety on the biotin-linked poly-U mRNA capture/recovery molecule in the TIVA tag is used to affinity purify the annealed TIVA tag-mRNA complexes away from the untagged mRNA populations. Once purified, cell-specific TIVA-captured mRNAs represent a

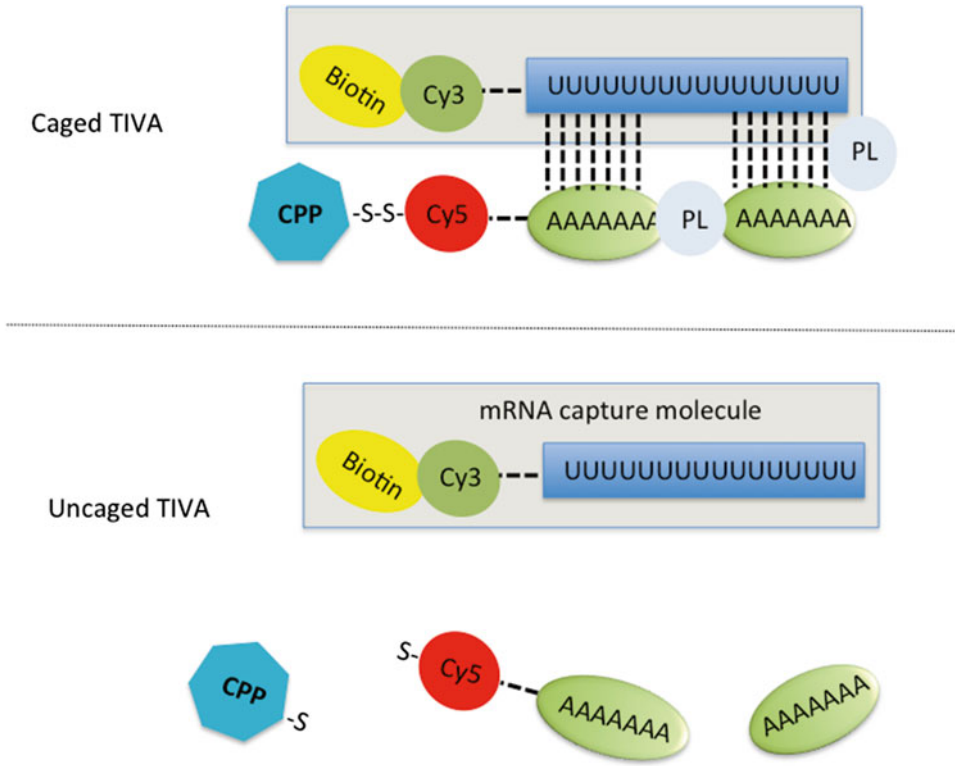

Fig. 1 *TIVA procedure can isolate cell-specific transcriptomes from tissues with heterogeneous cell populations. This cartoon shows the different functional components on the TIVA-capture tag:* 1) CCP to provide access to cytoplasm, 2) a pair of fluorophores (Cy3 and Cy5) that provide fluorescence resonance energy transfer (FRET) to permit cell-specific uncaging of TIVA tag in live tissue slices, and 3) a biotin-linked poly-U mRNA capture molecule (*shaded blue area*). The caged TIVA tag (*upper*) and uncaged (*lower*) versions of the tag are shown

microenvironment-associated biologically accurate transcriptome that is suitable for next-generation transcriptome sequencing or other mRNA analysis methods.

1.5 TIVA-Mediated Transcriptome Isolation Summary

Over the next few years, investigators will identify the single-cell transcriptomes in hundreds of different cell types. The biological accuracy of the data from these sequencing efforts will be directly linked to the initial mRNA capture methods. Due to the single cell's transcriptome sensitivity to external and internal environment changes, the most valuable data will undoubtedly come from studies that maintain the natural cellular connections and extracellular environment. The TIVA approach was developed to overcome this common experimental limitation and provide a more truthful measure of each cell-specific transcriptome by providing a method to capture single-cell mRNA population under natural in vivo conditions.

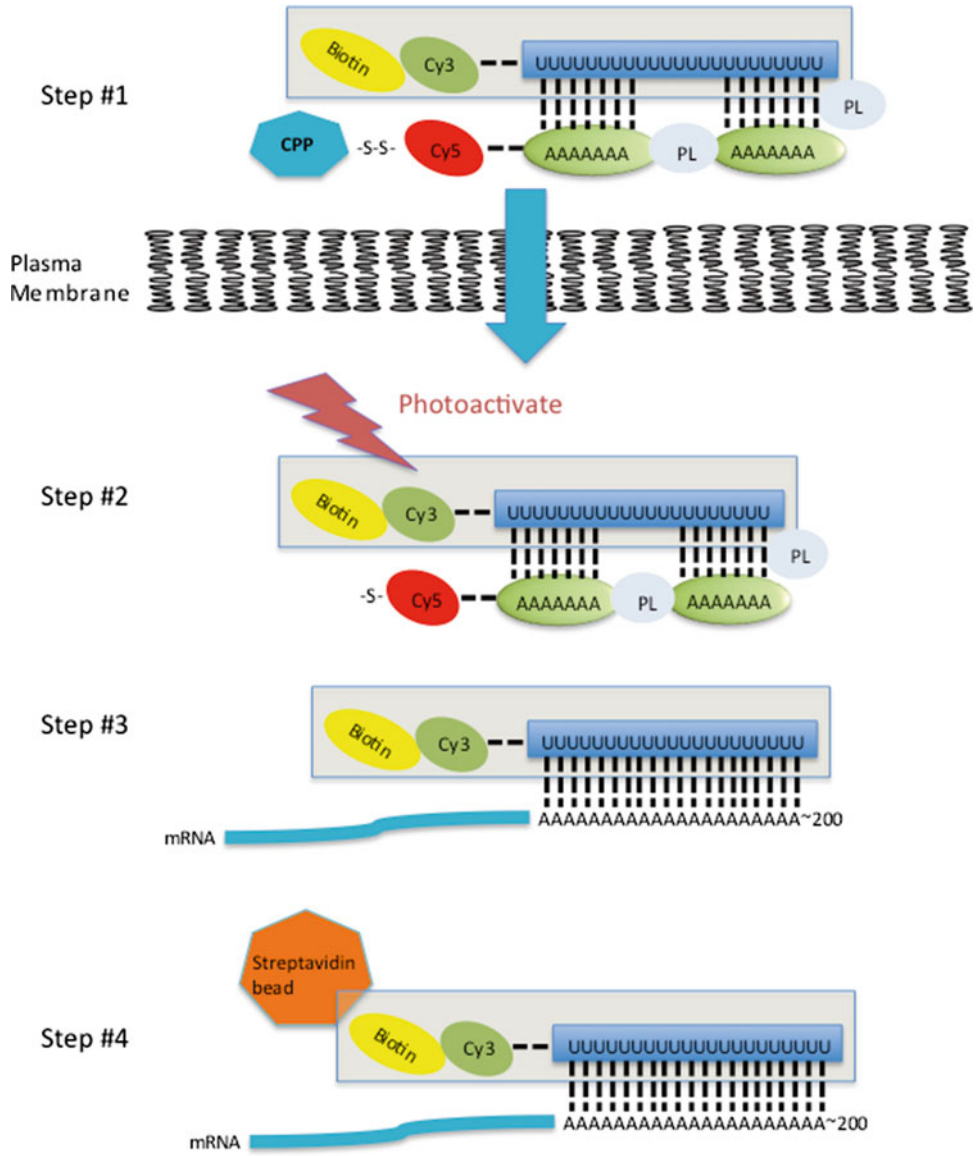

Fig. 2 *A schematic of the TIVA procedure.* **Step 1**: A cell-penetrating peptide (CPP) gets the TIVA-capture tag across the plasma membrane. Once inside the cell, the cytoplasmic environment drives the dissociation of the caged TIVA tag from the CCP. **Step 2**: Laser-mediated photoactivation of the caged TIVA tag enables investigators to selectively activate and uncage the TIVA tags in individual target cells or subcellular regions of interested. **Step 3**: Once the TIVA tag is uncaged, a poly-U mRNA capture molecule is free to bind the poly-A tails of mRNAs in the cytoplasm of the target cells. **Step 4**: After the cellular mRNAs and the poly-U mRNA capture molecules of the TIVA tag anneal, the photolysed region containing both photolysed and non-photolysed cells is collected via glass pipette aspiration or another collection method. **Step 4**: A lysis buffer is used to release the mRNAs from the cytoplasm and the biotin moiety on the biotin-linked poly-U mRNA capture/recovery molecule in the TIVA tag is used to affinity purify the annealed TIVA tag-mRNA complexes away from the untagged mRNA populations. The cell-specific TIVA-captured mRNAs are suitable for next-generation transcriptome sequencing or other mRNA analysis methods

2 Materials

2.1 Buffers

1. Artificial cerebrospinal fluid (aCSF): 122 mM NaCl, 28 mM $NaHCO_3$, 5.5 mM glucose, 10 mM HEPES, 3.5 mM KCl, 1 mM $MgCl_2$, 2 mM $CaCl_2$ 2, pH 7.4 with 5 % CO_2/95 % O_2 gas mixture. Filter sterilize. Store at −20 °C.
2. Dulbecco's phosphate-buffered saline (1×), ph 7.4. Store at 4 °C.
3. HEPES-buffered saline (HBS), ph 7.4: 25 mM HEPES, 075 mM Na_2HPO_4, 70 mM $NaCl_2$. Filter sterilize. Store at −20 °C.
4. Lysis buffer: 10 mM Tris–HCl pH 7.5, 300 mM NaCl, 10 mM $MgCl_2$, 0.1–0.5 % NP40, 1 U/μL Superase-In RNase inhibitor. Filter sterilize. Store at 4 °C.
5. Streptavidin magnetic bead storage buffer: Dulbecco's phosphate-buffered saline (1×), 0.1 % bovine serum albumin (BSA), 0.2 % NaN_3.
   Store at −20 °C.
6. Blocking nonspecific buffer for streptavidin magnetic bead: Dulbecco's phosphate-buffered saline (1×), 0.1 % BSA.
   Store at 4 °C.
7. Dulbecco's phosphate-buffered saline (1×), ph 7.4. Store at 4 °C.

2.2 Other Reagents

1. TIVA capture tag (UPENN, Custom synthesis)
2. Dynabeads M-270 Streptavidin magnetic beads (Invitrogen).
3. NP40 (Sigma).
4. Superase-In RNase inhibitor (1 U/μL) (Invitrogen).
5. Nuclease-free water.
6. Microcentrifuge tubes.
7. Microcentrifuge.
8. Brain tissue slices: The procedure can be performed in any cell system including dispersed cells in culture, the live acute and organotypic slice culture, as well as intact tissue. For cells in culture, we typically use rat cortical neurons plated in 35 mm dishes in ~12 ml of media at 400,000 cells/ml (~4.8×10^6 cells in each plate). For slice cultures, the slices are typically cut on a tissue slicer at a thickness of 300 μm. These slices are then moved to a slice culture chamber on a microscope slide for acute culturing and TIVA imaging, activation, and TIVA-RNA isolation.
9. Cultured cells: The procedure can be performed in any cell culture system. We typically use cells plated on glass poly-L-lysine-coated cover slip in 12-well plates at 200,000 cells/ml.

3 Methods

3.1 TIVA tag Loading in Brain Tissue Slices (Option #1)

1. Standard brain slice processing methods should be used to prepare the specimens.
2. Transfer the brain slices to aCSF.
3. Incubate the brain slices in aCSF for 90 min.
4. Add 30 mM TIVA tag in aCSF to the brain slices.
5. Incubate for 90 min at room temperature (RT).

3.2 TIVA Tag Uncaging (Option #1)

1. Transfer to imaging chamber in 1× PBS.
2. Immediately perform imaging and photolysis with a confocal microscope (Zeiss 710 Meta, 40× water objective (N.A. 1.0)).
3. Confirm loading by detecting Cy5 signal in the emission range excited by 561 nm.
4. Perform uncaging via the 405 nm laser (80 % power and 100.85 μs per pixel) while recording FRET excited by 514 nm and simultaneous capturing in Cy3 (538–599 nm) and Cy5 (637–704 nm) emission ranges.
5. The photolysed region (both photolysed and non-photolysed cells) is collected via glass pipette aspiration or another collection method.

(Potential stopping point)

3.3 TIVA Tag Loading in Cell Cultures (Option #2)

1. Standard cell culture methods should be used to prepare the samples. We typically use cells plated on glass poly-L-lysine-coated cover slip in 12-well plates at 200,000 cells/ml.
2. Rinse the cover slips 2× with rinse in prewarmed 1× PBS.
3. Remove the 1× PBS.
4. Add 50 μL of 10 μM TIVA tag in 1× PBS to cover slip.
5. Incubate for 15 min at room temperature (RT).
6. Rinse the cover slips 2× with rinse in prewarmed 1× PBS.

3.4 TIVA Tag Uncaging (Option #2)

1. Transfer to imaging chamber in PBS.
2. Immediately perform imaging and photolysis with a confocal microscope (Zeiss 710 Meta, 40× water objective (N.A. 1.0)).
3. Confirm loading by detecting Cy5 signal in the emission range excited by 561 nm.
4. Perform uncaging via the 405 nm laser (30 % power and 50 ms per pixel) while recording FRET excited by 514 nm and simultaneous capturing in Cy3 (538–599 nm) and Cy5 (637–704 nm) emission ranges.

5. The photolysed region (both photolysed and non-photolysed cells) is collected via glass pipette aspiration or another collection method.

3.5 Collecting Photolysed and Non-photolysed Samples via Glass Pipette Aspiration

1. Wearing gloves, fill the tip of collection pipette with 1× PBS by holding the tip of the pipette tip in 1× PBS for ~3 s.
2. Checking the collection pipette:
   - Good collection pipettes should have approximately first 5 mm of the pipette filled with 1× PBS after **step 1**.
   - Poor/non-usable collection pipettes will not detect PBS in the pipette after **step 1**.
3. Carefully load the collection pipette in the pipette holder.
4. Open the suction line and apply positive pressure as the tip of the pipette is lowered into the bath.
5. Once the pipette in the bath, close the suction line.
6. Place the pipette tip as close as possible to your region of interest.
7. To collect the sample, open the suction line and begin to slowly apply negative pressure.
8. Continue to increase the amount of negative pressure until the region of interest moves into the collection pipette.
9. Once the cell completely enters the pipette, it will get pulled out of the visual field. At this point, stop applying negative pressure and close the stopcock.
10. Immediately lift the pipette out of the bath and remove the pipette from the pipette holder

3.6 Harvesting Samples from the Collection Pipette to the Collection Tube

1. Collection microcentrifuge tube should be kept on ice or in the –20 °C freezer until needed.
2. Remove the pipette from the pipette holder.
3. Hold the pipette close to the tip just like you would hold a pen when writing.
4. Aim the pipette ~25 % away from the top of the microcentrifuge tube (e.g., in region that contains 1.5 ml marking on a standard microcentrifuge tube).
5. Break the first ~5 mm of the tip on the side of the microcentrifuge tube.
6. Spin the microcentrifuge tube briefly and to force all contents (your sample with some glass) to the bottom of the tube.
7. The samples can be stored at –80 °C until needed; however, we typically process the cells within 4 weeks of collection.

(Potential stopping point)

3.7 Magnetic Bead Preparation

1. Take 30 μL (300 μg) of the magnetic beads (10 mg/ml), magnetically separate for 10 min on magnetic stand, and then remove the buffer.
2. Rinse 2× with 1 ml lysis buffer.
3. Rotate for 10 min at RT.
4. Centrifuge briefly.
5. Magnetically separate for 10 min on magnetic stand, and then remove the buffer.
6. Remove from magnetic stand and add 30 μL of the lysis buffer to the magnetic beads.

(Note: The beads can be prepared in advance. The washed beads can be stored at 4 °C for a week.)

3.8 TIVA Tag Affinity Purification and mRNA Isolation

1. Prechill the lysis buffer (10 mM Tris-HCl pH 7.5, 300 mM NaCl, 10 mM $MgCl_2$, 0.1–0.5 % NP40, 1 U/μL Superase-In RNase inhibitor) on ice.
2. Lyse the cells or tissue in a final volume of 200 μL lysis buffer.
3. Incubate for 5 min on ice and in the dark (wrap the tube in aluminum foil).
4. Add 10 μL prewashed MyOne T1 or C1 streptavidin magnetic Dynabead.
5. Mix and incubate for 15 min on ice in the dark (wrap the tube in aluminum foil).
6. Add 200 μL of wash buffer (20 mM Tris–HCl pH 7.5, 50 mM NaCl) to the TIVA-mRNA/bead complexes.
7. While magnetized, aspirate the wash buffer from the TIVA-mRNA/bead complexes.
8. Rewash the samples two more times by repeating **steps 6** and **7**.
9. After the final wash, resuspend the TIVA-mRNA/bead complexes in 6 μL of nuclease-free water.

3.9 Eluting the TIVA-Captured mRNAs from the Magnetic Beads

1. Incubate the beads at 70 °C in a benchtop water bath for 5 min to release the TIVA-captured mRNAs from the beads.
2. Place on a magnetic stand for 2 min to magnetically separate the beads from the TIVA-captured mRNAs.
3. While magnetized, aspirate the supernatant with the TIVA-captured mRNAs.
4. Transfer the supernatant to a new microcentrifuge.
5. The supernatant with TIVA-captured mRNAs can be either immediately frozen or proceed to the amplification procedure.

(Potential stopping point)

4 Amplification, Library Construction, and RNA-seq

1. To generate 100 ng and 1000 ng of amplified aRNA for library construction, the TIVA-captured mRNAs should be subjected to two to three rounds of linear in vitro transcription-based amplification.
2. The population size and sample concentration should be determined via a Bioanalyzer nanochip.
3. Once 100 ng and 1000 ng of aRNA is achieved, proceed to Tru-Seq library construction and RNA-seq analysis according to the manufacturer's instructions.

5 Notes

1. No mRNAs captured or low mass smears:
   RNA degradation can occur from nuclease contamination in the original sample or in the reagents used during the procedure. TIVA procedures permit for the transcriptome analysis of very small quantities of mRNAs (e.g., single-cell or subcellular regions of select cells), so extremely high-quality general lab practices are essential to yield experimental success. Gloves need to be worn when handling the samples and reagents to avoid contamination by nucleases. All solutions, reagents, glassware, and dissecting instruments need to be prepared RNase free. Using control RNA samples (nanograms of mRNA from commercial vendors) as a positive technical control can help identify the issue. If both the control and TIVA samples appear as low-molecular-mass smears on the Bioanalyzer, RNA degradation is the issue. If both the control and TIVA samples yield no RNA signal, one of the reagents or experiment steps were omitted or not executed appropriately. To help reduce variability from the reagents, the reagents should be divided into aliquots to screen single cells in large groups (~50 cells) with identical stocks of reagents. If the source of the contamination cannot be identified, the quickest solution is to move forward with a fresh set of reagents. Lastly if the controls (nanograms of mRNA from commercial vendors) and samples work, but the TIVA samples fail, either the cell uncaging (Subheadings 3.2 and 3.4, **step 2**) or cell isolation (Subheadings 3.2 and 3.4, **step 5**) steps were not executed correctly.
2. Verifying the TIVA results:
   Control samples that were treated with TIVA tag but not subjected to photo-uncaging should be processed in parallel with photoactivated samples (Subheadings 3.2 and 3.4, **step 5**). Cell-specific expression of select mRNAs of interest can be

verified by in situ hybridization [4]. This approach will also identify the subcellular expression patterns for a given mRNA, which would not be captured via the subsequent transcriptome analysis if the whole cell was subjected to TIVA tag uncaging.

References

1. Eberwine J, Sul JY, Bartfai T, Kim J (2014) The promise of single-cell sequencing. Nat Methods 11:25–27
2. Wu AR, Neff NF, Kalisky T, Dalerba P, Treutlein B, Rothenberg ME, Mburu FM, Mantalas GL, Sim S, Clarke MF, Quake SR (2014) Quantitative assessment of single-cell RNA-sequencing methods. Nat Methods 11(1):41–6
3. Lovatt D, Ruble BK, Lee J, Dueck H, Kim TK, Fisher S, Francis C, Spaethling JM, Wolf JA, Grady MS, Ulyanova AV, Yeldell SB, Griepenburg JC, Buckley PT, Kim J, Sul JY, Dmochowski IJ, Eberwine J (2014) Transcriptome in vivo analysis (TIVA) of spatially defined single cells in live tissue. Nat Methods 11:190–196
4. Eberwine J, Belt B, Kacharmina JE, Miyashiro K (2002) Analysis of subcellularly localized mRNAs using in situ hybridization, mRNA amplification, and expression profiling. Neurochem Res 27:1065–1077

Chapter 31

Live Cell Genomics: RNA Exon-Specific RNA-Binding Protein Isolation

Thomas J. Bell and James Eberwine

Abstract

RNA-binding proteins (RBPs) are essential regulatory proteins that control all modes of RNA processing and regulation. New experimental approaches to isolate these indispensable proteins under in vivo conditions are needed to advance the field of RBP biology. Historically, in vitro biochemical approaches to isolate RBP complexes have been useful and productive, but biological relevance of the identified RBP complexes can be imprecise or erroneous. Here we review an inventive experimental to isolate RBPs under the in vivo conditions. The method is called peptide nucleic acid (PNA)-assisted identification of RBP (PAIR) technology and it uses cell-penetrating peptides (CPPs) to deliver photo-activatible RBP-capture molecule to the cytoplasm of the live cells. The PAIR methodology provides two significant advantages over the most commonly used approaches: (1) it overcomes the in vitro limitation of standard biochemical approaches and (2) the PAIR RBP-capture molecule is highly selective and adaptable which allows investigators to isolate exon-specific RBP complexes. Most importantly, the in vivo capture conditions and selectivity of the RBP-capture molecule yield biologically accurate and relevant RBP data.

Key words RNA-binding protein, Cell-penetrating peptide, Alternatively spliced exons, Posttranscriptional regulation

1 Introduction

1.1 Introduction to Live Cell RNA-Binding Protein Capture Methodology (PAIR)

Posttranscriptional control of gene expression requires specific RNA-binding protein (RBP) interactions with key regulatory sequences in their respective target mRNAs. Although RBP-mRNA interactions control multiple posttranscriptional events, only a relatively small number of RBPs and their respective target mRNA-binding sequences have been identified. Fragile X syndrome has highlighted the complexity and the clinical importance of RBPs; this well-studied neurological disease is caused by mutations in the RBPs called fragile-x mental retardation proteins (FMRPs). The mutated forms of FMRP do not regulate the respective RNA cargoes correctly, which ultimately yields alterations in the biology associated with the target mRNAs [1, 2].

Ülo Langel (ed.), *Cell-Penetrating Peptides: Methods and Protocols*, Methods in Molecular Biology, vol. 1324,
DOI 10.1007/978-1-4939-2806-4_31,

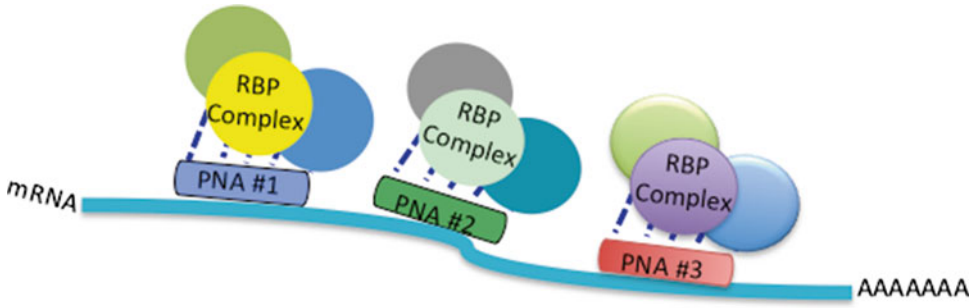

Fig. 1 PAIR procedure can isolate exon-specific RBP complexes. This cartoon shows how PAIR procedure can be used to identify exon-specific RBP complexes within the same mRNA. PNA#1 is designed to identify the RBP complex that regulates the expression of an alternatively spliced exon. In contrast, PNA#2 targets the RBP complex that regulates the expression of the non-alternatively spliced exon and PNA#3 identifies the RBP complex that regulates the expression of a retained intron within the same mRNA

1.2 PAIR Technology Isolates RBP Complexes in an Exon-Specific Manner

A single mammalian cell transcriptome contains 4000–12,000 mRNAs [3, 4]. For a given mRNA, a large number of different RBP complexes coat the entire topography of an mRNA to regulate a diverse range of posttranscriptional events such as alternative splicing (exon utilization), subcellular localization, and RNA stability. The PAIR technology allows investigator to identify RBP complexes in select gene regions or exons in live cells [5, 6]. Equivalent to designing PCR primers, investigators can directly target exons in their mRNA of interest with peptide nucleic acid analogs (PNAs) as probes. PNAs are used as probes instead of nucleic acids because they are more stable under in vivo conditions. The PNA probe design strategy is straightforward. The PNA probes need to be (1) complementary to their target mRNA sequence, (2) ~12–18 in length to be exon specific, (3) limit the GC content to ~50 %, and (4) the PNA sequence should not have three consecutive purine nucleotides. A database search should be used to verify that each PNA probe is specific for their respective targets. To elevate the stringency level of the RBP screen, it is highly recommended that a minimum of two PNA probes should be designed for each target exon and multiple PAIR capture concentrations are tested. Figure 1 shows a strategy to isolate RBP complexes that regulate two distinct forms of posttranscriptional regulation in the BKCa channel mRNAs: intron retention [7, 8] and activity-dependent alternative splicing [9].

1.3 How Does PAIR Technology Work

An overview of the PAIR procedure is provided in Fig. 2. The PAIR capture tag has three distinct functional components: (1) a cell-penetrating peptide (CPP), (2) a photo-activatible compound p-benzoylphenylalanine (Bpa), and (3) a distinct PNA sequence to target select mRNAs. The cell-penetrating peptide is used to get

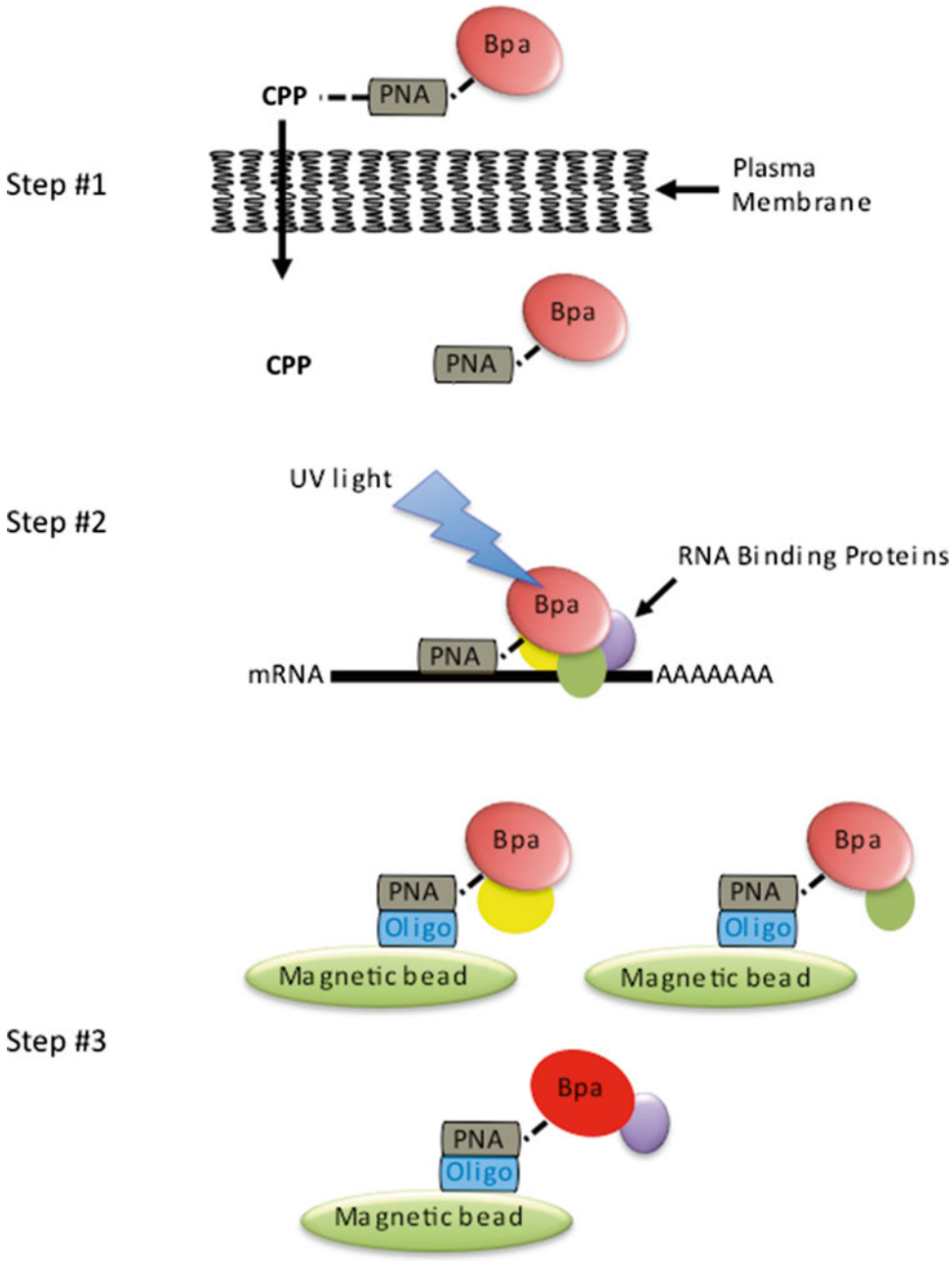

Fig. 2 A schematic of the PAIR procedure. **Step 1**: A cell-penetrating peptide (CPP) gets the PNA-Bpa complexes across the plasma membrane. **Step 2**: The PNAs hybridize to their target mRNA in live neurons and UV light stimulation activates p-benzoylphenylalanine (Bpa) and cross-links the PNA-Bpa-RBP complexes. **Step 3**: The cells are collected and magnetic beads are used to isolate the PNA-Bpa-RBP complexes. The eluted RNA-RBP complexes are purified by chloroform-methanol precipitation. SDS-PAGE and silver staining are used to visualize the isolated RBPs. The protein bands of interest will be excised and subjected to mass spectrometry analysis

the PAIR capture tag efficiently into the cellular cytoplasm. Once the PAIR capture tag is taken up into the cellular cytoplasm, the CPP component of the complex is reduced and dissociates from the PAIR capture tag. The remaining molecules in the PAIR capture tag, PNA-Bpa, bind to their respective target mRNA sequences under in vivo conditions.

Once the PNA-Bpa complex anneals with the target mRNA, the cells are subjected to UV light to activate the Bpa molecule and physically link PNA-Bpa to nearby RBP complexes. After UV cross-linking, the cells are treated with Triton-100 lysis buffer to disrupt the cellular membranes. To release the mRNA-PNA-Bpa complexes, lysates are next subjected to RNase A treatment. The PNA-RBP complexes are separated from cellular lysates via magnetic beads coupled to oligonucleotide primers that are complementary to the PNA probes. After eluting the RNA-RBP complexes from the beads, the RBPs are purified by chloroform-methanol precipitation. The purified RBPs are separated and visualized by a combination of SDS-PAGE and silver staining. Distinct protein bands or select regions of interest on the gel are excised and partially sequenced by mass spectrometry to identify the purified RBPs.

1.4 Summary

RBPs are fundamental regulatory proteins for all cells but only a few functionally significant RBPs have been identified. To advance the field, investigators need novel experimental approach to identify RBPs in their live cellular environment. The PAIR procedure gives investigators a major advantage over other techniques because it allows the isolation of exon-specific RBP complexes for any mRNA under in vivo conditions and does not require random cross-linking that will increase the number of false positives.

2 Materials

2.1 Buffers

1. HEPES-buffered saline (HBS), ph 7.4: 25 mM HEPES, 075 mM Na_2HPO_4, 70 mM $NaCl_2$. Filter sterilize and store at –20 °C.
2. TX-100 lysis buffer, pH 8.0: 25 mM HEPES, 0.1 % Triton X-100, 300 mM $NaCl_2$, 20 mM glycerophosphate, 1.5 mM $MgCl_2$, 1 mM DTT, 2 mM EDTA. Filter sterilize and store at 4 °C. Add fresh protease inhibitors to the TX-100 lysis buffer before each experiment. As per the manufacturer's recommendations, 10 μl protease inhibitor cocktail per 1 ml cell extracts. The final concentration of PMSF should be 1 mM.
3. Salt-free lysis buffer, pH 8.0: 25 mM HEPES, 0.1 % Triton X-100, 20 mM glycerophosphate, 1.5 mM $MgCl_2$, 1 mM DTT, 2 mM EDTA. Filter sterilize and store at 4 °C. Add fresh protease inhibitors to the salt-free lysis buffer before each

experiment. As per the manufacturer's recommendations, 10 μl protease inhibitor cocktail per 1 ml cell extracts. The final concentration of PMSF should be 1 mM.

4. Ammonium bicarbonate buffer, pH 8.0; 25 mM NH_4HCO_3. Filter sterilize. Store at −80 °C.
5. Streptavidin magnetic bead storage buffer: Dulbecco's phosphate-buffered saline (1×), 0.1 % bovine serum albumin (BSA), 0.2 % NaN_3. Store at −20 °C.
6. Blocking nonspecific buffer for streptavidin magnetic bead: Dulbecco's phosphate-buffered saline (1×), 0.1 % BSA. Store at 4 °C.
7. Dulbecco's phosphate-buffered saline (1×), ph 7.4. Store at 4 °C.
8. GnHCl buffer for dissolving protein pellets: 3 M GnHCl. Filter sterilize and store at 4 °C.

2.2 Protease Inhibitors

1. Protease inhibitor cocktail (Sigma).
   Store at −20 °C.
2. Phenylmethanesulfonyl fluoride solution (PMSF) (Fluka).
   Store at 4 °C.

2.3 Chemicals for Buffers

1. Sodium hydroxide (NaOH).
2. Sodium phosphate dibasic dihydrate ($Na_2HPO_4 \cdot 2H_2O$).
3. Ethylenediaminetetraacetic acid disodium salt dihydrate.
4. Ammonium bicarbonate (NH_4HCO_3).
5. 1 M Tris–HCl pH 8.0.
6. 4-(2-Hydroxyethyl)piperazine-1-ethanesulfonic acid ($C_8H_{18}N_2O_4S$).
7. Sodium chloride ($NaCl_2$).
8. Triton X-100.
9. Glycerol 2-phosphate disodium salt hydrate ($C_3H_7O_6Na_2P \cdot xH_2O$).
10. Magnesium chloride hexahydrate ($MgCl_2 \cdot 6H_2O$).
11. Calcium chloride dihydrate ($CaCl_2 \cdot 2H_2O$).
12. Potassium chloride (KCl_2).
13. Potassium dihydrogen phosphate (KH_2PO_4).
14. Sodium azide (NaN_3).
15. Purified BSA (New England BioLabs).

2.4 Chemicals for Protein Precipitation

1. Methanol (MeOH).
2. Chloroform ($CHCl_3$).
3. Guanidine hydrochloride (GnHCl) (Life Technologies, Inc.).

2.5 Protein Gel Reagents

1. NuPAGE 10 % Bis-Tris Gel 1.0 mm × 12 well (Invitrogen).
2. NuPAGE Sample Reducing Agent (Dithiothreitol) (Invitrogen).
3. NuPAGE LDS Sample Buffer (Lauryl alcohol sulfate, lithium salt) (Invitrogen).
4. NuPAGE Antioxidant (*N*,*N*-dimethylformamide and sodium bisulfite ($NaHSO_3$)) (Invitrogen).
5. SilverQuest Silver staining kit (Invitrogen).

2.6 Other Reagents

1. RNase A (Roche).
2. Dynabeads M-270 Streptavidin magnetic beads (Invitrogen).
3. Biotinylated sense oligonucleotide complementary to the PNA sequence.
4. Nuclease-free water.
5. Cell scrapers.
6. 15 ml capped tubes.
7. Microcentrifuge tubes.
8. Microcentrifuge.
9. Centrifuge for 15 ml tubes.
10. Cultured cells: The procedure can be performed in any cell culture system. We typically use rat cortical neurons plated in 35 mm dishes in ~12 ml of media at 400,000 cells/ml (~4.8×10^6 cells in each plate). For each PNA, we use minimum of 1.4×10^7 cells per experiment. However, the number of cells required for PAIR analysis depends on the abundance of the target mRNA. Lower abundant mRNAs may require increasing the number of cells.

3 Methods

3.1 In Vivo Formation of PNA-RNA-Binding Protein Complexes

A representative PAIR experiments

Sample name	Treatment
PNA #1 low concentration	20 μl of PNA #1
PNA #1 high concentration	40 μl of PNA #1
Negative control low concentration	20 μl of HEPES buffer saline
Negative control high concentration	40 μl of HEPES buffer saline

1. Collect 4 ml of media from each plate into a 15 ml tube. Aspirate the rest of the medium from the plate.
2. Add the 4 ml back to the plate.
3. Directly add 20 μl or 40 μl of each treatment (*see* chart above) to a plate.
4. Mix by slowly moving the plates in circles for ~20 s.
5. Incubate for 90 min at 37 °C in tissue culture incubator.
6. Rinse the cells 2× with 4 ml HBS (at room temperature).
7. UV cross-link for 2.5 min with UV light source.
8. Replace the HBS with 4 ml ice-cold TX-100 lysis buffer (*with freshly added protease inhibitors: PI and PMSF).
9. Scrape the cells and collect the cell lysate in a 15 ml tube.
10. Remove 30 μl of each sample and save for protein gel analysis. Label the tubes Total Cell Lysate for each sample. Store at −80 °C.
11. Place the cell lysates in the 15 ml tubes on dry ice for 60 min. Either proceed to the next step or store the samples at −80 °C.

(Potential stopping point)

3.2 Liberating the PNA-RNA-Binding Protein Complexes from the Cellular mRNAs

1. Thaw the cell lysates in RT water bath.
2. Add 12 μl of RNase A (1 mg/ml) to the cell lysates. Rotate the tubes at 37 °C for 20 min.
3. Place the cell lysates on dry ice for 60 min. Store the samples at −80 °C.

(Potential stopping point)

3.3 Linking of Biotinylated Sense Oligonucleotide to Streptavidin Magnetic Beads

1. Put 1 ml (=10 mg) of streptavidin magnetic beads into a micro-centrifuge tube.
2. Place the tube in the magnetic stand for 10 min, and then remove the buffer.
3. Add 1 ml of D-PBS and rotate for 10 min at room temperature.
4. Place the tube in the magnetic stand for 10 min, and then remove the buffer.
5. Wash the beads again with 1 ml D-PBS (repeat **steps 2–3**).
6. Dissolve the oligonucleotide (1 mg/ml in Tris-EDTA buffer.
7. Add 50 μl (=50 μg) of each oligonucleotide solution to 950 μl of 1× D-PBS.
8. Remove the buffer from the beads and resuspend them in 1 ml 1× D-PBS containing 50 μg biotinylated sense oligonucleotide (**step 7**).
9. Rotate the solution at room temperature for 1 h.

10. Magnetically separate the beads from the solution and wash the beads five times with 1 ml 1× D-PBS (*see* **step 2–3**).
11. Resuspend the beads in 1 ml D-PBS containing 0.2 % (wt/vol) BSA to block nonspecific binding to the beads.
12. Rotate the tubes at RT for 1 h.
13. Place the tube in the magnetic stand for 10 min, and then remove the buffer.
14. Briefly, wash the bead-streptavidin-biotin-oligo complex with D-PBS. For this wash, add 1 ml of D-PBS and vortex for 10 s at room temperature.
15. Place the tube in the magnetic stand for 10 min, and then remove the buffer.
16. Second brief wash (repeat **steps 7–9**).
17. Resuspend the bead complex in 1 ml (a final concentration of 10 mg/ml) storage buffer (0.1 % BSA (wt/vol), 0.2 % NaN_3 (wt/vol) in PBS, pH 7.4) and store at 4 °C.

3.4 Magnetic Bead Preparation

1. Take 30 μl (300 μg) of the magnetic beads (10 mg/ml), magnetically separate for 10 min on magnetic stand, and then remove the buffer.
2. Rinse 2× with 1 ml TX-100 lysis buffer containing freshly added protease inhibitors.
3. Rotate for 10 min at RT.
4. Centrifuge briefly.
5. Magnetically separate for 10 min on magnetic stand, and then remove the buffer.
6. Remove from magnetic stand and add 30 μl of the TX-100 lysis buffer (with protease inhibitors) to the magnetic beads.

(Note: The beads can be prepared in advance. The washed beads can be stored at 4 °C for a week.)

3.5 Purifying PNA-RNA-Binding Protein Complexes from the Cell Lysate

1. Thaw the cell lysate in water bath (RT).
2. Add 30 μl of the pre-washed magnetic beads from Section A to the cell lysates.
3. Rotate the tubes at 37 °C for 30 min and at RT for 30 min. The beads with sense oligo should now be annealed to the PNAs cross-linked to RBPs.
4. Centrifuge the supernatant tubes at 5000 RPM for 1 min.
5. Save a 30 μl aliquot (labeled as FT for flow-through) of the supernatant of each PNA sample for protein gel analysis. Store at −80 °C.
6. Without disturbing the pelleted beads, remove the supernatant until 500 μl of the lysate remains.

7. Transfer the PNA-coupled beads to a microcentrifuge tube.
8. Magnetically separate the beads from the lysate for 10 min and aspirate the supernatant.
9. While magnetized, rinse the beads 2× with 1 ml TX-100 lysis buffer containing freshly added protease inhibitors to remove any uncoupled lysate proteins.
10. Rotate for 20 min at RT, centrifuge briefly, magnetically separate for 10 min, and remove the buffer.

3.6 RBP Complex Elution from the Magnetic Beads

1. Resuspend the beads in 100 μl of salt-free TX-100 lysis buffer (with freshly added protease inhibitors) pre-warmed to 50 °C to elute the PNA-RBP complex.
2. Incubate the beads at 50 °C in a benchtop water bath flicking the tube periodically for 20 min.
3. Centrifuge the beads for 1 min at RT at maximum speed (13,200 RPM) in a benchtop centrifuge.
4. Transfer the eluate to a new microcentrifuge. The eluate now contains the RBPs bound to the specific PNA.

(Potential stopping point)

3.7 Methanol-Chloroform Precipitation of RBP Complexes

1. Add 400 μl of methanol to each microcentrifuge containing the eluate. Vortex for 10 s and centrifuge at 10,000 RPM for 10 s.
2. Add 100 μl chloroform, vortex for 10 s, and centrifuge at 10,000 RPM for 10 s.
3. Add 300 μl nuclease-free water, vortex for 10 s, and centrifuge at 10,000 RPM for 3 min at 4 °C.
4. The interphase now contains the proteins. Aspirate and discard the upper phase and leave ≤20 μl of the upper phase in the tube.
5. Add 300 μl methanol, vortex for 10 s, and centrifuge at 13,200 RPM for 10 min at 4 °C.
6. Decant the supernatant and air-dry the pellet for ~5 min.
7. Add 50 μl of 25 mM ammonium bicarbonate buffer.
8. Store at −80 °C for protein gel analysis. Alternatively the entire RBP precipitation can be used for mass spectrometry analysis.

(Potential stopping point)

3.8 Final Separation and Visualization of RBP Complexes via SDS-PAGE, Silver Staining, Mass Spectrometry Analysis

1. Run SDS-PAGE gels to analyze the PAIR results for each PNA. Load three samples for each PNA: (1) the total cell lysate, (2) flow-through, and (3) RBP complex precipitation.
2. Stain the gel with silver staining kit.
3. Excised protein bands of interest are analyzed by mass spectrometry.

4 Notes

1. *Contaminants in the mass spec analysis*
   Keratin- and protein-based experimental reagents, such as BSA and trypsin, are commonly detected in the mass spectrometry analysis. To eliminate keratin, investigators should avoid any direct experimental exposure to their skin by always wearing gloves and lab coats. Protein reagents should simply be removed from the mass spectrometry data. Lastly, restricting the opening of the tissue culture dishes to well-ventilated tissue culture hoods will prevent the introduction of other contaminants.
2. *Low yields*
   Some PNAs may not isolate a sufficient quantity of RBP complexes to perform the mass spectrometry analysis. Therefore, multiple PNAs should be designed and a few different concentrations of each PNA (*see* Subheading 3.1) should be tested for each exon of interest. Additionally it may be appropriate to use more cells to increase the yield.
3. *Verifying results*
   For any experimental result, using multiple experimental methodologies to verify initial findings is always a prudent approach. Therefore, before pursuing PAIR-identified mRNA-RBP complexes in more complex experimental systems (transgenetic animals) or functional studies (physiology or imaging experiments), investigators should consider confirming their results with other RBP isolation methodologies, such as immunoprecipitation. However, the in vitro biochemical approaches may not replicate the PAIR results, because they do not replicate the in vitro PAIR conditions. Also, other methods depend on antibodies to the target RBP to perform the experiments; this could be a limiting factor in using antibody-based methods. Investigators should be aware that it may not be possible to verify all PAIR results by traditional biochemical approaches and some PAIR results may not be reproduced by these approaches.
4. *Predicting results*
   The limited number of known neuronal RBPs makes it somewhat difficult to predict the potential identities of the proteins that will be identified with PAIR analysis. However, investigators should be open to pursuing a wide range of candidate proteins (tradition and nontraditional RBPs) for their exons of interest. PAIR analysis could yield novel RNA-binding proteins, signaling proteins that regulate RBP complexes associated with their exon, proteins that bind to RBPs and are close to where the PNA bound, as well as known RNA-binding proteins (such as FRMP) that regulate the RNA metabolism of their exon of interest.

5. *Identifying functional roles for the isolated RBPs*
   The PAIR procedure isolates exon-specific RBP complexes. The next challenge is to identify the functional impacts of the PAIR-identified RBPs. Most molecular, imaging, and electrophysiological techniques are compatible with cell culture-based model systems. This allows investigators to perform a diverse range functional screens in same model systems to rapidly transition from PAIR RBP screening to functional studies. RNA interference (RNAi) in conjunction with different functional screens is one to test the functional impacts of PAIR-identified RBP complexes. Three examples are described below:
   (a) *Do the PAIR-identified RBPs regulate subcellular distribution patterns of the exon of interest?* The combination of RNA interference and in situ hybridization (ISH) can be used to determine whether PAIR-identified RBP complexes regulate the localization patterns of your exon of interest. Via RNA interference (RNAi), the levels of PAIR-identified RBP can be selectively reduced and ISH can be used to screen for changes in the localization patterns of your exon of interest.
   (b) *Do the PAIR-identified RBPs regulate protein levels and expression patterns of your target mRNA?* RNAi and immunostaining can be used to determine whether PAIR-identified RBP plays a role in regulating the protein patterns of your target mRNA. Again, the levels of PAIR-identified RBP can be selectively reduced by RNAi and Western blot or immunostaining analysis can be used to identify changes in your target protein levels or subcellular distribution patterns.
   (c) *Do the PAIR-identified RBPs regulate the excitability of neurons?* RNAi and patch clamp analysis can be combined to determine if PAIR-identified RBP plays a role in regulating the membrane properties of neurons.
6. *Future experiments*
   One advantage of using a cell culture-based model experimental systems is that the cells are easily manipulated by pharmacological treatments. Therefore, investigators can combine the PAIR procedure with pharmacological manipulations to screen for activity-dependent changes in their PAIR-identified RBP complexes.

References

1. Miyashiro K, Dichter M, Eberwine J (1994) On the nature and differential distribution of mRNAs in hippocampal neurites: implications for neuronal functioning. Proc Natl Acad Sci U S A 91:10800–10804
2. Sidorov MS, Auerbach BD, Bear MF (2013) Fragile X mental retardation protein and synaptic plasticity. Mol Brain 6:15
3. Eberwine J, Belt B, Kacharmina JE, Miyashiro K (2002) Analysis of subcellularly localized mRNAs

using in situ hybridization, mRNA amplification, and expression profiling. Neurochem Res 27(10):1065–1077

4. Lovatt D, Ruble BK, Lee J, Dueck H, Kim TK, Fisher S, Francis C, Spaethling JM, Wolf JA, Grady MS, Ulyanova AV, Yeldell SB, Griepenburg JC, Buckley PT, Kim J, Sul JY, Dmochowski IJ, Eberwine J (2014) Transcriptome in vivo analysis (TIVA) of spatially defined single cells in live tissue. Nat Methods 11:190–196
5. Zeng F, Peritz T, Kannanayakal TJ, Kilk K, Eiriksdottir E, Langel U, Eberwine J (2006) A protocol for PAIR: PNA-assisted identification of RNA binding proteins in living cells. Nat Protoc 1:920–927
6. Zielinski J, Kilk K, Peritz T, Kannanayakal T, Miyashiro KY, Eiriksdottir E, Jochems J, Langel U, Eberwine J (2006) In vivo identification of ribonucleoprotein-RNA interactions. Proc Natl Acad Sci U S A 103:1557–1562
7. Bell TJ, Miyashiro KY, Sul JY, Buckley PT, Lee MT, McCullough R, Jochems J, Kim J, Cantor CR, Parsons TD, Eberwine JH (2010) Intron retention facilitates splice variant diversity in calcium-activated big potassium channel populations. Proc Natl Acad Sci U S A 107:21152–21157
8. Bell TJ, Miyashiro KY, Sul JY, McCullough R, Buckley PT, Jochems J, Meaney DF, Haydon P, Cantor C, Parsons TD, Eberwine J (2008) Cytoplasmic BK(Ca) channel intron-containing mRNAs contribute to the intrinsic excitability of hippocampal neurons. Proc Natl Acad Sci U S A 105:1901–1906
9. Xie J, Jan C, Stoilov P, Park J, Black DL (2005) A consensus CaMK IV-responsive RNA sequence mediates regulation of alternative exons in neurons. RNA 11:1825–1834

INDEX

A

Actin cytoskeleton 248–252, 257
Alpha helix 296
Alternatively spliced exons 458
AMP. *See* Antimicrobial peptides (AMP)
Amphipathic..... 5–11, 13, 17, 33, 76, 134, 164, 177, 225, 227–229, 231, 233–234, 284–285, 350, 418, 421–422, 428–429, 435
ANNs. *See* Artificial neural networks (ANNs)
Anticancer efficacy 283–285
Antimicrobial peptides (AMP) 48, 224–236, 239, 283–285
ANTS..... 90, 91, 94–97, 100–103
ApoE. *See* Apolipoprotein E (ApoE)
Apolipoprotein B (ApoB)..... 331–336
Apolipoprotein E (ApoE) 332
Arginine-rich cell-penetrating peptide..... 13, 49, 165, 235, 238, 389, 390
Artificial neural networks (ANNs)..... 40, 51, 53–54

B

Bacteriorhodopsin 77, 79–80, 82
BBB. *See* Blood–brain barrier (BBB)
Bilayer permeabilization 90–94
Bioportide..... 178, 180–188
Blood–brain barrier (BBB)..... 206, 236, 331–333, 349–352
Botulinum toxin 397–414
Brain delivery 349–354
Brain tumor..... 206–207, 212–213, 215, 350–351

C

Caco-2..... 261–265, 268–272
Calcein leakage..... 79, 81–82, 292–293
CD. *See* Circular dichroism (CD)
Cell culture 14, 113–114, 118, 137–140, 143–145, 152, 155–156, 166–167, 179–180, 185–186, 207, 210, 216–218, 236, 238, 249, 250, 261–265, 268–272, 281–282, 286, 289, 296–297, 304, 306, 309, 319–320, 322, 352–354, 361, 391–394, 436, 438–439, 451, 452, 462, 467
Cell-penetrating peptides (CPP) 3–21, 33–34, 39–57, 59–68, 73–85, 89, 90, 92, 102–103, 107–120, 123–130, 133–147, 149–152, 160, 163–172, 177–188, 206, 210, 218, 223–239, 247–258, 261–275, 279–299, 304–310, 312, 314, 317–346, 349–354, 357–367, 387–395, 397–414, 418–419, 423–424, 426–431, 435–444, 448–450, 458–460
Cell-penetrating peptides as carriers 7, 14, 16, 109, 163, 231, 236, 261–275, 351, 358–359, 370–371, 401–402, 405–406, 413–414, 426, 430–431
Cell trafficking 424
Cell viability 7, 118, 135, 137–140, 144, 185, 217, 263–271, 273–274, 281, 285, 373
Cell wall 229, 418–422, 424, 428–429
Circular dichroism (CD) 73–75, 79, 81, 91, 112, 291, 294–295, 298, 439, 443
CNS delivery..... 331–332, 351
Confocal microscopy 31, 126–129, 179, 183–184, 187, 209, 216, 249–252, 254, 362–363, 365–366, 391, 452
Counteranion 389–390
CPP. *See* Cell-penetrating peptides (CPP)
CPP classes..... 6
CPP kinetics..... 134
CPP mechanisms 12, 103, 107–120
CXCR1 ..... 18, 193, 198–199
CXCR2 ..... 18, 193, 198–199
CXCR4 ..... 12, 18, 165, 193–195, 198–199, 233–234
Cytochalasin D..... 15, 249, 421

D

Delivery..... 3, 29, 60, 77, 89, 133, 149, 164, 177, 206, 223, 248, 261, 279, 303, 317, 331, 339, 349, 357, 369, 388, 397, 417, 435, 448
Direct membrane penetration..... 40, 394, 418

Ülo Langel (ed.), *Cell-Penetrating Peptides: Methods and Protocols*, Methods in Molecular Biology, vol. 1324,
DOI 10.1007/978-1-4939-2806-4, © Springer Science+Business Media New York 2015

DLS. *See* Dynamic light scattering (DLS)
DNA 4–5, 7, 17–18, 30, 31, 33, 150, 220, 229, 281, 289, 303–304, 308–309, 311, 313, 320, 324, 326, 334–335, 339–340, 346, 394, 417–418, 423, 425–427, 429–431, 435–444
DPX 90–91, 94–95, 97, 100–101, 103
Drug delivery 60, 68, 134, 234–236, 261–275
Drug delivery system 235, 249, 266, 273
Dynamic light scattering (DLS) 74, 81, 84–85, 112, 165, 266, 291–292, 295, 364, 382, 383

E

Electrostatic interaction 32–33, 51, 53, 56, 75, 279–280, 370, 390, 400, 418, 429, 431
ELISA. *See* Enzyme-linked immunosorbent assay (ELISA)
Endosomal escape 19–20, 68, 77–78, 80, 82, 150, 224, 305, 351, 371–373, 380
Enzyme-linked immunosorbent assay (ELISA) 136–138, 140–142, 171, 274, 404
Exine 421–422, 424
Exon skipping 20, 317–328
Ex vivo 34, 206, 208, 211–212, 214, 218–219

F

Fillapodia 252, 256
Fluorescence 15–16, 19, 73–77, 79–82, 84–85, 91, 96–101, 103, 112, 124, 127–128, 130, 137, 149–150, 209, 217, 252, 281, 286–290, 292–293, 296–298, 311, 320–321, 323–324, 327, 341–344, 346, 365, 383, 387–388, 392, 423, 428, 448–449

G

GAGs. *See* Glycosaminoglycans (GAGs)
Gene delivery 306, 308, 339–346, 417–418, 425–427, 430–431
Glioblastoma 206, 281, 287, 350–352
Glycosaminoglycans (GAGs) 10, 33–34, 111–112, 123–127, 129–130, 206, 280, 305, 429
G-protein-coupled receptors (GPCRs) 18, 178, 191–193, 195–196, 199

H

HCV. *See* Hepatitis C virus (HCV)
Hepatitis C virus (HCV) 166, 236–237
High-throughput screening 60, 266, 285
HIV. *See* Human immunodeficiency virus (HIV)
Homeodomain 30–31, 34, 111
Homeoprotein 3, 5–7, 29–30, 32
Human immunodeficiency virus (HIV) 5, 7, 8, 29, 30, 230, 232, 233, 236–237, 239, 257, 357
Hyperhidrosis 397–398, 403, 407, 411

I

Incubation 76–77, 109, 111, 115–116, 118–120, 126–130, 141, 143, 145, 152, 156, 160, 211–212, 216, 218, 254, 257, 267, 269, 271–275, 286, 288, 313, 320, 323–324, 327, 342–343, 365, 367, 378–379, 383, 420, 429, 436, 439, 441–444
Immunofluorescence 124–125
Immunogenicity 133–147, 370, 408
Intracellular trafficking 149–151
In vitro 4, 55, 89, 112, 134, 136–137, 206, 221, 223, 261–275, 285, 304, 306, 316–328, 340, 348, 350–352, 359, 361, 382, 397, 401, 403, 407, 425, 455, 466
In vivo 4, 13–14, 18, 20, 34, 55, 133–134, 142, 204–221, 223, 230, 236, 262, 304, 306, 314, 317, 339–346, 349, 351, 358–359, 366–367, 371, 397, 400–401, 403, 424, 448–449, 458, 460, 462
In vivo reporter gene induction 339, 346
Ionic 12, 32, 160, 193, 382, 400–401, 405

K

Kinetic uptake studies 14, 133–147, 150

L

Lamellapodia 254–258
Large unilamellar vesicles (LUVs) 74–85, 96–98, 100, 102, 290–295
Lateral canthal lines (LCLs) 398, 403, 407–410, 412–414
LCLs. *See* Lateral canthal lines (LCLs)
LDLR. *See* Low-density lipoprotein receptor (LDLR)
Leakage assay 91, 94–95
Lipidated CPPs 112, 191–200
Lipopeptides 110, 195–196
Liposomes 133, 167–168, 171, 290–292, 350–351, 358–364, 366–367
Low-density lipoprotein receptor (LDLR) 331–336
LUVs. *See* Large unilamellar vesicles (LUVs)

M

Machine learning approach 40, 51–55
Macropinocytosis 12–13, 16, 34, 146, 165, 248, 254, 258, 327, 422, 428–429
Mass spectrometry 16, 107–120, 304, 322, 393, 459–460, 465–466
Mast cell 5, 178, 185, 188, 198
Metabolic degradation 265, 272
Metabolic labeling 124, 126, 128
Metabolic stability 262–263
Microspore 420–426, 430
Mitochondrial membrane permeability 281

Mitochondrial Network organization..... 281, 287–288
Molecular docking..... 40, 55–56
Molecular dynamics..... 40, 56–57
Mucus..... 261–263, 265, 270, 272, 274
Multifunctional nanocarriers..... 361, 363, 365–366
Multivariate statistics..... 40

N

Nanogold-labeled oligonucleotides..... 151–156, 158–160
Nanoparticle formation..... 163–172, 206
NickFect..... 9, 17–18, 75, 150, 160, 165, 303–314, 436
NMR. *See* Nuclear magnetic resonance (NMR)
Noncovalent complexes..... 340
Nuclear magnetic resonance (NMR)..... 32, 47, 73–75, 112, 196, 378–379, 384, 390
Nude mice..... 197

O

Oligonucleotide delivery..... 34, 149–151, 169
Oligonucleotides (ONs)..... 17–18, 34, 89, 150–155, 158–160, 163, 166, 168–170, 303–308, 333–334, 352, 431, 460, 462–464
ONs. *See* Oligonucleotides (ONs)

P

PAR1..... 9, 18, 192, 194–198
PAR2..... 192, 195, 198
PAR4..... 192–193, 196–198
PB. *See* Pyrenebutyrate (PB)
Penetratin..... 5, 7, 10, 14–16, 29–35, 40–41, 77, 110, 120, 134, 177, 225, 230, 236–237, 285–287, 318, 350, 357, 370, 418–420
Penetration-accelerating sequence (PAS)..... 389–392, 394
Pepducins..... 18, 191–200
PepFect..... 9, 17–18, 75, 150–151, 155, 160, 238, 303–314, 341, 351
Peptide/lipid interaction..... 33, 224, 298
Peptide quantification..... 107
Peptides deduced from vascular epithelial cadherin (pVEC)..... 5, 8, 10–11, 15–16, 206, 230, 232, 233, 418–422
Permeability..... 16, 19, 20, 29, 84–85, 90–94, 103–104, 178, 181, 185, 206, 226, 229–230, 237, 250, 269, 271, 273, 275, 281, 351–354, 358, 421, 424–425
Phage display..... 19–20, 205–221, 232, 234, 351
PH gradient..... 32, 77, 79–80, 82–84
Phosphorodiamidate morpholino oligomers (PMO)..... 13, 20, 230, 237–238, 317–318, 320–321, 323–324, 327–328
Plant cells..... 417–418, 420–430
Plasmid DNA (pDNA)..... 17–18, 150–151, 303–304, 306–312, 314, 339–340, 342–346, 352–354, 370, 425, 429–431, 436, 438, 440–442
PMO. *See* Phosphorodiamidate morpholino oligomers (PMO)
Polymer conjugates..... 370
Polymeric micelles..... 358–360, 363
Polyplex..... 340, 370–373, 375, 381–383, 385, 418
Pore formation..... 90, 93, 228, 231
Pore size..... 79, 81, 82, 90, 94–95, 212, 273, 319, 353, 362–363
Posttranscriptional regulation..... 457–458
Prediction..... 39–57, 60–63, 65, 68, 178, 180, 340
Protein–protein interaction..... 387–388
Proteins..... 3, 29, 48, 59, 74, 89, 108, 125, 133, 150, 163, 177, 191, 205, 223, 258, 261, 283, 303, 320, 331, 341, 349, 357, 369, 387, 399, 418, 435, 457
Protein transport..... 331–332
Proton pumping..... 77–78, 83
PVEC. *See* Peptides deduced from vascular epithelial cadherin (pVEC)
Pyrenebutyrate (PB)..... 76, 389–392, 394

R

Recombinant protein production..... 436
Resonance..... 47, 73, 448–449
RNA..... 4–5, 7, 12, 49, 150, 166, 197, 236–239, 303, 317, 320, 324–326, 328, 350, 369–385, 418, 426–427, 436, 447, 451, 455
RNA-binding protein..... 7, 457–467

S

SCARA. *See* Scavenger receptor (SCARA)
SCARA3..... 166–168, 170
SCARA5..... 166–168, 170
Scavenger receptor (SCARA)..... 18, 55, 151, 163–172, 305, 308, 350
Screening..... 59–68, 112, 178, 195, 206, 209, 211, 214, 234, 263–264, 266, 285, 305, 308, 342, 382, 397, 401, 448, 455, 458, 467
Second-generation CPPs..... 17–19
Secretion..... 180, 185–186, 188, 198, 221, 224, 262, 352, 354, 399
Silencing RNA (siRNA)..... 4, 12, 18, 20, 56, 140, 141, 143, 150, 163, 165–170, 172, 237, 303, 306–308, 350, 370–372, 374–375, 380–383, 427, 428
Single-cell transcriptome..... 447–449
Single-chain antibody fragments..... 124, 125
SiRNA. *See* Silencing RNA (siRNA)
Splice-correction..... 168, 170, 238, 303, 306

Stable isotopically labeled internal standard 108
Stimulus-sensitive nanoparticles..... 364–366
Support..... 34, 40, 54, 55, 61, 90, 209, 224, 226, 248, 257, 258, 290–291, 349, 370, 375, 400, 413, 414
Support vector machine (SVM) 40, 51, 54, 61–66, 68
SVM. *See* Support vector machine (SVM)

T

T7..... 206, 208–210, 213, 217–220
TAT..... 30, 31, 76, 134, 164, 165, 225, 349, 350, 357–367, 370, 400, 418–426, 428, 429
Tat..... 5, 7, 8, 11–17, 20, 29, 33, 110, 124, 177, 230, 232, 233, 235–239, 257
TAT2..... 420, 421, 423–426, 428, 429
TATp. *See* TAT peptide (TATp)
TAT peptide (TATp)..... 357–366
TEM. *See* Transmission electron microscopy (TEM)
Terbium..... 95, 98, 101
Therapeutics..... 20, 34, 59, 133, 134, 191–200, 206, 223, 229, 234–239, 261, 279, 305, 306, 331, 339, 357–359, 366, 369–385, 397, 398, 400, 401, 410, 413, 423, 427
Toxicity..... 33, 133–147, 159, 171, 227, 231, 263, 290, 297, 311, 339, 358, 359, 369, 370, 372, 373, 403, 425, 436, 443, 444
TP. *See* Transportan (TP)
Transcriptomics..... 447–456
Transcytosis..... 331, 350, 351
Transepithelial drug delivery 261–275
Transfection..... 4, 29, 144, 146, 147, 160, 167–169, 171, 237, 238, 288, 289, 297, 304, 306, 308, 312–314, 320, 333, 336, 339, 340, 350, 382, 425, 429–431, 435–444
Transfection reagent..... 167, 168, 171, 237, 289, 312, 313, 333, 339, 435–444
Transient leakage..... 93
Transmission electron microscopy (TEM)..... 150–154, 156, 157, 160, 364
Transportan (TP) 5, 8, 10, 14, 15, 76, 129, 134, 177, 231–233, 236, 357, 419–422
Transwell..... 351–353
Tumor-homing CPP..... 206, 283, 285
Tumor targeting..... 206, 215, 285, 424

U

Uptake mechanism..... 6, 12, 61, 75, 134, 139, 144, 150, 151, 164, 235, 279, 318, 357

V

Vasculature 205, 221, 358
Vector machines 40, 54, 61
Vesicle leakage..... 75, 91
Virtual 52, 59–68, 349
Virtual screening 59–68